ADVANCES IN WELL DELIVERABILITY AND PRODUCTION FORECASTING

MIKE J. FETKOVICH

THE UNIVERSITY OF TRONDHEIM
NORWEGIAN INSTITE OF TECHNOLOGY
DEPARTMENT OF PETROLEUM ENGINEERING
1989

ADVANCES IN WELL DELIVERABILITY AND PRODUCTION FORECASTING

Submitted by
Mike J. Fetkovich

to
The University of Trondheim
Norwegian Institute of Technology
Department of Petroleum Engineering

as fulfillment of
requirements for the degree
doctor of the technical sciences

December 1988

DEDICATION

To Emily, my wife and support for the past 35 years.

FOREWORD

This thesis is a compilation of independent research performed during the period 1965 to 1988. The research and subsequent publications really started when I transferred to Phillips Computing Department as an Engineering Analyst in 1963. This was the period that I was given total responsibility and Computing Department support for developing general purpose gas reservoir and production engineering computer programs for company-wide use. My previous nine years of experience as a gas reservoir and production engineer in the Natural Gas Department, which include three years of field experience, were the principal source of many of my ideas for computer program development and future publications.

It is to M. H. (Doc) Cullender that I am most indebted to for taking a chance on me after graduating from the University of Pittsburgh in 1954 (at that time a truly confirmed stutterer) for offering me an engineering position with Phillips Petroleum Company's Natural Gas Department. My first three years were as a gas well test engineer in the Texas and Oklahoma Panhandle gas fields. The methods of testing and analyzing gas well performance that M. H. Cullender, C. W. Binckley, and R. V. Smith had developed and implemented within Phillips to this day have not been surpassed by the rest of the industry. My next six years as a natural gas reservoir and production engineer were in the Bartlesville office under the direct supervision of R. V. Smith and M. H. Cullender where I was able to grow technically through exposure to a variety of engineering assignments.

My transfer to the Computing Department under the supervision of B. L. Giles and H. W. Hennigan was virtually the start of a new career. With the aid of the computer, I was able to accomplish one to two orders of magnitude more productive work. Having developed and maintained most of the natural gas reservoir and production engineering computer programs, I began to be called on as a consultant to our International and Domestic Exploration and Production Departments. These practical applications to real field problems led to many modifications and enhancements to our existing computer programs. Work on several of the projects eventually led to some of my later publications.

While with the Computing Department, I had the opportunity to attend an advanced reservoir engineering school at Texas A&M University. It was there that I first met Professor H. J. Ramey, Jr. Later, working with him when he was consulting with me on pressure transient analysis of our early Ekofisk Field discovery wells, he introduced me to the graphical type curve analysis approach and several other significant pressure transient concepts. Through his encouragement, I began to publish some of the papers I had been sitting on; the "Decline Curve Analysis Using Type Curves" and "The Isochronal Testing of Oil Wells" papers.

After 10 years in the Computing Department, I transferred to the newly organized World Wide Natural Resources Group in 1973 as Staff Director of Reservoir Engineering under the direction of A. F. Bertuzzi. The past 15 years have been spent on solving practical field problems with simple basic concepts and approaches.

Some of the colleagues I have had the pleasure of working with and exchanging ideas are, A. F. Bertuzzi, D. J. Ebbs, and L. K. Thomas all with Phillips Petroleum Company, Raj Raghavan and Curtis Whitson with academia, and Flavio da Silva with Petrofina.

Special thanks to J. L. Whitmire and J. F. Griggs for giving me the time and resources to put together this thesis. Also to K. Patton and S. Baughman for their efforts in typing, re-drafting, and assembling the final product.

Finally, I would like to honor my parents, Mike and Anna Fetkovich, for their encouragement and assistance to go to college in the first place. It was my father who first suggested that I consider taking Petroleum Engineering to escape the steel mills of Pennsylvania.

Contents

ADVANCES IN WELL DELIVERABILITY AND PRODUCTION FORECASTING

INTRODUCTION

The one common simple concept that appears throughout all of my writings is - given a rate equation and a material balance equation, one can produce a production forecast. Production forecasts of wells or fields may have a period of constant rate production followed by a constant wellbore pressure period of declining production. These concepts were developed and applied as a result of my early years working as a natural gas reservoir and production engineer in the West Panhandle and Texas and Oklahoma Hugoton gas fields.

An understanding of the gas material balance equation was developed from the analysis of literally thousands of pressure-cumulative production graphs developed from both official state tests and informational shut-in pressure data. Rate equation concepts, both transient and pseudo-steady state behavior, were developed as a result of personally conducting numerous isochronal tests, official state tests, and maintaining thousands of well performance curves, log $(\bar{p}^2 - p_{wf}^2)$ vs log q backpressure curves, with which the maximization of allowable and production from gas wells was achieved. As with pressure-cumulative production graphs, both official state tests and routine monthly informational spot flow performance data were used to maintain the individual well backpressure performance curves. With the gas-in-place indicated from a pressure cumulative production graph and the stabilized performance curve established from actual field performance data, production forecasts were routinely made for various future production schemes.

What follows will be a brief summary of each of my papers, both published and unpublished, along with some insight into my thinking at the time. All of my papers were a result of attempts to understand and solve actual field problems. The papers will be discussed in chronological order.

SUMMARY

The Effect of Water Influx on P/z - Cumulative Gas Production Curves

This paper was a result of a field study conducted on a large moderately overpressured gas reservoir in the Texas Gulf Coast area. Investments were made on the basis of an early performance linear extrapolation of the field $P/z - G_p$ graph to an apparent original gas-in-place that was later found to be 200 Bscf overstated. Figure 5, Run 20 of this paper representing a small finite aquifer system, $R_a/R_r = 5$, illustrates the actual behavior of our field of study.

The gas material balance equation in terms of $P/z - G_p$ was modified to include the effect of water influx. This was also my first exposure to the constant wellbore pressure solutions of van Everdingen-Hurst that would later be utilized in developing rate-time decline curve analysis concepts. The rate equation used in this study was a total field wellhead backpressure curve developed by summing up each individual well's wellhead backpressure curve.

Limited Aquifer Performance

This paper immediately followed the previous paper but was based on an investigation of overpressured gas reservoirs which by their nature of being overpressured normally consist of limited aquifers. A complete material balance derivation that included the expansion effects of rock and water and gas in solution in the water resulted in a new linear form of the gas material balance equation. The cumulative compressibility term, $\overline{C}_e$, is based on the expansion of rock, water, and gas in solution in the water from the initial reservoir pressure, p_i, to any subsequent reservoir pressure, p_n. Normally, $\overline{C}_e$ is fairly constant down to normal abandonment pressures used for overpressured gas reservoirs.

A Simplified Approach to Water Influx Calculations - Finite Aquifer Systems

As pointed out in the published abstract of this paper, "The separation of the water influx problem into a rate equation and a material balance equation, not requiring superposition, makes the concepts and calculations quite simple and easy to apply." The approach used in this paper utilizes the stabilized or pseudosteady-state aquifer productivity index and an aquifer material balance equation to represent the finite compressible system. By combining the two equations, we obtain an equation expressing the instantaneous rate of water influx as a function of time and the inner boundary constant pressure, p_{wf}. Simply changing the variables from water to oil results in the constant wellbore pressure exponential decline equation used in oil well rate-time decline analysis.

The technical note "Conversion of van Everdingen-Hurst B and t_D to values of PI_w and W_{ei} for use in the Simplified Approach to Water Influx Calculations" illustrates with a field example how to obtain the aquifer PI and original water in place when the van Everdingen-Hurst solution is used to determine the original gas-in-place for a range of finite aquifer systems.

The Isochronal Testing of Oil Wells

This work was initiated as a result of Vogel's computer simulation work on inflow performance for solution gas drive reservoirs. His proposed empirical relationship for oil well inflow performance was presented in the same dimensionless form as that developed for gas wells by Phillips engineers in the early 1950's for sizing orifice plates to obtain a good spread of flow points on multi-point isochronal tests. When Vogel's relationship was plotted on the gas well dimensionless curve, it fell very close to that for a gas well backpressure curve with a slope n = 1. In fact, Fig. 17 of the paper "Case Study of a Low-Permeability Volatile Oil Field Using Individual-Well Advanced Decline Curve Analysis" illustrates that the gas well Δp^2 form of the equation with n = 1 better fits Vogel's computer calculated IPR over the entire range of depletion than his own dimensionless empirical form of the IPR equations.

From some 40 oil well backpressure tests examined in this study, the exponent n, for the Δp^2 form of the oil well backpressure equation, was found to lie between 0.568 and 1.0, very near the limits commonly accepted for gas well backpressure curves. This paper clearly demonstrated that gas wells and oil wells behave very similarly and should be tested and analyzed using the same basic flow equations. The pressure function $1/\mu_o B_o$ and $1/\mu_o B_g$ are shown to be very similar and suggest a real oil potential approach analogous to the real gas potential approach now used for gas wells. Further, a non-Darcy flow term or rate dependent skin was detected in some of the oil well tests conducted even in the single phase liquid region. For wells at or below the bubble point pressure, a rate and time dependent skin due to near wellbore gas blockage was also identified and quantified.

For the oil well backpressure curve relationship to be useful for simple production forecasting or developing rate-time decline curve equations, the change in k_{ro} with depletion must be accounted for. Through personal observations from many conventional material balance forecasts for solution gas drive reservoirs, k_{ro} was found to be approximately linear with reservoir pressure resulting in the following equation

$$q_o = J_{oi}' \left(\frac{\bar{p}_R}{p_{Ri}} \right) (\bar{p}_R^2 - p_{wf}^2)^n$$

This equation with n = 1 was tested using Vogel's computer simulation results and also those computer simulation results reported by Levine and Pratts with good results. Some limited unpublished data on a field in Venezuela also supports the above relationship. This final form of an oil well rate equation that accounts for drawdown and depletion was used to develop oil well decline equations and define the limits of the decline exponent b in terms of the backpressure slope n and to determine its range of expected values.

A technical note: Oil Wells Inflow Performance was prepared to illustrate more clearly through examples the use of the various forms of inflow performance equations. The write-up was later furnished to SPE for inclusion in the Production Engineering Volume update.

Decline Curve Analysis Using Type Curves

This paper demonstrates that both the analytical constant wellbore pressure infinite and finite reservoir single phase liquid solutions can be placed on a common dimensionless log-log type curve with all the standard "empirical" exponential, hyperbolic and harmonic decline curve equations developed by Arps. Simple combinations of material balance equations and gas well and oil well inflow performance rate equations illustrate under what circumstances specific values of the hyperbolic decline exponent b should result for gas wells and oil wells.

The main contribution of this paper to rate-time production analysis and forecasting was the inclusion of the early transient period along with the Arps depletion stems ranging between a b = 0 to 1.0. The widespread misuse of Arps equation with transient rate-time data generally results in technically incorrect overly optimistic forecasts with indicated b values in excess of 1. To date, there has been no realistic physical system found that results in values of the depletion decline exponent b in excess of 1 that can be maintained throughout the life of a well.

Another important contribution from this work is the demonstrated ability to calculate kh and skin from routine monthly production data. Not brought out in this or subsequent papers is the concept that the decline exponent is a reflection of the efficiency of the drive mechanism for volumetric solution gas drive single layer reservoirs. The lower the recovery efficiency, the lower the value of b. This can be envisioned from the fact that regardless of the ultimate recovery efficiency of a reservoir, the early transient performance will be the same before boundary effects are felt. Future projection of rate-time data past the transient period results in higher recoveries for increasing values of b. Thus, b = 0 is an indication of a low recovery efficiency and a b = 0.5 would yield the highest recovery efficiency. For a single layered, or equivalent, system, a maximum value of b = 0.5 appears to be applicable to gas wells, oil wells, and full water drive oil fields.

Multipoint Testing of Gas Wells

This paper outlines the various methods of testing gas wells to establish their transient or stabilized well performance curves. In the case of very low permeability reservoirs where the wells have been stimulated, a single long duration flow, with rates and pressures recorded frequently, is recommended over multipoint testing to obtain maximum useful information for establishing a well's deliverability curves. The concept of rate normalization to analyze drawdown data is introduced at this time and will be discussed in more detail in a later section.

Transient and pseudo-steady state or stabilized deliverability equations are given at reservoir conditions and defined in terms of the laminar and non-Darcy (turbulent) flow component pressure drops. In this form, it becomes obvious that low permeability gas wells will have a slope n approaching 1 whereas high permeability gas wells yield slopes more nearly approaching 0.5. This concept is useful in establishing a well's deliverability curve when multipoint data are not available to directly determine the back-pressure curve slope n.

Since gas is sold at the surface, the bottomhole curve is given at a surface datum where the effects of tubing and gathering line friction pressure drops can be included. The form of equation to express pressure drops thru tubing gathering lines and surface equipment is shown to be identical to that of the reservoir non-Darcy flow term.

Examination of the total pressure drop equations indicates that in wells with large bottomhole potentials, we should expect the slope of the wellhead deliverability curve to approach 0.5, the slope of all pipe flow and turbulent pressure drop components. The wellhead curve could, in some instances, be totally described by the pressure drop through the tubing string. The well could then be defined as being tubing limited. Once tubing limited, always tubing limited i.e., the wellhead curve cannot shift to the right with decreasing reservoir pressure and corresponding decreased flow rates. These types of wells are candidates for tubing change outs to larger diameters providing the production casing string will allow.

This paper is the documentation of the reservoir engineering approaches used in the late 1960's to develop and forecast the production performance of the Hewett Gas Field located in the U.K. sector of the North Sea. The field was developed with 7 inch tubing in all wells drilled with an 8 well cluster radius of only 900 feet with an equivalent total field radius approaching 9000 feet.

Well Testing and Analysis in Indonesian Reef Reservoirs

This paper presents procedures and methods of testing and analyzing oil and gas wells drilled in naturally fractured reef reservoirs to determine the formation characteristics, stimulation skins, and well deliverabilities. Buildup plots are shown that indicate a constant pressure boundary (active bottom water drive) could be detected from initial test analysis. This was later confirmed several years later when the fields were abandoned.

The multi-point oil well tests obtained in wells with a totally undersaturated oil clearly indicated non-Darcy flow behavior in these high permeability naturally fractured reef reservoirs. A decline exponent b of 0.5 was indicated from the historical rate-time performance data for these full water drive fields.

Decline Curve Analysis Using Type Curves - Case Histories

This paper presents numerous case history studies that demonstrate methods of analyzing rate-time data to predict future production and to determine reservoir variables. For the first time, the ability to calculate reservoir pore volume from rate time analysis is presented.

Case histories for individual oil and gas wells are presented along with groups of wells in a field and total field studies. The field studies include a one-well full water drive field, a low permeability solution gas drive field, and a field with both primary and secondary (waterflood) history. Examples are given for the "trap" of fitting transient rate-time data to Arps' equation resulting in technically unsound and optimistic forecasts of future production rates. To identify transient rate-time data and its end, a log-log plot of the rate-time data must be made. Arps' equation must only be applied to rate-time data that indicates depletion.

Rate Normalization of Buildup Pressure By Using Afterflow Data

This study illustrates the utility of two basic methods of normalizing transient rate and pressure data. Rate-normalized pressure ($\Delta p/q$) for constant rate analysis and pressure normalized rate ($q/\Delta p$) for constant wellbore pressure analysis. The successful application of normalization techniques to rate-time decline curve analysis require that both rate and pressure data be recorded frequently and that only fixed choke tests be conducted so that rate and pressure data decline smoothly and monotonically.

Shape Factor, C_A, Expressed as a Skin, s_{CA}

This work was developed in an attempt to calculate reservoir interference effects of well locations on production forecasts utilizing pseudo-steady state or stabilized backpressure curves. When using backpressure or deliverability curves based on pseudosteady-state flow equations, the effect of a well not located in the center of a radial or square drainage area becomes immediately apparent when the shape factor C_A is expressed as a skin term. This work evolved from a study of drilling additional well location in the North of Hewett Gas Fields in the U.K. sector of the North Sea.

A somewhat similar approach was used in determining the development drilling cluster pattern finally selected for the Hewett Gas Field located in the same area. In this case, however, Muskat's Cluster Wells Equation was used to develop a skin effect for a well located at a cluster radius r in a field with n wells and a total field drainage radius R.

Both these papers illustrate the use of simple concepts in developing a well's deliverability or backpressure curve for production forecasting in what may first appear to be a complex problem solvable only by computer reservoir simulation studies.

Case Study of a Low-Permeability Volatile Oil Field Using Individual-Well Advanced Decline Curve Analysis

This paper presents a detailed case history study of a low permeability volatile oil field. The field was analyzed on an individual well basis using advanced decline curve analysis for 40 wells. Well permeabilities, skins, original oil-in-place (OOIP), and production forecasts are calculated for each well from rate-time analysis using constant wellbore pressure type curve analysis techniques.

Multi-well decline curve analysis shows the validity of the variables s (skin), k, OOIP, ultimate fractional recovery, and gas-oil ratio versus fractional recovery evaluated from each well's type curve evaluation. These variables must all give consistent and reasonable numbers when compared with each other. A single well analysis can easily give results that are not recognized as being invalid unless compared with other wells in the field.

The study also illustrates flowing and pumping well backpressure changes in a well's decline, the method of handling such changes, and their effect on ultimate recoverable reserves predictions. Conventional decline curve analysis cannot handle backpressure changes because of its constraint that

what controls the decline in the past will also continue in the future. The oil inflow performance relationship used to handle backpressure changes is thus utilized over the entire production forecasts, not just at an instant in time.

Oil and Gas Relative Permeabilities Determined From Rate-Time Performance Data

This study presents a method of determining k_g/k_o, oil relative permeability, k_{ro}, and gas relative permeability, k_{rg}, using oil and gas rate-time performance data from individual wells and from a total field. Advanced decline curve analysis is used to obtain original oil-in-place, N, and thus saturation; the Δp^2 form of an oil inflow performance equation is used to determine k_{ro} below the bubble point pressure.

The procedure was used on production data from several wells in a North Sea naturally fractured limestone volatile oil field. Results indicate the calculated oil and gas relative permeability curves differ from laboratory and correlation calculated curves. By analyzing the oil and gas relative permeability curves of each of the seven wells in the field, it was found that the degree of natural fracturing of a specific well influences the position of the oil and gas relative permeability curves. The results expressed as k_g/k_o curves appear to be consistent with the field case history findings of Arps for limestone reservoirs - i.e., as the degree of fracturing increases, the k_g/k_o curve become more unfavorable with respect to oil recovery. The calculated k_g/k_o curves can be extrapolated to allow the calculation of future rates of gas production to correspond with the future oil production rates developed from the rate-time decline analysis.

Depletion Performance of Layered Reservoirs Without Crossflow

This study, initiated by real field data, typifies the whole concept of the use of a simple rate and material balance equation approach being used to solve what has been considered a very complex problem - no crossflow layered reservoir production performance. Rigorous and simplified approaches to the problem result in essentially the same results. Both constant wellbore pressure and constant rate depletion performance are examined as a part of this study.

Two simple correlating parameters (q_{MAX}/G_i] ratio and volume ratio, G_{i1}/G_{i2}, can be used to describe the production performance of no-crossflow layered reservoirs. A physical basis for the Arps' decline exponent b between 0.5 and 1.0 is now available where the magnitude of b may even provide an indication of the layer permeability contrast and the layer volume ratio. Also demonstrated from this study is that different combinations of layer skins can exhibit similar rate-time and pressure-cumulative production differential depletion responses.

By means of graphical presentations of rate-time and pressure cumulative production, this study illustrates some of the depletion performance characteristics that identify no-crossflow layered reservoirs. These graphical presentations show very clearly the effect of changes in the layer volume, permeability, and skin on the depletion performance of no-crossflow layered reservoirs.

M. J. FETKOVICH PUBLICATIONS

Bruns, J. R., Fetkovich, M. J., and Meitzen, V. C.: "The Effect of Water Influx on p/z-Cumulative Gas Production Curves," Journal of Petroleum Technology (March, 1965) 287-291.

Fetkovich, M. J.: "Limited Aquifer Performance".

Fetkovich, M. J.: "A Simplified Approach to Water Influx Calculations-Finite Aquifer Systems," Journal of Petroleum Technology (July, 1971) 814-828, first presented as SPE paper 2603 at the SPE 44th Annual Fall Meeting held in Denver, Colorado, September 28-October 1, 1969.

Fetkovich, M. J.: "Conversion of van Everdingen-Hurst B and t_D to Values of PI_W and W_{ei} For Use in the Simplified Approach to Water Influx Calculations."

Fetkovich, M. J.: "The Isochronal Testing of Oil Wells," SPE Reprint Series No. 14 (1980), 265-288, first presented as SPE paper 4529 at the SPE 48th Annual Fall Meeting held in Las Vegas, Nevada, September 30-October 3, 1973.

Fetkovich, M. J.: "Oil Wells Inflow Performance."

Fetkovich, M. J.: "Decline Curve Analysis Using Type Curves," Journal of Petroleum Technology (June, 1980) 1065-1077, first presented as SPE paper 4629 at the 48th Annual Fall Meeting held in Las Vegas, Nevada, September 30-October 3, 1973.

Fetkovich, M. J.: "Multipoint Testing of Gas Wells," SPE Mid-Continent Section Continuing Education Course, Well Test Analysis, March 17, 1975.

Ziara, B. A. and Fetkovich, M. J.: "Well Testing and Analysis in Indonesian Reef Reservoirs," presented at the 7th IPA Annual Convention, Jakarta, Indonesia, June 6-7, 1978.

Fetkovich, M. J., Vienot, M. E., Bradley, M. D., and Kiesow, U.G.: "Decline Curve Analysis Using Type Curves - Case Histories," Journal of Petroleum Technology (December, 1987) 637-656, first presented as SPE paper 13169 presented at the 59th Annual Fall Meeting held in Houston, Texas, September 16-19, 1984.

Fetkovich, M. J. and Vienot, M. E.: "Rate Normalization of Buildup Pressure Using Afterflow Data," Journal of Petroleum Technology (December, 1984) 2211-2224, first presented as SPE paper 12179 at the SPE 58th Annual Fall Meeting held in San Francisco, California, October 5-8, 1983.

Fetkovich, M. J. and Vienot, M. E.: "Shape Factor, C_A, Expressed as a Skin, s_{CA}" Journal of Petroleum Technology (February, 1985) 321-322, first appearing as SPE paper 13304.

Fetkovich, M. J.: "Muskat's Cluster Wells Equation."

Fetkovich, M. J., Vienot, M. E., Johnson, R. D., and Bowman, B.A.: "Case Study of Low-Permeability Volatile Oil Field Using Individual-Well Advanced Decline Curve Analysis," SPE paper 14237 presented at the SPE 60th Annual Fall Meeting held in Las Vegas, Nevada, September 22-25, 1985.

Fetkovich, M. D., Guerrero, E. T., Fetkovich, M. J., and Thomas, L. K.: "Oil and Gas Relative Permeabilities Determined From Rate-Time Performance Data," SPE paper 15431 presented at the SPE 61st Annual Fall Meeting held in New Orleans, Louisiana, October 5-8, 1986.

Fetkovich, M. J., Bradley, M. D., Works, A. M., and Thrasher, T. S.: "Depletion Performance of Layered Reservoirs Without Crossflow," SPE paper 18266 presented at the SPE 63rd Annual Fall Meeting held in Houston, TX, October 2-5, 1988.

THE EFFECT OF WATER INFLUX ON p/z-CUMULATIVE GAS PRODUCTION CURVES

by

J. R. Bruns
Member AIME
M. J. Fetkovich
Junior Member AIME
V. C. Meitzen

Phillips Petroleum Co.
Bartlesville, Okla.

Original manuscript received in Society of Petroleum Engineers office July 13, 1964. Revised manuscript received Feb. 2, 1965. Paper presented at SPE 39th Annual Fall Meeting held in Houston, Tex., Oct. 11-14, 1964.

THE EFFECT OF WATER INFLUX ON p/z-CUMULATIVE GAS PRODUCTION CURVES

Abstract

The relationship between p/z and cumulative gas production for typical gas reservoirs was studied by calculating pressure response to various modes of gas production and water encroachment. Water encroachment methods considered were Schilthuis, Hurst simplified and van Everdingen-Hurst. In the method, the assumptions normally made in water encroachment calculations were accepted. Normally, pressures are measured and the gas reserves and water encroachment found implicitly. Conversely, in this work various encroachment factors, reserves and reservoir-aquifer geometry were assumed and the pressures solved implicitly.

The results show the spectrum of p/z shapes that can be expected for real reservoirs. With normal encroachment rates for closed aquifers the p/z chart exhibits the typical inflection at early times. This has sometimes been interpreted as all measurement error. These studies have shown that a new look should be taken at interpretation. It is rather dangerous to extrapolate "straight-line" p/z charts if encroachment from an aquifer is suspected.

Introduction

A common method of predicting gas reserves is the graphical solution to the gas material balance equation. A special case of the material balance equation is linear in p/z with cumulative gas production (G_p) which predicts the initial in-place gas when p/z is extrapolated to zero. Derivation of this form is based on the equation of state, corrected for compressibility ($pV = znRT$), and, particularly, on the reservoir being closed (no water encroachment). A straight line on the p/z chart results when these conditions hold. However, an apparent straight line on the chart does not assure that the reservoir is closed. Many of the curves show a rapid decline in the early stages of production after which they flatten out. Confusion arises as to whether these characteristics are caused totally by pressure measurements. To answer this question in part, a series of controlled mathematical experiments was performed in which a typcial gas field was produced subject to various forms of water encroachment. These runs were specifically designed to eliminate measurement errors by calculating pressures at the inner boundary of the aquifer. The resultant p/z charts were thus made available for study and direction in predicting reserves and to indicate the curvature that can be expected in addition to that caused by normal measurement error.

Solution of the Basic Equation for p/z

The basic equation solved for p and p/z is derived in Appendix A. It is

$$G_a = G_r + \frac{K_e S(p,t)}{B_g - B_{gi}} \quad \ldots\ldots\ldots\ldots\ldots\ldots (1)$$

G_a and G_r are the apparent and real values of original gas in place and are derived by assuming a closed reservoir for G_a, and one open to an aquifer for G_r. The function $S(p,t)$ is defined by three methods--Schilthuis, Hurst simplified or van Everdingen-Hurst.[1-4] The definitions of these functions are given in Appendix B.

Eq. 1 is the linear function that is commonly plotted (G_a vs $S(p,t)/B_g-B_{gi}$) with the intercept predicting the original gas in place and slope predicting the water encroachment factor.[5,6] This is a graphical solution of Eq. 1 when histories on pressure and cumulative productions are known. In some cases the equation has been rearranged so a plot can be made such that the encroachment factor is predicted by the intercept and the reserve by the slope.[7]

In the calculations presented in this paper, in-place values, water encroachment factors, rock fluid properties, and cumulative production were set. Eq. 1 was solved implicitly for p/z.

The equivalent of Eq. 1 in terms of p/z is

$$p/z = \frac{p_i}{z_i}\left[\frac{G_r - G_p}{G_r - \dfrac{z_i T p_{sc}}{T_{sc} p_i K_e S(p,t)}}\right] \quad \ldots\ldots\ldots\ldots (2)$$

Setting $K_e S(p,t) = 0$ (no water encroachment), produces the linear form. Obviously, whether the p/z curve is linear or not when $K_e S(p,t) \neq 0$ depends upon the $S(p,t)$ function.

The cumulative productions were determined from production rates calculated from wellhead operating curves subject to the maximum allowables.[8] The wellhead curve is defined by

$$q_g = C(p_{swh}^2 - p_{tf}^2)^n, \quad \ldots\ldots\ldots\ldots\ldots\ldots (3)$$

where q_g = the production rate, Mscf/D
C = the performance coefficient
p_{swh} = the wellhead shut-in pressure, psia
p_{tf} = the tubing flowing pressure, psia
n = the back-pressure exponent.

Shut-in wellhead pressures were determined after the reservoir pressure p was chosen by calculating the static head by the method of Cullender and Smith.[9] The static head was subtracted from p to p_{swh}.

A general flow scheme of the calculation technique is given in Fig. 1, and the field conditions are given in Table 1.

Compressibilities were interpolated from the 1952 API tables. Tables 2 and 3 list conditions that were varied for individual runs.

Discussion of Results

The results of the calculations are shown in Figs. 2 through 9. All of the curves show p/z as a function of cumulative gas produced and are labeled with the numbers corresponding to the data in Tables 2 and 3. Each plotted point represents two years.

Fig. 2 gives the results when the aquifer was assumed to be unlimited, or when original aquifer pressure was assumed to remain constant at some outer boundary (Schilthuis). As the encroachment factor was increased the pressure was maintained at a higher and higher level. The dotted line at the bottom represents no encroachment and the top dotted line shows complete pressure maintenance by a very active water drive.

Fig. 3 shows the results of increasing the Hurst simplified encroachment factor from 2.5×10^4 to 2.5×10^6 (cu ft) in (mo)/psi/year.

The van Everdingen-Hurst encroachment factors were assumed for runs shown in Figs. 4 through 9, and the aquifer was assumed closed and radial. Combinations of three variations in relative aquifer size, two water compressibilities and nine aquifer permeabilities were represented in the runs.

Curves with inflections, which have been observed in practice, were produced for the closed aquifers.

In most cases the families of curves appear to approach a common slope at zero time. At zero time this slope will represent the p/z line for no water encroachment.

Runs with the Schilthuis method and Hurst-simplified method converge at or near a horizontal line as water encroachment factors increase. This means that pressure drops in the aquifer are approaching zero.

In the van Everdingen-Hurst runs the curves respond to the mobility (k/μ) and compressibility of the water, and the relative size of the aquifer. For R_a/R_r of 1.5, the effect of the aquifer is negligible for a given water compressibility regardless of the permeability (Fig. 4). However, for a higher water compressibility an effect is felt for comparable mobilities (Fig. 7).

In general the pressure is maintained at higher levels as the water compressibility, aquifer size or water mobility is increased. Yet, even with increases in mobility an extreme curve was approached for the closed aquifers (Runs 25 and 26, Fig. 6). In these cases pressure drops in the aquifer were small and the shapes were controlled by the water compressibilities.

Conclusions

Fig. 10 illustrates the increasing error that occurs if a p/z curve is extrapolated with no regard for water encroachment. As the relative size of

the aquifer increases from $R_a/R_r = 1.5$ to 10, the error increases from a negligible amount to an estimate of over 100 per cent of the actual initial gas in place. This estimate would be made after 65 per cent of the initial gas in place is produced.

This leads to the principal conclusion that it is dangerous to extrapolate p/z charts on a straight line without considering the possibility of water influx.

Runs performed here eliminated measurement error and the curved portions were produced under realistic production schedules. Thus, curved portions at the start of production history can be caused by the unsteady-state nature of the aquifer and not solely by measurement errors. So, these curved portions should not be neglected, but ought to be regarded as an indication of possible water encroachment.

These results make a case for accelerated early production so that the inflections will be accentuated, permitting better early estimates of gas in place.

Acknowledgment

The authors thank the Phillips Petroleum Co. for permission to publish this work. Special thanks are due R. V. Smith for his cooperation and assistance.

References

1. Schilthuis, R. J.: "Active Oil and Reservoir Energy", Trans., AIME (1936) 118, 33.

2. van Everdingen, A. F. and Hurst, W.: "The Application of the Laplace Transformation to Flow Problems in Reservoirs", Trans., AIME (1949) 186, 305.

3. Hurst, W.: "Water Influx into a Reservoir and Its Application to the Equation of Volumetric Balance", Trans., AIME (1943) 151, 57.

4. van Everdingen, A. F., Timmerman, E. H. and McMahon, J. J.: "Application of the Material Balance Equation to a Partial Water Drive Reservoir", Trans., AIME (1953) 198, 51.

5. Pirson, S. J.: Oil Reservoir Engineering, 2nd Ed. McGraw-Hill Book Co., Inc., New York (1958) 608.

6. Stanley, L. T.: "Curve-Fitting Cuts Material Balance Calculations", Pet. Eng. (Aug., 1961) 90.

7. Hubbard. R. M. and Elenbaas. J. R.: "Determining Gas-Filled Pore Volume in a Water-Drive Gas Storage Reservoir", Jour. Pet. Tech. (April, 1964) 383.

8. Frick, T. C.: Petroleum Production Handbook. Vol. II, McGraw-Hill Book Co., Inc., New York (1962) 30.

9. Cullender, M. H. and Smith, R. V.: "Practical Solution of Gas-Flow Equations for Wells and Pipelines with Large Temperature Gradients", Trans., AIME (1956) 207, 281.

Appendix A

Derivation of the Basic Equations

The apparent reserves for a gas field are those determined when no water encroachment is assumed, or,

$$V_p = V_{pi}, \quad \ldots\ldots\ldots\ldots\ldots\ldots\ldots\ldots \quad (A\text{-}1)$$

where V_{pi} is the original pore volume, cu ft.

V_p is the pore volume containing gas at some later time.

$$V_p = (G_a - G_p)B_g \quad \ldots\ldots\ldots\ldots\ldots\ldots\ldots\ldots \quad (A\text{-}2)$$

$$V_{pi} = G_a B_{gi}, \quad \ldots\ldots\ldots\ldots\ldots\ldots\ldots\ldots \quad (A\text{-}3)$$

where G_a = the apparent original gas in place, scf

G_p = cumulative gas produced, scf

B_{gi} and B_g are the gas formation volume factors, cu ft/scf.

$$B_{gi} = \frac{p_{sc} T_i Z_i}{p_i T_{sc}} \quad \ldots\ldots\ldots\ldots\ldots\ldots\ldots\ldots \quad (A\text{-}4)$$

$$B_g = \frac{p_{sc} T z}{p\ T_{sc}} \quad \ldots\ldots\ldots\ldots\ldots\ldots\ldots\ldots \quad (A\text{-}5)$$

Substituting Eqs. A-2 and A-3 into Eq. A-1 and solving for G_a gives

$$G_a = G_p \left(\frac{B}{B_g - B_{gi}} \right) \quad \ldots\ldots\ldots\ldots\ldots\ldots\ldots\ldots \quad (A\text{-}6)$$

When water encroachment is considered, Eq. A-1 is replaced by

$$V_p = V_{pi} - W_e \quad \ldots\ldots\ldots\ldots\ldots\ldots\ldots\ldots \quad (A\text{-}7)$$

to account for the water influx W_e.

Under these conditions, G_a in Eqs. A-2 and A-3 is defined as G_r (real initial in place gas), or,

$$V_p = (G_r - G_p)B_g, \quad \ldots \quad (A\text{-}8)$$

and

$$V_{pi} = G_r B_{gi} \quad \ldots \quad (A\text{-}9)$$

Substitution of Eqs. A-8, A-9, and

$$W_e = K_e S(p,t) \quad \ldots \quad (A\text{-}10)$$

into Eq. A-7 gives

$$G_r = \frac{G_p B}{(B_g - B_{gi})} - \frac{K_e S(p,t)}{(B_g - B_{gi})} \quad \ldots \quad (A\text{-}11)$$

where K_e is the water encroachment factor and S(p,t) is a function of pressure and time and describes the unsteady-state water influx.

Substraction of Eq. A-11 from Eq. A-6 results in the basic equation

$$G_a = G_r + \frac{K_e S(p,t)}{(B_g - B_{gi})} \quad \ldots \quad (A\text{-}12)$$

Appendix B

Definition of S(p,t)

Schilthuis Method

$$S(p,t) = \sum_{i=2}^{n} \Delta p_i \Delta t_i \quad \ldots \quad (B\text{-}1)$$

$$\text{where } \Delta p_i = p_1 - \frac{(p_i + p_{i-1})}{2} \quad \ldots \quad (B\text{-}2)$$

$$\text{and } \Delta t_i = t_i - t_{i-1} \quad \ldots \quad (B\text{-}3)$$

where n = number of pressure points
t_i = time in years
p = aquifer pressure (inner boundary) psia.

Hurst-Simplified Method

$$S(p,t) = \sum_{i=2}^{n} \frac{\Delta p_i \Delta t_i}{\ln(12t_i)} \quad , \quad \text{(B-4)}$$

where Δp_i and Δt_i are still defined by Eqs. B-2 and B-3

van Everdingen-Hurst Method

$$S(p,t) = \sum_{i=1}^{n-1} \Delta p_i q_{\Delta t_d i} \quad , \quad \text{(B-5)}$$

where

$$\Delta p_i = \frac{p_{i+1} - p_i}{2} \quad , \quad \text{(B-6)}$$

for i = 1, and

$$\Delta p_i = \frac{p_{i+1} - p_{i-1}}{2} \quad , \quad \text{(B-7)}$$

for i = 2 to n - 1.

$q\Delta t_{di}$ is the dimensionless flow rate and is a function of Δt_{di} (the dimensionless time increment) and aquifer geometry.

$$t_{di} = 2.309 \left(\frac{k \, \Delta t}{\phi \mu C_w (R_r)^2} \right) \quad , \quad \text{(B-8)}$$

with k in millidarcies, t in years, ϕ a fraction, μ in cp, C_w in 1/psi, R_r in ft.

$q\Delta t_{di}$ is defined under the following conditions. All $\Delta t_{di} < 0.01$, or the linear system

$$q\Delta t_{di} = 2\sqrt{\Delta t d_i / \pi} \quad , \quad \text{(B-9)}$$

Infinite Radial System

$(0.01 < \Delta t_{di} \leq 10^8)$

$$q_{\Delta t_{di}} = e^{(A_1(\ln\Delta t_{di})+A_2(\ln\Delta t_{di})^2+A_3(\ln\Delta t_{di})^3+A_4(\ln\Delta t_{di})^4+A_5)} \quad . . \quad (B\text{-}10)$$

where $A_1 = 0.647692$

$A_2 = 0.0177318$

$A_3 = 0.0002737391$

$A_4 = 0.4318125 \times 10^{-5}$

$A_5 = 0.4506432.$

Finite Radial Systems

The finite radial systems are defined by the infinite radial Eq. B-10, where $\Delta t_{di} > 0.01$ and less than the middle range defined in Table 4. In the middle range the dimensionless flow is defined by an equation of the same form as Eq. B-10, but with constants shown in Table 4. Table 4 also gives the steady-state values applicable above the middle range.

J. R. BRUNS (left) is a senior mathematical engineer in the Phillips Petroleum Co.'s Computing Dept. For the past seven years he has worked in reservoir engineering computer applications. He has a BS in chemical engineering from the U. of Missouri, an MS in chemical engineering from Illinois Institute of Technology, and a Master of Gas Technology degree from the Institute of Gas Technology. M. J. FETKOVICH (right) is a reservoir engineering and gas technology analyst in the Reservoir and Production Project Groups of Phillips. He graduated from the U. of Pittsburgh in 1954 with a BS degree in petroleum and natural gas engineering and soon joined Phillips. V. C. MIETZEN (center) is a senior electronic computer programmer for Phillips at Bartlesville, OK. He joined Phillips after receiving his BS degree in petroleum engineering from the U. of Texas in 1960. He worked as a staff engineer in the Pauls Valley, OK. Area Office before joining the Computer Dept. in 1963.

TABLE 1

FIELD CONDITIONS

Area = 2,500 acres
Pay = 100 ft
Porosity = 0.25
Connate water = 0.3
Original BHP = 5,000 psia
Formation temperature = 250F
Depth = 10,000 ft
Gas Gravity = 0.68 (No N_2, CO_2 or H_2S)
$(\text{Radius})^2 = 34.7 \times 10^6$ sq ft
Initial wellhead shut-in pressure = 4,200 psia
Wellhead shut-in temperature = 100F
Back-pressure curve slope = 0.7
Open flow potential = 74.4 MM scf/D
Minimum wellhead flowing pressure = 100 psia
Maximum allowable field rate = 47.2 MM scf/D

TABLE 2

VARIABLE CONDITIONS FOR RUNS 1 THROUGH 14

Run No.	Type Encroachment Factor	Encroachment Factor
1		5,900
2		18,000
3	Schilthuis	36,000
4	(cu ft/psi/year)	59,000
5	Radial Infinite	100,000
6		200,000
7		590,000
8		25,000
9		90,000
10	Hurst Simplified	150,000
11	(cu ft in (month)/psi/year)	250,000
12	Radial Infinite	340,000
13		610,000
14		2,500,000

TABLE 3

VARIABLE CONDITIONS FOR RUNS 15 THROUGH 38

Type Encroachment Factor	Ratio of Aquifer Radius to Field Radius	Aquifer Permeability (md)	Dimensionless Time to Real Time Ratio (1/year)	Water Compressibility (1/psi)
	1.5	1	.089	3.0×10^{-6}
	1.5	10	.89	3.0×10^{-6}
	1.5	100	8.9	3.0×10^{-6}
	5.0	1	.089	3.0×10^{-6}
van Everdingen	5.0	10	.89	3.0×10^{-6}
Hurst Radial Finite	5.0	100	8.9	3.0×10^{-6}
16,350 cu ft/psi	5.0	1000	89.	3.0×10^{-6}
	10.0	1	.089	3.0×10^{-6}
	10.0	10	.89	3.0×10^{-6}
	10.0	100	8.9	3.0×10^{-6}
	10.0	1000	89.	3.0×10^{-6}
	10.0	10000	890.	3.0×10^{-6}
	1.5	10	.089	30×10^{-6}
	1.5	100	.89	30×10^{-6}
	5.0	10	.089	30×10^{-6}
	5.0	18	.16	30×10^{-6}
van Everdingen	5.0	39.3	.35	30×10^{-6}
Hurst Radial Finite	5.0	100	.89	30×10^{-6}
163,500 cu ft/psi	10.0	10	.089	30×10^{-6}
	10.0	15.8	.141	30×10^{-6}
	10.0	31.5	.28	30×10^{-6}
	10.0	100	.89	30×10^{-6}
	10.0	1000	8.9	30×10^{-6}
	10.0	10000	89.	30×10^{-6}

TABLE 4

R_a/R_r	Middle Range of Δtd_i From	To	Equation B-10—A Constants A_1	A_2	A_3	A_4	A_5	Stabilized State Values Above the Middle Range
1.5	.1206	0.7	- 0.03255975	- 0.02485001	0.03179695	0.007970778	0.6164517	0.6235899
2.0	.418	2.5	0.3852062	- 0.09626595	-0.05244533	-0.004754152	1.281475	1.509915
2.5	.815	6.0	0.7919653	0.05396428	-0.06348801	-0.01234595	1.534877	2.634689
3.0	1.33	11.0	1.046089	0.2388103	-0.08575203	-0.008445356	1.574667	3.994681
3.5	1.12	25.0	0.4178854	1.292179	-0.4404957	0.03704949	1.630682	5.650575
4.0	2.05	34.0	- 2.231692	3.177286	-0.8411667	0.06444676	2.779082	7.499222
4.5	2.62	46.0	- 6.108747	5.413047	-1.266439	0.09235701	4.890919	9.619498
5.0	3.06	60.0	- 6.429505	4.823608	-0.8503674	0.03632684	5.599367	11.97866
6.0	5.85	110.0	-24.90336	12.44925	-2.042113	0.1044283	20.58242	17.48006
7.0	8.48	160.0	-43.33130	17.84979	-2.486980	0.1043855	39.95260	23.95055
8.0	9.29	240.0	-51.48727	19.26185	-2.365595	0.08228036	50.46776	31.66351
9.0	9.96	280.0	-31.97360	8.612722	-0.05276312	-0.08174990	38.52328	39.96676
10.0	14.52	360.0	-20.55106	0.6903652	1.759464	-0.2079732	37.02682	49.14654

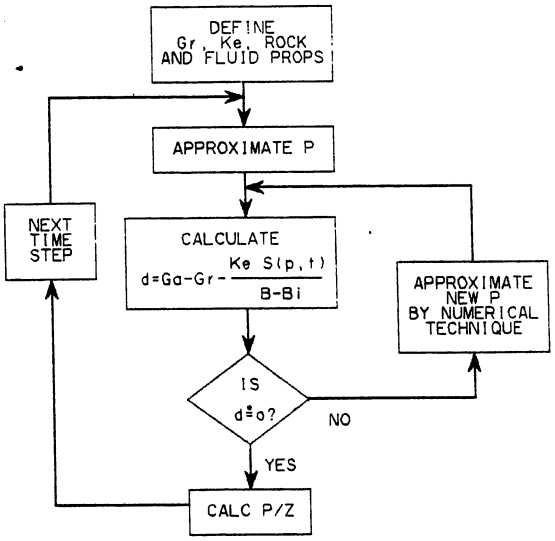

FIG. 1 - SOLUTION OF EQ. A-12 FOR P/Z.

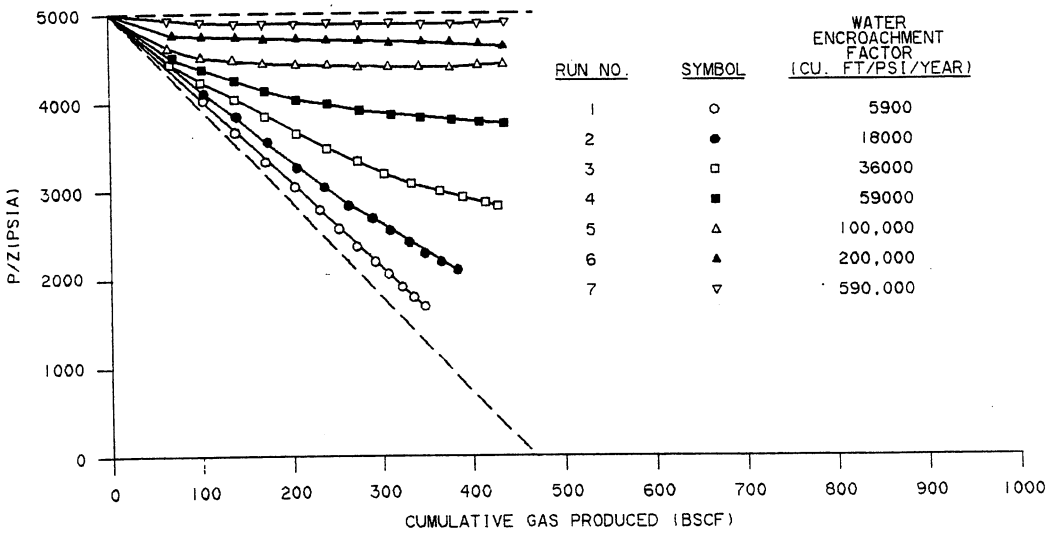

FIG. 2 - CURVES OF P/Z FOR GAS RESERVOIRS WITH WATER INFLUX, SCHILTHUIS METHOD.

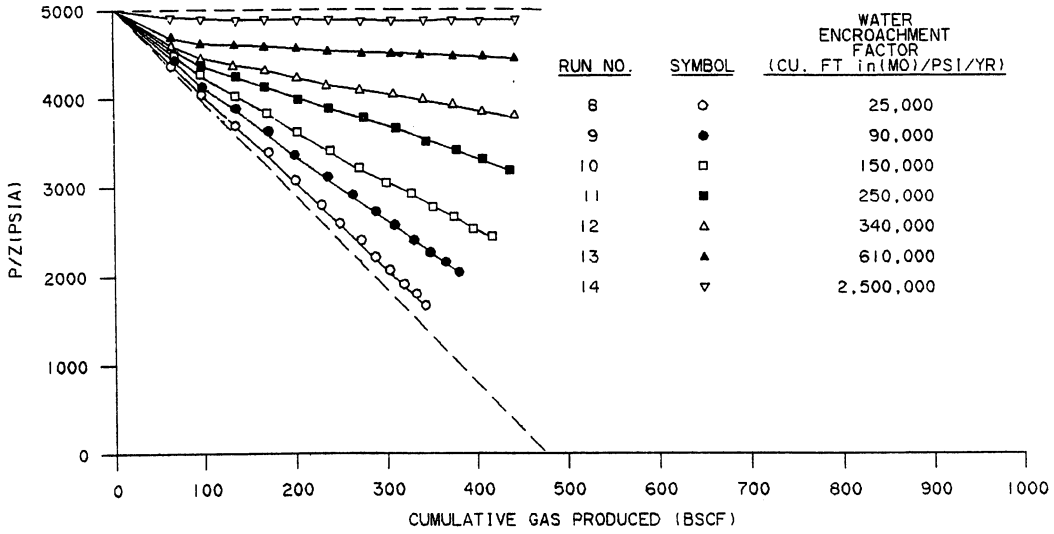

FIG. 3 - CURVES OF P/Z FOR GAS RESERVOIRS WITH WATER INFLUX, HURST SIMPLIFIED METHOD.

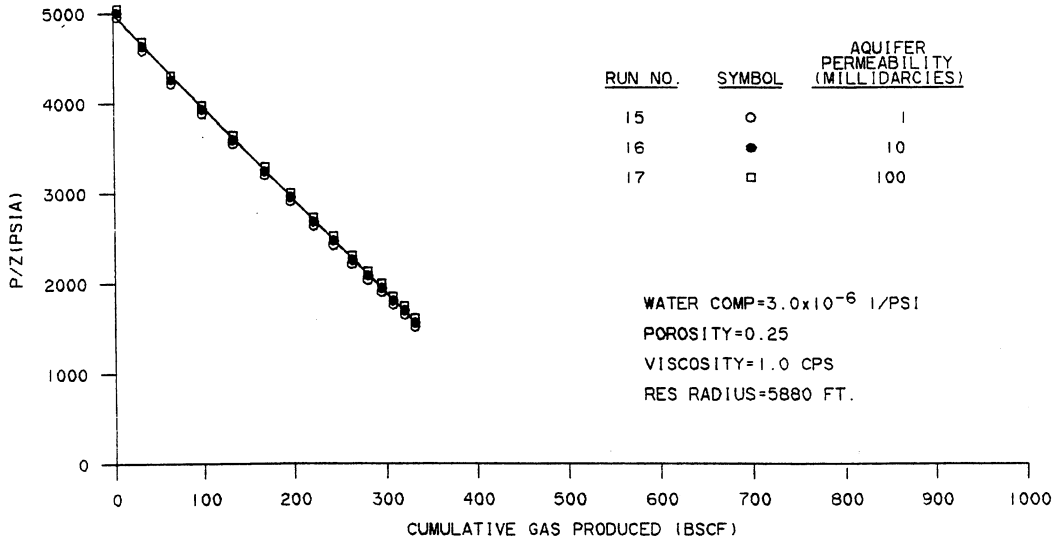

FIG. 4 - CURVES OF P/Z FOR GAS RESERVOIRS WITH WATER INFLUX, VAN EVERDINGEN-HURST METHOD, FINITE, $R_d/R_r = 1.5$.

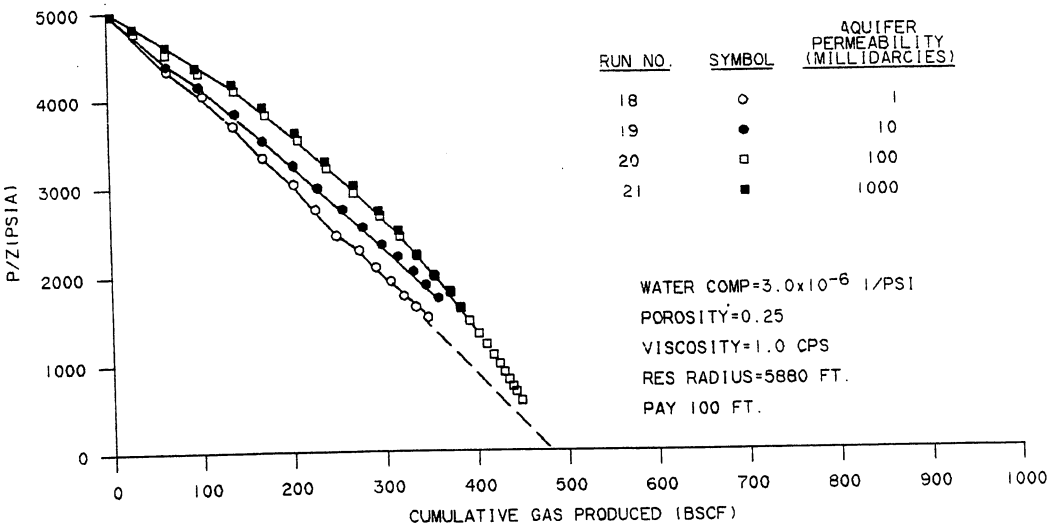

FIG. 5 - CURVES OF P/Z FOR GAS RESERVOIRS WITH WATER INFLUX, VAN EVERDINGEN-HURST METHOD, FINITE, $R_a/R_r = 5$.

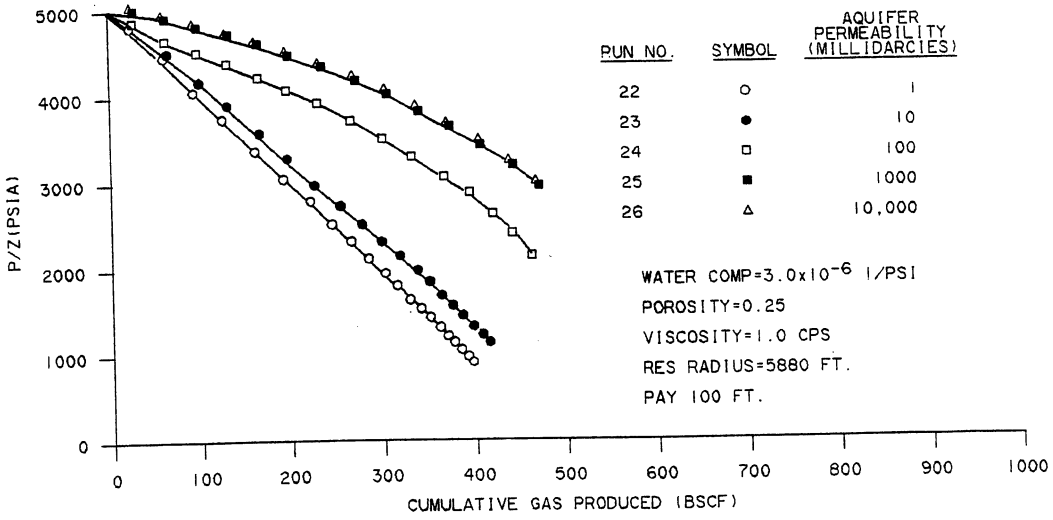

FIG. 6 - CURVES OF P/Z FOR GAS RESERVOIRS WITH WATER INFLUX, VAN EVERDINGEN-HURST METHOD, FINITE, $R_a/R_r = 10$.

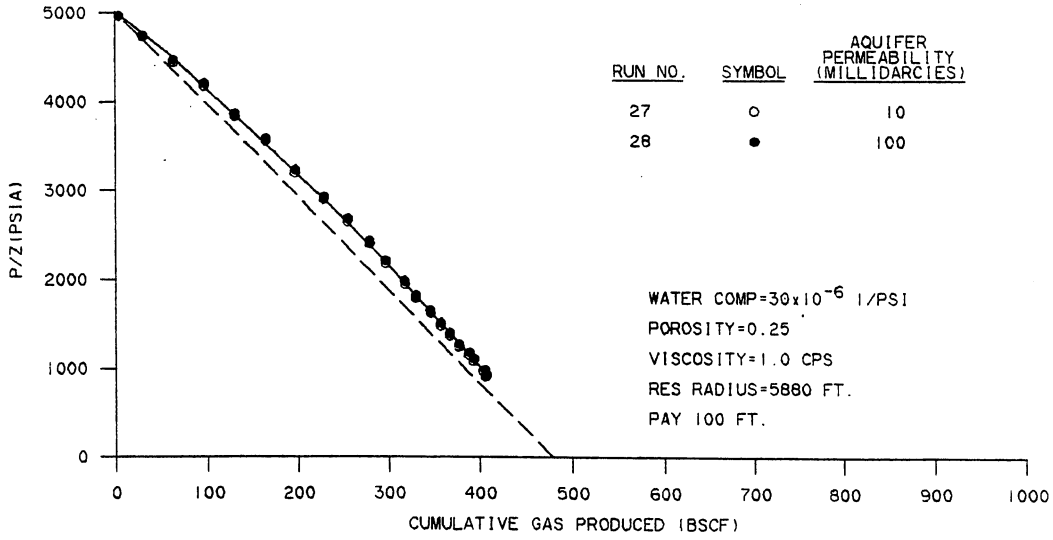

FIG. 7 - CURVES OF P/Z FOR GAS RESERVOIRS WITH WATER INFLUX, VAN EVERDINGEN-HURST METHOD, FINITE, $R_a/R_r = 1.5$.

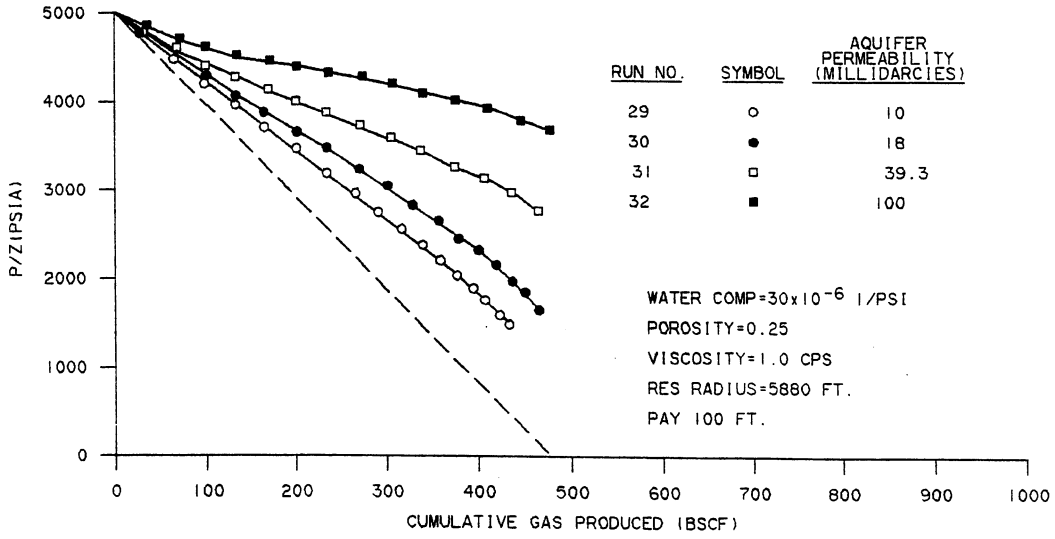

FIG. 8 - CURVES OF P/Z FOR GAS RESERVOIRS WITH WATER INFLUX, VAN EVERDINGEN-HURST METHOD, FINITE, $R_a/R_r = 5$.

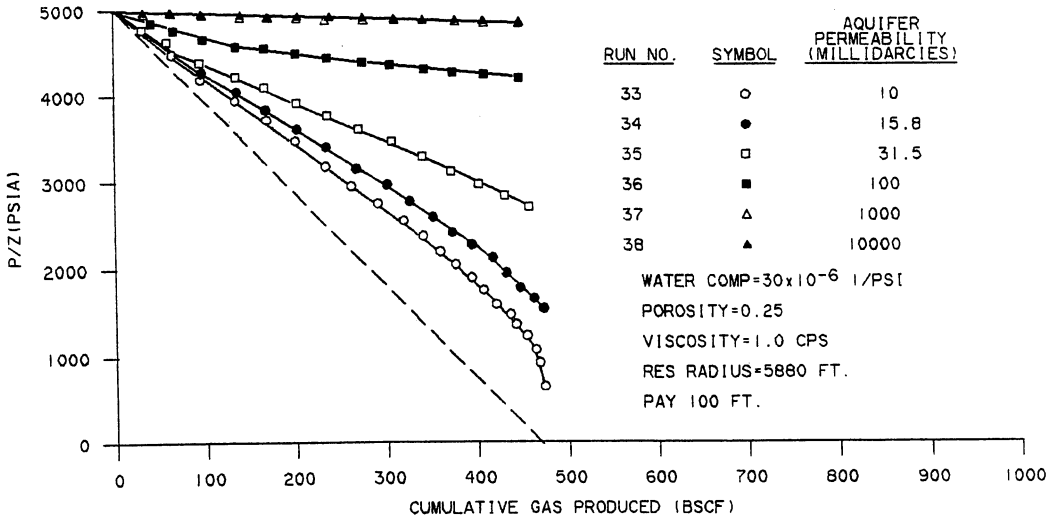

FIG. 9 - CURVES OF P/Z FOR GAS RESERVOIRS WITH WATER INFLUX, VAN EVERDINGEN-HURST METHOD, FINITE, $R_a/R_r = 10$.

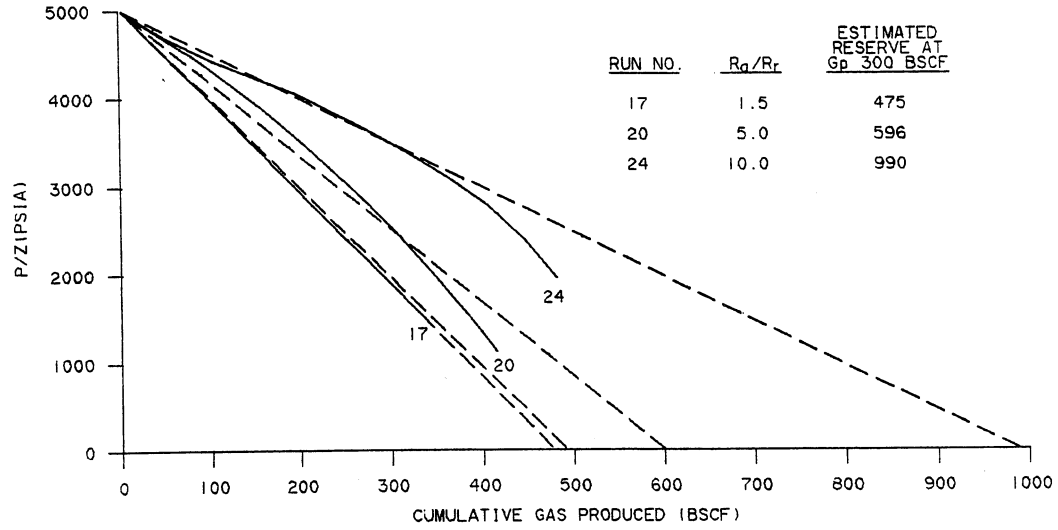

FIG. 10 - COMPARISON OF P/Z CURVES FOR INCREASING AQUIFER SIZES, VAN EVERDINGEN-HURST, RADIAL FINITE.

LIMITED AQUIFER PERFORMANCE

by

M. J. Fetkovich

LIMITED AQUIFER PERFORMANCE

The objective of this derivation was to determine the extent to which p/z vs G_p behaviour could be accounted for by using a cumulative compressibility for the rock and water associated with the gas pay (within the gross interval) and the rock and water surrounding the gas pay. The concept of cumulative compressibility as used herein assumes transient effects within the aquifer to be negligible. It can readily be shown that this method is equivalent to that of ODEH and HAVLENA for material balance calculations involving small aquifers.

The following formula accounts for pressure support attributable to cumulative compressibility, $\bar{C}_e$ $(p_i - p)$, where $\bar{C}_e$, which is really a function of pressure will be treated as a constant, C_e, for simplicity of presentation.

$$\frac{p}{z}\left[1 - C_e\,(p_i - p)\right] = \frac{p_i}{z_i} - \left(\frac{p_i/z_i}{G}\right) G_p \quad \ldots\ldots\ldots\ldots \quad (1)$$

where

$$C_e = \frac{S_{wi}\,C_w + C_f + M\,(C_w + C_f)}{(1 - S_{wi})}$$

with

S_{wi} = initial connate water saturation

C_w = water compressibility

C_f = rock compressibility

$$M = \frac{\text{pore volume aquifer}}{\text{pore volume gas reservoir}}$$

(Aquifer pore volume can be considered to also consist of any 100 percent saturated sands and shales within the gross reservoir interval.)

As is evident from equation 1, $p/z\,[1 - C_e\,(p_i - p)]$ versus G_p on co-ordinate paper should result in a straight line if transient effects are negligible and the correct C_e (actually M) is chosen. This involves a trial and error procedure to arrive at the correct C_e. This, however, is much simpler than the HAVLENA-ODEH procedure for limited aquifers.

(I use a rule of thumb that an $\frac{r_a}{r_r} \leq 3.0$ can be considered a limited aquifer.)

A SIMPLIFIED APPROACH TO WATER INFLUX CALCULATIONS - FINITE AQUIFER SYSTEMS

by

M. J. Fetkovich
SPE-AIME, Phillips Petroleum Co.

SPE 2603

Original manuscript received in Society of Petroleum Engineers office Aug. 5, 1969. Revised manuscript received April 8, 1971. Paper was presented at SPE 44th Annual Fall Meeting, held in Denver, Colo., Sept 28 - Oct. 1, 1969.

A SIMPLIFIED APPROACH TO WATER INFLUX CALCULATIONS-FINITE AQUIFER SYSTEMS

Introduction

All gas and oil reservoirs are associated to varying extents with formation waters. The inclusion of the effects of expansion or invasion of this water into oil and gas reservoirs has taken many forms, from recognizing the effects of the expansion of the connate water[1] within the gas or oil reservoir itself, to calculating water influx or efflux across a boundary (with the boundary usually being that of an oil or gas reservoir).

There are four currently popular methods used for calculating water influx into reservoirs. They are:

1. Schilthuis, steady state[1-3]
2. Hurst Simplified, unsteady state[1,2]
3. Resistance or Influence Function, unsteady state[4-6]
4. van Everdingen-Hurst Radial, unsteady state[7]

The first three methods have proved useful for predicting water drive performance after sufficient historical data have been obtained to fix the necessary influx constants. With what some consider to be disappointing results,[1,8] the van Everdingen-Hurst Radial method is often used with geological and core data when little or no performance history is available. It has also been used to predict reservoir performance after enough historical data have been accumulated to develop values of the influx constants, t_D and C.

In an attempt to include geometries other than radial, derivations for both limited and infinite systems have been made to cover linear,[7,9,10] spherical,[11] elliptical,[12] thick-sand,[13] and wedge-shaped[13] reservoir-aquifer models.

The many rigorous geometrical representations that have been developed cannot readily handle the effect of interference between reservoirs. Electric analyzer studies of the Smackover Limestone aquifer in Arkansas by Bruce,[14] of the Woodbine aquifer in East Texas by Rumble et al.,[15] and of the Ellenberger in West Texas by Moore and Truby[16] have shown that reservoirs sharing a common aquifer can severely interfere with each other, and that, for individual reservoirs in a common aquifer, water drive performance calculations that do not consider interference can be greatly in error.

Mortada[17] developed a mathematical method with which to handle interference in a basically infinite radial aquifer system. The method has been applied to field cases.[18,19] Coats concluded from his own study that, "In predicting the pressure-volume behavior of gas reservoirs situated on the common aquifer the effect of interference from other reservoirs on the common aquifer must be accounted for."

Another aquifer problem more recently presented in the literature[20] is that of flank water injection for pressure maintenance, either to initiate or to supplement edge-water influx. A case history[21] shows that we need to be able to study the effects of injecting water into the aquifer instead of merely including it in the hydrocarbon material balance equation.

Little wonder that efforts[17,22,23] have been made to simplify the water drive performance prediction methods, even to the point frequently of using the infinite solution without trying to define fairly clearly the limits and characteristics of the aquifer.

If we are to predict realistically the performance of water drive reservoirs, then, a simple method must be developed that can readily handle all the basic geometries, interference from other reservoirs, and water injection and production from the aquifer; the method should also be flexible enough that it can be further improved or added to as a problem requires.

We shall present here an approach that utilizes the "stabilized", or pseudosteady-state aquifer productivity index and an aquifer material balance to represent the finite compressible system. Much of this has been treated in the literature in the form of solutions to individual well problems and reservoir material balance derivations. For some reason -- possibly a concern for the early transient effects -- any earlier efforts to extend this available technology to aquifer or water drive problems have not been reported.

We hope to develop the idea that this simplified approach is accurate enough for engineering purposes, especially for field production forecasting of times involving some 10 to 20 years, by comparing the PI-Aquifer Material Balance solution with the van Everdingen-Hurst solution through the use of example problems. Solutions mainly involve finding a reasonable rate equation for the problem, and considering the aquifer encroachable water volume represented in the material balance equation as being independent of geometry only to the extent that basic mensuration equations can be applied.

Basic Equations

The generalized rate equation for an aquifer without regard to geometry or defining a specific type of flow is:

$$q_w = J_w (\overline{p} - p_{wf})^n, \qquad ..(1)$$

with n usually being represented as unity (1) when the flow obeys Darcy's law and is at pseudosteady state or steady state. J_w is defined as the productivity index (PI) of the aquifer and is analogous to the PI of an oil well or the gas well backpressure curve coefficient.

The aquifer material balance for a constant compressibility can be written in its simplest form as

$$\overline{p} = - \left(\frac{p_i}{W_{ei}} \right) W_e + p_i , \qquad ..(2)$$

where $\bar{p}$ is the average aquifer pressure (shut-in), W_{ei} is the initial encroachable water in place at initial pressure p_i, and W_e is the cumulative water efflux from the aquifer or influx into a reservoir.

By combining Equations 1 and 2 (see Appendices A and B for complete derivation), we can obtain the equation expressing the instantaneous rate of water influx as a function of time, and the inner boundary pressure p_{wf}.

$$e_w(t) = \frac{J_w(p_i - p_{wf})}{e^{[(q_{wi})max/W_{ei}]t}} \quad . \qquad ..(3)$$

$(q_{wi})_{max}$ is defined as the initial open-flow potential of the aquifer, again analogous to the open-flow potential of an oil well or gas well. Figure 1 is a graphical representation of the generalized rate equation expressed as Equation 1 and the aquifer open-flow potential described above. Note that if we let W_{ei} become large, Equation 3 reduces to the Schilthuis steady-state equation

$$e_w = J_w (p_i - p_{wf}) \qquad ..(4)$$

The final form of the cumulative water influx equation (given also in Appendix B)

$$W_e = \frac{W_{ei}}{p_i} (p_i - p_{wf}) \{1 - e^{-[(q_{wi})max/W_{ei}]t}\} \qquad ..(5)$$

is not useful by itself, because it cannot handle a changing inner boundary pressure p_{wf} while representing the aquifer pressure always at its initial value. Hurst[24] and others have handled this problem by the method of superposition.

We can rewrite the equation to represent the cumulative water influx over an interval of time Δt, then start the problem again after every time interval (as can be done for any material balance problem). With the aid of the aquifer material balance equation, we can redetermine a new aquifer shut-in pressure $\bar{p}_n$, then solve over a new time interval Δt. This reevaluation of the aquifer shut-in pressure each time eliminates the need for superposition.

A significant point here is that we need not always go back to the initial pressure to start a water influx calculation. We can conveniently start it at any time provided we can obtain a value to represent the aquifer shut-in pressure.

The interval equation is

$$\Delta W_{en} = \frac{W_{ei}}{p_i} [\bar{p}_{(n-1)} - \bar{p}_{wfn}] \cdot \left[1 - e^{-[(q_{wi})max/W_{ei}] \Delta tn}\right] \qquad ..(6)$$

The ratios W_{ei}/p_i and $(q_{wi})_{max}/W_{ei}$ can be further simplified to eliminate p_i from the expressions, which then do not need to be initialized again to new aquifer shut-in pressures. These forms are retained so as to keep their physical meanings.

The time interval is determined by

$$\Delta tn = t_n - t_{(n-1)} \; ; \qquad ..(7)$$

and the average pressure

$$\overline{P}_{wfn} = \frac{P_{wf(n-1)} + P_{wf(n)}}{2} \qquad ..(8)$$

represents the constant pressure used at the reservoir-aquifer boundary during the time interval Δtn. Figure 2 depicts this pressure-time relationship and the step curve that attempts to approximate it. This method of representing the average pressure, $\overline{P}_{wfn}$, is applicable to both past and future performance predictions.

To start the calculation again for the aquifer shut-in pressure $\overline{p}$, we will make use of the general aquifer material balance equation derived in Appendix B.

$$\overline{p} = -\left[\frac{W_e + \sum_{2}^{j} W_{ej} + (W_p - W_i)\, B_w}{W_{ei}}\right] p_i + p_i, \qquad ..(9)$$

where $W_e = \sum_{1}^{n} W_{en}$, the total cumulative influx (to time tn) into the reservoir of interest. The term $\sum_{2}^{j} W_{ej}$ is the total cumulative influx into other reservoirs within the common aquifer and is further discussed under Aquifer Interference. All other terms have the conventional definition or have previously been defined.

The realistic water influx rate and cumulative water influx relationship during an interval of time Δt is depicted in Figure 3 along with that which results from using a step-function constant pressure as an approximation in any water influx instantaneous rate equation.

Step-Function Solutions

It now appears that the simplification of the water influx problem is still none too simple. In reality, though, we have reduced the problem so that we can recognize that a simple time-incremented step-function solution using the rate equation $q_w = J_w (\overline{p} - p_{wf})$ to establish a constant rate over a time interval, and the aquifer material balance equation $\overline{p} = -\left(\frac{p_i}{W_{ei}}\right) W_e + p_i$ to evaluate the aquifer shut-in pressure after efflux from the aquifer, will give the analytical solutions to the problem when Δt is allowed to become small.

A Δt of a month in a normal reservoir problem does reproduce these analytical solutions. (Constant rate steps over a Δt of 1 year for all cases of $r_a/r_r \geq 5$ reported in this study gave results identical with those obtained using Equation 6.) Figure 4 illustrates this straightforward step-function approach.

For a time interval Δtn, from $t_{(n-1)}$ to t_n, the working equation for the rate equation would be

$$q_w = J_w(\overline{p}_{(n-1)} - \overline{p}_{wfn}) \qquad ..(10)$$

The cumulative efflux during the time interval Δtn would be

$$\Delta W_{en} = \Delta tn(q_w), \qquad ..(11)$$

and the total cumulative efflux to time tn would be

$$W_{en} = \sum_{1}^{n} \Delta W_{en}. \qquad ..(12)$$

Then to update the aquifer average pressure for the next time interval,

$$\overline{p}_n = -\left(\frac{p_i}{W_{ei}}\right) W_{en} + p_i \qquad ..(13)$$

Rate Equations

In all derivation methods that attempt to predict water influx and that assume a constant compressibility, it is necessary to start with the same volume of initial encroachable water in place for a given set of variables. Therefore, to predict water influx accurately with PI-Aquifer Material Balance approach, we need only find a suitable rate equation.

Aquifer Productivity Index J_w

The aquifer productivity index J_w values used in this study were calculated from a stabilized backpressure equation for finite radial flow conditions (θ=360°). The early transient period was neglected. For the finite, slightly compressible, radial aquifers studied, we used the "stabilized" pseudosteady-state rate equation:

$$q_w = \frac{7.08\ kh\ (\overline{p} - p_{wf})}{\mu\left[\ln\left(\frac{r_a}{r_r}\right) - \frac{3}{4}\right]} \qquad ..(14)$$

We have then a productivity index for radial "stabilized" flow

$$J_w = \frac{7.08\ kh}{\mu\left[\ln\left(\frac{r_a}{r_r}\right) - \frac{3}{4}\right]} \qquad ..(15)$$

The initial aquifer potential, $(q_{wi})_{max}$, then is

$$(q_{wi})_{max} = J_w (p_i - 0) \qquad ..(16)$$

The initial encroachable water in place, W_{ei}, for radial geometry (ϕ=360°) is determined by

$$W_{ei} = \frac{\pi}{5.61} (r_a^2 - r_r^2) \theta h c_t p_i \qquad ..(17)$$

Table 4 summarizes the rate equations from which PI can be calculated for finite radial and linear systems for pseudosteady-state and steady-state conditions. Also included in this table are the unsteady-state equations for radial and linear transient flow that can be used for a system that does not reach pseudosteady state or steady state during the period of interest (see Figure 20). Note that the infinite radial flow equation given in Table 4 is nothing more than the Hurst Simplified water influx equation defined.

As in individual well problems, we could also introduce the concept of skin into the equations to allow theory to fit the observed data. Where changing the internal aquifer radius, r_r, would also cause a change in the aquifer volume, W_{ei}, the concept of skin would allow us to vary PI without changing r_r. This would take on special significance if we attempt to match historical influx data from a best combination of J_w - W_{ei} while trying to conform with the existing geometry of the system.

As a guide to the times at which pseudosteady state and steady-state are reached in a radial system, we can use this equation[1] for pseudosteady state:

$$t_{ps} \cong \frac{0.02 \mu c_t \phi r_a^2}{k} \quad ; \qquad ..(18)$$

and this equation[1] for steady-state:

$$t_s \cong \frac{0.04 \mu c_t \phi r_a^2}{k} \qquad ..(19)$$

The equations for a linear system could be derived like those for the radial system. All units in the above equations are in terms of days, centipoises, psi^{-1}, feet, and darcies.

In estimating times, we must remember to consider the drainage boundaries that are established when there is interference from other reservoirs in the same aquifer.

Selection of Rate Equations

Figure 21 lists some possible types of aquifer flow systems that could be used as a guide in selecting appropriate rate equations. Many problems can be expressed in terms of essentially linear or radial flow.

Figure 21a describes a flow system that is obviously linear but whose distances between sealing faults describe the cross-sectional area to be used with the aquifer rate equation. In water influx calculations we are trying to describe the flow in the aquifer itself. The cross-sectional area at the aquifer-reservoir boundary is not necessarily applicable, especially after pseudosteady state or steady-state has been established.

Figure 21b describes flow in a long, narrow reservoir. That this type of flow could be classed as linear has been demonstrated by Havlena and Odeh[25] from an analysis of a gas reservoir 11 miles long and 1.5 miles wide. Their analysis, using the material balance as an equation of a straight line, indicated that the influx rate was proportional to the square root of time.

Figure 21c is an extension of the concept developed by Figure 21b but in an additional dimension. Bottomwater drive in a long, narrow field could be better approximated by radial flow in the vertical direction, with h being the length of the reservoir.

Figure 21d would be represented by most engineers as a radial flow system of 180°, using a radius to flow equivalent to r_r. However, by redefining the system to consider the dashed lines to be the new boundaries and by treating the volume of water between the fault reservoir (so that the expansion of this portion to the aquifer would take place with no resistance to flow) we can readily see that it is, for practical purposes, a linear flow situation. This approach should give an optimistic answer, but not so optimistic as it would be if the problem were treated as a radial flow system.

Figure 21e illustrates a reservoir located between two parallel sealing faults that terminate in a large aquifer. Flow into the reservoir would be linear, and there would be an essentially constant pressure at the outer boundary. This would require a steady-state approximation with the productivity index, J_w, being a function of the length of the sealing faults and the distance between.

Figure 21f depicts a wedge sand. Solutions to this problem have been reported in the literature[9,13] in terms of an extension of linear flow. Turned on end, it can also be treated as radial flow, with an angle θ and the width represented by the distance h.

These illustrations are given only as a guide to show that many reservoir-aquifer systems can be defined in terms of radial or linear flow. Both the simplified method and the van Everdingen-Hurst solutions are applicable if we view the problems in terms of finding the proper representation of a rate equation. However, the simplified method allows us to use different dimensions or geometries when defining the aquifer productivity index and the aquifer volume for a given problem.

Aquifer Interference

By separating the water influx problem as we have into a rate equation and a material balance equation, we can examine each individually as to its effect on interference. Consider an aquifer or radius r containing two similar fields, A and B (they need not be similar when applying the simplified method). We assume Field A has been producing long enough to reach steady state. Let the productivity index of Field A be $J_w = f(r)$. When Field B begins producing, the productivity index of Field A will <u>increase</u>, becoming $J_w = f(r/2)$. From the standpoint of the rate equation, the deliverability of the aquifer for Field A will be <u>increased</u> after Field B begins producing. As pointed out by Bruce[14] in his study of the Smackover aquifer, the interference effect is totally one of "competition among pools for the common water supply".

From the aquifer material balance standpoint, Field A would initially have an aquifer volume of W_{ei} bbl available to it for water influx. However, after Field B begins producing, the aquifer drainage volume available to Field A is reduced. It can be approximated by the basic relationship given by Matthews et al.[26] -- "at (pseudo) steady-state the drainage volumes in a bounded reservoir are proportional to the rates of withdrawal from each drainage volume".

$$W_{eiA}(t) = \frac{J_{wA}\,(\bar{p} - p_{wfA})}{J_{wA}\,(\bar{p} - p_{wfA}) + J_{wB}\,(\bar{p} - p_{wfB})} \cdot [W_{ei} - W_{eA}(t)] , \quad ..(20)$$

where

$W_{eiA}(t)$ = encroachable water in place available to Field A at time t.

If for simplicity we are assuming equal inner boundary pressures and equal PI values for Fields A and B (equal influx rates),

$$W_{eiA}(t) = \frac{W_{ei}(t)}{2} , \quad ..(21)$$

after Field B starts production and reaches pseudosteady state. The transient time will now be shorter than the transient period of Field A producing alone.

In our aquifer material balance equation, the interference term for other reservoirs with respect to a given reservoir is given by the summation term $\sum_{2}^{j} W_{ej}$, which represents the sum of the cumulative influx into all other reservoirs in the common aquifer. This results in additional depletion, or decline in the average pressure of the common aquifer as a result of these fields also having water influx.

The expanded expression is more easily visualized in the time-incremented step-function approach for a time interval Δt. The cumulative influx into all reservoirs from Fields 2 to j (the field of interest is Field 1) is

$$\Delta W_e\ (\Delta t) = J_{w(2)}\ [\overline{p} - p_{wf(2)}]\ \Delta t + J_{w(3)}\ [\overline{p} - p_{wf(3)}]\ \Delta t + \ldots + J_{w(j)}\ [\overline{p} - p_{wf(j)}]\ \Delta t \quad . \qquad ..(22)$$

Also, when handling the problem from a time-incremented standpoint, we could even, for completeness, include to some extent the change in compressibility of the total system by allowing each field, including all reservoirs within the common aquifer, to contribute to the total compressibility:

$$c_t = S_o c_o + S_g c_g + S_w c_w + c_f \quad . \qquad ..(23)$$

If we include all except the reservoir of interest (Reservoir 1) this becomes

$$c_t = \sum_{2}^{j} \left(\frac{N\beta_o c_o + G\beta_g c_g}{V_p} \right)_j + S_w c_w + c_f \ , \qquad ..(24)$$

where V_p is the total pore volume of the aquifer and nonproducing fields. Muskat[27] points out that the indicated abnormally high compressibility, $c_t = 36 \times 10^{-6}\ psi^{-1}$ of the East Texas Woodbine aquifer could be due to gas fields or gas caps of oil fields distributed in the aquifer.

If we do not wish to include the compressibility of the other reservoirs within the aquifer, Equation 24 reduces to the simple expression

$$c_t = c_w + c_f \ . \qquad ..(25)$$

Water Injection Into The Aquifer

The usual method of treating water injection for studying pressure maintenance is to include a water injection term in the hydrocarbon material balance equation. A form of the material balance equation for a gas reservoir is

$$G_p\beta_g = G(\beta_g - \beta_{gi}) + W_e + \beta_w(W_i - W_p) \ . \qquad ...(26)$$

The basic assumption here with respect to water injection is that all water injected is instantly available to the reservoir, which would be realistic if the water was injected uniformly throughout the reservoirs as in pattern waterflooding. However, when the purpose is to maintain pressure, we generally use a flank water injection, with the injection wells located in the aquifer.

A more realistic approach is to include a water injection term in the aquifer material balance equation so as to incorporate the effects of the resistance to flow across the reservoir-aquifer boundary. For high permeability boundaries, the results would be essentially the same. However, where the permeability at the boundary is low, over a realistic time period little or no water may enter the reservoir. The option should be available, at least, to

study it both ways or in combination. Equation 9 includes water injection into the aquifer in such a manner that the total water influx, W_e is also a function of the water injected, $W_e = f(W_i)$.

In an interesting case history[21] of the Pegasus Ellenberger reservoir, we are told of an attempt to maintain pressure by using flank water injection to supplement edgewater influx. The peripheral project failed to maintain pressure, resulting in very high pressures around the injection wells. Injection into the central producing area was required to halt the pressure decline. The water influx constants from the edgewater drive were established before water injection was begun. The PI-Aquifer Material Balance approach would have been more successful in predicting the final outcome.

Historical Data

There are two differing treatments of historical data from reservoirs subject to water drive. They are usually referred to as

1. The Material Balance as an Equation of a Straight Line[25], and
2. The Resistance or Influence Function.[4,6]

They differ mainly in their primary objectives. The straight-line approach attempts to determine the original gas or oil in place using the historical data, whereas the resistance or influence-function approach fixes a best estimate of gas or oil in place and then attempts to determine a best fit of the data to arrive at a resistance or influence function F(t) with which to predict future performance.

When the objective is to determine recoverable reserves, a precise value for oil or gas originally in place may not be justified because of the inaccuracies involved in arriving at reliable values for residual gas or oil saturation and sweep efficiency. If, however, in determining original in-place values the resulting influx coefficients, C and t_D, are to be used to make future performance predictions (reservoir pressures and producing rates) the two treatments will accomplish the same thing.

With the simplified procedure, where the problem has been separated into its two basic components -- productivity index and aquifer material balance -- we can approach the problem the way we would approach it to determine the resistance or influence function. For a gas reservoir:

1. We can fix a best estimate of gas in place, G.
2. Using the incremental form of the reservoir material balance equation for a time interval Δt_n and two historical reservoir pressures, p_{wfn} and $p_{wf(n-1)}$, we can solve for a water influx volume

$$\Delta W_{en} = \Delta(G_p\beta_g) - G\Delta\beta_g + \Delta(W_p\beta_w) \quad . \qquad ..(27)$$

Then the average influx rate during the time interval is

$$\bar{e}_w(\Delta tn) = \frac{\Delta W_{en}}{\Delta tn} \quad , \qquad ..(28)$$

which is represented at time $\frac{t_n + t_{n-1}}{2}$ ..(29)

3. We can plot the average influx rate $\bar{e}_w(\Delta tn)$ as a function of time.

4. We can calculate water influx rates as functions of time, using various combined values of aquifer productivity index and encroachable water in place. These rates of water influx are plotted with those calculated using the material balance equation.

5. We can select the best combination of J_w - W_{ei} to fit the problem. Although a statistical approach could be used to make a selection, an engineer's analysis based on intimate knowledge of each data point and field history would be preferable.

A good starting point for J_w and W_{ei} should be based on the basic geometry of of the reservoir-aquifer system being studied. For a strictly radial geometry the productivity index of the aquifer, J_w, the water in place, W_{ei}, and the original gas in place, G, are all functions of common variables in that $J_w = f(\ln r_r, \ln r_a)$; $W_{ei} = f(r_r^2, r_a^2)$; and $G = f(r_r^2)$. If aquifer interference occurs at a later time, J_w will change as a result of a change in drainage radius r_a, but only as the $\ln r_a(t)$, whereas the water in place $W_{ei}(t)$ will change as the square of $r_a(t)$, with the gas in place remaining the same. Therefore, it is possible to have more than one value of water in place as a solution during the producing life of a field.

During the early times, before pseudosteady state is established, the aquifer productivity index, $J_w(t)$ plotted vs the ln t and $\sqrt{t}$ for radial and linear flow, respectively, should be straight lines.[4,6] No fixed value of J_w and $W_{ei}(t)$ exists during the early transient period.

Discussion of Results

The method chosen with which to illustrate a comparison between the PI-Aquifer Material Balance approach and the more rigorous solutions of van Everdingen-Hurst is a hypothetical gas reservoir surrounded by a finite radial aquifer. Using a gas reservoir does not require the introduction of variables such as k_g/k_o relationships that may later be suspected of contributing to some of the basic responses shown by the water drive performance.

The properties used for the gas reservoir and aquifer are listed in Table 1. So that the effect of the early transient period could be investigated, we chose a range of permeabilities and external radii of the aquifer. In each case, the aquifer inner boundary pressure was represented by the average

pressure determined from the solution of the gas reservoir material balance. Values used for water viscosity and the total compressibility are typical of those often used in the literature for water influx calculations.

A typical gas withdrawal rate of take of 1 MMcf/D to 8.59 Bcf in place (1 MMcf/D to 7.3 Bcf recoverable with an 85-percent recovery factor) was used so as to obtain realistic water influx values. A more rapid gas withdrawal rate would result in less water influx for the same reservoir and aquifer properties used in this study. No attempt has been made to determine recoverable reserves at abandonment based on residual gas and sweep efficiencies. This could be handled, however, by the methods suggested by Agarwal et al.[28] All forecasts are carried out for a full period of 20 years, that time defined by a 1-to-7.3 rate of take. A constant field wellhead potential for the gas reservoir was used for all cases.

Figures 6 through 10 illustrate the water drive performance for an aquifer with a permeability of 1,000 md at four different external aquifer radii -- 30,000, 50,000, 70,000, and 100,000 ft (19 miles). In all cases, the PI-Aquifer Material Balance solutions match identically the gas producing rates, reservoir pressure, and cumulative water influx determined using the van Everdingen-Hurst solutions.

The simplified approach does not utilize superposition, whereas the van Everdingen-Hurst solution does. To investigate the effects of superposition when producing rates are varied severely, a variable producing rate situation was studied (Figure 10). This was done for the largest aquifer radius. Excellent agreement was obtained for this 1,000-md permeability case.

Figures 11 through 14 illustrate the water drive performance when the aquifer permeability is changed to 100 md. In these cases, the departure from the van Everdingen-Hurst solutions is quite small with respect to reservoir pressure and cumulative water influx and is well within engineering accuracy. The gas producing rates are identical.

Figure 12 includes the additional points representing results using the van Everdingen-Hurst radial infinite solution. After early times, their solution departs from the $r_a/r_r = 10$ case about as much above the line as the simplified does below. What is interesting here is that within the limits of field data, it would be difficult to determine the actual extent of the aquifer. That is, we could easily maintain that the performance data indicates an infinite radial aquifer. There would be enough room to adjust the internal boundary pressures to force a fit to an infinite solution.

Figure 14, showing the performance of the aquifer, illustrates why the cumulative water influx as calculated by the PI-Aquifer Material Balance method departs constantly from that calculated by the van Everdingen-Hurst method. The departure results, not unexpectedly, from a difference in influx rates during the early transient period. After this period, the influx rates agree quite well.

Figures 15 and 16 illustrate the water drive performance for an aquifer of 50-md permeability. The departure of the cumulative water influx from that derived by the van Everdingen-Hurst solution is most pronounced for the

aquifer-to-reservoir ratio of $r_a/r_r = 10$, an aquifer external radius of 100,000 ft. The constant departure indicates that the difference occurs as a result of the early transient period, as shown in Figure 14. Still, the reservoir pressure and gas producing rate agree quite well.

Figures 17 through 20 give the water drive performance using a 10-md aquifer permeability. In Figure 17, $r_a/r_r = 3$, the cumulative water influx for the PI-Aquifer Material Balance solution is always greater, indicating that the van Everdingen-Hurst solution was dominated by linear flow, resulting in a lower influx rate than the radial flow determination.

Figure 19, $r_a/r_r = 7$, shows a continuously increasing departure of the cumulative water influx as a result of transient flow effect throughout. In these cases as in all previous cases, the gas producing rates agree. In all the 10-md aquifer permeability cases, the gas reservoir is behaving essentially as a volumetric reservoir.

From a check of the time it takes to establish pseudosteady state, it was found that the productivity index representing the fixed dimensions of 100,000 ft for r_a of the aquifer, could not become established during the 20-year period of the forecast. Therefore, the Hurst-Simplified (Defined) equation given in Table 4 was used. The results obtained using this equation are quite good (see Figure 20). As in individual well forecasts, the Hurst-Simplified (Defined) equation could be used until pseudosteady state is established; then, after applying the material balance equation to determine the aquifer shut-in pressure, we could use the pseudosteady-state rate equation for the rest of the forecast.

Because the results presented in this study were based on finite aquifer systems, it would be appropriate to discuss briefly the terms "finite" and "infinite" as applied to water influx problems. "Finite", as used in this study, indicates only that finite dimensions were used for defining the aquifer productivity index, J_w, and the aquifer volume, W_{ei}. "Infinite", when applied to an aquifer, can take on at least three different meanings.

1. The aquifer volume W_{ei} is very large (infinite). This can result in a Schilthuis steady-state aquifer behavior.

2. The deliverability or productivity index, J_w, is very large (infinite). As a special case of water influx, an infinite productivity index is always assumed when the expansion of the water within the hydrocarbon reservoir itself is included in the reservoir material balance equation by the addition of a water compressibility term.

3. Transient flow exists during the entire period of interest, with the result that an infinite <u>solution</u> is applicable.

For the studies involving the largest aquifer radius used -- 100,000 ft -- the 10-md aquifer permeability case was the only one that could be classed as infinite --and then only because the infinite <u>solution</u> could be applied. Its volume of water influx was so insignificant as to cause the gas reservoir

to behave like a volumetric reservoir. The 100-md case response as a finite aquifer (even with no transients being considered for the simplified solution) was such that it appeared to behave like an infinite aquifer solution (see Figure 12). The term "infinite" when applied to water influx problems should always be qualified as to which of the above definitions is meant.

In review, the good results obtained with the PI-Aquifer Material Balance approach are surprising when we consider that the additional flow contributions from the early transient period have been omitted and that there exists the condition $r_r << r_a$, imposed in the derivation of the pseudosteady state radial flow equation. Variations of the constant in the term $[\ln (r_a/r_r) - 3/4]$ were studied by using -1/2 and -1, as well as some of the other suggested methods of expressing the inner boundary pressure, P_{wf}. In all cases, the results obtained were significantly poorer than those reported in this study.

Certainly in many cases the additional capabilities of the PI-Aquifer Material Balance, when properly included instead of omitted, can far outweigh any early transient effects omitted. In many cases where the transient is of long duration, as for the 10-md cases given in this study, it make little difference whether the transient effects are included or not.

Example Calculations

An example of a water drive performance prediction for a gas reservoir using the PI-Aquifer Material Balance approach is given in detail in Table 5. The calculations were performed on a desk calculator using the simple trial-and-error procedure of iterative substitution. The iterative calculations are shown only for Years 1 and 20. During the period of constant producing rate, the second trial was always within 1 psi of the final answer. When the producing rate was limited by the backpressure curve, an additional iteration was required.

Conclusions

The PI-Aquifer Material Balance approach to water influx calculations offers a very useful and flexible method for forecasting and analyzing the performance of water drive reservoirs. The separation of the water influx problem into a rate equation and a material balance equation, not requiring the use of superposition, makes the concepts and calculations quite simple and easy to apply.

Acknowledgements

I wish to thank Phillips Petroleum Co. for permission to publish this paper. The assistance of M. W. Canon, who programmed the calculations and helped with all the computer runs, is gratefully acknowledged.

Nomenclature

b = width, ft
β_g = gas formation volume factor, reservoir bbl/scf
β_o = oil formation volume factor, reservoir bbl/surface bbl
β_w = water formation volume factor, reservoir bbl/surface bbl
c_f = formation (rock) compressibility, psi^{-1}
c_g = gas compressibility, psi^{-1}
c_o = oil compressibility, psi^{-1}
c_t = total or effective aquifer compressibility, psi^{-1}
c_w = water compressibility (includes the effect of dissolved gas), psi^{-1}
C_g = gas well backpressure curve coefficient (gas well productivity index)
e = natural logarithm base 2.71828
e_w = water influx or efflux rate, reservoir bbl/D
$\overline{e}_w(\Delta tn)$ = average influx or efflux rate during time interval (Δtn), reservoir bbl/D
G = initial gas in place, Bscf
G_p = cumulative gas production, Bscf
h = aquifer thickness, ft
i = subscript to denote initial value or conditions (except for cumulative water injected, W_i)
J_w = aquifer productivity index, reservoir bbl/D/psi
k = aquifer permeability, darcies
L = length, ft
n = exponent of backpressure curve, also used as a subscript to denote the end of an interval
$\overline{p}$ = average aquifer pressure (shut-in pressure), psia
$\overline{p}_{(n-1)}$ = average aquifer pressure (shut-in pressure) at the beginning of an interval, psia
p_e = external boundary pressure, psia
p_i = initial aquifer pressure, psia
$\overline{p}_R$ = gas reservoir average pressure (shut-in pressure), psia
p_{tf} = wellhead tubing flowing pressure, psia
p_{ts} = wellhead shut-in pressure, psia
p_{wf} = inner aquifer boundary pressure, psia
$\overline{p}_{wf}$ = a constant inner boundary pressure for a time interval (Δtn)(see Equation 8), psia
PI = productivity index, reservoir bbl/D/psi
q_g = gas flow rate, Mscf/D
$\overline{q}_g$ = average gas flow rate during an interval, Mscf/D
q_{gc} = constant gas flow rate, Mscf/D
$(q_{wi})_{max}$ = initial open-flow potential of the aquifer, reservoir bbl/D
r_a = external radius of aquifer, ft
r_r = internal radius of aquifer, ft
t = time, days
Δtn = time interval n
t_{ps} = time to establish pseudosteady state, days
t_s = time to establish steady state, days
V_p = pore volume
W = initial water in place, surface bbl
W_e = cumulative water influx into a reservoir or efflux from the aquifer, reservoir bbl

ΔW_{en} = cumulative water influx or efflux during an interval, reservoir bbl
W_{ej} = cumulative water influx or efflux into reservoir (j) within the common aquifer, reservoir bbl
W_{ei} = initial encroachable water in place at pressure p_i, reservoir bbl
$W_{ei}(t)$ = encroachable water in place at time (t), reservoir bbl
W_i = cumulative water injected, surface bbl
W_p = cumulative water produced, surface bbl
z = gas deviation factor
ϕ = porosity, fraction
μ = viscosity of water, cp

References

1. Craft, B.C. and Hawkins, M. F., Jr.: Applied Petroleum Reservoir Engineering, Prentice-Hall, Inc., Englewood Cliffs, N.J. (1959) 126, 206, 224

2. Frick, T.C.: Petroleum Production Handbook, McGraw-Hill Book Co., Inc., New York (1962) II, Chap. 32, 5-22.

3. Pirson, S. J.: Elements of Oil Reservoir Engineering, 2nd ed., McGraw-Hill Book Co., Inc., New York (1958) 608.

4. Hutchinson, T. S. and Sikora, V. J.: "A Generalized Water-Drive Analysis", Trans., AIME (1959) **216**, 169-178

5. Hicks, A. L., Weber, A. G., and Ledbetter, R. L.: "Computing Techniques for Water-Drive Reservoirs", Trans., AIME (1959) 216, 400-402.

6. Coats, K. H., Rapoport, L. A., McCord, J. R., and Drews, W. P.: "Determination of Aquifer Influence Functions from Field Data", J. Pet. Tech. (Dec., 1964) 1417-1424.

7. van Everdingen, A. F. and Hurst, W.: "The Application of the Laplace Transformation to Flow Problems in Reservoirs", Trans., AIME (1949) **186**, 305-324.

8. Lowe, R. M.: "Performance Predictions of the Marg Tex Oil Reservoir Using Unsteady-State Calculations", J. Pet. Tech. (May, 1967) 595-600.

9. Mueller, T. D.: "Transient Response of Nonhomogenous Aquifers", Soc. Pet. Eng. J. (March, 1962) 33-43.

10. Nabor, G. W. and Barham, R. H.: "Linear Aquifer Behavior", J. Pet. Tech. (May, 1964) 561-563.

11. Chatas, A. T.: "Unsteady Spherical Flow in Petroleum Reservoirs", Soc. Pet. Eng. J. (June, 1966) 102-114.

12. Coats, K. H., Tek, M. R. and Katz, D. L.: "Unsteady-State Liquid Flow Through Porous Media Having Elliptic Boundaries", Trans., AIME (1959) **216**, 460-464.

13. Katz, D. L., Tek, M. R., Coats, K. H., Katz, M. L., Jones, S. C., and Miller, M. C.: Movement of Underground Water in Contact with Natural Gas, Monograph -- Project NO-31, AGA, New York (1963).

14. Bruce, W. A.: "A Study of the Smackover Limestone Formation and the Reservoir Behavior of Its Oil and Condensate Pools", Trans., AIME (1944) **155**, 88-119.

15. Rumble, R. C., Spain, H. H., and Stamm, H. E.: "Reservoir Analyzer Study of the Woodbine Basin", Trans., AIME (1951) **192**, 331-340.

16. Moore, W. D. and Truby, L. G., Jr.,: "Pressure Performance of Five Fields Completed in a Common Aquifer", Trans., AIME (1952) **195**, 297-302.

17. Mortada, M.: "A Practical Method for Treating Oilfield Interference in Water-Drive Reservoirs", Trans., AIME (1955) **204**, 217-226.

18. Coats, K. H., Tek, M. R. and Katz, D. L.: "Method for Predicting the Behavior of Mutually Interfering Gas Reservoirs Adjacent to a Common Aquifer", Trans., AIME (1959) **216**, 247-251

19. Robinson, M. P.: "Pressure Interference Correction to the Material Balance Equation for Water-Drive Reservoirs Using a Digital Computer", Trans., AIME (1958) **213**, 418-422.

20. Bonet, E. J. and Crawford, P. B.: "Aquifer Behavior with Injection", J. Pet. Tech. (Sept., 1969) 1210-1216.

21. Cargile, L. L.: "A Case History of the Pegasus Ellenburger Reservoir", J. Pet. Tech. (Oct., 1969) 1330-1336.

22. Carter, R. D. and Tracey, G. W." "An Improved Method for Calculating Water Influx", Trans., AIME (1960) **219**, 415-417.

23. Stanley, L. T.: "Curve-Fitting Cuts Material Balance Calculations", Pet Eng. (Aug., 1961) 90.

24. Hurst, W.: "Water Influx into a Reservoir and Its Application to the Equation of Volumetric Balance", Trans., AIME (1943) **151**, 57-72.

25. Havlena, D. and Odeh, A. S.: "The Material Balance as an Equation of a Straight Line -- Part II, Field Cases", J. Pet Tech. (July, 1964) 815-822.

26. Matthews, C. S., Brons, F. and Hazebroek, P.: "A Method for Determination of Average Pressure in a Bounded Reservoir", Trans., AIME (1954) **201**, 182-191.

27. Muskat, M.: Physical Principles of Oil Production, McGraw-Hill Book Co., Inc., New York (1949) 583.

28. Agarwal, R. G., Al-Hussainy, R., and Ramey, H. J., Jr.: "The Importance of Water Influx in Gas Reservoirs", J. Pet Tech. (Nov., 1965) 1336-1342.

29. Russell, D. G. and Prats, M.: "Performance of Layered Reservoirs with Crossflow -- Single-Compressible-Fluid Case", Soc. Pet. Eng. J. (March, 1962) 53-67.

30. Manual of Back-Pressure Testing of Gas Wells, Interstate Oil Compact Commission, Oklahoma City, Okla. (1966).

Appendix A

Aquifer Material Balance

A material balance equation may be developed for a finite aquifer system as follows.

Total Volume at Pressure $\bar{p}$

$$\left[\begin{pmatrix}\text{Volume of}\\ \text{Initial Contents}\\ \text{at } \bar{p}\end{pmatrix} + \begin{pmatrix}\text{Volume of all Injected}\\ \text{and Encroached Fluids}\\ \text{at } \bar{p}\end{pmatrix}\right]$$

Pore Volume at Pressure $\bar{p}$

$$\underset{\text{Original Pore Volume}}{\left[\begin{pmatrix}\text{Volume of}\\ \text{Initial Contents}\\ \text{at } p_i\end{pmatrix}\right.} - \underset{\text{Lost Pore Volume}}{\left.\begin{pmatrix}\text{Loss of}\\ \text{Pore Volume}\\ \text{at } \bar{p}\end{pmatrix}\right]}$$

Total Voidage Volume at Pressure $\bar{p}$

$$= \left[\begin{pmatrix}\text{Volume Effluxed and Produced}\\ \text{at } \bar{p}\end{pmatrix}\right] \qquad ..(A\text{-}1)$$

In the algebraic form using the standard AIME nomenclature,

$$\{[W\ \beta_w] + [W_i\ \beta_w]\} - \{[W\ \beta_{wi}] - [c_f\ (p_i - \bar{p})W\ \beta_{wi}]\} = \{[W_e] + [W_p\ \beta_w]\} \quad (A\text{-}2)$$

Dividing through by β_{wi},

$$\left\{\left[W\frac{\beta_w}{\beta_{wi}}\right]+\left[W_i\frac{\beta_w}{\beta_{wi}}\right]\right\}-\left\{W-\left[c_f(p_i-\bar{p})W\right]\right\}$$
$$=\left\{\left[\frac{W_e}{\beta_{wi}}\right]+\left[W_p\frac{\beta_w}{\beta_{wi}}\right]\right\} \qquad ..(A\text{-}3)$$

Substituting

$$\frac{\beta_w}{\beta_{wi}} = 1 + c_w(p_i - \bar{p}) , \qquad ..(A\text{-}4)$$

we obtain

$$W[1 + c_w(p_i - \bar{p})] - W[1 - c_f(p_i - \bar{p})] = \frac{1}{\beta_{wi}}[W_e + \beta_w(W_p - W_i)], \qquad ..(A\text{-}5)$$

or

$$W\,\beta_{wi}\,\{[1 + c_w(p_i - \bar{p})] - [1 - c_f(P_i - \bar{p})]\} = W_e + \beta_w(W_p - W_i)]; \qquad ..(A\text{-}6)$$

collecting terms

$$W\,\beta_{wi}\,[(c_w + c_f)(p_i - \bar{p})] = W_e + (W_p - W_i)\,\beta_w. \qquad ..(A\text{-}7)$$

Rearranging Equation A-7, we have

$$\bar{p} = -\left[\frac{W_e + (W_p - W_i)\beta_w}{(c_w + c_f)W\,\beta_{wi}}\right] + p_i . \qquad ..(A\text{-}8)$$

To further generalize the equation to include interference effects of other reservoirs in a common aquifer,

$$\bar{p} = -\left[\frac{W_e + \sum_{2}^{j} W_{ej} + (W_p - W_i)\beta_w}{(c_w + c_f)W\,\beta_{wi}}\right] + p_i, \qquad ..(A\text{-}9)$$

where W_e represents the cumulative water influx for the reservoir of interest, and W_{ej} represents cumulative water influx into reservoir (j) within the common aquifer. The water compressibility can be considered then as effective compressibility, which includes the compressibility of the other nonproducing hydrocarbon reservoirs.

Equation A-9 is the general equation, but to simplify the further derivation we will set the interference, water production, and water injection terms to zero; that is, $\Sigma W_{ej} = 0$, $W_p = 0$, and $W_i = 0$.

We then have

$$\overline{p} = - \left[\frac{1}{(c_w + c_f)W \beta_{wi}} \right] W_e + p_i. \qquad ..(A\text{-}10)$$

Defining $[(c_w + c_f)W \beta_{wi}]p_i = W_{ei}$, as the initial encroachable water in place, we can write for the aquifer material balance equation

$$\overline{p} = - \left(\frac{p_i}{W_{ei}} \right) W_e + p_i, \qquad ..(A\text{-}11)$$

which can be represented in graphical form as shown in Figure 5.

Note that the term W_{ei} is <u>not</u> total water in place, $W \beta_{wi}$ (which represents the total aquifer pore volume). The aquifer will still be 100-percent saturated with water when all the aquifer pressure is depleted; that is, when $\overline{p} = 0$. Note, too, that the determination of W_{ei}, the initial encroachable water in place, is not basically geometry-dependent except to the extent that fundamental mensuration rules can be applied. Isopachous planimetry would be the most rigorous of all approaches.

Appendix B

Water Influx Equations

Aquifer Rate Equation

The aquifer rate equation independent of geometry is

$$q_w = J_w(\overline{p} - p_{wf})^{1.0} \qquad ..(B\text{-}1)$$

The aquifer rate equation when graphically depicted is analogous to the productivity index curve of the oil wells and to the backpressure curve of the gas wells (see Figure 1).

The rate-time relationship for water influx against an increasing Δp is shown graphically in Figures 3 and 4.

The cumulative influx into the reservoir or efflux from the aquifer is determined by

$$W_e = \int_0^t q_w \, dt \qquad ..(B\text{-}2)$$

Differentiating we have

$$dW_e = q_w\, dt, \qquad ..(B\text{-}3)$$

or

$$\frac{dW_e}{dt} = q_w \qquad ..(B\text{-}4)$$

Using the aquifer rate equation, we obtain

$$q_w = J_w(\bar{p} - p_{wf}); \qquad ..(B\text{-}1)$$

then

$$\frac{dW_e}{dt} = J_w(\bar{p} - p_{wf}) \qquad ..(B\text{-}5)$$

At initial conditions we can define the maximum capacity or initial open-flow potential of the aquifer, when $p_{wf}=0$, as

$$(q_{wi})_{max} = J_w(p_i), \qquad ..(B\text{-}6)$$

or

$$J_w = \frac{(q_{wi})_{max}}{p_i} \quad . \qquad ..(B\text{-}7)$$

Therefore,

$$q_w = \frac{(q_{wi})_{max}}{p_i}\,(\bar{p} - p_{wf}) \quad . \qquad ..(B\text{-}8)$$

Then

$$\frac{dW_e}{dt} = \frac{(q_{wi})_{max}}{p_i}\,(\bar{p} - p_{wf}), \qquad ..(B\text{-}9)$$

or

$$dW_e = \frac{(q_{wi})_{max}}{p_i}\,(\bar{p} - p_{wf})dt \quad . \qquad ..(B\text{-}10)$$

From the material balance equation slope,

$$\frac{d\bar{p}}{dW_e} = -\left(\frac{p_i}{W_{ei}}\right), \qquad ..(B\text{-}11)$$

or

$$d\bar{p} = -\left(\frac{p_i}{W_{ei}}\right) dW_e \quad . \qquad ..(B\text{-}12)$$

Combining Equations B-10 and B-12,

$$d\bar{p} = - \frac{p_i}{W_{ei}} \left[\frac{(q_{wi})_{max}}{p_i} (\bar{p} - p_{wf}) dt \right] \qquad ..(B-13)$$

Simplifying and separating variables,

$$\frac{d\bar{p}}{(\bar{p} - p_{wf})} = - \frac{(q_{wi})_{max}}{W_{ei}} dt \ . \qquad ..(B-14)$$

Then

$$\int_{p_i}^{\bar{p}} \frac{d\bar{p}}{(\bar{p} - p_{wf})} = - \frac{(q_{wi})_{max}}{W_{ei}} \int_o^t dt \ . \qquad ..(B-15)$$

Rearranging and changing limits on p, we obtain

$$\frac{(q_{wi})_{max}}{W_{ei}} \int_o^t dt = \int_{\bar{p}}^{p_i} \frac{d\bar{p}}{(\bar{p} - p_{wf})} \ . \qquad ..(B-16)$$

Integrating between limits gives us

$$\left[\frac{(q_{wi})_{max}}{W_{ei}} \right] t = \ln \left[\frac{p_i - p_{wf}}{\bar{p} - p_{wf}} \right] , \qquad ..(B-17)$$

which can be expressed as

$$\frac{p_i - p_{wf}}{\bar{p} - p_{wf}} = e^{[(q_{wi})_{max}/W_{ei}]t} \ ; \qquad ..(B-18)$$

but

$$q_w = J_w(\bar{p} - p_{wf}) \ , \qquad ..(B-19)$$

or

$$\frac{q_w}{J_w} = (\bar{p} - p_{wf}) \ . \qquad ..(B-20)$$

Therefore,

$$\frac{J_w (p_i - p_{wf})}{q_w} = e^{[(q_{wi})_{max}/W_{ei}]t} \qquad ..(B-21)$$

Now, defining $e_w = q_w$,

$$e_{w(t)} = \frac{J_w(p_i - p_{wf})}{e^{[(q_{wi})_{max}/W_{ei}]t}} \quad , \qquad ..(B\text{-}22)$$

which is the final form expressing the instantaneous rate of water influx as a function of time and the internal boundary pressure, (p_{wf}). The equation is quite general and totally independent of geometry, and will use any consistent set of units.

Cumulative Water Influx Equation

Now we can derive the more useful cumulative water influx equation. If we combine the equations

$$W_e = \int_o^t e_w \, dt \qquad ..(B\text{-}2)$$

and

$$e_w = \frac{J_w(p_i - p_{wf})}{e^{[(q_{wi})_{max}/W_{ei}]t}} \quad , \qquad ..(B\text{-}23)$$

then

$$W_e = \int_o^t \frac{J_w(p_i - p_{wf})}{e^{[(q_{wi})_{max}/W_{ei}]t}} \, dt, \qquad ..(B\text{-}24)$$

or

$$W_e = J_w(p_i - p_{wf}) \int_o^t e^{-[(q_{wi})_{max}/W_{ei}]t} \, dt \, , \qquad ..(B\text{-}25)$$

Equation B-25, when integrated between limits

$$W_e = J_w(p_i - p_{wf}) \left\{ \frac{e^{-[(q_{wi})_{max}/W_{ei}]t}}{-\left[\frac{(q_{wi})_{max}}{W_{ei}}\right]} \right\}_o^t \, , \qquad ..(B\text{-}26)$$

gives

$$W_e = \frac{J_w(p_i - p_{wf})}{\left[\frac{(q_{wi})_{max}}{W_{ei}}\right]} \{1 - e^{-[(q_{wi})_{max}/W_{ei}]t}\} \; ; \qquad ..(B\text{-}27)$$

but

$$(q_{wi})_{max} = J_w(p_i) \qquad ..(B\text{-}6)$$

Substituting and rearranging, we arrive at the final form of the cumulative water influx equation.

$$W_e = \frac{W_{ei}}{p_i} (p_i - p_{wf}) \{1 - e^{-[(q_{wi})_{max}/W_{ei}]t}\} \quad ..(B-28)$$

It is interesting to note that both the instantaneous water influx rate equation and the cumulative influx equation are identical in form with equations derived by Russell and Prats[29] for predicting the performance of layered reservoirs. Their results and conclusions should be directly applicable when the simplified water influx approach is used.

TABLE 1

HYPOTHETICAL GAS RESERVOIR AND AQUIFER PROPERTIES.

Gas Reservoir Properties

Initial gas reservoir pressure, psia	2,000
Porosity, fraction	0.20
Pay thickness, ft	100
Water saturation, fraction PV	0.20
Initial formation volume factor for gas, scf/reservoir cf	154.26
Reservoir radius, ft	10,000
Gas gravity (to air)	0.700
Pseudo critical temperature for gas, °R	392
Pseudo critical pressure for gas, psia	668
Reservoir depth, ft	7,000
Reservoir temperature, °F	130
Initial gas-law deviation factor	0.780
Initial gas in place, Bcf	776
Rate of take (1 MMcf/D to 8.59 Bcf gas in place), Mscf/D	90,338
Total field wellhead potential, Mscf/D	250,000
Initial wellhead shut-in pressure, psia	1,600
Slope of wellhead backpressure curve	0.700
Line pressure, psia	200

Aquifer Properties

Inital pressure in aquifer, psia	2,000
Permeability, md	10, 50, 100, 1,000
r_a/r_r	3, 5, 7, 10
r_a (using r_r = 10,000 ft), thousands of ft	30, 50, 70, 100
Porosity, fraction	0.20
Aquifer thickness, ft	100
Total compressibility for aquifer, 1/psi	6×10^{-6}
Viscosity of water, cp	0.50

TABLE 2

RADIAL FLOW WATER INFLUX VARIABLES USED FOR THE PI-AQUIFER MATERIAL BALANCE SOLUTIONS FOR A 20-YEAR FORECAST OF THE HYPOTHETICAL GAS RESERVOIR

r_a/r_r	Radius of Aquifer (ft)	Initial Encroachable Water in Place (10^6 bbl)	k = 0.010 darcy (pseudosteady state) J_w (B/D/psi)	Initial Potential (B/D)	Stabilization Time (years)	k = 0.050 darcy (pseudosteady state) J_w (B/D/psi)	Initial Potential (B/D)	Stabilization Time (years)
3	30,000	107.52	40.620	81,240	3.0	203.10	406,200	0.6
5	50,000	322.56	16.477	32,954	8.2	82.385	164,770	1.6
7	70,000	645.12	11.840	23,680	16.1	59.200	118,400	3.2
10	100,000	1,330.56	9.1202	18,240	32.9*	45.601	91,202	6.6

			k = 0.100 darcy (pseudosteady state) J_w (B/D/psi)	Initial Potential (B/D)	Stabilization Time (years)	k = 1.000 darcy (pseudosteady state) J_w (B/D/psi)	Initial Potential (B/D)	Stabilization Time (years)
3	30,000	107.52	406.20	812,400	0.3	4,062.0	8,124,000	0.03
5	50,000	322.56	164.77	329,540	0.8	1,647.7	3,294,000	0.08
7	70,000	645.12	118.40	236,800	1.6	1,184.0	2,368,000	0.16
10	100,000	1,330.56	91.202	182,400	3.3	912.02	1,824,000	0.33

* Stabilization time for this value of J_w exceeds duration of forecast.

TABLE 3

RADIAL FLOW WATER INFLUX VARIABLES USED
FOR THE VAN EVERDINGEN-HURST SOLUTIONS FOR A
20-YEAR FORECAST OF THE HYPOTHETICAL GAS RESERVOIR

Aquifer Permeability (darcies)	Ratio of Dimensionless Time to Real Time (1/year)	Water Influx Constant (cu ft/psi)
0.010	0.38483	75,396
0.050	1.9242	75,396
0.100	3.8483	75,396
1.000	38.483	75,396

TABLE 4

RADIAL AND LINEAR AQUIFER RATE EQUATIONS[2]

Type of Boundary	Radial Flow	Linear Flow
Finite - closed (no flow) at outer boundary	$q_w = \dfrac{7.08\ kh(\bar{p} - p_{wf})}{\mu\left[\ln\left(\dfrac{r_a}{r_r}\right) - \dfrac{3}{4}\right]}$	$q_w = \dfrac{3(1.127)\ kbh(\bar{p} - p_{wf})}{\mu L}$
Finite - constant pressure at outer boundary	$q_w = \dfrac{7.08\ kh(p_e - p_{wf})}{\mu\left[\ln\left(\dfrac{r_a}{r_r}\right)\right]}$	$q_w = \dfrac{1.127\ kbh(p_e - p_{wf})}{\mu L}$
Infinite	$q_w = \dfrac{7.08\ kh(p_i - p_{wf})}{\mu\left[\ln\sqrt{\dfrac{14.23\ kt}{\phi\mu c_t\ r_r^2}}\right]}$ [Hurst Simplified (Defined)]	$q_w = \dfrac{kbh(p_i - p_{wf})}{\mu\sqrt{\dfrac{6.33kt}{\phi\mu c_t}}}$

TABLE 5—EXAMPLE OF A WATER DRIVE PERFORMANCE PREDICTION FOR A GAS RESERVOIR USING THE PI-AQUIFER MATERIAL BALANCE APPROACH

RESERVOIR MATERIAL BALANCE CALCULATIONS | PI – AQUIFER MATERIAL BALANCE CALCULATIONS (AQUIFER K = 100 md; $^{r}a/r_{r}$ = 10)

n	TIME t	$\Delta t_n = (t_n - t_{n-1})$	q_{gc} or $\bar{q}_g$	ΔG_p	G_p	$G - G_p$	$G = \left(\frac{W_e}{B_{gi}}\right)' +$	$\left[\frac{G - G_p}{G - \frac{W_e}{B_{gi}}}\right]$	$\frac{\bar{p}_n}{\bar{z}}$	$Z\ (p)^{**}$	$\bar{p}_n$ and p_{wf}	$p_{ts} = \frac{\bar{p}_n}{\sqrt{e^x}}$ ***	$C_g(p_{ts}^2 - p_{tf}^2)^n$	$\bar{q}_g = \frac{(q_{gc} + q_{gc})}{2}$	$\bar{p}_{wf} = \frac{(p_{wf\,n-1} + p_{wf\,n})}{2}$	$\bar{p}_{n-1}$	$(\bar{p}_{n-1} - \bar{p}_{wf})$	$-\left[\frac{(q_{wc})_{max}}{W_{ei}}\right]\Delta t_n$ $1 - e$	ΔW_e Eq. 6	W_e	$\frac{W_e}{B_{gi}}$	$p_i - \bar{p} = \left(\frac{p_i}{W_{ei}}\right) W_e$	$\bar{p}_n$
		$(t)_n - (t)_{n-1}$	90,338 or (15)	(3) x (4) x 10^{-6}	Σ (5)	776,000 – (6)	776,000 – (22)	(7) ÷ (8)	2565 x (9)	USING (10)	(10) x (11)	(12) ÷ $\sqrt{e^x}$	$\left(\frac{p_{ts}^2 - 200^2}{1000}\right)^{0.7}$ 1028.4 x	$\frac{(14)_{n-1} + (14)_n}{2}$	$\frac{(12)_{n-1} + (12)_n}{2}$	(24)$_{n-1}$	(17) – (16)	0.04881	665,280 x (18) x (19)	Σ (20)	(21) ÷ 1.1545 x 10^6	1.503 $^{r}2 \times 10^6$ x (21)	2000.0 – (23)
(1)	DAYS (2)	DAYS (3)	Mscfd (4)	Bscf (5)	Bscf (6)	Bscf (7)	Bscf (8)	Bscf (9)	PSIA (10)	(11)	PSIA (12)	PSIA (13)	Mscfd (14)	Mscfd (15)	PSIA (16)	PSIA (17)	PSI (18)	(19)	RES BBL (20)	RES BBL (21)	Bscf (22)	PSI (23)	PSIA (24)
															2000.0				0	0	0	0	2000.0
1 a	0	0	0	0	0	776,000	776,000	1.00000	2565	0.780	2000	1600	>90,338										
b	365	365	90,338	32.973	32.973	743.027	776,000	0.95751	2456	0.782	1921				1960.5	2000.0	39.5	0.04881	1,282,644	1,282,644	1.111		
c					32.973	743.027	774.889	0.95888	2460	0.783	1926				1963.0	2000.0	37.0		1,201,464	1,201,464	1.041	1.8	1998.2
					32.973	743.027	774.958	0.95880	2459	0.783	1925	1535	>90,338		1962.5	2000.0	37.5		1,217,700	1,217,700	1.055		
2	730		90,338	32.973	65.946	710.054	771.916	0.91586	2359	0.786	1855	1482	>90,338		1890.0	1998.2	108.2		3,513,470	4,731,170	4.098	7.1	1992.9
3	1095		90,338	32.973	98.919	677.081	767.095	0.88266	2264	0.790	1788	1431	>90,338		1822.0	1992.8	170.8		5,549,465	10,280,635	8.905	15.5	1984.5
4	1460		90,338	32.973	131.892	644.108	760.696	0.84674	2172	0.794	1725	1382	>90,338		1757.9	1984.5	226.5		7,387,380	17,668,015	15.304	26.6	1973.4
5	1825		90,338	32.973	164.865	611.135	752.824	0.81178	2082	0.798	1661	1333	>90,338		1693.8	1973.4	279.4		9,105,149	26,773,164	23.180	40.2	1959.8
6	2190		90,338	32.973	197.838	578.112	743.548	0.77750	1994	0.803	1601	1288	>90,338		1631.0	1958.8	328.8		10,676,794	37,449,958	32.438	56.3	1943.7
7	2555		90,338	32.973	230.811	545.189	733.065	0.74371	1907	0.808	1541	1242	>90,338		1571.8	1943.7	372.7		12,102,314	49,552,272	42.921	74.5	1925.5
8	2920		90,338	32.973	263.784	512.216	721.292	0.71004	1821	0.812	1479	1194	>90,338		1510.0	1925.5	415.5		13,492,116	63,044,388	54.608	94.8	1905.2
9	3285		90,338	32.973	296.757	479.243	708.589	0.67633	1735	0.819	1421	1150	>90,338		1450.0	1905.2	455.2		14,781,254	77,825,642	67.411	117.0	1883.0
10	3650		90,338	32.973	329.730	448.270	694.709	0.64238	1648	0.824	1358	1100	>90,338		1389.5	1883.0	493.5		16,024,932	93,850,574	81.291	141.1	1858.9
11	4015		90,338	32.973	362.703	413.297	679.734	0.60803	1560	0.830	1295	1052	>90,338		1326.5	1858.9	532.4		17,288,093	111,138,667	96.266	167.1	1832.9
12	4380		90,338	32.973	395.676	380.324	663.705	0.57303	1470	0.837	1230	1001	>90,338		1262.5	1832.9	570.4		18,522,029	129,660,696	112.308	184.9	1805.1
13	4745		90,338	32.973	428.649	347.351	648.559	0.53723	1378	0.843	1182	948	>90,338		1196.0	1805.1	609.1		19,778,695	148,439,391	129.441	224.6	1775.4
14	5110		90,338	32.973	461.622	314.378	628.308	0.50036	1283	0.850	1091	892	>90,338		1126.5	1775.4	648.9		21,071,081	170,510,472	147.692	256.3	1743.7
15	5475		90,338	32.973	494.595	281.405	608.937	0.46212	1185	0.858	1018	834	>90,338		1054.5	1743.7	689.2		22,379,702	192,890,174	167.077	289.9	1710.1
16	5840		88,362	32.252	526.847	249.153	588.402	0.42344	1086	0.868	943	775	86,386	88,362	980.5	1710.1	729.6		23,691,571	216,581,745	187.598	325.5	1674.5
17	6205		81,578	29.776	556.623	219.377	566.801	0.38704	993	0.877	871	717	78,770	81,578	907.0	1674.5	767.5		24,922,260	241,504,005	209.185	363.0	1637.0
18	6570		72,528	26.473	583.096	192.904	544.328	0.35439	909	0.885	804	664	68,286	72,528	837.5	1637.0	799.5		25,961,364	267,465,369	231.672	402.0	1597.0
19	6935		64,502	23.543	606.639	189.361	521.152	0.32497	834	0.892	744	616	60,717	64,502	774.0	1598.0	824.0		26,756,928	294,222,297	254.848	442.3	1557.7
20 a	7300	365	60,717	22.162	628.801	147.199	521.152	0.28245	724	0.903	654	543	48,744	55,230	699.0	1557.7	858.7	0.04881	27,883,706	322,106,003	279.000		
b			55,230	20.159	626.798	149.202	487.000	0.30021	770	0.899	692	574	54,300	57,508	718.0	1557.7	839.1		27,266,738	321,489,035	278.466		
c			57,508	20.990	627.629	148.371	497.534	0.25821	765	0.900	688	570	53,775	57,246	716.0	1557.7	841.7		27,331,682	321,553,979	278.522	483.3	1516.7
d			57,246	20.895	627.534	148.466	497.478	0.29844	765	0.900	688	570	53,775	57,246	716.0	1557.7	841.7		27,331,682	321,553,979	278.522		

EQUATIONS:

$$\frac{\bar{p}_n}{\bar{z}} = \frac{\bar{p}_i}{\bar{z}_i}\left[\frac{G - G_p}{G - \left(\frac{W_e}{B_{gi}}\right)}\right]$$; GAS RESERVOIR MATERIAL BALANCE EQUATION WITH WATER INFLUX.

$$q_g = C_g(p_{ts}^2 - p_{tf}^2)^n$$; TOTAL FIELD WELLHEAD BACK PRESSURE CURVE EQUATION.

$$p_{ts} = \bar{p}_n / \sqrt{e^x} \quad \text{WHERE } x = 0.0375\,\gamma_g\,D / \bar{T}\,\bar{Z}$$

$$\Delta W_e = \frac{W_{ei}}{\bar{p}_i}(\bar{p}_{n-1} - \bar{p}_{wf})\left\{1 - e^{-\left[\frac{(q_{wc})_{max}}{W_{ei}}\right]\Delta t_n}\right\}$$; EQUATION 6 IN PAPER.

$$\bar{p} = \left(\frac{p_i}{W_{ei}}\right) * p_i$$; EQUATION 2 IN PAPER.

NOTES.

*THE PRIMED QUANTITY IS OBTAINED FROM THE PREVIOUS TRAIL WITHIN A TIME INTERVAL.

** GAS DEVIATION FACTORS OBTAINED FROM REFERENCE 30.

*** A PLOT OF $\bar{p}_n$ VS $\sqrt{e^x}$ FOR A GIVEN RESERVOIR IS USED FOR THIS CALCULATION.

ALL BASIC DATA FOR THIS PROBLEM APPEAR IN TABLES 1 AND 2.

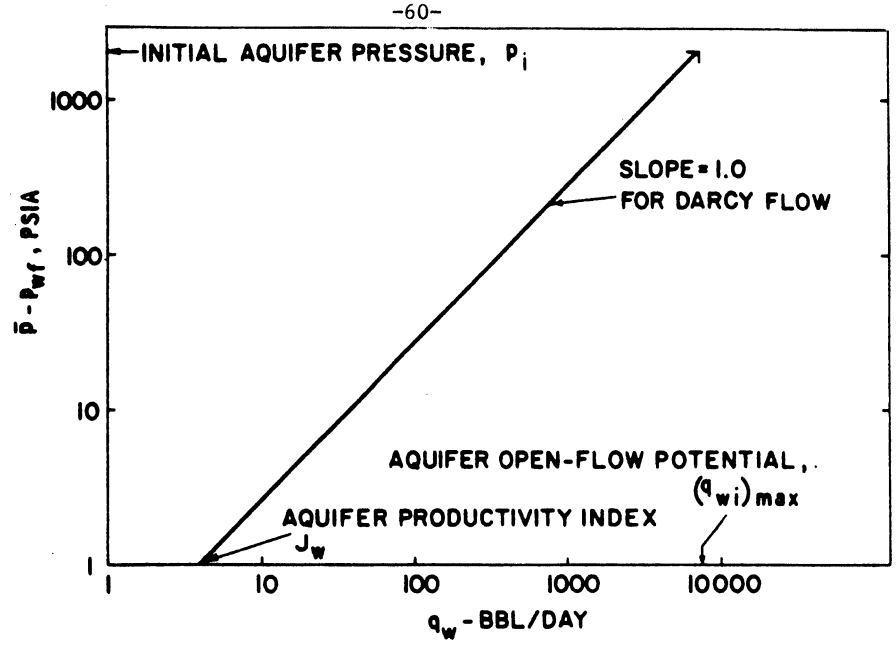

Fig. 1—Aquifer "backpressure curve" with open-flow potential, log-log plot.

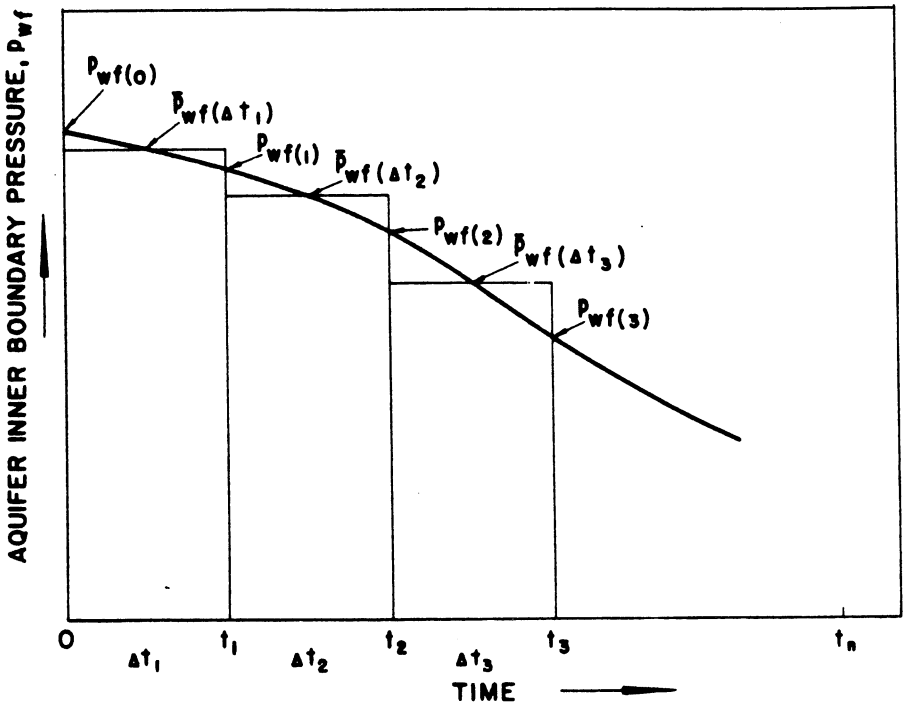

Fig. 2—Pressure-time relationship at aquifer inner boundary as a step-function approximation.

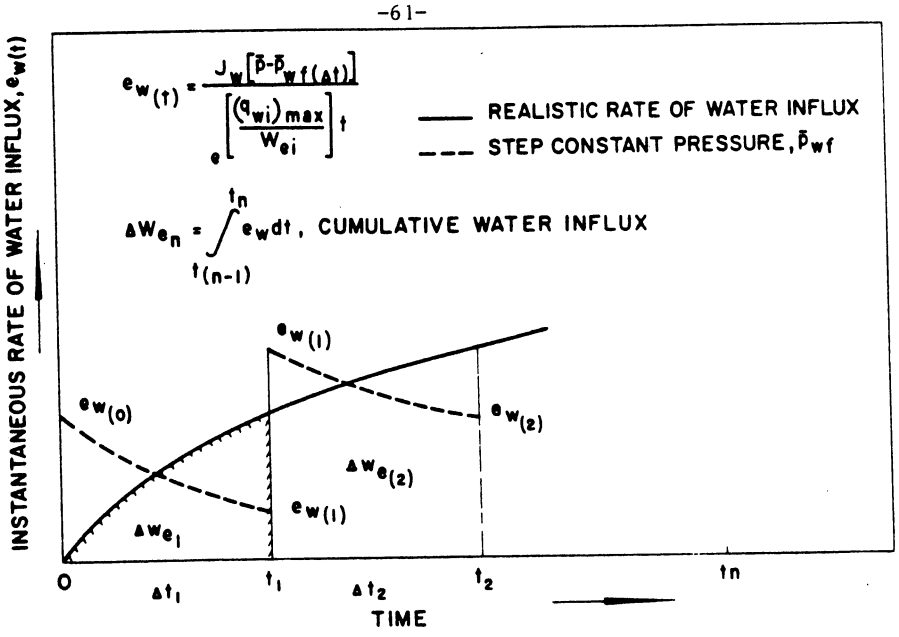

Fig. 3—Calculated rate of water influx using a step-constant pressure at the aquifer inner boundary compared with a realistic representation.

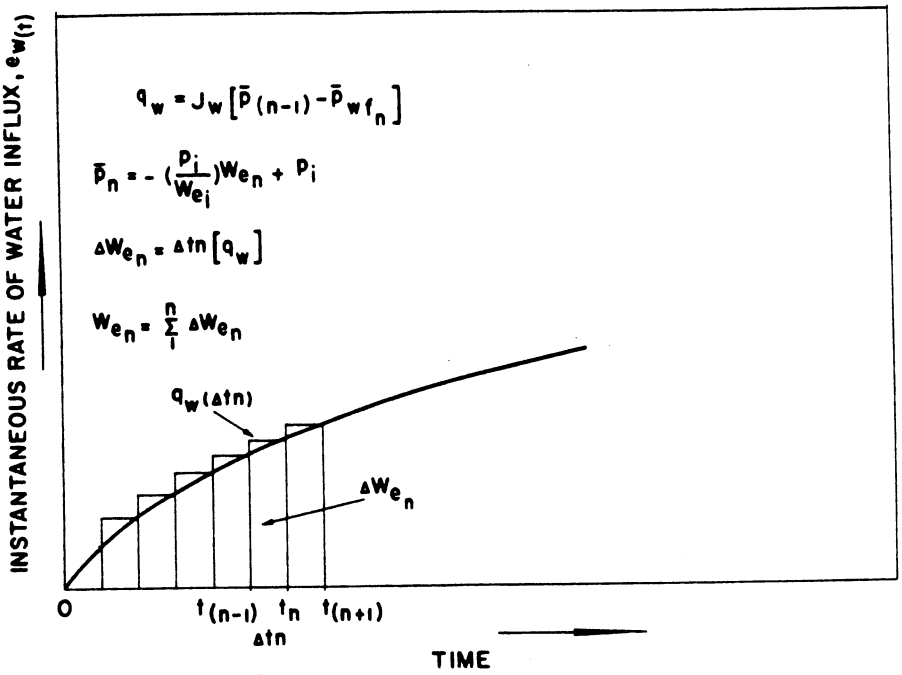

Fig. 4—A constant rate step-function approximation to water influx over short time intervals.

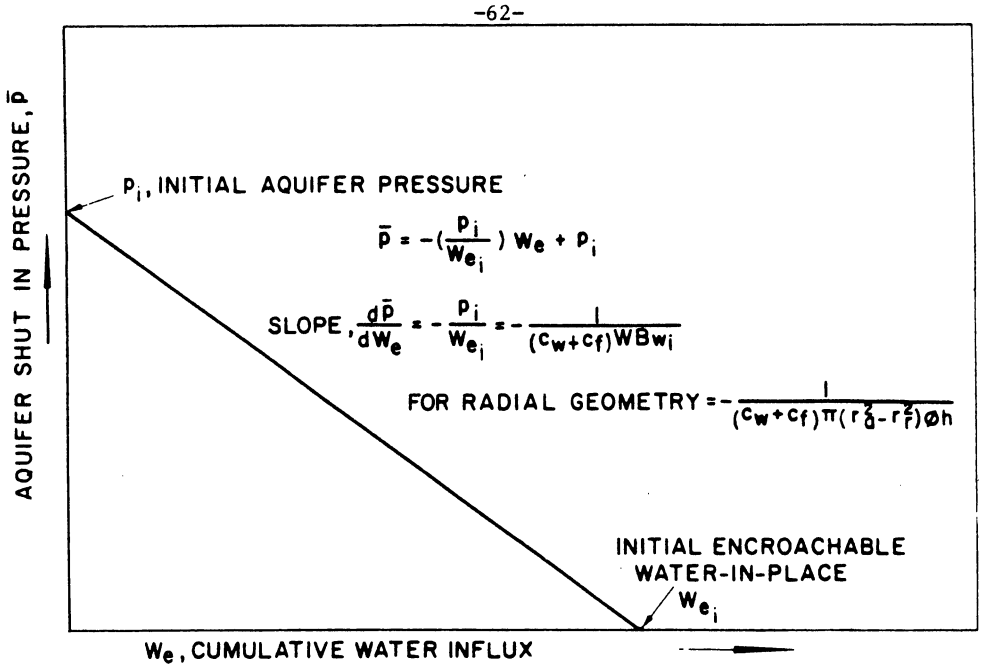

Fig. 5—Graphical representation of the aquifer material balance equation.

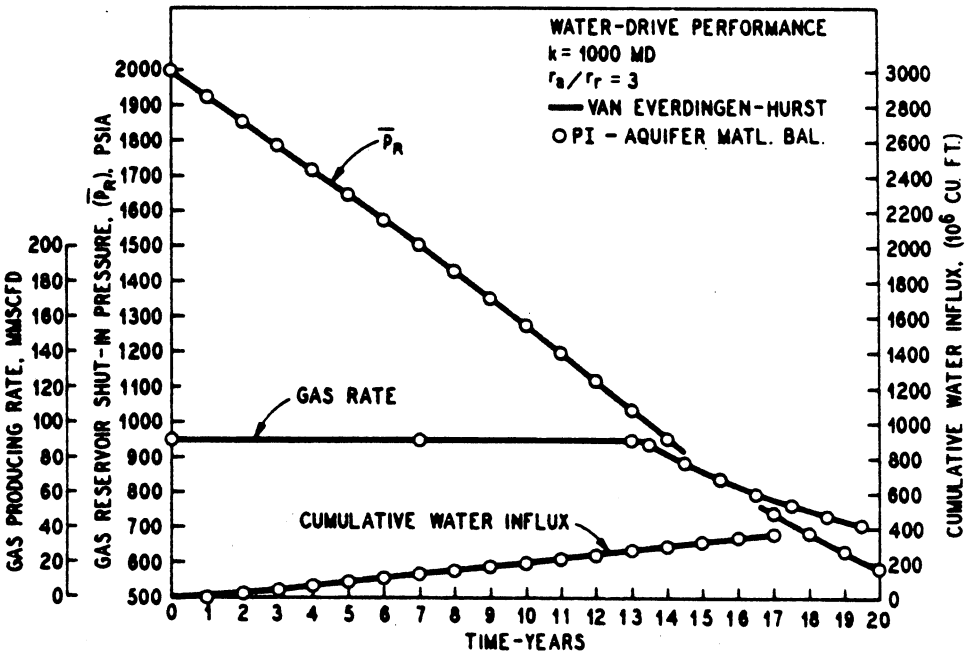

Fig. 6

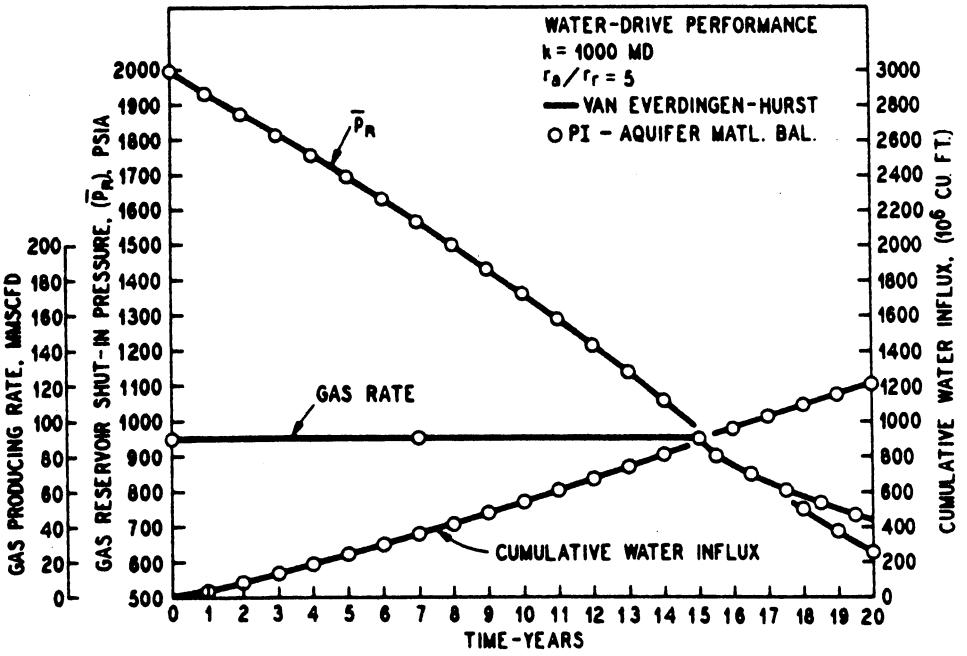
WATER-DRIVE PERFORMANCE
k = 1000 MD
r_a/r_r = 5
VAN EVERDINGEN-HURST
PI - AQUIFER MATL. BAL.
$\bar{P}_R$
GAS RATE
CUMULATIVE WATER INFLUX
GAS PRODUCING RATE, MMSCFD
GAS RESERVOIR SHUT-IN PRESSURE, $(\bar{P}_R)$, PSIA
CUMULATIVE WATER INFLUX, (10^6 CU. FT.)
TIME-YEARS

Fig. 7

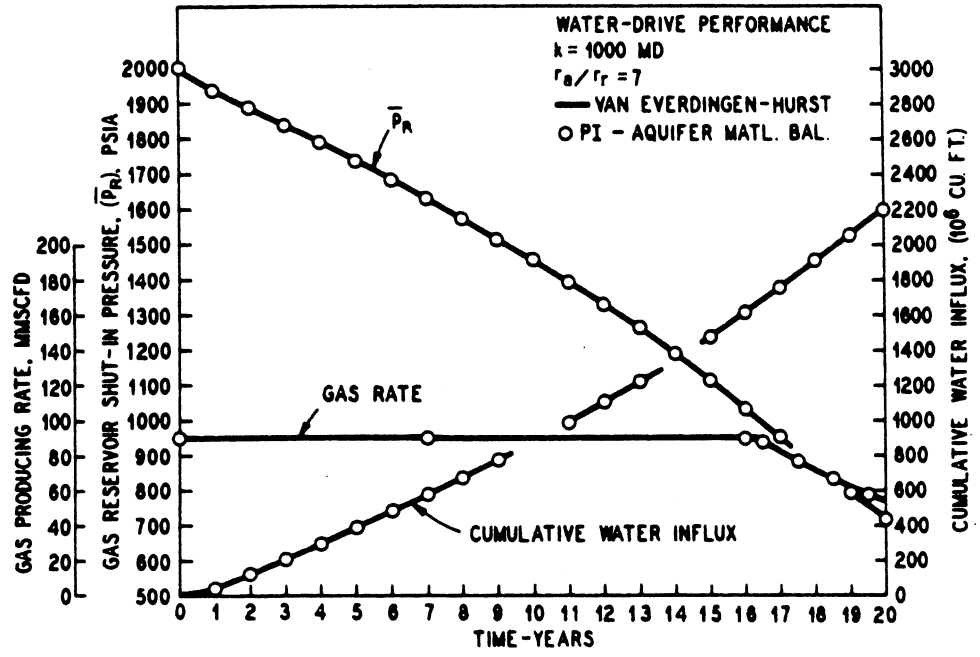
WATER-DRIVE PERFORMANCE
k = 1000 MD
r_a/r_r = 7
VAN EVERDINGEN-HURST
PI - AQUIFER MATL. BAL.
$\bar{P}_R$
GAS RATE
CUMULATIVE WATER INFLUX
GAS PRODUCING RATE, MMSCFD
GAS RESERVOIR SHUT-IN PRESSURE, $(\bar{P}_R)$, PSIA
CUMULATIVE WATER INFLUX, (10^6 CU. FT.)
TIME-YEARS

Fig. 8

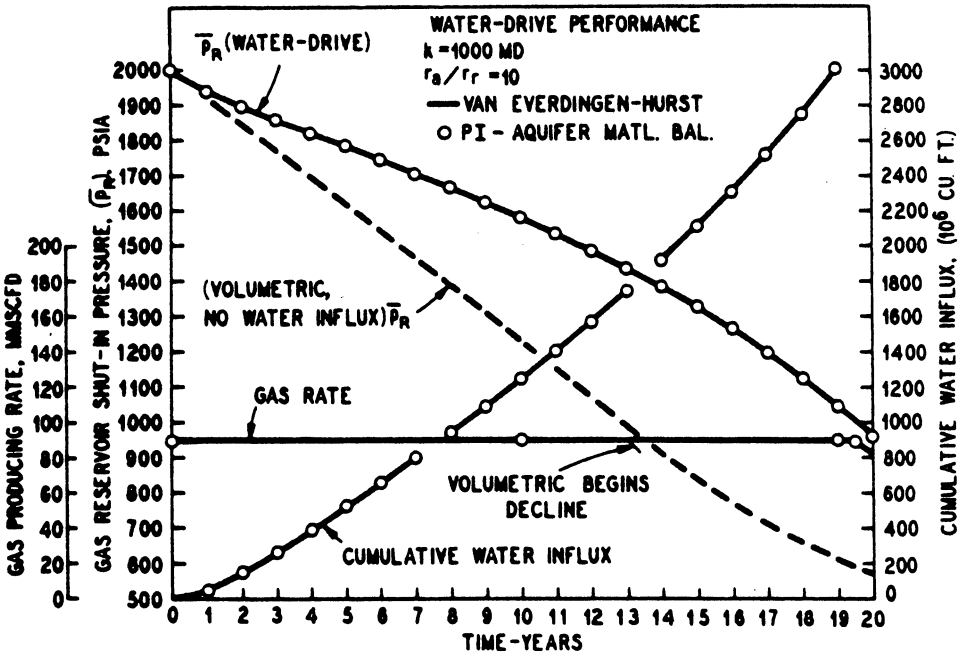
WATER-DRIVE PERFORMANCE
$\bar{p}_R$ (WATER-DRIVE)
k = 1000 MD
r_a/r_r = 10
VAN EVERDINGEN-HURST
PI - AQUIFER MATL. BAL.
(VOLUMETRIC, NO WATER INFLUX) $\bar{p}_R$
GAS RATE
VOLUMETRIC BEGINS DECLINE
CUMULATIVE WATER INFLUX
GAS PRODUCING RATE, MMSCFD
GAS RESERVOIR SHUT-IN PRESSURE, $(\bar{p}_R)$, PSIA
CUMULATIVE WATER INFLUX, (10^6 CU. FT.)
TIME-YEARS

Fig. 9

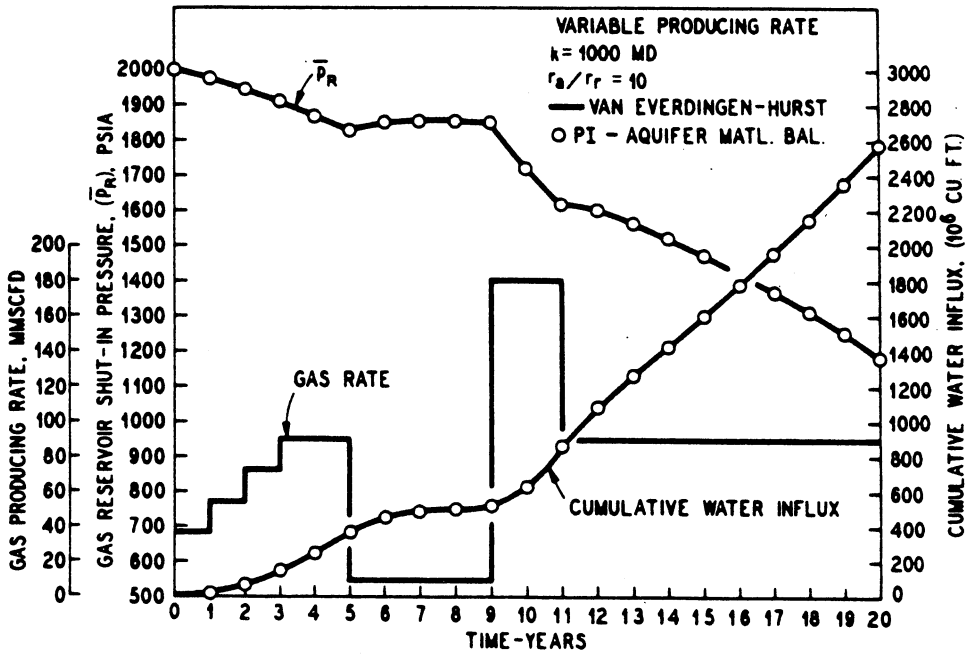
VARIABLE PRODUCING RATE
k = 1000 MD
r_a/r_r = 10
VAN EVERDINGEN-HURST
PI - AQUIFER MATL. BAL.
$\bar{p}_R$
GAS RATE
CUMULATIVE WATER INFLUX
GAS PRODUCING RATE, MMSCFD
GAS RESERVOIR SHUT-IN PRESSURE, $(\bar{p}_R)$, PSIA
CUMULATIVE WATER INFLUX, (10^6 CU FT.)
TIME-YEARS

Fig. 10

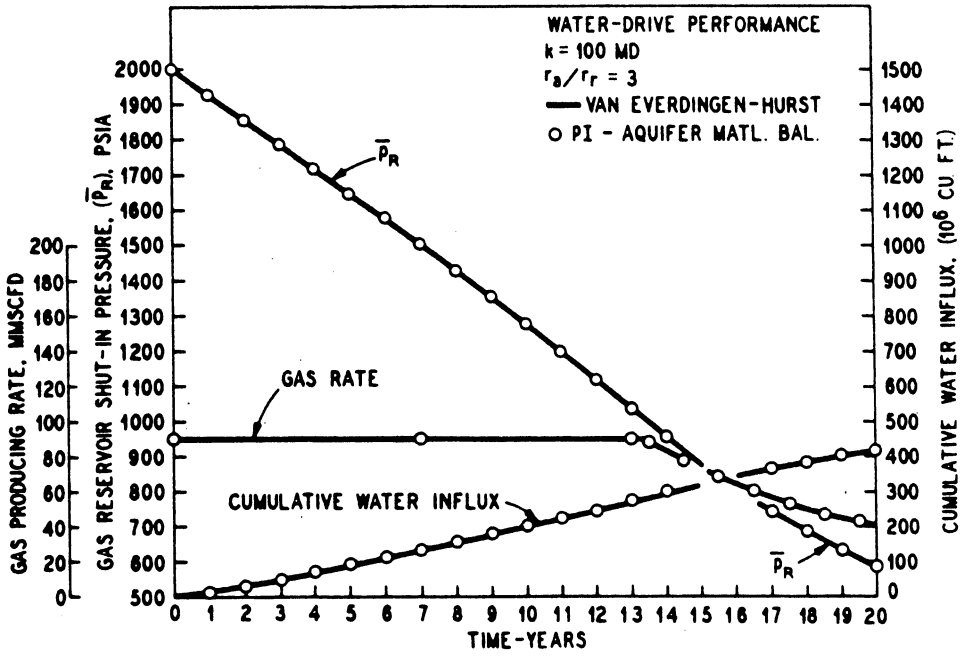
WATER-DRIVE PERFORMANCE
k = 100 MD
r_a/r_r = 3
VAN EVERDINGEN-HURST
PI - AQUIFER MATL. BAL.
$\bar{p}_R$
GAS RATE
CUMULATIVE WATER INFLUX
GAS PRODUCING RATE, MMSCFD
GAS RESERVOIR SHUT-IN PRESSURE, $(\bar{p}_R)$, PSIA
CUMULATIVE WATER INFLUX, (10^6 CU FT.)
TIME-YEARS

Fig. 11

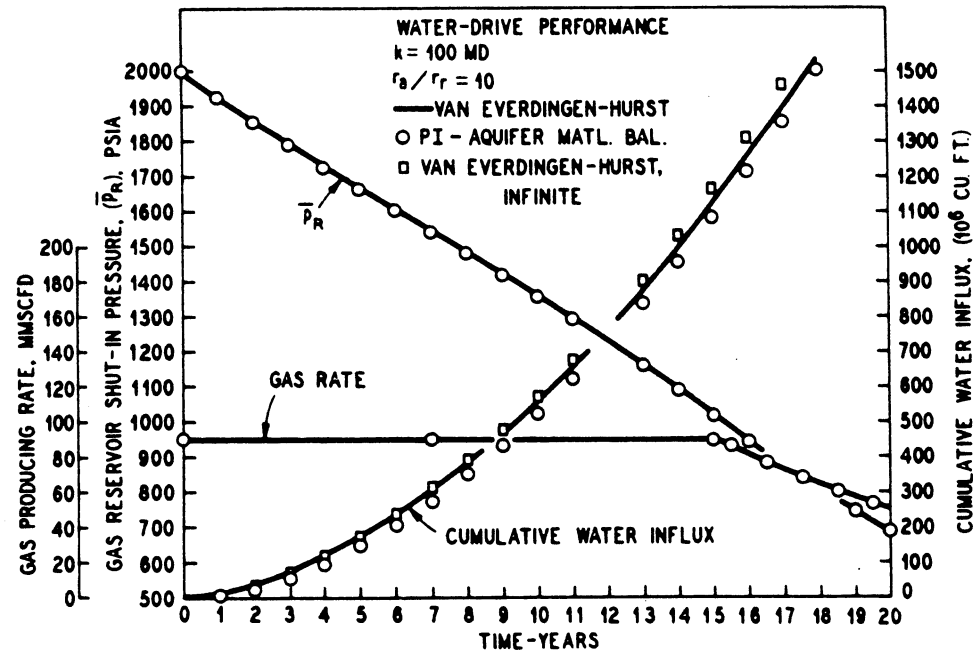
WATER-DRIVE PERFORMANCE
k = 100 MD
r_a/r_r = 10
VAN EVERDINGEN-HURST
PI - AQUIFER MATL. BAL.
VAN EVERDINGEN-HURST, INFINITE
$\bar{p}_R$
GAS RATE
CUMULATIVE WATER INFLUX
GAS PRODUCING RATE, MMSCFD
GAS RESERVOIR SHUT-IN PRESSURE, $(\bar{p}_R)$, PSIA
CUMULATIVE WATER INFLUX, (10^6 CU FT.)
TIME-YEARS

Fig. 12

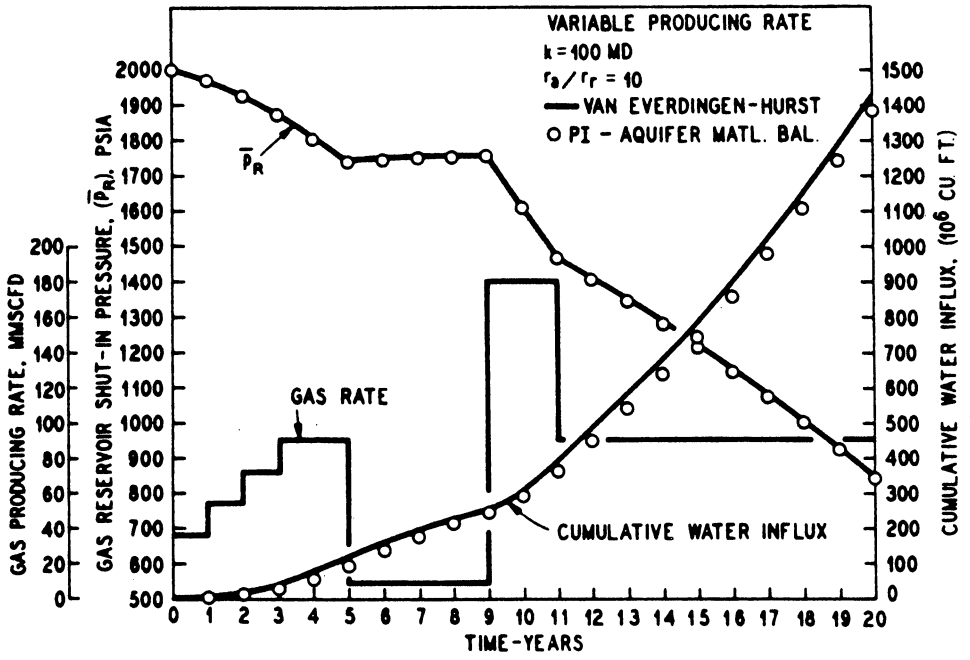
VARIABLE PRODUCING RATE
k = 100 MD
r_a/r_r = 10
VAN EVERDINGEN-HURST
O PI - AQUIFER MATL. BAL.
$\bar{p}_R$
GAS RATE
CUMULATIVE WATER INFLUX
GAS PRODUCING RATE, MMSCFD
GAS RESERVOIR SHUT-IN PRESSURE, $(\bar{p}_R)$, PSIA
CUMULATIVE WATER INFLUX, (10^6 CU. FT.)
TIME-YEARS

Fig. 13

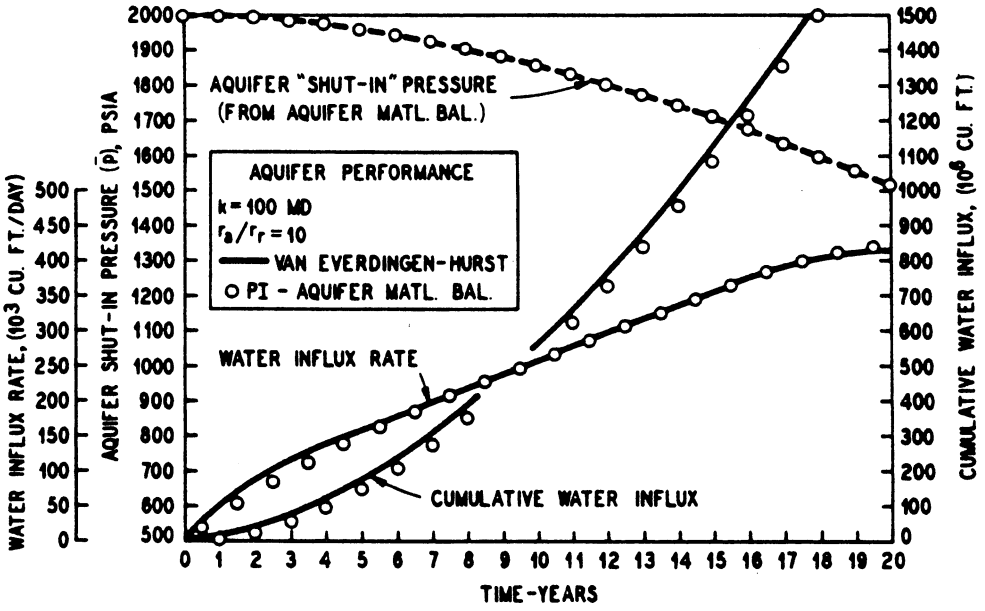
AQUIFER "SHUT-IN" PRESSURE
(FROM AQUIFER MATL. BAL.)
AQUIFER PERFORMANCE
k = 100 MD
r_a/r_r = 10
VAN EVERDINGEN-HURST
O PI - AQUIFER MATL. BAL.
WATER INFLUX RATE
CUMULATIVE WATER INFLUX
WATER INFLUX RATE, (10^3 CU. FT./DAY)
AQUIFER SHUT-IN PRESSURE $(\bar{p})$, PSIA
CUMULATIVE WATER INFLUX, (10^6 CU. FT.)
TIME-YEARS

Fig. 14

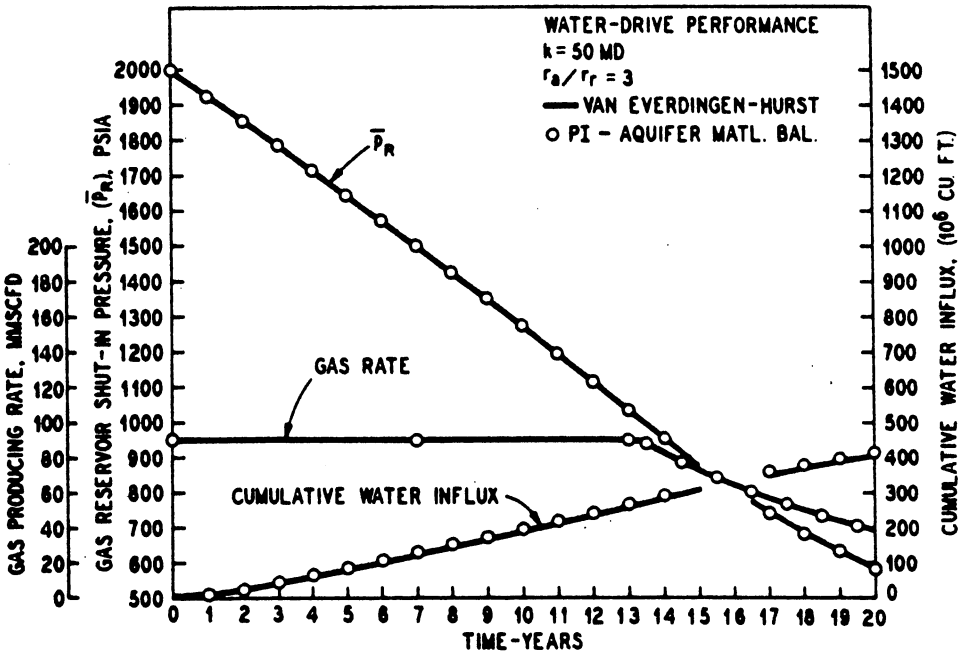
WATER-DRIVE PERFORMANCE
k = 50 MD
r_a/r_r = 3
VAN EVERDINGEN-HURST
PI - AQUIFER MATL. BAL.
$\bar{p}_R$
GAS RATE
CUMULATIVE WATER INFLUX
GAS PRODUCING RATE, MMSCFD
GAS RESERVOIR SHUT-IN PRESSURE, $(\bar{p}_R)$, PSIA
CUMULATIVE WATER INFLUX, (10^6 CU. FT.)
TIME-YEARS

Fig. 15

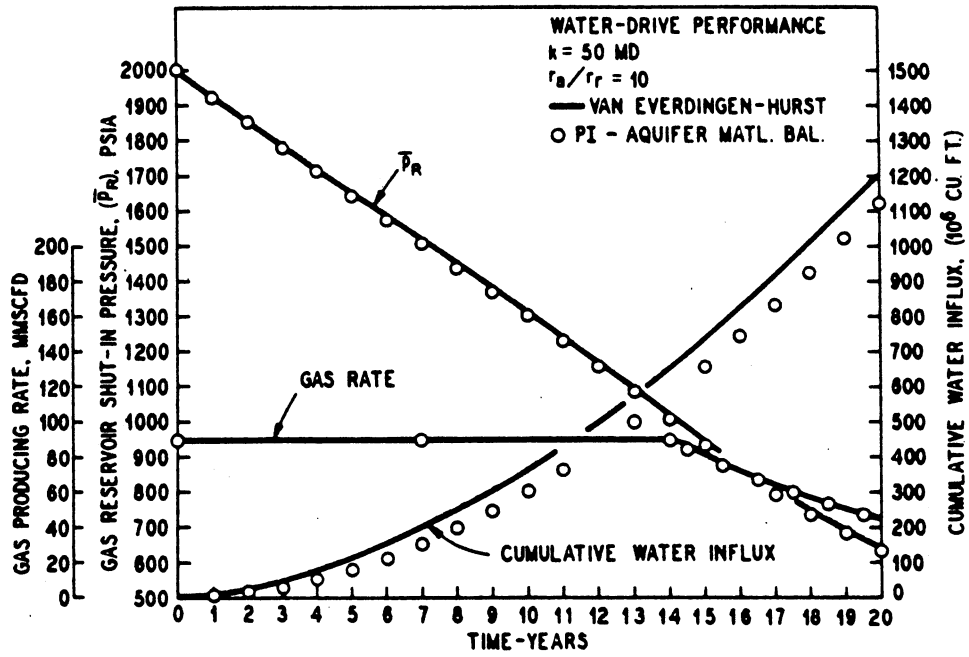
WATER-DRIVE PERFORMANCE
k = 50 MD
r_a/r_r = 10
VAN EVERDINGEN-HURST
PI - AQUIFER MATL. BAL.
$\bar{p}_R$
GAS RATE
CUMULATIVE WATER INFLUX
GAS PRODUCING RATE, MMSCFD
GAS RESERVOIR SHUT-IN PRESSURE, $(\bar{p}_R)$, PSIA
CUMULATIVE WATER INFLUX, (10^6 CU. FT.)
TIME-YEARS

Fig. 16

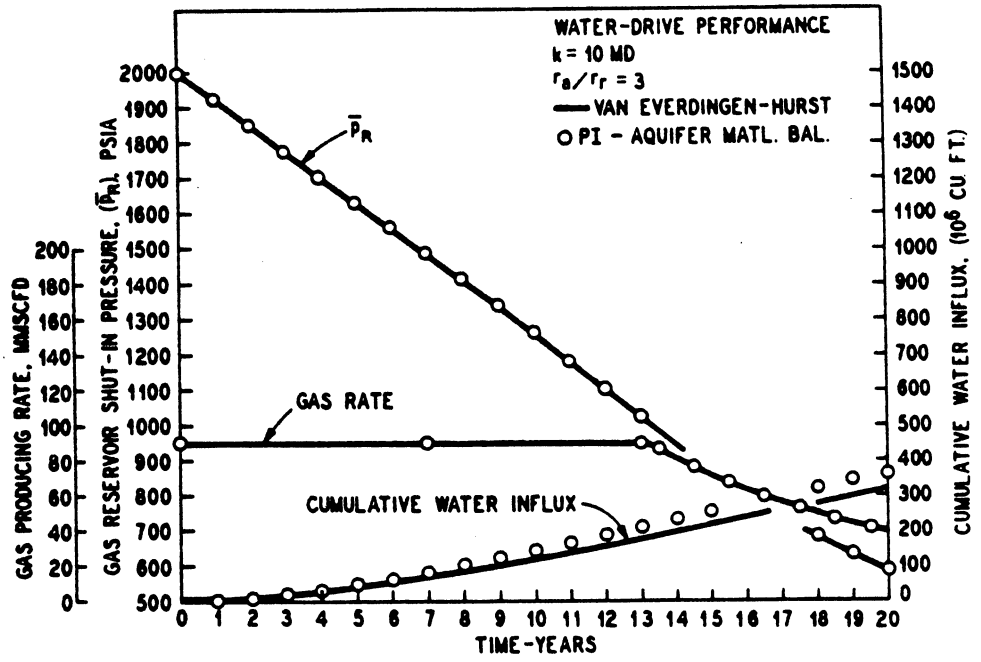
WATER-DRIVE PERFORMANCE
k = 10 MD
r_a/r_r = 3
VAN EVERDINGEN-HURST
PI - AQUIFER MATL. BAL.
$\bar{P}_R$
GAS RATE
CUMULATIVE WATER INFLUX
GAS PRODUCING RATE, MMSCFD
GAS RESERVOIR SHUT-IN PRESSURE, ($\bar{P}_R$), PSIA
CUMULATIVE WATER INFLUX, (10^6 CU FT.)
TIME-YEARS

Fig. 17

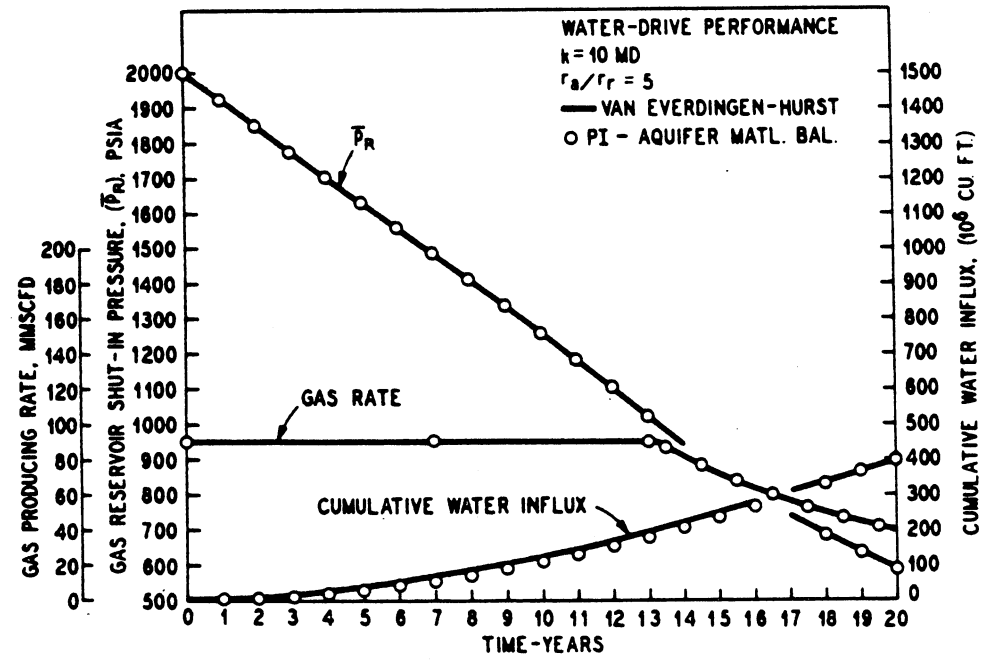
WATER-DRIVE PERFORMANCE
k = 10 MD
r_a/r_r = 5
VAN EVERDINGEN-HURST
PI - AQUIFER MATL. BAL.
$\bar{P}_R$
GAS RATE
CUMULATIVE WATER INFLUX
GAS PRODUCING RATE, MMSCFD
GAS RESERVOIR SHUT-IN PRESSURE, ($\bar{P}_R$), PSIA
CUMULATIVE WATER INFLUX, (10^6 CU FT.)
TIME-YEARS

Fig. 18

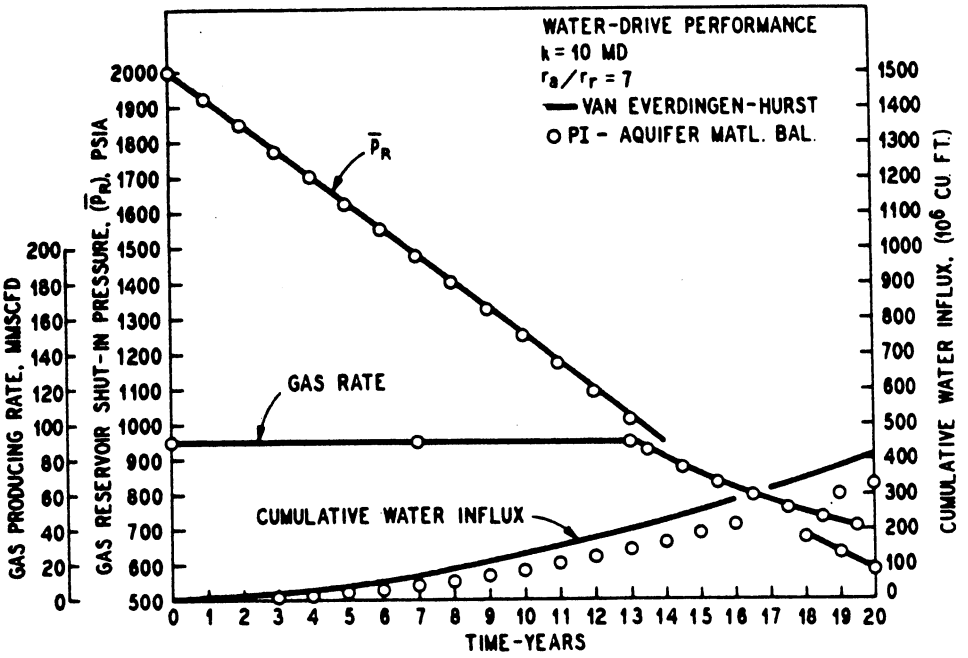
WATER-DRIVE PERFORMANCE
k = 10 MD
r_a/r_r = 7
VAN EVERDINGEN-HURST
PI - AQUIFER MATL. BAL.
$\bar{P}_R$
GAS RATE
CUMULATIVE WATER INFLUX
GAS PRODUCING RATE, MMSCFD
GAS RESERVOIR SHUT-IN PRESSURE, ($\bar{P}_R$), PSIA
CUMULATIVE WATER INFLUX, (10^6 CU. FT.)
TIME-YEARS

Fig. 19

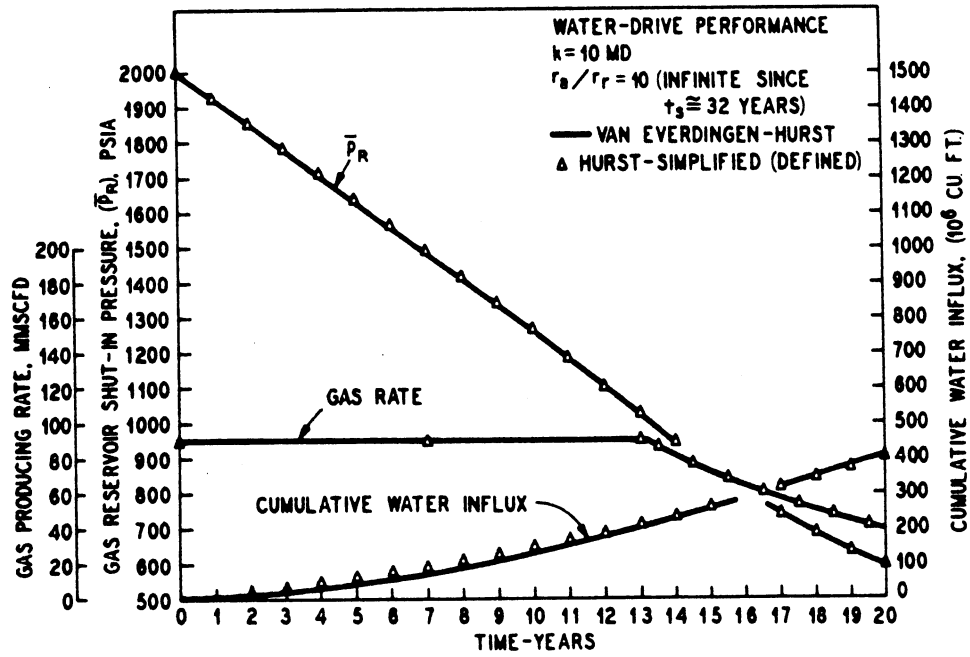
WATER-DRIVE PERFORMANCE
k = 10 MD
r_a/r_r = 10 (INFINITE SINCE
$t_s \cong$ 32 YEARS)
VAN EVERDINGEN-HURST
HURST-SIMPLIFIED (DEFINED)
$\bar{P}_R$
GAS RATE
CUMULATIVE WATER INFLUX
GAS PRODUCING RATE, MMSCFD
GAS RESERVOIR SHUT-IN PRESSURE, ($\bar{P}_R$), PSIA
CUMULATIVE WATER INFLUX, (10^6 CU. FT.)
TIME-YEARS

Fig. 20

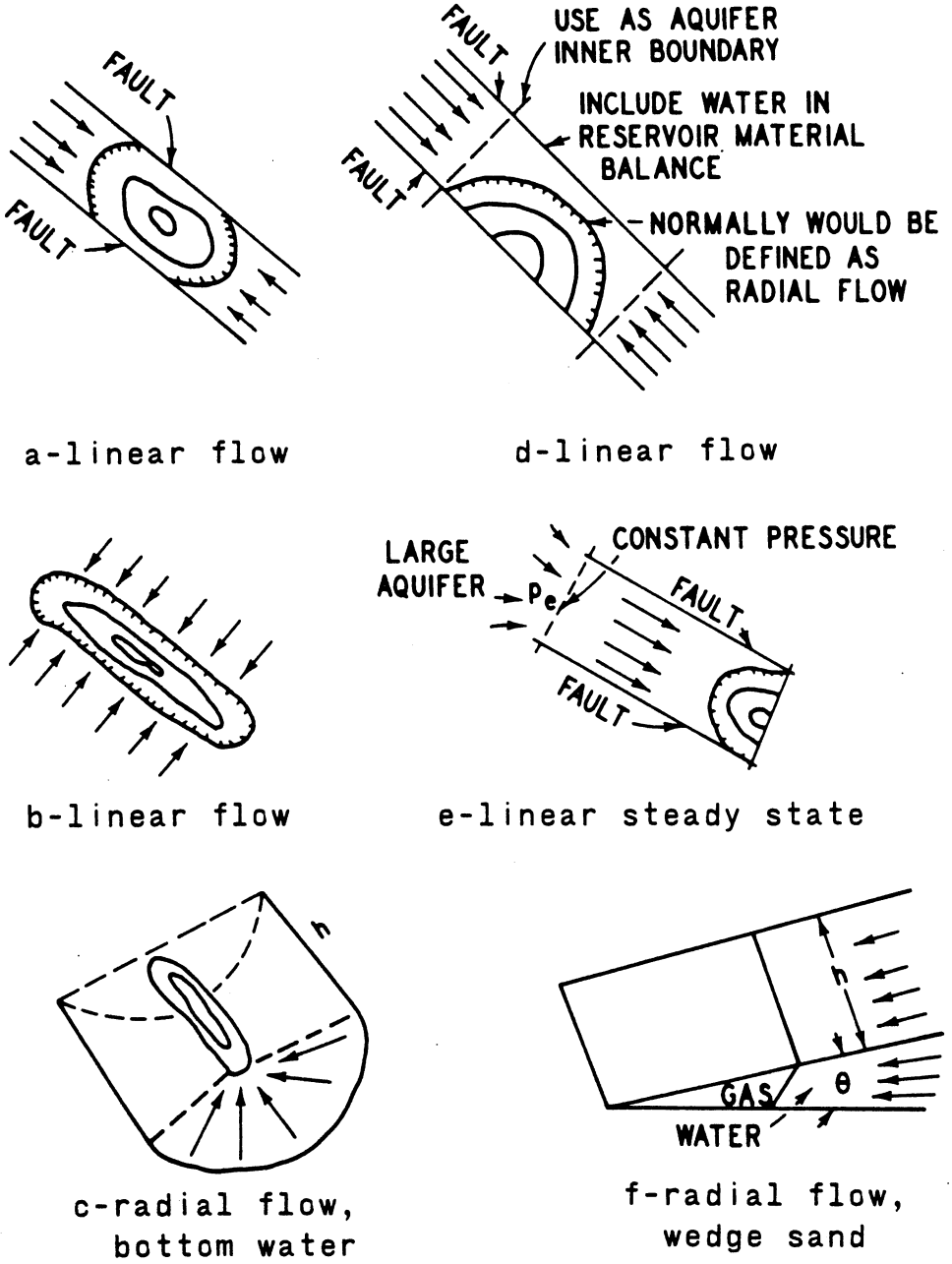

Fig. 21—Types of flow systems for rate equation.

CONVERSION OF van EVERDINGEN-HURST B AND t_D TO VALUES OF PI_w AND We_i FOR USE IN THE SIMPLIFIED APPROACH TO WATER INFLUX CALCULATIONS

by

M. J. Fetkovich

CONVERSION OF van EVERDINGEN-HURST B AND t_D TO VALUES OF PI_w AND W_{ei} FOR USE IN THE SIMPLIFIED APPROACH TO WATER INFLUX CALCULATIONS

The van Everdingen-Hurst influx constant B is defined by the following equation: (For convenience, cgs units are used so as to avoid confusion with regard to conversion constants.)

$$B = 2\,\pi\phi\, c_t\, h\, r_r^2 \left(\frac{\theta}{360}\right) \quad \ldots\ldots\ldots\ldots \quad (1)$$

In the Simplified Approach, the initial encroachable water-in-place is defined by the equation:

$$W_{ei} = \pi\phi\ \ c_t\, h\, (r_a^2 - r_r^2)\, p_i \left(\frac{\theta}{360}\right) \quad \ldots\ldots\ldots \quad (2)$$

We can define W_{ei} in terms of B by the following equation (a simple substitution of equation (1) into (3) will reduce it to equation (2)):

$$W_{ei} = B\,\frac{1}{2}\left[\left(\frac{r_a}{r_r}\right)^2 - 1\right] p_i \quad \ldots\ldots\ldots\ldots \quad (3)$$

Note that:

$$\frac{r_a^2 - r_r^2}{r_r^2} = \left(\frac{r_a}{r_r}\right)^2 - 1$$

The Simplified Approach to Water Influx Calculations makes use of term $\left(\frac{Q_{wi}}{W_{ei}}\right)\cdot t$ which is defined in paper SPE 2603. Note that this term resembles the dimensionless time term used in the van Everdingen-Hurst solutions.

Let us take the ratio $\frac{Q_{wi}}{W_{ei}}$ and define it in the basic variables for radial flow.

$$\frac{Q_{wi}}{W_{ei}} = \frac{PI_w\,(p_i)\left(\frac{\theta}{360}\right)}{\pi\phi\, c_t\, h\, (r_a^2 - r_r^2)\, p_i \left(\frac{\theta}{360}\right)}$$

$$\frac{Q_{wi}}{W_{ei}} = \frac{\dfrac{2\pi kh\,(p_i)}{\mu\left[\ln\left(\dfrac{r_a}{r_r}\right) - \dfrac{3}{4}\right]} \cdot \left(\dfrac{\theta}{360}\right)}{\pi\phi\, c_t\, h\,(r_a^2 - r_r^2)\, p_i \left(\dfrac{\theta}{360}\right)} \quad \ldots\ldots\ldots\ldots (4)$$

Simplifying and multiplying the denominator by $\left(\dfrac{r_r}{r_r}\right)^2$ we obtain

$$\frac{Q_{wi}}{W_{ei}} = \frac{2k}{\phi\mu\, c_t\,(r_a^2 - r_r^2)\left(\dfrac{r_r}{r_r}\right)^2} \cdot \frac{1}{\left[\ln\left(\dfrac{r_a}{r_r}\right) - \dfrac{3}{4}\right]}$$

$$\frac{Q_{wi}}{W_{ei}} = \frac{k}{\phi\mu\, c_t\, r_r^2} \cdot \frac{1}{\frac{1}{2}\left[\left(\dfrac{r_a}{r_r}\right)^2 - 1\right]\left[\ln\left(\dfrac{r_a}{r_r}\right) - \dfrac{3}{4}\right]} \quad \ldots\ldots (5)$$

Now $$\frac{t_D}{t} = \frac{k}{\phi\mu\, c_t\, r_r^2} \quad \ldots\ldots\ldots\ldots\ldots\ldots (6)$$

Therefore substituting (6) into (5) we have:

$$\frac{Q_{wi}}{W_{ei}} = \left(\frac{t_D}{t}\right)\left[\frac{1}{\frac{1}{2}\left[\left(\dfrac{r_a}{r_r}\right)^2 - 1\right]\left[\ln\left(\dfrac{r_a}{r_r}\right) - \dfrac{3}{4}\right]}\right] \quad \ldots\ldots (7)$$

or in terms of $\dfrac{t_D}{t}$:

$$\frac{t_D}{t} = \frac{Q_{wi}}{W_{ei}} \cdot \frac{1}{2}\left[\left(\frac{r_a}{r_r}\right)^2 - 1\right]\left[\ln\left(\frac{r_a}{r_r}\right) - \frac{3}{4}\right] \quad \ldots\ldots (8)$$

Using the equation:

$$Q_{wi} = PI_w\ (p_i) \quad \ldots\ldots\ldots\ldots\ldots \quad (9)$$

and substituting into equation (7) and rearranging we obtain:

$$PI_w = \frac{t_D}{t} \cdot \frac{W_{ei}}{p_i} \left[\frac{1}{\frac{1}{2}\left[\left(\frac{r_a}{r_r}\right)^2 - 1\right]\left[\ln\left(\frac{r_a}{r_r}\right) - \frac{3}{4}\right]} \right] \quad \ldots \quad (10)$$

The units on PI_w will depend on the units used for W_{ei}, t_D/t, and p_i. For example, if W_{ei} is in bbls, t_D/t in yrs^{-1}, and p_i in psi, PI_w will have units of bbl/yr/psi. Alternately we can express PI_w in terms of t_D/t and B by substituting equation (3) into equation (10) and simplifying:

$$PI_w = \frac{B \times \left(\frac{t_D}{t}\right)}{\left[\ln\left(\frac{r_a}{r_r}\right) - \frac{3}{4}\right]} \quad \ldots\ldots\ldots \quad (11)$$

It should be pointed out that this conversion is rigorous when the t_D/t and B for the van Everdingen-Hurst solutions are primarily those lying on the pseudo-steady state solution. In the majority of the cases, this will be so. This can be verified by a simple check of where the t_D/t at early times of 1 to 3 years lies for the given r_a/r_r ratio on the Q_{t_D} vs t_D curves. (See Craft and Hawkins, pages 213-216.)

Williams No. 2
15600 NAG Zone, Mystic Bayou Field
St. Martin Pa. La.

Type Bound.	Minimum Std Dev	Dimensionless Time Ratio t_D/t-(yrs^{-1})	Final Water Encroachment Factor B - (ft^3/psi)	Cum Water Encroached Based on Final Encrmt. Factor (ft^3)	Gas in Place Real (Using All Points) (BCF)
Volumetric	-	-	-	- 0 -	43.5
Schilt.	$.82188 \times 10^9$	-	-	$.10703 \times 10^7$	43.9
Hurst Simp	$.80251 \times 10^9$	-	-	$.14842 \times 10^7$	43.5
r_a/r_r					
1.5	$.67281 \times 10^9$	.10936	786.49	$.31871 \times 10^7$	41.7
3.0	$.67308 \times 10^9$	2.6367	123.75	$.32391 \times 10^7$	41.6
5.0	$.67325 \times 10^9$	16.238	41.473	$.32994 \times 10^7$	41.4
7.0	$.67262 \times 10^9$	41.823	20.610	$.32776 \times 10^7$	41.4
10.0	$.66794 \times 10^9$	100.000	9.8412	$.32006 \times 10^7$	41.6
∞ Radial	$.76157 \times 10^9$	.0065395	1670.7	$.22491 \times 10^7$	42.8

$$W_{ei} = B\,\frac{1}{2}\left[\left(\frac{r_a}{r_r}\right)^2 - 1\right] p_i \quad \text{and } p_i = 12887 \text{ psi}; \quad \frac{p_i}{2} = 6443.5 \text{ psi}$$

$\frac{r_a}{r_r}$	$\left[\left(\frac{r_a}{r_r}\right)^2 - 1\right]$	$\frac{p_i}{2}\left[\left(\frac{r_a}{r_r}\right)^2 - 1\right]$	B $\left(\frac{ft^3}{psi}\right)$	W_{ei} (ft^3)	W_{ei} (bbl)
1.5	1.25	8054.4	786.49	6334705	1128175
3.0	8	51548	123.75	6379065	1136076
5.0	24	154644	41.473	6413551	1142217
7.0	48	309288	20.610	6374426	1135250
10.0	99	637906	9.8412	6277761	1118034

$$PI = k(t)\,\frac{W_{ei}}{p_i}\,\frac{1}{\frac{1}{2}\left[\left(\frac{r_a}{r_r}\right)^2 - 1\right]\left[\ln\left(\frac{r_a}{r_r}\right) - \frac{3}{4}\right]}$$

$\frac{r_a}{r_r}$	"A" $\frac{1}{2}\left[\left(\frac{r_a}{r_r}\right)^2 - 1\right]$	$\frac{W_e}{p_i} = B\,\frac{1}{2}\left[\left(\frac{r_a}{r_r}\right)^2 - 1\right]$	"C" $\left[\ln\left(\frac{r_a}{r_r}\right) - \frac{3}{4}\right]$	A x C	$\frac{1}{A \times C}$	$\frac{W_{ei}}{p_i}\,\frac{1}{A \times C}$
1.5	.625	498.49		-	-	-
3.0	4	495.00	.3487	1.3944	.71715	354.99
5.0	12	497.68	.8594	10.3128	.0969669	48.258
7.0	24	494.64	1.1959	28.7016	.0348413	17.234
10.0	49.5	487.14	1.5526	76.8537	.0130117	6.3385

$\frac{r_a}{r_r}$	k(t) (t_D/t, yr^{-1})	$PI = k(t)\left[\frac{W_{ei}}{p_i}\left(\frac{1}{A \times C}\right)\right]$ ($ft^3/yr/psi$)	PI bbl/day/psi
3	2.6367	936.00	.4567
5	16.238	783.61	.38324
7	41.823	720.78	.35169
10	100.00	633.85	.30927

THE ISOCHRONAL TESTING OF OIL WELLS

by

M. J. Fetkovich
Member AIME, Phillips Petroleum Co.

SPE 4529

This paper was prepared for the 48th Annual Fall Meeting of the Society of Petroleum Engineers of AIME, to be held in Las Vegas, Nev., Sept. 30 - Oct. 3, 1973.

THE ISOCHRONAL TESTING OF OIL WELLS

Abstract

This paper presents the results and methods of analyzing isochronal and flow after flow multipoint back-pressure tests conducted on oil wells. Tests were conducted in reservoirs with permeabilities ranging from 6 md to > 1000 md. Reservoirs in which oil well multipoint back-pressure tests were obtained ranged from highly undersaturated, to saturated at initial reservoir pressure, to a partially depleted field with a gas saturation existing above the critical. Each of these three reservoir fluid states can result in different interpretation methods. Back-pressure tests were run to pseudo-steady state in the field where the saturation was above the critical gas saturation.

In all cases, oil well back-pressure curves were found to follow the same general form as that used to express the rate-pressure relationship of a gas well:

$$q_o = J'_o \, (\bar{p}_R^2 - p_{wf}^2)^n$$

From some 40 oil well back-pressure tests examined, the exponent n was found to lie between 0.568 and 1.000, very near the limits commonly accepted for gas well back-pressure curves. Flow point alignment to establish an oil well back-pressure curve on the customary log q_o vs. log $\Delta(p^2)$ plot is considered to be as good as that obtained on gas well back-pressure tests.

This paper demonstrates that gas wells and oil wells behave very similarly and should be tested and analyzed using the same basic flow equations.

Introduction

Multipoint back-pressure testing of gas wells is an accepted procedure for establishing a gas well's performance curve. Flow after flow[1] and isochronal[2] testing are the two basic methods commonly used. In high permeability reservoirs, either method can be employed. In low permeability reservoirs, the Isochronal method of testing eliminates the transient effects that can severely distort the results obtained from a flow after flow test. Methods for analyzing and calculating gas well performance curves have been the subject of numerous investigations. The bulk of these investigations have examined non-Darcy flow behavior, the primary reason that multipoint tests are conducted.

Multipoint testing of oil wells is not now a current practice. As early as 1930, however, T. V. Moore[3] reported the results of an oil well multipoint test conducted on the Humble Smith A-2 in the Yates Field. The purpose of the

back-pressure test was to demonstrate a method of establishing a well's open flow potential without producing the well wide open.

The need for establishing an accurate performance curve for an oil well is as important as determining one for a gas well. In the search for new oil, the industry is turning to remote areas such as the Arctic and offshore. Critical questions of whether to develop, and if so, how to develop a field hinge on the ability to accurately predict a well's deliverability. Often, because of equipment limitations, the rates of production obtained during drillstem testing are much less than those planned for full development.

The traditional method for predicting production rates and drawdowns for oil wells has been based on the concept of the productivity index (PI), which has been used in the industry for many years. The usual form of the equation

$$q_o = J_o (p_e - p_{wf}) \qquad ..(1)$$

is valid only for systems producing an ideal homogeneous liquid obeying Darcy's law. This condition normally holds for oil wells when the oil is undersaturated throughout the producing formation. It has long been recognized that in reservoirs existing at or below the bubble-point pressure, producing wells do not follow this simple equation. Actual field tests indicate that oil flow rates obtained at increasing drawdowns decline much faster than would be predicted by Equation 1.

Evinger and Muskat[4] first derived a theoretical productivity index for steady state radial flow in an attempt to account for the observed non-linear flow behavior of oil wells and arrived at the following equation

$$q_o = \frac{7.08\ kh}{\ln\left(\frac{r_e}{r_w}\right)} \int_{p_{wf}}^{p_e} f(p)\, dp \qquad ..(2)$$

$$\text{where } f(p) = \frac{k_{ro}}{\mu_o \beta_o}$$

Calculations using Equation 2 based on typical reservoir and fluid properties indicated that PI at a fixed reservoir pressure p_e (as defined from Equation 1) decreases with increasing drawdown.

In a computer study by Vogel[5], results based on two-phase flow theory were presented to indicate that a single empirical inflow performance relationship (IPR) equation might be valid for most solution-gas drive reservoirs. He found that a single dimensionless IPR equation approximately held for several hypothetical solution-gas drive reservoirs even when using a wide range of oil PVT properties and reservoir relative permeability curves. The fact that his study covered a wide range of fluid properties and relative permeability curves to obtain a single reference curve, can not be over emphasized. Vogel then proposed that his equation be used to take the place of the linear productivity index relationship for solution-gas drive reservoirs when the reservoir pressure is at or below the bubble-point pressure.

The proposed empirical reference equation (IPR) in dimensionless form was given as

$$\frac{q_o}{(q_o)_{max}} = 1 - 0.20\left(\frac{p_{wf}}{\bar{p}_R}\right) - 0.80\left(\frac{p_{wf}}{\bar{p}_R}\right)^2 \qquad ..(3)$$

A comparison was made of IPR's for liquid flow, gas flow (n=1) and two-phase flow (his reference curve) on a dimensionless basis, (Fig. 1). As is evident from Fig. 1, the position of the two-phase reference curve relative to liquid and gas flow indicates that oil wells producing as if in a solution-gas drive reservoir should actually behave more like a gas well, i.e., $(\bar{p}_R^2 - p_{wf}^2)$ vs. q_o should plot as a straight line on log-log paper with a slope (n) near unity.

This paper presents the results of multipoint back-pressure tests taken at a single reservoir pressure level ($\bar{p}_R$). These results show that the performance curve for an oil well can be expressed by a more general and familiar equation similar to that used for gas wells,

$$q_o = J_o' (\bar{p}_R^2 - p_{wf}^2)^n \qquad ...(4)$$

Reservoirs in which oil well multipoint back-pressure tests were obtained ranged from highly undersaturated, to saturated at initial reservoir pressure, to a partially depleted field with a gas saturation existing above the critical (equilibrium) gas saturation. Equation 4 was found to be valid for tests conducted in all three reservoir fluid states, even for the conditions where flowing pressures were well <u>above</u> the bubble-point pressure. Permeabilities of the reservoirs ranged from 6 to > 1000 millidarcys. Flow point alignment to establish an oil well back-pressure curve on the customary log q_o vs. log $\Delta(p^2)$ was found to be as good as that obtained on gas well back-pressure tests.

Basic Equations and Pressure Functions

The basic flow equation given by Evinger and Muskat[4] for steady-state flow, applicable to either oil or gas flow, is

$$q_o = \frac{7.08\ kh}{\ln\left(\frac{r_e}{r_w}\right)} \int_{p_{wf}}^{p_e} f(p)\ dp \qquad ..(2)$$

where f (p) can be any function of pressure. Using the typical pressure function depicted in Fig. 2 it is obvious that we can evaluate the total integral in two parts and write

$$q_o = \frac{7.08\ kh}{\left[\ln\left(\frac{r_e}{r_w}\right) + s'\right]}\left[\int_{p_{wf}}^{p_b} \frac{k_{ro}\ (S,p)}{\mu_o \beta_o}\ dp + \int_{p_b}^{p_e} \frac{k_{ro}\ (p)}{\mu_o \beta_o}\ dp\right] \qquad ..(5)$$

For flow in the region where the pressures are above the bubble point pressure if we assume $k_{ro} = 1$ (neglecting the pressure dependent permeability term for simplicity of presentation only) and treat $(\mu_o\beta_o)$ evaluated at the average pressure $(p_e + p_b)/2$ we can write

$$q_o = \frac{7.08\ kh}{\left[\ln\left(\frac{r_e}{r_w}\right) + s'\right]}\left[\int_{p_{wf}}^{p_b} \frac{k_{ro}\ (S,p)}{\mu_o\beta_o}\ dp + \frac{(p_e - p_b)}{\overline{\mu_o\beta_o}}\right] \qquad ..(\ 6)$$

Except for the addition of the necessary skin term, s' (discussed later in the paper) Equation 6 is identical to that derived by Handy[21].

Figure 2 illustrates a plot of $1/\mu_o\beta_o$ as a function of pressure for an undersaturated oil reservoir. Also, drawn on this figure is a dashed line representing the effect of relative permeability (k_{ro}) on drawdowns below the bubble-point pressure. It is assumed for purposes of demonstration that $k_{ro}/(\mu_o\beta_o)$ is linear and its intercept is 0 at 0 pressure. The simplifying assumption of the 0 intercept for $k_{ro}/(\mu_o\beta_o)$ approximately defines Vogel's IPR curve and exactly defines Equation 4 when n=1. Also, drawn on Fig. 2 is a hypothetical pressure function $k_{ro}/(\mu_o\beta_o)$ represented as a constant for all pressures. It is clear that a constant value of $k_{ro}/(\mu_o\beta_o)$ over the entire pressure drawdown range is required to obtain a constant productivity index (PI).

Figure 3 illustrates plots of $1/(\mu_g\beta_g)$ for two high pressure gas reservoirs. Curve A was obtained from calculations using the reservoir gas analysis and standard correlations of Z and μ_g as functions of critical pressure and temperature. Curve B was obtained directly from a PVT study. One striking feature of curve A is the fact that it resembles that of an undersaturated oil reservoir with an apparent or pseudo bubble-point pressure near 2500 psia, the normal inflection point of a Z curve. A further observation that can be made from curves A and B is that a region exists where a gas well can be considered to behave as a liquid, i.e., $1/(\mu_g\beta_g)$ is nearly constant or only slightly changing with pressure as is the case for the pressure function of an undersaturated oil reservoir above the bubble-point pressure.

For the region where the pressure function is a constant, or nearly so, we can immediately write upon integration of Equation 2 the well known steady-state single phase flow equation:

$$q = \frac{7.08\ kh}{\left[\ln\left(\frac{r_e}{r_w}\right) + s'\right]} \cdot \frac{(p_e - p_{wf})}{(\mu\beta)} \qquad ..(\ 7)$$

Note that this equation would approximately hold for gas wells represented by curves A and B in Fig. 3 over a considerable range of pressure drawdowns. q_g will then be proportional to Δp instead of $\Delta(p^2)$. This, in fact was found to be the case for isochronal tests conducted on two wells in a reservoir with fluid properties represented by curve B.

Now considering the entire pressure function from p_e to 0, for either the oil or gas curves, (the dashed line in Fig. 2) we note that f (p) can be represented approximately by two separate straight line segments. The approximate flow equation then, over the total pressure interval, can be written as: (See Appendix)

$$q = \frac{7.08\ kh}{\left[\ln\left(\frac{r_e}{r_w}\right) + s'\right](\overline{\mu\beta})_{p_e,p_b}} \cdot \left[\frac{(\overline{\mu\beta})_{p_e,p_b}\, a_2}{2}\,(p_b^2 - p_{wf}^2) + (p_e - p_b)\right] \qquad ..(8)$$

$$\text{or} \quad q = J'\,(p_b^2 - p_{wf}^2) + J\,(p_e - p_b) \qquad ..(8A)$$

For drawdowns both above and below the bubble-point pressure, a back-pressure curve plot will appear as two line segments, with the intersection yielding an approximate value for the reservoir bubble-point pressure. This then offers an approach for determining a reservoir's bubble-point pressure from an isochronal test. For an isochronal test, a constant reservoir radius of investigation is obtained for each flow-an insitu constant volume cell.

If the degree of undersaturation is slight, the two line segments may not be definable. Unstable flow conditions in the tubing at the low flow rates necessary to define the single-phase flow conditions may preclude defining two straight lines. Further, as will be demonstrated later, non-Darcy flow can exist even when all flowing pressures are above the bubble-point pressure. Conceivably then this could lead to even three line segments.

For the case of all drawdowns below the bubble-point pressure $J(p_e - p_b)$ is a constant, while the remaining term varies non-linearly with flowing pressure, p_{wf}.

The composite effect results in an equation of the form

$$q = C\,(p_e^2 - p_{wf}^2)^n \qquad ..(9)$$

As p_e decreases to the pressure p_b, $n \rightarrow 1.0$ and $C \rightarrow J'$ such that for the oil well case, only the two-phase flow term remains. We thus obtain the basic equation suggested from Vogel's results for $p_e \leq p_b$:

$$q_o = J_o'\,(p_e^2 - p_{wf}^2)^{1.0} \qquad ..(10)$$

A significant conclusion to be drawn from Equation 9 is that a gas well or an oil well can have a slope less than 1.0 on a log q vs. log $\Delta(p^2)$ plot without non-Darcy flow existing. The slope (n) in this case is strictly a result of the shape of the wells pressure function. This possibility, for a gas well, was recognized and reported by Rowan and Clegg[6].

Equation 10 must be further generalized with an exponent (n) in light of results obtained from multipoint back-pressure tests conducted on oil wells for <u>both</u> single-phase and two-phase flow to

$$q_o = J'_o \ (p_e^2 - p_{wf}^2)^n \qquad ..(11)$$

Equation 11 is identical in form to the gas well back-pressure equation. For constant rate transient gas flow, the gas well back-pressure equation is usually expressed by[7,8].

$$\frac{7.08\ kh\ (p_i - p_{wf})}{q\ (\overline{\mu\beta})} = \ln \sqrt{\frac{14.23\ k_i t}{\phi\ (\mu c_t)_i\ r_w^2}} + s + Dq \qquad ..(12)$$

Other than for the unique fluid property cases discussed above, or a pressure dependent permeability effect, the non-Darcy flow term in Equation 12 is required to obtain an exponent (n) less than 1.0.

In terms of a pseudo-pressure[9] m(p)

$$\frac{7.08\ kh\ [m(p_i) - m(p_{wf})]}{q} = \ln \sqrt{\frac{14.23\ k_i t}{\phi\ (\mu c_t)_i\ r_w^2}} + s + Dq \qquad ..(13)$$

where m (p) can also include a pressure dependent permeability [10,11]

$$m(p) = \int_o^p \frac{k_{ro}\ (S,p)}{\mu\beta}\ dp \qquad ..(14)$$

(The effect of a pressure dependent permeability could readily be displayed in Figures 2 and 3.)

Equations 12 or 13 then should be applicable for analyzing both oil well and gas well back-pressure tests.

Rate and Time Dependent Skin, s (q,t)

Slopes much less than 1 were consistently obtained from isochronal tests conducted on oil wells in saturated reservoirs. For undersaturated reservoirs, the shape of the pressure function was shown to be capable of accounting for slopes less than 1. Since Vogel's work based on two-phase flow theory indicated back-pressure curve slopes should be unity or even greater, a near well bore effect was suspected. (All of Vogel's results show the first calculated IPR curve after 0.1% of original oil-in-place is recovered. The effect of initial gas saturation build-up around the wellbore may not have been present in his results.) Handy[21] studied the adverse effect on PI of two-phase flow in the vicinity of the wellbore for undersaturated oils. Muskat[12,13] presented a simple approach to study the effect of two-phase flow about the well bore for a gas condensate well that could be applied to a saturated or undersaturated gas condensate or oil well.

s, (q,t) for Condensate Wells

Muskat's equation to calculate the rate of change of liquid saturation taking place about the wellbore for a producing condensate well is:

$$\frac{dS}{dt} = \frac{q_g}{2\pi rh\phi} \frac{dp}{dr} \frac{dc}{dp} \quad ..(15)$$

Saturation is assumed to build up only to the limiting equilibrium liquid saturation; its radius then expanding with time. For a steady state pressure distribution, and saturation S equal to 0 at t=0, we can obtain an equation in terms of the approximate radius of the equilibrium two-phase flow region. In engineering units, it is

$$r_a^2 = \frac{.1135\ q_g^2\ \mu ZYt}{h^2\ \phi k\ \bar{p}\ S_{clh}} \quad ..(16)$$

where Y is expressed as reservoir cubic feet of condensate accumulation in the reservoir per Mscf of full wellstream gas produced per psi, dc/dp. Y can be calculated using the retrograde liquid volume data determined from PVT studies. The term S_{clh} is the critical hydrocarbon liquid saturation to reach equilibrium, or mobil liquid saturation. The other pertinent units are Mscfd, cps, days, ft, and Darcy.

The definition of skin effect (s) in terms of the radius of an altered zone r_a (equilibrium two-phase flow region), and the reduced permeability of the altered zone k_a, can be expressed as

$$s = \frac{(k - k_a)}{2k_a} \ln \left(\frac{r_a}{r_w}\right)^2 \quad ..(17)$$

Substituting Equation 16 into 17 we obtain

$$s\ (q,t) = \frac{(k - k_a)}{2k_a} \ln \left[\frac{.1135\ q_g^2\ \mu ZYt}{h^2\ \phi k\ \bar{p}\ S_{clh}\ r_w^2} \right] \quad ..(18)$$

Equation 18 defines a rate and time dependent skin term that can give the appearance of non-Darcy flow. The equation, although approximate, gives a simple analytical expression with which to estimate the effects of two-phase flow in the vicinity of the wellbore. The significance of this effect in condensate wells has been demonstrated by others.[14,15,16,17] Equation 18 has been used to successfully analyze the results obtained from isochronal tests on condensate wells. A significant portion of the skin was attributed to s(q,t).

s (q,t) for Oil Wells

In the studies of West et al.[18], Perrine[19] and Weller[20], an analogous behavior around the wellbore has been shown to exist in an oil well. Under constant rate production for initially saturated solution-gas drive reservoirs, their results show that the gas saturation quickly builds up to the equilibrium gas

saturation (critical gas) and remains constant at its equilibrium value. Its radius increases with time until the wells drainage volume is above the critical gas saturation (see Fig. 4). This gas saturation build-up in the vicinity of the wellbore is commonly referred to as "gas block". The corresponding oil permeability reduction in this region is therefore constant, with its radius increasing with time. This damaged zone within which the relative permeability has been reduced has been referred to as pseudo-skin by Weller. Utilizing Equation 18 with the appropriate variable substitution, the rate and time dependent skin s (q,t) for an oil well is

$$s\,(q,t) = \frac{(k - k_a)}{2k_a} \ln \left[\frac{.0226\ q_o^2\ \beta_o \mu_o\ Xt}{h^2\ \phi\ k\ Scg\ r_w^2} \right] \qquad ..(19)$$

where X is expressed as reservoir cubic feet of gas evolved in the reservoir per stock tank barrel of oil produced per psi, dc/dp. X is readily obtained from a standard PVT study using the liberated gas data R_L as a function of pressure. Scg is the equilibrium or critical gas saturation, fraction of pore volume. Other pertinent units are STK BOPD, cps, day, ft, Darcy and RES BBL/STK BBL.

The results of West et al. were first used to determine whether Equation 19 would reasonably predict the radius of the "pseudo-skin" for times before boundary effects became significant. Using the basic data given in their paper and Equation 19, a calculated r_a = 1.6 ft versus their 1.5 ft was obtained at 2.21 days, and r_a = 4.6 ft versus their 6.0 ft at 16.8 days.

Equations 18 or 19 are applicable to initially saturated and partially undersaturated reservoirs. Once an oil wells' drainage volume exceeds the equilibrium gas saturation, Equation 19 is no longer applicable. For condensate wells, Equation 18 will apply for a much longer period of time, at least until revaporization begins to take place. Then r_a will begin to recede.

Only in the case of undersaturated reservoirs, we could assume that the two-phase region is at the equilibrium gas saturation and exists out to where the pressure is equal to the bubble-point pressure. This simpler approach, developed by Handy[21] for wells producing from undersaturated reservoirs, leads to the maximum reduction of PI which could be expected from a gas saturation build-up around a well producing with a flowing pressure below the bubble-point pressure. By analogy, the same approach could be used for treating undersaturated gas condensate wells.

For completeness then, Equations 12 and 13 should be written to include a rate and time dependent skin, s(q,t). We would then have

$$\frac{7.08\ kh\ (p_i - p_{wf})}{q(\overline{\mu\beta})} = \ln \sqrt{\frac{14.23\ k_i t}{\phi\ (\mu c_t)_i\ r_w^2}} + s + s(q,t) + Dq \qquad ...(20)$$

and

$$\frac{7.08\ kh\ [m(p_i) - m(p_{wf})]}{q} = \ln \sqrt{\frac{14.23\ k_i t}{\phi\ (\mu c_t)_i\ r_w^2}} + s + s(q,t) + Dq \quad .(21)$$

After Ramey[22], we can define

$$s' = s + Dq \quad ..(22)$$

and

$$s'' = s + s\ (q,t) + Dq \quad ..(23)$$

Well Test Results

The basic results obtained from isochronal back-pressure tests and flow after flow multipoint tests conducted on oil wells are summarized in Tables 1 and 2.

Reservoir fluid states in which multipoint well tests were obtained are, in chronological order,

1. Gas saturation existed throughout the reservoir above the critical or equilibrium gas saturation.

2. Undersaturated reservoir with flowing pressures obtained both above and below the bubble-point pressure.

3. Saturated reservoirs with the reservoir pressure at or very near the bubble-point pressure.

4. Undersaturated reservoir with all flowing pressures above the bubble-point pressure.

Gas Saturation Above Equilibrium

Stabilized flow after flow multipoint back-pressure tests were available on 16 wells producing from a solution-gas drive carbonate reservoir, Field A. Reservoir conditions were ideal for testing the hypothesis that q_o vs. ($\overline{p}_R^2 - p_{wf}^2$) would plot as a straight line on log-log graph paper with a slope (n) of 1. The reservoir variables in this field closely approximated those used by Vogel in his study, (see Table 3). Average gas saturation in the reservoir at the time the tests were conducted was estimated to be between 10 or 12 percent. Producing gas-oil ratios when compared to the initial solution gas-oil ratio of 684 SCF/BBL indicates that the reservoir was well above the equilibrium (critical gas) saturation at the time the tests were conducted. Gas-oil ratios increased only moderately at increasing drawdowns for most tests.

Although the unit slope did predominate, four wells exhibited back-pressure curve slopes much less than 1. A slope less than 1 results in an even more rapid decline in rate q with drawdown than would be predicted from Vogel's IPR equation.

The test on Well 6, Field A (Fig. 5) consisted of seven individual flows, each to apparent stabilization. The first four flow rates were run in a normal increasing sequence. Following the fourth flow at 229 BOPD, the rate was reduced to 93 BOPD then again followed by an increasing sequence of flows. All points essentially fell on the same line, indicating that transient effects were not the cause of the deviation from the linear relationship predicted by the productivity index concept. Note that the flow points define a performance curve with a slope of 1 almost to its absolute open flow potential (AOFP). Table 1 shows that for all wells tested in this field, the maximum flow rate was very near the extrapolated absolute open flow potential. In the other fields in which multipoint tests were conducted, equipment limitation precluded defining the entire curve, requiring a greater degree of extrapolation to AOFP.

Well No. 3, Field A, (Fig. 6) illustrates the most significant result of this first group of tests. With an excellent alignment of five stabilized flows, the slope of the back-pressure curve is 0.648. The results obtained from this test first suggested the possible existence of the same lower limit of the exponent (n) as exists for gas wells (n = 0.500), and a non-Darcy flow effect.

Well No. 14, Field A, (Fig. 7) exhibited the maximum increase in gas-oil ratio with increasing drawdown of all the wells tested. Even with the gas-oil ratio increasing with rate, the slope n of the performance curve was 1.0.

Undersaturated Reservoir ($p_{wf} > p_b$ and $p_{wf} < p_b$)

In an attempt to utilize the oil well back-pressure testing method to more accurately predict full development well performance from wildcat well tests, an isochronal test program was initiated. The first known oil well isochronal test was conducted on April 14, 1970, on the Phillips Ekofisk 2/4-2X well. Surprising results were obtained from these first tests. Two straight lines were obtained when a log q vs. log ($\bar{p}_R^2 - p_{wf}^2$) plot was prepared. Figure 8 illustrates the results obtained from a 6-hour isochronal test conducted on Zone 2.

Handy's[21] work led to the conclusion that the two straight lines were a result of the reservoir being undersaturated, with the intersection point indicating the apparent reservoir bubble-point pressure. Using the first two flow rates and the constant PI approach, an apparent absolute open flow potential of 13,000 BOPD is indicated. The true potential established by extrapolation of drawdown data below the bubble-point pressure is 5200 BOPD. Calculated permeability from build-up data following the first single phase flow was 6.1 md with a skin s = 0. For flows at pressure drawdowns below the bubble-point pressure, a rate dependent skin was indicated. The rate dependent skins extrapolated to a skin of 0 at the point single phase flow ended, $q_o \cong 2100$

BOPD, as should be expected, (see Fig. 9). Single-phase skins of -4 are normally obtained from tests following acid stimulations. This favorable response usually precluded obtaining drawdowns below the bubble-point pressure after acid, because of equipment limitations. As a result, no after acid isochronal tests have been obtained which could demonstrate whether the nature of the performance curve is substantially different than that obtained before acid. Isochronal tests conducted on two other zones in this well, before stimulation, yielded similar results.

Starting with Equation 8A, we can outline the procedure used to calculate the bubble-point pressure from the pre-acid test

$$q_o = J'_o \ (p_b^2 - p_{wf}^2) + J_o \ (p_e - p_b) \qquad ..(8A)$$

If we then define

$$q(2) = J'_o \ (p_b^2 - p_{wf}^2) \qquad ..(24)$$

and

$$q(1) = J'_o \ (p_e - p_b) \qquad ..(25)$$

then

$$q_o = q \ (2) + q \ (1) \qquad ..(26)$$

(No physical significance should be attached to q(1) or q(2) since it is obvious that for the steady state assumption upon which it was derived, the total q_o must be flowing through both regions.)

When combined two-phase and single phase flow are occurring in a well

$$q(1) = \text{CONSTANT} = J_{o,p_e,p_b} \ (p_e - p_b) \qquad ..(25)$$

therefore $q(2) = q_o$ (measured) - q (1) =

$$J'_o \ (p_b^2 - p_{wf}^2) \qquad ..(27)$$

With the correct value of a bubble-point pressure, p_b, a plot of q(2) vs. $(p_b^2 - p_{wf}^2)$ should plot a straight line on either cartesian or a log-log plot. On a log-log plot, the slope is 1.0 and the intercept J'_o.

The 1.0 slope was assumed for the two-phase term at this stage of development because of the computer results obtained by Vogel and the results obtained from tests in Field A. However, the fact that slopes less than 1.0 are indicated from other tests where two-phase flow existed in the reservoir, suggests the more general form of Equation 8A to be

$$q_o = J'_o \ (p_b^2 - p_{wf}^2)^n + J_o \ (p_e - p_b) \qquad ..(28)$$

A trial and error calculation assuming various values of p_b was performed until a slope of 1 was obtained, (see Fig. 10). This resulted in a calculated bubble-point pressure of 5874 psia. A bubble-point pressure of 5885 psia was determined from a PVT study of the reservoir fluid obtained from this well.

A simple graphical estimate of the bubble-point pressure from the apparent intersection point is probably adequate because of the uncertainties introduced by n, the exponent of the two-phase term, being a variable. Once the true bubble-point pressure is determined from PVT data, n can be directly calculated.

Saturated Reservoirs

Most of the reservoirs in Fields C through H are saturated at initial reservoir pressure. The reservoirs are very similar in nature at corresponding depths since the fields are in close proximity to each other. All reservoirs are relatively clean Tertiary sandstones ranging in depth from 7800 to 11200 ft. Permeabilities determined from build-up tests ranged from 130 to 2500 md with net pays ranging from 20 to 180 feet in thickness. Typical porosities are 22 percent with water saturations of around 30 percent. Relative permeability measurements exhibited critical gas saturations ranging from 7 to 13 percent.

Humping effects, wellbore storage, flat pressure build-up curves and the short duration of the build-ups made the determination of permeabilities difficult on several wells. For those wells not having permeabilities listed in the tables, its order of magnitude is reflected by the wells AOFP. A summary of all the isochronal test results obtained appears in Table 2.

The standard isochronal test in these fields consisted of a four hour flow followed by a four hour shut-in. Occasionally, a flow after flow test was also conducted. Increasing and decreasing sequences of flows were performed on most tests to check reproducibility. Because of the rather high permeabilities in these reservoirs, flow after flow tests often duplicated the isochronal test performance curve. Performance curve slopes obtained from these tests are seen to range from 0.568 to 0.875. Not one single well exhibited the 1 slope that was so predominant in Field A. Several of the well test performance curves obtained in initially saturated reservoirs are shown in Figs. 11-21. In general, flow point alignment to establish an oil well's performance curve is as good as that obtained from gas well back-pressure tests. Shut-in pressure recovery between isochronal flows on these tests is sufficient to establish true isochronal conditions. Gas-oil ratio variations are considered to be more a function of separator pressure than reservoir drawdown pressure effects. The most significant observation to be made from these tests is that flow after flow data fall on the same performance curve as that established by isochronal data points. The lowest permeability of this group of wells is 130 md. Test results for Well No. 3-C, Field C, (Fig. 12 and Table 4) demonstrate the flow after flow and isochronal test performance curve reproducibility by two separate tests conducted one week apart.

The test on Well No. 5-C in Field D was selected to apply Equation 20 to analyze the well performance data. The four hour isochronal well performance

curve was established by two separate tests six months apart. Nearly 100 psi reservoir pressure drop occurred between these two tests. No detectable shift in the position of the well's performance curve was noted. Well No. 5-C was the only one of the saturated reservoir wells that had a fully perforated interval, thus eliminating yet another variable, partial penetration effects. Further, the permeability calculated from build-up data was consistent with measured core permeabilities for this well. Tables 5 and 6 summarize the reservoir and test data used in the calculations and the results obtained. The rate dependent skin term s(q,t), for this well, was found to be insignificant at even the high flow rate of 2308 BOPD. Both s' and s" were plotted as a function of q_o. In either case, a line can be drawn thru the plotted points to q = 0 yielding a formation skin s = 0. Non-Darcy flow appears to be significant for this well.

The isochronal performance curve obtained on Well No. 7-e, Field D, (Fig. 16), exhibits the steepest slope of all the tests conducted in a saturated reservoir. Any of the flow rates would be reasonable for a normal single flow drillstem test. A comparison of calculated absolute open flow potential (AOFP) is made using the PI method and Vogel's IPR method for each of the flow rates. The maximum error in AOFP is of course obtained with the lowest flow rate - AOFP = 57,200 BOPD PI method, 31,990 BOPD IPR method and actual isochronal AOFP = 7250 BOPD. Even though the error in AOFP, using the PI or IPR methods is reduced when determined at the highest flow rate, the error in evaluating skin and flow efficiency will be increased.

Well No. 8-e, Field D, (Fig. 17 and Table 7) demonstrates the change in the wells performance curve as a result of increasing the perforated interval from 20 ft. to 60 ft.; net pay is 182 ft. The well's potential nearly doubled and the slope of the performance curve increased only slightly.

Undersaturated Reservoir ($p_{wf} > p_b$)

Of all the isochronal tests conducted, the most surprising results were those obtained on Wells 1-a and 2-b in Field G (Figs. 22 and 24 respectively). With all flowing pressures well above the reservoir bubble-point pressure, (single-phase liquid flow), slopes of 0.813 and 0.712 were obtained from a log q vs. log $\Delta(p^2)$ plot.

Conclusive evidence of the occurrence of non-Darcy flow in an oil well is demonstrated from a detailed analysis of the isochronal test data obtained on Well No. 1-a. PVT studies conducted on two bottom-hole samples and a recombination of surface samples indicated bubble-point pressures of 4495, 4756 and 4785 psia respectively. The lowest flow pressure obtained on this test was 5669 psia at a flow rate of 2973 STK BOPD. Net pay for this well is 25 feet with a perforated interval of 10 feet.

The isochronal performance curve for Well No. 1-a (Fig. 22) indicates a slope n of 0.813 with an excellent alignment of 8 separate flow rates. Three decreasing sequence flows were followed by five more decreasing flows. Table 8 summarizes the data obtained for each flow rate. The fact that alignment was obtained following repeated flows and shut-ins, and flow reversals tend to

indicate that a pressure dependent permeability would not account for the non-linear flow behaviour[23]. The normal hysteresis effect[24,25] in a pressure dependent permeability caused by repeated pressure reversals, as occurred during this isochronal test, should not have allowed the flows to retrace the back-pressure curve.

Analyses performed on build-ups obtained after four of the flows yielded consistent permeabilities of 222 md. The skin effect calculated from these build-up analyses was found to be rate dependent. When s was plotted as a function of q, a skin at q = 0 of + 2.2 and a non-Darcy flow coefficient D_o = .00233 $BOPD^{-1}$ was obtained (Fig. 23). From Reference[26], a partial penetration skin s_b was calculated to be +2.5, in very close agreement with that obtained extrapolating to q_o = 0. The reservoir skin damage (s) therefore is concluded to be 0.

A further verification of non-Darcy flow in this well was made by checking the Reynolds number

$$R_e = \frac{\rho v\ d}{\mu} \qquad ..(29)$$

A Reynolds number of 8 was obtained for the well under its flowing condition of 2973 BOPD with a flash formation volume factor of 2.70, a density of 0.48 gm/cc, 0.22 cps viscosity, and assuming a grain diameter of 0.5 mm. According to Muskat[12], turbulent flow can be expected for Reynolds numbers greater than 1.

The necessity for conducting multi-rate tests on oil wells for the correct evaluation of well performance, PI, reservoir damage, flow efficiency and potential is particularly emphasized by this example. One can also conclude that non-Darcy flow would also exist in the presence of a gas saturation around the wellbore and would be even more severe than is indicated for the single-phase liquid flows. For Well No. 1-a, a break in the performance curve should occur for flows below the bubble-point pressure, with the absolute open flow potential being even less than that indicated by the extrapolation on Fig. 22.

Change in Performance Curves with Depletion

Perhaps the biggest impediment to an earlier development of a multipoint testing of oil wells was the realization that a well's performance curve changes with changing oil saturation and pressure in a complex manner. Standing[27] extended the utility of Vogel's IPR equation (performance curve) by illustrating a simple method to correct a known IPR curve position to some future position as a result of a change in $k_{ro}/\mu_o\beta_o$. The future value of k_{ro} in his example was obtained from a Tarner material balance calculation using a Corey-type correlation for k_{ro}. The inability to define a real k_{ro} curve for a specific well still makes this approach only approximate.

It has been observed that in many material balance calculations for solution-gas drive reservoirs, k_{ro} is approximately linear with reservoir pressure. As

an approximation to the change in oil permeability with pressure depletion we could then write

$$\frac{k\ (\bar{p}_R)}{k_i} = \frac{\bar{p}_R}{\bar{p}_{Ri}} \qquad ..(30)$$

or

$$k_{ro}\ (\bar{p}_R) = \frac{\bar{p}_R}{\bar{p}_{Ri}} \qquad ..(31)$$

where k_{ro} is with respect to k_i and is defined at a vanishing Δp, zero drawdown. $\bar{p}_{Ri}$ is also assumed to be equal to, or less than, the bubble-point pressure. Then $k_{ro}\ (\bar{p}_R)/(\mu_o\beta_o), \bar{p}_R$ plotted as a function of pressure defines locus of values at zero drawdown. Using Equation 10 to define drawdown, and Equation 31 to correct for depletion, we obtain a simple empirical equation to predict the flow rate q_o for both drawdown and reservoir pressure depletion.

$$q_o = J'_{oi} \left(\frac{\bar{p}_R}{\bar{p}_{Ri}}\right) (\bar{p}_R^2 - p_{wf}^2) \qquad ..(32)$$

The subscript i defines any arbitrary initial condition at or below bubble-point pressure.

Equation 32 was tested using the results shown in Vogel's Figure 7. A comparison of his results with that using Equation 32 is given in tabular and graphical form on Fig. 25. The pressure ratio correction was also applied to results published in Ref. 28 with good results, (see Table 9). J'_{oi} was determined using both basic reservoir variables and an initial reported flow with about equal success. No field data exist at this time with which to check the above relationship, or the more general form

$$q_o = J'_{oi} \left(\frac{\bar{p}_R}{\bar{p}_{Ri}}\right) (\bar{p}_R^2 - p_{wf}^2)^n \qquad ..(33)$$

suggested by the results of the multipoint tests conducted to date. Well No. 5-C in Field D developed a 100 psi decline in reservoir pressure between the two isochronal tests conducted six months apart. With or without the pressure ratio correction, the performance curves are essentially the same.

Fig. 26 graphically illustrates the various states of the pressure function $k_{ro}/(\mu_o\beta_o)$ under the conditions of pressure depletion and drawdown. Pertinent comments are included on the figure.

Discussion

The forty multipoint tests reported in this study, isochronal and flow after flow, cover a wide range of reservoir fluids, fluid states, and reservoir variables. Vogel's computer study of inflow performance using two-phase flow theory covered a wide range of fluid properties and relative permeability relationships. The combined results of theoretical and field studies indicate

that multipoint tests are as necessary for oil wells as for gas wells. The fact that non-Darcy flow effects were found to be significant in field tests suggests that future theoretical computer studies need to include a non-Darcy flow effect. The exact nature of the non-Darcy flow and Reynolds number for two-phase flow in terms of reservoir and fluid variables needs further investigation.

To the author's knowledge, none of the wells included in this study were hydraulically fractured; true radial flow was obtained. Further field tests are needed to study the performance curves of fractured wells. They can be dominated by linear flow in the vicinity of the wellbore, the region in which non-Darcy flow should be most pronounced. West et al.[18] in their study of linear and radial two-phase flow point out that "The linear system does not exhibit the constriction effects which were observed in the radial system." However, since gas well and oil well tests have been shown to exhibit similar behaviour, and a significant number of tests on hydraulically fractured gas wells have been conducted without a breakdown in the log q vs. log $\Delta(p^2)$ relationship, no real departure is expected for tests conducted in hydraulically fractured oil wells.

All tests reported in this study were taken at essentially one pressure level. A change in slope of the portion of the back-pressure curve, consisting of all flows at drawdowns below the bubble-point pressure, can be predicted with reservoir shut-in pressure decline to the bubble-point pressure for undersaturated reservoirs. Vogel's computer results (not including a non-Darcy flow effect) suggested a simple empirical reservoir shut-in pressure ratio factor to establish a single performance curve for both drawdown and pressure depletion for a volumetric reservoir without fluid injection. The nature of the change in the well performance curve with pressure depletion requires field study.

Conclusions

The results obtained from the forty oil well multipoint back-pressure tests reported in this study, isochronal and flow after flow, leads to the following conclusions:

1. Multipoint tests for oil wells are required to accurately determine flow rates as a function of drawdown, reservoir damage, flow efficiency, and a well's true absolute open-flow potential.

2. Oil wells can behave very similar to gas wells on multipoint back-pressure tests and should therefore be tested and analyzed using the same basic flow equations.

3. The exponent (n) for oil wells tests determined from a log q vs. log $\Delta(p^2)$ plot was found to lie between 0.568 and 1.000, very near the limits commonly accepted for gas well back-pressure curves.

4. Flow-point alignment to establish an oil well back-pressure curve on a log q vs. log $\Delta(p^2)$ plot is as good as that normally obtained from gas well back-pressure tests.

5. A non-Darcy flow-term is generally required to account for slopes (n) less than 1 obtained on oil well back-pressure performance curves.

6. Back-pressure curve slopes less than 1 can be obtained on wells in undersaturated reservoirs without a non-Darcy flow term because of the shape of the pressure function $(k_{ro}/\mu_o\beta_o)$.

7. In some cases, it is possible to determine the bubble-point pressure of an undersaturated reservoir from multipoint tests when a sufficient range of flow rates is taken.

8. Flow after flow tests or isochronal tests on oil wells will yield the same performance curve in high permeability reservoirs.

9. With a single data point, a simple empirical equation predicts flow rates as a function of drawdown and pressure depletion for wells in a volumetric solution-gas drive reservoir, (no fluid injection). Field verification is obviously needed.

Nomenclature

a = slope of pressure function f(p), $(psi - cp)^{-1}$
b = intercept of pressure function f(p), cp^{-1}
B = formation volume factor, reservoir vol/surface vol
c_t = total compressibility, psi^{-1}
C = back-pressure curve coefficient
D = non-Darcy flow constant, $(STK\ BOPD)^{-1}$
h = thickness, ft
J = productivity index, STK/BBL/DAY/psi
J' = productivity index (back-pressure curve coefficient) $STK/BBL/DAY/(psi)^{2n}$
k = effective permeability, Darcy
k_a = permeability of altered or damaged zone, Darcy
k_{ro} = relative permeability to oil, fraction
$m(p)$ = pseudo-pressure, (see Equation 14), psi/cp
n = exponent of back-pressure curve
$\overline{p}$ = average pressure, psia
p_b = bubble point pressure, psia
p_e = external boundary pressure, psia
$\overline{p}_R$ = reservoir average pressure (shut-in pressure), psia
p_i = initial formation pressure, psia
p_{wf} = bottom-hole flowing pressure, psia
PI = productivity index (J), STK BBL/DAY/PSI
q = surface rate of flow, STK BOPD
r_a = radius of altered or damaged zone, ft
r_e = external boundary radius, ft
r_w = wellbore radius, ft
R_L = gas-oil ratio liberated per barrel of residual oil, SCF/STK BBL
s = skin effect, dimensionless
s_b = skin effect caused by partial penetration of formation, dimensionless
s' = total effective skin effect (see Equation 22), dimensionless

s'' = total effective skin effect (see Equation 23), dimensionless
$s(q,t)$ = rate and time dependent skin effect (see Eqs. 18 and 19) dimensionless
S = saturation, fraction of pore volume
S_{clh} = hydrocarbon liquid saturation to achieve mobility, fraction of pore volume
t = time, days
T = reservoir temperature, °R
X = reservoir cu ft of gas evolved in the reservoir/STK BBL produced/psi, (dc/dp) in Equation 15
Y = reservoir cu ft of condensate accumulation in the reservoir/MSCF full wellstream gas produced/psi, (dc/dp) in Equation 15
z = gas deviation factor, dimensionless
μ = viscosity, cp
ϕ = porosity, fraction of bulk volume

Subscripts

i = initial
o = oil
g = gas

Acknowledgements

I wish to thank Phillips Petroleum Company for permission to publish this paper. The support and assistance of numerous people in our International Department is gratefully acknowledged.

References

1. Rawlins, E. L., and Schellhardt, M. A.: "Back-Pressure Data on Natural Gas Wells and Their Application to Production Practices", U. S. Bureau of Mines Monograph 7, 1936.

2. Cullender, M. H.: "The Isochronal Performance Method of Determining the Flow Characteristics of Gas Wells", Trans. AIME (1955) 204, 137.

3. Moore, T. V.: "Determination of Potential Production of Wells Without Open Flow Test", API Production Bulletin 206, (1930), 27.

4. Evinger, H. H. and Muskat, M.: "Calculation of Theoretical Productivity Factor", Trans. AIME (1942) 146, 126.

5. Vogel, J. V.: "Inflow Performance Relationships for Solution-Gas Drive Wells", J. Pet. Tech. (Jan., 1968), 83.

6. Rowan, G. and Clegg, M. W.: "An Approximate Method for Non-Darcy Radial Gas Flow", Soc. Pet. Eng. J. (June, 1964), 96.

7. Smith, R. V.: "Unsteady-State Gas Flow into Gas Wells", J. Pet. Tech. (Nov., 1961), 1151.

8. Swift, G. W. and Kiel, O. G.: "The Prediction of Gas Well Performance Including the Effect of Non-Darcy Flow", J. Pet. Tech. (July, 1962) 791.

9. Al-Hussainy, R. and Ramey, H. J., Jr.,: "Application of Real Gas Flow Theory to Well Testing and Deliverability Forecasting," J. Pet. Tech. (May, 1966) 637.

10. Al-Hussainy, R., Ramey, H. J., Jr. and Crawford, P. B.: "The Flow of Real Gases Through Porous Media", J. Pet. Tech. (May, 1966) 624.

11. Raghavan, R., Scorer, J. D. T. and Miller, F. G.: "An Investigation by Numerical Methods of the Effect of Pressure-Dependent Rock and Fluid Properties on Well Flow Tests", Soc. Pet. Eng. J. (June, 1972), 267.

12. Muskat, M.: Physical Principles of Oil Production, McGraw-Hill Book Co., Inc., New York (1949) 793, 126.

13. Muskat, M.: "Some Theoretical Aspects of Cycling-Part 2, Retrograde Condensation About Well Bores", Oil & Gas Journal, Reprint (Circa 1950).

14. Eilerts, C. K. et al: "Integration of Partial Differential Equations for Transient Radial Flow of Gas-Condensate Fluids in Porous Structures", Soc. Pet. Eng. J. (June, 1965) 141.

15. Gondouin, M., Iffly, R. and Husson, J.: "An Attempt to Predict the Time Dependence of Well Deliverability in Gas Condensate Fields", Soc. Pet. Eng. J. (June, 1967) 113.

16. O'Dell, H. G. and Miller, R. N.: "Successfully Cycling a Low Permeability, High-yield Gas Condensate Reservoir", J. Pet. Tech. (January, 1967) 41.

17. Fussell, D. D.: "Single-Well Performance Predictions for Gas Condensate Reservoirs", paper SPE 4072 presented at the 47th Annual Fall Meeting, San Antonio, Texas, (October 8-11, 1972).

18. West, W. J., Garvin, W. W. and Sheldon, J. W.: "Solution of the Equations of Unsteady-State Two-Phase Flow in Oil Reservoirs", Trans., AIME (1954) 201, 217.

19. Perrine, R. L.: "Analysis of Pressure-Buildup Curves", Drilling and Prod. Practice, API (1956) 482.

20. Weller, W. T.: "Reservoir Performance During Two-Phase Flow", J. Pet. Tech. (February, 1966) 240.

21. Handy, L. L.: "Effect of Local High Gas Saturations on Productivity Indices", Drilling and Prod. Practice, API (1957) 111.

22. Ramey, H. J., Jr.,: "Non-Darcy Flow and Wellbore Storage Effects in Pressure Build-up and Drawdown of Gas Wells", J. Pet. Tech. (February, 1965) 223.

23. Vairogs, J. and Vaughan, W. R.: "Pressure Transient Tests in Formations Having Stress-Sensitive Permeability", paper SPE 4050 presented at the 47th Annual Fall Meeting, San Antonio, Texas, (October 8-11, 1972).

24. McLatchie, L. S., Hemstock, R. A. and Young, J. W.: "Effective Compressibility of Reservoir Rocks and Its Effects on Permeability", Trans. AIME (1958) 213, 386.

25. Vairogs, J., Hearn, C. L., Dareing, D. W. and Rhoades, V. W.: "Effect of Rock Stress on Gas Production from Low-Permeability Reservoirs", J. Pet. Tech. (September, 1971) 1161.

26. Brons, F. and Marting, V. E.: "The Effect of Restricted Fluid Entry on Well Productivity", J. Pet. Tech. (February, 1961) 172.

27. Standing, M. B.: "Concerning the Calculation of Inflow Performance of Wells Producing From Solution Gas Drive Reservoirs", J. Pet. Tech. (September, 1971) 1141.

28. Levine, J. S. and Prats, M.: "The Calculated Performance of Solution-Gas-Drive Reservoirs", Soc. Pet. Eng. J. (September 1961) 142.

Appendix

Equation 6

$$q_o = \frac{7.08\ kh}{\left[\ln\left(\frac{r_e}{r_w}\right) + s'\right]} \cdot \left[\int_{p_{wf}}^{p_b} \frac{k_{ro}\,(S,p)}{\mu_o \beta_o}\, dp + \frac{(p_e - p_b)}{\left(\overline{\mu_o \beta_o}\right)}\right] \qquad ..(\ 6)$$

can be used to describe all three possible flow conditions that could exist for a producing well at some time during the life of an initially undersaturated oil reservoir by eliminating any terms that do not apply over appropriate pressure ranges.

I Single-Phase Flow: $p_{wf} > p_b$, $p_e > p_b$ or $\overline{p}_R > p_b$

A. STEADY-STATE FLOW, Constant Pressure at Outer Boundary

$$q_o = \frac{7.08\ kh}{\left[\ln\left(\frac{r_e}{r_w}\right) + s'\right]} \left[\frac{(p_e - p_{wf})}{(\overline{\mu_o \beta_o})}\right] \qquad ..(A\text{-}1)$$

B. PSEUDO-STEADY STATE FLOW, Closed (NO FLOW) at Outer Boundary

a) Boundary Pressure p_e is known at r_e (Initial Isochronal Test)

$$q_o = \frac{7.08\ kh\ (p_e - p_{wf})}{\left[\ln\left(\frac{r_e}{r_w}\right) - \frac{1}{2} + s'\right](\overline{\mu_o \beta_o})} \qquad ..(A\text{-}2)$$

b) Average pressure $\bar{p}_R$ is known ($\bar{p}_R$ = shut-in pressure)

$$q_o = \frac{7.08\ kh\ (\bar{p}_R - p_{wf})}{\left[\ln\left(\frac{r_e}{r_w}\right) - \frac{3}{4} + s'\right](\overline{\mu_o \beta_o})} \qquad ..(A\text{-}3)$$

C. TRANSIENT FLOW

$$q_o = \frac{7.08\ kh\ (p_i - p_{wf})}{\left[\ln\sqrt{\frac{14.23\ k_i t}{\phi\ (\mu c_t)_i r_w^2}} + s'\right](\overline{\mu_o \beta_o})} \qquad ..(A\text{-}4)$$

II Two-Phase Flow: $p_{wf} < p_b$, $p_e \leq p_b$ or $\bar{p}_R \leq p_b$, and $S_g > S_{gc}$

A. STEADY-STATE FLOW, [Constant Pressure at Outer Boundary]

$$q_o = \frac{7.08\ kh}{\left[\ln\left(\frac{r_e}{r_w}\right) + s'\right]} \int_{p_{wf}}^{p_e} \frac{k_{ro}\ (S,p)}{\mu_o \beta_o}\ dp \qquad ..(A\text{-}5)$$

B. PSEUDO-STEADY STATE FLOW, [Closed (No Flow) at Outer Boundary]

a) Boundary Pressure p_e is known at r_e (Initial Isochronal Test)

$$q_o = \frac{7.08\ kh}{\left[\ln\left(\frac{r_e}{r_w}\right) - \frac{1}{2} + s'\right]} \int_{p_{wf}}^{p_e} \frac{k_{ro}\ (S,p)}{\mu_o \beta_o}\ dp \qquad ..(A\text{-}6)$$

b) Average pressure $\bar{p}_R$ is known ($\bar{p}_R$ = shut-in pressure)

$$q_o = \frac{7.08\ kh}{\left[\ln\left(\frac{r_e}{r_w}\right) - \frac{3}{4} + s'\right]} \int_{p_{wf}}^{\bar{p}_R} \frac{k_{ro}\ (S,p)}{\mu_o \beta_o}\ dp \qquad ..(A\text{-}7)$$

C. TRANSIENT FLOW

$$q_o = \frac{7.08\ kh}{\left[\ln\sqrt{\frac{14.23\ k_i t}{\phi(\mu c_t)_i r_w^2}} + s'\right]} \cdot \int_{p_{wf}}^{p_i} \frac{k_{ro}\ (S,p)}{\mu_o \beta_o}\ dp \qquad ..(A\text{-}8)$$

III Two-Phase and Single-Phase Flow: $p_{wf} < p_b$, $p_e > p_b$ or $\bar{p}_R > p_b$

A. STEADY-STATE FLOW, (Constant Pressure at Outer Boundary)

$$q_o = \frac{7.08\ kh}{\left[\ln\left(\frac{r_e}{r_w}\right) + s'\right]} \left[\int_{p_{wf}}^{p_e} \frac{k_{ro}\ (S,p)}{\mu_o \beta_o}\ dp + \frac{(p_e - p_b)}{(\mu_o \beta_o)_{\ p_e, p_b}}\right] ..(A\text{-}9)$$

B. PSEUDO-STEADY STATE FLOW, [Closed (No Flow) at Outer Boundary]

a) Boundary Pressure p_e is known at r_e (Initial Isochronal Test)

$$q_o = \frac{7.08\ kh}{\left[\ln\left(\frac{r_e}{r_w}\right) - \frac{1}{2} + s'\right]} \left[\int_{p_{wf}}^{p_b} \frac{k_{ro}\ (S,p)}{\mu_o \beta_o}\ dp + \frac{(p_e - p_b)}{(\mu_o \beta_o)_{\ p_e, p_b}}\right] ..(A\text{-}10)$$

b) Average pressure $\bar{p}_R$ is known ($\bar{p}_R$ = shut-in pressure during depletion)

$$q_o = \frac{7.08\ kh}{\left[\ln\left(\frac{r_e}{r_w}\right) - \frac{3}{4} + s'\right]} \cdot \left[\int_{p_{wf}}^{p_b} \frac{k_{ro}\ (S,p)}{\mu_o \beta_o}\ dp + \frac{(\bar{p}_R - p_b)}{(\mu_o \beta_o)_{\ \bar{p}_R, p_b}}\right] ..(A\text{-}11)$$

C. TRANSIENT FLOW

$$q_o = \frac{7.08\ kh}{\left[\ln\sqrt{\frac{14.23\ k_i t}{\phi(\mu c_t)_i r_w^2}} + s'\right]} \cdot \left[\int_{p_{wf}}^{p_b} \frac{k_{ro}\ (S,p)}{\mu_o \beta_o}\ dp + \frac{(p_i - p_b)}{(\mu_o \beta_o)_{\ p_i, p_b}}\right] ..(A\text{-}12)$$

All of the preceding flow equations could be more simply expressed in terms of a pseudo-pressure[9] $m_o\ (p)$

where

$$\int_{p_{wf}}^{p_e} \frac{k_{ro}\ (S,p)}{\mu_o \beta_o}\ dp = \int_{o}^{p_e} \frac{k_{ro}\ (S,p)}{\mu_o \beta_o}\ dp - \int_{o}^{p_{wf}} \frac{k_{ro}\ (S,p)}{\mu_o \beta_o}\ dp \qquad ..(A\text{-}13)$$

$$\text{or} \quad \int_{p_{wf}}^{p_e} \frac{k_{ro}\,(S,p)}{\mu_o \beta_o}\, dp = m_o\,(p_e) - m_o\,(p_{wf}) \qquad ..(A\text{-}14)$$

For the limiting case of at least using known PVT properties ($\mu_o\beta_o$), -- (assuming $k_{ro}\,(S,p) = 1$) we have

$$m_o\,(p_e) - m_o\,(p_{wf}) = \frac{p_b - p_{wf}}{(\overline{\mu_o\beta_o})_{p_b,p_{wf}}} + \frac{p_e - p_b}{(\overline{\mu_o\beta_o})_{p_e,p_b}} = \frac{p_e - p_{wf}}{(\mu_o\beta_o)_{avg}} \qquad ..(A\text{-}15)$$

Note that $(\mu_o\beta_o)$ normally evaluated at the average pressure $(p_e + p_{wf})/2$ would not result in a properly weighted average. But for the decline in $k_{ro}(S,p)$, a plot of q_o vs. $(p_e - p_{wf})/(\mu_o\beta_o)_{avg}$ would plot a straight line with a slope of $7.08\ kh/[\ln (r_e/r_w) + s']$ and intercept 0.

Let us now consider the case where $k_{ro}\,(S,p)$ decreases with increased drawdown, k_{ro} should approach 0, resulting in $k_{ro}/(\mu_o\beta_o)$ approaching 0. Assuming $k_{ro}/(\mu_o\beta_o)$ could be approximated by straight line functions as depicted in Fig. 2, we could write for the two-phase region.

$$\int_{p_{wf}}^{p_b} f(p)dp = \int_{p_{wf}}^{p_b} [a_2\, p + b_2]\, dp \qquad ..(A\text{-}16)$$

which when integrated between limits yields

$$\int_{p_{wf}}^{p_b} f\,(p)\, dp = \frac{a_2}{2}\,(p_b{}^2 - p_{wf}{}^2) + b_2\,(p_b - p_{wf}) \qquad ..(A\text{-}17)$$

To approximate Vogel's IPR equation we set $b_2 = 0$, then

$$\int_{p_{wf}}^{p_b} f\,(p)\, dp = \frac{a_2}{2}\,(p_b{}^2 - p_{wf}{}^2) \qquad ..(A\text{-}18)$$

Replacing p_b with $\overline{p}_R$ for the two-phase flow equation ($\overline{p}_R \leq p_b$), we have

$$q_o = \frac{7.08\ kh}{\left[\ln\left(\frac{r_e}{r_w}\right) + s'\right]}\left[\frac{a_2}{2}\,(\overline{p}_R{}^2 - p_{wf}{}^2)\right] \qquad ..(A\text{-}19)$$

The slope a_2, for $b_2 = 0$, is simply $(k_{ro}/\mu_o\beta_o)/\overline{p}_R$. We can then write

$$q_o = \frac{7.08\ kh}{\left[\ln\left(\frac{r_e}{r_w}\right) + s'\right]} \cdot \left[\left(\frac{k_{ro}}{\mu_o\beta_o}\right)_{\overline{p}_R} \frac{(\overline{p}_R{}^2 - p_{wf}{}^2)}{2\overline{p}_R}\right] \qquad ..(A\text{-}20)$$

Defining

$$J_o' = \frac{7.08\ kh}{\left[\ln\left(\frac{r_e}{r_w}\right) + s'\right]} \cdot \left[\left(\frac{k_{ro}}{\mu_o\beta_o}\right)_{\bar{p}_R} \left(\frac{1}{2\bar{p}_R}\right)\right] \quad ..(A\text{-}21)$$

then

$$q_o = J_o' (\bar{p}_R^2 - p_{wf}^2) \quad ..(A\text{-}22)$$

Similarly treating the single-phase flow region as depicted in Fig. 2. ($p_{wf} \geq p_b$)

$$q_o = \frac{7.08\ kh}{\left[\ln\left(\frac{r_e}{r_w}\right) + s'\right]} \cdot \left[b_1 (p_e - p_{wf}) - \frac{a_1}{2} (p_e^2 - p_{wf}^2)\right] \quad ..(A\text{-}23)$$

In terms of PI at a vanishing Δp,

$$\Delta p\ J_o' = \frac{7.08\ kh}{\left[\ln\left(\frac{r_e}{r_w}\right) + s'\right]} [b_1 - a_1 p_e] \quad ..(A\text{-}24)$$

where a_1 or b_1, if $a_1 = 0$, is simply $(k_{ro}/\mu_o\beta_o)$ evaluated at p_e.

For the combined single-phase and two-phase flow case we can write

$$q_o = \frac{7.08\ kh}{\left[\ln\left(\frac{r_e}{r_w}\right) + s'\right] (\overline{\mu_o\beta_o})_{p_e,p_b}} \cdot \left[\frac{(\overline{\mu_o\beta_o})_{p_e,p_b}\ a_2}{2} (p_b^2 - p_{wf}^2) + (p_e - p_b)\right] \quad ..(A\text{-}25)$$

where $(\overline{\mu_o\beta_o})_{p_e,p_b}$ is evaluated at the average pressure $(p_e + p_b)/2$.

In terms of PI definition

$$q_o = J_o \left(\overline{\mu_o \beta_o}\right)_{p_e, p_b} \left(\frac{a_2}{2}\right) \quad (p_b^2 - p_{wf}^2) + J_o (p_e - p_b) \qquad ..(A\text{-}26)$$

or

$$q_o = J'_o (p_b^2 - p_{wf}^2) + J_o (p_e - p_b) \qquad ..(A\text{-}27)$$

TABLE 1

FIELD A - CARBONATE RESERVOIR AT 5,100 FT. AND 108°F, SUMMARY OF STABILIZED FLO AFTERFLOW BACKPRESSURE TEST RESULTS. GAS SATURATION ABOVE CRITICAL OR EQUILIBRIUM GAS SATURATION. AVERAGE STABILIZATION TIME 48 HOURS, FLOWS IN INCREASING SEQUENCE.

Well No.	Number Of Flows	Shut-in Pressure P_R psia	Maximum Flow Rate			Back-Pressure Curve	
			q_o STK BOPD	Pwf psia	GOR SCF/STK BBL	Slope n	AOFP BOPD
1	5	1339	370	619	2745	1.000	420
2	5	1347	468	739	3102	0.875	670
3	5	1200	292	530	2572	0.648	340
4	5	1307	345	563	2181	1.000	425
5	5	1281	238	548	3571	1.000	310
6	7	1345	341	638	3945	1.000	445
7	5	1215	222	520	4485	0.771	275
8	4	881	116	375	2019	1.000	143
9	5	1159	202	436	3219	1.000	243
10	7	1430	261	491	1056	1.000	295
11	5	1284	126	395	4008	1.000	165
12	4	1474	321	578	1003	1.000	375
13	4	878	71	379	5979	0.707	83
14	4	1410	208	632	4607	1.000	260
15	5	1366	108	370	3805	1.000	123
16	5	1217	106	357	3397	1.000	110

TABLE 2

FIELDS C THROUGH H (TERTIARY SANDSTONES). SUMMARY OF 4-HOUR ISOCHRONAL BACKPRESSURE TEST RESULTS, SATURATED AND UNDERSATURATED RESERVOIRS (NO STIMULATION)

Field		Number	Reservoir		Shut-in Pressure	Maximum Flow Rate				Back-Pressure Curve			Net		Perm.
Well No.	Reservoir	Of Flows (Tests)	Depth ft.	Temp. °F	$\bar{P}_R$ PSIA	q_o STK BOPD	P_{wf} PSIA	GOR SCF/STK BBL	Gravity °API	Slope n	AOFP BOPD	Reservoir Fluid	Pay ft.	Perforations ft.	K MD
Field C															
1	a	4	8080	180	3535.3	2488	3451.6	588	37.3	0.813	30000	2905 B.P.	90	37	
2	b	7	9100	204	3778.9	2530	2988.2	1363	45.0	0.832	5750	saturated	11	6	200 B.U.
3	c	14(2)	9100	205	3926.2	2520	3192.1	1397	45.4	0.613	5000	saturated	32	8	180 B.U.
4	d	6	10450	220	4342.8	2303	4167.2	1896	46.7	0.752	15700	saturated	82	75	
5	e	5	10600	220	4396.4	2022	4171.8	1900	44.2	0.644	9100	saturated	97	10	240 B.U.
Field D															
1	a	6	7550	174	3187.4	2634	2676.7	1235	47.9	0.644	5900	saturated	41	20	
2	b	7	8300	194	3507.1	2993	3167.3	1516	45.3	0.580	8000	saturated	97	37	
3	b	7	8320	196	3763.9	2495	3593.0	1705	42.8	0.694	12500	saturated	58	26	450 Avg. Core
4	b	7	8620	196	3486.4	3753	3346.0	1545	47.2	0.645	20000	saturated	92	74	
5	c	8(2)	8600	200	3695.5	2308	3539.0	1309	43.7	0.580	9800	saturated	20	20	2470 B.U.
6	d	9(2)	8700	200	3766.8	3236	3519.9	1431	43.8	0.792	16300	saturated	36	14	1600 B.U.
7	e	5	8650	200	3913.0	3060	3448.0	1460	43.8	0.568	7250	saturated	52	18	470 B.U.
8	e	7	8830	205	3948.6	2502	3776.5	1348	43.5	0.602	10700	saturated	182	20	130 B.U.
8	e	5	8830	205	3899.2	2620	3823.3	1358	43.8	0.658	20300	saturated	182	60	
9	e	5	9000	205	3981.1	2321	3747.1	1367	42.8	0.613	8700	saturated	35	16	860 B.U.
Field E															
1	a	9	8440	217	3695.3	3689	3375.1	1290	43.9	0.875	17600	saturated	80	38	
Field F															
1	a	7	7830	156	3420.2	2800	3097.5	418	25.5	0.596	7800	saturated	42	8	
2	b	5	8450	164	3693.8	3088	3433.9	575	29.8	0.628	10600	saturated	41	16	
Field G															
1	a	8	11200	238	6454.2	2973	5669.1	2670	47.8	0.813	9600	4765 B.P.	25	10	222 B.U.
2	b	7	11230	238	6477.6	3519	5956.3	2991	46.3	0.712	13300	5035 B.P.	44	42	
Field H															
1	a	7	7940	174	3486.3	2626	3279.5	132	34.2	0.803	15000	N. A.	47	20	

TABLE 3

COMPARISON OF RESERVOIR VARIABLES OF FIELD A WITH VOGEL'S[5] HYPOTHETICAL SOLUTION GAS DRIVE RESERVOIR

	Field A	Vogel's[5] Figure 7
P_i	2020	2130
P_b	2020	2130
B_{oi}	1.39	1.35
$1/B_{gi}$	150	150
μ_{oi}	0.86	1.0
μ_{gi}	0.02	0.02
S_{wc}	11.5	19.4
ϕ	13.2	13.9
h	114	23.5
k-MD	31	20
R_{si}	684	600
Spacing-Acres	40	20

TABLE 4

SUMMARY OF 4-HOUR FLOW AFTER FLOW AND ISOCHRONAL TEST RESULTS,
OIL WELL 3-C, FIELD C

Flow No.	Shut-in Pressure $\bar{P}_R$-psig	Flowing Pressure P_{wf}-psig	q_o STK BOPD	GOR SCF/STK BBL	Separator Pressure psig
----------Flow After Flow Test 11/28/71----------					
1	3908.2	3180.1	2518	1397	572
2		3409.3	2064	1322	500
3		3610.8	1535	1200	490
4		3817.6	687	1607	290
5		3636.5	1394	1478	300
6		3834.5	711	1612	252
7		3847.8	534	1512	262
8		3177.4	2520	1397	572
SI 7 HR.	3907.3				
----------Isochronal Test 12/5/71----------					
9	3907.1	3440.4	2077	1379	450
10	N. A.	3759.2	1064	1555	258
11	3905.2	3434.7	2010	1502	467
12	3898.6	3654.5	1390	1490	305
13	3897.9	3811.5	709	1538	230
14	3901.0	3681.2	440	1611	154

TABLE 5

EXAMPLE CALCULATIONS OF S′ AND S" FOR SATURATED RESERVOIR, OIL WELL 5-C, FIELD D

Reservoir Data

K = 2469 MD, Build-up & Core Data

K_a = 1284 MD, K_{ro} = 0.52 at 10 percent critical gas saturation, S_{cg}

h = 20 ft

ϕ = 0.21

S_{wc} = 0.32

C_t = 25 x 10^{-6} psi^{-1}

r_w = 0.33 ft

μ_o = 0.27 cps

β_o = 1.94 RES BBL/STK BBL

t = 0.167 Days

X_o = 8.223 x 10^{-3} RES ft^3/STK BBL/psi, from PVT data

Summary of Results

q_o STK BOPD	(Eq. 19) S (q, t)	S" (Eq. 20) [S+S (q,t) + Dq]	S′ [S + D q]
2308	1.67	36.6	34.9
1452	1.24	26.6	25.4
757	0.64	11.1	10.4

An S′ or S" versus q_o plot yields S = 0 when extrapolated to q = 0.

TABLE 6

SUMMARY OF 4-HOUR ISOCHRONAL TEST RESULTS OF OIL WELL 5-C, FIELD D

Flow No.	Shut-in Pressure $\bar{P}_R$-psig	Flowing Pressure P_{wf}-psig	q_o STK BOPD	GOR SCF/STK BBL	Separator Pressure psig
----------Flow After Flow Test 12/23/71----------					
1	3680.8	3524.3	2308	1211	422
2	3672.1	3604.0	1452	1309	260
3	3670.5	3658.4	757	1375	139
4	3672.9	3665.8	419	1383	92
SI 4 HR.	3672.9				
----------Isochronal Test 6/10/72----------					
1	3583.9	3565.0	669	1406	115
2	3577.6	3535.1	1035	1333	160
3	3580.5	3513.7	1413	1357	215
4	3580.0	3430.9	2303	1217	370
SI 4 HR.	3570.7				

TABLE 7

SUMMARY OF 4-HOUR ISOCHRONAL TEST RESULTS OF OIL WELL 8-E, FIELD D

Flow No.	Shut-in Pressure $\bar{P}_R$-psig	Flowing Pressure P_{wf}-psig	q_o STK BOPD	GOR SCF/STK BBL	Separator Pressure psig
----------20 Ft. Perforations, 12/14/71----------					
1	3934.0	3912.5	701	1452	160
2	3930.6	3759.4	2447	1369	480
3		3852.8	1648	1383	350
4	3920.9	3761.8	2502	1348	480
5	3927.9	3835.5	1775	1476	350
6	3921.4	3901.4	787	1496	160
7	3913.5	3910.2	490	1413	170
SI 4 HR.	3933.9				
----------60 Ft. Perforations 6/1/72----------					
1	3899.2	3820.8	2490	1418	462
2		3884.3	766	1413	298
3	3897.9	3887.6	727	1503	167
4	3896.1	3854.7	1591	1483	280
5	3892.2	3808.6	2620	1358	456

TABLE 8

SUMMARY OF 4-HOUR ISOCHRONAL TEST RESULTS OF OIL WELL 1-A, FIELD G

Flow No.	Shut-in Pressure $\bar{P}_R$-psig	Flowing Pressure P_{wf}-psig	q_o STK BOPD	GOR SCF/STK BBL	Separator Pressure psig	Separator Temp. °F
1	6439.5	5654.4	2973	2670	405	107
2		6148.4	1328	2615	310	84
3	6427.1	6301.6	722	2680	215	68
4	6432.8	5660.1	2871	2835	445	106
5	6427.0	5947.0	2120	2668	395	96
6	6427.1	6181.2	1236	2593	380	82
7	6428.1	6249.9	992	2683	285	72
8	6427.1	6320.1	665	2591	240	68

TABLE 9

USE OF PRESSURE RATIO TO FORECAST RATE OF FLOW WITH PRESSURE DEPLETION[28]

RESERVOIR DATA USED

$p_i = p_b = 2075$ psia; $\phi = 0.139$; $s_{wc} = 0.177$; $h = 23.5$ ft; $r_w = 0.33$ ft; $r_e = 1053$ ft (80 acres); $\mu_{oi} = 0.99$ cp.; $\beta_{oi} = 1.33$ RES BBL/STK BBL; $k = 25$ and 2.5 MD; $S_{cg} = .02$ (assumed to be established rapidly), $k_{ro} = 0.444$ @ S_{cg}.

RESULTS

$\bar{p}_R$	p_{wf}	$\bar{p}_R^2$	p_{wf}^2	$\bar{p}_R$	$\bar{p}_R^2 - p_{wf}^2$	q_o - STK BOPD		
psia	psia	(Thousands)	(Thousands)	$\bar{p}_{Ri}$	(Thousands)	Ref. 28	Eq. 32	After Eq. (A-21)
80 acres, $k = 25$ MD; $J'_{oi} = 0.03735$ and 0.03717 BOPD/(Thousand psia^2)								
1708	65	2917	4	1.000	2913	108.8	108.8*	108.3
1377	65	1896	4	.8062	1892	53.3	57.0	56.7
1054	65	1111	4	.6171	1107	24.6	25.5	25.4
519	65	269	4	.3039	265	5.12	3.0	3.0
80 acres, $k = 2.5$ MD; $J'_{oi} = 0.004118$ and 0.003870 BOPD/(Thousand psia^2)								
1778	65	3161	4	1.0000	3157	13.0	13.0*	12.2
1567	65	2455	4	.8813	2451	7.88	8.90	8.36
1297	65	1682	4	.7295	1678	4.32	5.04	4.74
1112	65	1237	4	.6254	1233	2.82	3.18	2.99
871	65	759	4	.4899	755	1.54	1.52	1.43

$$\text{Eq. 32, } q_o = J'_{oi}\left(\frac{\bar{p}_R}{p_{Ri}}\right)(p_R^2 - p_{wf}^2) \; ; \; *J'_{oi} = \frac{q_{oi}}{(\bar{p}_{Ri}^2 - p_{qf}^2)}$$

$$J'_{oi} = \frac{7.08k\,(k_{ro})_{cg}h}{\left[\ln\left(\frac{r_e}{r_w}\right) - \frac{1}{2}\right](\mu_o\beta_o)_i\; 2p_i} \cdot \frac{\bar{p}_{Ri}}{p_i} \; ; \; J'_{oi} \text{ at } \bar{p}_{Ri} \text{ of examples}$$

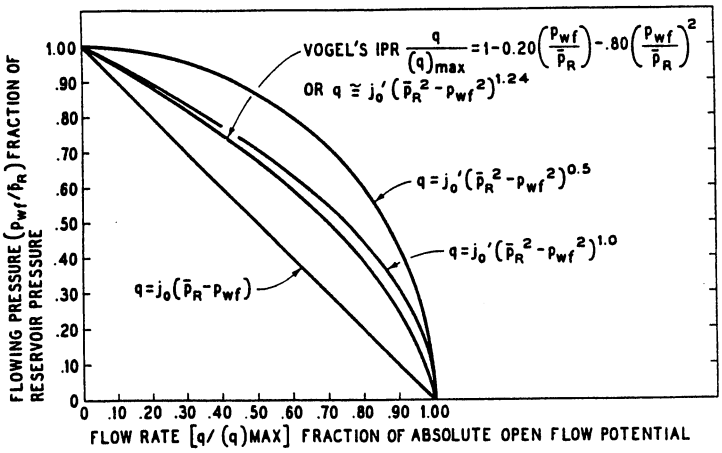

FIG. (1)

INFLOW PERFORMANCE RELATIONSHIPS FOR VARIOUS FLOW EQUATIONS (AFTER VOGEL[5])

$$q_o = \frac{7.08kh}{\ln\left(\frac{r_e}{r_w}\right)} \int_{p_{wf}}^{p_e} f(p)\,dp = \frac{7.08kh}{\ln\left(\frac{r_e}{r_w}\right)} \int_{p_{wf}}^{p_b} \frac{k_{ro}}{\mu_o B_o}\,dp + \int_{p_b}^{p_e} \frac{1}{\mu_o B_o}\,dp$$

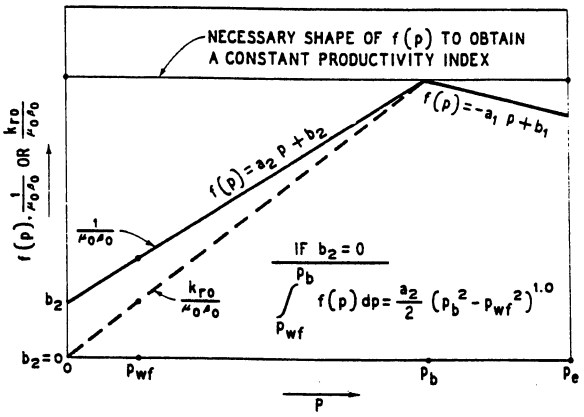

TWO PHASE

$$\text{AREA} = \int_{p_{wf}}^{p_b} \frac{k_{ro}}{\mu_o B_o}\,dp$$

SINGLE PHASE

$$\text{AREA} = \int_{p_b}^{p_e} \frac{1}{\mu_o B_o}\,dp$$

FIG. (2)

BASIC PRESSURE FUNCTION UNDERSATURATED OIL RESERVOIR

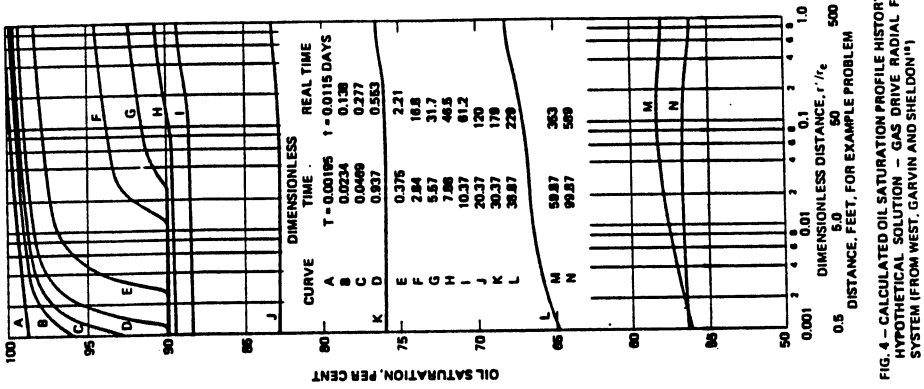

FIG. 4 – CALCULATED OIL SATURATION PROFILE HISTORY OF HYPOTHETICAL SOLUTION – GAS DRIVE RADIAL FLOW SYSTEM (FROM WEST, GARVIN AND SHELDON[18])

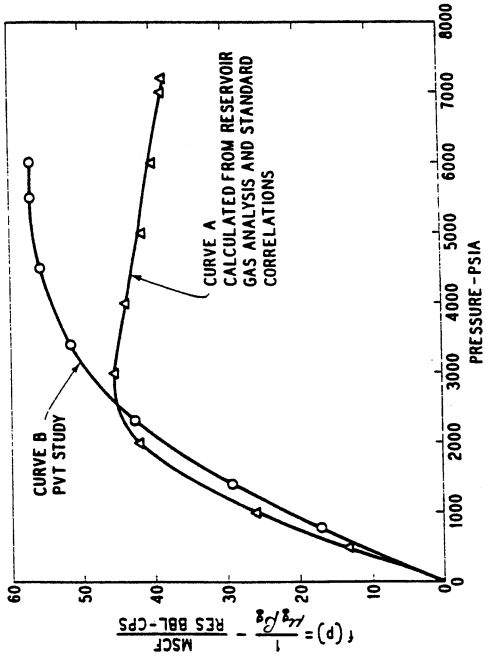

FIG. (1)

BASIC PRESSURE FUNCTION FOR
TWO HIGH PRESSURE GAS RESERVOIRS

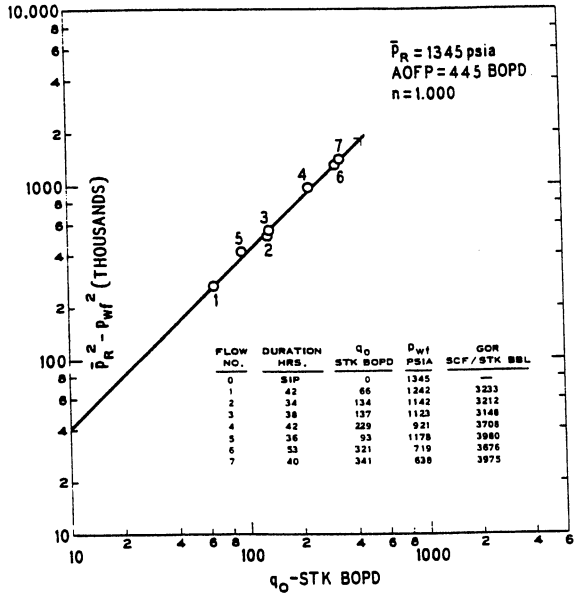

FLOW NO.	DURATION HRS.	q_o STK BOPD	P_{wf} PSIA	GOR SCF/STK BBL
0	SIP	0	1345	—
1	42	66	1242	3233
2	34	134	1142	3212
3	38	137	1123	3148
4	42	229	921	3708
5	36	93	1178	3980
6	53	321	719	3676
7	40	341	638	3975

FIG. (5)

STABILIZED PERFORMANCE CURVE
OF OIL WELL NO. 6, FIELD "A"

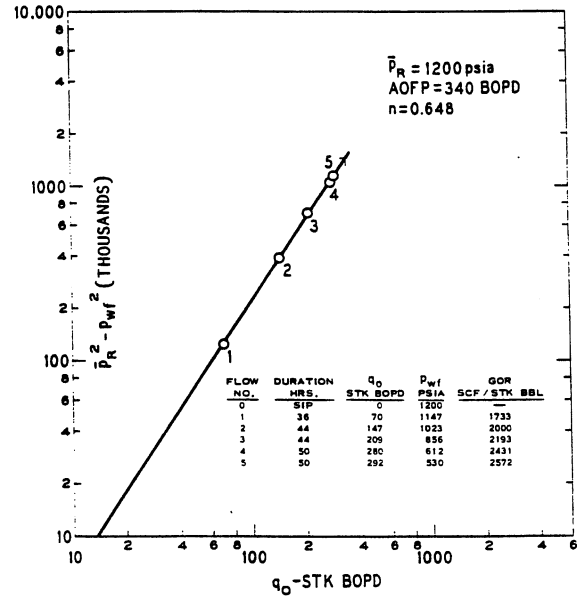

FLOW NO.	DURATION HRS.	q_o STK BOPD	P_{wf} PSIA	GOR SCF/STK BBL
0	SIP	0	1200	—
1	36	70	1147	1733
2	44	147	1023	2000
3	44	209	856	2193
4	50	280	612	2431
5	50	292	530	2572

FIG. (6)

STABILIZED PERFORMANCE CURVE
OF OIL WELL NO. 3, FIELD "A"

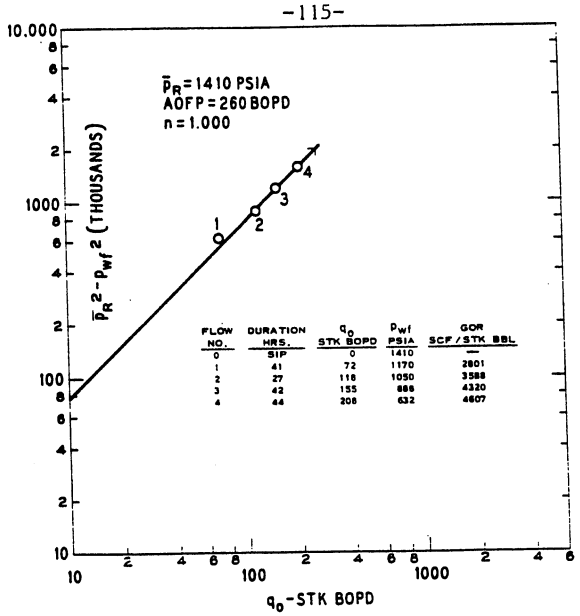

FIG. (7) STABILIZED PERFORMANCE CURVE OF OIL WELL NO. 14. FIELD A

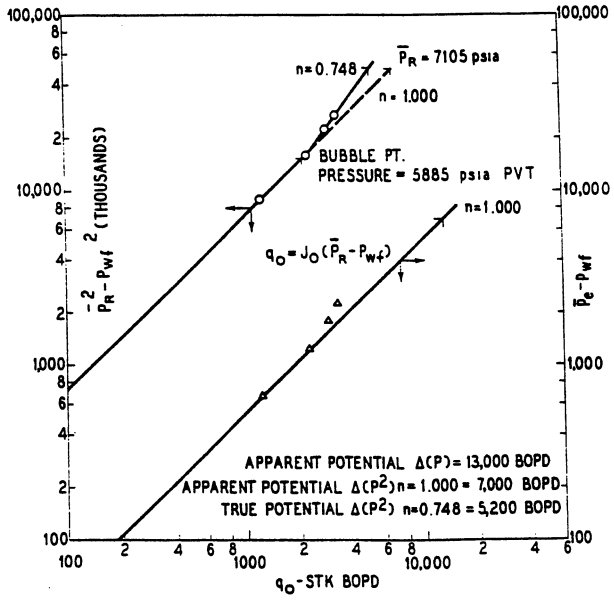

FIG. (8)

6 HR. ISOCHRONAL PERFORMANCE CURVE OF EKOFISK 2/4-2X WELL, ZONE 2, 4/14/70

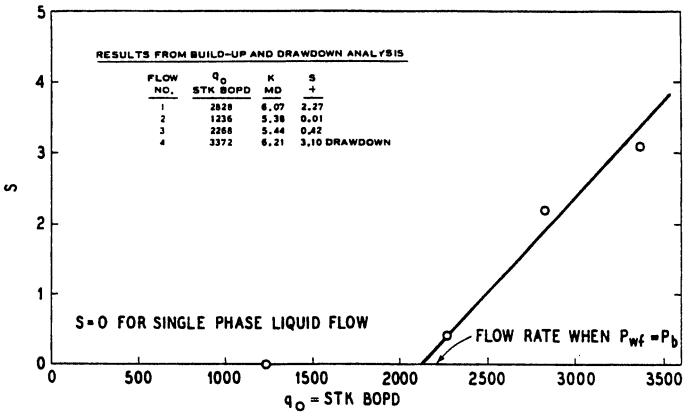

FIG. (9)

RATE DEPENDENT SKIN EFFECT FOR FLOWING PRESSURES LESS THAN BUBBLE POINT PRESSURE. EKOFISK 2/4 – 2X WELL, ZONE 2, BEFORE ACID.

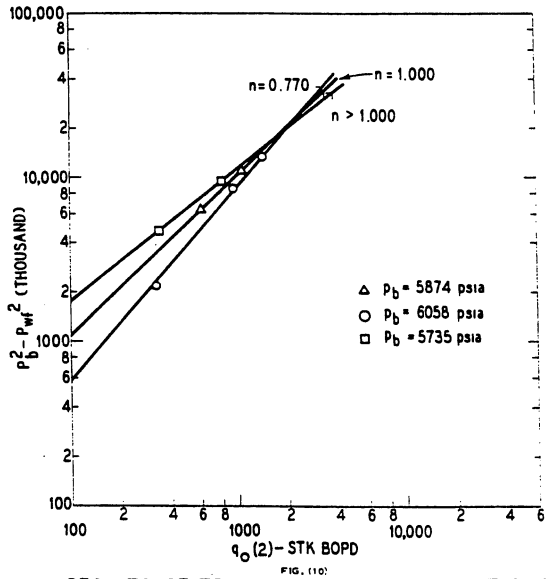

FIG. (10)

RESULTS OF TRAIL AND ERROR CALCULATIONS TO DETERMINE BUBBLE POINT PRESSURE OF 5874 psia FOR EKOFISK 2/4 – 2X WELL TEST ON ZONE 2.

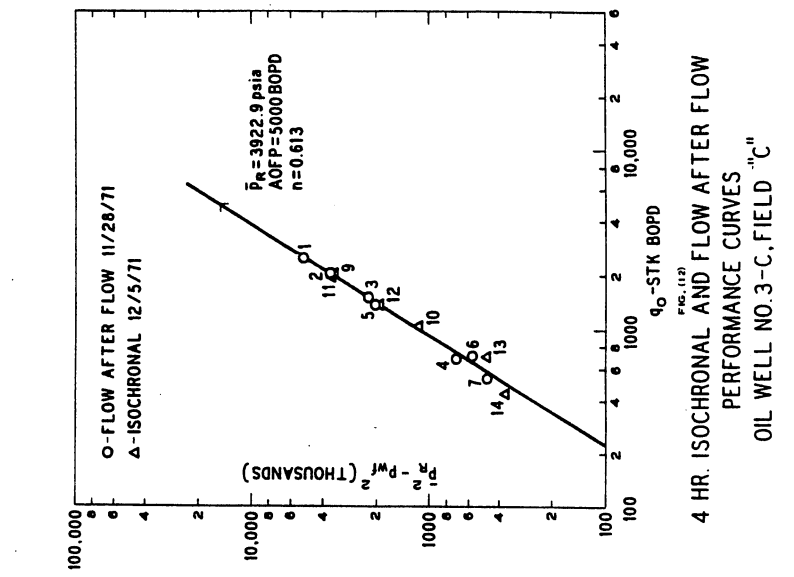

4 HR. ISOCHRONAL AND FLOW AFTER FLOW PERFORMANCE CURVES OIL WELL NO.3-C, FIELD "C"

FIG. (12)

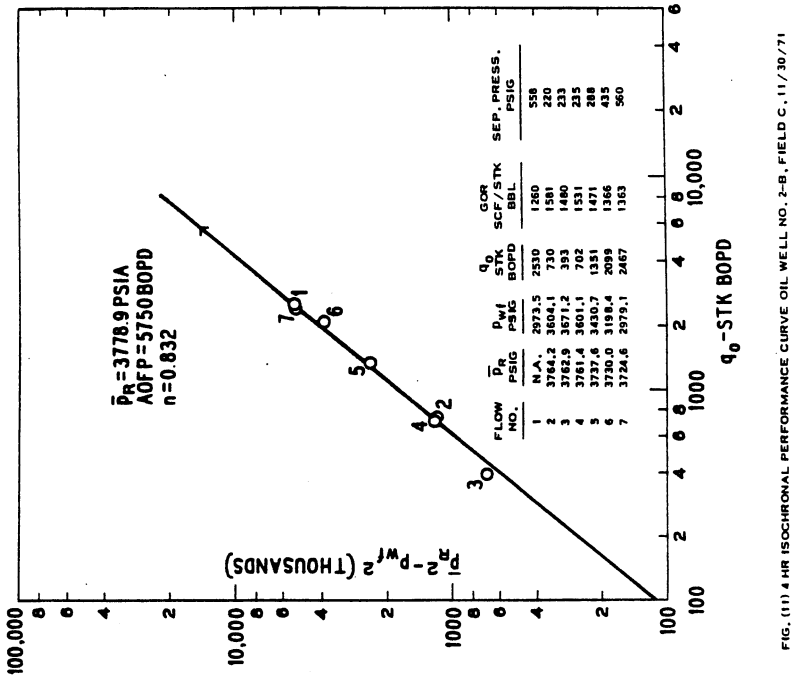

FLOW NO.	$\bar{P}_R$ PSIG	P_{wf} PSIG	q_o STK BOPD	GOR SCF/STK BBL	SEP. PRESS. PSIG
1	N.A.	2973.5	2530	1260	558
2	3764.2	3604.1	730	1581	220
3	3762.9	3671.2	393	1480	233
4	3761.4	3601.1	702	1531	235
5	3737.6	3430.7	1351	1471	288
6	3730.0	3198.4	2099	1366	435
7	3724.6	2979.1	2467	1363	560

FIG. (11) 4 HR ISOCHRONAL PERFORMANCE CURVE OIL WELL NO. 2-B, FIELD C, 11/30/71

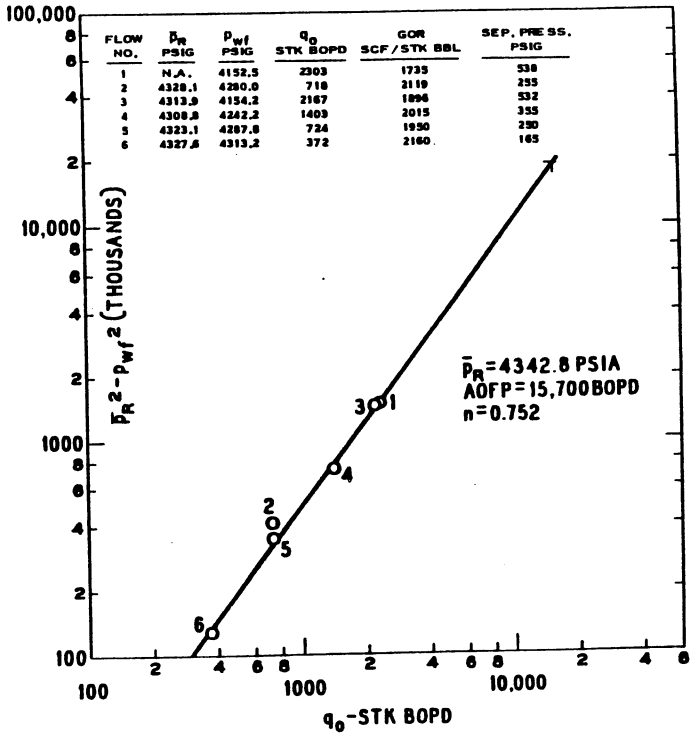

FIG. (13) 4 HR ISOCHRONAL PERFORMANCE CURVE OIL WELL NO. 4-d, FIELD C, 12/10/71

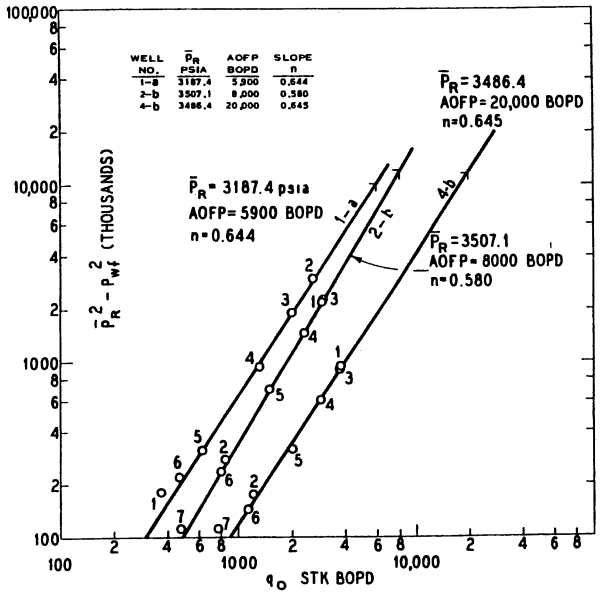

FIG. (14)

4 HR ISOCHRONAL PERFORMANCE CURVES OF OIL WELLS NO. 1-a, 2-b, AND 4-b, FIELD D DEMONSTRATING FLOW POINT ALIGNMENT.

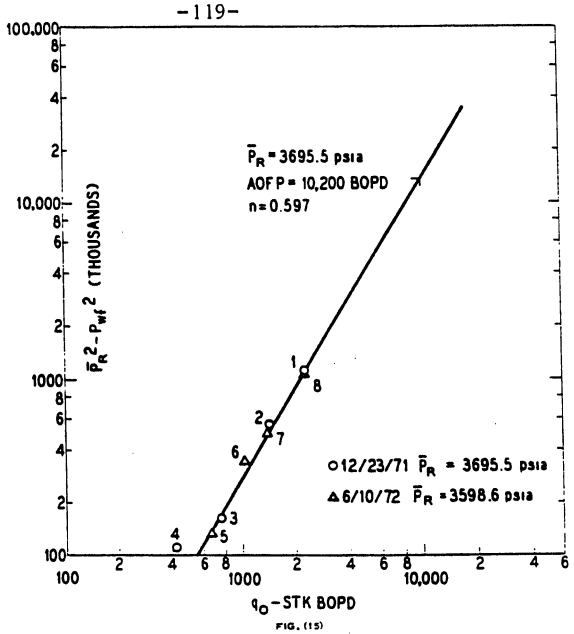

FIG. (15)

4 HR ISOCHRONAL PERFORMANCE CURVES OF WELL 5-C, FIELD D

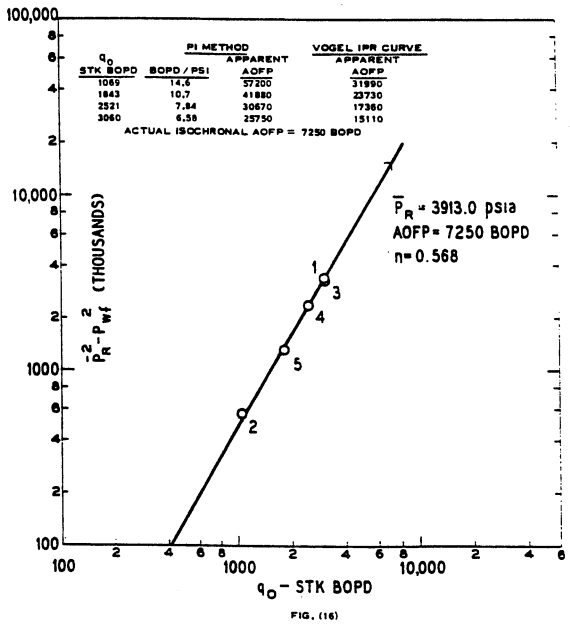

FIG. (16)

4 HR. ISOCHRONAL PERFORMANCE CURVE OIL WELL NO. 7-e, FIELD D, 12/25/71 WITH COMPARISONS OF CALCULATED AOFP'S USING PI AND VOGEL METHODS

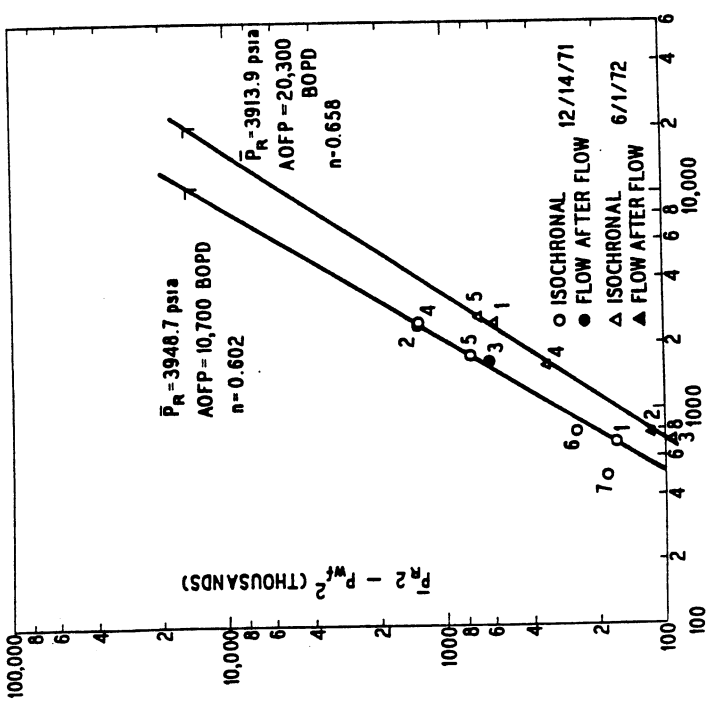

FIG. (17)
4HR ISOCHRONAL PERFORMANCE CURVES OF OIL WELL NO. 8-e, FIELD D
12/14/71 W/20 FT OF PERFORATIONS AND 6/1/72 W/60 FT OF PERFORATIONS

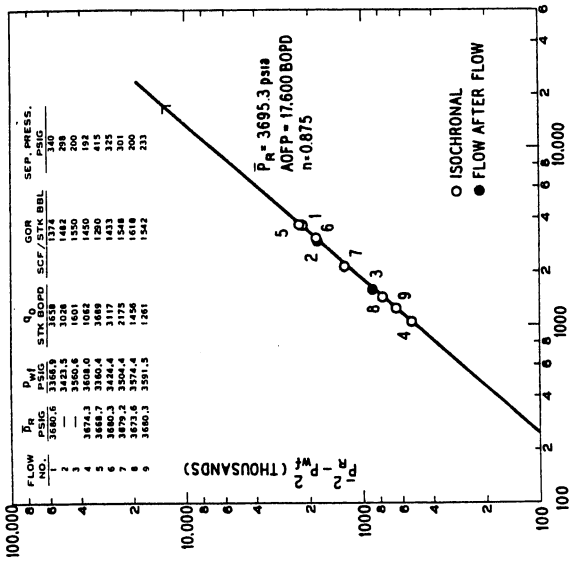

FIG. (18)
4HR ISOCHRONAL PERFORMANCE CURVE OF OIL WELL NO. 1-a, FIELD E, 3/16/72

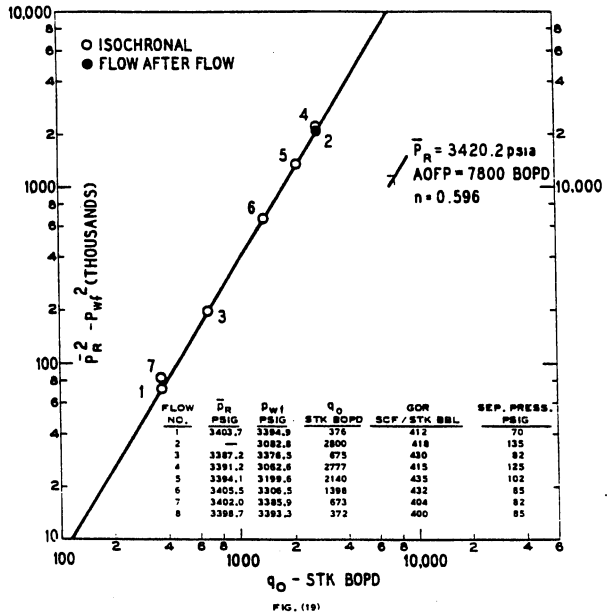

FLOW NO.	$\bar{P}_R$ PSIG	P_{wf} PSIG	q_o STK BOPD	GOR SCF/STK BBL	SEP. PRESS. PSIG
1	3403.7	3394.9	376	412	70
2	—	3082.8	2800	418	135
3	3387.2	3376.5	675	430	82
4	3391.2	3062.6	2777	415	125
5	3394.1	3199.6	2140	435	102
6	3405.5	3308.5	1398	432	85
7	3402.0	3385.9	673	404	82
8	3398.7	3393.3	372	400	85

FIG. (19)

4 HR. ISOCHRONAL PERFORMANCE CURVE OF OIL WELL NO. 1-a, FIELD F, 1/2/72

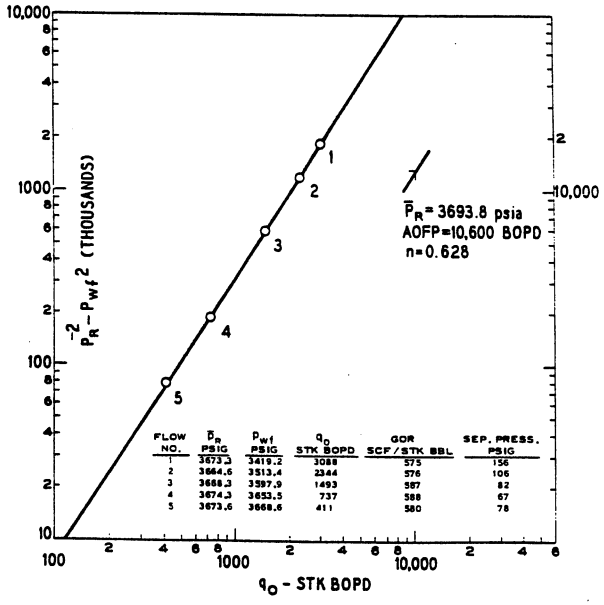

FLOW NO.	$\bar{P}_R$ PSIG	P_{wf} PSIG	q_o STK BOPD	GOR SCF/STK BBL	SEP. PRESS. PSIG
1	3673.3	3419.2	3088	575	156
2	3664.6	3513.4	2344	576	106
3	3668.3	3597.9	1493	587	82
4	3674.3	3653.5	737	588	67
5	3673.6	3668.6	411	580	78

FIG. (20)

4 HOUR ISOCHRONAL PERFORMANCE CURVE OF OIL WELL NO. 2-b, FIELD F, 1/7/72

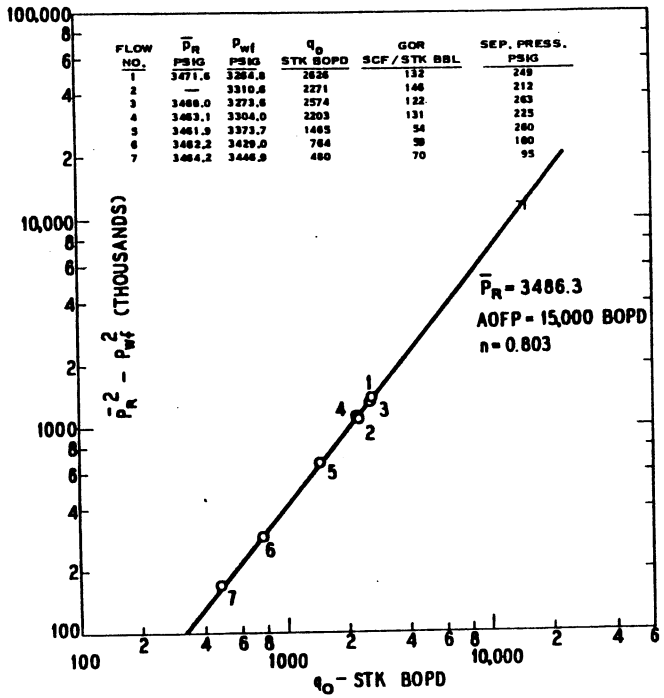

FIG. (21)
4HR ISOCHRONAL PERFORMANCE CURVE OF OIL WELL NO. 1-8, FIELD H, 7/24/72

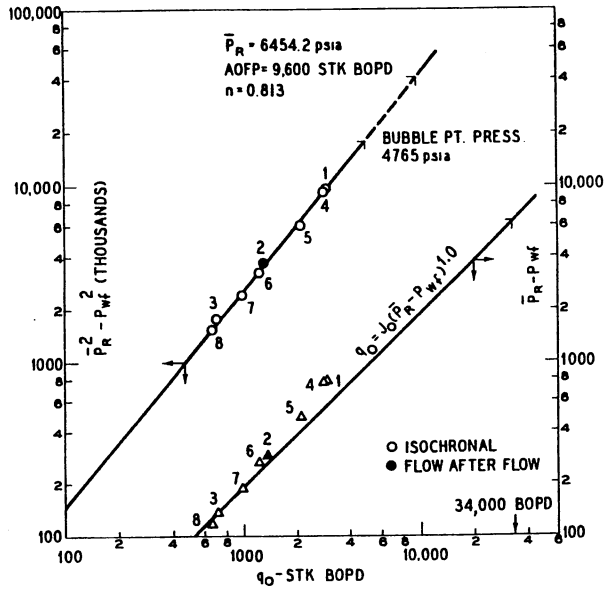

FIG. (22)
4 HR. ISOCHRONAL PERFORMANCE CURVE OF OIL WELL NO. 1 - a, FIELD G, 1/18/72

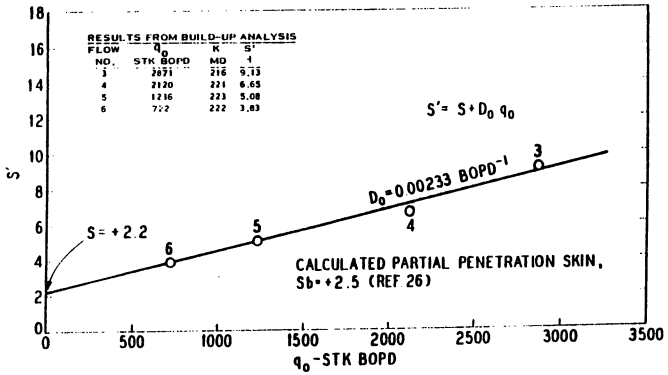

FIG. (23)

NON-DARCY FLOW EFFECT
SINGLE-PHASE LIQUID FLOW OIL WELL NO 1-a, FIELD G

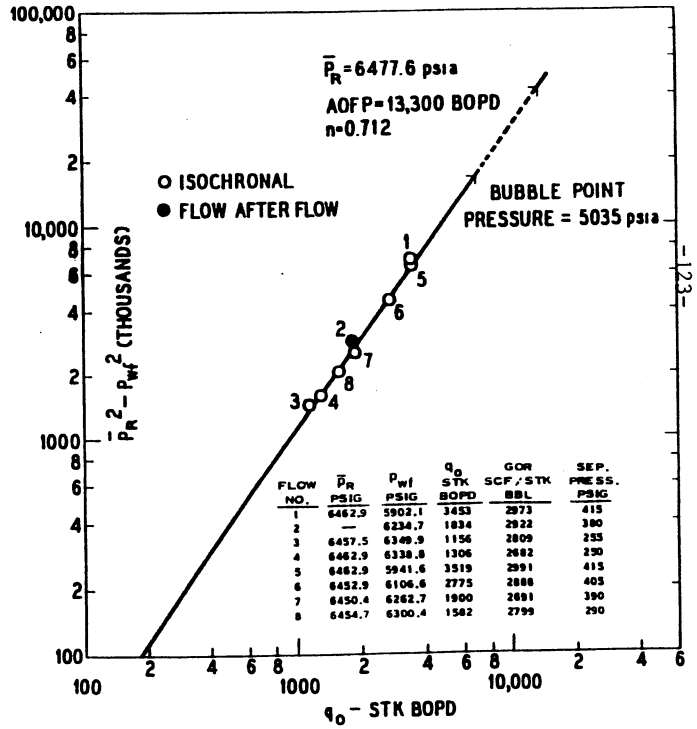

FIG. (24) 4 HOUR ISOCHRONAL PERFORMANCE CURVE OF OIL WELL 2-b, FIELD G, 1/8/72

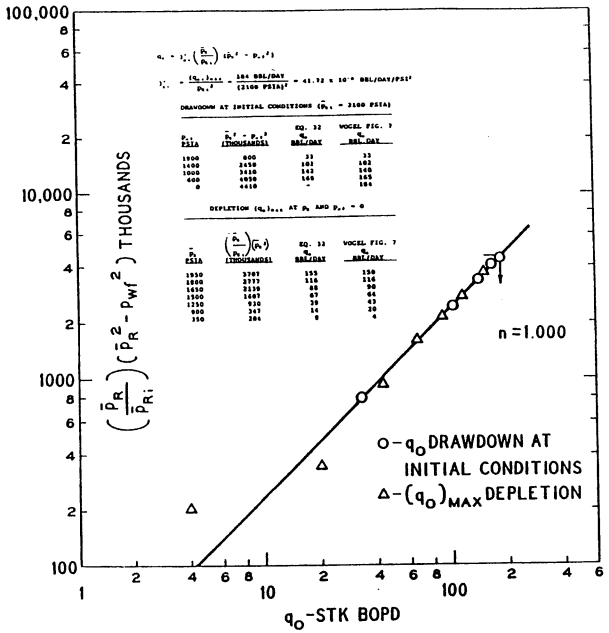

FIG. (25)

DISSOLVED GAS DRIVE DRAWDOWN AND DEPLETION PERFORMANCE CURVE. (AFTER VOGELS[5] FIG. 7)

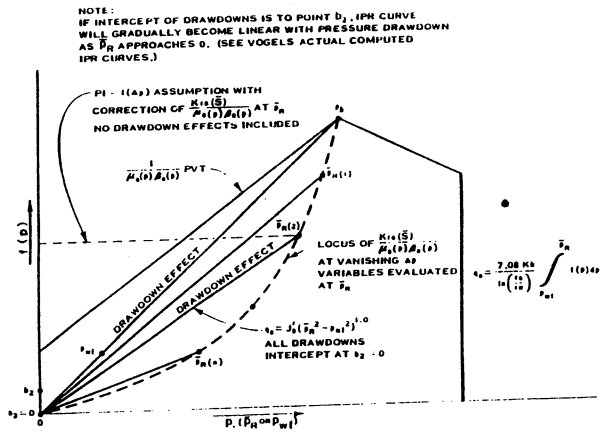

FIG. (26)

PRESSURE FUNCTION f(p) ILLUSTRATING DEPLETION AND DRAWDOWN

OIL WELLS

INFLOW PERFORMANCE

by

M. J. Fetkovich

OIL WELLS

Inflow Performance

•

The simplest and most widely used inflow performance or backpressure equation used to determine stabilized or pseudo-steady state flow at any backpressure p_{wf} is given by the productivity index or PI equation as

$$q_o = J\,(\bar{p}_R - p_{wf}) \qquad \ldots\ldots\ldots\ldots \quad (1)$$

In terms of measured data, the PI is represented as

$$J = \frac{q_o}{\bar{p}_R - p_{wf}} \qquad \ldots\ldots\ldots\ldots \quad (2)$$

where J = stabilized productivity index, STB/D-psi
q_o = measured stabilized surface oil flow rate, STB/D
p_{wf} = wellbore stabilized flowing pressure, psia
$\bar{p}_R$ = average reservoir pressure, psia

J is specifically defined as a productivity index determined from flow rate and pressure drawdown measurements. It normally varies with increasing drawdown -- i.e., is not a constant value. In terms of reservoir variables, the stabilized or pseudo-steady state productivity index J* at zero drawdown or as $p_{wf} \longrightarrow \bar{p}_R$ can be written as

$$J^* = \frac{7.08\ kh}{\left[\ln\left(\frac{r_e}{r_w}\right) - \frac{3}{4} + s\right]} \cdot \left(\frac{k_{ro}}{\mu_o \beta_o}\right)_{\bar{p}_R} \qquad \ldots\ldots\ldots\ldots \quad (3)$$

where J^* = stabilized productivity index at zero drawdown, STB/D-psi
k = effective permeability, Darcy
k_{ro} = relative permeability to oil, fraction
h = formation thickness, ft
μ_o = oil viscosity, cp (evaluated at $\bar{p}_R$)
β_o = oil formation volume factor, res bbl/STB (evaluated @ $\bar{p}_R$)
r_e = external boundary radius, ft
r_w = wellbore radius, ft
s = skin effect, dimensionless

J* is the special definition of productivity index J at a vanishing pressure drawdown, i.e., as p_{wf} approaches $\bar{p}_R$. Productivity index for a well is defined uniquely only at a zero drawdown.

Although this discussion will be limited to the pseudo-steady state, a transient form of the flow coefficient $J^*_{(t)}$ is also given for completeness.

$$J^*_{(t)} = \frac{7.08\ kh}{\left[\ln\sqrt{\frac{14.23\ kt}{\phi\mu\ c_t\ r_w^2}} + s\right]} \cdot \left(\frac{k_{ro}}{\mu_o\beta_o}\right)_{\bar{p}_R} \qquad \ldots\ldots\ldots \quad (4)$$

where t = time, days
ϕ = porosity, fraction
c_t = total compressibility, psi^{-1}

The above equations are perfectly valid for single-phase flow, i.e., $\bar{p}_R$ and p_{wf} are always greater than the reservoir bubble point pressure p_b. However, it has long been recognized that in reservoirs existing at or below the bubble point pressure, producing wells do not follow the simple PI Eqs. 1 and 2. Actual field tests indicate that oil flow rates obtained at increasing drawdowns decline much faster than would be predicted by Eq. 1.

Evinger and Muskat[1] first derived a theoretical productivity index for steady state radial flow in an attempt to account for the observed non-linear flow behavior of oil wells and arrived at the following equation

$$q_o = \frac{7.08\ kh}{\ln\left(\frac{r_e}{r_w}\right)} \int_{p_{wf}}^{p_e} f(p)dp \qquad \ldots\ldots\ldots\ldots \quad (5)$$

where p_e = reservoir pressure at the external boundary, psia

$$f(p) = \left(\frac{k_{ro}}{\mu_o\beta_o}\right)$$

Calculations using Eq. 5 with typical reservoir and fluid properties indicated that PI at a fixed reservoir pressure p_e decreases with increasing drawdown. This apparently complex form of an IPR equation found little use in the field.

In a computer study by Vogel[2], results based on two-phase flow theory were presented to indicate that a single empirical inflow performance relationship (IPR) equation might be valid for most solution-gas drive reservoirs. He found that a single dimensionless IPR equation approximately held for several hypothetical solution-gas drive reservoirs even when using a wide range of oil PVT properties and reservoir relative permeability curves. The fact that his study covered a wide range of fluid properties and relative permeability curves to obtain a single reference curve, cannot be over emphasized. Vogel proposed that his simple equation be used in place of the linear productivity index relationship for solution-gas drive reservoirs when the reservoir pressure is at or below the bubble-point pressure.

The proposed equation (IPR) in dimensionless form was given as

$$\frac{q_o}{q_{o(max)}} = 1 - 0.20\left(\frac{P_{wf}}{\bar{p}_R}\right) - 0.80\left(\frac{P_{wf}}{\bar{p}_R}\right)^2 \quad \ldots\ldots\ldots \quad (6)$$

where $q_{o(max)}$ = maximum producing rate at P_{wf} = 0 psia.

Fetkovich[3], in an attempt to verify the Vogel IPR relationship, obtained isochronal and flow-after-flow multi-point backpressure test field data on some 40 different oil wells. The reservoirs in which oil well multi-point backpressure tests were obtained ranged from highly undersaturated, to saturated at initial reservoir pressure, to a partially depleted field with a gas saturation existing above the critical (equilibrium) gas saturation. A form of an IPR equation similar to that used for gas wells was found to be valid for tests conducted in all three reservoir fluid states, even for the conditions where flowing pressures were well above the bubble point pressures. Permeabilities of the reservoirs ranged from 6 to > 1000 millidarcies.

In all cases, oil well backpressure curves were found to follow the same general form as that used to express the rate-pressure relationship of a gas well

$$q_o = J'\,(\bar{p}_R^{\,2} - P_{wf}^{\,2})^n \quad \ldots\ldots\ldots\ldots\ldots \quad (7)$$

For the 40 oil well backpressure tests examined, the exponent n was found to lie between 0.568 and 1.000, that is, within the limits commonly accepted for gas well backpressure curves.

In terms of measured data J' is defined by

$$J' = \frac{q_o}{(\bar{p}_R^{\,2} - P_{wf}^{\,2})^n} \quad \ldots\ldots\ldots\ldots\ldots \quad (8)$$

where J'= stabilized productivity index, STB/D-$(psi)^{2n}$.

The exponent n is usually determined from a multipoint or isochronal backpressure test and is an indicator of the existence of non-Darcy flow. If n = 1, non-Darcy flow is assumed not to exist.

With productivity index expressed in terms of pressures squared, $\bar{p}_R^2$ and p_{wf}^2

$$J' = \frac{J^*}{2\bar{p}_R} \qquad \ldots\ldots\ldots\ldots\ldots\ldots \quad (9)$$

Expressing the pseudo-steady state J' in terms of reservoir variables

$$J' = \frac{7.08\ kh}{2\bar{p}_R\left[\ln\left(\frac{r_e}{r_w}\right) - \frac{3}{4} + s\right]} \cdot \left(\frac{k_{ro}}{\mu_o\beta_o}\right)_{\bar{p}_R} \qquad \ldots\ldots\ldots \quad (10)$$

$$\text{or} \quad q_o = \frac{7.08\ kh}{\left[\ln\left(\frac{r_e}{r_w}\right) - \frac{3}{4} + s\right]} \cdot \left(\frac{k_{ro}}{\mu_o\beta_o}\right)_{\bar{p}_R} \frac{(\bar{p}_R^2 - p_{wf}^2)^{1.0}}{2\bar{p}_R} \qquad \ldots \quad (11)$$

Expressed in a form with reservoir variables and a non-darcy flow term, D, where the resulting n would be less than 1.0 and a function of D.

$$q_o = \frac{7.08\ kh}{\left[\ln\left(\frac{r_e}{r_w}\right) - \frac{3}{4} + s + Dq_o\right]} \cdot \left(\frac{k_{ro}}{\mu_o\beta_o}\right)_{\bar{p}_R} \frac{(\bar{p}_R^2 - p_{wf}^2)}{2\bar{p}_R} \qquad \ldots \quad (12)$$

When $\bar{p}_R$ is equal to or less than the bubble point pressure p_b and n is less than 1, a non-Darcy flow term D is indicated. When D = 0, n = 1. The term D is normally developed from multi-point test data. As will be indicated in a later example, it is possible to have D = 0 and n less than 1.0 for undersaturated wells producing at flowing pressures below the bubble point pressure. (See Figure 8 of Reference 3.) This is strictly a result of the shape of the $\frac{k_{ro}}{\mu_o\beta_o}$ pressure function.

Expressing the backpressure form of the IPR equation in terms similar to that of Vogel's equation (instead of Vogel's equation in terms of the backpressure curve) we have from Eq. 7

$$q_o = J' (\bar{p}_R^{\,2} - p_{wf}^{\,2})^n$$

and $$q_{o(max)} = J' (\bar{p}_R^{\,2})^n \text{ or } J' = \frac{q_{o(max)}}{(\bar{p}_R^{\,2})^n} \quad \ldots\ldots\ldots\ldots (13)$$

Substituting and rearranging yields

$$\frac{q_o}{q_{o(max)}} = \left[\frac{\bar{p}_R^{\,2} - p_{wf}^{\,2}}{\bar{p}_R^{\,2}} \right]^n = \left[1 - \left(\frac{p_{wf}}{\bar{p}_R} \right)^2 \right]^n \quad \ldots\ldots (14)$$

For n = 1, we have the simplest possible form of a multi-phase IPR equation based on results obtained from actual field data

$$\frac{q_o}{q_{o(max)}} = 1 - \left(\frac{p_{wf}}{\bar{p}_R} \right)^2 \quad \ldots\ldots\ldots\ldots (15)$$

Comparing Eq. 15 to vogel's Eq. 6, which was derived only from computer simulation data, we see that the coefficient for $p_{wf}/\bar{p}_R$ is 0 and the coefficient for $(p_{wf}/\bar{p}_R)^2$ is equal to 1. This results in an IPR Eq. 15 that yields a slightly more conservative answer than given by Vogel's original equation. (Actually, Vogel's Figure 7 shows computer model calculated IPR results less than obtained from his reference equation.) Not included in any of Vogel's simulation runs were effects of non-Darcy flow in the reservoir or perforation restrictions which in the field result in n values less than 1.0 and an even more severe IPR rate reduction relationship.

IPR Example Problem

The following example problem illustrates the various possible methods of computing inflow rates.

An oil well is producing at a stabilized rate of 70 STB/D at a bottomhole flowing pressure p_{wf} = 1147 psia. The average reservoir shutin static pressure, $\bar{p}_R$ = 1200 psia. Calculate the maximum possible flow rate, q_o at 0 psig, and the producing rate if artificial lift were installed to lower the bottomhole flowing pressure to 550 psia. Make the calculations using the PI Eq. 1, Vogel's method and the backpressure curve method with n = 1.0 and n = 0.650. (The data is from an actual IPR test reported in Reference 3.)

Productivity Index (PI).

$$J = \frac{70 \text{ BOPD}}{1200 - 1147} = 1.32 \text{ STB/D-psi}$$

$$q_o \text{ (15 psi)} = J (\bar{p}_R - p_{wf}) = 1.32 (1200 - 15) = \underline{1564 \text{ STB/D}}$$

$$q_o \text{ (550 psi)} = 1.32 (1200 - 550) = \underline{858 \text{ STB/D}}$$

Vogel IPR.

$$q_o = 70 \text{ BOPD} ; \frac{p_{wf}}{\bar{p}_R} = \frac{1147}{1200} = 0.9558; \left(\frac{p_{wf}}{\bar{p}_R}\right)^2 = 0.9136$$

$$\frac{q_o}{q_{o(max)}} = 1 - 0.20 \left(\frac{p_{wf}}{\bar{p}_R}\right) - 0.80 \left(\frac{p_{wf}}{\bar{p}_R}\right)^2$$

$$\frac{q_o}{q_{o(max)}} = 1 - 0.19116 - 0.73088 = 0.07796$$

$$q_{o(max)} = \frac{70 \text{ BOPD}}{0.07796} = 898 \text{ BOPD}$$

q_o @ p_{wf} = 15 psia

$$\frac{q_o \text{ (15 psi)}}{q_{o(max)}} = 1 - 0.20 \left(\frac{15}{1200}\right) - 0.80 \left(\frac{15}{1200}\right)^2 = 0.99738$$

$$q_o \text{ (15 psi)} = q_{o(max)} (0.99738) = 898 \text{ BOPD } (0.99738) = \underline{896 \text{ BOPD}}$$

q_o @ p_{wf} = 550 psia

$$\frac{q_o \text{ (550 psi)}}{q_{o(max)}} = 1 - 0.20 \left(\frac{550}{1200}\right) - 0.80 \left(\frac{550}{1200}\right)^2 = 0.740277$$

$$q_o \text{ (550 psi)} = q_{o(max)} \text{ (0.740277)} = 898 \text{ BOPD (0.740277)} = \underline{665 \text{ BOPD}}$$

Backpressure curve (n = 1.0) IPR.

$$q_o = 70 \text{ BOPD} \; ; \; \bar{p}_R^2 = (1200)^2 = 1{,}440{,}000$$
$$p_{wf}^2 = (1147)^2 = 1{,}315{,}609$$

$$J' = \frac{70 \text{ BOPD}}{(1200)^2 - (1147)^2} = \frac{70}{124{,}391} = 0.00056274 \text{ STB/D-psi}^2$$

$$q_o \text{ (15 psi)} = J' (\bar{p}_R^{\,2} - p_{wf}^2) = 0.00056274 \text{ (1,440,000 - 225)} = \underline{810 \text{ BOPD}}$$

$$q_o \text{ (550 psi)} = 0.00056274 \text{ (1,440,000 - 302,500)} = \underline{640 \text{ BOPD}}$$

Using the dimensionless backpressure curve form in terms of $q_o/q_{o(max)}$ and $p_{wf}/\bar{p}_R$ with n = 1.0

$$q_o = 70 \text{ BOPD} \; ; \left(\frac{p_{wf}}{\bar{p}_R}\right)^2 = \left(\frac{1147}{1200}\right)^2 = 0.9136$$

$$\frac{q_o}{q_{o(max)}} = 1 - \left(\frac{p_{wf}}{\bar{p}_R}\right)^2 = 1 - 0.9136 = 0.0864$$

$$q_{o(max)} = \frac{70 \text{ BOPD}}{0.0864} = 810 \text{ BOPD}$$

q_o @ p_{wf} = 550 psia

$$\frac{q_o \text{ (550 psi)}}{q_{o(max)}} = 1 - \left(\frac{550}{1200}\right)^2 = 1 - 0.168056 = 0.78993$$

$$q_o \text{ (550 psi)} = 810 \text{ (0.78993)} = \underline{640 \text{ BOPD}}$$

Backpressure equation (n = 0.650) IPR.

$$q_o = 70 \text{ BOPD} \; ; \; \bar{p}_R = (1200)^2 = 1{,}440{,}000$$
$$p_{wf} = (1147)^2 = 1{,}315{,}609$$

$$J' = \frac{70 \text{ BOPD}}{(1{,}440{,}000 - 1{,}315{,}609)^{0.650}} = \frac{70 \text{ BOPD}}{2049.3} = 0.0341580 \text{ STB/D-psi}^{2n}$$

$$q_o \text{ (15 psi)} = J' (\bar{p}_R^{\,2} - p_{wf}^{2})^{0.650} = 0.0341580 \text{ (1,440,000 - 225)}^{0.650}$$

$$q_o \text{ (15 psi)} = 0.0341580 \text{ (10066.8)} = \underline{344 \text{ BOPD}}$$

$$q_o \text{ (550 psi)} = 0.0341580 \text{ (1,440,000 - 302,500)}^{0.650} = \underline{295 \text{ BOPD}}$$

Using the dimensionless backpressure curve form in terms of $q_o/q_{o(max)}$, $p_{wf}/\bar{p}_R$ and n = 0.650

$$q_o = 70 \text{ BOPD}; \left(\frac{p_{wf}}{\bar{p}_R}\right)^2 = \left(\frac{1147}{1200}\right)^2 = 0.9136$$

$$\frac{q_o}{q_{o(max)}} = \left[1 - \left(\frac{p_{wf}}{\bar{p}_R}\right)^2\right]^{0.650} = \left[1 - 0.9136\right]^{0.650} = 0.203579$$

$$q_{o(max)} = \frac{70 \text{ BOPD}}{0.203579} = 344 \text{ BOPD}$$

$\underline{q_o \text{ @ } p_{wf} = 550 \text{ psia}}$

$$\frac{q_o \text{ (550 psi)}}{q_{o(max)}} = \left[1 - \left(\frac{550}{1200}\right)^2\right]^{0.650} = 0.857892$$

$$q_o = 344 \text{ BOPD } (0.857892) = \underline{295 \text{ BOPD}}$$

Again, this example problem is based on field data where several rates were measured to establish the real IPR relationship of the well. The real absolute open flow of the well was 340 BOPD. This is 38% of the rate predicted by Vogel's IPR equation and 42% of the rate predicted by the backpressure equation with n = 1. A value of n = 0.650 as illustrated in this example is required to match the field data. A non-Darcy flow term D is indicated for this test.

Single-Phase and Two-Phase IPR Equation

Fetkovich[3] gives a general equation that treats flow both above and below the bubble point pressure for an undersaturated oil well.

$$q_o = J^* (\bar{p}_R - p_b) + J' (p_b^2 - p_{wf}^2) \quad \ldots\ldots\ldots\ldots (16)$$

where $$J' = J^* (\mu_o\beta_o)_{\bar{p}_R,\ p_b} \cdot \left(\frac{a_2}{2}\right) \quad \ldots\ldots\ldots\ldots (17)$$

Assuming $(\mu_o\beta_o)$ is a constant value above the bubble point pressure equal to $(\mu_o\beta_o)_b$ (the basis of the constant PI assumption for flow above the bubble point pressure, p_b) then $a_2 = \dfrac{1}{p_b(\mu_o\beta_o)_b}$ (see Appendix of Reference 3).

Then

$$J' = \frac{J^* (\mu_o\beta_o)_b}{2p_b (\mu_o\beta_o)_b} = \frac{J^*}{2p_b} \quad \ldots\ldots\ldots\ldots (18)$$

Substituting Eq. 18 into 16 we obtain the final form of the single phase and two phase IPR equation

$$q_o = J^* (\bar{p}_R - p_b) + \frac{J^*}{2p_b} (p_b^2 - p_{wf}^2) \quad \ldots\ldots\ldots (19)$$

Example Problem

The following example problem illustrates the method of computing inflow rates for flows both above and below the bubble point pressure of an undersaturated oil well.

An oil well is producing at a rate of 50 STB/D at a bottomhole flowing pressure of 2100 psia. The reservoir average shutin pressure is 3200 psia with a bubble point pressure of 1800 psia.

Calculate the maximum possible flow rate, q_o at p_{wf} = 0 psig and the producing rate at 550 psia bottomhole flowing pressure. (For flows above p_b, J = J*.)

$$J = J^* = \frac{q_o}{(\bar{p}_R - p_{wf})}$$

$$J^* = \frac{50 \text{ BOPD}}{(3200 - 2100)} = \frac{50 \text{ BOPD}}{1100} = 0.045454 \text{ STB/D-psi}$$

$$q_o \text{ (15 psi)} = J^* (\bar{p}_R - p_b) + \frac{J^*}{2p_b} (p_b^2 - p_{wf}^2)$$

$$q_o \text{ (15 psi)} = 0.045454 \text{ (3200 - 1800)} + \frac{0.045454}{2 \text{ (1800)}} (1800^2 - 15^2)$$

$$q_o \text{ (15 psi)} = 64 \text{ BOPD} + 0.00012626 \text{ (3,240,000 - 225)}$$

$$q_o \text{ (15 psi)} = 64 \text{ BOPD} + 41 \text{ BOPD} = \underline{105 \text{ BOPD}}$$

Compares to 145 BOPD if regular (PI) productivity index equation assumed valid to 15 psia.

q_o @ p_{wf} = 550 psia

$$q_o \text{ (550 psi)} = J^* (\bar{p}_R - p_b) + \frac{J^*}{2p_b} (p_b^2 - p_{wf}^2)$$

$$q_o \text{ (550 psi)} = 0.045454 \text{ (3200 - 1800)} + \frac{0.045454}{2 \text{ (1800)}} (1800^2 - 550^2)$$

$$q_o \text{ (550 psi)} = 64 \text{ BOPD} + 0.000012626 \text{ (3,240,000 - 302,500)}$$

$$q_o \text{ (550 psi)} = 64 \text{ BOPD} + 37 \text{ BOPD} = \underline{101 \text{ BOPD}}$$

The additional 535 psi pressure drop from 550 psia to 15 psia results in only 4 BOPD increase. It is significant to point out that if several flows, all with flowing pressure p_{wf} below the bubble pressure p_b, were calculated using the above equation and example then plotted as a backpressure curve but with $\bar{p}_R^2 - p_{wf}^2$, it would indicate a value of n = 0.820. We would have an indicated n less than 1.0 without a non-Darcy flow term D. With the uncertainty involved in really knowing the <u>true</u> bubble point pressure of a particular well, we could obtain test n values less than 1.0 without non-Darcy flow existing.

To more clearly illustrate a case of drawdown data obtained at flowing pressures below the bubble point pressure to obtain J* we will use the 550 psia rate obtained above and the previously specified data. Actual unrounded calculated rate is 100.73 BOPD.

$$q_o = J^* (\bar{p}_R - p_b) + \frac{(p_b^2 - p_{wf}^2)}{2p_b}$$

$$J^* = \frac{q_o}{\left[(\bar{p}_R - p_b) + \frac{(p_b^2 - p_{wf}^2)}{2p_b}\right]}$$

$$J^* = \frac{100.73 \text{ BOPD}}{\left[(3200 - 1800) + \frac{(3{,}240{,}000 - 302{,}500)}{2\,(1800)}\right]}$$

$$J^* = \frac{100.73 \text{ BOPD}}{[1400 + 816]} = \frac{100.73 \text{ BOPD}}{2216 \text{ psi}} = 0.045450 \text{ STB/D psi (Good Check)}$$

Future Inflow Performance

Standing[4] presented a method for adjusting IPR utilizing Vogel's equation from a measured condition to a future reservoir pressure $\bar{p}_R$. It is based on the fact that productivity index can be defined uniquely only at a zero drawdown, $p_{wf} \longrightarrow \bar{p}_R$.

$$J^* = \lim_{\Delta p \to 0} J \qquad \ldots\ldots\ldots\ldots\ldots\ldots (20)$$

Applying the limit condition using Vogel's equation yielded

$$J^* = \frac{1.8\, q_{o(max)}}{\bar{p}_R} \qquad \ldots\ldots\ldots\ldots\ldots (21)$$

Using the same approach with the backpressure equation and n = 1

$$\frac{q_o}{q_{o(max)}} = \left[1 - \left(\frac{p_{wf}}{\bar{p}_R}\right)^2\right]^{1.0}$$

yields

$$J^* = \frac{2\, q_{o(max)}}{\bar{p}_R} \qquad \ldots\ldots\ldots\ldots\ldots (22)$$

If we define $q_o*_{(max)}$ as that absolute open flow potential, we would obtain assuming conventional Δp productivity index were used

$$q_o*_{(max)} = J* (\bar{p}_R - 0)$$

$$q_o*_{(max)} = J* \bar{p}_R = 2\, q_{o(max)} \qquad \ldots\ldots\ldots\ldots\ldots\ldots (23)$$

Note that the "real" $q_{o(max)}$ is 1/2 that assuming a Δp productivity index relationship. This is more clearly seen from the figure below and Eq. 24.

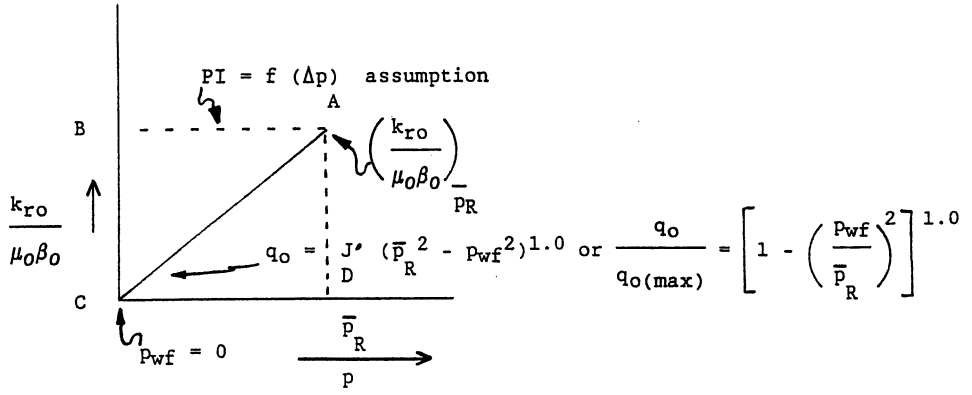

Fig. 34-5. Simple pressure function $\left(\frac{k_{ro}}{\mu_o\beta_o}\right)$ for Δp^2 relationship and n = 1.0

In terms of the Evinger-Muskat equation

$$q_o = J* \int_{p_{wf}}^{\bar{p}_R} \frac{k_{ro}}{(\mu_o\beta_o)}\, dp = J* \text{ (area under curve)} \qquad \ldots (24)$$

For the n = 1.0 IPR relationship, the area under the curve (A, C, D) is exactly 1/2 that area (A, B, C, D) assuming Δp productivity index relationship when $p_{wf} = 0$.

Example Problem

Using Standing's example problem data we will

(1) Calculate $J*_p$ present from present flow data.
(2) Adjust $J*_p$ to a future $J*_f$.
(3) Calculate a future rate at p_{wf} = 1200 psig.

The following was given in Standing's[4] example. The present productivity index, J, has been determined to be 0.92 at a flow rate of 400 BOPD with p_{wf} = 1815 psig. Average reservoir pressure, $\bar{p}_R$, at this time is 2250 psig. Future reservoir pressure $\bar{p}_R$ will be 1800 psig. $(k_{ro}/\mu_o\beta_o)$ = 0.2234 present and 0.1659 future.

$$q_{o(max)} = \frac{q_o}{\left[1 - \left(\frac{p_{wf}}{\bar{p}_R}\right)^2\right]} = \frac{400}{\left[1 - \left(\frac{1830}{2265}\right)^2\right]} = 1152 \text{ BOPD}$$

$$J^* = \frac{2\, q_{o(max)}}{\bar{p}_R} = \frac{2\,(1152)}{2265} = 1.017$$

$$J^*_f = J^*_p \frac{\left(\frac{k_{ro}}{\mu_o\beta_o}\right)_f}{\left(\frac{k_{ro}}{\mu_o\beta_o}\right)_p} = 1.017 \quad \frac{0.1659}{0.2234} = 0.755$$

$$q_{o(max)f} = \frac{J^*_f\,(\bar{p}_R)}{2} = \frac{0.755\,(1800 + 15)}{2} = 685 \text{ BOPD}$$

$$q_{of}\ (1200 \text{ psig}) = q_{o(max)f}\left[1 - \left(\frac{p_{wf}}{\bar{p}_R}\right)^2\right] = 685\left[1 - \left(\frac{1215}{1815}\right)^2\right] = 378 \text{ BOPD}$$

REFERENCES

1. Evinger, H. H. and Muskat, M.: "Calculation of Theoretical Productivity Factor," Trans, AIME (1942) 146, 126.

2. Vogel, J. V.: "Inflow Performance Relationships for Solution Gas Drive Wells," J. Pet. Tech. (Jan. 1968), 83.

3. Fetkovich, M.J.: "The Isochronal Testing of Oil Wells," Paper SPE 4529 Presented at the 48th Annual Fall Meeting, Las Vegas, Nev., Sept 30 - October 3, 1973. (SPE Reprint Series No. 14, 265.)

4. Standing, M.B.: "Concerning the Calculation of Inflow Performance of Wells Producing from Solution Gas Drive Reservoirs," J. Pet. Tech. (Sept. 1971) 1141.

DECLINE CURVE ANALYSIS USING TYPE CURVES

by

M. J. Fetkovich
SPE, Phillips Petroleum Co.

SPE 4629

Original manuscript received in Society of Petroleum Engineers office Aug. 3, 1973. Paper accepted for publication Aug. 7, 1974. Revised manuscript received March 31, 1980. Paper first presented at the SPE 48th Fall Meeting held in Las Vegas, Sept. 30 - Oct. 3, 1973.

DECLINE CURVE ANALYSIS USING TYPE CURVES

Introduction

Rate-time decline curve extrapolation is one of the oldest and most often used tools of the petroleum engineer. The various methods used always have been regarded as strictly empirical and generally not scientific. Results obtained for a well or lease are subject to a wide range of alternate interpretations, mostly as a function of the experience and objectives of the evaluator. Recent efforts in the area of decline curve analysis have been directed toward a purely computerized statistical approach, its basic objective being to arrive at a unique "unbiased" interpretation. As pointed out in a comprehensive review of the literature by Ramsay,[1] "In the period from 1964 to date (1968), several additional papers were published which contribute to the understanding of decline curves but add little new technology."

A new direction for decline curve analysis was given by Slider[2] with his development of an overlay method to analyze rate-time data. Because his method was rapid and easily applied, it was used extensively by Ramsay in his evaluation of some 200 wells to determine the distribution of the decline curve exponent b. Gentry's[3] Fig. 1 displaying the Arps'[4] exponential, hyperbolic, and harmonic solutions all on one curve also could be used as an overlay to match all of a well's decline data. However, he did not illustrate this in his example application of the curve.

The overlay method of Slider is similar in principle to the log-log type curve matching procedure presently being employed to analyze constant-rate pressure buildup and drawdown data.[5-9] The exponential decline, often used in decline curve analysis, readily can be shown to be a long-time solution of the constant-pressure case.[10-13] It followed then that a log-log type curve matching procedure could be developed to analyze decline curve data.

This paper demonstrated that both the analytical constant-pressure infinite (early transient period for finite systems) and finite reservoir solutions can be placed on a common dimensionless log-log type curve with all the standard "empirical" exponential, hyperbolic, and harmonic decline curve equations developed by Arps. Simple combinations of material balance equations and new forms of oilwell rate equations from the recent work of Fetkovich[14] illustrate under what circumstances specific values of the hyperbolic decline exponent b should result in dissolved-gas-drive reservoirs. Log-log type curve analysis then is performed using these curves with declining rate data completely analogous to the log-log type curve matching procedure presently being employed with constant-rate case pressure transient data.

Arps' Rate-Time Equations

Nearly all conventional decline curve analysis is based on the empirical rate-time equations given by Arps[4] as

$$\frac{q(t)}{q_i} = \frac{1}{\left[1 + bD_it\right]^{1/b}} \quad \ldots\ldots\ldots\ldots (1)$$

For b = 0, we can obtain the exponential decline equation from Eq. 1,

$$\frac{q(t)}{q_i} = \frac{1}{e^{D_it}} , \quad \ldots\ldots\ldots\ldots (2)$$

and for b = 1, referred to as harmonic decline, we have

$$\frac{q(t)}{q_i} = \frac{1}{[1 + D_it]} \quad \ldots\ldots\ldots\ldots (3)$$

A unit solution (D_i = 1) of Eq. 1 was developed for values of b between 0 and 1 in 0.1 increments. The results are plotted as a set of log-log type curves (Fig. 1) in terms of a decline curve dimensionless rate,

$$q_{Dd} = \frac{q(t)}{q_i} , \quad \ldots\ldots\ldots\ldots (4)$$

and a decline curve dimensionless time,

$$t_{Dd} = D_it . \quad \ldots\ldots\ldots\ldots (5)$$

From Fig. 1 we see that when all the basic decline curves and normal ranges of b are displayed on a single graph, all curves coincide and become indistinguishable at $t_{Dd} \cong 0.3$. Any data existing before a t_{Dd} of 0.3 will appear to be an exponential decline regardless of the true value of b and, thus, plot as a straight line on semilog paper. A statistical or least-squares approach could calculate any value of b between 0 and 1.

Analytical Solutions

(Constant-Pressure at Inner Boundary)

Constant well pressure solutions to predict declining production rates with time were published first in 1933 by Moore, Schilthuis and Hurst,[10] and Hurst.[11] Results were presented for infinite and finite, slightly compressible, single-phase plane radial flow systems. The results were presented in graphical form in terms of a dimensionless flow rate and a dimensionless time. The dimensionless flow rate q_D can be expressed as

$$q_D = \frac{141.3\ q(t)\ \mu\beta}{kh(p_i - p_{wf})}\ , \quad \ldots\ldots\ldots\ldots \quad (6)$$

and the dimensionless time t_D as

$$t_D = \frac{0.00634\ kt}{\phi\mu c_t r_w^2}\ . \quad \ldots\ldots\ldots\ldots \quad (7)$$

The original publications did not include tabular values of q_D and t_D. For use in this paper infinite solution values were obtained from Ref. 15, while the finite values were obtained from Ref. 16. The infinite solution and finite solutions for r_e/r_w from 10 to 100,000 are plotted in Figs. 2a and 2b.

Most engineers utilize the constant-pressure solution not in a single constant-pressure problem but as a series of constant-pressure step functions to solve water influx problems using the dimensionless cumulative production Q_D.[13]. The relationship between Q_D and q_D is

$$\frac{d(Q_D)}{dt_D} = q_D\ . \quad \ldots\ldots\ldots\ldots \quad (8)$$

Fetkovich[17] presented a simplified approach to water influx calculations for finite systems that gave results that compared favorably with the more rigorous analytical constant-pressure solutions. Eq. 3 of his paper for a constant-pressure p_{wf}, can be written as

$$q(t) = \frac{J_o(p_i - p_{wf})}{e^{\left[\frac{(q_i)_{max}}{N_{pi}}\right]t}}\ , \quad \ldots\ldots\ldots\ldots \quad (9)$$

but

$$q_i = J_o(p_i - p_{wf})\ , \quad \ldots\ldots\ldots\ldots \quad (10)$$

and

$$J_o = \frac{(q_i)_{max}}{p_i}\ . \quad \ldots\ldots\ldots\ldots \quad (11)$$

Substituting Eq. 11 into Eq. 10 we can write

$$(q_i)_{max} = \frac{q_i}{\left[1 - \frac{p_{wf}}{p_i}\right]} \quad \ldots\ldots\ldots\ldots (12)$$

Now substituting Eqs. 10 and 12 into Eq. 9 we obtain

$$\frac{q(t)}{q_i} = e^{-\left[\frac{q_i t}{\left(1 - \frac{p_{wf}}{p_i}\right) N_{pi}}\right]} \quad \ldots\ldots\ldots\ldots (13)$$

Eq. 13 can be considered as a derivation of the exponential decline equation in terms of reservoir variables and the constant-pressure imposed on the well. For the same well, different values of a single constant backpressure p_{wf} always will result in an exponential decline - i.e., the level of backpressure does not change the type of decline. For $p_{wf} = 0$, a more realistic assumption for a well on true wide-open decline, we have

$$\frac{q(t)}{q_i} = e^{-\left[\frac{(q_i)_{max}}{N_{pi}}\right] t} \quad \ldots\ldots\ldots\ldots (14)$$

In terms of the empirical exponential decline curve, Eq. 2, D_i is then defined as

$$D_i = \frac{(q_i)_{max}}{N_{pi}} \quad \ldots\ldots\ldots\ldots (15)$$

In terms of a dimensionless time for decline curve analysis we have from Eqs. 5 and 15

$$t_{Dd} = \left[\frac{(q_i)_{max}}{N_{pi}}\right] t \quad \ldots\ldots\ldots\ldots (16)$$

Defining N_{pi} and $(q_i)_{max}$ in terms of reservoir variables

$$N_{pi} = \frac{\pi(r_e^2 - r_w^2)\phi c_t h p_i}{5.615\ \beta}, \quad \ldots\ldots\ldots\ldots (17)$$

and

$$(q_i)_{max} = \frac{khp_i}{141.3\ \mu\beta\left[\ln\left(\frac{r_e}{r_w}\right) - \frac{1}{2}\right]} \quad \ldots\ldots\ldots (18)$$

The decline curve dimensionless time, in terms of reservoir variables, becomes

$$t_{Dd} = \frac{0.00634\ kt}{\phi\mu c_t r_w^2} \cdot \frac{1}{\frac{1}{2}\left[\left(\frac{r_e}{r_w}\right)^2 - 1\right]\left[\ln\left(\frac{r_e}{r_w}\right) - \frac{1}{2}\right]}, \quad \ldots (19)$$

or

$$t_{Dd} = \frac{t_D}{\frac{1}{2}\left[\left(\frac{r_e}{r_w}\right)^2 - 1\right]\left[\ln\left(\frac{r_e}{r_w}\right) - \frac{1}{2}\right]} \quad \ldots\ldots\ldots (20)$$

To obtain a decline curve dimensionless rate q_{Dd} in terms of q_D,

$$q_{Dd} = \frac{q(t)}{q_i} = q_D\left[\ln\left(\frac{r_e}{r_w}\right) - \frac{1}{2}\right], \quad \ldots\ldots\ldots\ldots (21)$$

or

$$q_{Dd} = \frac{q(t)}{\frac{kh(p_i - p_{wf})}{141.3\ \mu\beta\left[\ln\left(\frac{r_e}{r_w}\right) - \frac{1}{2}\right]}} \quad \ldots\ldots\ldots\ldots (22)$$

Thus, the published values of q_D and t_D for the infinite and finite constant-pressure solutions were transformed into a decline curve dimensionless rate

and time, q_{Dd} and t_{Dd}, using Eqs. 20 and 21. Fig. 3 is a plot of the newly defined dimensionless rate and time, q_{Dd} and t_{Dd}, for various values of r_e/r_w.

At the onset of depletion (a type of pseudosteady state), all solutions for various values of r_e/r_w develop exponential decline and converge to a single curve. Fig. 4 is a combination of the constant-pressure analytical solutions and the standard "empirical" exponential, hyperbolic, and harmonic decline curve solutions on a single dimensionless curve. The exponential decline is common to both the analytical and empirical solutions. Note from the composite curve that rate data existing only in the transient period of the constant terminal pressure solution, if analyzed by the empirical Arps approach, would require values of b much greater than 1 to fit the data.

Solutions From Rate and Material Balance Equations

The method of combining a rate equation and material balance equation for finite systems to obtain a rate-time equation was outlined in Ref. 17. The rate-time equation obtained using this simple approach, which neglects early transient effects, yielded surprisingly good results when compared with those obtained using more rigorous analytical solutions for finite aquifer systems. This rate-equation material balance approach was used to derive some useful and instructive decline curve equations for solution-gas-drive reservoirs and gas reservoirs.

Rate Equations

Until recently, no simple form of a rate equation existed for solution-gas-drive reservoirs with which to predict rate of flow as a function of both flowing pressure and declining reservoir shut-in pressure. Fetkovich[14] has proposed a simple empirical rate equation for solution-gas-drive reservoirs that yields results that compare favorably with computer results obtained using two-phase flow theory. The proposed rate equation was given as

$$q_o = J'_{oi}\left(\frac{\bar{p}_R}{p_{Ri}}\right)\left(\bar{p}_R^2 - p_{wf}^2\right)^n, \quad \ldots\ldots\ldots\ldots\ldots (23a)$$

Where n will be assumed to lie between 0.5 and 1.0.

Although the above equation has not been verified by field results, it offers the opportunity to define the decline exponent (1/b) in terms of the backpressure curve slope (n) and to study its range of expected values. Also, the initial decline rate D_i can be expressed in terms of reservoir variables. One further simplification used in the derivations is that $p_{wf} = 0$. For a well on decline, p_{wf} usually will be maintained at or near zero to maintain maximum flow rates. Eq. 23a then becomes

$$q_o = J'_{oi}\left(\frac{\bar{p}_R}{p_{Ri}}\right)\left(\bar{p}_R^{2n}\right), \quad \ldots\ldots\ldots\ldots\ldots (23b)$$

The form of Eqs. 23a and 23b also could be used to represent gas-well behavior with a pressure dependent interwell permeability effect defined by the ratio (p_R/p_{Ri}). The standard form of the gas-well rate equation usually is given as

$$q_g = C_g \left(p_R^2 - p_{wf}^2\right)^n. \quad \ldots\ldots\ldots\ldots\ldots (24)$$

Material Balance Equations

Two basic forms of a material balance equation are investigated in this study: p_R is linear with N_p or G_p, and p_R^2 is linear with N_p or G_p (Figs. 5A and 5B). The linear p_R relationship for oil is

$$\bar{p}_R = -\left(\frac{\bar{p}_{Ri}}{N_{pi}}\right) N_p + \bar{p}_{Ri}, \quad \ldots\ldots\ldots\ldots (25)$$

and for gas

$$\bar{p}_R = -\left(\frac{\bar{p}_{Ri}}{G}\right) G_p + \bar{p}_{Ri}. \quad \ldots\ldots\ldots\ldots (26)$$

Eq. 25 is a good approximation for totally undersaturated oil reservoirs or is simply assuming that during the decline period $\bar{p}_R$ vs. N can be approximated by a straight line. For gas reservoirs, Eq. 26 is correct for the assumption of gas compressibility Z = 1.

In terms of $\bar{p}_R^2$ being linear with cumulative production, we would have

$$\bar{p}_R^2 = -\left(\frac{\bar{p}_{Ri}^2}{N_{pi}}\right) N_p + \bar{p}_{Ri}^2. \quad \ldots\ldots\ldots\ldots (27)$$

This form of equation results in the typical shape of the pressure $\bar{p}_R$ vs. cumulative production N_p relationship of a solution-gas-drive reservoir as depicted in Fig. 5B. Applications would be more appropriate in nonprorated fields - i.e., wells are produced wide open and go on decline from initial production. This more likely would be the case for much of the decline curve data analyzed by Cutler[18] obtained in the early years before proration.

Rate-Time Equations for Oil Wells

Rate-time equations using various combinations of material balance and rate equations were derived as outlined in Appendix B of Ref. 17. Using Eqs. 23b and 25, the resulting rate-time equation is

$$\frac{q_o(t)}{q_{oi}} = \frac{1}{\left[2n\left(\frac{q_{oi}}{N_{pi}}\right)t + 1\right]^{\frac{2n+1}{2n}}} \quad \ldots\ldots\ldots (28)$$

A unit solution, $q_{oi}/N_{pi} = 1$, of Eq. 28 is plotted as a log-log type curve for various values of n (Fig. 6) in terms of the decline curve dimensionless time t_{Dd}. For these derivations with $p_{wf} = 0$, $q_{oi} = (q_{oi})_{max}$. For the limiting range of backpressure curve slopes n of 0.5 and 1.0, the Arps empirical decline curve exponent 1/b is 2.0 and 1.5, respectively, or b = 0.500 and 0.667, respectively - a surprisingly narrow range. To achieve an exponential decline, n must be equal to zero, and a harmonic decline requires $n \longrightarrow \infty$. In practical applications, if we assume an n of 1.0 dominates in solution-gas (dissolved gas) drive reservoirs and $\bar{p}_R$ vs. N is linear for nonuniquely defined rate-time data, we simply would fit the rate-time data to the n = 1.0 curve. On the Arps' solution type curves (Fig. 1), we would use (1/b) = 3/2 or b = 0.667.

The rate-time equations obtained using Eqs. 23b and 27 are

$$\frac{q_o(t)}{q_{oi}} = \frac{1}{\left[\frac{2n-1}{2}\left(\frac{q_{oi}}{N_{pi}}\right)t + 1\right]^{\frac{2n+1}{2n-1}}} \quad \ldots\ldots (29a)$$

for all oil well backpressure curve slopes where n > 0.5.

For n = 0.5, the exponential decline is obtained:

$$\frac{q_o(t)}{q_{oi}} = e^{-\left(\frac{q_{oi}}{N_{pi}}\right)t} \quad \ldots\ldots (29b)$$

The unit solution of Eqs. 29a and 29b are plotted as a log-log type curve for various values of n (Fig. 7). For the limiting range of backpressure curve slopes n of 0.5 and 1.0, the Arps empirical decline curve exponent 1/b is ∞ and 3 or b = 0 (exponential) and 0.333, respectively. This range of b values also fits Arps' findings using Cutler's decline curve data. He found that more than 90% of the values of b lie in the range $0 \leq b \leq 0.5$. Ramsay[1] found a different distribution of the value of b analyzing modern rate decline data from some 202 leases. His distribution may be more a function of analyzing wells that have been subject to proration and are better represented by the assumptions underlying the rate-time solution given by Eq. 28 - i.e., $\bar{p}_R$ vs. N_p was linear over the decline period.

Decline Curve Analysis of Gas Wells

Decline curve analysis of rate-time data obtained from gas wells has been reported in only a few instances.[19,20] Using equation 24 with $p_{wf} = 0$ and Eq. 26, the rate-time equation for a gas well is

$$\frac{q_g(t)}{q_{gi}} = \frac{1}{\left[(2n-1)\left(\frac{q_{gi}}{G}\right)t + 1\right]^{\frac{2n}{2n-1}}} \quad . \quad . \quad . \quad . \quad (30)$$

for all backpressure curve slopes where $n > 0.5$.

For $n = 0.5$, the exponential decline is obtained:

$$\frac{q_g(t)}{q_{gi}} = e^{-\left(\frac{q_{gi}}{G}\right)t} \quad . \quad . \quad . \quad . \quad . \quad . \quad . \quad . \quad . \quad . \quad . \quad . \quad (31)$$

The unit solutions of Eqs. 30 and 31 are plotted as a log-log type curve in Fig. 8. For the limiting range of backpressure curve slopes n of 0.5 and 1.0, the Arps decline curve exponent (1/b) is ∞ and 2, or b = 0 (exponential) and 0.500, respectively.

The effect of backpressure on a gas well is demonstrated for a backpressure curve slope n = 1.0 in Fig. 9. The backpressure is expressed as a ratio of p_{wf}/p_i. Note that as $p_{wf} \longrightarrow p_i$ ($\Delta p \longrightarrow 0$), the type curve approaches exponential decline, the liquid case solution. Whereas backpressure does not change the type of decline for the liquid case solution, it does change the type of decline in this case.

Using the more familiar rate and material balance equations for gas wells, we can obtain the cumulative-time relationship by integrating the rate-time Eqs. 30 and 31 with

$$G_p = \int_o^t q_g(t)dt \quad . \quad . \quad . \quad . \quad . \quad . \quad . \quad . \quad . \quad . \quad . \quad . \quad (32)$$

For $n > 0.5$ we obtain

$$\frac{G_p}{G} = 1 - \left[1 + (2n-1)\left(\frac{q_{gi}}{G}\right)t\right]^{\frac{1}{(1-2n)}} \quad , \quad . \quad . \quad . \quad . \quad . \quad . \quad (33)$$

and for $n = 0.5$,

$$\frac{G_p}{G} = 1 - e^{-\left(\frac{q_{gi}}{G}\right)t} \quad . \quad . \quad . \quad . \quad . \quad . \quad . \quad . \quad . \quad . \quad . \quad (34)$$

Log-log type curves of Eqs. 33 and 34 could be prepared for convenience in obtaining cumulative production.

Type Curve Analysis

Recent papers by Agarwal et al.,[5] Ramey,[6] Raghavan et al.,[7] and Gringarten et al.,[8] have demonstrated or discussed the application and usefulness of a type curve matching procedure to interpret constant-rate pressure buildup and drawdown data. Van Poollen[21] demonstrated the application of the type curve procedure in analyzing flow-rate data obtained from an oil well producing with a constant pressure at the wellbore. All of his data, however, were in the early transient period. No depletion was evident in his examples. This same type curve matching procedure can be used for decline curve analysis.

The basic steps used in type curve matching of declining rate-time data are as follows:

1. Plot the actual rate vs. time data in any convenient units on log-log tracing paper of the same size cycle as the type curve to be used. (For convenience all type curves should be plotted on the same log-log scale so that various solutions can be tried.)

2. The tracing paper data curve is placed over a type curve, the coordinate axes of the two curves being kept parallel and shifted to a position that represents the best fit of the data to a type curve. More than one of the type curves presented in this paper may have to be tried to obtain a best fit of all the data.

3. Draw a line through and extending beyond the rate-time data overlain along the uniquely matched type curves. Future rates then simply are read from the real-time scale on which the rate data is plotted.

4. To evaluate decline curve constants or reservoir variables, a match point is selected anywhere on the overlapping portion of the curves, and the coordinates of this common point on both sheets are recorded.

5. If none of the type curves will fit all the data reasonably, the departure curve method[15,22] should be attempted. This method assumes that the data is a composite of two or more different decline curves. After a match of the late time data has been made, the matched curve is extrapolated backward in time and the departure, or difference, between the actual rates and rates determined from the extrapolated curve at corresponding times is replotted on the same log-log scale. An attempt then is made to match the departure curve with one of the type curves. (At all times some consideration of the type of reservoir producing mechanism should be considered.) Future predictions then should be made as the sum of the rates determined from the two (or more if needed) extrapolated curves.

Type Curve Matching Examples

Several examples will be presented to illustrate the method of using type curve matching to analyze typical declining rate-time data. The type curve approach provides solutions on which engineers can agree or shows when a unique solution is not possible with a type curve only. In the event of a

nonunique solution, a most probable solution can be obtained if the producing mechanism is known or indicated.

Arps' Hyperbolic Decline Example

Fig. 10 illustrates a type curve match of Arps' example of hyperbolic decline.[4] Every single data point falls on the b = 0.5 type curve. This match was found to be unique in that the data would not fit any other value of b. Future producing rates can be read directly from the real-time scale on which the data is plotted. If we wish to determine q_i and D_i, use the match points indicated on Fig. 10 as follows.

$$q_{Dd} = 0.033 = \frac{q(t)}{q_i} = \frac{1{,}000 \text{ BOPM}}{q_i} .$$

$$q_i = \frac{1{,}000 \text{ BOPM}}{0.033} = 30{,}303 \text{ BOPM} .$$

$$t_{Dd} = 12.0 = D_i t = D_i \ 100 \text{ months} .$$

$$D_i = \frac{12.0}{100 \text{ months}} = 0.12 \text{ months}^{-1} .$$

The data also could have been matched using the type curves in Figs. 6 and 7. In both cases the match would have been obtained with a backpressure curve slope n = 0.5, which is equivalent to b = 0.5. Match points determined from these curves could have been used to calculate q_i and q_i/N_{pi} and finally N_{pi}.

The fact that this example was for a lease, a group of wells, and not an individual well raises an important question. Should there be a difference in results between analyzing each well individually and summing the results or simply adding all wells' production and analyzing the total lease production rate? Consider a lease or field with fairly uniform reservoir properties, b or n is similar to each well, and all wells have been on decline at a similar terminal wellbore pressure p_{wf} for a sufficient period of time to reach pseudosteady state. According to Matthews et al.,[23] "at (pseudo) steady state the drainage volumes in a bounded reservoir are proportional to the rates of withdrawal from each drainage volume." It follows then that the ratio q_i/N_{pi} will be identical for each well and, thus, the sum of the results from each well will give the same results as analyzing the total lease or field production rate. Some rather dramatic illustrations of how rapidly a readjustment in drainage volumes can take place by changing the production rate of an offset well or drilling an offset well is illustrated in a paper by Marsh.[24] Similar drainage volume readjustments in gas reservoirs also have been demonstrated by Stewart.[25]

For the case where some wells are in different portions of a field separated by a fault or a drastic permeability change, readjustment of drainage volumes

proportional to rate cannot take place among all wells. The ratio q_i/N_{pi} then may be different for different groups of wells. A total lease or field production analysis then would give different results than summing the results from individual well analysis. A similar situation also can exist for production from stratified reservoirs[26,27] (no crossflow).

Arps' Exponential Decline Example

Fig. 11 shows the results of a type curve analysis of Arps' example of a well with an apparent exponential decline. In this case, there are not sufficient data to establish uniquely a value of b. The data essentially fall in the region of the type curves where all curves coincide with the exponential solution. As shown in Fig. 11, a value of b = 0 (exponential) or b = 1.0 (harmonic) appear to fit the data equally well. (Of course all values in between also would fit the data.) The difference in forecasted results from the two extreme interpretations would be great in later years. For an economic limit of 20 BOPM, the exponential interpretation gives a total life of 285 months, the harmonic 1,480 months. This points out yet a further advantage of the type curve approach; all possible alternate interpretations conveniently can be placed on one curve and forecasts made from them. A statistical analysis, of course, would yield a single answer, but it would not be necessarily the correct or most probable solution. Considering the various producing mechanisms, we could select (1) b = 0 (exponential) if the reservoir is highly undersaturated, (2) b = 0 (exponential) for gravity drainage with no free surface,[28] (3) b = 0.5 for gravity drainage with a free surface,[28] (4) b = 0.667 for a solution-gas-drive reservoir (n = 1.0) if $\overline{p}_R$ vs. N_p is linear, or (5) b = 0.333 for a solution-gas-drive reservoir (n = 1.0) if $\overline{p}_R^2$ vs. N_p is approximately linear.

Fractured Well Example

Fig. 12 is an example of type curve matching for a well with declining rate data available both before and after stimulation. (The data were obtained from Ref. 1.) This type problem usually presents some difficulties in analysis. Both before- and after-fracture log-log plots are shown in Fig. 12 with the after-fracture data reinitialized in time. These before and after log-log plots will overlie each other exactly, indicating that the value of b did not change for the well after the fracture treatment. (The before-fracture plot can be considered as a type curve itself, with the after-fracture data overlaid and matched on it.) Thus, all the data were used in an attempt to define b. When a match is attempted on the Arps unit solution type curves, it was found that a b of between 0.6 and 1.0 could fit the data. Assuming a solution-gas drive, a match of the data was made on the Fig. 6 type curve with n = 1.0 and b = 0.667.

Using the match points for the before-fracture data, we have from the rate match point

$$q_{Dd} = 0.243 = \frac{q(t)}{q_{oi}} = \frac{1{,}000 \text{ BOPM}}{q_{oi}},$$

and

$$q_{oi} = \frac{1{,}000 \text{ BOPM}}{0.243} = 4{,}115 \text{ BOPM} .$$

From the time match point,

$$t_{Dd} = 0.60 = \left(\frac{q_{oi}}{N_{pi}}\right) t = \frac{(4{,}115 \text{ BOPM})(100 \text{ months})}{N_{pi}} ,$$

and

$$N_{pi} = \frac{(4{,}115 \text{ BOPM})(100 \text{ months})}{0.60} = 685{,}833 \text{ bbl.}$$

Then,

$$\frac{q_{oi}}{N_{pi}} = \frac{4{,}115 \text{ BOPM}}{685{,}833} = 0.006000 \text{ months}^{-1}.$$

Now using the match points for the after-fracture data, we have from the rate match point

$$q_{Dd} = 0.134 = \frac{q(t)}{q_{oi}} = \frac{1{,}000 \text{ BOPM}}{q_{oi}} ,$$

and

$$q_{oi} = \frac{1{,}000 \text{ BOPM}}{0.134} = 7{,}463 \text{ BOPM} .$$

From the time match point,

$$t_{Dd} = 1.13 = \left(\frac{q_{oi}}{N_{pi}}\right) t = \frac{(7{,}463 \text{ BOPM})(100 \text{ months})}{N_{pi}} ,$$

and

$$N_{pi} = \frac{(7{,}463 \text{ BOPM})(100 \text{ months})}{1.13} = 660{,}442 \text{ bbl} .$$

Then,

$$\frac{q_{oi}}{N_{pi}} = \frac{7{,}463 \text{ BOPM}}{660{,}442 \text{ bbl}} = 0.011300 \text{ months}^{-1} .$$

We now can check the two limiting conditions to be considered following an increase in rate after a well stimulation:

1. Did we simply obtain an acceleration of production, the well's reserves remaining the same?

2. Did the reserves increase in direct proportion to the increase in producing rate as a result of a radius of drainage readjustment?[23] Before treatment, N_{pi} was found to be 685,833 bbl. Cumulative production determined from the rate data before stimulation was 223,500 bbl. Then N_{pi} at the time of the fracture treatment is

$$N_{pi} = 685{,}833 \text{ bbl} - 223{,}500 \text{ bbl} = 462{,}333 \text{ bbl} .$$

If only accelerated production was obtained and the reserves remained the same, q_i/N_{pi} after the fracture treatment should have been

$$\frac{7{,}463 \text{ BOPM}}{462{,}333 \text{ bbl}} = 0.016142 \text{ months}^{-1} .$$

Actual q_{oi}/N_{pi} after treatment was 0.011300 months^{-1}. If the reserves increased in direct proportion to the flow rate, the ratio q_{oi}/N_{pi} should have remained the same as that obtained before treatment or 0.006000 months^{-1}. This then would have indicated that

$$N_{pi} = \frac{7{,}463 \text{ BOPM}}{0.006000 \text{ months}^{-1}} = 1{,}243{,}833 \text{ bbl} .$$

Actual increase in reserves as a result of the fracture treatment appears to lie between the two extremes. Based on the method of analysis used, the actual increase in reserves attributable to the fracture treatment is 198,109 bbl (660,442 bbl - 462,333 bbl).

Stratified Reservoir Example

This example illustrates a method of analyzing decline curve data for a layered (no crossflow) or stratified reservoir using type curves. The data are taken from Ref. 18 and are for the East Side Coalinga field. Ambrose[29] presented a cross section of the field, showing an upper and lower oil sand separated by a continuous black shale. This layered description for the field along with the predictive equation for stratified reservoir presented in Ref. 27 led to the idea of using the departure curve method (differencing) to analyze decline curve data.

After Russell and Prats,[27] the production rate of a well (or field) at pseudosteady state producing a single-phase liquid at the same constant wellbore pressure (p_{wf} = 0 for simplicity) from two stratified layers is

$$q_T(t) = q_{i1} e^{-\left(\frac{q_i}{N_{pi}}\right)_1 t} + q_{i2} e^{-\left(\frac{q_i}{N_{pi}}\right)_2 t} , \quad \ldots\ldots\ldots (35)$$

or

$$q_T(t) = q_1(t) + q_2(t) \quad . \quad . \quad . \quad . \quad . \quad . \quad . \quad . \quad . \quad . \quad . \quad . \quad . \quad . \quad . \quad (36)$$

The total production from both layers then is simply the sum of two separate forecasts. Except for the special case of the ratio q_i/N_{pi} being equal for both layers, the sum of two exponentials will not result, in general, in another exponential.

In attempting to match the rate-time data to a type curve, it was found that the late time data can be matched to the exponential (b = 0) type curve. Fig. 13 shows this match of the late time data designated as Layer 1. With this match, the curve was extrapolated backward in time, and the departure, or difference between the actual rates determined from the extrapolated curve was replotted on the same log-log scale. See Table 1 for a summary of the departure curve results. The difference or first departure curve, Layer 2, itself resulted in a unique fit of the exponential type curve, thus satisfying Eq. 35, which now can be used to forecast the future production. Using the match points indicated in Fig. 13 to evaluate q_i and D_i for each layer, the predictive equation becomes

$$q_T(t) = 58{,}824 \text{ BOPY } e^{-(0.200)t} + 50{,}000 \text{ BOPY } e^{-(0.535)t} ,$$

where t is in years.

Higgins and Lechtenberg[30] named the sum of two exponentials the double semilog. They reasoned that the degree of fit of empirical data to an equation increases with the number of constants.

This interpretation is not claimed to be the only interpretation possible for this set of data. A match with b = 0.2 can be obtained fitting nearly all of the data points but cannot be explained by any of the drive mechanisms so far discussed. The layered concept fits the geologic description and offered the opportunity to demonstrate the departure curve method. The departure curve method essentially places an infinite amount of combinations of type curves at the disposal of the engineer with which to evaluate rate-time data.

Effect of a Change in Backpressure

The effect of a change in backpressure is illustrated best by a hypothetical single-well problem. The reservoir variables and conditions used for this example are given in Table 2. The analytical single-phase liquid solution of Fig. 3 is used to illustrate a simple graphical forecasting superposition procedure. The inverse procedure, the departure or differencing method, can be used to analyze decline-curve data affected by backpressure changes.

After Hurst,[12] superposition for the constant-pressure case for a simple single-pressure change can be expressed by

$$q(t) = \frac{kh(p_i - p_{wf1})}{141.3(\mu\beta)\left[\ln\left(\frac{r_e}{r_w}\right) - \frac{1}{2}\right]} q_{Dd}(t_{Dd})$$

$$+\frac{kh(p_{wf1} - p_{wf2})}{141.3(\mu\beta)\left[\ln\left(\frac{r_e}{r_w}\right) - \frac{1}{2}\right]} q_{Dd}(t_{Dd} - t_{Dd1}) ,$$

or

$$q(t) = \frac{kh(p_i - p_{wf1})}{141.3(\mu\beta)\left[\ln\left(\frac{r_e}{r_w}\right) - \frac{1}{2}\right]}$$

$$\cdot\left\{ q_{Dd}(t_{Dd}) + \left[\frac{p_{wf1} - p_{wf2}}{p_i - p_{wf1}}\right] q_{Dd}(t_{Dd} - t_{Dd1}) \right\} . \quad . . . . . (37)$$

Up to the time of the pressure change p_{wf2} at t_{Dd1}, the well production is simply q_1 as depicted on Fig. 14. The q_1 forecast as a function of time is made simply by evaluating a single set of match points using the reservoir variables given in Table 2. At p_{wf1} and r_e/r_w' = 100: t = 1 day, t_{Dd} = 0.006967, $q_1(t)$ = 697 BOPD, and q_{Dd} = 2.02.

Plot the rate 697 BOPD and time of 1 day on log-log tracing paper on the same size cycle as Fig. 3. Locate the real-time points over the dimensionless time points in Fig. 3 and draw in the r_e/r_w' curve of 100 on the tracing paper. Read flow rates as a function of time directly from the real-time scale.

When a change in pressure is made to p_{wf2} at t_1, t = 0 for the accompanying change in rate q_2 (really a Δq for superposition), this rate change retraces the q_{Dd} vs. t_{Dd} curve and is simply a constant fraction of q_1:

$$q_2 = q_1 \frac{p_{wf1} - p_{wf2}}{p_i - p_{wf1}} ,$$

or at t - 1 day after the rate change,

$$q_2 = 697 \text{ BOPD} \quad \frac{1{,}000 \text{ psi} - 50 \text{ psi}}{4{,}000 \text{ psi} - 1000 \text{ psi}} = 221 \text{ BOPD} .$$

The total rate q_T after the pressure change is $q_T = q_1 + q_2$ as depicted in Fig. 14. Flow rates for this example were read directly from the curves in Fig. 14 and summed at times past the pressure change p_{wf2}.

The practical application of this example in decline curve analysis is that

the departure or difference method can be used on rate-time data affected by a change in backpressure. The departure curve represented by q_2 in Fig. 14 should overlie exactly the curve represented by q_1. If it does in an actual field example, the future forecast is made correctly by extending both curves and summing them at times beyond the pressure change.

Calculation of kh From Decline Curve Data

Pressure buildup and decline curve data were available from a high-pressure, highly undersaturated, low-permeability sandstone reservoir. Initial reservoir pressure was estimated to be 5,790 psia at -9,300 ft with a bubble-point pressure of 2,841 psia. Two fieldwide pressure surveys were conducted while the reservoir was still undersaturated. Table 3 summarizes the reservoir properties and basic results obtained from the pressure buildup analysis on each well. Note that nearly all wells had negative skins as a result of hydraulic fracture treatments. Also appearing in this table are results obtained from an attempt to calculate kh using decline curve data available for each of the wells.

Ten of the 22 wells started on decline when they first were placed on production. As a result, the early production decline data existed in the transient period, and a type curve analysis using Fig. 3 was matched to one of the r_e/r_w stems. Other wells listed on the table, where an r_e/r_w match is not indicated, were prorated wells and began their decline several months after they first were put on production. For the decline curve determination of kh, the reservoir pressure existing at the beginning of decline for each well was taken from the pressure history match of the two fieldwide pressure surveys. The constant bottomhole flowing pressure for the wells ranged between 800 and 900 psia.

A type curve match using decline curve data to calculate kh for Well 13 is illustrated in Fig. 15. A type curve match using pressure buildup data obtained on this same well is illustrated in Fig. 16. The constant-rate type curve of Gringarten et al.[8] for fractured wells was used for matching the pressure buildup data. The buildup kh of 47.5 md-ft compares very well with the kh of 40.5 md-ft determined by using the rate-time decline curve data.

In general, the comparison of kh determined from decline curve data and pressure buildup data tabulated in Table 3 is surprisingly good. (The pressure buildup analysis was performed independently by another engineer.) One fundamental observation to be made from the results obtained on wells where a match of r_e/r_w was not possible is that the effective wellbore radius r_w' (obtained from the buildup analysis) is used to obtain a good match between buildup and decline curve calculated kh.

Type Curves for Known Reservoir and Fluid Properties

All the type curves discussed so far were developed for decline curve analysis using some necessary simplifying assumptions. For specific reservoirs, where PVT data, reservoir variables, and backpressure tests are available, type curves could be generated for various relative permeability curves and backpressure. These curves developed for a given field would be more accurate for analyzing decline data in that field. Conventional material balance programs or more sophisticated simulation models could be used to develop

dimensionless constant-pressure type curves as was done by Levine and Pratts[31] see their Fig. 11).

Conclusions

Decline curve analysis not only has a solid fundamental base but provides a tool with more diagnostic power than has been suspected previously. The type curve approach provides unique solutions upon which engineers can agree or shows when a unique solution is not possible with a type curve only. In the event of a nonunique solution, a most probable solution can be obtained if the producing mechanism is known or indicated.

Nomenclature

b = reciprocal of decline curve exponent (1/b)
β = formation volume factor, res vol/surface vol
c_t = total compressibility, psi^{-1} (pa^{-1})
C_g = gas-well backpressure curve coefficient
D_i = initial decline rate, t^{-1}
e = natural logarithm base 2.71828
G = initial gas-in-place, surface measure
G_p = cumulative gas production, surface measure
h = thickness, ft(m)
J_o = productivity index, STB/D/psi (stocktank m^3/d/kPa)
J_o' = productivity index (backpressure curve coefficient) STB/D/$(psi)^{2n}$ [stock-tank m^3/d/$(kPa)^{2n}$]
k = effective permeability, md
n = exponent of backpressure curve
N_p = cumulative oil production, STB (stock-tank m^3)
N_{pi} = cumulative oil production to a reservoir shut-in pressure of 0, STB (stock-tank m^3)
p_i = initial pressure, psia (kPa)
p_R = reservoir average pressure (shut-in pressure), psia (kPa)
p_{wf} = bottomhole flowing pressure, psia (kPa)
q_D = dimensionless rate (Eq. 6)
q_{Dd} = decline curve dimensionless rate (Eq. 4)
q_i = initial surface rate of flow at t = 0
$(q_i)_{max}$ = initial wide-open surface flow rate at p_{wf} = 0
$q(t)$ = surface rate of flow at time t
Q_D = dimensionless cumulative production
r_e = external boundary radius, ft(m)
r_w = wellbore radius, ft(m)
r_w' = effective wellbore radius, ft(m)
t = time, days for t_D
t_D = dimensionless time (Eq. 7)
t_{Dd} = decline curve dimensionless time (Eq. 5)
Z = gas compressibility factor
μ = viscosity, cp (Pa.s)
ϕ = porosity, fraction of bulk volume

Acknowledgment

I thank Phillips Petroleum Co. for permission to publish this paper.

References

1. Ramsay, H. J. Jr.: "The Ability of Rate-Time Decline Curves to Predict Future Production Rates," MS thesis, U. of Tulsa, Tulsa, OK (1968).

2. Slider, H. C.: "A Simplified Method of Hyperbolic Decline Curve Analysis," J. Pet. Tech. (March 1968) 235-236.

3. Gentry, R. W.: "Decline-Curve Analysis," J. Pet. Tech. (Jan. 1972) 38-41.

4. Arps, J. J.: "Analysis of Decline Curves," Trans., AIME (1945) 160, 228-247.

5. Ramey, H. J. Jr.: "Short-Time Well Test Data Interpretation in the Presence of Skin Effect and Wellbore Storage," J. Pet. Tech. (Jan. 1970) 97-104; Trans., AIME, 249.

6. Agarwal, R., Al-Hussainy, R., and Ramey, H. J. Jr.: "An Investigation of Wellbore Storage and Skin Effect in Unsteady Liquid Flow: I. Analytical Treatment," Soc. Pet. Eng. J. (Sept. 1970) 279-290; Trans., AIME, 249.

7. Raghavan, R., Cady, G. V., and Ramey, H. J. Jr.: "Well-Test Analysis for Vertically Fractured Wells," J. Pet. Tech. (Aug. 1972) 1014-1020; Trans., AIME, 253.

8. Gringarten, A. C., Ramey, H. J. Jr., and Raghavan, R.: "Unsteady-State Pressure Distributions Created by a Well With a Single Infinite-Conductivity Vertical Fracture," Soc. Pet. Eng. J. (Aug. 1974) 347-360; Trans., AIME, 257.

9. McKinley, R. M.: "Wellbore Transmissibility from Afterflow-Dominated Pressure Buildup Data," J. Pet. Tech. (July 1971) 863-872; Trans., AIME, 251.

10. Moore, T. V., Schilthuis, R. J., and Hurst, W.: "The Determination of Permeability from Field Data," Bull., API (May 1933) 211, 4.

11. Hurst, R.: "Unsteady Flow of Fluids in Oil Reservoirs," Physics (Jan. 1934) 5, 20.

12. Hurst, W.: "Water Influx into a Reservoir and Its Application to the Equation of Volumetric Balance," Trans., AIME (1943) 151, 57-72.

13. van Everdingen, A. F. and Hurst, W.: "The Application of the Laplace Transformation to Flow Problems in Reservoirs," Trans., AIME (1949) 186, 305-324.

14. Fetkovich, M. J.: "The Isochronal Testing of Oil Wells," paper SPE 4529 presented at the SPE 48th Annual Fall Meeting, Las Vegas, Sept. 30 - Oct. 3, 1973.

15. Ferris, J., Knowles, D. B., Brown, R. H., and Stallman, R. W.: "Theory of Aquifer Tests," U.S. Geol. Surv., Water Supply Paper 1536E (1962) 109.

16. Tsarevich, K. A. and Kuranov, I.F.: "Calculation of the Flow Rates for the Center Well in a Circular Reservoir Under Elastic Conditions," Problems of Reservoir Hydrodynamics, Leningrad (1966) Part I, 9-34.

17. Fetkovich, M. J.: "A Simplified Approach to Water Influx Calculations-Finite Aquifer Systems," J. Pet. Tech. (July 1971) 814-823.

18. Cuttler, W. W. Jr.: "Estimation of Underground Oil Reserves by Oil-Well Production Curves," Bull., USBM (1924) 228.

19. Stewart, P. R.: "Low-Permeability Gas Well Performance at Constant Pressure," J. Pet. Tech. (Sept. 1970) 1149-1156.

20. Gurley, J.: "A Productivity and Economic Projection Method - Ohio Clinton Sand Gas Wells," J. Pet. Tech. (Nov. 1963) 1183-1185.

21. van Poollen, H. K.: "How to Analyze Flowing Well-Test Data...with Constant Pressure at the Well Bore," Oil and Gas J. (Jan. 16, 1967) 98-101.

22. Witherspoon, P. A., Javandel, I., Neuman, S. P., and Freeze, P. A.: Interpretation of Aquifer Gas Storage Conditions from Water Pumping Tests, Monograph, AGA, New York City (1967) 110.

23. Matthews, C. S., Brons, F., and Hazebroek, P.: "A Method for Determination of Average Pressure in a Bounded Reservoir," Trans., AIME (1954) 201, 182-191.

24. Marsh, H. N.: "Method of Appraising Results of Production Control of Oil Wells," Bull., API (Sept. 1928) 202, 86.

25. Stewart, P. R.: "Evaluation of Individual Gas Well Reserves," Pet. Eng. (May 1966) 85.

26. Lefkovits, H. C. and Matthews, C. S.: "Application of Decline Curves to Gravity-Drainage Reservoirs in the Stripper Stage," Trans., AIME (1958) 213, 275-284.

27. Russel, D. G. and Prats, M.: "Performance of Layered Reservoirs With Crossflow - Single-Compressible Fluid Case," Soc. Pet. Eng. J. (March 1962) 53-67.

28. Matthews, C. S. and Lefkovits, H. C.: "Gravity Drainage Performance of Depletion-Type Reservoirs in the Stripper Stage," Trans., AIME (1956) 207, 265-274.

29. Ambrose, A. W.: "Underground Conditions in Oil Fields," Bull., USBM (1921) 195, 151.

30. Higgins, R. V. and Lechtenberg, H. J.: "Merits of Decline Equations Based on Production History of 90 Reservoirs," paper SPE 2450 presented at the SPE Rocky Mountain Regional Meeting, Denver, May 25-27, 1969.

31. Levine, J. S. and Prats, M.: "The Calculated Performance of Solution-Gas Drive Reservoirs," Soc. Pet. Eng. J. (Sept. 1961) 142-152.

SI Metric Conversion Factors

acre	x	4.046 873	E	+ 03	=	m^2
bbl	x	1.589 873	E	- 01	=	m^3
cp	x	1.0*	E	- 03	=	Pa.s
ft	x	3.048*	E	- 01	=	m
md-ft	x	3.008 142	E	+ 02	=	μm^2.
psi	x	6.894 757	E	+ 00	=	kPa
psi^{-1}	x	1.450 377	E	- 04	=	Pa^{-1}

*Conversion factor is exact.

TABLE 1

SUMMARY OF RATE-TIME DATA FROM EAST SIDE COALINGA FIELD[18] WITH THE RESULTS FROM THE DEPARTURE CURVE METHOD

Time (years)	(1) Total Field Rate, q_T (BOPY)	(2) Layer 1 Rate, q_1 (BOPY)	(1) - (2) Layer 2 Rate, q_2 (BOPY)
0.5	90,000	52,000*	38,000
1.5	64,000	42,500*	21,500
2.5	48,000	34,500*	13,500
3.4	36,000	28,500*	7,500
4.5	27,500	23,000*	4,500
5.5	21,250	18,600*	2,650
6.5	16,250	15,000*	1,250
7.5	13,000	12,500*	500
8.5	10,500	10,500	0
9.5	8,500	8,500	
10.5	6,900	6,900	
11.5	5,600	5,600	
12.5	4,550	4,550	
13.5	3,800	3,800	
14.5	3,200	3,200	
15.5	2,750	2,750	

* Taken from Layer 1 curve in Fig. 13.

TABLE 2

DATA FOR EXAMPLE PROBLEM OF A CHANGE IN BACKPRESSURE

p_i = 4,000 psia
p_{wf1} = 1,000 psia
p_{wf2} = 50 psia
k = 1 md
h = 100 ft
μ_o = 1 cp
β_o = 1.50 RB/STB
c_t = 20 x 10^{-6} psi^{-1}
r_e = 1,053 ft (80 acres)
r_w' = 10.53 ft (stimulated well)

$$t_D = \frac{0.00634\ kt}{\phi\mu c_t r_w'^2} = \frac{0.00634\ (1)\ t}{(0.20)(1.0)(20 \times 10^{-6}(10.53)^2} = 14.30\ t$$

$$t_{Dd} = \frac{14.30\ t}{1/2\ [(100)^2 - 1][\ln (100) - 0.5]} = 0.0006967\ t_{days}$$

$$q_{Dd} = \frac{q(t)}{\dfrac{kh\ (p_i - p_{wf})}{141.3(\mu B)\left[\ln\left(\dfrac{r_e}{r_w}\right) - \dfrac{1}{2}\right]}} = \frac{q(t)}{\dfrac{100\ (3{,}000)}{141.3(1)(1.5)(4.105)}} = \frac{q(t)}{345}$$

$q(t) = q_{Dd}\ (t_{Dd})\ 345$ or $q(t) = 2.02\ (345)$ at t = 1 day
$q(t)$ = 697 BOPD

TABLE 3

COMPARISONS OF kh DETERMINED FROM BUILDUP AND DECLINE CURVE ANALYSIS, FIELD A (SANDSTONE RESERVOIR); 160-ACRE SPACING, r_e = 1,490 ft, r_w = 0.25 ft

				Pressure Buildup Results			Decline Curve Analysis Results				
Well No.	h (ft)	ϕ (%)	S_{wc} (%)	Skin s	r_w' (ft)	kh (md-ft)	r_e/r_w' Matched	q_{Dd} (10,000 BOPM)	$\frac{P_i - P_{wf}}{(\mu_o \beta_o)}$	kh (md-ft)	k (md)
1	34	9.4	32.9	-0.23	0.3	120.5	*	0.52	6658	108	3.18
2	126	10.5	18.3	-2.65	3.5	56.7	*	0.68	7979	48	0.38
3	32	9.9	20.4	-3.71	10.3	63.0	*	0.43	8048	60	1.88
4	63	9.5	18.6	-3.41	7.6	28.5	40	0.58	8273	31	0.49
5	67	10.2	15.1	-4.29	18.3	44.4	20	0.57	6296	32	0.48
6	28	10.3	12.6	-2.07	2.0	57.9	*	0.60	7624	62	2.21
7	17	10.0	17.5	-3.41	7.6	16.8	10	1.30	7781	8.3	0.49
8	47	9.1	24.2	-3.74	10.6	16.6	10	1.14	7375	10	0.21
9	87	10.2	18.0	-4.19	16.5	104.7	*	0.435	5642	76	0.87
10	40	10.4	21.7	-5.80	82.9	363.2	*	0.36	1211	255	6.38
11	29	11.5	19.2	-1.00	2.0	59.9	*	0.56	7669	66	2.28
12	19	11.1	17.0	-3.97	13.3	8.9	50	3.30	5045	9.5	0.50
13	121	10.1	18.8	-3.85	11.8	47.5	50	0.54	7259	40.5	0.33
16	74	9.4	20.4	-4.10	15.0	224.8	*	0.32	5737	104	1.41
15	49	10.9	28.6	-3.59	9.1	101.9	*	0.43	4312	115	2.35
16	35	10.0	25.6	-4.57	24.2	14.3	20	0.96	5110	24	0.69
17	62	8.8	22.4	-3.12	5.7	27.2	*	0.82	8198	35	0.56
18	75	9.4	18.1	-1.50	1.2	65.1	*	0.52	6344	93	1.24
19	38	8.9	19.2	-2.11	2.1	40.5	20	0.54	6728	32	0.84
20	60	9.6	24.6	-5.48	60.1	88.1	*	0.345	5690	64	1.07
21	56	11.1	16.5	-2.19	2.2	39.1	20	0.72	5428	30	0.54
22	40	8.9	22.5	-3.79	11.1	116.0	100	0.46	8114	51	1.28

*r_w' used from buildup analysis with r_e of 1,490 ft.

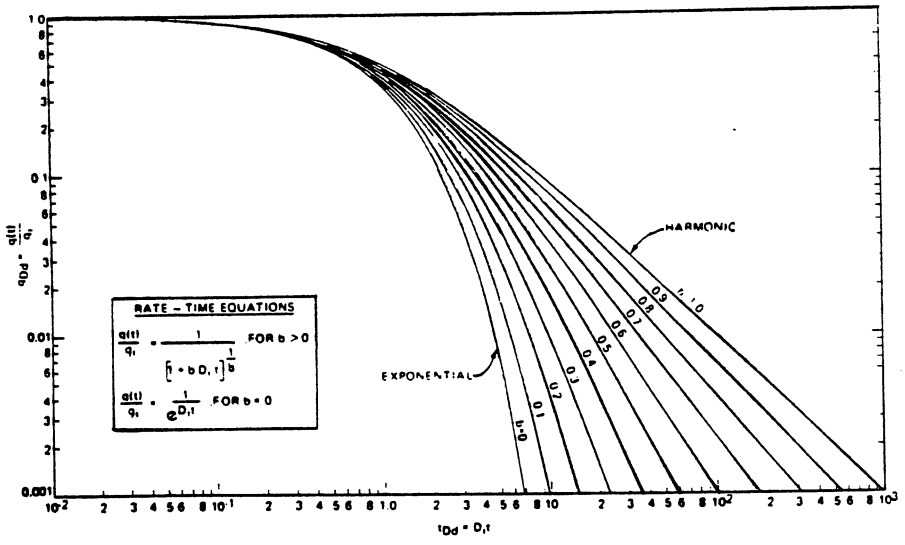

Fig. 1 – Type curves for Arps' empirical rate-time decline equations, unit solution ($D_i = 1$).

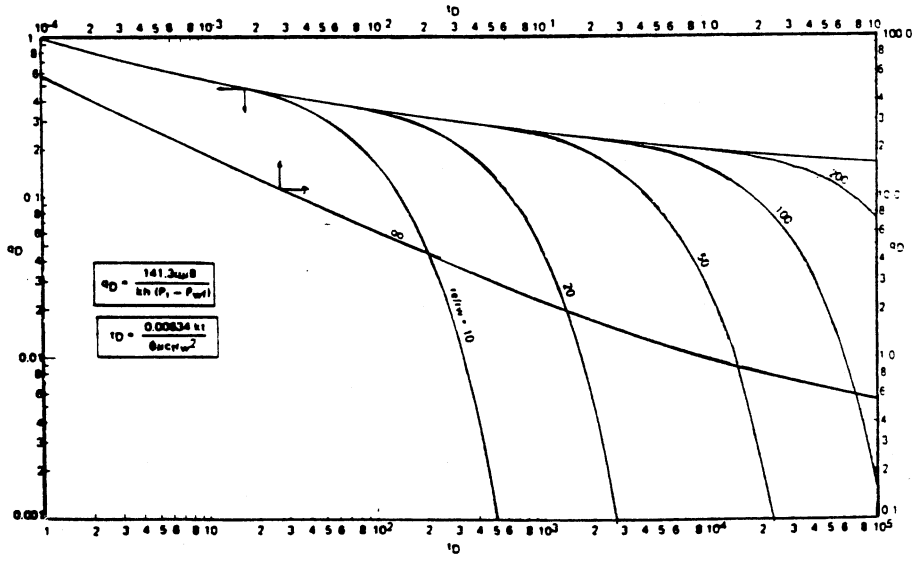

Fig. 2A – Dimensionless flow rate functions for plane radial system, infinite and finite outer boundary, constant pressure at inner boundary.[10,11,15,16]

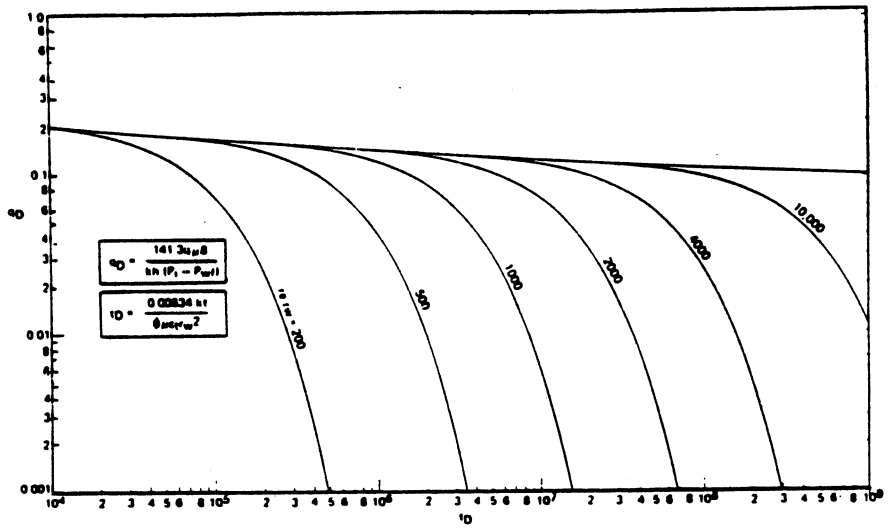

Fig. 2B – Dimensionless flow rate functions for plane radial system, infinite and finite outer boundary, constant pressure at inner boundary.[10,11,15,16]

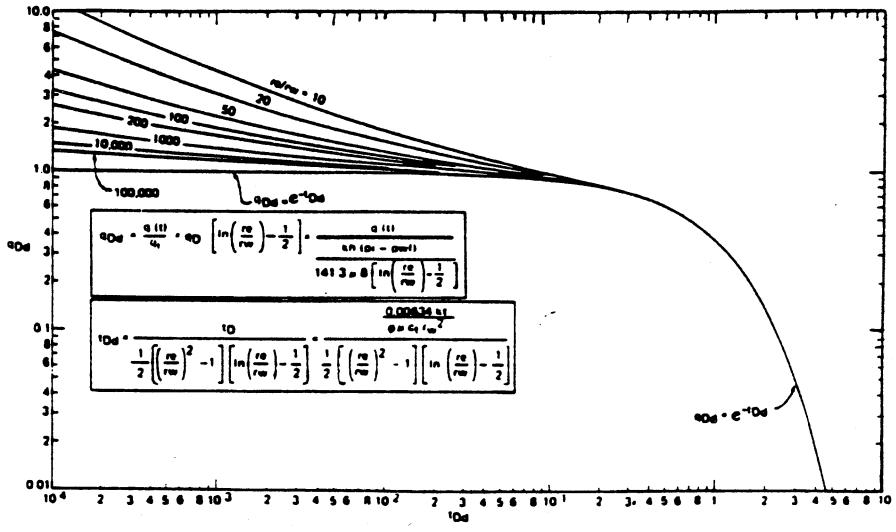

Fig. 3 – Dimensionless flow rate functions for plane radial system, infinite and finite outer boundary, constant pressure at inner boundary.

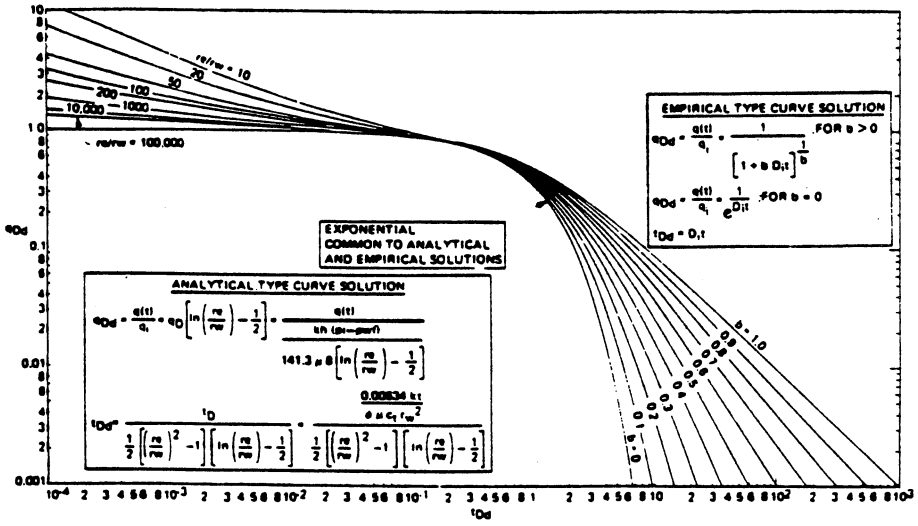

Fig. 4 – Composite of analytical and empirical type curves of Figs. 1 and 3.

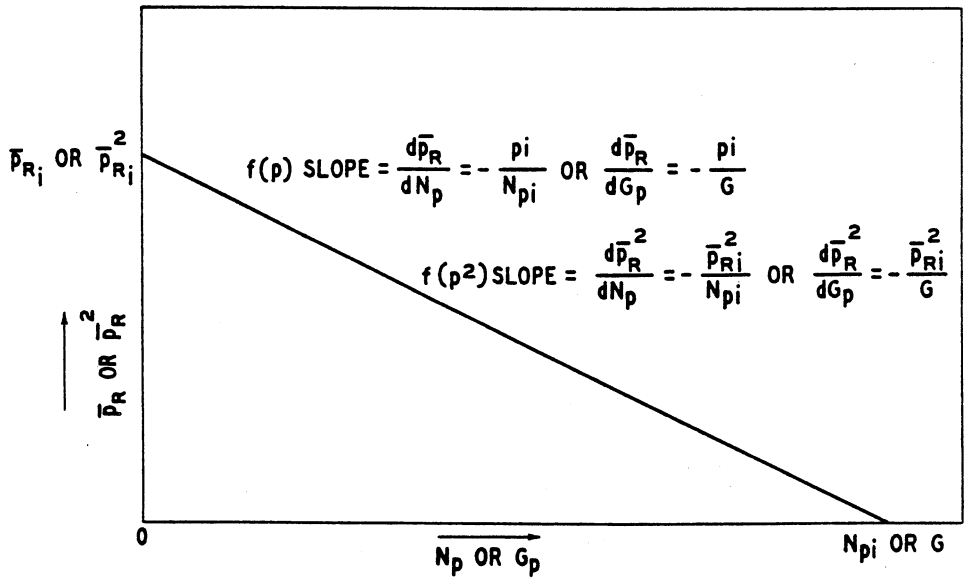

Fig. 5A – Graphical representation of material balance equation.

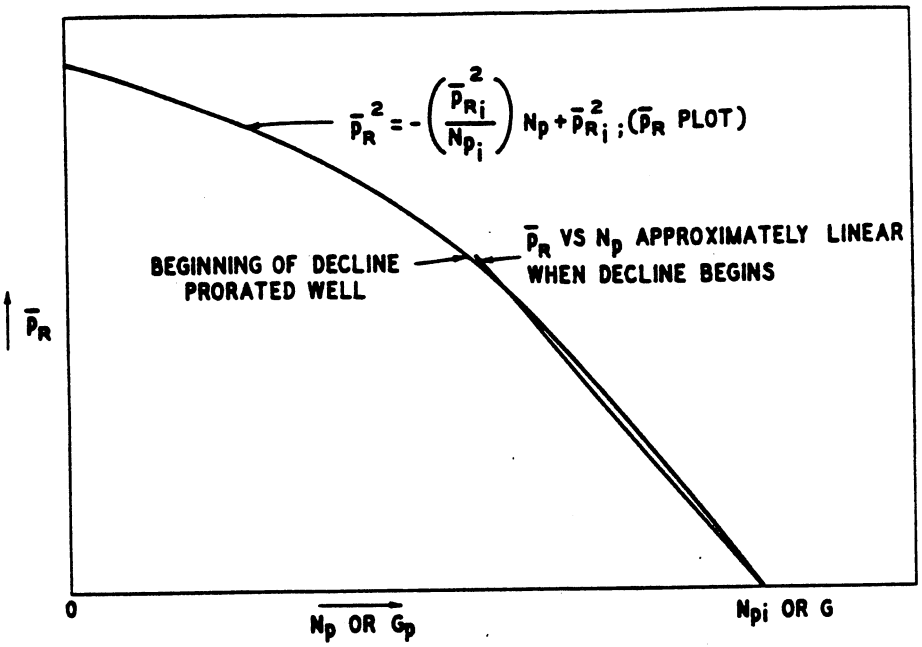

Fig. 5B – Graphical representation of material balance equation.

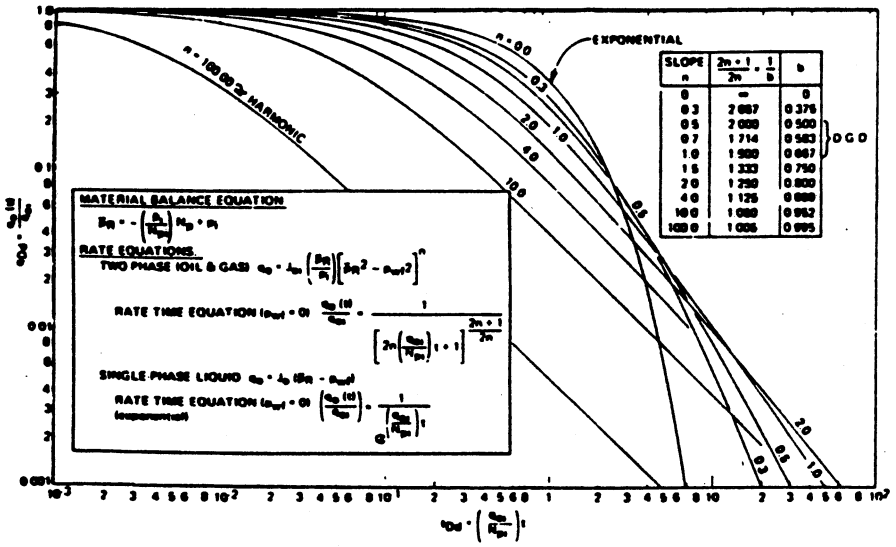

Fig. 6 – Dissolved-gas-drive reservoir rate decline type curves for finite system with constant pressure at inner boundary ($p_{wf} = 0$ @ r_w); early transient effects not included.

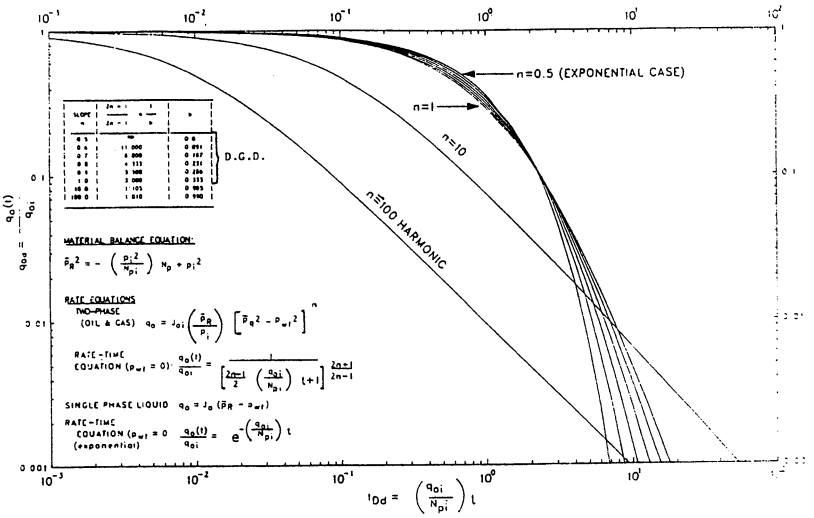

Fig. 7 – Dissolved-gas-drive reservoir rate decline type curves for finite system with constant pressure at inner boundary (p_{wf} = 0 @ r_w); early transient effects not included.

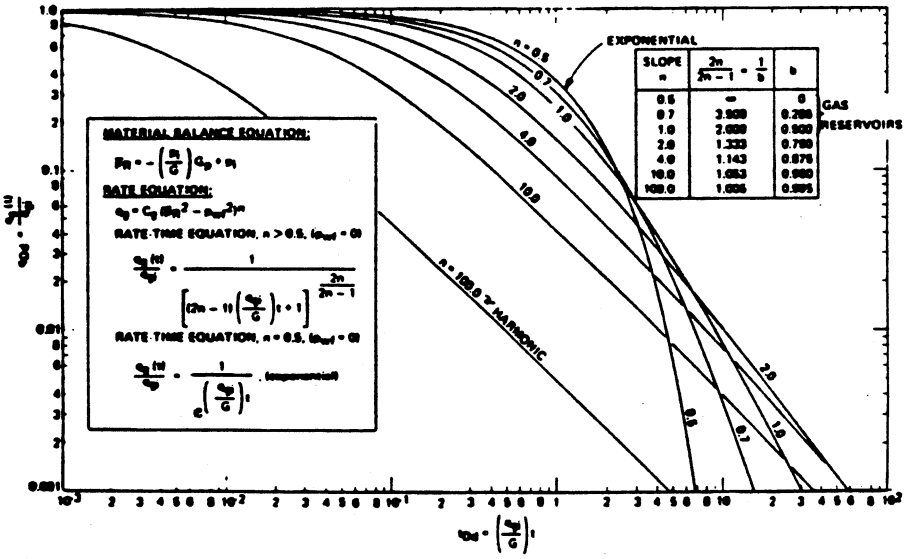

Fig. 8 – Gas reservoir rate decline type curves for finite system with constant pressure at inner boundary (p_{wf} = 0 @ r_w); early transient effects not included.

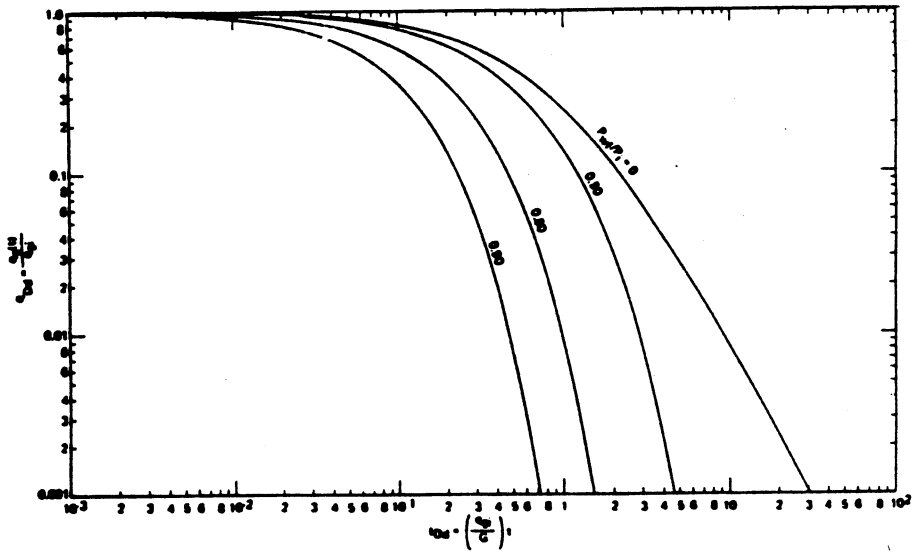

Fig. 9 – Gas reservoir rate decline type curves with backpressure for finite system with constant pressure at inner boundary (p_{wf} = constant @ r_w); early transient effects not included and Z = 1 (based on gas well backpressure curve slope, n = 1).

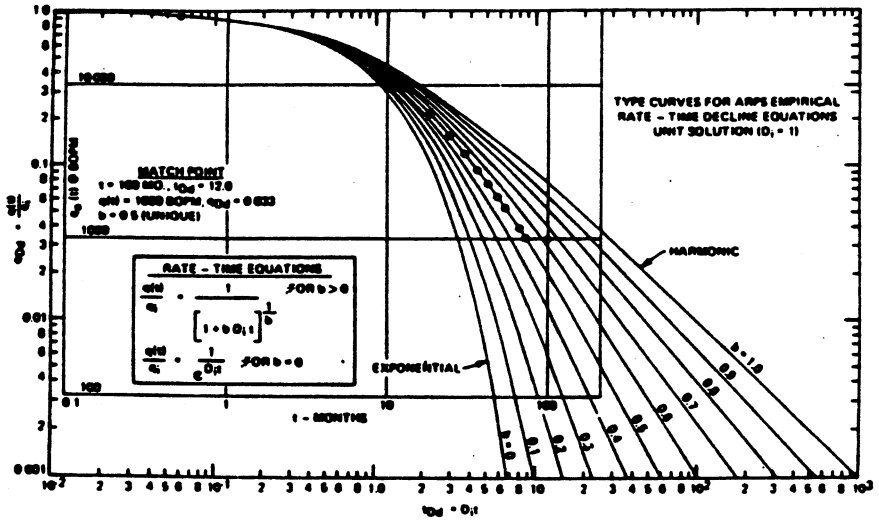

Fig. 10 – Type curve match of Arps' hyperbolic decline example[4] (unique match).

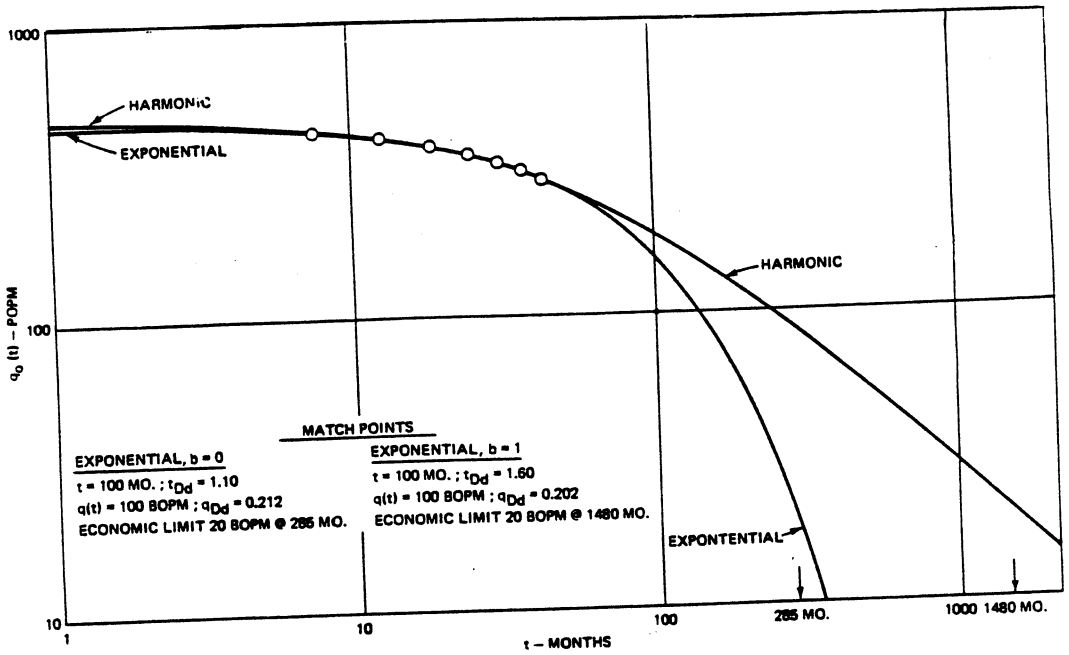

Fig. 11 – Type curve analysis of Arps' exponential decline example.[4]

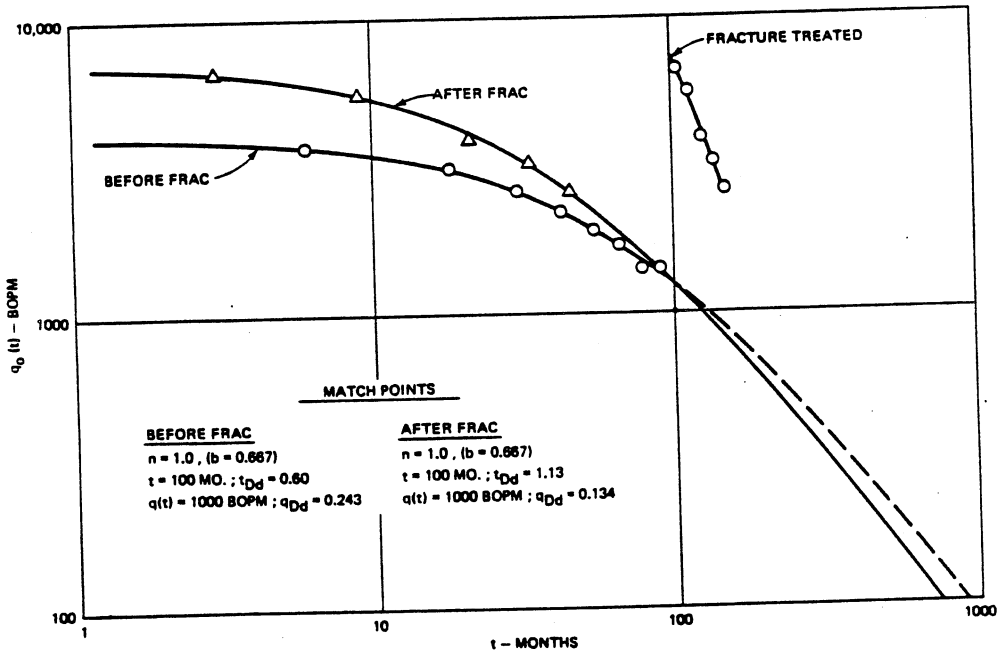

Fig. 12 – Type curve analysis of a stimulated well before and after fracture treatment.

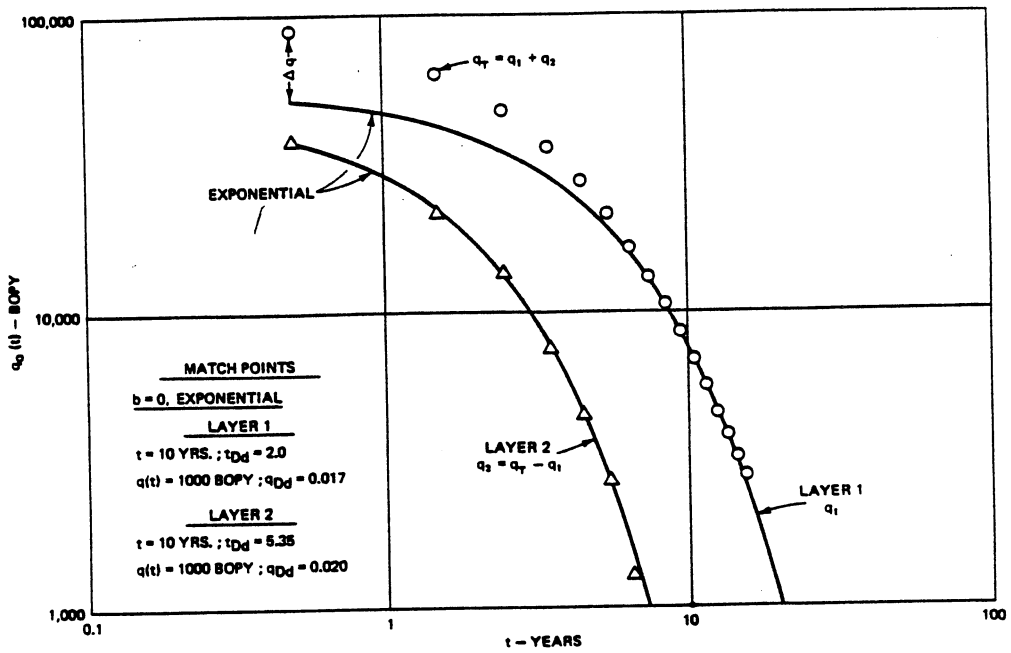

Fig. 13 – Type curve analysis of a layered reservoir (no crossflow) by differencing.

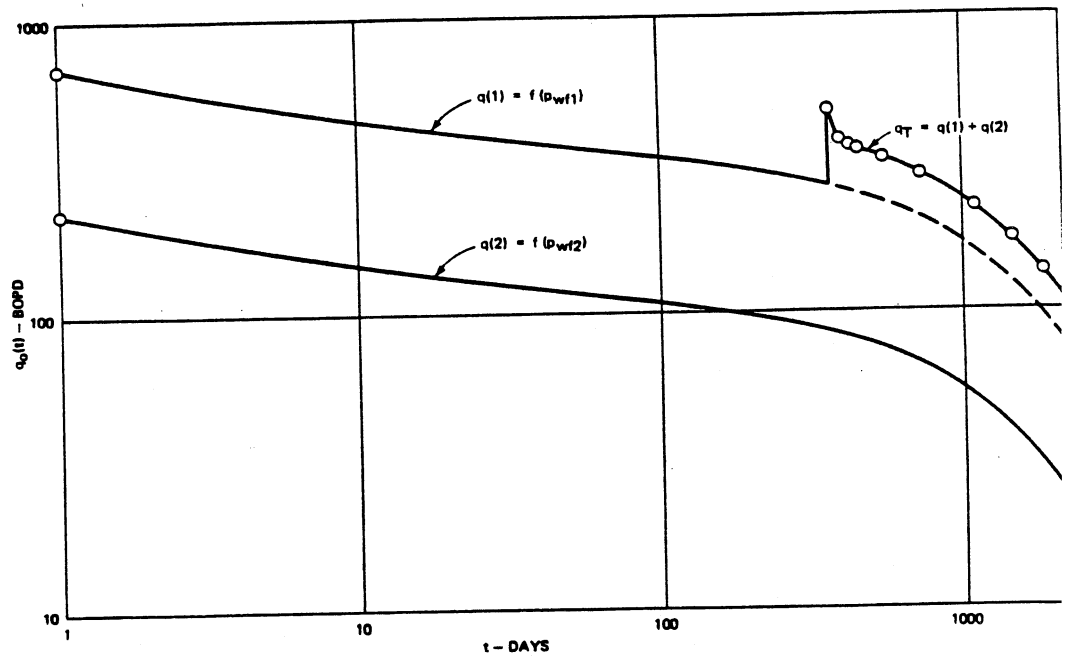

Fig. 14 – Effect of a change in backpressure on decline using graphical superposition.

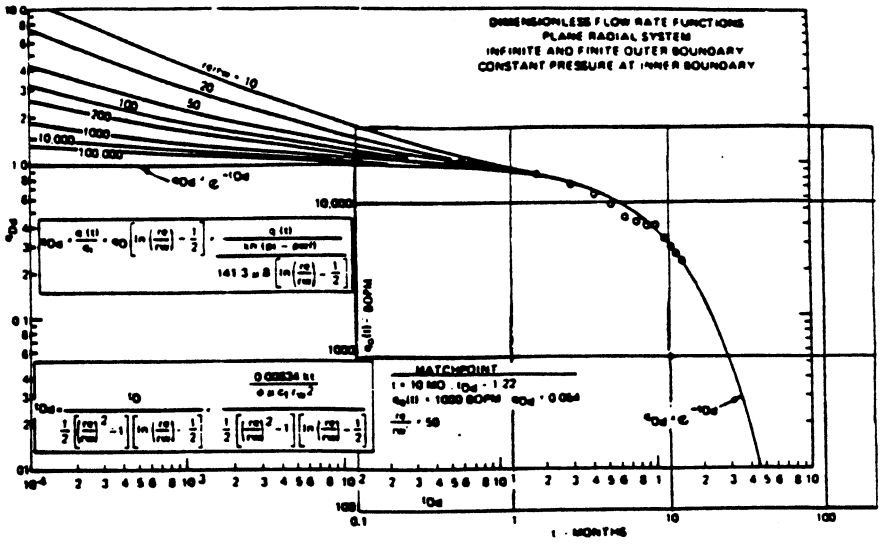

Fig. 15 – Type curve matching example for calculating *kh* using decline curve data, Well 13, Field A.

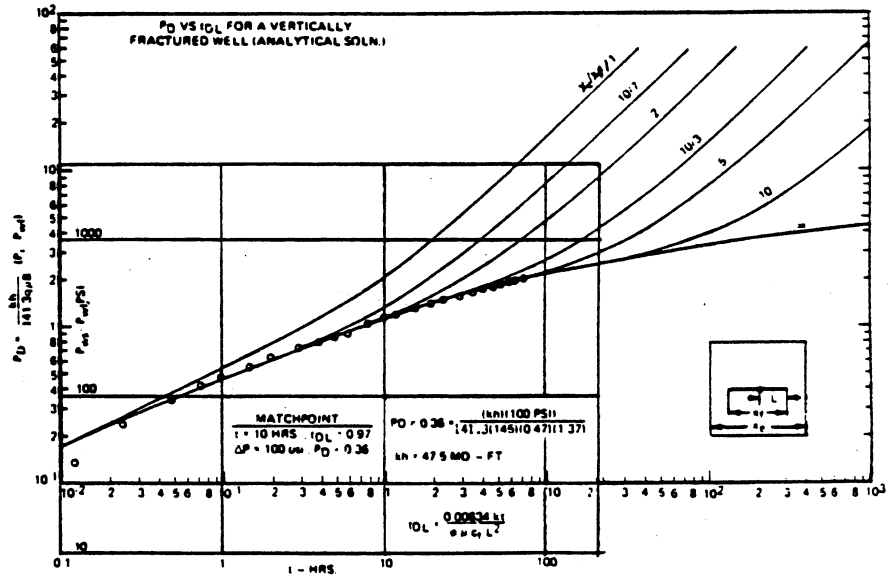

Fig. 16 – Type curve matching example for calculating *kh* from pressure buildup data, Well 13, Field A (type curve from Ref. 8).

MULTIPOINT TESTING OF GAS WELLS

by

M. J. Fetkovich

Phillips Petroleum Company

SPE MID-CONTINENT SECTION
CONTINUING EDUCATION COURSE
WELL TEST ANALYSIS
MARCH 17, 1975

MULTIPOINT TESTING OF GAS WELLS

Multipoint tests consist of a series of at least three or more flows with pressures, rates and other data being recorded as a function of time. The tests are usually conducted for one of the following reasons:

1. Required by a state regulatory body for proration purposes or to obtain an allowable.
2. Required for a pipeline connection.
3. Company policy.
4. Obtain sufficient information for reservoir and production engineering studies which can consist of:
   a. Production forecasting (deliverability type or reservoir simulation).
   b. Determining number of wells and location for development of the field.
   c. Sizing tubing.
   d. Sizing gathering lines.
   e. Sizing trunklines.
   f. Designing compression requirements.
   g. Determining necessity for stimulation.
   h. Correctly evaluating damage (skin effect).
   i. Establish base performance curves for future comparison.

We will limit our present discussion on multipoint testing to Item 4.

There are two basic types of multipoint tests:

1. Flow After Flow Test [1] (No shut-in between flows)
   a. Normal sequence (Fig. 1)
   b. Reverse sequence (Fig. 2)
2. Isochronal Test (Well is shut-in between flows)
   a. True isochronal [2] (Fig. 3)
   b. Modified isochronal [3] (Fig. 4)

Flow After Flow

The flow after flow test starts from a shut-in condition after which a series of increasing flows (normal sequence) or decreasing flows (reverse sequence) is imposed upon the well. No (or very small) shut-in periods occur between each of the flows. Flow times are usually arbitrary or can be set by a regulatory body when conducted for that purpose.

If "stabilized" flows are obtained, the test may be considered to be as valid as if one were to have conducted a true isochronal test. This condition is normally obtained in high permeability reservoirs. Stabilization is defined in the IOCC Manual[4]: "A constant flowing wellhead pressure or static column wellhead pressure and rate of flow for a period of at least 15 minutes shall constitute stabilization . . .". If a well is tubing capacity limited, a pseudo-stabilization can occur if one uses only flowing tubing pressures as the criteria. Pseudo-stabilization can also occur as a result of flowing tubing temperature increase. Therefore, bottomhole or static column pressure stabilization is preferable for this definition.

The different performance curves one could obtain on the same well from an increasing or decreasing sequence multipoint test and an isochronal test is demonstrated by the results shown[2] in Fig. 5. These type of results are normally limited to tests conducted in low permeability reservoirs.

Isochronal Tests

The isochronal method of multipoint testing gas wells is the only certain way of obtaining reliable performance curves. Each flow starts from a comparable shut-in condition. The shut-in must be close enough to a fully built up condition that any pressure rise still occurring will not affect pressure during the drawdown of the subsequent flow; i.e., no prior transits exist during any flow period. Although the flow periods for an isochronal test are usually of equal duration, they need not be. However, when a performance curve is plotted, data from flow periods of the same duration are plotted to obtain the correct value of slope (n), Fig. 6. Note that rates and pressures at a specific time are plotted - NOT AVERAGE RATE.

The isochronal test is based on the principle that the drainage radius established during a flow period is a function only of dimensionless time and is independent of the flow rate; i.e., for equal flow times the same drainage radius is established for different rates of flow. It follows then that an isochronal test would yield a valid performance curve if conducted as either a constant rate or constant flowing pressure test. In fact, many low permeability gas well tests that exhibit severe rate declines on test are really constant wellbore pressure cases and should be analyzed as such. (In a paper by Winestock and Colpitts[5], their rate decline data analyzed as constant pressure case gives the same permeability value as a build-up test.) A constant rate is not required for a valid isochronal test. If one is attempting to short-cut the isochronal test using superposition, then and only then could a constant rate flow condition be required - but only for the purpose of using superposition.

Modified Isochronal Test

In very low permeability reservoirs it may require days to obtain a completely built-up pressure after even relatively short periods of flow (2 to 3 hours). In an attempt to shorten testing time, the modified isochronal test was proposed. It is conducted with shut in periods equal to the flow periods. The unstabilized shut-in pressures are used to calculate the difference in pressure relationship used with the next flow rate. This method of testing has never been adequately justified, either theoretically or by field comparisons with true isochronal tests. What little discussion published justifying this method theoretically has been based on the assumption that flowing pressure behavior with time (superposition) is a function of the log of time $P = f(\ln t)$. Practically however, most low permeability wells where the modified test would be practically applied require stimulation (hydraulic or acid fracs) to be commercial. In these cases pressures are more likely to be a function of the square root of time, $P = f\sqrt{t}$. Modified tests under these conditions can have flowing pressure behavior as functions of $\sqrt{t}$, transitional or ln t each for different flow rates. Fig. 7 is a type curve plot of drawdown data from a 3 hr isochronal flow, note the linear flow behavior for the entire period of flow. For maximum reservoir information purposes, the author does not recommend the modified isochronal test, nor any other method that depends on the application of superposition techniques to shorten test times for low permeability wells. If time is of such importance in low permeability formations, one can be further ahead by simply conducting one long duration flow period (making certain we are out of wellbore storage, $\sqrt{t}$ and transitional period prior to ln (t) behavior) and assuming a back-pressure curve slope (n) of one. Better still, the Two Flow Method[6] of Carter, Miller and Riley would be preferred - i.e., two isochronal points.

Isochronal Testing

For maximum information and minimum confusion, the writer prefers and recommends the isochronal test method when multipoint tests are required - particularly on wildcat or initial development wells. Once the basic characteristics of the reservoir and fluid properties have been defined from valid isochronal tests, one should consider the possibility of reducing testing time without sacrificing information.

The number of flows and flow and shut in times can often be reduced with shut in periods even eliminated in some cases.

Without getting into the detailed mechanics of testing and taking data, a few remarks on test procedure are appropriate. Whenever possible bottom hole pressure gauges should be used. Surface pressures should be recorded with a dead weight tester and measured on both the tubing and annulus along with flowing temperatures. The frequency of taking the surface drawdown and buildup data should be sufficient for type curve analysis, i.e., early time data is critical for this analysis. Similarly, with about the same frequency, flow rate data should be recorded and reported. A constant wellbore pressure analysis or a Winestock and Colpitts analysis ($\Delta p^2/Q$ vs time) may be

required. Plotting and analysis of the test data, drawdown, buildup and back-pressure curves on site during the test are rather critical to obtaining valid tests. Most important of all, the well must be cleaned up prior to conducting the test. The importance of a clean up flow is dramatically illustrated by the test results obtained on Well C, Fig. 8. As a general rule for selecting rates one should attempt to flow the well at or near the expected continuous sales rate. If sand, water coning or other problems could develop, now is the time to find out.

Following is a typical isochronal test procedure used on a wildcat or early development well:

1. Initial Flow (± 15 min)
2. Initial Shut-in (± 2 hrs)
3. Clean Up Flow at Maximum Separator Capacity (± 10 hrs)
4. Shut-in Period (± 12 hrs)
5. Flow at ± 1/4 Maximum Rate (± 6 hrs)
6. Shut-in Period (± 9 hrs)
7. Flow at ± 1/2 Maximum Rate (± 6 hrs)
8. Shut-in Period (± 9 hrs)
9. Flow at ± 3/4 Maximum Rate (± 6 hrs)
10. Shut-in Period (± 9 hrs)
11. Flow at Maximum Rate (± 6 hrs)

The above time periods are subject to change depending on an on-site analysis of the initial data. Severe wellbore storage effects or total linear flow as demonstrated in Figs. 9 and 7 respectively would cause the multipoint test to be aborted, and one would then settle for a single long duration drawdown and buildup.

Conventional Well Test Analysis ($\bar{p}_R$ < 2500 psi)

Gas well analysis can be divided into two pressure regions, low to medium pressure and high pressure wells. Much of the basic theory of testing and analysis was developed from well tests with reservoir pressure levels under 2500 psi. This resulted in the familiar back pressure curve plotting of log q vs log $\Delta(p^2)$ and pressure build-up and drawdown analysis using p^2 vs $\log\left(\frac{t + \Delta t}{\Delta t}\right)$ plot and p^2 vs log t.

With the advent of deeper drilling, gas wells have been discovered with reservoir pressures approaching 10,000 psi. In these cases, and down to about 2500 psi the conventional methods of analysis break down and the real gas potential theory approach must be resorted to. (This will be discussed later.)

Basic Equations (Reservoir and Surface Datums)

The familiar transient gas flow equation is usually given in standard engineering units as:

$$\bar{p}_{Ri}^2 - p_{wf}^2 = \frac{1424\ (\bar{\mu}\bar{z})T}{Kh}\left\{\left[\frac{1}{2}(\ln t_D + 0.809) + S\right]Q + \left[\frac{2.226 \times 10^{-15}\ \beta KG}{hr_w\mu}\right]Q^2\right\} \quad \ldots (1)$$

Where Q = gas flow rate, Mscfd
K = effective permeability to gas, md
h = net pay, ft
T = reservoir temperature, °R
$\bar{p}_R$ = static reservoir pressure, psia
p_{wf} = bottom hole flowing pressure, psia
G = gas gravity
μ = gas viscosity, cps (evaluated at $\bar{p}_R$)
$\bar{\mu}$ = gas viscosity, cps [evaluated at average pressure, $(\bar{p}_R + p_{wf})/2$]
β = turbulence factor, ft^{-1}
S = <u>laminar</u> flow skin effect, dimensionless
r_w = wellbore radius, ft
t_D = dimensionless time

The dimensionless time equation, with time t in days is:

$$t_D = \frac{6.33 \times 10^{-3}\ K\ \bar{p}_R\ t}{\phi\mu r_w^2} \quad \ldots (2)$$

The basic equation used to describe reservoir drawdown when stabilized flow exists is given as:

$$\bar{p}_R^2 - p_{wf}^2 = \frac{1424\ (\bar{\mu}\bar{z})\ T}{Kh}\left\{\left[\ln\left(\frac{.472\ r_e}{r_w}\right) + S\right]Q + DQ^2\right\} \quad \ldots (3)$$

For further discussion if we define:

$$B = \frac{1424\ (\bar{\mu}\bar{z})\ T}{Kh}\ D \quad \ldots (4)$$

we can obtain

$$\bar{p}_R^2 - p_{wf}^2 = \frac{1424\ (\overline{\mu z})\ T}{Kh} \left[\ln\left(\frac{.472 r_e}{r_w}\right) + S \right] Q + BQ^2 \qquad ..(5)$$

Defining

$$A = \frac{1424\ (\overline{\mu z})\ T}{Kh} \left[\ln\left(\frac{.472\ r_e}{r_w}\right) + S \right] \qquad ..(6)$$

or for the transient period

$$A(t) = \frac{1424\ (\overline{\mu z})\ T}{Kh} \left[\frac{1}{2} (\ln t_D + 0.809) + S \right] \qquad ..(7)$$

We obtain the familiar form of the Forscheimer equation (either A or A(t) is applicable in all that follows)

$$\bar{p}_R^2 - p_{wf}^2 = AQ + BQ^2 \qquad ..(8)$$

Which can also be written in the more familiar form as an approximation to the above equation as:

$$Q \cong C_{bh}\ (\bar{p}_R^2 - p_{wf}^2)^n \qquad ..(9)$$

Breaking the total pressure drop into the laminar and turbulent pressure drop contributions we have

Total Drop		Laminar Drop		Turbulent Drop	
$\bar{p}_R^2 - p_{wf}^2$	=	$(\bar{p}_R^2 - p_{Lf}^2)$	+	$(p_{Lf}^2 - p_{wf}^2)$	..(10)

The laminar contribution equation can then be written at reservoir datum as

$$Q = \frac{1}{A} (\bar{p}_R^2 - p_{Lf}^2)^{1.0} = \frac{Kh\ (\bar{p}_R^2 - p_{Lf}^2)^{1.0}}{1424\ (\overline{\mu z})\ T \left[\ln\left(\frac{.472\ r_e}{r_w}\right) + S \right]} \qquad ..(11)$$

for the laminar drop and

$$Q = \frac{1}{\sqrt{B}} (p_{Lf}^2 - p_{wf}^2)^{0.5} \qquad ..(12)$$

for the turbulent drop.

Rearranging equation (8) we obtain

$$\frac{\bar{p}_R^2 - p_{wf}^2}{Q} = A + BQ \qquad ..(13)$$

A plot of $(\bar{p}_R^2 - p_{wf}^2)/Q$ vs Q of the back-pressure test data will readily yield A from the intercept and B from the slope. Plotting transient flow data the intercept would be A(t) from which we could readily calculate skin (s). Fig. 10 and Table 1 illustrate the plot and calculations for Well C. A separate back pressure curve plot, **that is a straight line**, can be made for both the turbulent and laminar pressure drop contribution. The laminar curve will have a slope n = 1.0 and the turbulent curve a slope n = 0.5. A composite or total pressure drop curve can then be readily constructed by summing the pressure drops from each curve at the same value of rate of flow. The composite curve or total pressure drop curve may then be a curved line except for the limiting slopes of n = 0.5 and n = 1.0. In most cases, however, the composite will yield a dominant slope n between 0.5 and 1.0 with its actual value being a function of the relative contribution of laminar and turbulent flow.

Slopes of the Back Pressure Performance Curves

Examination of field performance curves indicates that low permeability gas wells will normally yield bottom-hole back pressure curves with slopes more nearly approaching 1.0, while high permeability gas wells yield slopes more nearly approaching 0.5. Popular belief has usually been based simply on the concept of permeability value, i.e., low permeability develops turbulent flow (β is large), high permeability laminar flow. Also, it is often stated that the value of the exponent n is 0.5 for completely turbulent flow. In a radial flow system, there is no possible way of physically having turbulent flow throughout the drainage radius.

Returning again to the Forscheimer equation[8]

$$\bar{p}_R^2 - p_{wf}^2 = AQ + BQ^2 \qquad ..(8)$$

When Kh is large, the term AQ becomes small and we would have

$$Q \cong \frac{1}{\sqrt{B}}(\bar{p}_R^2 - p_{wf}^2)^{0.5} \qquad ..(14)$$

Similarly when Kh is small, the AQ becomes large and the BQ^2 term can become negligible (not necessarily zero) when compared to the laminar pressure drop term. We could then write

$$Q \cong \frac{1}{A}(\bar{p}_R^2 - p_{wf}^2)^{1.0} \qquad ..(15)$$

It is clear then that it is not necessary for flow to be completely turbulent throughout the reservoir for the slope (n) to be equal to 0.5.

The following table summarizes results obtained from isochronal tests on a few high and low permeability wells. All tests were run with sub-surface gauges in the well.

BOTTOMHOLE CURVE

Well	Formation	Potential Mscfd	Slope (n)	Build-Up K - md
1	Sandstone	57,000	0.554	960
2	Sandstone	170,000	0.532	1331
3	Sandstone	310,000	0.658	978
4	Sandstone	88,000	1.000	12
5	Sandstone	68,000	1.000	7

Back Pressure Curves at Surface Datum, "Wellhead Curves"

Gas cannot be sold at the bottom of the hole. It must first be produced through tubing (or casing, of course) surface equipment, a gathering line, then finally through a pipeline. Until the gas enters a trunkline, we must continue to predict the pressure drops through the entire system to obtain the ability of a well to deliver gas to a pipeline.

We can carry the discussion about back pressure curves and slopes one step further to include the tubing pressure drop effect and the resulting wellhead back pressure curve and its slope. If we divide the Forscheimer form of the bottom hole flow equation by the gas well hydrostatic head term e^s, we obtain

$$\frac{\bar{p}_R^{\,2}}{e^s} - \frac{p_{wf}^{\,2}}{e^s} = \frac{A}{e^s} Q + \frac{B}{e^s} Q^2 \qquad ..(16)$$

where $S = 0.0375\ GH/T_a\ Z_a$ (This S should not be confused with skin)
and e = natural log
G = gas gravity
H = vertical depth, ft
T_a = average temperature, °R
Z_a = gas deviation factor at average pressure
$p_c^{\,2} = \bar{p}_R^{\,2}/e^s$
$p_w^{\,2} = p_{wf}^{\,2}/e^s$

P_c is the wellhead shut-in pressure and p_w is the wellhead static column flowing pressure. p_w is that pressure that would be recorded on the annulus while flowing if there were no packer in the well. Even if there is a packer in a well, it is a useful pressure to evaluate and a useful concept to use in back pressure curve performance analysis. (The simplifying assumption of a constant e^s does not introduce serious errors and we end up with some very useful equations that can be easily manipulated.)

We can now write the reservoir flow equation in terms of the more convenient wellhead pressures and now at a surface datum

$$p_c^2 - p_w^2 = A_{wh}\, Q + B_{wh}\, Q^2 \qquad ..(17)$$

which can also be written in the more familiar form as

$$Q \cong C_{wh}\, (p_c^2 - p_w^2)^n \qquad ..(18)$$

where now

$$A_{wh} = \frac{1424\ (\overline{\mu z})\ T}{Kh\ e^s} \left[\ln\left(\frac{.472\ r_e}{r_w}\right) + S \right] \qquad ..(19)$$

$$B_{wh} = \frac{B}{e^s} \qquad ..(20)$$

Tubing Friction Curves

The basic equation relating wellhead static column pressure p_w and the wellhead flowing tubing pressure P_t as given in the IOCC Manual[4] is

$$p_{wf}^2 = e^s\, P_t^2 + \left(\frac{F_r\, Q\, T_a\, Z_a}{31.62}\right)^2 (e^s - 1) \qquad ..(21)$$

where

$$F_r = \frac{0.10797}{D^{2.612}} \qquad \text{with D in inches.}$$

Dividing both sides by e^s, we obtain

$$\frac{p_{wf}^2}{e^s} = P_t^2 + \left(\frac{F_r\, Q\, T_a\, Z_a}{31.62}\right)^2 \frac{(e^s - 1)}{e^s} \qquad ..(22)$$

with $p_{wf}^2/e^s = p^2{}_w$ we can rearrange and obtain

$$Q = \left[\frac{31.62\ e^{s/2}}{\sqrt{(e^s - 1)}\ F_r\ T_a\ Z_a}\right] (p_w^2 - P_t^2)^{0.5} \qquad ..(23)$$

The general form is simply

$$Q = T\ (P_w^2 - P_t^2)^{0.5} \qquad ..(24)$$

$$\text{or } P_w^2 - P_t^2 = (Q/T)^2 \qquad ..(25)$$

that will plot as a straight line on log-log paper with a slope of 0.5. Thus $(1/T^2)\ Q^2 = (P_w^2 - P_t^2)$ defines the pressure drop through the tubing string. (For convenience, in later discussions, let's define $T_{wh} = 1/T^2$.)

Combining the tubing pressure drop equation with the equation describing the pressure drops through the reservoir in terms of wellhead pressures, we obtain the wellhead back pressure curve equation that accounts for the total pressure drop through the system. The total pressure drop expressed at the tubing wellhead (surface datum) is then given by

$$(P_c^2 - p_w^2) + (p_w^2 - P_t^2) = A_{wh}\ Q + B_{wh}\ Q^2 + T_{wh}\ Q^2 \qquad ..(26)$$

or

$$(P_c^2 - P_t^2) = A_{wh}\ Q + (B_{wh} + T_{wh})\ Q^2 \qquad ..(27)$$

which can also be represented as

$$Q = C_{wht}\ (P_c^2 - P_t^2)^n \qquad ..(28)$$

Note that as a limiting condition, if T_{wh} is large compared to A_{wh} and/or B_{wh} (a very large bottom hole potential), the equation reduces to

$$Q = C_{wht}\ (P_c^2 - P_t^2)^{0.5} \qquad ..(29)$$

Figures 11, 12, and 13 illustrate the effects of tubing friction on wellhead deliverability.

This indicates that the wellhead curve could in some instances be totally described by the pressure drop through the tubing string. A significant point is that we can use this equation to establish, for flow through any given tubing size, a maximum position for a wellhead curve, its potential, and it will have a slope of 0.500. For other diameter flow strings one need only ratio $\frac{D^{2.612}_{New}}{D^{2.612}_{Present}}\ C_{wht}$ to draw in its curve. This approach of changing flow string diameter can also be used when compositing total drops from each of the pressure drop curves, laminar, turbulent and tubing.

Gathering Line or Pipeline Equation

A pressure drop equation for a gathering line and a pipeline can be developed using the general flow equation as given in the Natural Gas Processors Suppliers Association, Engineering Data Book, 1966. (The fact that we can often treat a total field as a single back pressure curve can even allow us to include the pipeline pressure drop in our analysis or forecasts.)

The flow equation (assuming negligible elevation differences between inlet and outlet) can be written as:

$$Q = \frac{5.487\ D^{2.5}}{\sqrt{T_a'\ Z_a\ GL}}\ \log_{10}\left(\frac{3.7\ D}{K_e}\right)\ [\ P_{up}^2 - P_{dwn}^2\ ]^{0.5} \qquad ..(30)$$

where Q = gas flow rate Mscfd @ 14.7 & 60° F
D = inside diameter, in
K_e = absolute roughness, in (K_e = 0.0015 is suggested)
T_a' = average flowing line temperature, °R
Z_a = gas deviation factor at average pressure
G = gas gravity
L = pipe length, miles
P_{up} = upstream pressure, psia (equal to P_t for gathering line connected to tubing)
P_{dwn} = downstream pressure, psia

$$Q = C_{PL} \ (P_{up}^2 - P_{dwn}^2)^{0.5}$$

In the general form we have

$$Q = L \ (P_t^2 - P_{dwn}^2)^{0.5} \qquad ..(30\text{-}A)$$

(Again for convenience, we will define $L_{wh} = 1/L^2$.) Now we can write equations at surface datum representing the total pressure drop through the system.

$$\Delta(P^2)_{total} = P_c^2 - P_{dwn}^2$$

$$= \Delta(P^2)_{darcy} + \Delta(P^2)_{skin} + \Delta(P^2)_{turb} + \Delta(p^2)_{tbg} + \Delta(P^2)_{line}$$

or

$$P_c^2 - P_{dwn}^2 = (P_c^2 - P_L^2) + (P_L^2 - p_w^2) + (p_w^2 - P_t^2) + (P_t^2 - P_{dwn}^2)$$

or

$$P_c^2 - P_{dwn}^2 = A_{wh} \ Q + (B_{wh} + T_{wh} + L_{wh})Q^2$$

recapitulating

$$A_{wh} = \frac{1424 \ (\overline{\mu z}) \ T}{Kh \ e^s} \left[\ln\left(\frac{.472 \ r_e}{r_w}\right) + S \right] \quad \text{or} \quad A(t) = f(t_D)$$

$$B_{wh} = B/e^s$$

$$T_{wh} = \frac{(e^s - 1) \ F_r^2 \ T_a'^2 \ Z_a^2}{(31.62)^2 \ e^s}$$

$$L_{wh} = \frac{T_a' \ Z_a \ GL}{(5.487)^2 \ D^5}$$

The total pressure drop equation finally can be represented as

$$Q = C_{total} \ (P_c^2 - P_{dwn}^2)^n \qquad ..(31)$$

For deliverability or production forecasting this is the equation that should be used.

Still further, to account for the pressure drop through a well's required well site surface equipment (separator and dehydrator), the basic flow equation $Q = C_E\ (p_1^2 - p_2^2)^{0.5}$ can be included into the above equations. A single data point on the equipment either measured or obtained from the manufacturer can be used to define C_E.

Note that all the above pressure drop components can be graphed individually as log Q vs log $\Delta(p^2)$. A total curve can then be constructed by a composition of all curves, thus relating pressure drop through the total system for a given flow rate.

Examination of the total pressure drop equations indicates that in wells with large bottom hole potentials we should expect the slope of the wellhead deliverability curve to approach 0.5, the slope of all pipe flow and turbulent flow pressure drop components. Conversely for small potential wells we would expect the slope of the wellhead curve to approach the slope of the bottom hole or Darcy flow curve, 1.0.

Real Gas Flow ($\bar{p}_R$ > 2500 psi)

Al Hussainy, Ramey and Crawford[7] showed that it was possible to consider gas physical property dependence on pressure by means of the real gas pseudo-pressure m(p). Although they indicated that it was important for the case of gas flow in tight high pressure formations with large drawdowns, it is equally important for high permeability formations with normal drawdowns.

The real gas pseudo-pressure m(p) was defined by them as:

$$m(p) = 2 \int_{P_m}^{P} \frac{P}{\mu(P)\ Z(P)}\ dp \qquad ..(32)$$

where P = pressure, psia
μ = gas viscosity, cps
Z = gas deviation factor
P_m = base pressure, psia (P = 0 is most convenient)

an m(p) could also be defined in a more familiar form as

$$m(p) = \int_{P_m}^{P} \frac{1}{\mu_g\ \beta_g}\ dp \qquad ..(33)$$

where $\beta_g = \frac{P_{sc}\ Z\ T}{T_{sc}\ P}$ (sub sc indicates standard conditions)

then

$$m(p) = \frac{T_{sc}}{P_{sc}\ T} \int_{P_m}^{P} \frac{P}{\mu(P)\ Z(P)}\ dp \qquad ..(34)$$

where temperature is in °R.

In all further discussions we will deal with the m(p) in terms of $1/\mu_g\ \beta_g$.

For simplicity of discussion, let us use the general steady state radial flow equation:

$$q = \frac{7.08kh}{\ln\left(\frac{r_e}{r_w}\right)} \int_{P_{wf}}^{P_e} f\ (p)\ dp \qquad ..(35)$$

where q = surface rate of flow, bbl/day
K = effective permeability, Darcy
h = thickness, ft
r_w = wellbore radius, ft
r_e = external boundary radius, ft
P_{wf} = bottom hole flowing pressure, psia
P_e = external boundary pressure, psia

It is perfectly general and is equally applicable to either liquid or gas flow. For gas flow we can simply write

$$q_g = \frac{7.08kh}{\ln\left(\frac{r_e}{r_w}\right)} \int_{P_{wf}}^{P_e} \frac{1}{\mu_g\ \beta_g}\ dp \qquad ..(36)$$

The integral can be expressed in terms of pseudo-pressures m(p)

$$\int_{P_{wf}}^{P_e} \frac{1}{\mu_g\ \beta_g}\ dp = \int_0^{P_e} \frac{1}{\mu_g\ \beta_g}\ dp - \int_0^{P_{wf}} \frac{1}{\mu_g\ \beta_g}\ dp \qquad ..(37)$$

or

$$\int_{P_{wf}}^{P_e} \frac{1}{\mu_g\ \beta_g}\ dp = m(P_e) - m(P_{wf}) \qquad ...(38)$$

The quantity $[m(P_e) - m(P_{wf})]$ is simply the area under the $1/\mu_g\ \beta_g$ curve from P_e to P_{wf}. $m(P_e)$ is the area under the curve from P_e to 0, and $m(P_{wf})$ is the area under the curve from P_{wf} to 0. The ABSOLUTE OPEN FLOW POTENTIAL can be expressed by

$$AOFP = \frac{7.08kh}{\ln\left(\frac{r_e}{r_w}\right)}\ m(P_e) \qquad ..(39)$$

Let us examine the basic shape of $1/\mu_g \beta_g$ with pressure. Fig. 14 is a plot of $1/\mu_g \beta_g$ for a gas reservoir with an initial shut in pressure of 5567 psia. At high pressures $1/\mu_g \beta_g$ is nearly constant, only slightly changing with pressure. Again, for simplicity of discussion, we can approximate the pressure function by two straight line sections as:

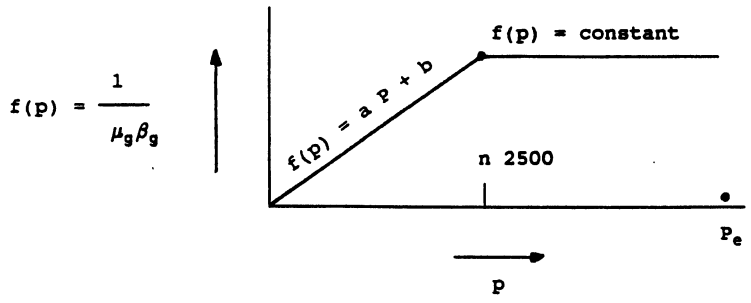

For the region where the pressure function is a constant ($1/\mu_g \beta_g$ is constant), we can evaluate the integral as

$$\int_{P_{wf}}^{P_e} f(p)\, dp = \frac{1}{\mu_g \beta_g} \int_{P_{wf}}^{P_e} dp \qquad ..(40)$$

which when integrated between limits, yields

$$\int_{P_{wf}}^{P_e} f(p)\, dp = \frac{P_e - P_{wf}}{\mu_g \beta_g} \qquad ..(40A)$$

Then

$$q_g = \frac{7.08kh}{\ln\left(\frac{r_e}{r_w}\right)} \frac{(P_e - P_{wf})}{\mu_g \beta_g} \qquad ..(41)$$

(Note that this is identical to the single phase liquid flow equation commonly used for oil wells.) A multipoint test conducted with drawdowns over the constant portion of the $1/\mu_g \beta_g$ curve should yield a straight line on a q_g vs Δp plot. This in fact is the case for a gas well isochronal test, Fig. 15, conducted in the reservoir represented by the $1/\mu_g \beta_g$ plot of Figure 14.

The same data when plotted in the conventional manner of log q vs log $\Delta(p^2)$ yields a back pressure curve with a slope n = 1.265, Fig. 16. This is greater than the normally accepted maximum value of 1.0. (A curve with slopes greater than 1 is characteristic of a Δp behavior plotted in the $\Delta(p^2)$ form.)

Neither a Δp nor a $\Delta(p^2)$ extrapolation of the multipoint test can be justified to define the remainder of the back-pressure curve and to determine its absolute open flow potential. (It's only coincidental that the $\Delta(p^2)$ extrapolation of the example results in the same AOFP as the m(p) plot. It should only be considered a result of trend plotting.) The only correct method of extrapolating the test results from Well D is by means of an m(p) plot, Fig. 17.

Even though we cannot extrapolate the $\Delta(p)$ plot of Well D to a correct AOFP, it can and was used to validate what "appeared" initially to be an invalid isochronal test. All high pressure gas well test data should be field checked with a Δp plot until m(p) data can be developed.

Let us next examine the pressure function at pressures below ~ 2500 psi. Approximating f(p) in this region with an equation of a straight line.

$$f(p) = a\,P + b$$

With the intercept b = 0, and P_e < 2500 psi

$$\int_{p_{wf}}^{P_e} f(p)\,dp = \int_{p_{wf}}^{P_e} a\,P\,dp = \frac{a}{2}\,(P_e^2 - p_{wf}^2) \qquad ..(42)$$

The slope a for b = 0, is simply $(1/\mu_g\,\beta_g)/P_e$. We can then write

$$q_g = \frac{7.08kh}{\ln\left(\frac{r_e}{r_w}\right)(\mu_g\,\beta_g)_{P_e}}\;\frac{(P_e^2 - p_{wf}^2)}{2\,p_e} \qquad ..(43)$$

with β_g evaluated at P_e, we obtain the familiar $\Delta(p^2)$ form of equation

$$q_g = \frac{3.54kh\,T_{sc}\;(P_e^2 - p_{wf}^2)}{\mu Z\,T\,P_{sc}\;\ln\left(\frac{r_e}{r_w}\right)} \qquad ..(44)$$

Clearly then in the high pressure region where flow is behaving as a liquid, one can plot p to analyze drawdown or buildup data. With all pressures over the low pressure region, one should plot p^2 to analyze drawdown or build-up data. If the pressure data covers both the high and low pressure regions, as one might expect in high pressure low permeability formations, one must plot m(p). When in doubt, always use m(p).

Table 1

Well C

ISOCHRONAL TEST (BOTTOM-HOLE GAUGE)

$\bar{p}_R$ = 1370 psia

Flow No.	Q Mscfd	p_{wf} psig	$\bar{p}_R^2 - p_{wf}^2$ psia^2	$\frac{\bar{p}_R^2 - p_{wf}^2}{Q}$ psia^2/Mscfd	Flow Duration Hours
1	11,300	1327	75,096	6,646	16
2	6,700	1343	32,376	4,832	2
3	11,850	1325	80,400	6,785	2
4	14,780	1318	98,901	6,692	2
5	52,500	1307	127,776	2,434	6
6	13,300	1349	16,224	1,220	1
7	20,650	1343	32,376	1,568	1
8	29,400	1335	53,800	1,830	1

Kh = 306,060 md-ft (From Build-Up); K = 978 md
h = 313 ft
$\bar{P}$ = 1346 psia
μ = 0.014 cps
$\bar{Z}$ = 0.868
T = 120°F
t = 1 hr
Q = 18.1
G = 0.655
r_w = .33 ft
hp = 70 ft (perforated at top)

EXAMPLE CALCULATIONS FROM ISOCHRONAL TEST

Well "C"

$$A(t) = \frac{1424\ (\overline{\mu z})\ T}{Kh}\left[\frac{1}{2}\ (\ln t_D + 0.809) + S\right] = 1.00\ \frac{psi^2}{Mscfd}$$

$$S = \frac{A(t)\ Kh}{1424\ (\overline{\mu z})\ T} - \left[\frac{1}{2}\ (\ln t_D + 0.809)\right]$$

With

$$t_D = \frac{0.00633\ K\ \bar{P}\ t}{\phi \mu r_w^2} = \frac{.00633\ (978)\ (1346)\ 1}{(.181)\ (.014)\ (.33)^2\ 24}$$

$$t_D = 1.258 \times 10^6$$

$$S = \frac{1.0\ (306{,}060)}{1424\ (.014)(.868)(580)} - [\ 7.43\ ] = +\ 22.8$$

PARTIAL PENETRATION SKIN (BRONS AND MARTING)[8]

TOP 70 ft PERFORATED OUT OF 313 ft PAY

$$b = \frac{70}{313} = 0.22$$

$$\frac{h}{r_w} = \frac{313}{.33} = 948$$

Sb = + 19 Good Check

EXAMPLE CALCULATIONS FROM ISOCHRONAL TEST

WELL "C"

$$B = \frac{1424\ (\overline{\mu z})\ T}{Kh} \qquad D = 27.322 \times 10^{-6} \left(\frac{psi^2}{Mscfd}\right)$$

$$D = \frac{2.226 \times 10^{-15}\ \beta\ K\ G}{h\ r_w\ \mu}$$

$$B = \frac{3.17 \times 10^{-12}\ Z\ G\ T}{h^2\ r_w}\ \beta$$

$$\beta = \frac{Bh^2\ r_w}{3.17 \times 10^{-12}\ Z\ G\ T} = \frac{27.322 \times 10^{-6}\ (313)^2\ (.33)}{3.17 \times 10^{-12}\ (.868)\ (.655)\ (580)}$$

$$\beta = 8.45 \times 10^{8}\ ft^{-1}$$

From Katz Curve, $\beta = 3.4 \times 10^{6}\ ft^{-1}$

NOTE: This difference is consistent with the author's in evaluating ß values from field data over a large range of permeabilities. Actual β's are usually 100 times larger than those obtained from Katz's Curve.(3)

CALCULATION OF m(p), WELL D

Pressure psia	ΔP psi	P avg psia	$\frac{1}{\mu_g \beta_g}$ @ P avg, Mscf / Res Bbl-cps	$\Delta P\left(\frac{1}{\mu_g \beta_g}\right)$, 10^3	$m(p) = \sum_{P=0}^{P} \Delta P\left(\frac{1}{\mu_g \beta_g}\right)$, Mscf-psi / Res Bbl-cps, 10^3
5600					227.52
	600	5300	56.70	34.02	
5000					193.50
	500	4750	56.00	28.00	
4500					165.50
	500	4250	54.80	27.40	
4000					138.10
	500	3750	53.00	26.50	
3500					111.60
	500	3250	50.80	25.40	
3000					86.20
	500	2750	47.30	23.65	
2500					62.55
	500	2250	42.00	21.00	
2000					41.55
	500	1750	34.80	17.40	
1500					24.15
	500	1250	26.20	13.10	
1000					11.05
	500	750	16.40	8.20	
500					2.85
	500	250	5.70	2.85	
0					0

REFERENCES

1. Rawlins, E. L., and Schellhardt, M. A., "Back-Pressure Data on Natural Gas Wells and Their Application to Production Practices", U.S. Bureau of Mines Monograph 7, 1936.

2. Cullender, M. H., "The Isochronal Performance Method of Determining the Flow Characteristics of Gas Wells", Trans. AIME (1955) 204, 137.

3. Katz, D. L., et al, Handbook of Natural Gas Engineering, McGraw-Hill Book Co., Inc., N. Y. (1959).

4. Interstate Oil Compact Commission, "Manual of Back-Pressure Testing of Gas Wells", Oklahoma City, Oklahoma.

5. Winestock, A. G., and Colpitts, G. P., "Advances in Estimating Gas Well Deliverability", The Journal of Canadian Petroleum Technology (1965) Vol. 4, 111-119.

6. Carter, R. D., Miller, S. C., and Riley, H. G., "Determination of Stabilized Gas Well Performance From Short Flow Tests", J. Pet. Tech. (June, 1963) 651.

7. Al-Hussainy, R., Ramey, H. J., Jr., and Crawford, P. B., "The Flow of Real Gases Through Porous Media", J. Pet. Tech. (May, 1966) 624.

8. Bron, F. and Marting, V. E., "The Effect of Restricted Fluid Entry on Well Productivity", J. Pet. Tech. (Feb. 1961) 172.

PURPOSE OF MULTIPOINT TESTING

1. Required by a state regulatory body for proration purposes, or to obtain an allowable.

2. Required to obtain a pipeline connection.

3. Company Policy.

4. Obtain sufficient information for reservoir and production engineering studies. Some of which are:

   a) Production forecasting (deliverability type or reservoir simulation).

   b) Determining number of wells for field development.

   c) Sizing tubing.

   d) Sizing gathering lines.

   e) Sizing trunklines.

   f) Compressor requirements.

   g) Determining necessity for stimulation.

   h) Proper evaluation of damage or skin effect.

   i) Establish a base performance curve for future comparison (Reconditioning Studies).

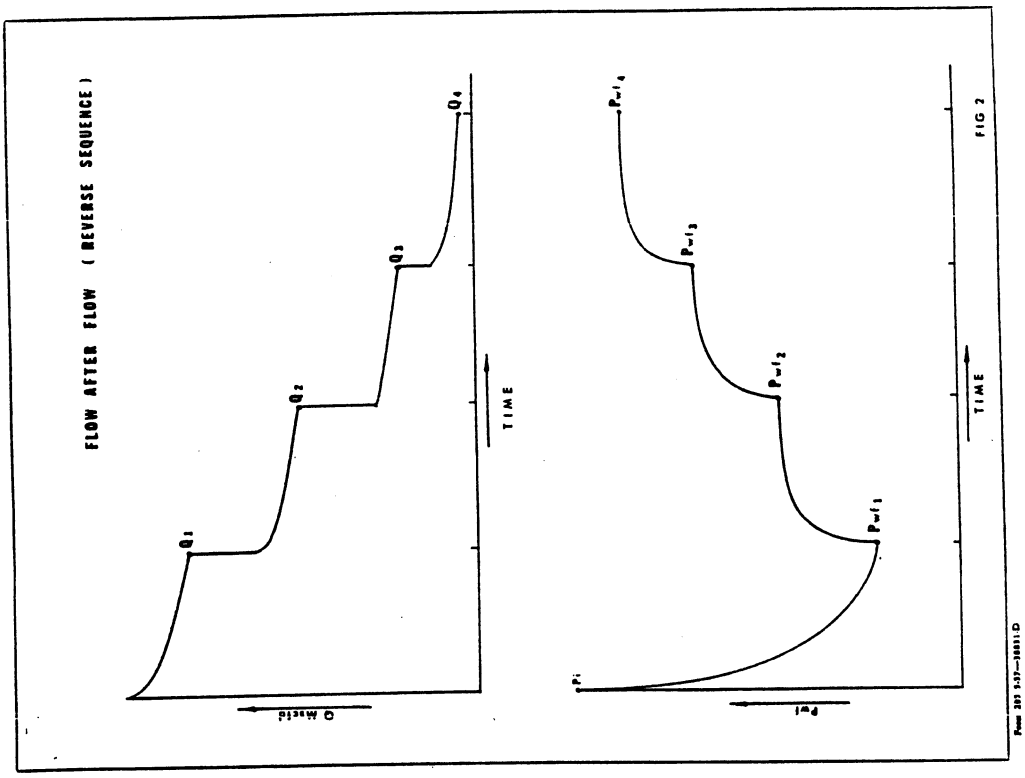
FLOW AFTER FLOW (REVERSE SEQUENCE)
Q1
Q2
Q3
Q4
Q Mscfd
TIME
Pwf4
Pwf3
Pwf2
Pwf1
Pi
Pwf
TIME
FIG 2

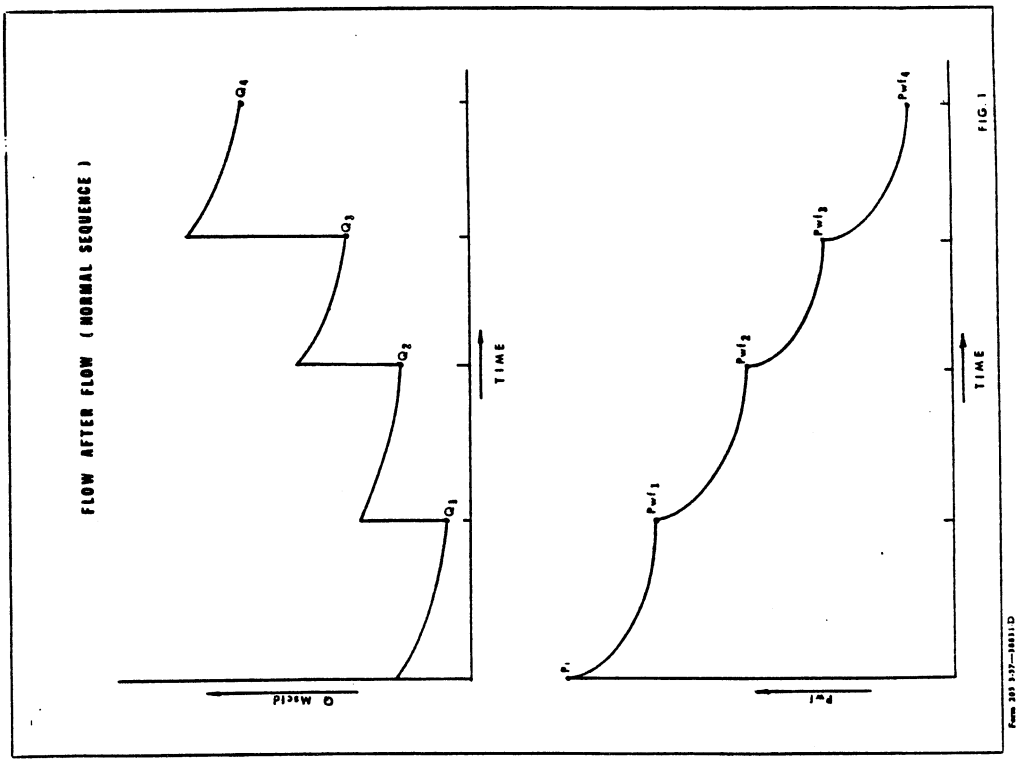
FLOW AFTER FLOW (NORMAL SEQUENCE)
Q4
Q3
Q2
Q1
Q Mscfd
TIME
Pwf4
Pwf3
Pwf2
Pwf1
Pi
Pwf
TIME
FIG. 1

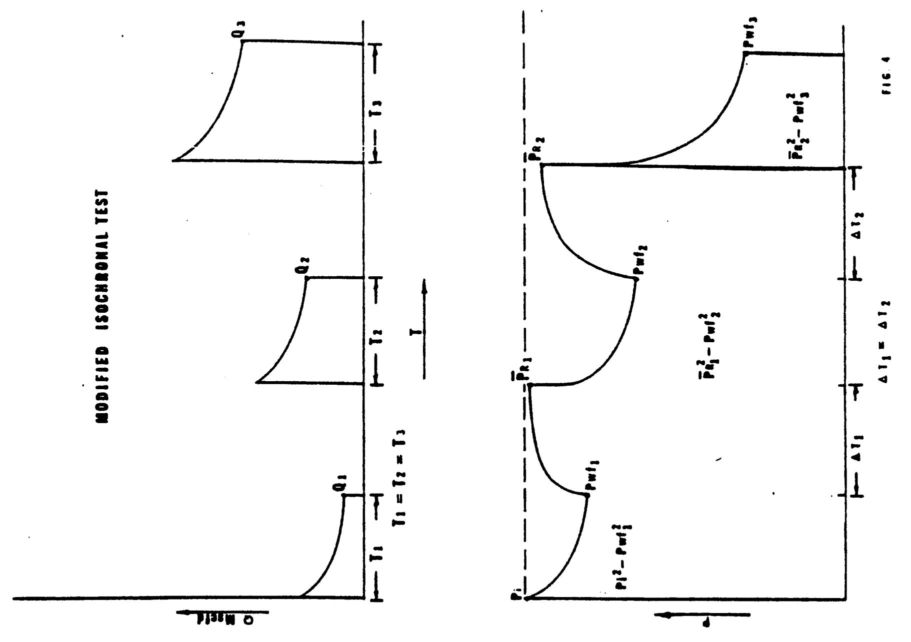
MODIFIED ISOCHRONAL TEST
Q Mscfd
Q1
Q2
Q3
T1
T2
T3
T1 = T2 = T3
T
P
Pi
Pwf1
P̄R1
Pwf2
P̄R2
Pwf3
Pi² − Pwf1²
P̄R1² − Pwf2²
P̄R2² − Pwf3²
ΔT1
ΔT2
ΔT1 = ΔT2

FIG 4

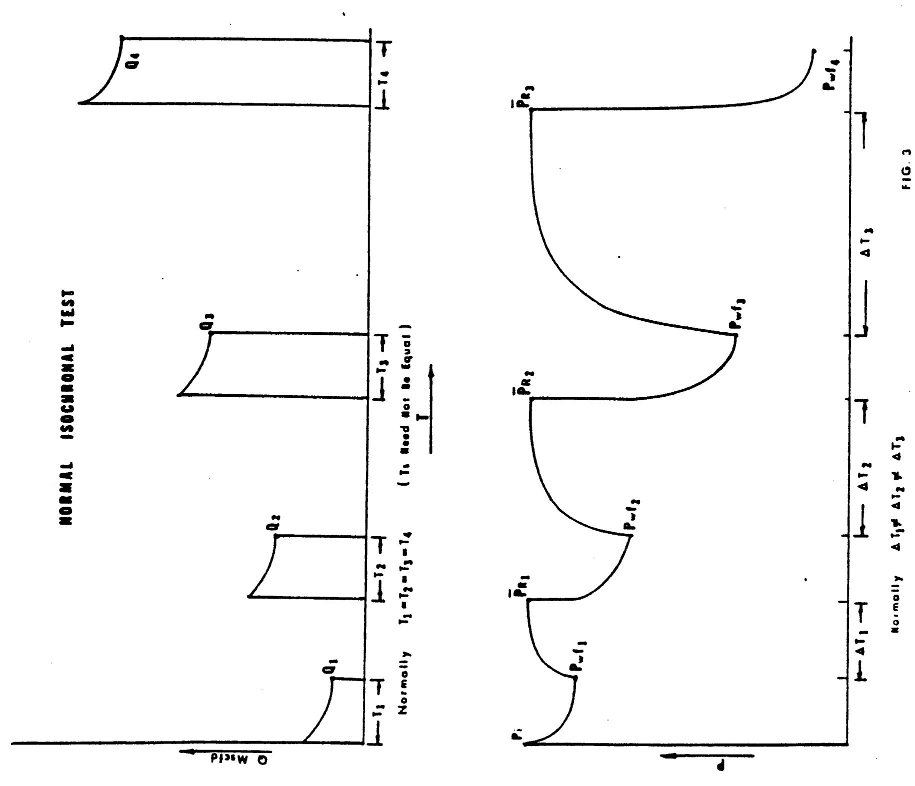
NORMAL ISOCHRONAL TEST
Q Mscfd
Q1
Q2
Q3
Q4
T1
T2
T3
T4
Normally T1 = T2 = T3 = T4
(T4 Need Not Be Equal)
T
P
Pi
Pwf1
P̄R1
Pwf2
P̄R2
Pwf3
P̄R3
Pwf4
ΔT1
ΔT2
ΔT3
Normally ΔT1 ≠ ΔT2 ≠ ΔT3

FIG. 3

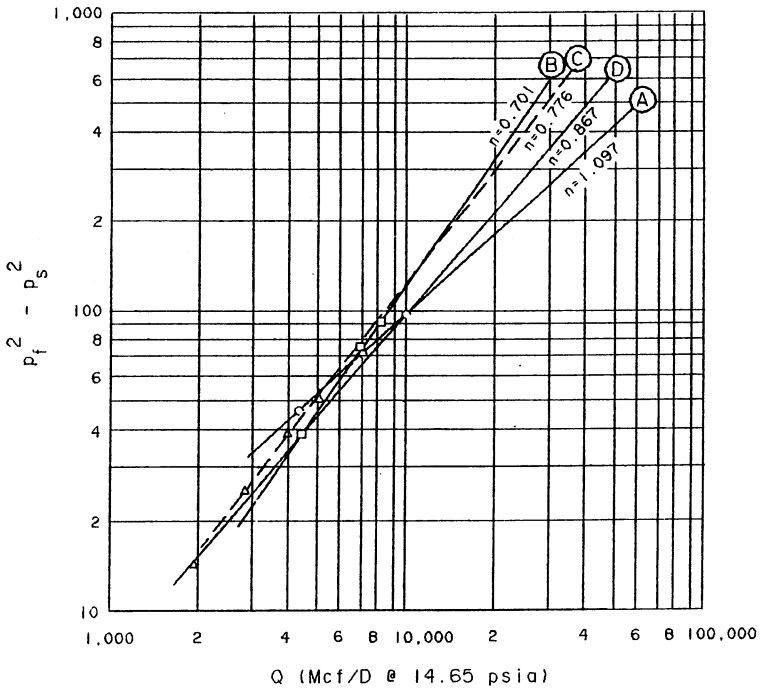

Figure 5.

Curve A: 24-hour, reverse sequence back-pressure test (slope=1.097).
Curve B: 24-hour, normal sequence back-pressure test (slope=0.7011).
Curve C: 24-hour, normal sequence back-pressure test (slope=0.7761).
Curve D: 24-hour, isochronal performance curve (slope=0.867).

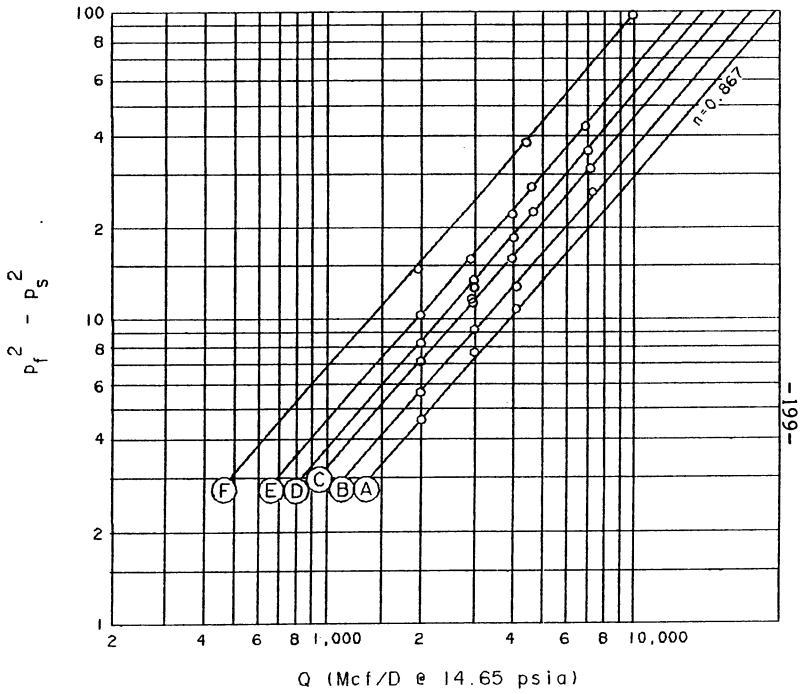

Figure 6.

Curve A: 0.1-hour duration of flow
Curve B: 0.2-hour duration of flow
Curve C: 0.5-hour duration of flow
Curve D: 1.0-hour duration of flow
Curve E: 3.0-hour duration of flow
Curve F: 24.0-hour duration of flow

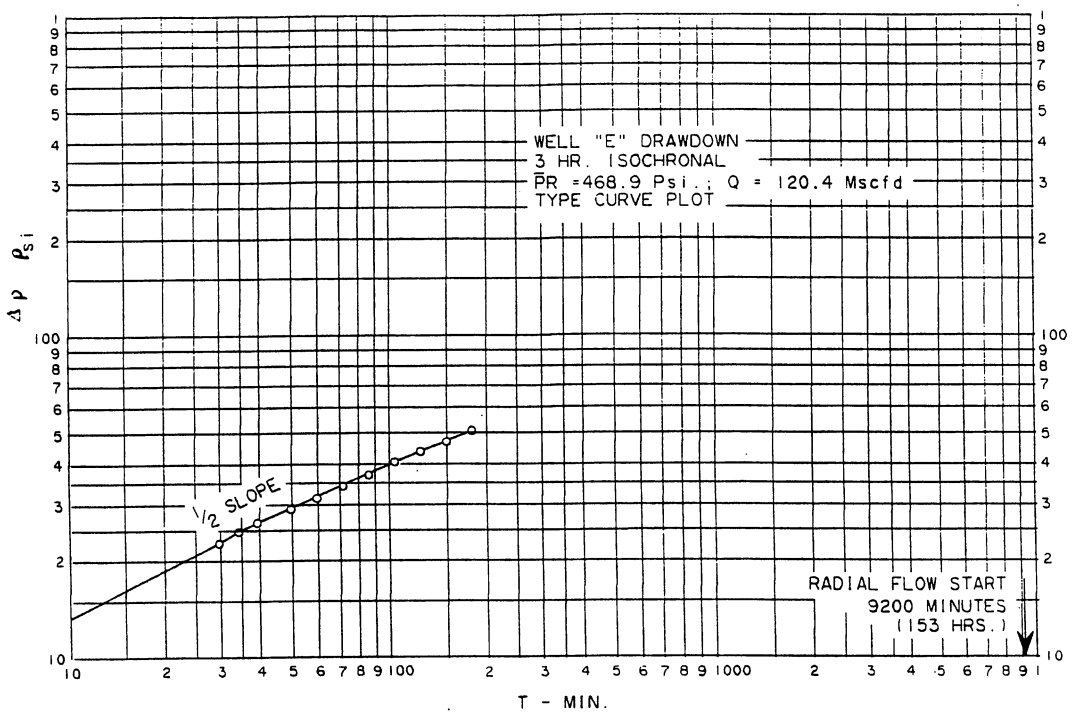

Figure 7.

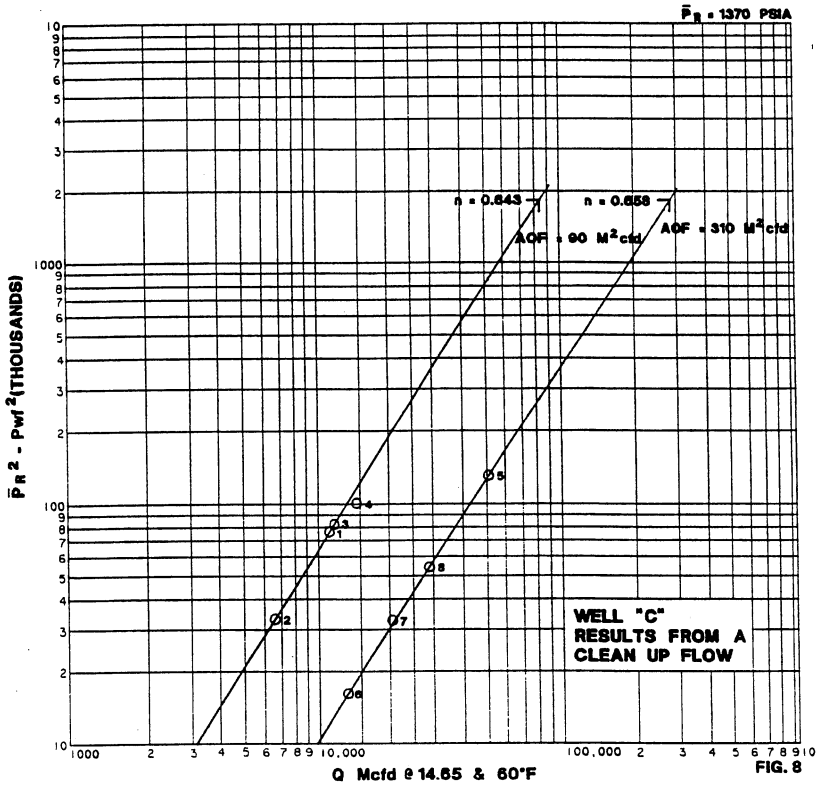

FIG. 8

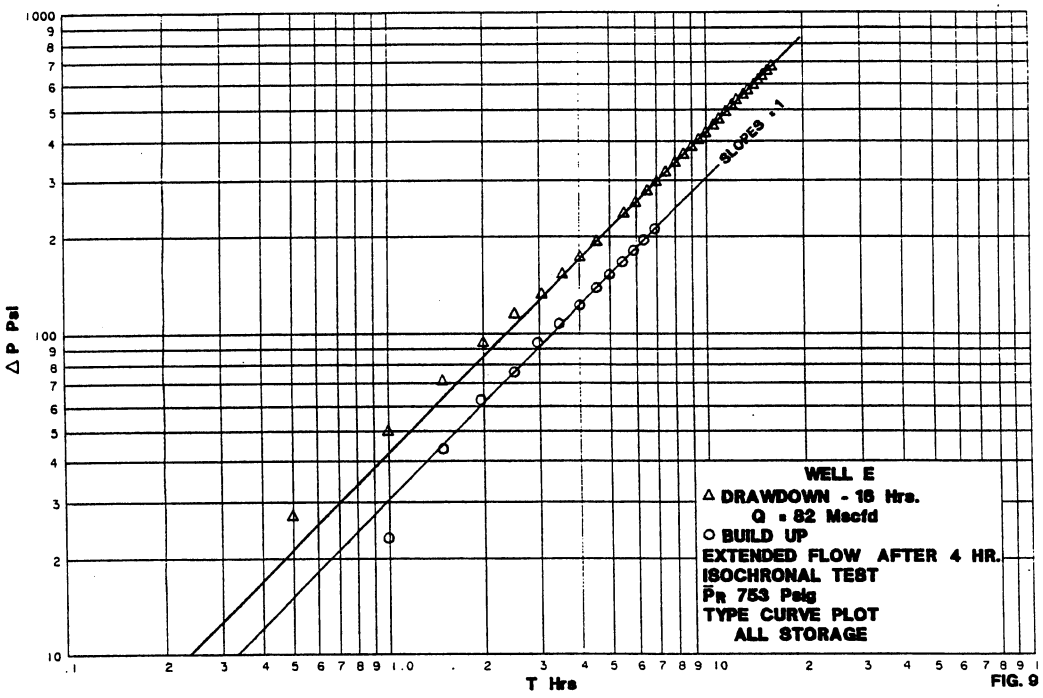
ΔP Psi
T Hrs
SLOPES = 1
WELL E
Δ DRAWDOWN - 16 Hrs.
Q = 82 Mscfd
○ BUILD UP
EXTENDED FLOW AFTER 4 HR.
ISOCHRONAL TEST
$\bar{P}_R$ 753 Psig
TYPE CURVE PLOT
ALL STORAGE

FIG. 9

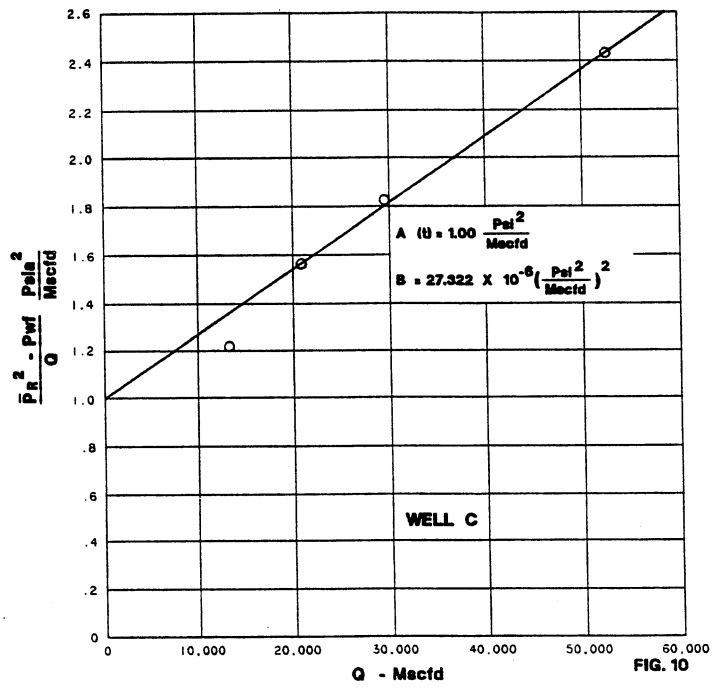
$\frac{\bar{P}_R^2 - P_{wf}^2}{Q}$ $\frac{Psia^2}{Mscfd}$
Q - Mscfd
A (t) = 1.00 $\frac{Psi^2}{Mscfd}$
B = 27.322 X 10^{-6} $(\frac{Psi^2}{Mscfd})^2$
WELL C

FIG. 10

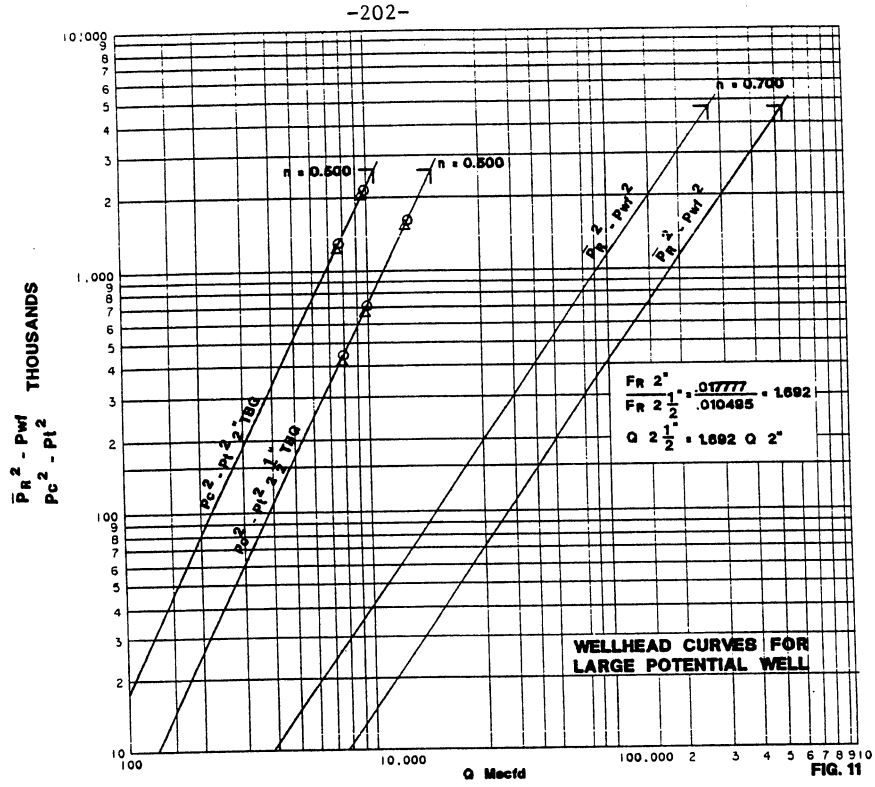
n = 0.700
n = 0.600
n = 0.500
$\bar{P}_R^2 - P_{wf}^2$
$P_c^2 - P_t^2$ 2" TBG
$P_c^2 - P_t^2$ 2½" TBG
F_R 2" / F_R 2½" = .017777 / .010495 = 1.692
Q 2½" = 1.692 Q 2"
WELLHEAD CURVES FOR LARGE POTENTIAL WELL
$\bar{P}_R^2 - P_{wf}^2$ THOUSANDS
$P_c^2 - P_t^2$
Q Mcfd
FIG. 11

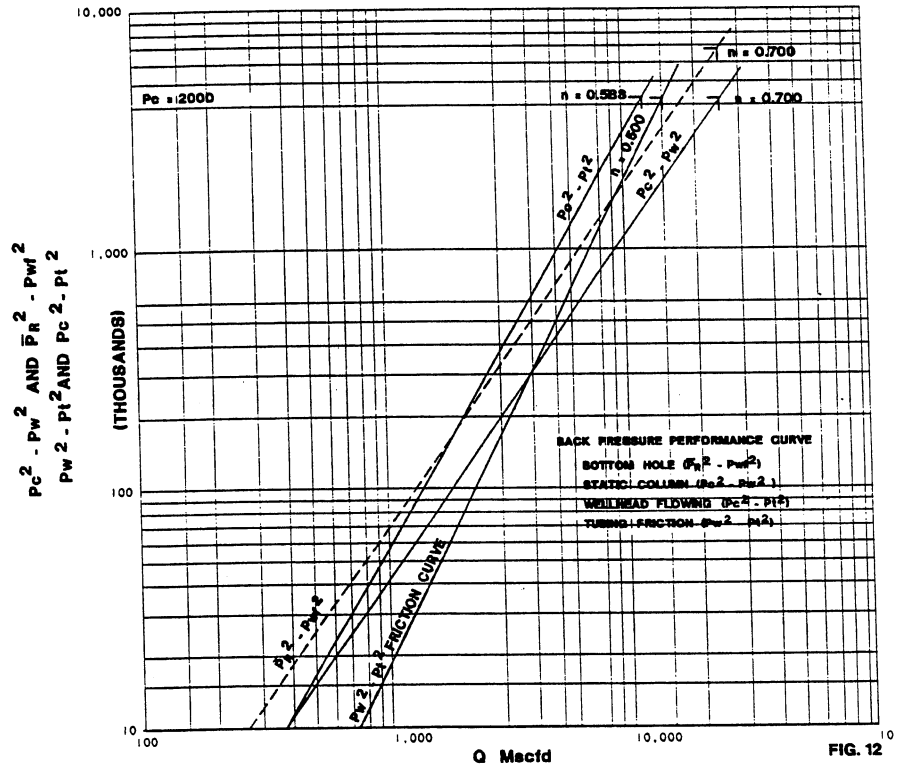
Pc = 1200
n = 0.588
n = 0.700
n = 0.600
$P_c^2 - P_t^2$
$P_c^2 - P_w^2$
BACK PRESSURE PERFORMANCE CURVE
BOTTOM HOLE ($\bar{P}_R^2 - P_{wf}^2$)
STATIC COLUMN ($P_c^2 - P_w^2$)
WELLHEAD FLOWING ($P_c^2 - P_t^2$)
TUBING FRICTION ($P_w^2 - P_t^2$)
$\bar{P}_R^2 - P_{wf}^2$
$P_w^2 - P_t^2$ FRICTION CURVE
$P_c^2 - P_w^2$ AND $\bar{P}_R^2 - P_{wf}^2$
$P_w^2 - P_t^2$ AND $P_c^2 - P_t^2$
(THOUSANDS)
Q Mcfd
FIG. 12

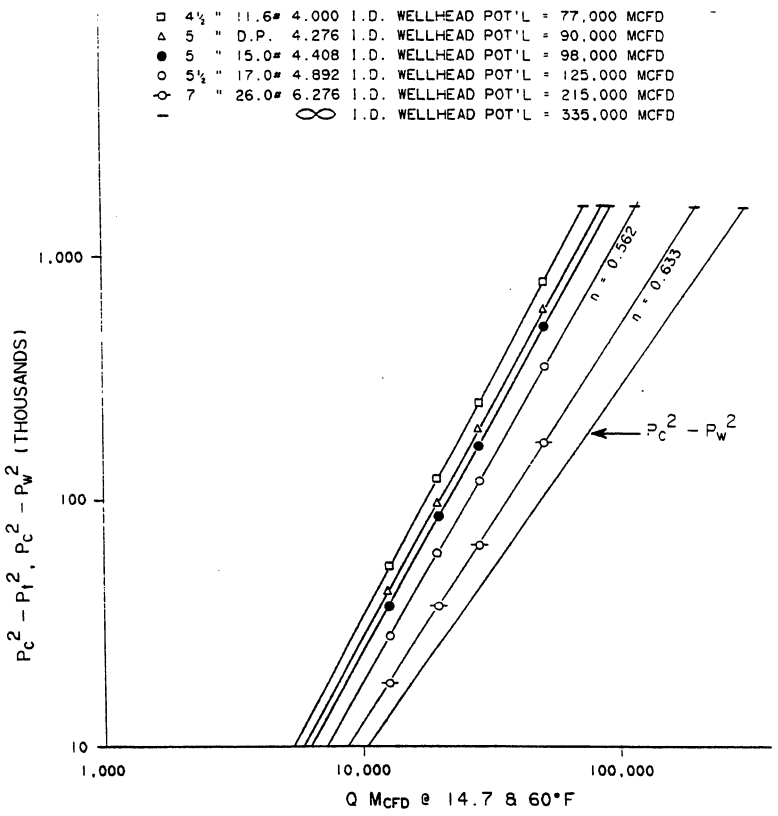
□ 4½ " 11.6# 4.000 I.D. WELLHEAD POT'L = 77,000 MCFD
△ 5 " D.P. 4.276 I.D. WELLHEAD POT'L = 90,000 MCFD
● 5 " 15.0# 4.408 I.D. WELLHEAD POT'L = 98,000 MCFD
○ 5½ " 17.0# 4.892 I.D. WELLHEAD POT'L = 125,000 MCFD
◇ 7 " 26.0# 6.276 I.D. WELLHEAD POT'L = 215,000 MCFD
— ⌀ I.D. WELLHEAD POT'L = 335,000 MCFD
n = 0.562
n = 0.633
$P_c^2 - P_w^2$
1,000
100
10
1,000
10,000
100,000
$P_c^2 - P_f^2$, $P_c^2 - P_w^2$ (THOUSANDS)
Q M_{CFD} @ 14.7 & 60°F
TUBING DESIGN

Figure 13.

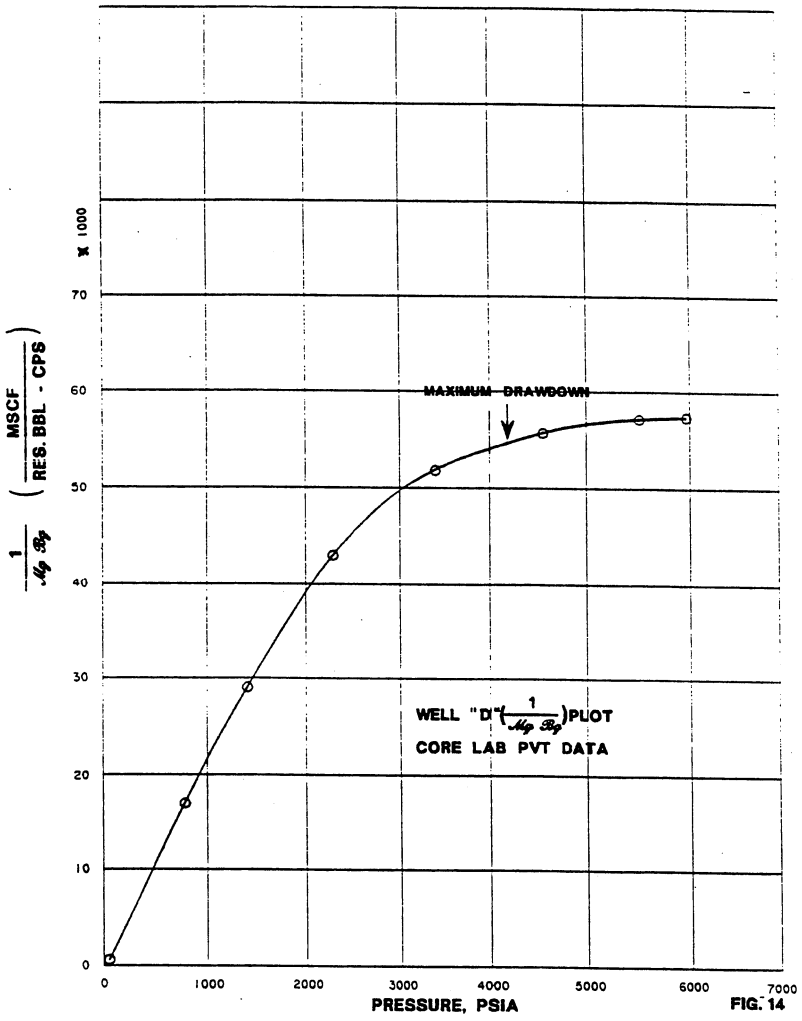
$\frac{1}{\mu_g B_g}$ $\left(\frac{\text{MSCF}}{\text{RES. BBL - CPS}}\right)$
x 1000
70
60
50
40
30
20
10
0
MAXIMUM DRAWDOWN
WELL "D" $\left(\frac{1}{\mu_g B_g}\right)$ PLOT
CORE LAB PVT DATA
0
1000
2000
3000
4000
5000
6000
7000
PRESSURE, PSIA

FIG. 14

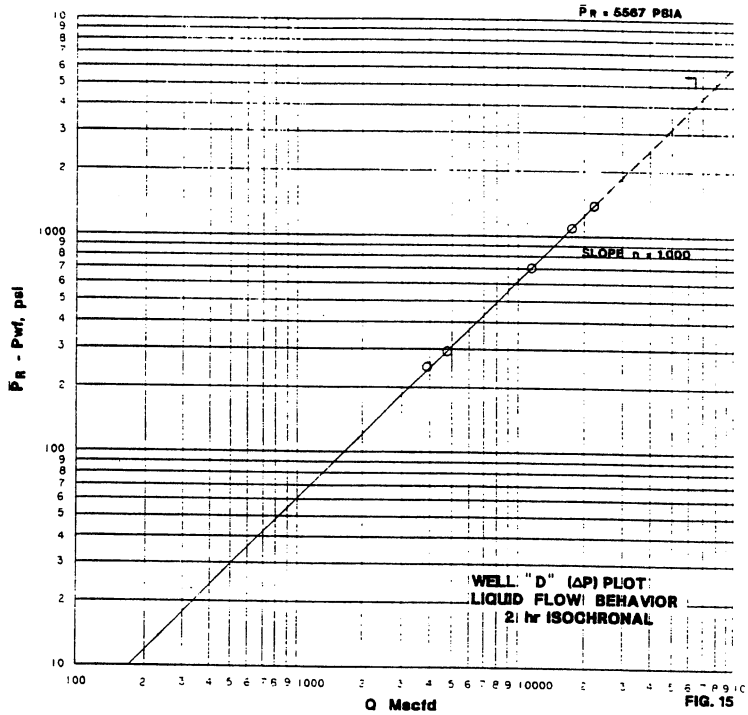
$\bar{P}_R$ = 5567 PSIA
SLOPE n = 1.000
WELL "D" (ΔP) PLOT
LIQUID FLOW BEHAVIOR
2 hr ISOCHRONAL
$\bar{P}_R$ - Pwf, psi
Q Mscfd

FIG. 15

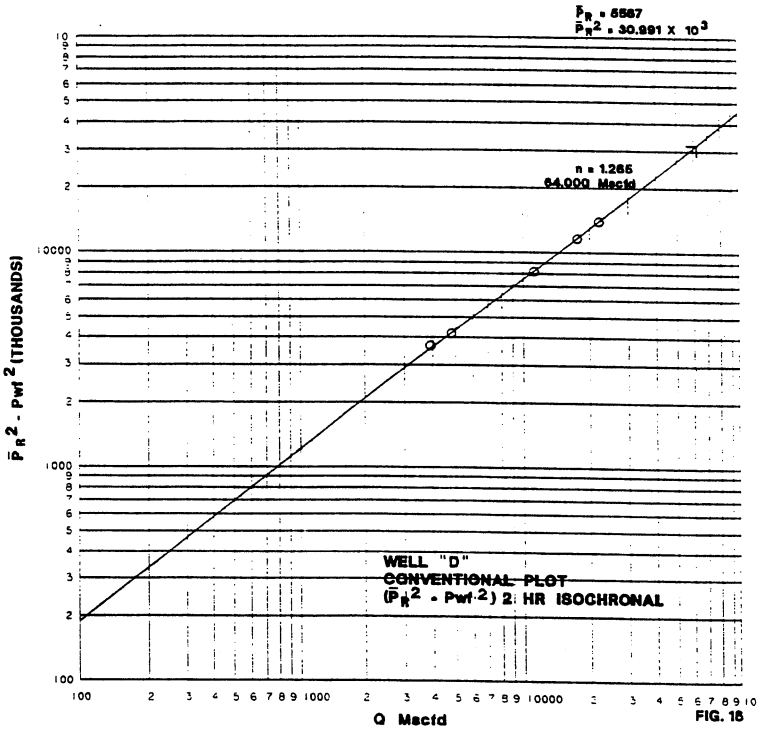
$\bar{P}_R$ = 5567
$\bar{P}_R^2$ = 30.991 X 10^3
n = 1.265
64,000 Mscfd
WELL "D"
CONVENTIONAL PLOT
($\bar{P}_R^2$ - Pwf^2) 2 HR ISOCHRONAL
$\bar{P}_R^2$ - Pwf^2 (THOUSANDS)
Q Mscfd

FIG. 16

$$m(P_I) = \frac{222.9}{} \times 10^6$$

$$m(P) = \int_{P_{wf}}^{\bar{P}_R} \frac{1}{\mu_g B_g} dP$$

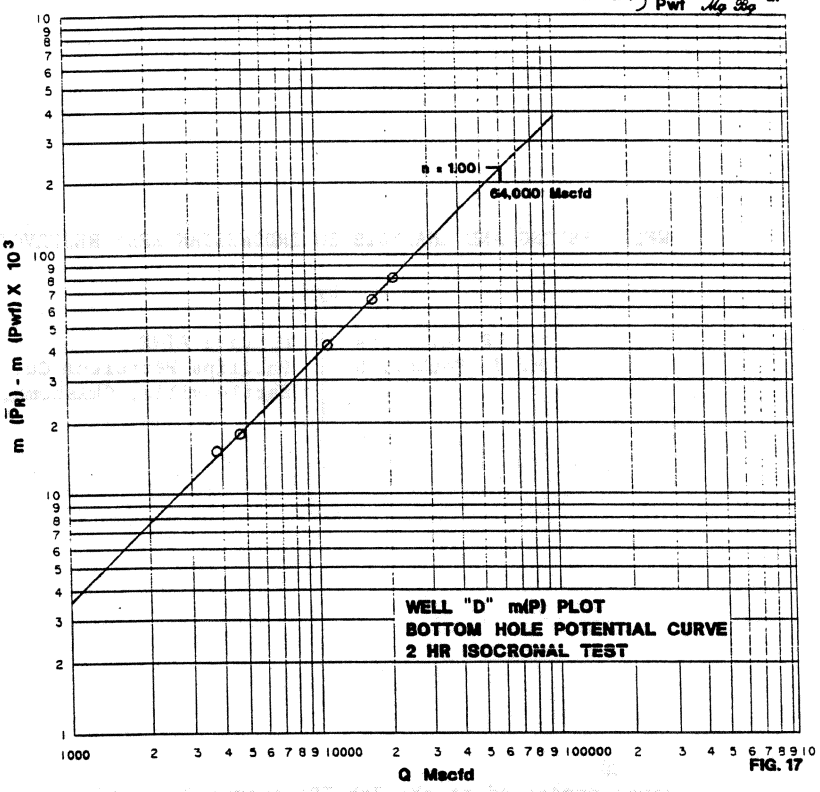

FIG. 17

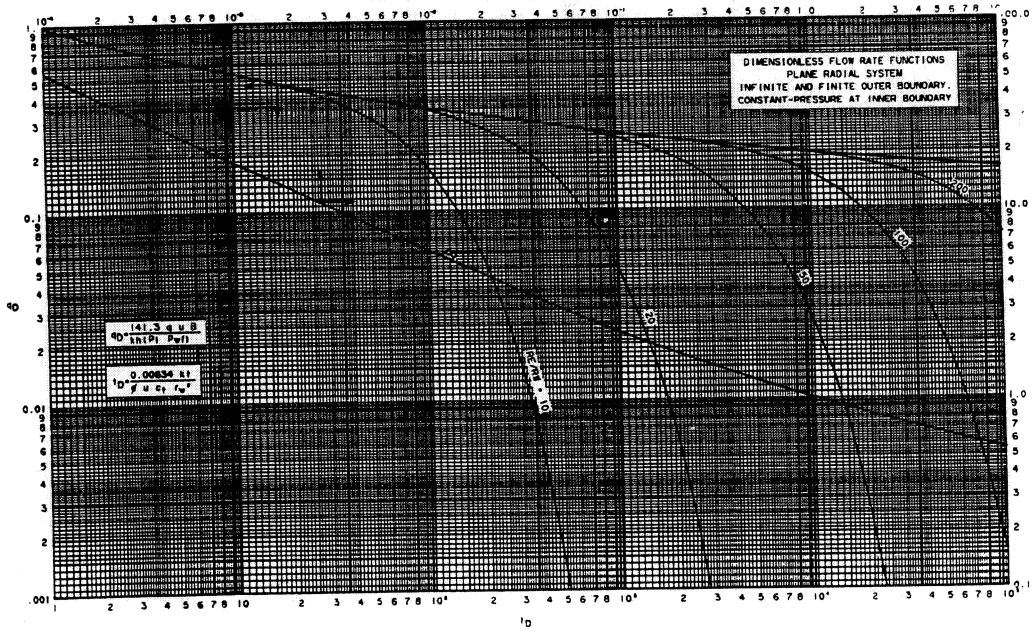

Figure 18.

WELL TESTING AND ANALYSIS IN INDONESIAN REEF RESERVOIRS

by

B. A. Ziara
M. J. Fetkovich

Membera AIME
Phillips Petroleum Co.
Bartlesville, Oklahoma, U.S.A.

Paper presented at the 7th IPA Annual Convention,
Jakarta, Indonesia, June 6-7, 1978

WELL TESTING AND ANALYSIS IN INDONESIAN REEF RESERVOIRS

Abstract

This paper presents procedures and methods of testing and analyzing Indonesian reef oil and gas wells to determine the formation characteristics and well deliverabilities. The well tests are in five different oil fields and one gas field. Most of the reservoirs have secondary porosity and permeability systems which allow high flow rates from individual wells. The bottomhole pressure drawdown on some of the best wells range from 2 to 15 psi at flow rates in excess of 10,000 BOPD. Conventional test analysis of individual drawdown and buildup are difficult even with high precision pressure recorders. Selection of correct pressure drawdown and Horner buildup slopes on these type of wells are difficult to determine. Test analysis for determining formation characteristics of these wells are based on multipoint tests.

Buildup plots of wells with permeabilities of 10 to 100 millidarcies are shown that indicate a constant pressure boundary (active water drive) could be detected from test analysis.

Three types of tests and their analysis are presented in this paper, (1) single flow and buildup, buildup with and without a constant outer boundary pressure case, (2) multipoint, isochronal and flow after flow, and (3) single flow of long duration and buildup with constant pressure at inner boundary, are discussed in this paper.

Introduction

All wells are completed in the Salawati Basin. Production in the basin comes from Upper Miocene Kais Formation stratigraphic or combination fault/stratigraphic traps. The traps consist of Kais reef or downslope carbonate mud accumulations, occasionally modified by normal faulting. Depths to the top of the Kais pay for the oil wells range from 5100 feet to 6700 feet, and 9500 feet for the gas well. The oil reservoirs are highly undersaturated, with an aquifer underlying these reservoirs. Primary porosities in the Kais pay are of the order of 14% - 18%. Most of the well tests examined in this paper were eventually completed in the upper third portion of the total pay thickness.

Types and Duration of Tests

Three types of tests, (1) single flow and buildup, (2) multipoint, isochronal and flow after flow and, (3) single flow of long duration and buildup were conducted in these wells. Each type of test was selected and designed to

provide information necessary for reservoir studies. Tests and durations were sometimes modified during testing operations to obtain specific data. The types of tests, its durations and purpose are discussed.

Single Flow and Buildup

1. Initial Flow (15 minutes)
2. Initial Shut in (2 hours) to determine original reservoir pressure
3. Clean up flow at maximum separator capacity (6 hours)
4. Shut in period (8 hours)
   Tests were usually conducted:
   a. In open hole before drilling to the oil-water contact
   b. Over separate parts of the productive interval
   c. To determine the oil-water contact

On the basis of results of these tests, decisions on completion procedures and further testing were made. The range of permeabilities determined from single flow tests would be used to help design the type and duration of multipoint testing required after the wells are completed. The skin effect calculated from pre-acid single flow and buildup tests would indicate the extent of the reservoir damage and the necessity for acidizing.

Isochronal Multipoint Tests

1. Acidize well. Shut in for acid contact time.
2. Clean up flow at maximum separator capacity (8 hours)
3. Shut in period (8 hours)
4. Flow at 1/3 of maximum after acid clean up rate (3 hours)
5. Shut in period (3 hours)
6. Flow at 2/3 of maximum after clean up rate (3 hours)
7. Shut in period (3 hours)
8. Flow at maximum separator capacity (3 hours)
9. Shut in period (3 hours)

The isochronal tests were usually conducted after the wells were completed and the drilling rigs were released. The durations of flow periods ranging from 3 to 5 hours varied on the basis of time required for clean up after acidization and stabilization. Shut in periods were determined from observations of when surface pressures stopped building up at a rate of less than 0.25 psi per hour. In cases of permeabilities in the range of 1,000 to 5,000 md, two hour shut in periods were sufficient for bottomhole pressure to build up to initial.

Flow after Flow Multipoint Tests

1. Acidize well. Shut in for acid contact time.
2. Clean up flow at maximum separator capacity (4 hours)
3. Shut in period (3 hours)
4. Flow at maximum after acid clean up rate (2 hours)
5. Flow at 2/3 of maximum after acid clean up rate (2 hours)
6. Flow at 1/3 of maximum after acid clean up rate (2 hours)

Only one test of this type was conducted in these wells. The test was performed in a second well in a given field with permeability of 2,000 md.

The flow after flow test was in decreasing flows (reverse sequence), but since stabilized flows were obtained in a short period, the performance curve obtained was almost identical to the one obtained from isochronal multipoint test.

The multipoint tests results are analyzed to determine the productivity indices, reservoir damage, flow efficiency, well's true bottomhole absolute open-flow potential and well head deliverability curves. With the small pressure drawdowns during flow periods, it is erroneous to rely on single flow and shut in periods for calculating permeabilities and skin.

Single Flow (long duration) and Buildup Test

1. Acidize well. Shut in for acid contact time.
2. Clean up flow at maximum separator capacity (24 hours)
3. Shut in period (24 hours)
   The rig was released and a wireline unit was mobilized for running 14 day bottomhole gauges
4. Shut in well. Made pressure traverse going in the hole at 1,000 ft stops for determining fluid pressure gradient
   Recorded initial shut in reservoir pressure
5. Flow well at maximum separator capacity (168 hours)
6. Shut in period (74 hours)

The long duration drawdown test of 168 hours was designed to define reservoir performance, its limits and whether it's volumetric or effective water drive. The decision to run such tests was determined after analyzing the rate-pressure data taken during the 24 hour flow and 24 hour buildup periods.

Methods of Test Analysis

Analysis of Drawdowns and Buildups

The traditional method for calculating permeability, skin, productivity and other formation characteristics is to analyze a single drawdown and/or build-up. Let us examine the buildup following the first drawdown of an isochronal test taken on a gas well 1, field A. The test was prior to acidization in open hole over pay thickness of 186 feet out of 585 feet of total pay thickness. The reservoir parameters used and a summary of the isochronal test results are shown in Table 1.

The slope of the buildup shown in Figure 1 is 47 psi/cycle:

$$kh = \frac{162.6\ q\ \mu_g \beta_g}{m}$$

$$q = 22385000\ \text{scfd}/5.61 = 3{,}986{,}643\ \text{BPD}$$

$$kh = \frac{162.6(3{,}986{,}643)(.0210)(.004559)}{47.00} = 1{,}322\ \text{md-ft, w/h} = 186\ \text{ft, k} = 7.2\ \text{md}$$

$$S' = S + D_q = 1.151 \left[\frac{P_{1hr} - P_{wf}}{m} - \log \frac{k}{\phi \mu c_t r_w^2} + 3.23 \right]$$

$$S' = 1.151 \left[17.49 - 8.25 + 3.23 \right] = +14.36$$

$$S' = S + D_q = +14.36$$

where $S = S_d + S_b$

Partial Penetration Skin (S_b) From Brons & Marting[1]

186 ft penetration out of 585 ft pay

$$b = \frac{186}{585} = .32$$

$$\frac{h}{r_w} \quad \frac{585}{.354} = 1653$$

From Brons & Marting[1] $S_b = +9.20$

S_d is the formation skin resulted from wellbore damage or acidization.

$S' = S_d + 9.20 + D_q = +14.36$ where D is the non-Darcy flow that should be evaluated from multipoint flow test. Multipoint analysis of this test will be discussed later.

Let's analyze the buildup following the first flow period using log-log type curve analysis. The techniques for analyzing pressure data using the type-curve method is discussed in great detail in chapter 3 of SPE Monograph Volume 5 "Advances in Well Test Analysis" by Robert D. Earlougher, Jr.

A type curve plot of Δp vs Δt is shown in Figure 2. The semi-log straight line period begins after 3.5 minutes. The data matched the infinite curve (Figure 3) and started dipping downward at Δt = 100 minutes or equivalent

$t + \Delta t = 8.00$ on a Horner plot. The second flatter slopes on Horner plots before and after acidization extrapolate to initial reservoir pressure. The type curve indicates a reduction of Δp below the infinite curve which indicates that a possible constant pressure source exists, i.e., a water drive is being reflected. This will be further analyzed using a dimensionless Horner Plot.

An After Acid Test Analysis of Well 1, Field A

Type curve analyses (Figure 2)

Match Points

$\Delta p = 10$ psia, $p_d = 1.92$

$\Delta t = 100$ mins, $t_d = 48$

$$p_d = \frac{kh\Delta p}{141.3\ q\ \mu\beta}$$

$$kh = \frac{p_d(141.3)\ q\overline{\mu\beta}}{\Delta p} = \frac{(1.92)\ (141.3)\ (9{,}882{,}000)\ (.02824)(0.004215),}{10\ (5.615)}$$

$kh = 5683$ md-ft, with $h = 585$ ft, $k = 9.71$ md

$$t_D = \frac{0.000264\ k\ t\ hrs}{\phi\mu\ c_t\ L^2}$$

$$L^2 = \frac{.000264\ k\ t\ hrs}{t_D\ \phi\ \mu\ c_t} = 220.72\ ft^2,\quad L = 14.35\ ft$$

$$S = -\ln\frac{L}{2r_w} = -\ln\frac{14.85}{2(.354)} = -3.04$$

Horner Plot (Figure 4)

$$kh = \frac{162.6\ q\ \mu\beta}{m} = \frac{162.6\ (9{,}882{,}000)\ (.02824)\ (.004215)}{6.0\ \text{psi/cycle}\ (5.615)} = 5677\ \text{md-ft}$$

With h = 585 ft, k = 9.70 md (excellent check with type curve analysis).

$$S' = 1.151\left[\frac{4201 - 4186.6}{6.0} - \log\frac{9.70\ (10^6)}{(.108)\ (.02824)\ (140)\ (.354)^2} + 3.23\right]$$

S' = -3.02, which is a good check with type curve analysis.

The formation skin $S = S' - D_q$. D_q from multipoint analysis of this is (.06295 x 9.882 = 0.622), therefore the formation skin factor resulted from acidization S = -3.64. Plots of drawdown followed by a buildup pressure data of an oil well 1, field B, are shown in Figures 5 and 6. Both plots yield approximately the same slope with approximately 80 md permeability and an after acid skin of -4.1.

Note again the second flatter slope on the Horner plot (Figure 6). The constant pressure at outer boundary case (water drive) is being reflected on this oil well test as well as the previous gas well analysis.

Analyses of individual drawdowns and buildups on wells with very high permeabilities (in the range of 2 to 17 Darcies) were difficult and inconsistent. Figures 7 and 8 are examples of buildups on two different wells with drawdowns of 2 and 7 psi producing at flow rates of 2025 BOPD and 4244 BOPD during 4 to 6 hours flow periods and permeabilities in the range 5 to 15 Darcies respectively.

For these types of wells, multipoint tests are useful for calculating reservoir characteristics.

Multipoint Testing (Bottomhole and Wellhead Curves)

Multipoint and backpressure testing of gas wells is an accepted procedure for establishing a gas well's performance curve and obtaining formation data for reservoir studies.

Fetkovich[2], in his paper, "The Isochronal Testing of Oil Wells," demonstrated that oil wells behave very similar to gas wells and should be tested and analyzed using the same basic flow equations.

The basic flow equations for oil or gas flow given in the literature are:

Transient Flow:

$$q = \frac{7.08\ kh}{\left[\ln\sqrt{\frac{14.23\ kt}{\phi\ (\mu\ c_t)\ i\ r_w^2}} + S + D_q\right]} \int_{P_{wf}}^{\bar{P}_R} f\ (p)\ dp$$

Pseudo-Steady State Flow:

$$q = \frac{7.08\ Kh}{\left[\ln\left(\frac{r_e}{r_w}\right) - \frac{3}{4} + S + D_q\right]} \int_{P_{wf}}^{\bar{P}_R} f\ (p)\ dp$$

Based on the flow equations, Fetkovich[2] established the validity of an oil well backpressure curve plot on log Q_o vs log (Δp^2) plot from some 40 oil well tests. The (Δp^2) is defined as $\bar{P}_R^2 - P_{wf}^2$.

The $\int_{P_{wf}}^{\bar{P}_R} f\ (p)\ dp$ was derived for oil and gas wells in two flow regions. One region is for high pressure gas wells and single liquid flow phase for undersaturated oil reservoirs above the bubble point pressure. The second flow region is for low pressure gas wells and two phase flow in oil reservoirs flowing below the bubble point pressures.

Fetkovich[3], in his presentation of "Multipoint Testing of Gas Wells," demonstrated that for the first flow region f(p) is constant and one should plot Δp to analyze drawdown or buildup data. For pressures over low pressure region, one should plot Δp^2 to analyze drawdown and buildup data. If pressure data taken from multipoint tests covers both high and low pressure regions, one must plot pseudo-pressure m(p). m(p) is defined as $\int_{P_{wf}}^{\bar{P}_R} \frac{dp}{\mu\beta}$ and can be obtained from PVT plot of $\frac{1}{\mu\beta}$ vs pressure for both oil and gas wells.

Therefore, the same basic flow equations can be written in terms of m(p) as follows:

Transient:

$$\frac{7.08\ kh\ [m(\bar{p}_R) - m(p_{wf})]}{q} = \ln\sqrt{\frac{14.23\ K_i\ t}{\phi\ (\mu c_t)\ i\ r_w^2}} + S + D_q$$

Pseudo-Steady State

$$\frac{7.08\ kh\ [m(\bar{p}_R) - m(p_{wf})]}{q} = \ln\left(\frac{r_e}{r_w}\right) - \frac{3}{4} + S + D_q$$

Flow equations for Δp and $\Delta(p^2)$ will be shown for individual analysis.

Multipoint tests, as previously described, consist of two types, "Isochronal" and "Flow After Flow".

The types of tests presented in this paper deal with the Isochronal method of testing. The durations of flow and shut in periods were previously discussed.

A. Gas Wells

A backpressure curve plot of an isochronal test results of gas well 1, field A presented in Table 1 is shown in Figure 9. With a good alignment of four stabilized flows, the slope of the backpressure curve is 0.740. The test was run in reverse sequence and not in the normal recommended increasing sequence. But since each flow period was followed by shut-in periods, transient effects are not considered to be a factor. The effect of non-Darcy flow to the Δp^2 should be calculated to determine its contribution to the effective skin possibly avoiding unnecessary stimulation efforts. The non-Darcy flow constant is determined from the plot of $(p^2)/Q$ versus Q (Figure 10).

The transient gas flow equation is:

$$\bar{p}_R^2 - p_{wf}^2 = \frac{1424\ (\overline{\mu z})\ T}{kh}\left[\left\{\frac{1}{2}(\ln t_D + 0.809) + S\right\} Q + \left\{\frac{2.226 \times 10^{-15}\ \beta KG}{hr_w\ \mu}\right\} Q^2\right]$$

$$\text{Let } A(t) = \frac{1424\ (\overline{\mu z})\ T}{kh}\left\{\frac{1}{2}(\ln t_D + 0.809) + S\right\}$$

$$D = \frac{2.226 \times 10^{-15}\ \beta KG}{hr_w\ \mu}$$

$$\text{and } B = \frac{1424\ (\overline{\mu Z})\ T\ D}{kh}$$

We obtain the familiar form of the Forscheimer equation:

$$\overline{p_R}^2 - p_{wf}^2 = A(t)\ Q + B\ Q^2$$

Then $$\frac{\overline{p_R}^2 - p_{wf}^2}{Q} = A(t) + B\ Q$$

A plot of $\frac{\overline{p_R}^2 - p_{wf}^2}{Q}$ vs Q (Fig. 10) will yield A (t) from the intercept and B from the slope.

Test Analysis of Well-1, Field-A, Before Acid-Open Hole

From plot of $\frac{\overline{p_R}^2 - p_{wf}^2}{Q}$ vs Q at Q = 0, A (t) = 159 $\frac{psia^2}{MSCFD}$ and

B = .005386 $(psia/MSCFD)^2$.

$$A\ (t) = 159 = \frac{1424\ (\overline{\mu Z})\ T}{kh} \left\{ \frac{1}{2} (\ln t_D + 0.809) + S \right\}$$

$$t_D = \frac{0.00633\ \overline{K}Pt}{\phi\ r_w^2} = \frac{0.00633\ k\ (3699)\ (4/24)}{(.102)\ (.0201)\ (.354)^2} = 15{,}189\ k$$

kh from Horner is 1322 md-ft, w/h = 186 ft, k = 7.2 md

$$t_D = 15189\ (7.2) = 109{,}361$$

$$S = \frac{A\ (t)\ kh}{1424\ (\mu Z)\ T} - \left[\frac{1}{2}\ (\ln t_D + 0.809) = \right] 11.77 - 6.20 = +5.57$$

$$\beta = \frac{Bh^2\ r_w}{3.17 \times 10^{12}}\ ZGT = \frac{0.005386\ (186)^2\ (.354)}{3.17 \times 10^{-12}\ (.905)\ (.745)\ (660)} = 4.64 \times 10^{10}$$

$$D = \frac{2.226\ (10^{15})\ \beta KG}{h\ r_w\ \mu} = \frac{2.226 \times 10^{-15}\ (4.64)\ (10^{10})\ 7.2\ (.745)}{1.86\ (.354)\ (.0210)}$$

$$D = 0.0004\ MSCD^{-1}$$

$$D_q = 0.0004 \times 22385 = 8.95$$

$$S' = S + D_q$$

$S' = 5.57 + 8.95 = 14.52$ which is a good check with S' of 14.36 determined from Horner analysis of buildup.

Based on this analysis, it is evident that the partial penetration skin S_b and the non-Darcy flow D_q attributed mostly to the total effective skin of +14.36.

A second multipoint test was conducted over completion intervals and after acidization. The backpressure curve and a plot of $\Delta(p^2)/Q$ vs Q are shown in Figures 11 and 12. Using the same type analysis of multipoint tests as previously discussed and a skin factor of -3.64, kh was calculated to be 5710 md-ft which is in close agreement with 5683 md-ft calculated from buildup analysis.

The non-Darcy flow constant is calculated with slope B from Figure 12 of 2.7829×10^{-4} as follows:

$$D = \frac{B\ kh}{1424\ (\mu z)\ T} = \frac{2.7829\ (10^{-4})\ (5710)}{1424\ (.02824)\ (.93)\ (675)} = 0.00006295\ MSCFD^{-1}$$

The non-Darcy flow constant after acidization is 0.06295 $MMSCFD^{-1}$ compared to pre-acid value of 0.400 $MMSCFD^{-1}$ which confirms a good acidization. Both tests, interval No. 1, which was an open hole before acid test and the total completion interval test were over essentially the same interval.

The wellhead backpressure curves before and after acid tests are shown in Figure 13. The absolute bottomhole potential after acidization increased by approximately nine (9) fold, but the wellhead potentials increased by only 1.5 times. This indicates that the wellhead curves are totally described by pressure drop through the tubing string resulted from tubing friction, i.e., the wellhead deliverability is tubing limited. The wellhead potential through 4.5" tubing (3.920") was calculated to be 2.3 times the one measured through 3.5" tubing.

B. Oil Wells

Test results on oil wells with very small drawdowns and permeabilities ranging from 2 to 17 Darcies are exhibited in Figures 7 and 8. Figure 7 is in field C, well No. 3, and Figure 8 is in field D, well 1. Both fields are highly undersaturated oil with bubble point pressures of 20 and 10 psig and initial reservoir pressures of 2387 psia and 2855 psia respectively. The flow regions are single phase oil and the pressure functions f(p) are nearly constant.

Figures 14 and 15 illustrate plots of $1/\mu_o\beta_o$ as a function of pressure obtained from PVT studies on both reservoirs field C and field D respectively.

Then $\int_{p_{wf}}^{\bar{p}_R} f(P)$ is merely $\dfrac{\bar{p}_R - p_{wf}}{\mu_o\beta_o}$ or $\dfrac{\Delta p}{\mu_o\beta_o}$ and the steady state flow equation is:

$$q_o = \frac{7.08\ kh}{\left[\ln\left(\frac{r_e}{r_w}\right) - \frac{3}{4} + S + D_q\right]} \frac{\Delta p}{\mu_o\beta_o}$$

This implies that multipoint tests conducted in these wells should yield a straight line on log q_o vs log Δp as shown in Figures 16 and 17 for well 3, field C and well 1, field D. The quantity under $\dfrac{1}{\mu_o\beta_o}$ from $\bar{p}_R$ to p_{wf} is th pseudo-pressure difference $[m(\bar{p}_R) - m(p_{wf})]$. For determining the absolute open flow potential by extrapolation, the only correct method is by the means of an m(p) plot. The steady state flow equation becomes:

$$q_o = \frac{7.08\ kh}{\left[\ln\left(\frac{r_e}{r_w}\right) - \frac{3}{4} + S + D_q\right]} [m(\bar{p}_R) - m(p_{wf})]$$

Or

$$\frac{m(\bar{p}_R) - m(p_{wf})}{q} = \frac{\left[\ln\left(\frac{r_e}{r_w}\right) - \frac{3}{4} + S\right]}{7.08\ kh} + \frac{D_q}{7.08\ kh}$$

$$\text{Let } B = \frac{D}{7.08\ kh},$$

Then a plot of $\frac{\Delta m(p)}{q}$ vs q of multipoint test data will readily yield $\left[\ln\left(\frac{r_e}{r_w}\right) - \frac{3}{4} + S\right]/7.08\ kh$ from the intercept and B from the slope. Let us examine a plot of $\frac{\Delta m(p)}{q}$ vs q for this test.

If we refer to the intercept as A (t), the equation becomes simply

$$\frac{\Delta m(p)}{q} = A\ (t) + Bq$$

Let us illustrate the method of analyzing multipoint test of well 1, field D using data shown in Figures 15 and 17.

A method of calculating m(p) as a function of pressure is presented in Table 2. Table 3 illustrates calculations of $\Delta m(p)/q$ for each flow rate which is graphically shown in Figure 18.

Method of Data Analysis

$$A(t) = .2730 \times 10^{-3} = \frac{1}{7.08\ kh}\left[\ln\left(\frac{900}{.354}\right) - 4.00 - 0.75\right] = \frac{3.10}{7.08\ kh}$$

kh = 1604 Darcy - ft, w/h = 133 ft, k = 12 Darcies

$$\frac{\Delta m(p)}{q} = .273 \times 10^{-3} + 1.4\ (10^{-8})\ q$$

In order to correctly define the remainder of the backpressure curve to determine absolute open flow potential, a plot of m(p) vs q is required.

$$\Delta m(p) = .273 \times 10^{-3}\ q + 1.4\ (10^{-8})\ q^2$$

A plot of $\Delta m(p)$ vs q at various rates is presented in Figure 19. The absolute bottomhole open flow potential is 245,000 BOPD. The wellhead potential of the well from the wellhead backpressure curve plot is 54,000 BOPD (Figure 20).

Dimensionless Horner Plot (Constant Pressure at Outer Boundary)

If these reservoirs are strong water-drive systems, then a dimensionless Horner solution for constant pressure boundary case suggested by Ramey[4] can be applied.

The Horner buildup curves for gas well 1; field A (Figures 1 and 4), and for the oil well 1, field B (Figure 6), show an early straight line section followed by a flatter straight line portion extrapolating back into initial reservoir pressure. A typical misinterpretation of this behavior is that a region of improved permeability exists in the vicinity of the well. A more logical interpretation for reef reservoirs is that a constant pressure source such as a water drive is being reflected.

A dimensionless Horner analysis is made using a plot of

$$\frac{kh}{141.3\ q\mu\beta}\ (p_i - p_{ws}) \text{ versus } \frac{t + \Delta t}{\Delta t}$$

on semilog paper. Solutions for closed and constant pressure boundaries for different situations and drainage shapes were published by Ramey (Ref. 4). In case of well 1, field A, the best match was obtained for a square system with a well located in the center of three closed boundaries and one constant pressure boundary. One possible source of the constant pressure is a recharge from water drive source (Figure 21). If the same system was completely closed (volumetric), p_d at $t + \Delta t$ of 1 is 0.15 which is more than 0. The fact that the second flatter slope extrapolates to initial reservoir pressure implies that the term p_d at $t + \Delta t/\Delta t$ of 1 is 0 or $p_i - p_{ws} = 0$ which is the case for this solution. Solutions for both cases are shown in Figures 22 and 23.

A similar plot for the oil well 1, field B was made and is shown in Figure 24 for a t_{da} of 0.011. Again, a good fit with a constant pressure boundary solution (Figure 25) was obtained.

The dimensionless Horner plot for constant pressure solutions can help confirm interpretations of the Horner plots and should be used as another tool to define the type of system we are dealing with.

Constant Pressure Case (At Inner Boundary)

So far, our analyses of well tests dealt with decline in bottomhole flowing pressure with the flow rate being essentially constant. There are cases where the wellbore flowing pressure remains constant and the producing rate declines. Fetkovich[5], in his paper, "Decline Curve Analysis Using Type Curves," presented log-log type curve analysis for these cases completely analogous to the log-log type curve matching procedure for constant rate case pressure transient data analysis (Figure 26).

The data obtained from a 24 hour after acid flow test on well 1, field G, exactly matched the constant flowing pressure solution. Based on results of this test, a seven (7) day flow test followed by a 3 day buildup test was performed on well 1, field G to help define reservoir performance, i.e., limits, volumetric behavior or effectiveness of the water drive system. Figure 27 is a log-log plot of the total fluid flow rate versus time data of the seven (7) day flow test. Using the dimensionless flow rate q_d versus dimensionless time t_d type curve, the best fit of the data was obtained with match points shown on Figure 28. Let us analyze the data.

Match Points

q = 10,000 BFPD, q_d = 0.192
t = 10 hours, t_d = 840
$q = q_o + q_w$ = 3900 BOPD + 6100 BWPD = 10,000 BFPD on Reservoir Data:

h = 143 ft	β_o = 1.000
ϕ = 17.6 pct	β_w = 1.025
$p_i - p_{wf}$ = 14.10 psi	c_t = 7.8 (10^{-6}) psi^{-1}
μ_o = 6 cps	r_w = 0.51 ft
μ_w = .36 cps	
S_w = 51 pct	

$$kh = \frac{141.3\ q\ \mu\beta}{q_D \Delta p} \qquad k = \frac{141.3\ q\ \mu\beta}{q_D \Delta p\ h}$$

For oil $$k_o = \frac{141.3\ (3900)\ (6)\ (1.000)}{0.192\ (14.10)\ (143)} = 8541 \text{ md}$$

For water $$k_w = \frac{141.3\ (6100)\ (.36)\ (1.025)}{0.192\ (14.10)\ (143)} = 821 \text{ md}$$

$$t_d = \frac{.00634\ kt}{\phi\mu\ c_t\ r_w'^2} \qquad r_w' = \sqrt{\frac{.00634\ kt}{\phi\mu\ c_t\ t_d}}$$

$$\left[\frac{k}{\mu}\right]_t = \frac{k_o}{\mu_o} + \frac{k_w}{\mu_w} = \frac{8541}{6} + \frac{821}{.36} = 3705\ \frac{md}{cps}$$

$$r_w' = \sqrt{\frac{0.00634\ (3705)\ (10)\ (10^6)}{(.176)\ (7.8)\ (24)\ (840)}} = 92'$$

$$S = -\ln\left(\frac{r_w'}{r_w}\right) = -\ln\left(\frac{92}{.510}\right) = -5.20$$

Let us compare results of this analysis to the analysis of the three (3) day buildup that followed this drawdown.

The Horner plot of the buildup test is shown in Figure 29.

m = .92 psi/cycle
q_o = 1221 BOPD
q_w = 4885 BWPD
p_{wf} = 2431.9 psig
p_1 = 2442.50 psig

Perforations = 41 ft
r_w = 0.51 ft

$$k_o = \frac{162.6\ q_o\ \mu_o\beta_o}{m\ h} = \frac{162.6\ (1221)\ (6)\ (1.00)}{.92\ (143)} = 9054\ md$$

which is a fair check with 8541 md determined from previous rate-time type curve decline analysis.

$$k_w = \frac{162.6\ (4885)\ (.36)\ (1.025)}{.92\ (143)} = 2227\ md$$

$$\left[\frac{k}{\mu}\right]_t = \frac{9054}{6} + \frac{2227}{.36} = 7695\ \frac{md}{cps}$$

$$S = 1.151\left[\frac{p_1 - p_{wf}}{m} - \log\left(\frac{k}{\phi\,\mu\,c_t\,r_w^2}\right) + 3.23\right]$$

$$S = 1.151\left[\frac{2442.50 - 2431.9}{.92} - \log\frac{7695\,(10^6)}{.176\,(7.8)\,(.26)} + 3.23\right]$$

$$S = 1.151\,[11.52 - 10.34 + 3.23] = 5.07$$

$$S = S_d + S_b,\quad S_d = S - S_b$$

where S_b is partial penetration skin

$$b = \frac{41}{143} = 0.287\ ,\qquad \frac{h}{r_w} = \frac{143}{0.51} = 280,\ S_b = +9.0$$

$S_d = 5.07 - 9.0 = -3.93$ which implies no communications behind the pipe. From the above calculations, the build-up kh and skin compares fairly well with the kh and skin determined by using the rate-time decline curve data.

Furthermore, the long duration drawdown test and rate-time decline curve analysis approach provides a tool for generating a production forecast by extending the r_e/r_w' curve and simply reading the rates from the real time scale.

Water Coning Calculations

Well 1, field G produced at initial rate of 18,000 BOPD with no water, then it started producing free water after 3 days. This lead to believe that the high initial oil rate of 18,000 BOPD might develop a cone and eventually water break through into the wellbore. Sobocinski and Cornelius[6] presented an analytical solution for predicting the critical coning rate and time to breakthrough.

$$q_o = \frac{0.00307\,\Delta\rho\,k_h\,h\,h_c}{z\,\mu_o\beta_o}$$

where z = dimensionless coning height
$\Delta\rho$ = water-oil density difference gm/cc
h = oil zone thickness, ft
h_c = height of apex of water cone above the average water oil contact, ft
q_o = oil production rate, STB/D
β_o = oil formation volume factor
μ_o = viscosity oil, cps

A Z of 3.5 is considered the limiting value for critical rate. Therefore q at Z of 3.5 is the critical coning rate.

$$q_o = \frac{0.00307\ (0.097)\ (9054)\ (143)\ (102)}{(3.5)\ (6.0)\ (1.00)} = 1873 \text{ BOPD}$$

This implies that the initial rate of 18,000 BOPD should develop the cone and water breakthrough should occur after a short period.

$$t = \frac{t_d\ \mu_o\ \phi\ F_k\ h}{0.00137\ \Delta\rho\ k_h\ (1 + M^{\alpha})} \qquad \text{where } F_k = \frac{k_{\text{horiz.}}}{k_{\text{vert.}}} \text{ and } M = \frac{\mu_o\ k_w}{\mu_w\ k_o}$$

An initial rate of 18,000 BOPD, Z equals 0.364 and t_d from Z vs t_d correlation is 0.17. Let's assume that ratio of $k_{horizontal}$ to $k_{vertical}$ equals 1, based on high permeabilities (9 Darcies) and core analysis

$$M = \frac{\mu_o\ k_w}{\mu_w\ k_o} = \frac{(6)\ (2227)}{(.36)\ (9054)} = 4.2$$

$$\alpha = 0.6 \text{ for } 1 < M < 10.$$

$$1 + M^{\alpha} = 1 + 4.2^{0.6} = 3.35$$

$$t = \frac{.17\ (6)\ (.176)\ (143)\ (1.00)}{(.00137)\ (.0097)\ (9054)\ (3.35)} = 6.37 \text{ days which compares closely with}$$

test results where free water was produced in large quantities after approximately 3 days.

Conclusions

The results obtained from testing and analyzing several Indonesian reef oil and gas wells leads to the following conclusions:

1. Multipoint tests are required for providing accurate determination of formation characteristics for those wells exhibiting high permeabilities and low pressure drawdowns even while flowing at high flow rates.

2. Single flow and buildup period type tests for wells with permeabilities ranging from 10 md to 100 md are adequate for determining reservoir parameters such as permeability, skin and productivity index. However, these tests above can not accurately determine flow rates as a function of drawdown, and well's true absolute open-flow potential. Multipoint tests are required to provide these data.

3. Multipoint tests (true isochronal or flow after flow) are useful for determining wellhead deliverabilities, true bottomhole deliverabilities (used for sizing tubing) and production forecasting.

4. The dimensionless Horner analysis provides an interpretation method for early detection of the possible presence of an active water drive in these reef reservoirs.

5. Decline rate-time type curve analysis for wells flowing at essentially a constant pressure at the wellbore provides a useful method for forecasting and calculating formation characteristics which closely agrees with conventional Horner analysis of the buildup.

Nomenclature

β = formation volume factor, reservoir vol/surface vol
C = total compressibility, psi^{-1}
D = non-Darcy flow constant, $(STK\ BOPD)^{-1}$
G = gas gravity
h = thickness, ft
k = effective permeability, md
m = slope of straight-line portion of buildup or drawdown curve, psi/cycle
m(p) = pseudo-pressure, $\int_{p_{wf}}^{p_R} dp/\mu\beta$, STKB-psi/Res B-cps
n = exponent of backpressure curve
ϕ = porosity, fraction of bulk volume
p_b = bubble point pressure, psia
P_c = wellhead shut in pressure, psia
pd = dimensionless pressure drop
p_i = initial reservoir pressure, psia
p_R = reservoir shut in pressure, psia
p_t = wellhead flowing pressure, psia
p_{wf} = bottomhole flowing pressure, psia
p_{ws} = pressure at time Δt after shut-in, psia
q_D = dimensionless rate
q = surface rate of flow, STK BOPD or MSCFD
r_e = external boundary radius, ft
r_w = wellbore radius, ft
r_w' = effective wellbore radius, ft
S = skin effect, dimensionless
S' = total effective skin effect, $S' = S_d + S_b + D_q$, dimensionless
S_w = water saturation, pot
t = time
T = reservoir temperature, R
t_D = dimensionless time
t_{Dd} = decline curve dimensionless time

μ = viscosity, cp
Z = gas deviation factor, dimensionless

Subscripts

i = initial
o = oil
g = gas
w = water

References

1. Brons, F. and Marting, V.E.: "The Effect of Restricted Fluid Entry on Well Productivity," J. Pet. Tech. (Feb. 1961) 172.

2. Fetkovich, M. J.: "The Isochronal Testing of Oil Wells," paper SPE 4529 presented at the 48th Annual Fall Meeting, Las Vegas, Nevada, (Sept. 30-Oct. 3, 1973).

3. Fetkovich, M. J.: "Multipoint Testing of Gas Wells," Presented at SPE Mid-Continent Sec. Continuing Educ. Course on Well Test Analysis, March 17, 1975.

4. Ramey, H. J., Jr., Kumar, A., and Gulati, S. M.: "Gas Well Test Analysis Under Water-Drive Conditions," Amer. Gas Assoc. Project 61-51 of the Pipeline Research Committee at Stanford Univ. 1973.

5. Fetkovich, M. J.: "Decline Curve Analysis Using Type Curves," paper SPE 4629 presented at the 48th Annual Fall Meeting, Las Vegas, Nevada (Sept. 30 - Oct. 3, 1973).

6. Sobocinski, D. P., Cornelius, A. J.: "A Correlation for Predicting Water Coning Time," presented at the Annual Fall Meeting held in Houston, Oct. 11-14, 1965.

Acknowledgement

We wish to thank Phillips Petroleum Company for permission to publish this paper.

About the Authors

B. A. Ziara - is a 1966 petroleum engineering graduate of the University of Tulsa. Ziara joined Phillips soon after graduation as a production engineer working in the Texas Panhandle. In 1968, he was transferred to the Company's Norwegian Operations in the North Sea where he held various engineering positions. In 1975, he was promoted to his current Bartlesville position as Reservoir Engineering Consultant for Worldwide Drilling and Production. He is a member of the AIME-SPE and International Toastmasters Club.

M. J. Fetkovich - A 1954 petroleum and natural gas engineering graduate of the University of Pittsburgh. Fetkovich joined Phillips as a gas well test engineer working in the Texas-Oklahoma Panhandle. In 1957 he became a gas reservoir engineer in Bartlesville, and six years later became reservoir engineering and gas technology specialist in Phillips' Computing Department. Fetkovich was promoted to his current Bartlesville position as Staff Director of Reservoir Engineering for Worldwide Drilling and Production in 1974. He served as 1977-1978 Distinguished Lecturer in the SPE's 17th Distinguished Lecturer series discussing Well Testing and Analysis.

TABLE 1

Field A, Well 1

Before Acid - Open Hole Test

$\bar{p}_R$ = 4117 psia $\bar{p}_R^2$ = 16,949,689 psia^2

Flow	Duration Hours	Q MSCFD	p_{wf} psia	$\bar{p}_R^2 - p_{wf}^2$ psia (thousands)	$\bar{p}_R^2 - p_{wf}^2/Q$ psia^2/MSCFD
1	4	22,385	3281	6185	276.3
2	4	17,391	3536	4446	255.7
3	4	12,930	3749	2895	223.9
4	4	7,950	3919	1591	200.1

hp = 232 ft (perforated at top)
h = 585 ft
r_w = .354 ft
μ = .0210 cps (at p avg)
Z = .905 (at p avg)
T = 200° F or 660° R
G = .745
t = 4 hrs flow time

$$\bar{p} = \frac{\bar{p}_R + p_{wf}}{2} \qquad \frac{4117 + 3281}{2} = 3699 \text{ psia}$$

ϕ = .102
c_t = 140 (10^{-6}) psia^{-1}
β_g = .004559 Res Bbl/Surface Bbl

TABLE 2

Field D, Well 1

m(p) Calculation

Pressure psia	ΔP psia	$1/\mu_o\beta_o$ @ P avg	$\Delta(1/\mu_o\beta_o)$ STKB - psi / Res B - cps	$m(p) = \sum^{p} \Delta p \left(\frac{1}{\mu_o\beta_o}\right)$ STKB - psi / Res B - cps
2858				562.45
	58	.1792	10.39	
2800				552.06
	300	.1830	54.90	
2500				497.16
	500	.1920	96.00	
2000				401.16
	500	.2136	61.80	
1500				339.36
	500	.2150	107.50	
1000				231.86
	500	.2260	113.00	
500				118.86
	300	.2355	70.65	
200				48.21
	100	.2400	24.00	
100				24.21
	100	.2421	24.21	
0				0

TABLE 3

Field D, Well 1

After Acid Multipoint Test

Duration of Each Flow Test = 4 Hours

$\bar{p}_R$ = 2857.7 psia $m(\bar{p}_R)$ = 562.45 STKB - psi/Res B-cps

q_o BOPD	p_{wf} psia	$\bar{p}_R - p_{wf}$ psia (Δp)	$m(p_{wf})$	$\Delta m(p)$ $m(\bar{p}_R) - m(p_{wf})$	$\Delta m(p)/q_o$
1994	2854.6	3.1	561.85	0.60	0.000301
4244	2850.2	7.5	561.05	1.40	0.000330
6670	2844.9	12.8	560.00	2.45	0.000367

h = 133 ft
ϕ = 16%
S_w = 27%
c_t = 7.7 (10^{-6}) psi^{-1}
r_w = .354 ft
T = 176° F or 636° R
r_e = 900 ft
S = -4

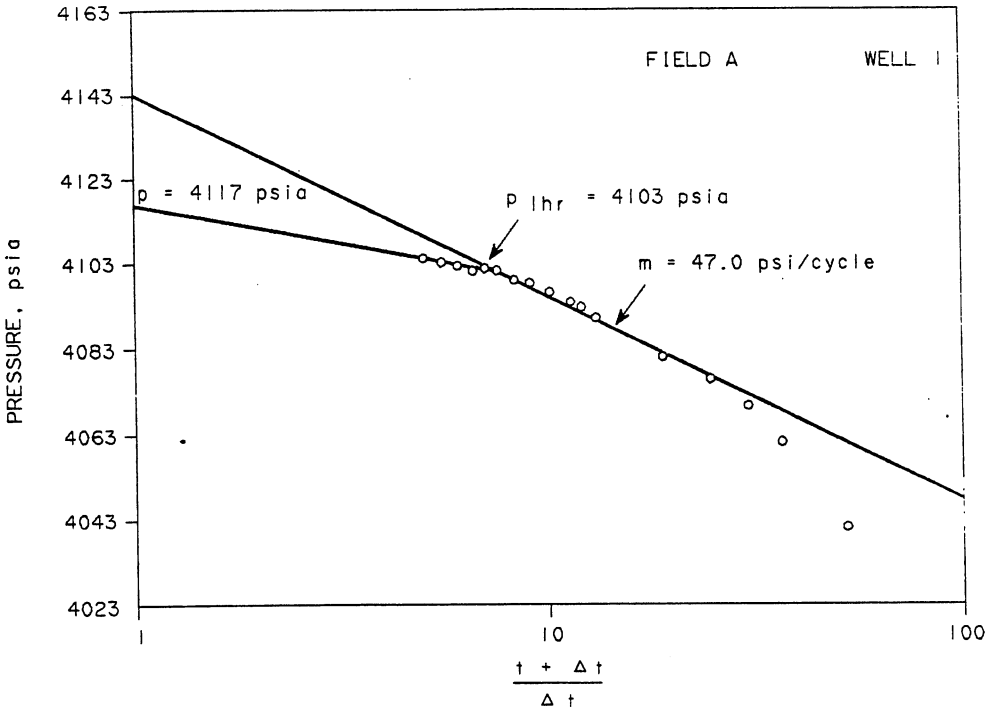

FIGURE 1 - BEFORE ACID BUILD UP - OPEN HOLE TEST

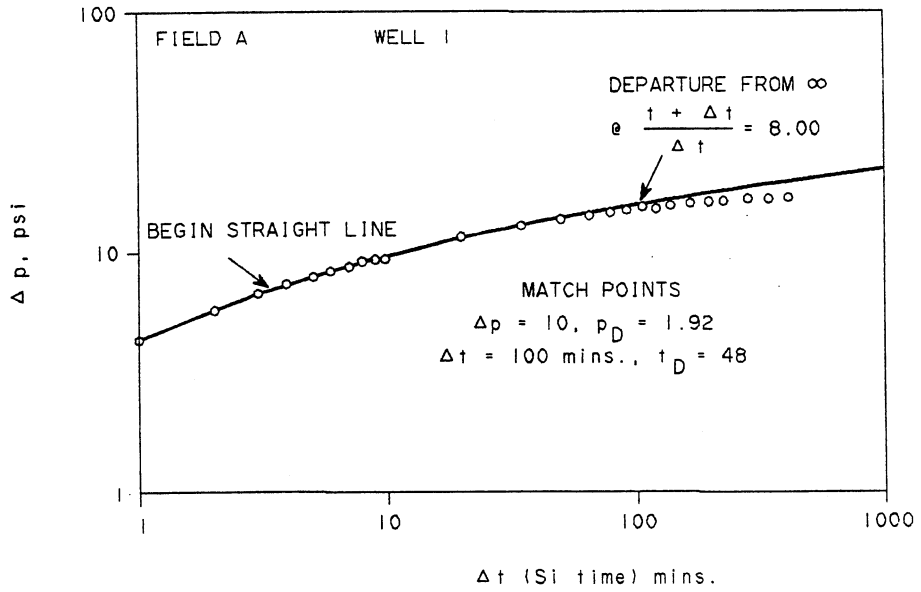

FIGURE 2 - AN AFTER ACID BUILD UP

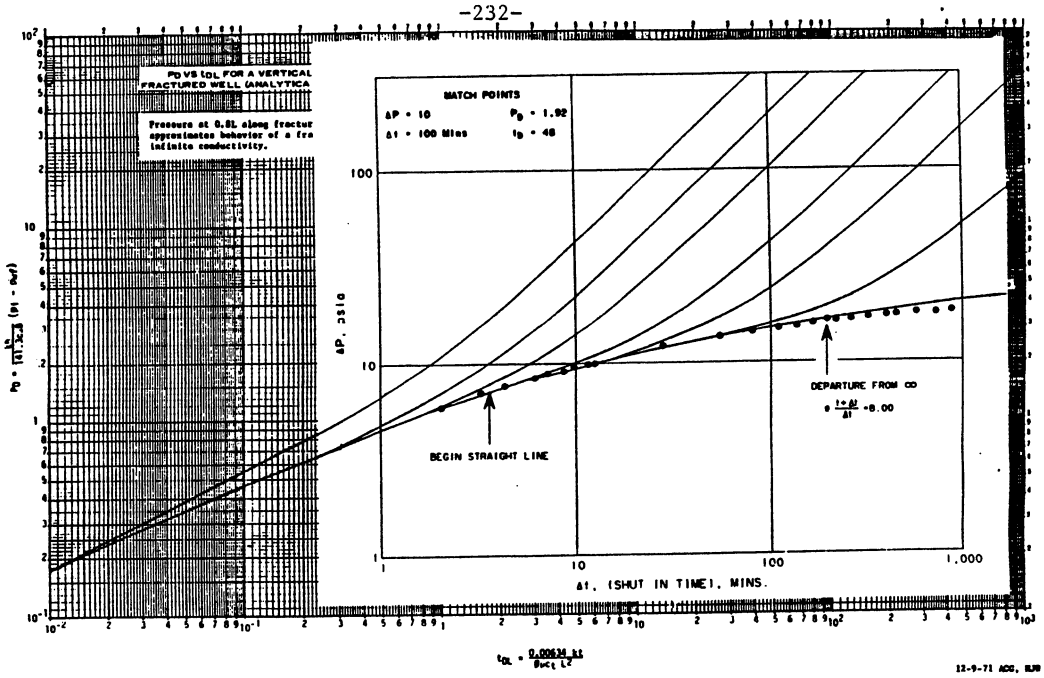

FIGURE NO. 3 FIELD A WELL 1

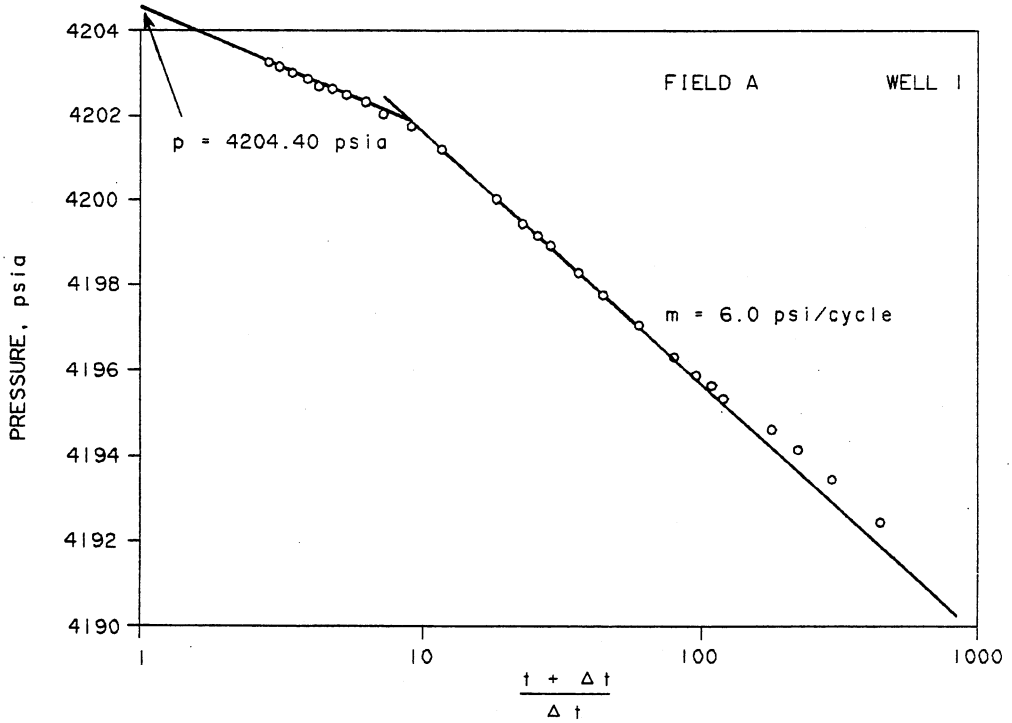

FIGURE 4 - AN AFTER ACID BUILD UP

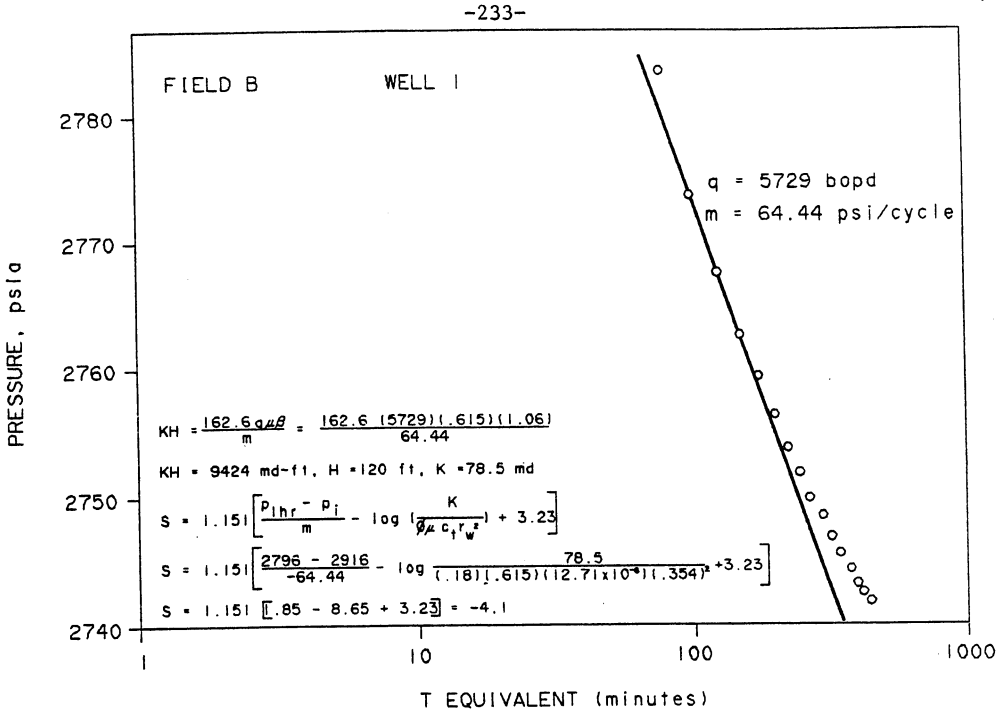

FIGURE 5 - AN AFTER ACID DRAWDOWN

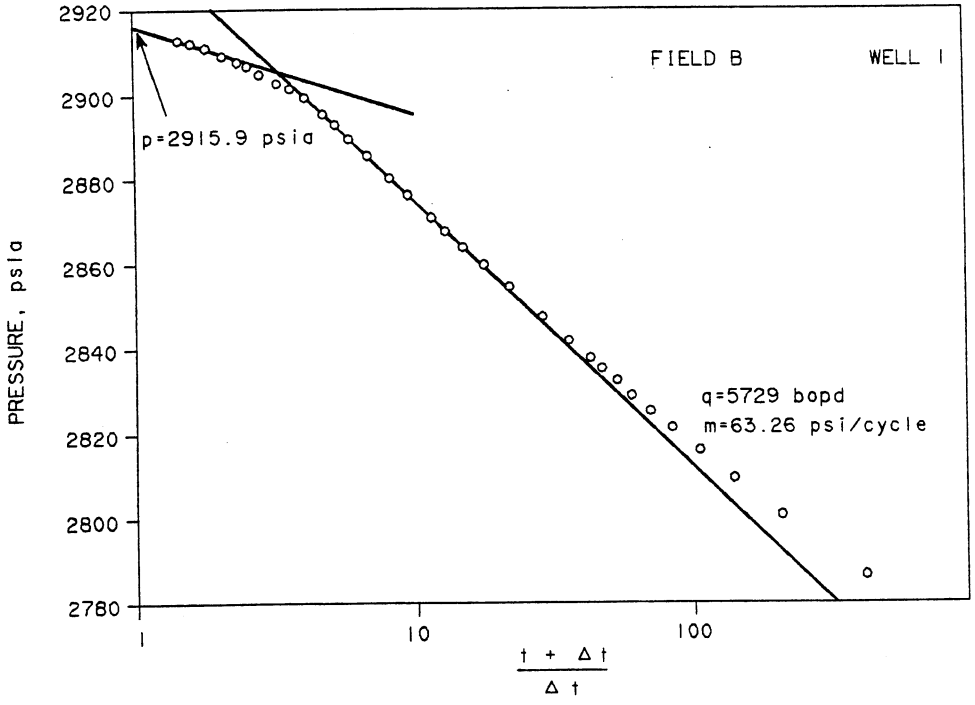

FIGURE 6 - AN AFTER ACID BUILD UP

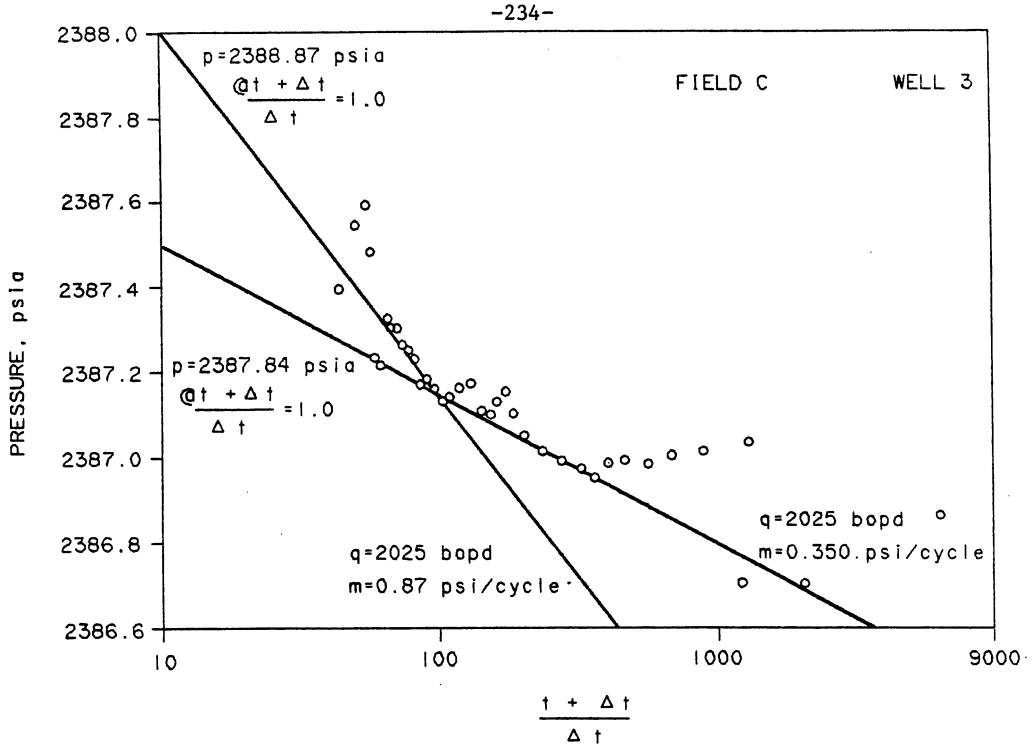

FIGURE 7 - AN AFTER ACID BUILD UP

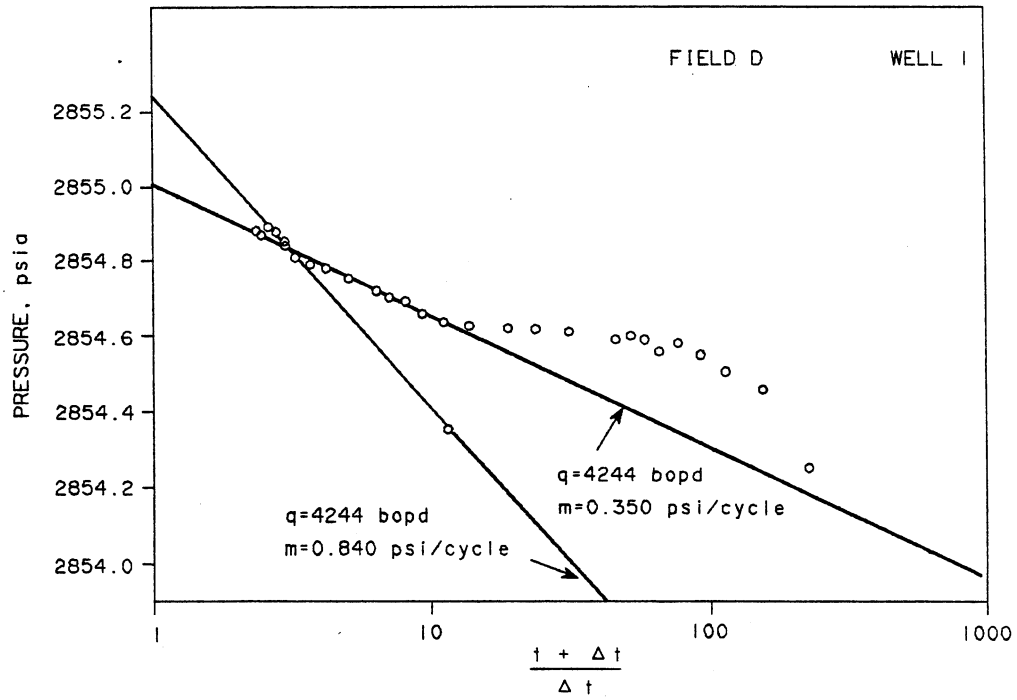

FIGURE 8 - AN AFTER ACID BUILD UP

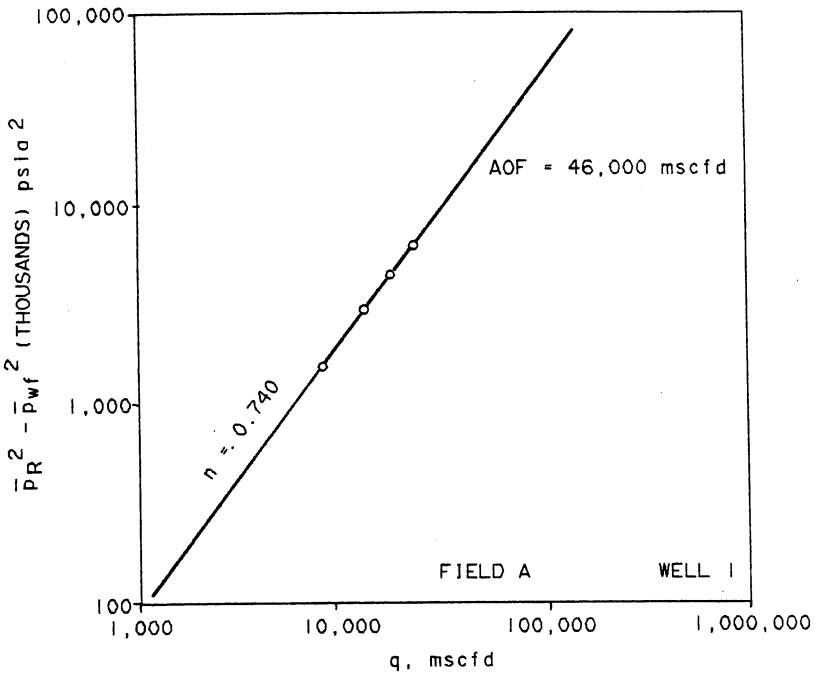

FIGURE 9 - BEFORE ACID OPEN HOLE ISOCHRONAL TEST

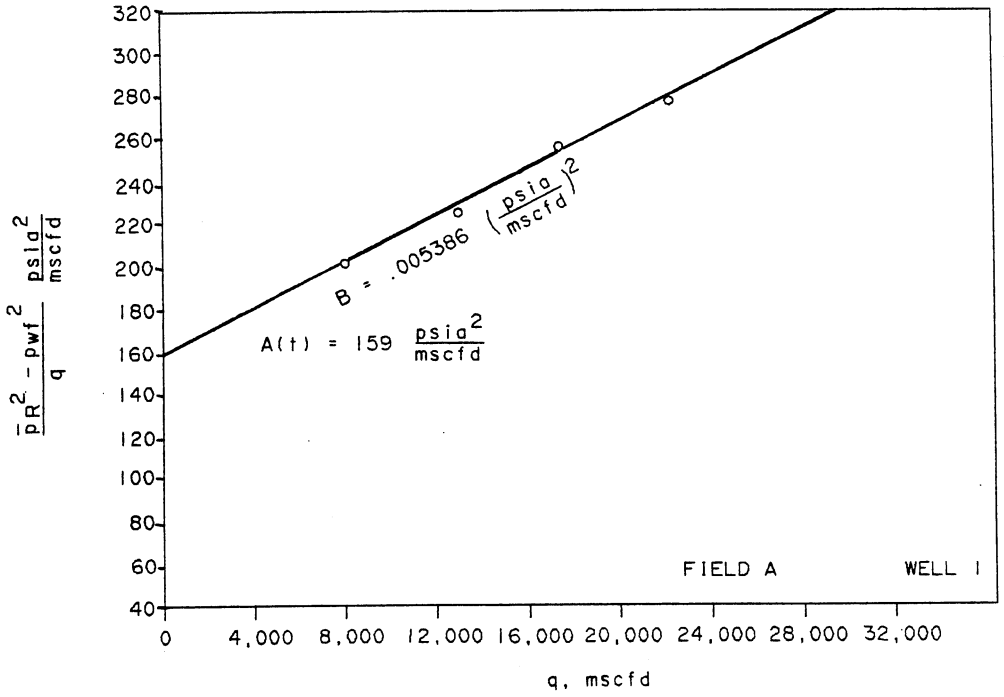

FIGURE 10 - BEFORE ACID OPEN HOLE ISOCHRONAL TEST

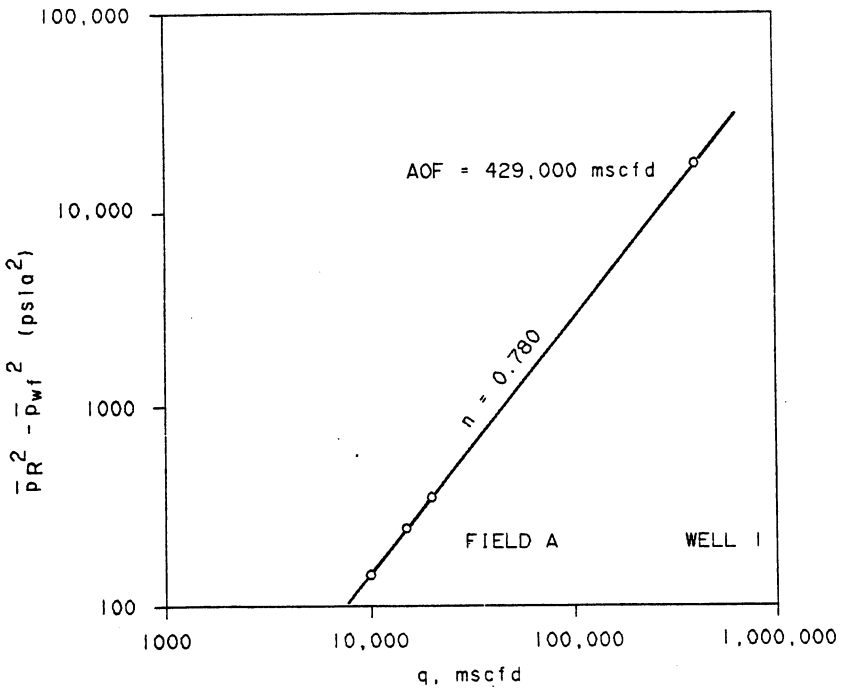

FIGURE 11 - BACK PRESSURE CURVE

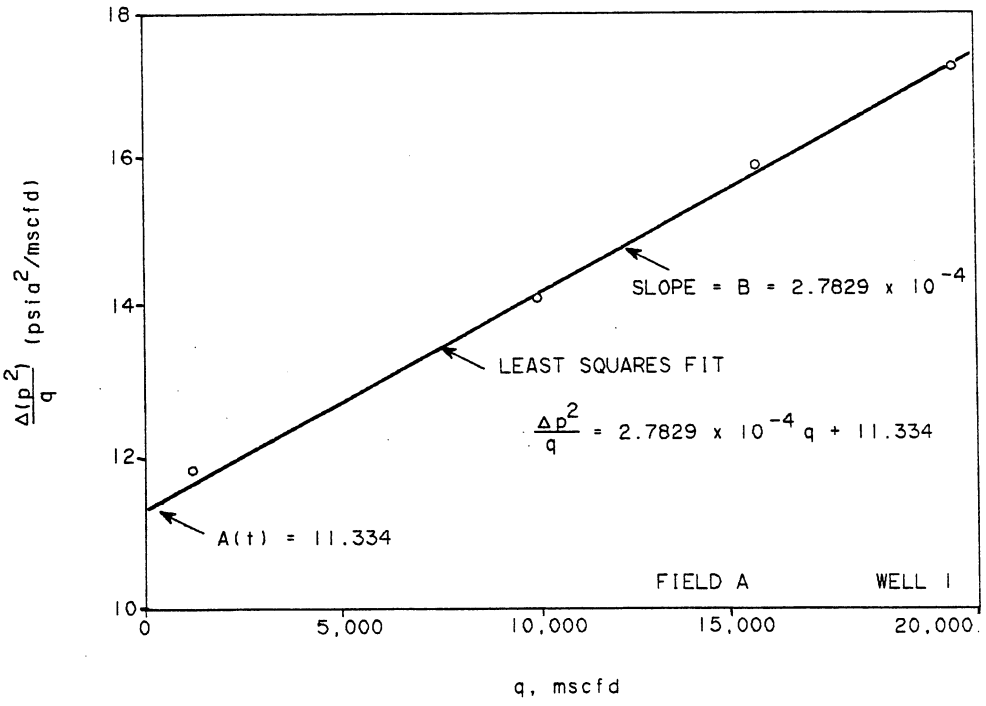

FIGURE 12

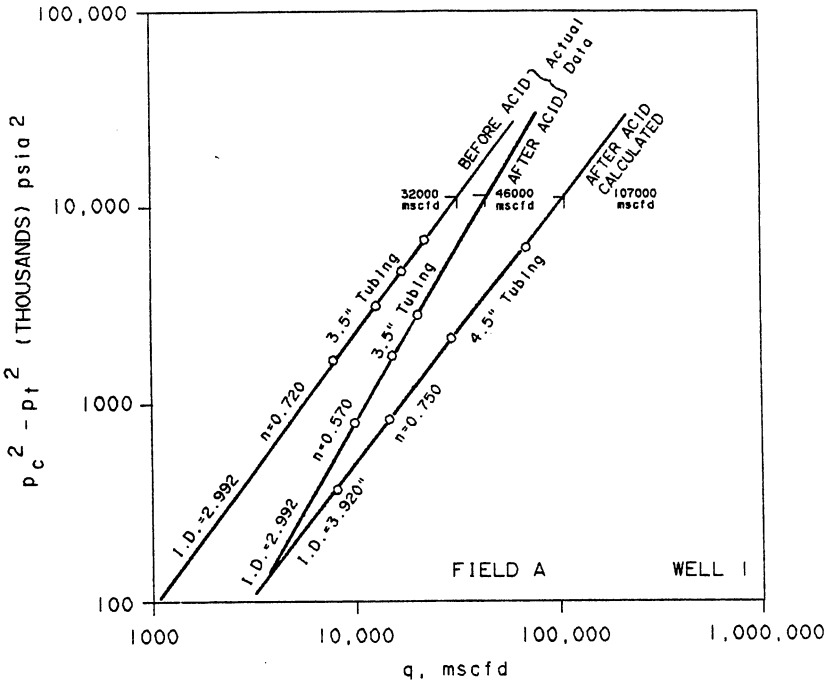

FIGURE 13 - WELLHEAD BACK PRESSURE CURVE

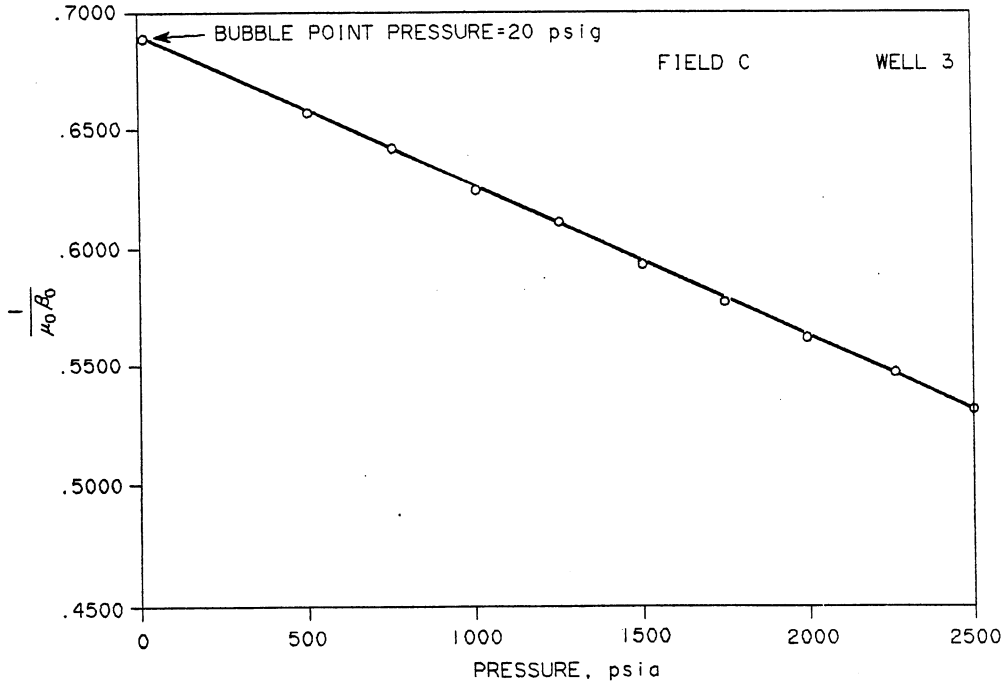

FIGURE 14 - FROM PVT STUDY

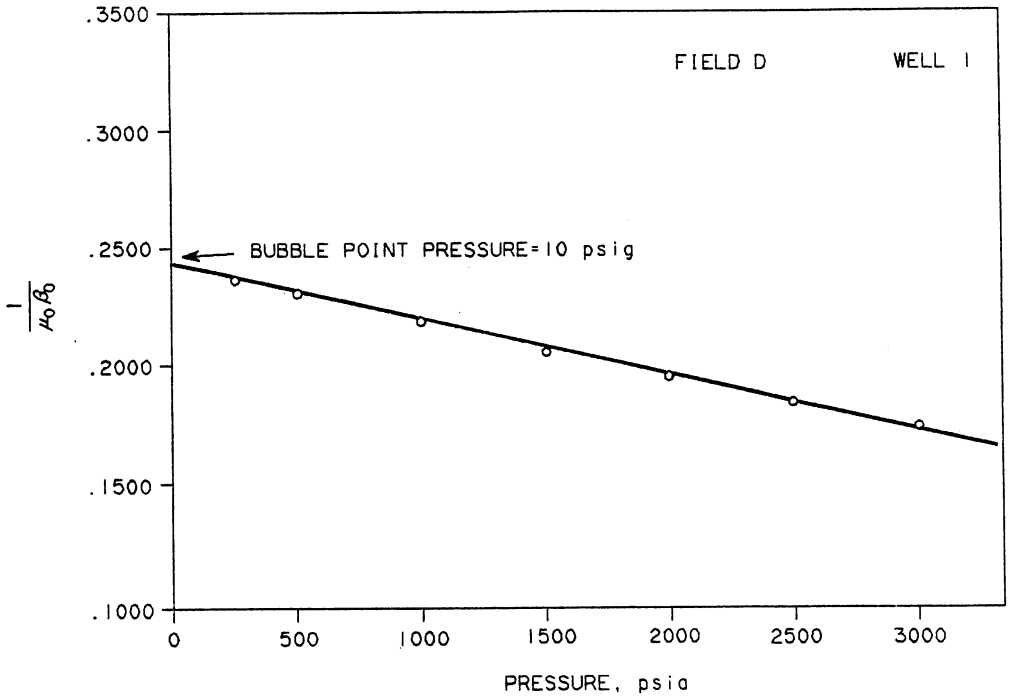

FIGURE 15 - FROM PVT STUDY

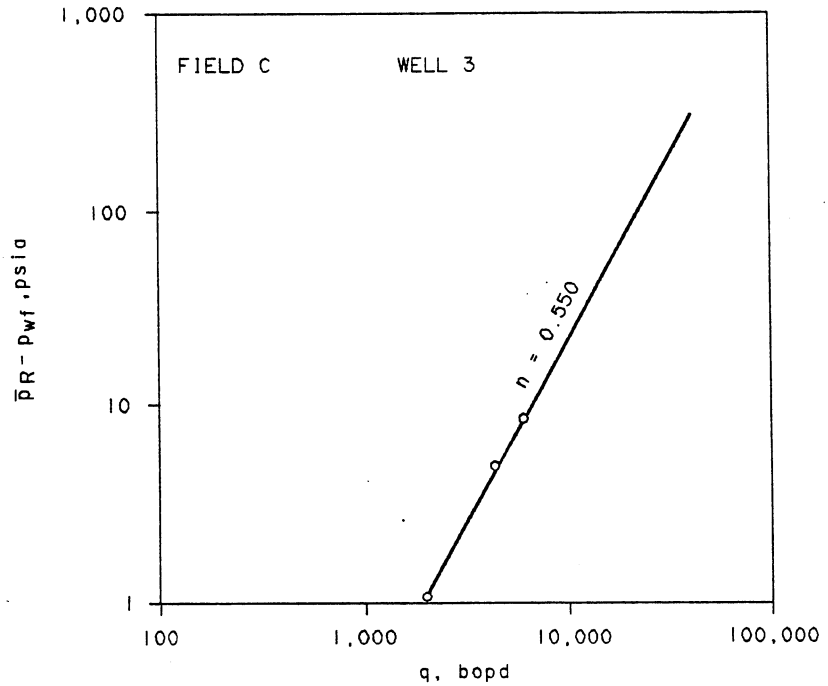

FIGURE 16 - AN AFTER ACID ISOCHRONAL TEST

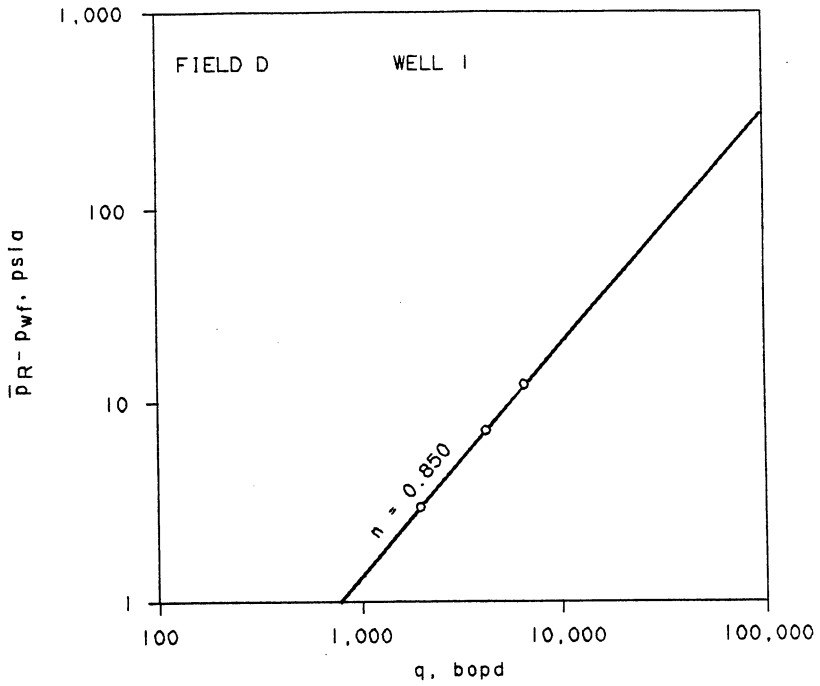

FIGURE 17 - AN AFTER ACID ISOCHRONAL TEST

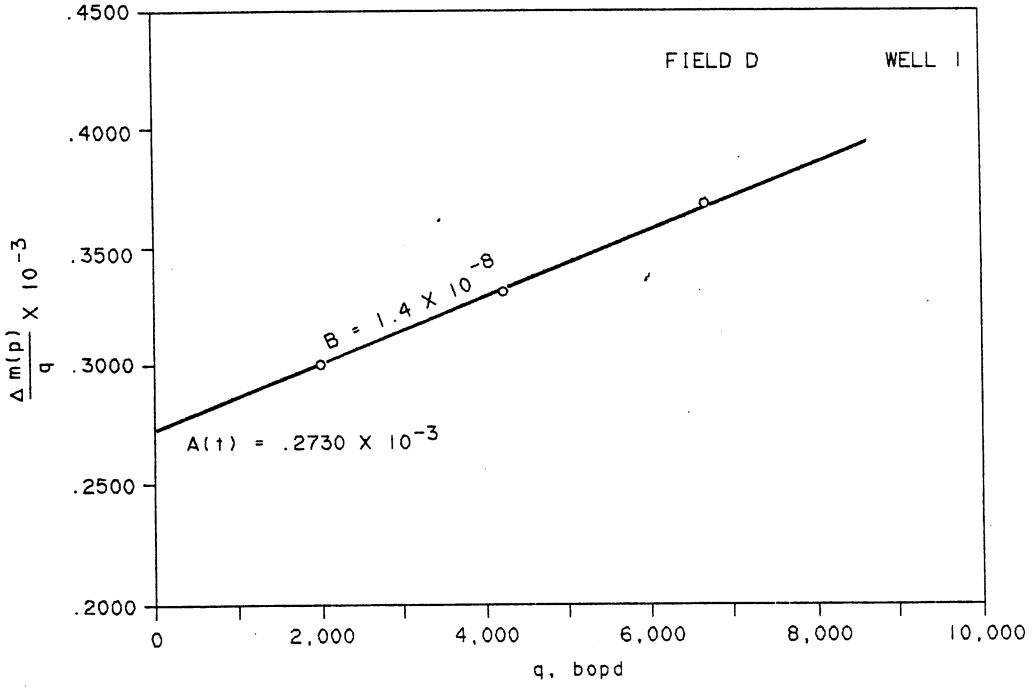

FIGURE 18

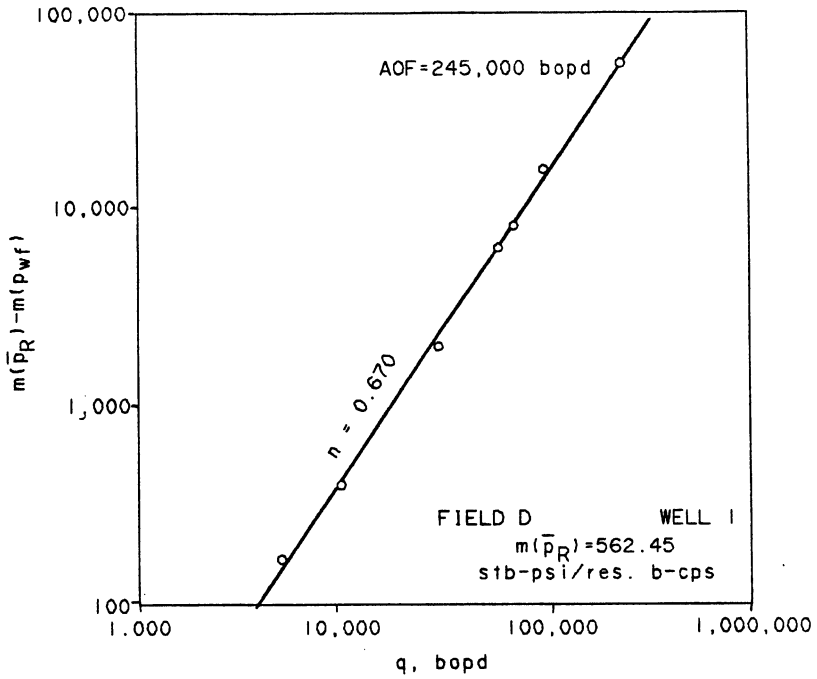

FIGURE 19 - BOTTOM HOLE BACK PRESSURE CURVE

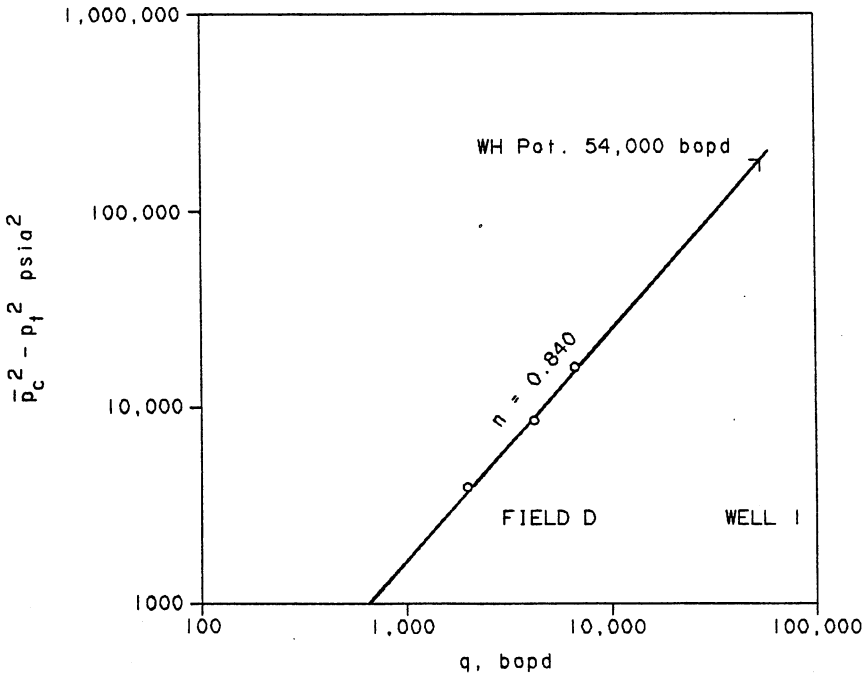

FIGURE 20 - WELLHEAD BACK PRESSURE CURVE

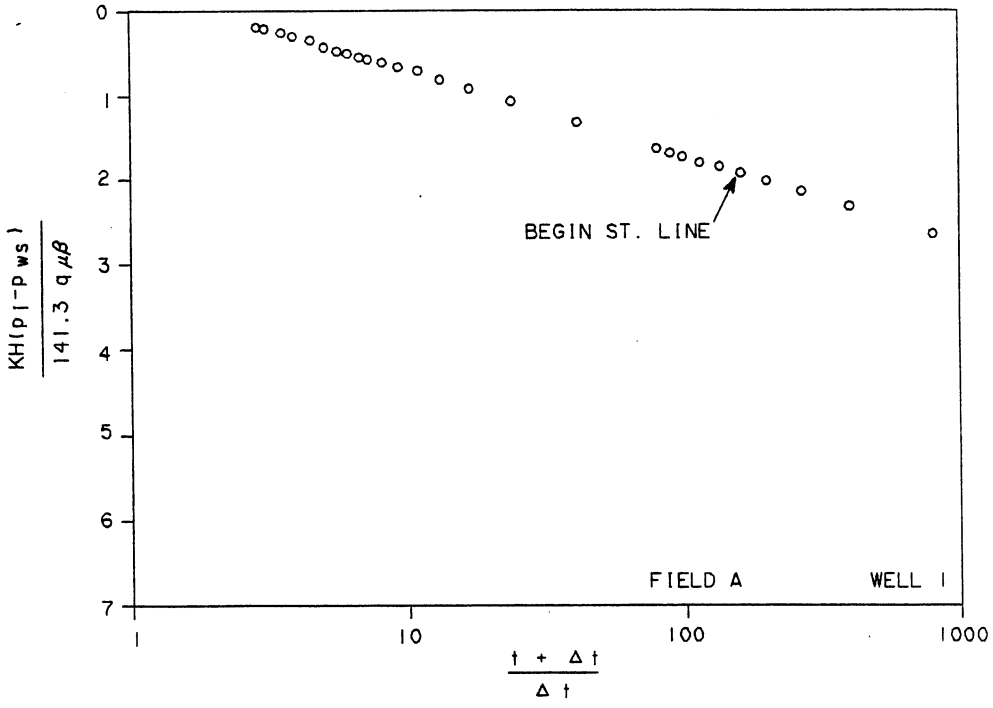

FIGURE 21

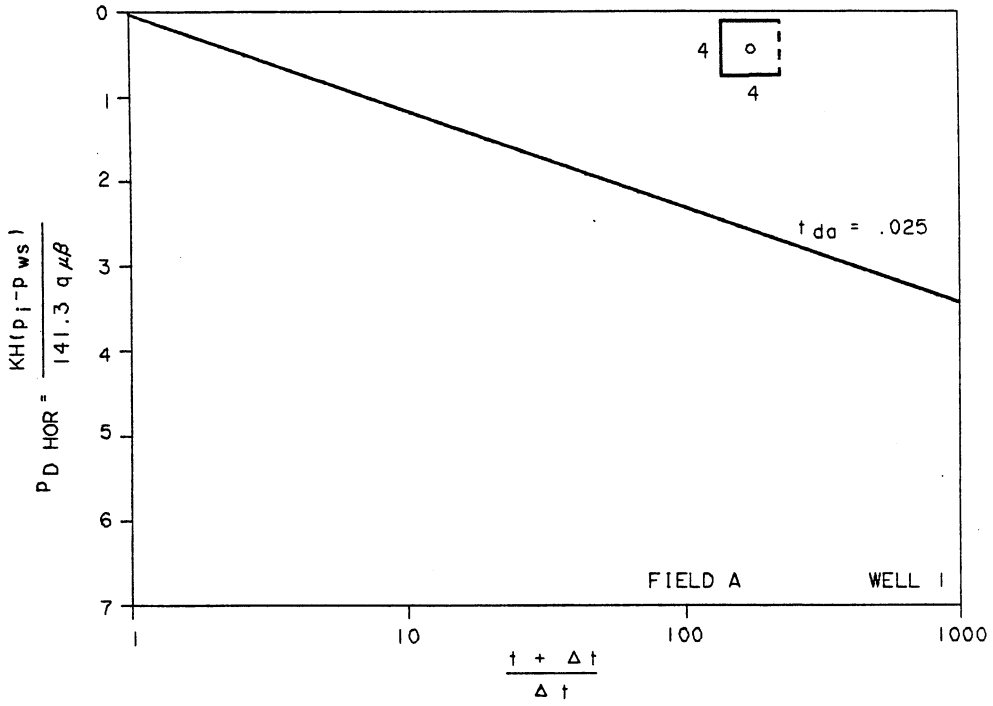

FIGURE 22

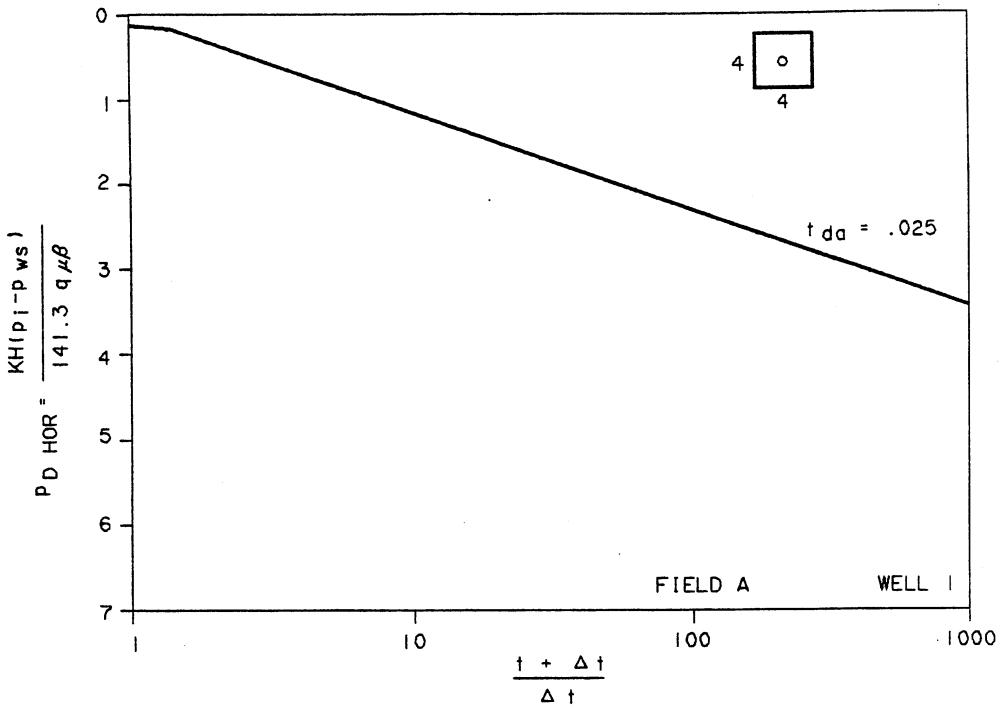

FIGURE 23

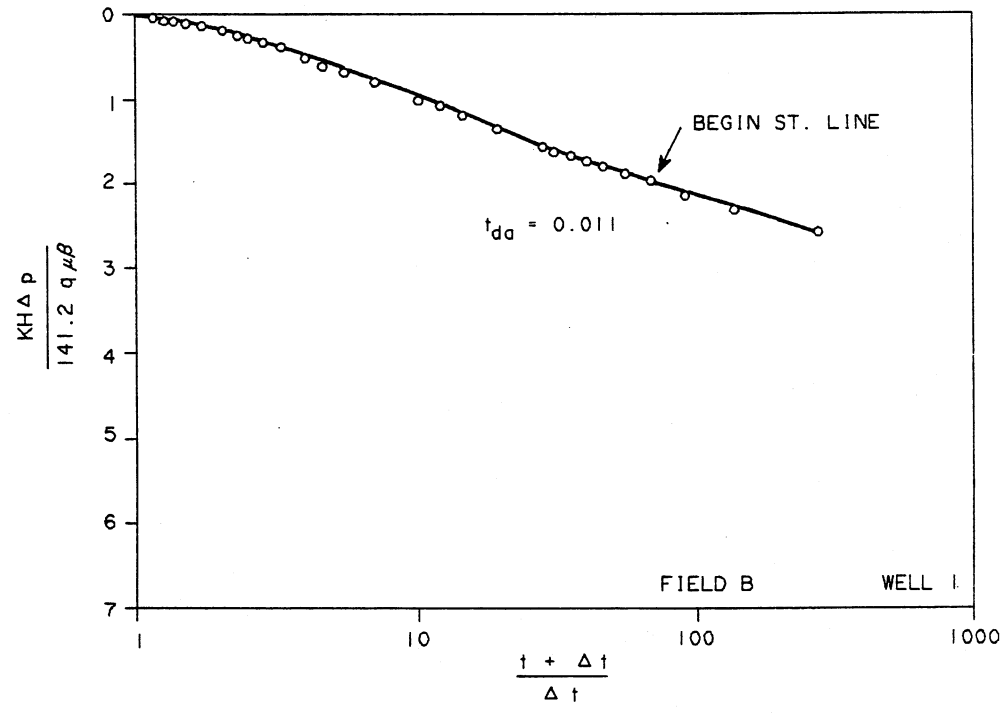

FIGURE 24

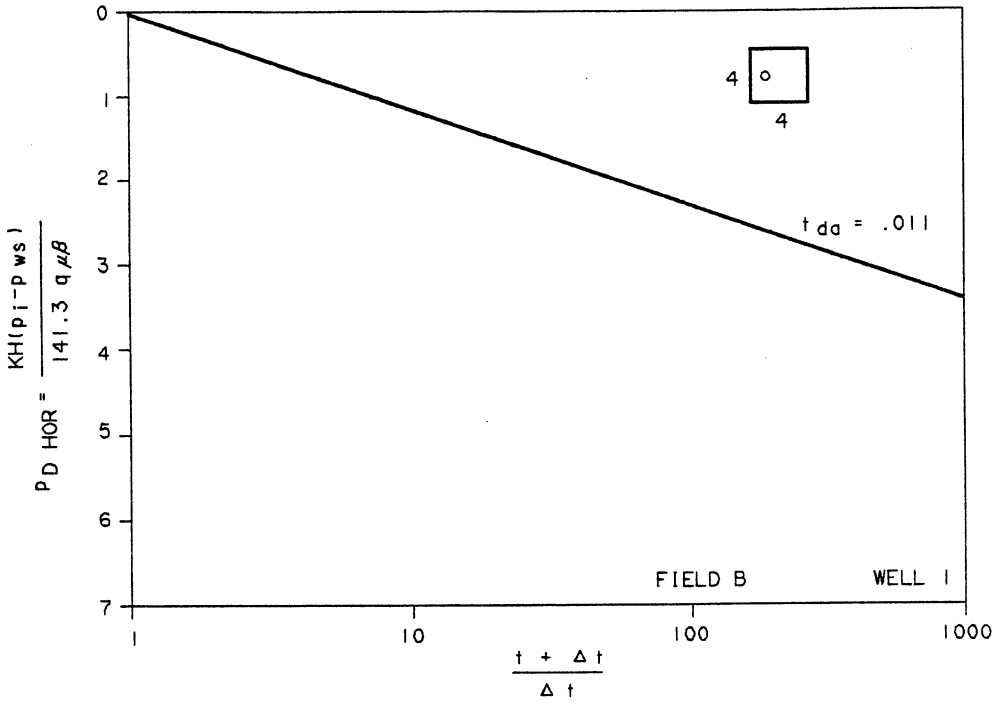

FIGURE 25

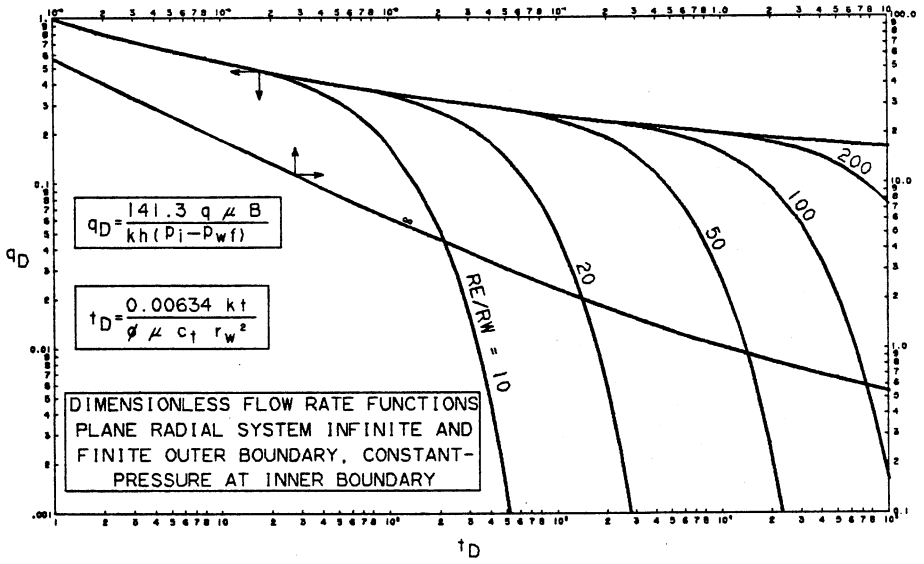

FIGURE 26

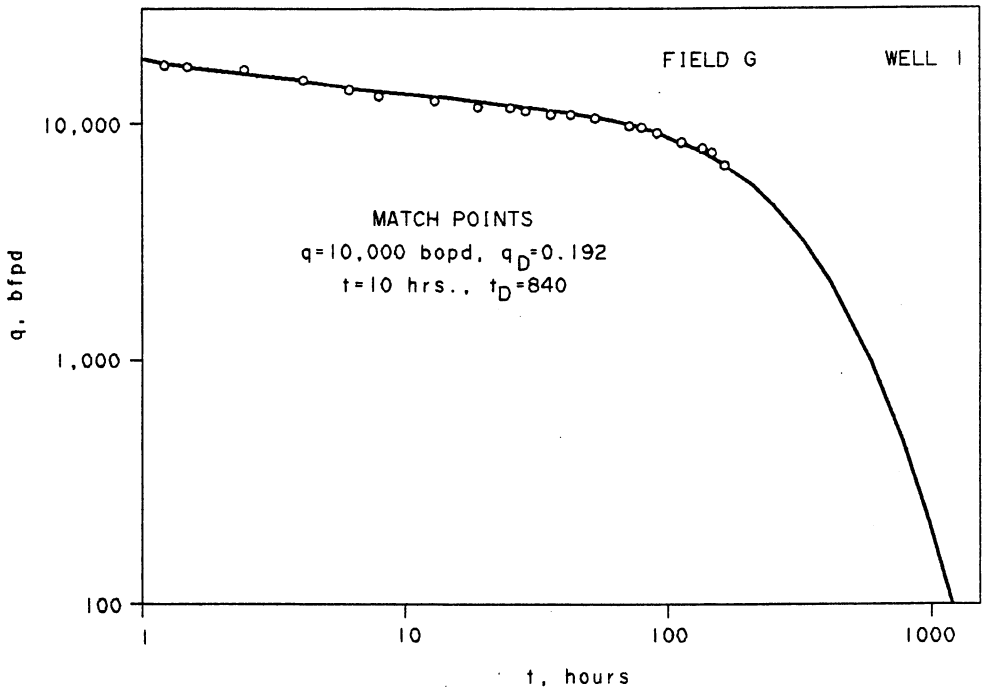

FIGURE 27 - LONG DURATION DRAWDOWN

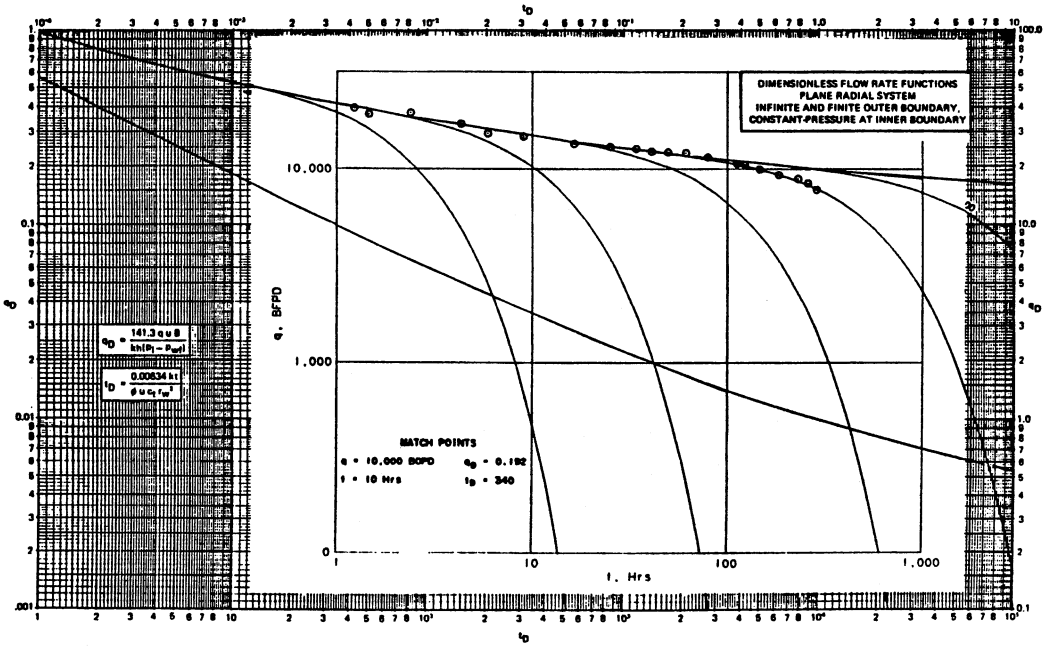

FIGURE NO. 28 FIELD G WELL 1

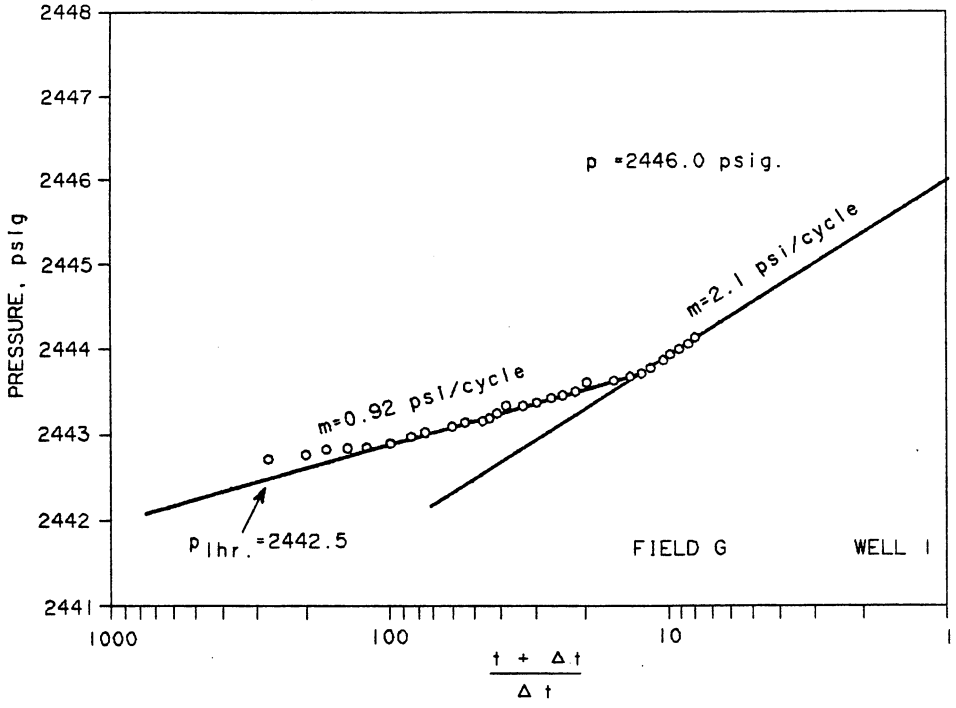

FIGURE 29 - BUILD UP TEST

DECLINE CURVE ANALYSIS USING TYPE CURVES: CASE HISTORIES

by

M. J. Fetkovich
M. E. Vienot
M. D. Bradley
U. G. Kiesow

Phillips Petroleum Co.
SPE Members

SPE 13169

This paper was presented at the 59th Annual Technical Conference and Exhibition held in Houston, Texas, September 16-19, 1984.

DECLINE CURVE ANALYSIS USING TYPE CURVES: CASE HISTORIES

Summary

The purpose of this paper is to present case history studies that demonstrate methods of analyzing rate-time data to predict future production and to determine reservoir variables. Constant wellbore pressure analysis techniques are demonstrated, using existing q_{dD} - t_{dD} type curves along with developing new q_{dD} - t_{dD} type curves from actual field data.

Case histories for individual oil and gas wells are presented, along with groups of wells in a field and total field studies. The field studies include a one-well full water drive field, a low-permeability solution gas drive field, and a field with both primary and secondary (waterflood) history. Field shut ins and backpressure changes are shown to retrace the early time rate data as would be expected from superposition principles. Reservoir variables developed from a total field rate-time match are compared to early well pressure buildup analysis results. Comparisons are excellent.

This work not only demonstrates the technique of analyzing rate-time data, it also presents a method whereby a reservoir or formation dimensionless type curve can be developed from rate-time field data. The resulting type curve can then be used to forecast wells or fields in the same reservoir or formation. Because such a type curve is dimensionless, changes in stimulation, spacing, and reservoir properties can also be accounted for.

Introduction

Since Fetkovich's[1] original presentation in 1973, many successful applications have been made with declining rate-time data using the type-curve approach. Case-history studies of individual oil and gas wells, groups of wells in a field, and total fields are presented in this follow-up paper. Additional papers[2-7] dealing with the constant-wellbore-pressure solution (which also include the depletion period) have since been published to aid analysis and understanding of what is now called "advanced decline curve analysis."

In essence, decline-curve analysis is a forecasting technique: rate-time data are history-matched on an appropriate type curve, and then a forecast is made. Complex simulation studies proceed similarly. By using basic reservoir engineering concepts and knowledge, we know what direction to take, what type curve(s) to choose, and where the rate-time data should fit.

Decline-curve analysis must work because it is founded on basic fluid-flow principles -- the same principles used in pressure-transient analysis. The problem most engineers have had and will continue to have with decline-curve analysis is bad, erratic, or insufficient data. Careful attention to obtaining accurate flow rates, flowing pressures, and downtime should help solve the problem. A good rate-time analysis not only will give the same results as conventional pressure-transient analysis, but also will allow a forecast to be made directly at no cost in lost production. For low-permeability stimulated wells, in particular, pressure-buildup testing could be eliminated in many cases as being of little value or economically unjustifiable because of the resulting production loss when compared with what can be obtained from properly conducted constant wellbore-pressure drawdown tests.

Rate-Time Type Curve Analysis Concepts

The Radial Flow Solution

The fundamental basis of advanced decline-curve analysis is an understanding of the constant-wellbore-pressure solutions and their corresponding log-log type-curve plots, which are the inverse of the constant rate solution. Figure 1 is a composite of the analytic constant-wellbore-pressure solution and the Arps[8] exponential, hyperbolic, and harmonic decline-curve solutions on a single dimensionless type curve. The depletion stem values of b range between 0 (exponential) and 1 (harmonic) which are the normally accepted limits. The exponential-depletion stem (b = 0) is common to the analytic solution and to the Arps equation.

Decline-curve dimensionless rate and dimensionless time in terms of reservoir variables are defined for the type curve as

$$q_{dD} = q_D \left[\ln\left(\frac{r_e}{r_w}\right) - \frac{1}{2} \right] \qquad ..(1)$$

or

$$q_{dD} = \frac{\dfrac{q(t)}{kh\,(p_i - p_{wf})}}{141.2\,\mu\beta \left[\ln\left(\frac{r_e}{r_w}\right) - \frac{1}{2} \right]} \qquad ..(2)$$

and

$$t_{dD} = \frac{0.00634kt}{\phi(\mu\, c_t)_i r_w^2} \cdot \frac{1}{\frac{1}{2}\left[\left(\frac{r_e}{r_w}\right)^2 - 1\right]\left[\ln\left(\frac{r_e}{r_w}\right) - \frac{1}{2}\right]} \qquad ..(3)$$

or

$$t_{dD} = \frac{t_D}{\frac{1}{2}\left[\left(\frac{r_e}{r_w}\right)^2 - 1\right]\left[\ln\left(\frac{r_e}{r_w}\right) - \frac{1}{2}\right]} . \qquad ..(4)$$

Published values of q_D and t_D for the infinite and finite constant-pressure solutions for single-phase radial flow were transformed into a defined decline curve dimensionless rate and time, q_{dD} and t_{dD}, by Equations 1 and 4. The values in Figure 2 were used to generate Figure 3, which is a plot of the decline-curve dimensionless rate and time, q_{dD} and t_{dD}, for various values of r_e/r_w down to 10.

The constant 1/2 was used in the final equations with p_i (after 1/2, 5/8, and 3/4 were tried), because a better correlation was obtained, particularly at small r_e/r_w stems; the constant-pressure-outer-boundary case during the transient period also overlies the closed-outer-boundary-case type curve.

The plotted type curves (Figures 1 and 3) generated from the <u>exact</u> q_D - t_D constant-wellbore-pressure solution are also exact by definition, although they were generated with the 1/2 value. The curves cannot be used by simply changing 1/2 to 3/4. One can only back-calculate the correct q_D - t_D from these curves with the value of 1/2. The r_e/r_w stems were discontinued at a value of 10 because the correlation begins to break down as linear instead of radial flow develops - i.e., as r_e approaches r_w.

In Figure 1, note that a t_{dD} between 0.2 and 0.3 separates the transient period from the depletion period. Fitting rate-time data to the Arps equation is valid only once depletion sets in and the transient period is over. If flowing pressures are available and are not reasonably constant but smooth and monotonically decreasing, the pressure-normalized rate, log $q/\Delta p$ vs. log t, should be used for analysis.

Rapidly declining rate data fitting the early transient r_e/r_w stems are characteristic of low-permeability stimulated wells and often result in a unique fit. Stimulation causes the rate data to appear on a small r_e/r_w stem, and the low permeability then allows them to remain on the stem for real-time periods. Data for high-permeability stimulated wells leave the transient stems and go to pseudosteady state almost immediately. Conversely, a well with a large positive skin producing at a truly constant wellbore pressure will yield very flat rate declines, indistinguishable from b = 0 to ∞, and will also look like a constant-rate situation. Just as we make a log Δp-log Δt type-curve plot to find the semilog straight line in pressure-build-up analysis, in decline-curve analysis we must make a log q - log Δt type-curve plot of rate-time data to see whether the data are transient.

With regard to the r_e/r_w transient stems, we will repeat a statement from the original paper[1]: "Note from the composite curve [Figure 1] that rate data existing only in the transient period of the constant terminal pressure solution, if analyzed by the empirical Arps approach, would require values of b much greater than 1 to fit the data." The principal objective of that paper was the development of Figure 1, which provided a method of analysis for

transient data. Transient data should not be interpreted by the Arps equation.

Figure 4 illustrates the effect of transposing the r_e/r_w stem of 10, indicative of a low-permeability stimulated well response, and the r_e/r_w stem of 10,000, indicative of a large positive skin or damaged well, to the depletion state where the Arps equation is applicable. An equivalent Arps b = 10 approximates the r_e/r_w stem of 10,000; a b = 3 approximates the r_e/r_w stem of 10. They appear equivalent and on log-log type-curve matching would be indistinguishable if the Arps exponent b were left unbounded. The same data, if fit on the transient portion to the left of t_{dD} = 0.2 and then extrapolated, must ultimately go down a depletion stem. The same data fit to an Arps equation with b > 1 will extrapolate to infinity with no rational basis of terminating the forecast. The exponent b must be bound between 0 and 1.

If we rearrange Equation 2, we can evaluate the productivity factor from the q_{dD} - q(t) match point:

$$\frac{kh}{\left[\ln\left(\frac{r_e}{r_{wa}}\right) - \frac{1}{2}\right]} = \left[\frac{141.2\ \mu\beta}{(p_i - p_{wf})}\right]\left[\frac{q(t)}{q_{dD}}\right], \qquad ..(\ 5)$$

where r_{wa} is the effective wellbore radius determined from the skin effect, $r_{wa} = r_w e^{-s}$. The skin term can also include the effect of shape factor C_A (see Reference 9).

Assuming that $(r_e/r_w)^2$ is large compared to 1 in the term $[(r_e/r_w)^2 - 1]$, reintroducing thickness, h, in the t_{dD} equation, Equation 3, thus $(kh/\phi h)$, and substituting Equation 5 into Equation 3, we can obtain the following equation in terms of the match point q_{dD} - q(t) and t_{dD} - t:

$$V_p = \pi\ r_e^2 h\ \phi = \left[\frac{\overline{\mu\beta}}{(\mu\ c_t)_i\ (p_i - p_{wf})}\right]\left(\frac{t}{t_{dD}}\right)\left[\frac{q_{(t)}}{q_{dD}}\right]. \qquad ..(\ 6)$$

This equation gives the PV at the start of the decline analysis.

It must be pointed out that Equation 6 is only valid for closed-outerboundary situations when the onset of depletion is indicated by the data showing evidence of starting down one of the depletion stems. In the case of water-drive reservoirs, there might be a sufficient delay in aquifer movement to detect depletion, which could then be evaluated. Transient data alone with no indication of depletion is not unique on the q_{dD} - t_{dD} type curve of Figure 1 or 3. Data only in the transient stage could fit on every stem. This is more easily seen if transient data were fit only on the q_D - t_D type curve (Figure 2) to the left of r_e/r_w = 10. Clearly, this portion of the curve is common to all r_e/r_w depletion stems from 10 to infinity.

Single-Vertical-Fracture Solution

The 1975 Locke and Sawyer constant-wellbore-pressure, infinite-conductivity, vertical-fracture solution type curve (Figure 5) begins, with regard to depletion stems, where the radial-flow solutions illustrated in Figures 1 through 3 leave off. In terms of effective wellbore radius ($r_{wa} = L_{xf}/2$), r_e/r_{wa} of 10 approximately equals $L_{xe}/L_{xf} = 5$, where the single-vertical-fracture solution more closely represents the physical situation.

With improved stimulation techniques, hydraulic fracture lengths, L_{xf}, can and do start approaching L_{xe} for 5- and 10-acre [2- and 4-ha] spacings, i.e., $L_{xe}/L_{xf} \rightarrow 1$. The r_e/r_w stems could easily be extended to include values less than 10 with little loss in the type-curve evaluation accuracy; see Reference 10 for q_D -t_D values of r_e/r_w less than 10.

In our experience, the basic type curves of Figures 1 through 3 and 5 have solved most of our decline-curve analysis problems.

With regard to the early transient period, the dashed line of Figure 6 illustrates the infinite-conductivity, vertical-fracture solution expressed in terms of $r_{wa} = L_{xf}/2$ -- i.e., t_{xfD} converted to t_{rwaD} by the following equation:

$$t_{rwaD} = 4t_{xfD} \cdot \qquad ..(7)$$

Rate-time data for a stimulated well can be matched and forecast on either the infinite-conductivity, vertical-fracture solution or the plane-radial-flow solution with r_{wa} or effective wellbore radius for skin, with little practical difference in the resulting forecast. A rapid decline in rate with time usually identifies a stimulated low-permeability well. Data fit on a single-vertical-fracture solution do not identify fracture volume depletion or a naturally fractured reservoir. Whether or not an induced stimulation fracture is propagated down a natural fracture is irrelevant in identifying a naturally fractured system.

The question of whether naturally fractured reservoirs can initially have negative values of skin without stimulation needs to be addressed because the rapid decay in rate resulting from a negative skin effect can be and has been misinterpreted as identifying a naturally fractured reservoir. We will discuss this again later with examples. If we examine Figure 7a, representing an intensely naturally fractured reservoir (similar to the Warren and Root[12] model), we see from the definition of skin that for a well drilled in a naturally fractured reservoir to have a negative skin, it must penetrate a region near the wellbore that has a permeability greater than that in the interwell region. The likelihood is remote that we could be so fortunate every time we drill a well in a naturally fractured hydrocarbon reservoir. Cutting a single vertical natural fracture with a vertical or subvertical well is equally remote. Wells drilled in a naturally fractured reservoir will initially have large positive skins because of heavy mud losses around the wellbore into the natural fractures. In an intensely naturally fractured limestone reservoir, an acid treatment generally removes the mud damage and results in good negative skins. Pressure-transient data obtained after such a stimulation fit the van Everdingen and Meyer[11] matrix-acid solution (a situation where the permeability near the wellbore is truly altered) as

opposed to the single-vertical-fracture solution based on the model shown in Figure 7b. In the case of the Greater Ekofisk development, the type-curve characteristics are noticeably different after stimulation. Data fit to the single-vertical-fracture solution usually result in a low fracture intensity index (FI), whereas data fit to the matrix-acid solution result in a high FI. The fracture volume associated with Figure 7a will be connected to the wellbore; in contrast, any fracture volume associated with Figure 7b may not be connected. In our experience, wells have never obtained a negative skin in a naturally fractured reservoir except after a stimulation treatment.

Naturally Fractured Reservoir (Warren and Root Model) Type Curves

Dual-porosity or naturally-fractured-reservoir type curves developed by Da Pratt et al.[6] were a significant and timely contribution to decline-curve analysis concepts. The unsupported statement "fracture depletion" with rapidly declining rate-time data is widely used. Careless use of the word "fractured" when dealing with hydraulically fractured wells and the corresponding rapid decline in rate associated with these successful fracture jobs have helped perpetuate the fracture-volume-depletion myth.

On the basis of the Da Pratt et al. naturally fractured (Warren and Root model), dual-porosity, constant-wellbore-pressure type curves, the only identifying characteristic is the double-exponential decline: depletion of the fracture volume followed by depletion of the matrix volume. Segments A to B in Figure 8 represent fracture depletion, and Segments B to C represent matrix depletion. This behavior is not equivalent to the two parallel straight lines from the constant-rate solution of Warren and Root[12] because theirs was an infinite-reservoir solution. Two semilog force-fits (double exponential) of early-time data can be and have been manufactured by unsuspecting engineers trying to smooth the rate-time data. There is no indication from the dual-porosity type curves of a $b > 1$ anywhere, except again in the transient portion, which is identical in character to the homogeneous-reservoir solution. The transient portion can yield only apparent values of $b > 1$. Also, the matrix-depletion stem can be so flat as to be easily misinterpreted as having a b much greater than 1 (see the misplaced r_e/r_w stem of 10,000 in Figure 4). Gas saturations within the matrix block for solution-gas-drive systems along with end effects (little or no oil flow from the matrix blocks) would appear as large positive skins with respect to oil flow, further creating long, flat, transient r_e/r_w stems. Stimulation or removal of matrix skins is not possible.

Log-Log Decline Curve Plot

If we closely examine Equations 2 and 3 expressing q_{dD} - t_{dD} and consider the nature of the log q_{dD} - log t_{dD} plot, we should recognize that real rate-time data, in any convenient units, when plotted as log q - log t can look exactly like one of the q_{dD} - t_{dD} type-curve plots previously discussed. The data in rate and time will be shifted from the unit solution only by the coefficient of q and t in q_{dD} and t_{dD}, respectively. Some basic reservoir knowledge usually suggests with which type curve, and where on the curve, we should expect to obtain a match. By overlaying rate-time data on Figure 1 or 3, for example, we can obtain a match of q_{dD}, t_{dD}, r_e/r_{wa}, and b and evaluate reservoir variables kh, r_e/r_{wa}, s, r_e, or PV. In a given field, all wells should normally be expected to match the same depletion type curve, although

skins could be different; the axis will be shifted in time and rate for each well only by the coefficient of q_{dD} and t_{dD}. For q_{dD} the coefficient is

$$\frac{141.2\ \mu\beta\left[\ln\left(\frac{r_e}{r_{wa}}\right) - \frac{1}{2}\right]}{kh\ (p_i - p_{wf})},$$

and for t_{dD}, the coefficient is

$$\left[\frac{0.00634k}{\phi(\mu\ c_t)_i r_{wa}^2}\right] \left\{\frac{1}{\frac{1}{2}\left[\left(\frac{r_e}{r_{wa}}\right)^2 - 1\right]\left[\ln\left(\frac{r_e}{r_{wa}}\right) - \frac{1}{2}\right]}\right\}.$$

The overlaying technique is a fundamental concept that leads to the idea of developing a field type curve from rate-time data alone. The type curve so developed may or may not appear anything like an existing solution. Figure 9 is the log q - log t plots of Wells A through D in the same field; the match results are given in Table 3 of Reference 1. First, note that the data from the four wells overlie each other and have developed a single log-log type curve at least to the range of existing data. Essentially, the shift in the rate axis reflects a different kh, while the shift in the time axis reflects a different k and r_{wa}. We could match and have matched this curve to a known analytic solution (Figure 3). By knowing or estimating reservoir variables from some source, such as a complete buildup analysis or early-time rate-time decline analysis on at least one of the wells, we can back-calculate values of q_{dD} and t_{dD}. Slight differences in r_e/r_{wa} stems appear to be reflected in the early transient period. The significance of the collapsed q_{dD} -t_{dD} plot (Figure 3) is illustrated by this example.

The next logical step in the use of type curve and log-log plot concepts is the development of the total field type curve. Total field production can be considered as an "average well" times the number of wells. Wells overlie wells within a field with the same drive mechanism, so why shouldn't field rate-time production data from the same formation with similar drive mechanisms overlie other fields in the same formation? The reservoir and fluid variables [k, h, r_e (spacing), r_{wa}, μ_o, β_o, p_i, p_{wf}, ϕ, s_w, and c_t] can be different for all fields. This concept will be demonstrated with the development of the Monterey type curve from historical production data from several Monterey fields in California.

Arps Limits of b

The Arps stems in Figure 1, b = 0 to 1, combined with the analytic transient stems, deserve some discussion. First, the data used by Arps to develop and test his original equations were from real fields and wells. They indicate that real-world data most often do not follow the single-phase analytic solution for depletion, the b = 0 solution. The limits to b that he found using Cutler's data were between 0 and 0.7, with over 90% of the cases having

values less than 0.5: no case was found with a b in excess of 0.7. Arps' own experience, however, indicated that b = 1 did occur, but only rarely.

If we consider the initial declining-rate period as nothing more than an extended drawdown test, then matching of the early-time data on the rate-time type curve for reservoir parameter evaluation yields initial permeability, k_i, and $(\mu c_t)_i$ at t = 0, the start of the decline analysis. A value of b > 0 reflects changing values of $(k_{ro}/\mu_o\beta_o)_p$ and $(\mu)_p$ $(c_t)_p$ during reservoir depletion. For a given drive mechanism, k_i, $(\mu c_t)_i$, and b should be sufficient to describe a type curve for a given field or formation. Theoretically, an oil pseudopressure, p_{ps}, and a pseudodimensionless time, t_{pdD}, could be developed from a history-matched k_{ro} - k_{rg} relationship to drive the rate-time data to the analytic solution b = 0; however, this is too complex a procedure and will find little practical use. Nevertheless, the pursuit may be worthwhile, perhaps leading to a better understanding of what causes the different values of b.

Carter's[5] study of the effect of pressure level and drawdown on gas well rate-time behavior provides some insight into what causes b values to be greater than 0. Examination of his Figure 1 shows that the early transient period is unaffected by a variation in $(\mu c_t)_p$, while the depletion stems increase from b = 0 for a λ = 1 to b = 0.3 for λ = 0.75, and b $\cong$ 0.5 for λ = 0.55. Carter's λ is defined as

$$\lambda = \frac{\mu(p_i)c_g\ (p_i)}{\overline{\mu c_g}} \qquad ..(\ 8)$$

or

$$\lambda = \left[\frac{\mu\ (p_i)c_g(p_i)}{2}\right] x \left[\frac{p_{pi} - p_{pwf}}{\left(\frac{p}{z}\right)_i - \left(\frac{p}{z}\right)_{wf}}\right]$$

One could interpolate between his λ values by interpolating between approximate b values.

A b > 0 for solution-gas-drive reservoirs should reflect an increasing total compressibility with increasing gas saturation. Later development of other supplemental drives -- such as gravity segregation, limited water movement, late-time crossflow from nonwellbore productive layers, and hydrocarbon influx from the periphery of the reservoir -- would tend to increase the value of b.

Decline-Curve Analysis Using Type Curves - Individual Well Cases

Well M-4X

Well M-4X was the fourth of five appraisal wells drilled on a carbonate Middle Cretaceous Mishrif structure in the Middle East. In January 1974, data for production rate vs. time, obtained on a long-duration production test after two separate acid treatments totaling 14,000 gal [53 m^3] 20% HCl, indicated a

severe decline in production rate. The initial rate declined steadily from 2,361 BOPD to 1,045 BOPD [375 to 166 m^3/d oil] after only 160 hours (6.7 days) of testing (see Figure 10). This high initial decline rate was generally interpreted to be depletion. More specifically, it was interpreted as fracture and vug porosity depletion because some vugs and fractures were identified in the initial core description.

First and foremost about the test is that it was recognized as a true constant-wellbore-pressure test where the rate must necessarily decline with time. The constant wellhead flowing pressure observed during the test of 53 to 55 psi [365.4 to 379.2 kPa], coupled with the fact that the reservoir fluid was highly undersaturated and should then have an essentially constant oil head, resulted in a constant bottomhole flowing pressure (BHFP) during the entire test. A constant-wellbore-flowing-pressure analysis was made by type-curve matching the rate-time data on Figure 2. The match shown in Figure 10 was unique and conclusively established that the rate-time decline was a transient phenomenon and not depletion; i.e., the rate-time data fit the transient portion of the analytic type curve. Depletion would be identified by the rate-time data overlying an r_e/r_w exponential-depletion stem (analogous to the reservoir limit test).

Because the identifying mark of dual-porosity depletion is an exponential-depletion stem (depletion of the fracture/vugs) followed later by another exponential-depletion stem (depletion of the matrix), we clearly cannot attribute the well's rapid decline in rate to the reservoir's being naturally fractured or vuggy. The rapid transient decline rate seen on the well is the expected behavior of a successfully stimulated well of moderate to low permeability. One should look at the ratio k/μ to see what is moderate or low permeability. For this well,

$$\frac{k_o}{\mu_o} = \frac{51 \text{ md}}{2.3 \text{ cp}} \cong 25 \text{ md/cp } [\sim 25{,}000 \text{ md/Pa·s}].$$

For a gas reservoir of 0.02 cp [0.02 mPa·s], the same ratio of 25 would yield a permeability of 0.5 md. Both would exhibit similar transient behavior.

Using the rate-time data from the 7-day production test, we forecast the well's future production rate as a function of time by drawing a line through the rate-time data overlaid on the uniquely matched portion of the type curve and down a premised r_e/r_{wa} stem for an assumed spacing, r_e. At an appropriate rate, the BHFP was lowered to 500 psia [3447.4 kPa] by use of the superposition method given in Reference 1.

Well Edda 10X

Well Edda 10X rate-time data taken in November 1973 were obtained on the second appraisal well drilled in the Upper Cretaceous chalk reservoir of the Edda field, one of several fields located in the Greater Ekofisk development of the Norwegian North Sea. A drillstem test taken in November 1973 after an acid fracture treatment, without the use of proppants, indicated a very severe decline in production rate during the drawdown test. The rate declined from 9,500 BOPD [1510 m^3/d oil] at 1 hour to 4,600 BOPD [731 m^3/d] after only 10 hours. The flowing tubing pressure varied from 896 psia [6177.9 kPa] at the

beginning of the test to 751 psia [5178.1 kPa] at the end, essentially a constant-wellbore-pressure condition. Again, as in the Well M-4X test, the rate decline was incorrectly assumed to be either natural fracture volume depletion, because the Greater Ekofisk development reservoirs are known to be naturally fractured, or closure of the induced fracture as a result of pressure drawdown -- both exotic and simplistic explanations.

Figure 11 illustrates the type-curve match on the plane-radial-flow, constant-wellbore-pressure solution with another unique match on the transient or infinite-acting period. No exponential depletion, fracture volume depletion, or any other type of depletion is indicated. It is not possible to determine whether the reservoir is naturally fractured from the rate-time decline. Again, the rapid decline in rate is the expected behavior of a successfully stimulated low-permeability well.

An Arps depletion stem match of the data gives an apparent b = 2.5, which, of course, is invalid.

An evaluation of the q_D - t_D match and the results obtained from the pressure-buildup analysis are summarized in Table 1. The values of permeability and skin obtained from the rate-time drawdown analyses and the Horner buildup are essentially the same. To determine whether the reservoir was naturally fractured, a fracture index, I_f, was calculated from a permeability value obtained from a matrix-plug permeability-porosity plot compared with a buildup or drawdown calculated permeability:

$$I_f = \frac{k_{BU} \text{ or } k_{DD}}{k\ (\phi - k)} = \frac{0.9 \text{ md}}{0.66 \text{ md}} = 1.4 \ . \qquad ..(\ 9)$$

For this well, there appears to be little natural fracturing at this location because the index is 1.4. This is not the case, however, for most of the development wells drilled later in this field. We will demonstrate this in a full-field rate-time analysis of the total field production.

Figure 12 illustrates a one-well forecast that was made before any development drilling by extrapolating down an r_e/r_w stem for the premised well spacing. Future rates were read from the real-time scale on which the rate data were plotted. Also shown in Figure 12 is an extrapolation of the same data fit on an Arps b = 2.5, which is clearly incorrect. Although one would not attempt an Arps equation fit and extrapolation on only 10 hours of production data, it serves as the only example in which, using transient data, false values of b > 1 would severely underestimate production.

To summarize, this example illustrated the ability to develop a sound technical decline-curve analysis prediction with basic reservoir engineering principles with only 10 hours of rate-time data.

MHF Well A

Agarwal et al.[13] presented 300 days of rate-time data for a massive hydraulically fractured (MHF) well. Figure 13 illustrates a type-curve match of their data on the radial-flow, constant-wellbore-pressure solution and the infinite-conductivity, single-vertical-fracture, constant-wellbore-pressure

solution. Clearly, all the data lie on the transient or infinite-acting period, and there is no evidence of depletion. An evaluation of the match points on the basic radial-flow, constant-wellbore-pressure solution yields k = 0.0081 md. This value is identical to the Agarwal et al. prefracture test result and is the same value obtained from matching on the vertical-fracture constant-wellbore-pressure solution. Calculated values of skin or L_{xf} are reasonably close. Table 2 lists the Agarwal et al. forecast results obtained when their type-curve analysis and reservoir and fluid properties were entered into their MHF simulator. Listed on the far left is the forecast read directly from the match on the basic radial-flow, constant-wellbore-pressure solution. The middle column is the forecast read directly from the match on the infinite-conductivity, vertical-fracture, constant-wellbore-pressure solution. Note the good agreement between the graphical extrapolation using the radial-flow, constant-wellbore-pressure solution and their simulator results. Our extended forecasts from the type-curve matches are, for practical purposes, the same.

Fitting the transient data to the Arps equation resulted in an apparent value of b = 2.2; in this case, for the 20-year forecast period, it would not have resulted in as severely different a forecast as in the previous Well Edda 10X example.

This example further serves as a classic graphical illustration of a case for infill drilling -- closer spacing than an r_e = 2,000 ft [610 m] -- to increase recoverable reserves in a reasonable time period. This example also illustrates that conventional deliverability forecasting of rate-time decline would be grossly in error, even if we correctly estimated a stabilized backpressure curve position from reservoir variables. On the curve of Figure 14, note the point at which the rate departs from the transient stem and starts down the depletion stem. This point represents the stabilized backpressure curve position. The rate at the given Δp^2 would establish a point on the stabilized backpressure curve.

All early transient production higher than this stabilized rate would be completely ignored in a conventional deliverability rate-time forecast. Further complicating a conventional deliverability approach is the inability to get valid reservoir pressures from reasonable-duration pressure-buildup tests in such a low-permeability well to determine original gas in place from a p/z-vs.-G_p graph. Additional discussion of this point occurs later in the San Juan example.

To illustrate more clearly the shifting of the backpressure curve with time to the stabilized curve position, Cullender's[14] Gas Well No. 3 backpressure curve coefficients -- C values for a 214-hour flow and C values from a four-point isochronal test and 72-hour deliverability tests covering a period of 9 years -- were plotted and matched on the infinite-conductivity, vertical-fracture, constant-wellbore-pressure solution (Figure 15). Figure 16 shows these same data plotted as a series of backpressure curves shifting with time. (See Table 3 of Reference 14 for the complete set of the data.) This well was initially acid-fractured. Note the near-perfect fit of all the data on the infinite-conductivity, vertical-fracture, constant-wellbore-pressure solution with no indication of wellbore performance deterioration. Even after 9 years of production and a 106-psi [730.9-kPa] reservoir shut-in pressure decline, the 72-hour values of C fall on the original curve trace.

West Virginia Gas Well A

Well A is a low-permeability gas well located in West Virginia. It produces from the Onondaga chert that has been hydraulically fractured with 50,000 gal [189 m^3] of 3% gelled acid and 30,000 lbm [13 608 kg] of sand. After initial completion, the well was placed on production for 200 days and then shut in for a 106-day pressure buildup in an attempt to obtain reservoir pressure. A conventional Horner analysis of the buildup data gave p_R = 3,268 psia [22 532 kPa], k = 0.082 md, and s = -5.4. A type-curve analysis of the same data indicated that the correct semilog straight line started at about 600 hours (25 days).

Figure 17 is a log-log plot of monthly production data. These are raw monthly production data obtained directly from production files, not data from special tests. The 8 years of rate-time data were matched on the radial-flow constant-wellbore-pressure solution (dashed line), the r_e/r_{wa} exponential stem of 20, and b = 0 to yield k = 0.0651 md, s = -5.38, and r_e = 1,547 ft [472 m]. The solid line through the same data shows a fit on the b = 0.5 and Carter's λ = 0.55 constant-wellbore-pressure solution on the r_e/r_{wa} stem of 20. Results from the match on a b = 0.5 resulted in a k = 0.0700 md, s = -5.17, and r_e = 1,242 ft [379 m]. These results compare closely with those obtained from the match on Carter's type curve, which gave k = 0.0678 md, s = -5.17, and r_e = 1,252 ft [382 m]. Carter's λ was calculated to be 0.555 for this example. For the pressure ratio p_{wf}/p_R = 500 psi/3,268 psi = 0.15 [3447 kPa/22 532 kPa], Figures 8 and 9 of Reference 1 also indicate that the expected depletion stem should have a b = 0.5 for this gas well.

Occasional shut-ins and blows to the atmosphere for dewatering the wellbore did occur during the normal production of the well. One would expect a b = 0.5 situation gradually to approach a b = 0 performance because liquid loading occurs when the flow rate declines and the wellbore deteriorates with time.

Evaluating the Match

The previous discussion of the match to the r_e/r_{wa} stem of 20 leaves some doubt as to whether the match to the 20 stem is unique or the best answer. We will investigate the sensitivity of results to stems of 10, 20, and 50 for the b = 0 and b = 0.5 match. To illustrate the complete evaluation of the matching technique, we will use the b = 0.5 match (Figure 17) to the composite type curve as an example. Table 3 lists all the pertinent reservoir variables for the well. For the match point of b = 0.5, q_{dD} = 0.58, q(t) = 1,000 Mscf/D [28 x 10^3 std m^3/d], t_{dD} = 0.126, and t = 100 days.

When Equation 5 is expressed in terms of gas units and pseudopressure, p_p, the productivity factor is

$$\frac{kh}{\left[\ln\left(\frac{r_e}{r_{wa}}\right) - \frac{1}{2}\right]} = \frac{q(t)\ p_{sc}\ T}{19.87 \times 10^{-6}\ q_{dD}\ T_{sc}\ (p_{pi} - p_{pwf})} \qquad ..(10)$$

$$= \frac{1{,}000\ (14.7)(620)}{(19.87 \times 10^{-6})(0.58)(520)(7{,}948 \times 10^5 - 208 \times 10^5)}$$

$$= \quad 1.965 \text{ md-ft } [0.599 \text{ md·m}]$$

Also expressing Equation 6 in terms of gas units and pseudopressure, p_p, we have

$$V_p = \pi\ r_e^2 h\ \phi\ = \left[\frac{2{,}000\ P_{sc}\ T}{(\mu\ c_t)_i\ T_{sc}\ (p_{pi} - p_{pwf})}\right]\left(\frac{t}{t_{dD}}\right)\ \left[\frac{q_{(t)}}{q_{dD}}\right] \qquad ..(11)$$

$$= \left[\frac{2{,}000\ (14.7)\ (620)}{0.0172\ (177 \times 10^{-6})\ (520)\ (7{,}948 \times 10^5 - 208 \times 10^5)}\right] \cdot \left(\frac{100}{0.126}\right)\left(\frac{1{,}000}{0.58}\right)$$

$$= 20.36 \times 10^6 \text{ ft}^3\ [0.5765 \times 10^6 \text{ m}^3]\ ,$$

and

$$r_e = \sqrt{\frac{V_p}{\pi\ h\ \phi}} = \sqrt{\frac{20.36 \times 10^6}{3.1416\ (70)\ (0.06)}} = 1{,}242 \text{ ft } [379 \text{ m}]\ . \qquad ..(12)$$

The gas in place, G, at p_i = 3,268 psia [22 533 kPa], with p_i being the pressure at the start of the decline analysis, is then

$$G = V_p\ (1 - S_w)\ \beta_g \qquad ..(13)$$

$$= 20.36 \times 10^6\ (1\text{-}0.35)(208.8)$$

$$= 2.763 \text{ Bscf } [78.2 \times 10^6 \text{ std m}^3]\ .$$

For comparison purposes, G at p_i = 3,268 psia [22 533 kPa] from the Carter type-curve match on λ = 0.55 is 2.807 Bscf [79.4 x 10^6 std m^3], while that obtained from the b = 0 match is 4.286 Bscf [121.3 x 10^6 std m^3].

Assuming little or no PV change resulting from rock and water expansion, at the original reservoir pressure of 4,175 psia [28 787 kPa], β_g = 253.9 scf/ft^3 [std m^3/m^3], an original gas in place, G_i, was then calculated to be 3.360 Bscf [95.1 x 10^6 std m^3]. The difference of 0.597 Bscf [17 x 10^6 m^3] compares well with the measured cumulative production of 0.580 Bscf [16 x 10^6 std m^3] between the two average reservoir pressure intervals.

With the productivity factor calculated as 1.965 md-ft [0.599 md·m] and r_e calculated as 1,242 ft [379 m], we can now investigate the sensitivity of k and s to r_e/r_{wa} stems (Table 4). Regardless of the r_e/r_{wa} stem chosen, once

the depletion stem is established by the rate-time data (the match points from the composite type curve Figure 1), q_{dD} - q(t) and t_{dD} - t are fixed and the PV is then fixed. The calculated initial permeability and skin are insensitive to the r_e/r_{wa} stem selection. In this case, we have the 106-day pressure-buildup analysis run just before the start of the decline-curve analysis with which to compare. From the Horner results, the correct r_e/r_{wa} stem appears to be ~ 20. If at early time we had taken more frequent, precise rates and flowing pressures, then we could have uniquely fit the stem. At the very least, kh and s could have been calculated from a short-duration constant wellbore pressure test, as opposed to calculating kh and s from a long-duration buildup test. This was done for West Virginia Gas Well B.[15,16] Figure 18 compares the pressure-normalized, constant-wellbore-pressure analysis (the rate data alone had no character) and the corresponding Horner analysis results for this well. Therefore, one need not have shut in Gas Well A for 106 days to obtain kh and s for selecting the proper r_e/r_{wa} stem.

Table 5 summarizes the pertinent results of matching the rate-time data on b = 0, b = 0.5, and Carter's λ = 0.55. By comparing the difference of 0.91 Bscf [25.8 x 10^6 std m^3] between a calculated G_i = 5.20 Bscf [147.2 x 10^6 std m^3] at 4,175 psia [28 787 kPa] and the G = 4.29 Bscf [121.5 x 10^6 std m^3] at 3,268 psia [22 533 kPa] with the real cumulative production of 0.58 Bscf [16.4 x 10^6 std m^3] between the two shut-in pressures, the b = 0 as a match is ruled out and the b = 0.5 must be selected.

San Juan Example

Early in 1982, a reservoir study of all wells completed in the Blanco Mesaverde pool in one entire township in Rio Arriba County, NM (San Juan basin), was initiated to quantify the reserve increase resulting from the infill drilling program begun in 1975. The initial spacing of 320 acres [130 ha], was halved through infill drilling.

The San Juan basin is located in northwestern New Mexico and extends into southwestern Colorado. The gas-producing formations in the basin are sandstones of Upper Cretaceous Age. The Mesaverde ranges in gross thickness from a few hundred to almost 1,800 ft [550 m]. Average porosity in the Mesaverde is about 10%, and the permeability ranges from 0.02 to 1.0 md. Initial pressure in the study area was about 1,200 psi [8274 kPa].

The area we investigated had 72 original wells, drilled two per section, plus 72 infill wells. Initial pressure for a majority of the infill wells was some 30 to 40% less than original reservoir pressure, indicating that drainage was occurring. A limited number of infill wells had initial pressures essentially equal to original pressure, indicating that drainage was not occurring at these locations.

The reserve determination method used in the past was the p/z plot. This method consisted of plotting annual 7-day shut-in pressures vs. cumulative gas produced. Although annual 7-day shut-ins were taken, the final shut-in pressure was well below the true static reservoir pressure. Because of the low-permeability stimulated character of the wells, the semilog straight line was seldom reached, making the determination of average reservoir pressure difficult. This essentially negated the p/z plot as a useful reservoir analysis tool until infill wells were drilled. Trend plotting of the short-

duration shut-in and its corresponding p/z was used without recognizing the need to pass through the initial p/z value (see Figure 19). The initial p/z value was ignored to prevent an apparent yearly increase in gas reserves.

A majority of the infill wells came in at pressures about 30 to 40% lower than the original reservoir pressure. In these cases, the infill original pressure could be used to provide a pressure point on the plot of p/z vs. cumulative gas produced of the original well. A reserve figure was determined for the original well by passing a line from the initial p/z through the infill-well p/z value with an abandonment pressure of 100 psi [690 kPa] assumed. This method could not be used, however, when the infill initial pressure essentially equaled the original reservoir pressure. In such cases, the most practical method available to determine the reserve was decline-curve analysis.

Figures 20 and 21 present the rate-time data and type-curve match of the original well, Well 58, and the offset infill well, Well 58A. The latter came in at near-original pressure. Data for both wells (as for all wells in the study area) were obtained from a commercially available data base. The character of the monthly rate-time data was erratic -- a problem not uncommon in rate-time analysis -- and average 6-month rates available from the data base were plotted at midpoint intervals as a form of data smoothing. The average 6-month data points appear as solid squares on the type-curve matches. Notice how the character of the production profile was enhanced by this smoothing technique.

A type-curve match of the rate-time data for Well 58 indicates the well to be on decline and going down a depletion stem. The calculated k and s are 0.36 md and -4.3, respectively, with a calculated drainage area of 225 acres [91 ha]. Although not apparent, a match on different r_e/r_{wa} stems would result in essentially the same calculated value of r_e. The drainage radius is fixed once depletion is evident. Table 6 illustrates this point for Well 58 matched on r_e/r_{wa} stems of 100 and 200. The rate-time data of Well 58A were matched to the Locke and Sawyer type curve and found to be entirely transient. The k and s were calculated to be 0.07 md and -6.4, respectively.

These results are consistent in that one would expect the infill well permeability to be less than the original well permeability, when the infill location had not been drained. The more negative skin factor for the infill well represents the improvement in hydraulic fracturing technology and design, because the original well was stimulated in the late 1950's. A production forecast for the infill well was developed by forecasting down a depletion stem of $L_{xe}/L_{xf} = 3.2$. This stem corresponds to the skin of -6.4 and a drainage area of 95 acres [38 ha] to keep the total drainage area of 320 acres [130 ha] whole.

A reserve forecast for all wells on decline in the study area was made from a rate-time analysis. These calculated reserves are within 9% of the p/z reserve determined with the infill-well original pressure. The reserve study of the township indicated that infill drilling resulted in an average reserve increase of 11%.

Reserve increases resulting from infill drilling have been postulated as a result of the flattening observed in the p/z trend after infill drilling.

If total field production remains essentially constant (fixed market demand) before and after infill drilling, a reduction in some of the original wells' flow rates will occur after the start of infill drilling. This reduction in flow rate will cause a corresponding increase in flowing pressure. When the well is next shut in for an annual 7-day test, the final buildup pressure will automatically reflect a higher final shut-in pressure than when the well was produced at the previously higher rate. The obvious limiting case is when a well is cut back to zero flow rate, and only then will 7-day shut-ins reflect true reservoir pressure. The rate-reduction effect is demonstrated both by a two-dimensional (2D), single-well, transient gas model simulation and actual field data. Also, examination of pressure production data from low-permeability gas wells in fields not subject to infill drilling shows the same increased shut-in pressure trend as a result of reduction in takes resulting from the current oversupply of gas.

The single-well simulation is based on an area of 320 acres [130 ha], a permeability of 0.05 md, and a 500-ft [152-m] infinite-conductivity vertical fracture corresponding to a -6.5 skin. In the simulation, the well produced at a constant rate of 240 Mscf/D [6.80 x 10^3 std m^3/d] for 10 years and then at 160 Mscf/D [4.53 x 10^3 std m^3/d] for 10 years. Annual 7-day shut-ins were simulated, and Figure 22 presents the resulting plot of p/z vs. cumulative gas produced. Note the rise in 7-day p/z values when the rate reduction took effect. It is this rise which can be misinterpreted as a reserve increase. Figure 23 is an actual well example illustrating this same problem. In this instance, the flow rates of the original wells were reduced because of the production of infill wells. Notice the effect of the reduced flow rate on the p/z plot, which is identical to that shown by the 2D, single-well model study.

In low-permeability reservoirs, transient effects may last for several years. Coupled with this problem are the extreme shut-in times required to establish useable average reservoir pressure and the difficulty in determining the stabilized backpressure curve. Decline type-curve analysis provides a reserve estimate and a production forecast, which can be easily updated without knowledge of reservoir pressures or the stabilized curve.

Reported Cases of b > 1.

Gentry and McCray[17] made a study attempting to determine why some wells exhibit decline-curve values of b > 1. The reservoir model described in their study did not include the effects of transient flow behavior.

The rate-time data presented as Field Example No. 2 (Figure 24) was plotted as log q - log t and yielded an almost perfect type-curve match of all the data on the Locke and Sawyer infinite-conductivity, single-vertical-fracture, constant-wellbore-pressure solution (see Figure 25). Note that the first year of data is in the transient or infinite-acting period.

All the data were expected to match this type curve because the well was described as being completed in the Mississippi limestone and the producing formation was stated to be fractured, with a tight matrix. No evidence of a double-depletion exponential decline indicative of a naturally fractured reservoir appears in the log-log data plot. "Fractured" may have simply meant hydraulically fractured. In any case, a well completed in a limestone reservoir would probably have been stimulated. Because oil wells are

generally drilled on small spacing, and because improved stimulation techniques result in hydraulic fracture lengths beginning to approach spacing, $L_{xe}/L_{xf} \longrightarrow 1$. In the unique match of Figure 25, $L_{xe}/L_{xf} = 1.5$. Figure 26 shows a match of the 2- to 6-year data, but they are reinitialized in time after depletion has clearly set in, at about 2 years. The data fit a decline with b = 0 and can even be recognized as such on their original semilog plot. Figure 27 shows the same rate-time data and their use of the Arps equation in a different form, leading to implied values of b between 1 and ∞. Once again, an attempt to fit transient-dominated data to the Arps depletion equation leads to apparent values of b > 1.

One further example from the literature illustrates a fit of transient data to the Arps equation with a least-squares computer model to "precisely determine optimum values for the coefficients a, b, and q_o."[18] Figure 28 is a log q - log t plot and match of Well No. 2., Wattenberg field, an example from Reference 18. The match is again made on the infinite-conductivity, vertical-fracture, constant-wellbore-pressure solution type curve. The Wattenberg field produces from a tight gas sand and is developed on 160-acre [65-ha] spacing with hydraulic fracture lengths averaging at least 1,500 ft [457 m].[19] Good engineering judgement indicates that with an L_{xe} = 1,320 ft [402 m] and a fracture length of 1,500 ft [457 m], the data should decline down an $L_{xe}/L_{xf} \cong 1.0$ stem on the type-curve match, which it does after a nearly 5-year-long transient flow period. The "unique and unbiased"[18] statistical extrapolation of the Arps equation fit of the data with b = 2.29 yields a life of 1,042 years to an economic limit of 200 Mscf/month [5.66 x 10^3 std m^3/month], which is unreasonable. The extrapolation on the vertical-fracture-solution type curve on the basis of basic reservoir information with spacing and fracture lengths gives a rational answer.

According to Reference 18, this application of the regression approach by use of the Arps equation was used on some 200 tight-gas wells. A correlation of b with fracture fluid volume on about 50 Wattenberg wells indicated that in nearly all cases, b > 1 and was as high as 3.5 in one instance.

All cases we have seen where b > 1 have been shown to be transient rate-time decline of low-permeability stimulated wells. Statistical approaches to decline-curve analysis that permit b > 1, the recognized upper limit to the Arps equation, can lead to bad results and bad decisions. The normal range of apparent b, from force fits of transient data to the Arps equation, appears to be between 2.2 and 2.5. To identify transient data and their end, a log-log plot of rate-time data must be made.

Decline Curve Analysis Using Type Curves - Field Cases

Field E

One of our earliest field type-curve analysis cases was a one-well field. The depletion mechanism was virtually a full bottomwater drive or, more specifically, a constant-pressure-outerboundary case. To date, no analytic work concerning the expected value of b with water displacement processes has been done.

Field E is located in the Far East and produces from a carbonate Upper Miocene Kais reef. The reservoir is highly undersaturated with a producing gas/oil

ratio (GOR) of ~ 3 scf/bbl [~ 0.54 std m^3/m^3] and a gravity of 47° API [0.79 g/cm^3], and is more than likely to be naturally fractured - a typical situation for developing a strong waterdrive. Only the upper 50% of the producing interval was perforated to avoid early water coning. The well was initially completed with 4 shots/ft [13 shots/m] and acidized with 6,100 gal [23 m^3] 30% HCl staged with ball sealers. The initial reservoir pressure was 2,921 psia [20 140 kPa]. As with most of the reef reservoirs in the area, later shut-in pressures return to within 10 to 20 psi [68.9 to 137.9 kPa] of the original reservoir pressure after a 24-hour shut-in.

Figure 29 is a semilog plot illustrating the production performance of the field in terms of oil production, total fluid production, and WOR. Gas rates were so small that the GOR is not plotted. The initial oil rate decline basically coincides with increasing water production when, after 1 year, gas-lift facilities were installed for all fields in the area. Successful gas lifting in this field began in July 1979 and resulted in the first BHFP change and another decline period. Gas injection rates were increased twice more to lower the BHFP, resulting in yet two more decline periods.

Figure 30 is the same oil production rate data now placed on a log q_o - log t plot in preparation for type-curve analysis. Each of the three additional decline periods following increased gas injection rates were reinitialized in time and log q - log t plots made for each one. They all exactly overlie the initial decline established during the natural-flow period. This should be expected from superposition principles; i.e., every new transient introduced into the well or field must go back and retrace the original q_{dD} - t_{dD} curve (Figure 31). (Referring back to the Cullender Gas Well No. 3 data log q - log t plot in Figure 15, note that the ten 72-hour annual tests taken between 1945 and 1953 with up to 106 psi [730.9 kPa] of pressure depletion exactly overlie the original type-curve match.)

A match was made with the composite q_{dD} - t_{dD} type curve (Figure 1) on a value of b = 0.5. Evaluation of the match point yielded k = 152 md and s = -4.1. This compares well with the initial well test Horner analysis of k = 143 md and s = -3.9. Table 7 compares the results and lists the reservoir and fluid properties used for the well.

Figure 31 shows the log q - log t match on the q_{dD} - t_{dD} type curve. If we now transfer the q_{dD} - t_{dD} axes onto the tracing paper of the real-time plot, we have a Kais Reef full waterdrive type curve that could be used to predict future performance with backpressure changes for any set of reservoir (k, ϕ, h, p_i) and fluid (μ, β, c_t) parameters with any well spacing (r_e) and any skin effect (r_{wa}) of another Kais Reef reservoir having no performance data at all. This grid transfer is equivalent to back-calculating q_{dD} - t_{dD} values for each of the plotted rate-time data from the known reservoir variables listed in Table 7 and the results obtained from the pressure buildup analysis.

Edda Field

The Edda field is the smallest of four overpressured volatile oil reservoirs within the Greater Ekofisk development in the Norwegian Sector of the North Sea. Table 8 lists the basic reservoir and fluid properties. Production is from seven wells completed in the Upper Cretaceous chalk (Maastrichtian) or

Tor formation. Slight to moderate natural fracturing is indicated from the FI derived from the pressure-buildup analysis (see Table 9). Note that Well C-5 indicates no natural fracturing while Well C-2 has the highest I_f of 28. All wells were acid-fractured without proppants on completion. As indicated by the skin values listed in Table 9, all wells appear to have been successfully stimulated.

Figure 32 illustrates the production performance of the field with time in terms of monthly average oil and gas production and GOR. Note that the field came on fairly rapidly, resulting in a classic field decline curve. The surface flowing pressure after the first few months has been virtually constant throughout the field's production history. The slight dips in production are a result of field shut-ins. Note also the slight production peaks that follow, discussed in detail later. Of special note is the flattening of the GOR curve starting in about mid-1982.

Figure 33 is the total field oil production rate plotted in terms of measured daily production rate vs. time on a log q - log t basis. To the best of our knowledge, this is the first time that daily production for a field was measured and available for decline-curve analysis over a 4-year period. Transient spikes after shut-ins are clearly visible and significant on this plot and are used in the decline analysis. There were several field shut-downs followed by an initial transient spike (flush production), as expected for such a low-permeability field with successfully stimulated wells. Theoretically, each of the transient spikes (if reinitialized in time) should retrace the field's initial q_{dD} - t_{dD} transient decline. Figure 34 is a plot of two of the transient spikes obtained after extended shut-ins and indeed they both virtually overlie the original field transient decline. The rate and time scales shown in Figure 34 are for the initial production period only; the rate and time scales for periods A and B have been omitted for clarity of presentation. Note that the field transient appears to end after about 100 days of production. Permeability, skin, and reservoir volumes were calculated for the total field match and each of the two production transients on an average-well basis also -- i.e., q_T divided by the number of wells. Table 8 summarizes the match results for r_e/r_{wa} = 50 and b = 0.6. Reservoir pressures and gas saturations for total-compressibility calculations for the decline analysis of the transient spikes following shut-ins were estimated from a total field pressure, GOR, and a field-deliverability-matched compositional material-balance study that is normally updated yearly. Note from the table the slightly declining values of effective permeability to oil values as a result of increasing gas saturation in the reservoir. The calculated reservoir PV's from all three matches are about the same.

A comparison of the calculated PV from the initial match of the total field rate-time data of 202.8 x 10^6 res bbl [32.2 x 10^6 res m^3] with that obtained from the total field compositional material-balance performance-matched PV of 201.1 x 10^6 res bbl [32.0 x 10^6 res m^3] is excellent.

Material-balance matching of the reservoir consisted of two distinct periods of interest with respect to the decline-curve analysis. The period before the GOR flattened out when forecasted gave rate-time data that fit a b = 0.3. The period after the flattening, because of more efficient indicated recovery (less gas voidage), now results in a b = 0.6, the same value of b indicated from the decline-curve match. Al-Kasim,[20] using data we furnished and a one-

dimensional radial model matched to the most current field performance data, also found an early b = 0.3, but b = 0.7 most of the time. Clearly, no double-depletion stems indicative of dual-porosity, naturally fractured reservoir can be observed in the rate-time decline data.

Evaluating the Match

We will again illustrate the evaluation of the matching technique and investigate the sensitivity of results to r_e/r_{wa} stems of 20, 50, and 100 for b = 0.6, now for an oilfield case. For a match point of b = 0.6, q(t) = 10,000 STB/D [1590 stock-tank m^3/d] oil, q_{dD} = 0.295, t = 100 days, and t_{dD} = 0.29.

With Equation 5, the field productivity factor is

$$\frac{kh}{\left[\ln\left(\frac{r_e}{r_{wa}}\right) - \frac{1}{2}\right] F} = \left[\frac{141.2\ (\overline{\mu_o \beta_o})}{(p_i - p_{wf})}\right] \left[\frac{q(t)}{q_{dD}}\right] \qquad ..(5)$$

$$= \left[\frac{141.2\ (0.416)}{(6{,}300\text{-}1{,}500)}\right] \left(\frac{10{,}000}{0.295}\right)$$

$$= 414.82 \text{ md-ft } [126.43 \text{ md·m}].$$

Because there are seven wells, q(t) is divided by seven and the average well productivity factor is

$$\frac{kh}{\left[\ln\left(\frac{r_e}{r_{wa}}\right) - \frac{1}{2}\right] W} = 59.26 \text{ md-ft } [18.1 \text{ md·m}].$$

Equation 6 will yield the total field PV:

$$V_{pF} = \left[\frac{(\overline{\mu_o \beta_o})}{(\mu\ c_t)_i\ (p_i - p_{wf})}\right] \left(\frac{t}{t_{dD}}\right) \left[\frac{q(t)}{q_{dD}}\right] \qquad ..(6)$$

$$= \left[\frac{(0.416)}{(0.185 \times 27 \times 10^{-6})(6{,}300 - 1{,}500)}\right] \left(\frac{100}{0.29}\right) \left(\frac{10{,}000}{0.295}\right)$$

$$= 202.8 \times 10^6 \text{ res bbl } [3.22 \times 10^7 \text{ res } m^3].$$

$$r_{eF} = \sqrt{\frac{V_p \times 5.615}{\pi\, h\, \phi}}$$

$$= \sqrt{\frac{202.8 \times 10^6\ (5.615)}{\pi\ 100\ (0.236)}} = 3{,}919 \text{ ft } [1195 \text{ m}].$$

Then the oil in place, N_s, at the start of the decline analysis when p_i = 6,300 psia [43 439 kPa] and β_O = 1.92 is

$$N_s = \frac{V_{pF}\ (1 - S_w)}{\beta_O}$$

or

$$= \frac{202.8 \times 10^6 \text{ bbl } (1 - 0.365)}{1.92}$$

$$= 67.08 \text{ MMSTB } [10.7 \times 10^6 \text{ stock-tank m}^3].$$

Because 1.2×10^6 STB [0.191×10^6 stock-tank m^3] had been produced before the start of the decline analysis, the original oil in place, N_s, is indicated to be 68.3 MMSTB [10.9×10^6 stock-tank m^3]. The pressure and GOR history-matched compositional material-balance program obtained an N_{si} of 67.4 MMSTB [10.7×10^6 stock-tank m^3]. The comparison is good.

Using the decline-curve analysis, N_{si} = 68.3 MMSTB [10.9×10^6 stock-tank m^3], and the cumulative recovery of 16.6 MMSTB [2.64×10^6 stock-tank m^3] to January 1, 1984, results in a 24.3% recovery rate to date. From the decline-curve projection to an economic limit, the indicated ultimate recovery of 22.6 MMSTB [3.59×10^6 stock-tank m^3] will result in a 33.1% recovery.

Table 10 shows the effect of several r_e/r_{wa} stems on k and s for the total field match, and the results are also expressed as an average well -- i.e., total field rate divided by number of wells. With the productivity factor and r_e fixed, the effect of varying r_e/r_{wa} stems is illustrated for the total field and the average well. The arithmetic average skin s = -4.2, determined from individual well tests (Table 9), might be used to select an r_e/r_{wa} of 50.

To test the match, the average well (k = 2.02 md, s = -4.43, r_e/r_{wa} = 50, b = 0.6) was forecast in terms of q_{dD} - t_{dD} and superposition, which included all the shutdown periods. The result multiplied by seven wells is compared with the actual total field performance in Figure 35.

Clyde Cowden

The Clyde Cowden lease is part of the Goldsmith (5,600-ft [1707-m]) field in Ector County, TX. The main development of the lease occurred between 1950 and early 1952, with 50 wells drilled on 40-acre [16-ha] spacing. An acid treatment of the dolomitic formation was a routine part of each completion. The dominant drive mechanism during the primary recovery period is understood to be solution gas drive.

Figure 36 shows the production history of the lease from 1949 to 1982. The primary decline period began in October 1951 and ended with the beginning of the waterflood program in August 1961. Between 1970 and 1972, most of the producing wells were hydraulically fractured. The secondary decline period began at about this time, in May 1971.

The 34-year production history shown in Figure 36 is replotted on a log-log scale in Figure 37. The primary recovery period (1951-61), matched to an r_e/r_{wa} stem of 1,000 and a b = 0.3, is shown in Figure 38. The reinitialized plot of the waterflood decline period is shown in Figure 39. Here, too, the match is on an r_e/r_{wa} stem of 1,000 and a b = 0.3. The primary and secondary decline period log-log plots overlie each other (Figure 40).

The results of type-curve analysis and relevant reservoir data are summarized in Table 11. The match-calculated average well permeability of 32 md is in good agreement with the permeability range of 20 to 30 md reported for the Upper Clearfork, and the negative skin of -0.8 is consistent with the perhaps only moderately effective acid treatment at completion.

With the method detailed earlier for Edda, the match-derived N_{si} value of 49.8 MMSTB [7.92 x 10^6 stock-tank m^3] agrees well with the 48 to 52 MMSTB [7.63 x 10^6 to 8.27 x 10^6 stock-tank m^3] N_{si} estimates from earlier material-balance calculations.[21]

Production forecasts were made for the primary decline and for Waterflood Period 2 on the basis of the decline match of b = 0.3 for both. A recovery of 9.8 MMSTB [1.56 x 10^6 stock-tank m^3] (or 20% of 49.8 MMSTB N_{si} [7.92 x 10^6 stock-tank m^3]) is forecast for primary recovery; the primary-plus-waterflood forecast is 18.4 MMSTB [2.93 x 10^6 stock-tank m^3] (or 37% of N_{si}). The incremental recovery of 8.6 MMSTB [1.37 x 10^6 stock-tank m^3] resulting from waterflooding represents 88% of primary recovery.

That the primary decline and the waterflood decline appear to fall on the same decline stem, b = 0.3, may be coincidental. While we can think of some possible explanation why this should occur, we can think of none why this must occur. As such, one of the main reasons for presenting this example is to encourage others to examine primary and waterflood histories for their decline exponents. We suppose that if we were asked to produce a waterflood forecast in one day given primary production history, we would as a first approximation forecast a waterflood decline on the same value of b as that established during primary recovery.

Monterey Type Curve

In an effort to determine the production performance characteristics of fields producing from the Monterey formation in California, production data from the Lompoc and Orcutt fields were obtained, and an average well rate-time curve was established for each field.[22,23]

A log q - log t tracing-paper plot was made from the data for each of the fields. If these two separate log q - log t plots are overlaid and the vertical and horizontal axis shifted as required, they exactly overlie. This was a surprise at first, yet was consistent with type-curve theory in that the plots should differ only by the coefficients involved in the definition of q_{dD} - t_{dD} -- i.e., reservoir and fluid variables. Further, the drive mechanisms, relative permeability relationships, and natural fracturing characteristics also must be similar.

The question of the correctness of the representative average well was immediately raised. Good-quality, unambiguous data available on a single lease within the Orcutt field were also plotted log q - log t, and that plot also exactly overlaid both of the field plots. This appeared to verify the total-field-averaging technique used to obtain our average well plot for each field. Each plot by itself was limited in range; however, all three plots combined virtually doubled the total range of data.

Although suggested by theory, this was the first test of the concept that fields within the same formation having similar drive mechanisms should overlie each other, regardless of the fact that they may have totally different fluid and rock properties, well spacing, stimulation response, and reservoir pressures.

Fluid and rock properties, spacing, and reservoir and flowing pressures were then estimated for the Lompoc and Orcutt fields and a q_{dD} - t_{dD} was calculated for each of the rate-time points to establish a dimensionless type curve for the Monterey formation. Our final dimensionless type-curve, which we refer to as the Monterey type curve, is shown in Figure 41. We further confirmed the type curve with the addition of rate-time data from the West Cat Canyon, the Santa Maria Valley, and the Zaca fields. Figure 42 shows the complete five-field overlay. This type curve essentially matches the harmonic decline stem b = 1.

The q_{dD} - t_{dD} type curve developed for the Monterey formation was converted to a p_{dD} - t_{dD} type curve to enable us to calculate how long a well or field could produce at a constant rate to a fixed flowing pressure before going on decline (see Figure 43). The late-time portion of the p_{dD} - t_{dD} type curve appears to be a 1/2 slope, a $\sqrt{t}$ relationship, which may or may not be significant. It is unlikely that linear flow is from the matrix blocks because the apparent linear flow period is too long and the matrix blocks are considered very small. The Monterey chert is generally overlain with a thick, very-low-permeability mudstone. Therefore, crossflow down from it could be a possible explanation.

The field or formation type curve represents the ultimate use of reservoir or field analogy. The q_{dD} - t_{dD} Monterey type curve is readily applied on an average well basis to develop forecasts for varying reservoir properties and

fluid properties, spacing, flowing pressure, and stimulation. Several wells with differing productivities could be used by proportioning total reservoir volume to correspond with each individual well productivity factor to arrive at an average well. Summing each well's forecast developed from the Monterey type curve would result in a more straightforward total field forecast.

Still further flexibility can be added by the use of two conventional one-cell, material-balance forecasts, which when combined match the Monterey type curve. Each material balance allows the inclusion of a drilling schedule, downtime, a relative permeability curve to predict gas rates, and oil and gas production limits. Two forecasts were generated with such a simple model, assuming there exists an intensely fractured area, or volume, and a slightly fractured or nonfractured area or volume with very contrasting deliverabilities. The contrasting deliverability areas can exist areally or vertically. (See Reference 24 for the effect of hydrocarbon influx of various degrees from a low-permeability outer-boundary region.) The percentage of fractured-area volume to nonfractured-area volume was arrived at by trial and error to get a composite decline rate-time data match of the Monterey type curve. Each separate forecast had the typical solution-gas drive of $b = 0.3$.

If one were to develop a sophisticated three-dimensional fracture model, it should first be history-matched to the Monterey type curve before being used to make production forecasts.

Figure 44 is a semilog plot of the Monterey type curve. Of special note is the precipitous early decline, which later flattens. This behavior can easily be misinterpreted as indicating depletion of the fracture volume followed by flow from only the matrix blocks. The log-log plot of the Monterey type curve does not exhibit in any way the double depletion stems characteristic of the constant-wellbore-pressure solution of the dual porosity Warren and Root model.

Conclusions

1. For decline-curve analysis, a log q - log t plot should be made to identify transient data and/or depletion data. The plot should be reinitialized in time to eliminate any constant-rate production period.

2. The Arps equation must be applied only to rate-time data that indicate depletion. The limits of the value of b, when the Arps equation applies, are between 0 (exponential) and 1 (harmonic). A forced fit of transient data to the Arps equation results in apparent values of $b > 1$; generally, these false values of b fall in the range of 2.2 to 2.5. Further, rapidly declining rate data are characteristic of low-permeability stimulated wells (apparent $b > 1$). Often a unique fit of such data can be obtained on the transient portion of a type curve. The misuse of the Arps equation with transient data generally results in overly optimistic forecasts and is technically incorrect.

3. With rate-time data, the double-depletion decline is the only indication of a dual-porosity system. The dual-porosity, constant-wellbore-pressure solution (Warren and Root model) does not anywhere indicate $b > 1$, except for the apparent b values from the early transient period; the character of this period is identical to the homogeneous-reservoir solution.

4. The pore volume and reservoir parameters kh and s at the start of decline analysis can be calculated from a type-curve match once depletion is indicated by the data and the decline exponent b is defined or reasonably estimated.

5. In low-permeability gas reservoirs, reserve estimates and production forecasts developed from rate-time data would be more appropriate than conventional p/z vs. cumulative production used with the calculated stabilized backpressure curve approach.

6. Superposition using q_{dD} - t_{dD} with values of b > 0 can be successfully applied to field problems.

7. Field or formation q_{dD} - t_{dD} type curves can be developed from basic reservoir data and declining rate-time production data.

8. Advanced decline-curve analysis should always be supported by and checked against already existing well and reservoir information.

Recommendations

An effort should be made to obtain accurate rate and surface flowing pressure data to improve the reliability of decline curve analysis. If these data are taken frequently at early times while producing wide open, if possible, or at a fixed choke setting, then an evaluation of initial reservoir parameters as kh and s can be made to assist in fixing the r_e/r_w decline-curve stem once depletion sets in. The Edda case history is a classic example of what can be done with good-quality data taken frequently.

Dimensionless type curves to characterize the more important producing formations should be developed from the vast amount of existing field data.

Finally, some analytic work needs to be done with regard to determining what values of b should result from a water displacement process. We need a stronger theoretical basis for waterflood decline-curve analysis.

Nomenclature

b = reciprocal of decline-curve exponent
β_g = gas FVF, surface vol/res vol
β_o = FVF, res vol/surface vol
c_g = gas compressibility, psi^{-1} [kPa^{-1}]
c_t = total compressibility, psi^{-1} [kPa^{-1}]
C = gas-well backpressure-curve coefficient
D_i = initial decline rate, t^{-1}
e = natural logarithm base, 2.71828
G = gas in place at start of decline analysis, surface-measured
G_i = initial gas in place, surface-measured
G_p = cumulative gas production, surface-measured
h = thickness, ft [m]
I_f = fracture index (Eq. 8)
k = effective permeability, md
L_{xe} = reservoir half-length, ft [m]

L_{xf} = fracture half-length, ft [m]
n = exponent of backpressure curve
N_p = cumulative oil production, STB [stock-tank m^3]
N_s = oil in place at start of decline analysis, STB [stock-tank m^3]
N_{si} = original oil in place, STB [stock-tank m^3]
p_i = initial pressure, at start of decline, psia [kPa]
p_p = gas pseudopressure, psi^2/cp [$kPa^2/mPa \cdot s$]
p_{po} = oil pseudopressure, psi/cp [kPa/mPa·s]
p_{wf} = bottomhole flowing pressure, psia [kPa]
q_{dD} = decline-curve dimensionless rate (Eq. 4)
q_D = dimensionless rate
$q(t)$ = surface rate of flow at time t
r_e = external-boundary radius, ft [m]
r_w = wellbore radius, ft [m]
r_{wa} = effective wellbore radius, ft [m]
s = skin
S_w = water saturation
t = time, days for t_D
t_{dD} = decline-curve dimensionless time
t_D = dimensionless time
T = reservoir temperature, °R [K]
V_p = reservoir PV, ft^3 or bbl (consistent units on q and β)
z = gas compressibility factor, dimensionless
Δ = change
λ = type-curve parameter used to characterize gas well drawdown, dimensionless
μ = viscosity, cp [Pa·s]
ϕ = porosity, fraction of bulk volume

Subscripts

BU = buildup
DD = drawdown
F = field
g = gas
i = initial
o = oil
p = production

Superscript

- = average

Acknowledgements

We wish to thank Phillips Petroleum Co. for permission to publish this paper. We also wish to thank our Stavanger office and our coventurers in the Greater Ekofisk development for permission to publish the Edda field data.

References

1. Fetkovich, M. J.: "Decline Curve Analysis Using Type Curves," JPT (June 1980) 1065-77.

2. Locke, C. D. and Sawyer, W. K.: "Constant Pressure Injection Test in a Fractured Reservoir - History Match Using Numerical Simulation and Type Curve Analysis," paper SPE 5594 presented at the 1975 SPE Annual Technical Conference and Exhibition, Dallas, Sept. 28-Oct. 1.

3. Uraiet, A. A. and Raghavan, R.: "Unsteady Flow to a Well Producing at a Constant Pressure," JPT (October 1980) 1803-12.

4. Ehlig-Economides, C. A. and Ramey, H. J. Jr.: "Transient Rate Decline Analysis for Wells Produced at Constant Pressure," SPEJ (Feb. 1981) 98-104.

5. Carter, R. D.: "Characteristic Behavior of Finite Radial and Linear Gas Flow Systems - Constant Terminal Pressure Case," paper SPE 9887 presented at the 1981 SPE/DOE Symposium on Low Permeability Gas Reservoirs, Denver, May 27-29.

6. Da Prat, G., Cinco-Ley, H., and Ramey, H. J. Jr.: "Decline Curve Analysis Using Type Curves for Two-Porosity Systems," SPEJ (June 1981) 354-62.

7. Carter, R. D.: "Type Curves for Finite Radial and Linear Gas-Flow Systems: Constant-Terminal-Pressure Case," SPEJ (Oct. 1985) 719-28.

8. Arps, J. J.: "Analysis of Decline Curves," Trans, AIME (1945) 160, 228-47.

9. Fetkovich, M. J. and Vienot, M. E.: "Shape Factor, C_A, Expressed as Skin, s_{CA}," JPT (Feb. 1985) 321-22.

10. Chatas, A. T. and Malekfam, H.: "The Estimation of Aquifer Properties from Reservoir Performance in Water-Drive Fields," paper SPE 2970 presented at the 1970 SPE Annual Meeting, Houston, Oct. 4-7.

11. van Everdingen, A. F. and Meyer, L. J.: "Analysis of Buildup Curves Obtained After Well Treatment," JPT (April 1971) 513-24; Trans., AIME, 251.

12. Warren, J. E. and Root, P. J.: "The Behavior of Naturally Fractured Reservoirs," SPEJ (Sept. 1963) 245-55; Trans., AIME, 228.

13. Agarwal, R. G., Carter, R. D., and Pollack, C. B.: "Evaluation and Performance Prediction of Low-Permeability Gas Wells Stimulated by Massive Hydraulic Fracturing," JPT (March 1979) 362-72; Trans., AIME, 267.

14. Cullender, M. H.: "The Isochronal Performance Method of Determining the Flow Characteristics of Gas Wells," Trans., AIME (1955) 204, 137-42.

15. Fetkovich, M. J. and Vienot, M. E.: "Rate Normalization of Buildup Pressure by Using Afterflow Data," JPT (Dec. 1984) 2211-24.

16. Fetkovich, M. J. and Thrasher, T. S.: "Constant Well Pressure Testing and Analysis in Low Permeability Reservoirs," paper SPE 7928 presented at the SPE Regional Meeting, Denver, Colorado, May 1979, (8 1/2 x 11 copies of the slide presentation, along with a type curve were distributed at the meeting).

17. Gentry, R. W. and McCray, A. W.: "The Effect of Reservoir and Fluid Properties on Production Decline Curves," JPT (Sept. 1978) 1327-41.

18. Bailey, W.: "Hyperbolic Decline Curve Analysis of Gas Wells," Oil & Gas J. (Feb. 15, 1982) 116-18.

19. Parrott, D. I. and Long, M. G.: "A Case History of Massive Hydraulic Refracturing in the Tight Muddy 'J' Formation," paper SPE 7936 presented at the 1979 SPE/DOE Symposium on Low Permeability Gas Reservoirs, Denver, May 20-22.

20. Al-Kasim, F.: "Decline Type Curve Analysis and Simulation of Edda Production Performance," MS thesis, Norwegian Inst. of Technology, Trondheim (Dec. 30, 1983).

21. Spradlin, B. C.: "Performance of the Goldsmith 5600' Zone, Clyde and Jessie Cowden Leases, Section 13, 14, 23, 24, 25, and 26, Block 44, T1S Ector County, Texas," Phillips Petroleum Co. Report, (July 1959).

22. Bradley, M. D. and Craig, D. A." "A Production History Evaluation of Lompoc Field, Santa Barbara County, California," Phillips Petroleum Co. Report, Denver (Feb. 12, 1981).

23. Bradley, M. D. and Craig, D. A.: "A Production History Evaluation of the Orcutt Field, Santa Barbara County, California," Phillips Petroleum Co. Report, Denver (March 2, 1981).

24. Bixel, H. C. and van Poollen, H. K.: "Pressure Drawdown and Buildup in the Presence of Radial Discontinuities," SPEJ (Sept. 1967) 301-09; Trans., AIME, 240.

SI Metric Conversion Factors

cp	x 1.0*	E+00	=	mPa·s
ft	x 3.048*	E-01	=	m
ft^3	x 2.831 685	E-02	=	m^3
^oF	$(^oF-32)/1.8$		=	^oC
md-ft	x 3.008 142	E-03	=	md·m
psi	x 6.894 757	E+00	=	kPa
psi^{-1}	x 1.450 377	E-01	=	kPa^{-1}

*conversion factor is exact

TABLE 1

EDDA 10X WELL

DST 2 SUMMARY OF ANALYSIS RESULTS (POSTACID) AND RESERVOIR DATA

	Horner	$q_D - t_D$ Constant p_{wf} Plane Radial System
k, md	0.95	0.89
s	-4.8	-5.1
r_{wa}, ft	40	54

Reservoir Data

ϕ	0.25
S_w	0.35
μ, cp	0.167
p_i, psia	7,043
β_o, RB/STB	1.992
h, ft	50
c_t, psi^{-1}	21.6×10^{-6}

TABLE 2

MHF GAS WELL A

COMPARISON OF PRODUCTION FORECASTS

Time (months)	Constant Pressure Solution (Mscf/D)	Infinite-Conductivity Vertical-Fracture Solution (Mscf/D)	SPE 6838 Simulator Results (Mscf/D)
12	182	182	190
18	157	157	165
24	140	136	150
30	130	128	140
36	122	120	135
42	117	112	130
48	110	108	120
54	108	103	110
60	104	100	105
(years)			
6	100	95	
7	96	89	
8	92	86	
9	89	83	
10	86	80	
11	84	78	
12	82	75	
13	80	73	
14	79	71	
15	77	69	
16	76	68	
17	74	67	
18	73	66	
19	72	65	
20	71	64	

TABLE 3

WEST VIRGINIA GAS WELL A

Reservoir and Fluid Properties

Gas specific gravity	0.57 (air = 1.00)
Porosity	0.06
Water saturation	0.35
Original pressure, psia	4,175
Pressure at start of decline, psia	3,268
Viscosity at 3,268 psia, cp	0.0171
System compressibility at 3,268 psia, psi^{-1}	177×10^{-6}
Thickness, ft	70
Temperature, ^{o}F	160
Wellbore radius, ft	0.354
Rate before 106-day pressure buildup, Mscf/D	2,181
Δp_p, psi^2/cp	774×10^6
β_g at 3,268 psia, scf/ft^3	208.8
β_g at 4,175 psia, scf/ft^3	253.9

TABLE 4

WEST VIRGINIA GAS WELL A: SENSITIVITY TO r_e/r_w

	r_e/r_{wa} = 10	r_e/r_{wa} = 20	r_e/r_{wa} = 50	Horner Analysis p_p Basis
kh, md-ft	3.542	4.902	6.705	5.635
k, md	0.0506	0.0700	0.0958	0.0805
V_p, 10^6 ft^3	20.36	20.36	20.36	
r_e, ft	1,242	1,242	1,242	
r_{wa}, ft	124.2	62.1	24.8	
s	-5.86	-5.17	-4.25	-5.52
G at 3,268 psia, Bscf	2.763	2.763	2.763	
G_i at 4,175 psia, Bscf	3.360	3.360	3.360	

TABLE 5

WEST VIRGINIA GAS WELL A
SUMMARY OF RATE-TIME ANALYSIS RESULTS

Match Points

Composite Type Curve b = 0		Composite Type Curve b = 0.5		Carter Type Curve λ = 0.55 (b = 0.5)	
q_{dD}	0.62	q_{dD}	0.58	q_{DR}	0.24
t_{dD}	0.075	t_{dD}	0.126	t_{DR}	60
q(t), Mscf/D	1,000	q(t), Mscf/D	1,000	q(t), Mscf/D	1,000
t, days	100	t, days	100	t, days	100

	r_e/r_{wa} = 10	r_e/r_{wa} = 20	r_e/r_{wa} = 50	Horner Analysis
		b = 0 Evaluation		
kh, md-ft	3.292	4.558	6.231	
k, md	0.047	0.065	0.089	0.0805
r_{wa}, ft	154.7	77.4	30.9	
s	-6.08	-5.38	-4.47	-5.52
r_e, ft	1,547	1,547	1,547	
		b = 0.5 Evaluation		
kh, md-ft	3.542	4.902	6.705	
k, md	0.0506	0.0700	0.0958	
r_{wa}, ft	124.2	62.1	24.8	
s	-5.86	-5.17	-4.25	
r_e, ft	1,242	1,242	1,242	
		Carter's λ = 0.55 Evaluation		
kh, md-ft	3.451	4.746	6.699	
k, md	0.0493	0.0678	0.0957	
r_{wa}, ft	126.4	62.6	24.8	
s	-5.88	-5.17	-4.25	
r_e, ft	1,264	1,252	1,240	

TABLE 6

SAN JUAN WELL 58: SENSITIVITY TO r_e/r_w

	r_e/r_{wa} = 100	r_e/r_{wa} = 200
k, md	0.34	0.40
s	-4.3	-3.6
r_e, ft	1,765	1,776

TABLE 7

FIELD E: RESERVOIR DATA AND COMPARISON OF ANALYSIS RESULTS

p_i, psia	2,921
p_{wf}, psia	2,760
μ, cp	0.615
β_o, RB/STB	1.06
c_t, psi^{-1}	12.7×10^{-6}
ϕ	0.18
S_w	0.26
h, ft	100
r_w	0.258

	Early Well Test	$q_{dD} - t_{dD}$ Type-Curve Match
k, md	143	152
s	-3.9	-4.1

TABLE 8

EDDA RESERVOIR DATA AND TYPE-CURVE MATCHING RESULTS
(r_e/r_{wa} = 50; b = 0.6)

	Total Production Period	Reinitialized Production Period 3	Reinitialized Production Period 6
kh, md-ft	202	178	127
k, md	2.0	1.8	1.3
r_{wa}, ft	29.62	28.53	29.21
s	-4.4	-4.4	-4.4
r_e, ft	1,481	1,427	1,461
V_p, MMbbl	29.0	27.0	28.0
ø	0.236	0.236	0.236
S_w	0.365	0.365	0.365
μ_o, cp	0.185	0.17	0.255
β_o, RB/STB	1.92	1.98	1.67
$\overline{\mu\beta}$, cp-RB/STB	0.416	0.44	0.50
c_t, psi^{-1}	27×10^{-6}	35×10^{-6}	105×10^{-6}
p_i, psia	6,300	5,200	3,800
p_{wf}, psia	1,500	1,500	1,500
h	100	100	100
r_w	0.354	0.354	0.354

Edda: Reservoir Data at Discovery

p_i, psia	7,115
p_b, psia	5,045
μ_{oi}, cp	0.2
β_{oi}, RB/STB	1.895
C_{ti}, psi^{-1}	24×10^{-6}
ϕ	0.236
S_w	0.365
h, ft	100

TABLE 9

EDDA: INITIAL COMPLETION WELL TEST RESULTS AND FRACTURE INTENSITY INDICES

Well	kh (md-ft)	h (ft)	k (md)	s	ϕ (%)	k matrix (ϕ -k plot) (md)	k well test / k matrix (ϕ -k)
C-2	2,028	110	18.4	-4.9	25.3	0.66	28
C-5	50	70	0.7	-4.0	23.8	0.50	1
C-9	1,119	120	9.3	-4.5	24.6	0.58	16
C-10	218	82	2.7	-4.7	24.0	0.50	5
C-11	510	90	5.7	-4.6	24.1	0.52	11
C-14	298	114	2.6	-3.0	22.6	0.40	7
C-15	201	115	1.7	-3.7	20.8	0.28	6
Total	4,424	701	41.1	29.4	165.2	3.44	74
Arithmetic Average Value *	632	100	5.9	-4.2	23.6	0.49	11

* k = 6.32 md

TABLE 10

EDDA SENSITIVITY TO r_e/r_{wa}

	r_e/r_{wa} = 20		r_e/r_{wa} = 50		r_e/r_{wa} = 100	
	Total Field	Average Well	Total Field	Average Well	Total Field	Average Well
kh, md-ft	1,035.2	147.90	1,415.4	202.2	1,702.9	243.3
k, md	10.35	1.48	14.15	2.02	17.03	2.43
V_p, 10^6 bbl	202.8	29.0	202.8	29.0	202.8	29.0
r_e	3,919	1,481	3,919	1,481	3,919	1,481
r_{wa}	195.95	74.05	78.38	29.62	39.19	14.81
s_F*	-5.34	-	-4.43	-	-3.73	-
s	-	-5.34	-	-4.43	-	-3.73
N_s, MMSTB	67.1	9.6	67.1	9.6	67.1	9.6
N_{si}, MMSTB	68.3	9.8	68.3	9.8	68.3	9.8
Material-Balance N_{si}, MMSTB	67.4	9.6	67.4	9.3	67.4	9.6

* $r_{wF} = \sqrt{\text{number of wells} \times r_w^2}$

$= \sqrt{7\ (0.354\ \text{ft})^2}$

$= 0.9366$ ft

TABLE 11

CLYDE COWDEN: RESERVOIR AND WELL DATA

p_i (at discovery), psig	2,250
p_i (match), psig	1,900
p_{wf}, psig	600
c_{ti} at 1,900 psig, 10^{-6} psi^{-1}	75
μ_o at 1,900 psig, cp	0.9
β_o at 1,900 psig, RB/STB	1.43
$\mu\beta$ at 1,250 psig, cp-RB/STB	1.2
ϕ	0.15
S_{wi}	0.33
h, ft	48
r_w, ft	0.33

Clyde Cowden: Analysis Results,
Average Well From Primary Decline Period Match

Match Point

q(t), bbl/month oil	10,000
t, months	10
r_e/r_{wa}	1,000
q_{dD}	0.11
t_{dD}	0.135
b	0.3

Average Well

kh, md-ft	1,519
k, md	32
V_p, 10^6 res bbl	2.07
r_e, ft	717
r_{wa}	0.717
s	-0.8
N_s (average well), MMSTB	0.97
N_{si} (base), MMSTB	48.5
Produced before decline, MMSTB	1.3
N_{si}, MMSTB	49.8
N_{si} (material-balance calculation), MMSTB	50

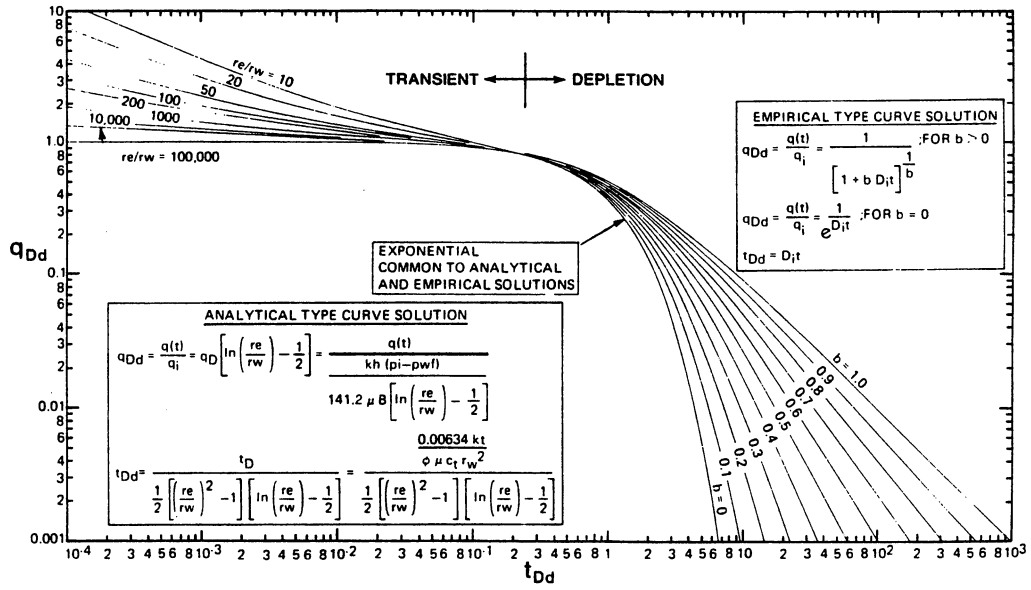

Fig. 1-Composite of analytic and empirical type curves (after Fetkovich[1]).

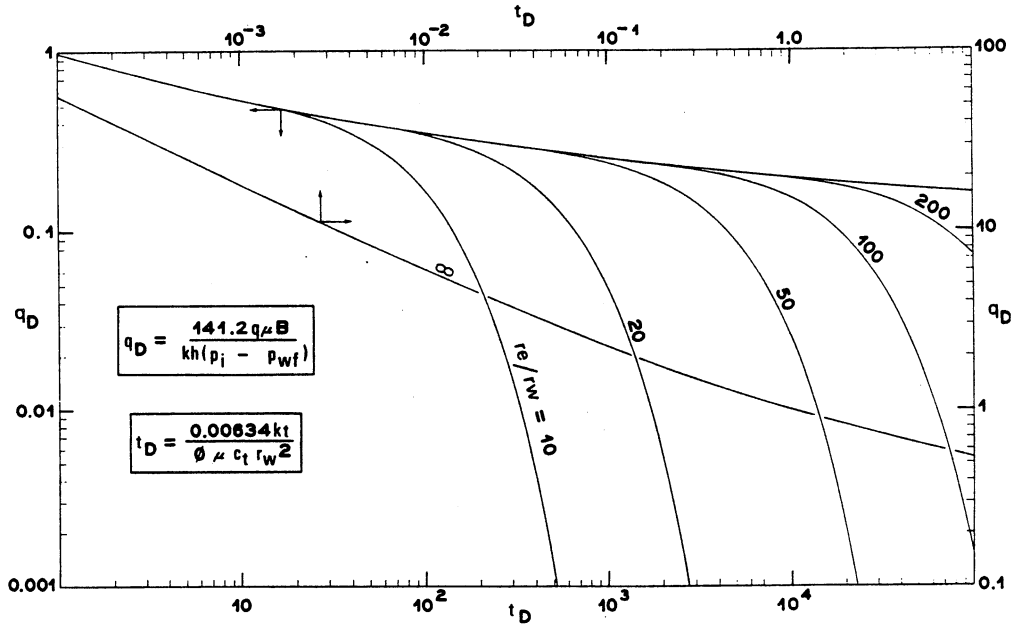

Fig. 2-Dimensionless flow-rate functions, q_D-t_D, for plane radial system, infinite and finite outer boundary, constant pressure at inner boundary (after Fetkovich[1]).

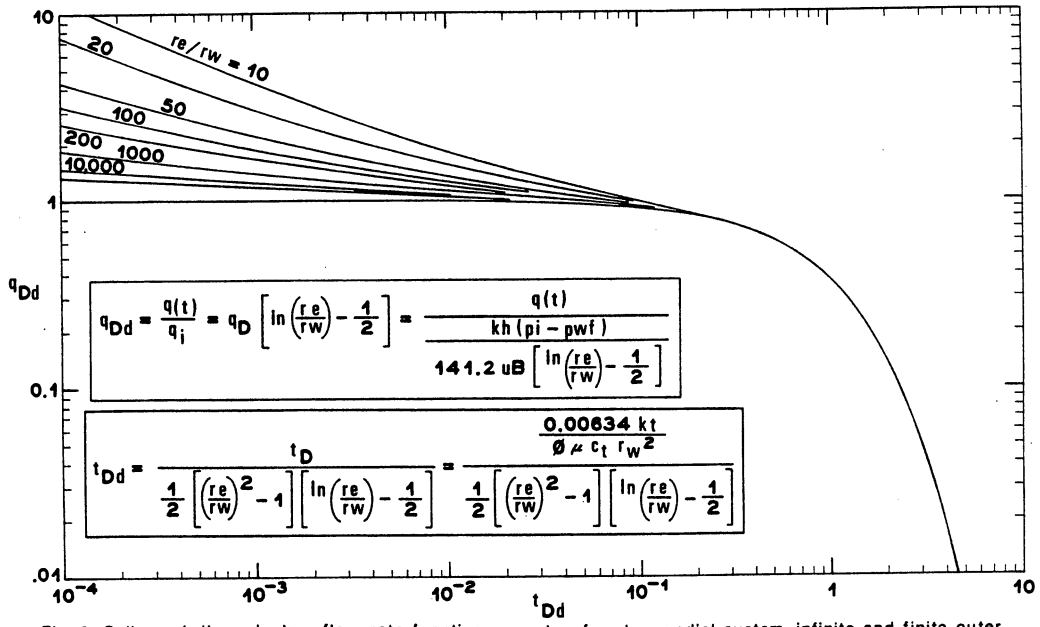

Fig. 3-Collapsed dimensionless flow-rate functions, q_{dD}-t_{dD}, for plane radial system, infinite and finite outer boundary, constant pressure at inner boundary (after Fetkovich[1]).

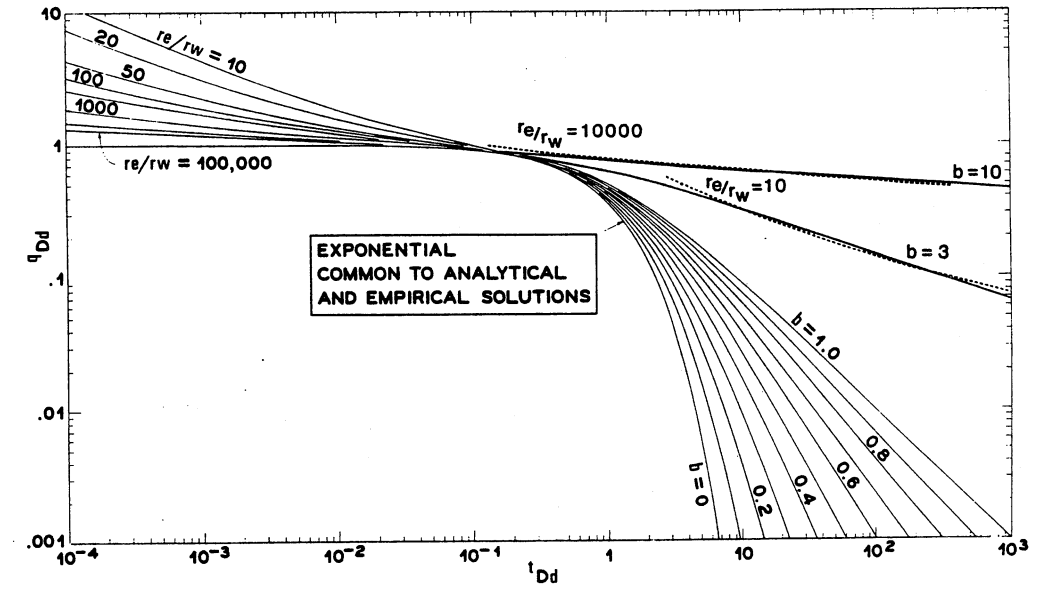

Fig. 4-Apparent b values in excess of 1 because of transient flow data.

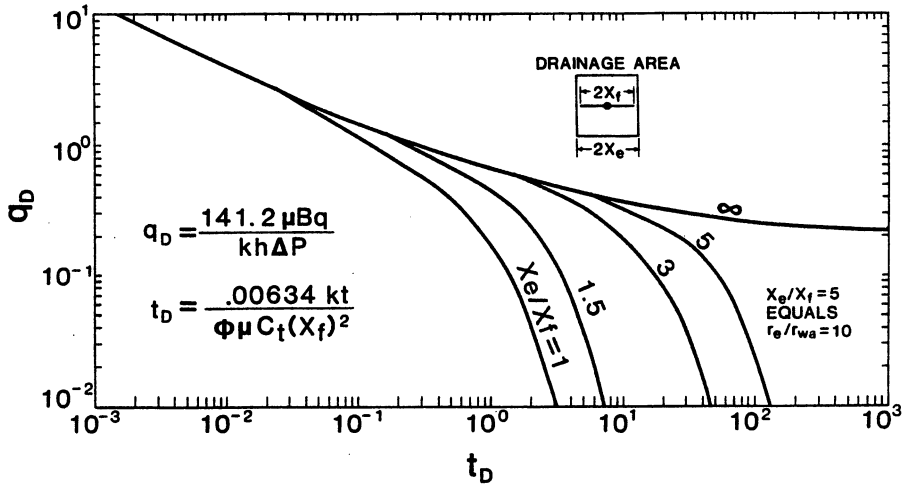

Fig. 5-Dimensionless flow-rate function for infinite-conductivity, vertical-fracture, constant-wellbore-pressure solution (after Locke and Sawyer[2]).

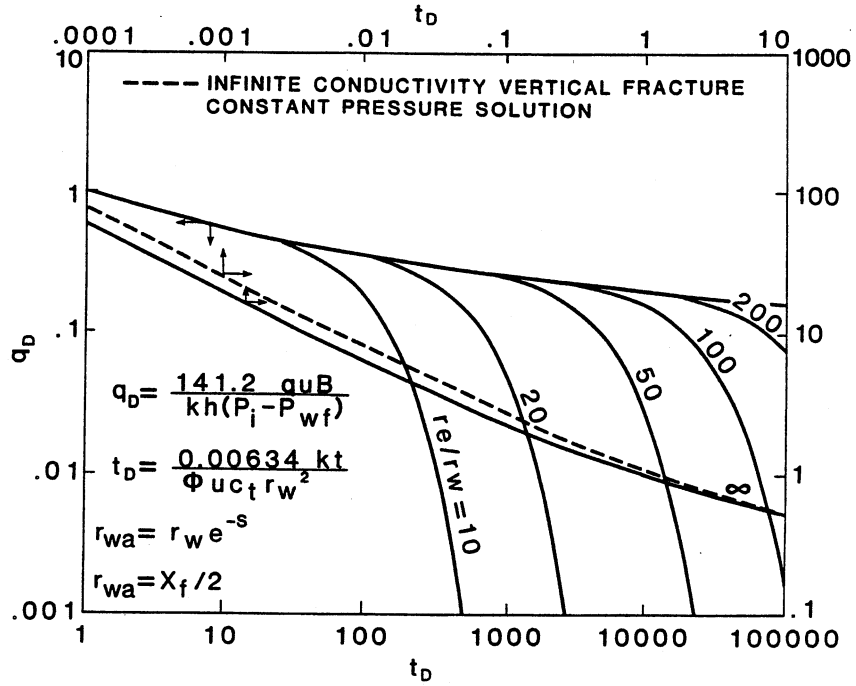

Fig. 6-Comparison of dimensionless flow rate for plane radial flow and infinite-conductivity, vertical-fracture, constant-pressure solutions.

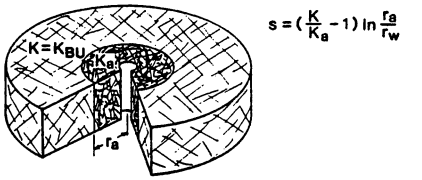

FIGURE 7A. INTENSE NATURAL FRACTURING AND MATRIX ACID EFFECT

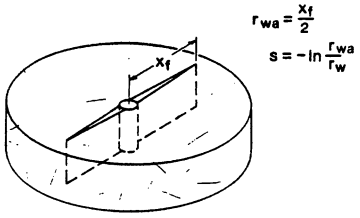

FIGURE 7B. INDUCED SINGLE VERTICAL FRACTURE FROM ACID FRAC

Fig. 7–Comparison of natural fracture and single-vertical-fracture models:
(a) intense natural fracturing and matrix acid effect;
(b) induced single vertical fracture from acid fracture.

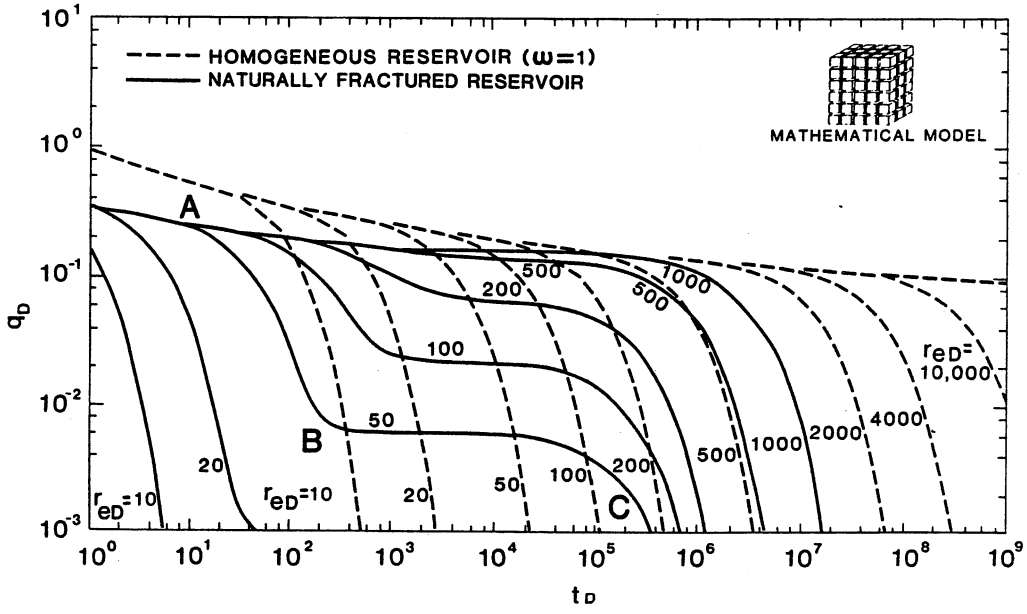

Fig. 8–q_d vs. t_d for constant-pressure production (after DaPrat et al.[6]).

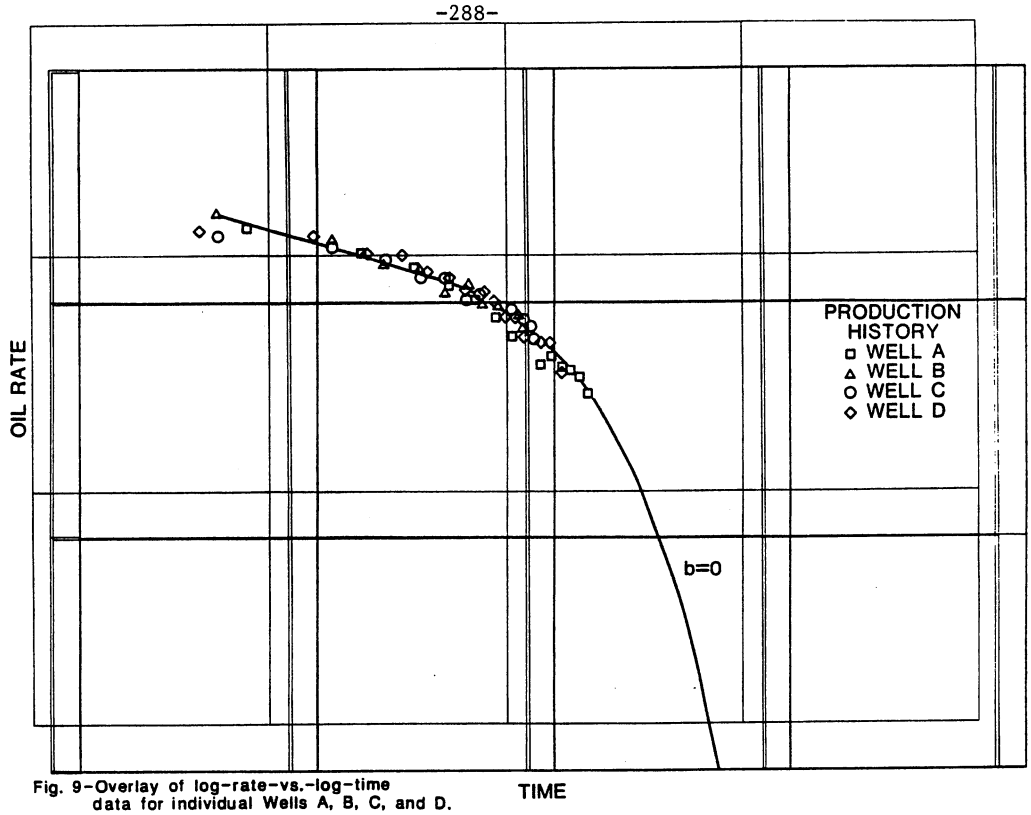

Fig. 9-Overlay of log-rate-vs.-log-time data for individual Wells A, B, C, and D.

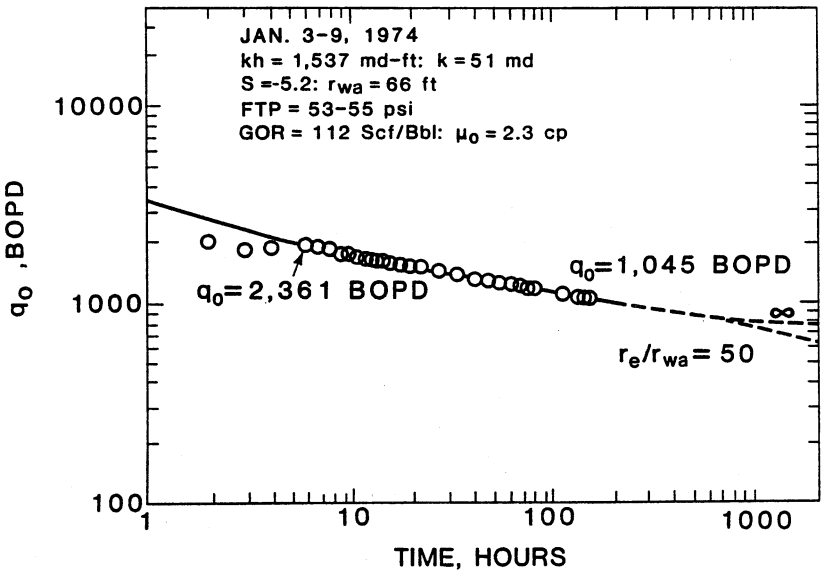

Fig. 10-Log-rate-vs.-log-time data for Well M-4X obtained from long-duration, constant-pressure production test.

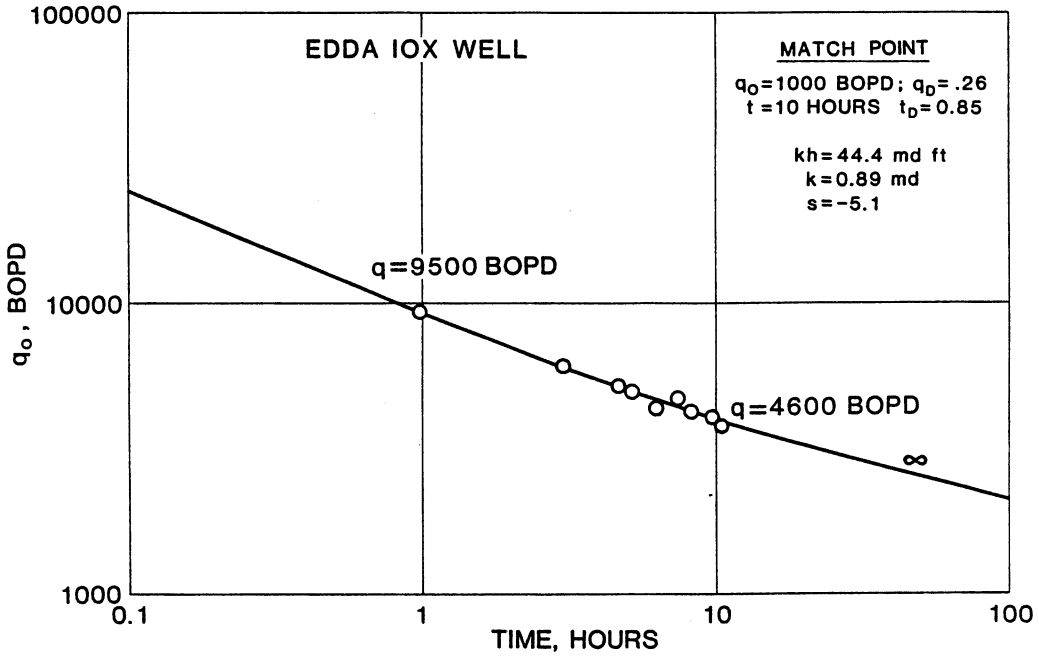

Fig. 11-Well Edda 10X rate-time type-curve match of 10-hour production test after stimulation.

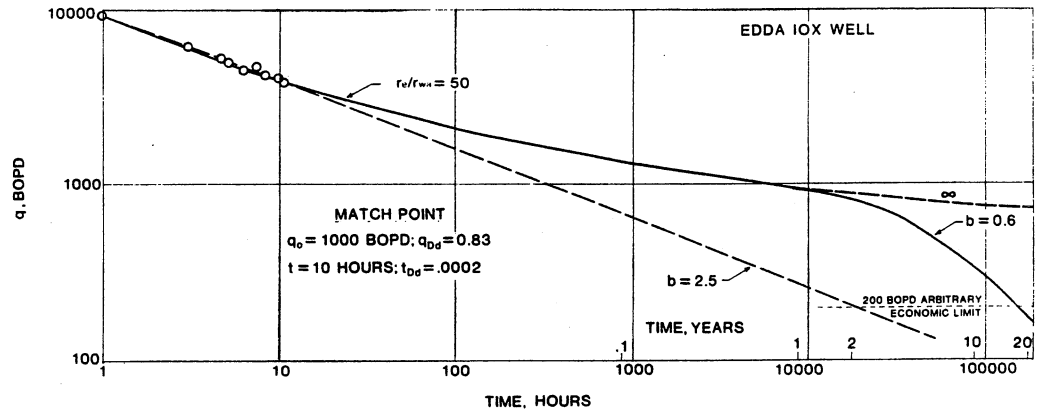

Fig. 12-Well Edda 10X-graphic production forecast compared to an Arps regression fit of b=2.5.

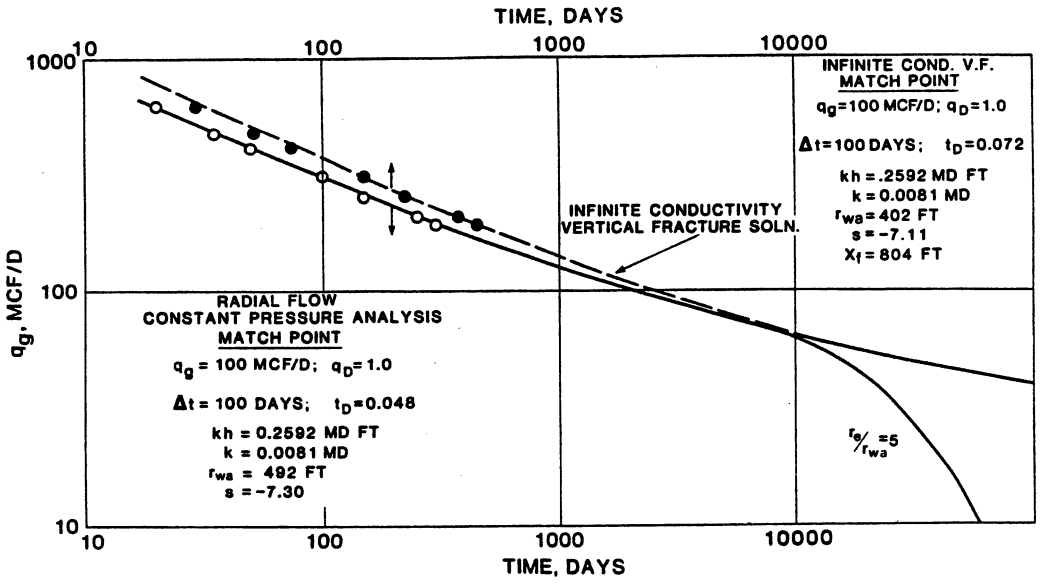

Fig. 13-MHF Well A-type curve match comparison of data fit on both the radial-flow, constant-wellbore-pressure solution and the infinite-conductivity, vertical-fracture solution.

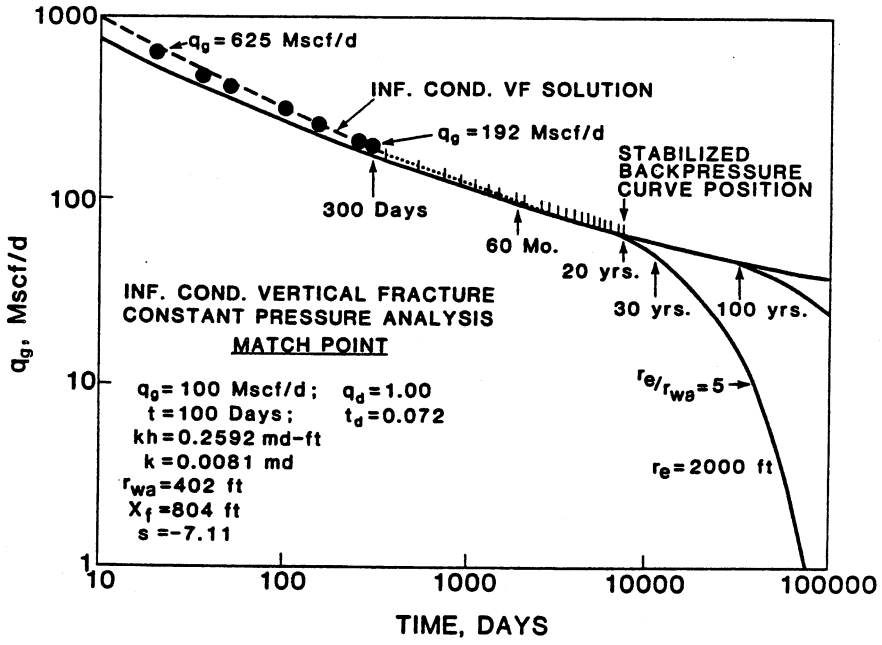

Fig. 14-MHF Well A graphic production forecast.

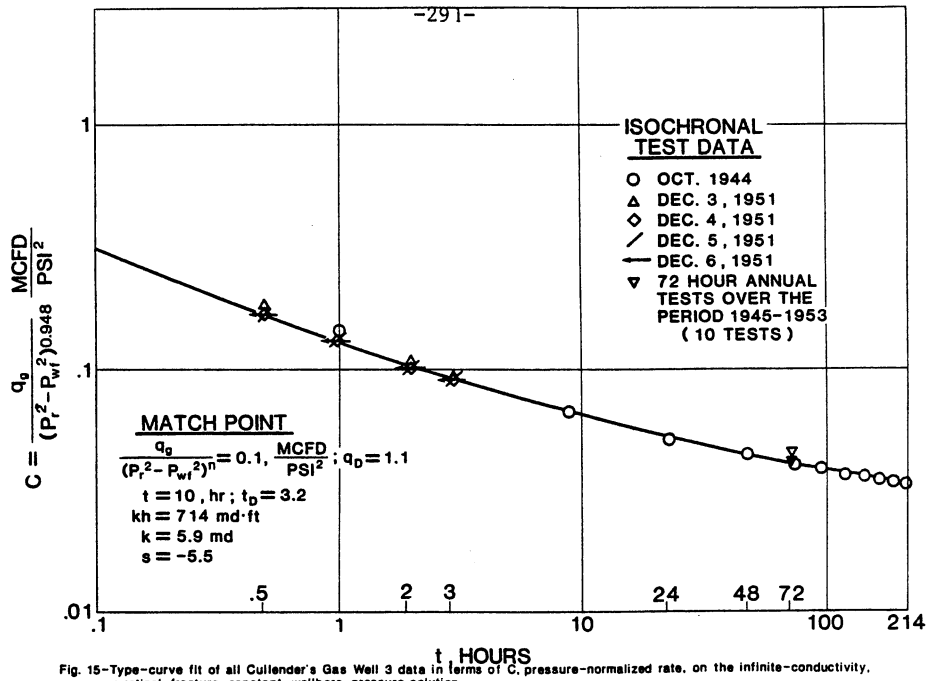

Fig. 15-Type-curve fit of all Cullender's Gas Well 3 data in terms of C, pressure-normalized rate, on the infinite-conductivity, vertical-fracture, constant-wellbore-pressure solution.

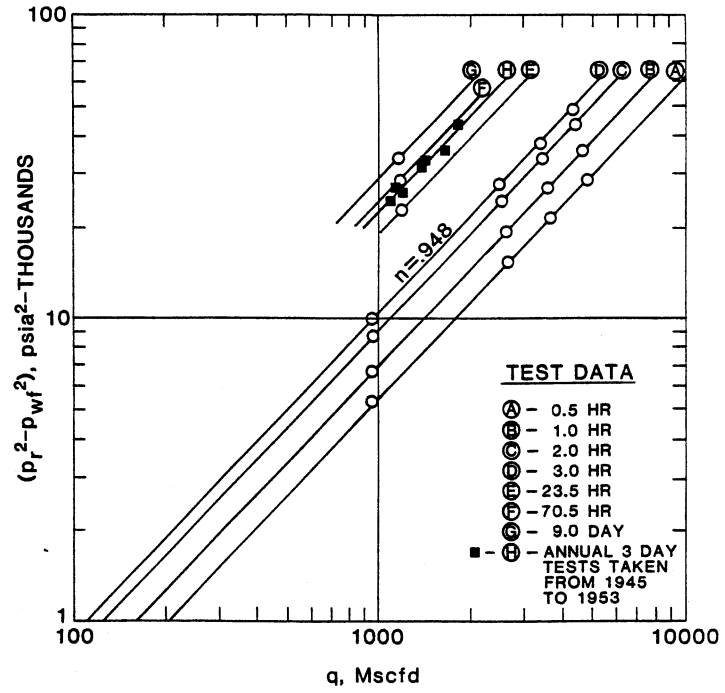

Fig. 16- Cullender's Gas Well 3 data expressed as transient backpressure curves.

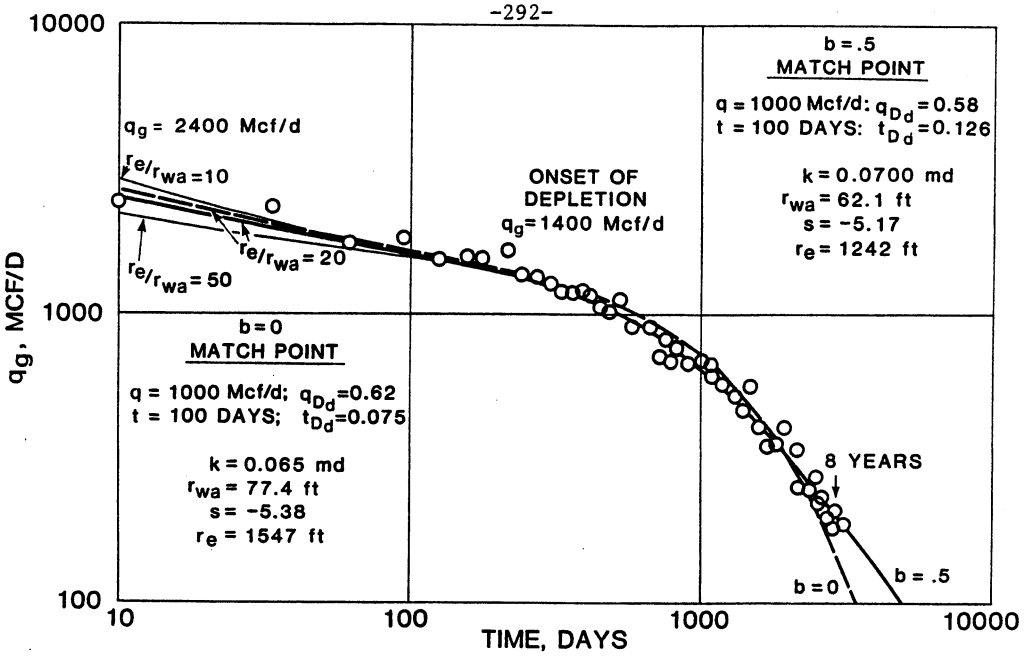

Fig. 17-West Virginia Gas Well A type-curve fit of 8 years of production data fit to a b=0 and b=0.5.

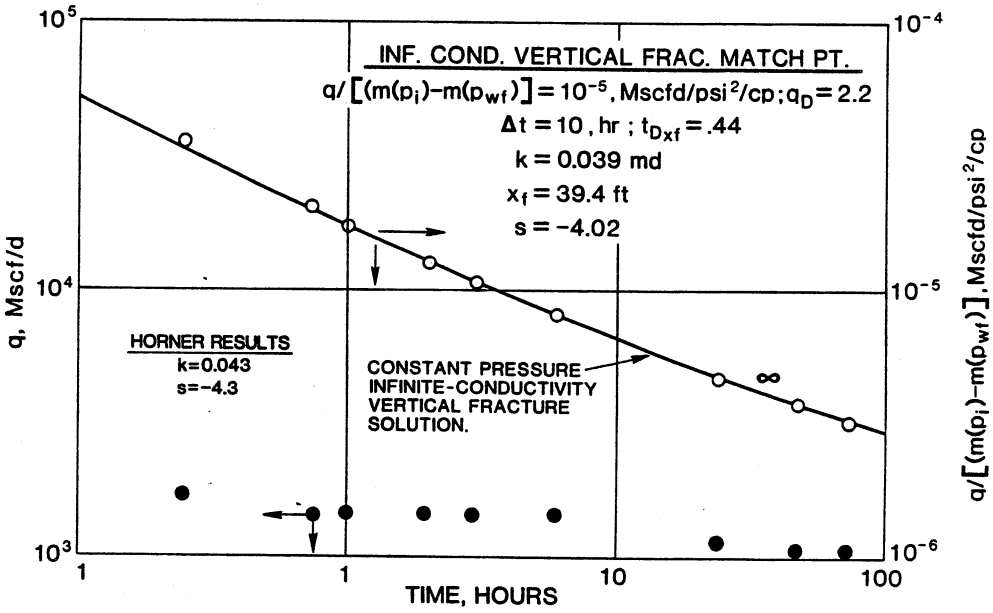

Fig. 18-West Virginia Gas Well B comparison of rate-time plot and pressure-normalized, rate-time plot of same data.[15]

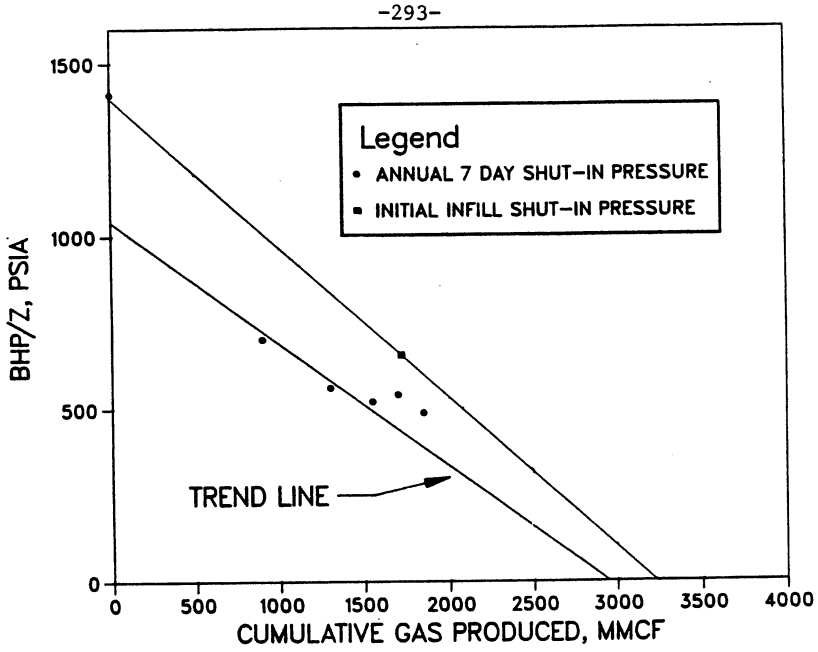

Fig. 19-Trend plot of p/z-vs.-cumulative-gas-production data for San Juan Gas Well 36.

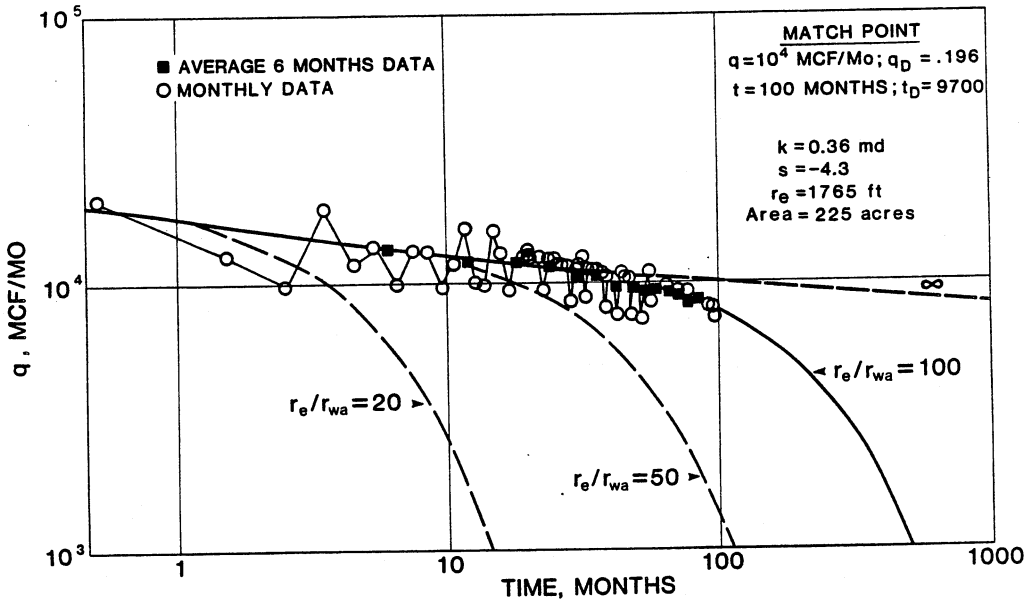

Fig. 20-San Juan Gas Well 58 rate-time type-curve match of production data on the radial-flow, constant-wellbore-pressure solution.

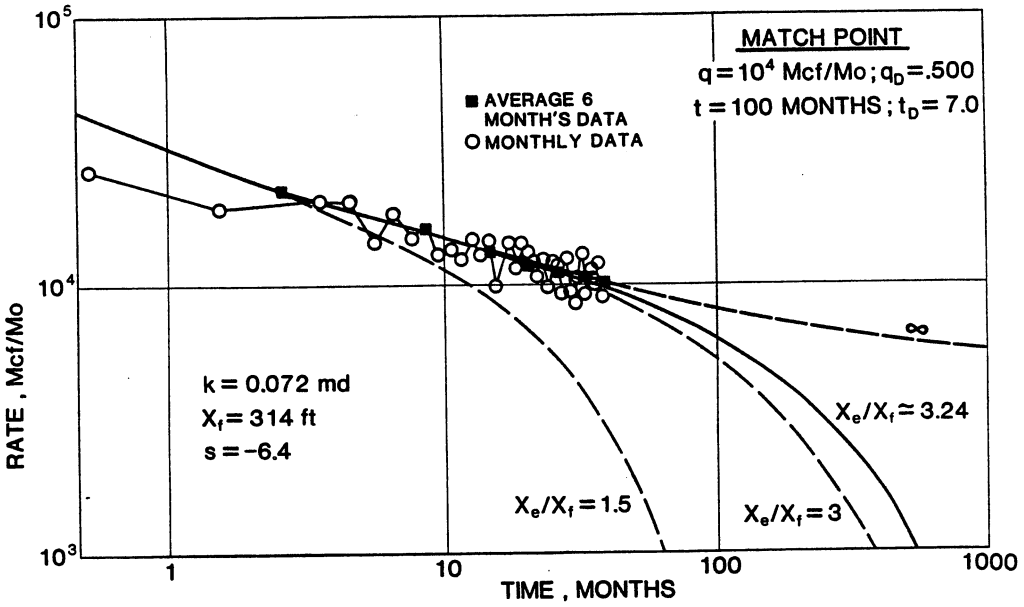

Fig. 21-San Juan Gas Well 58A rate-time type-curve match of production data on the Locke and Sawyer type curve.

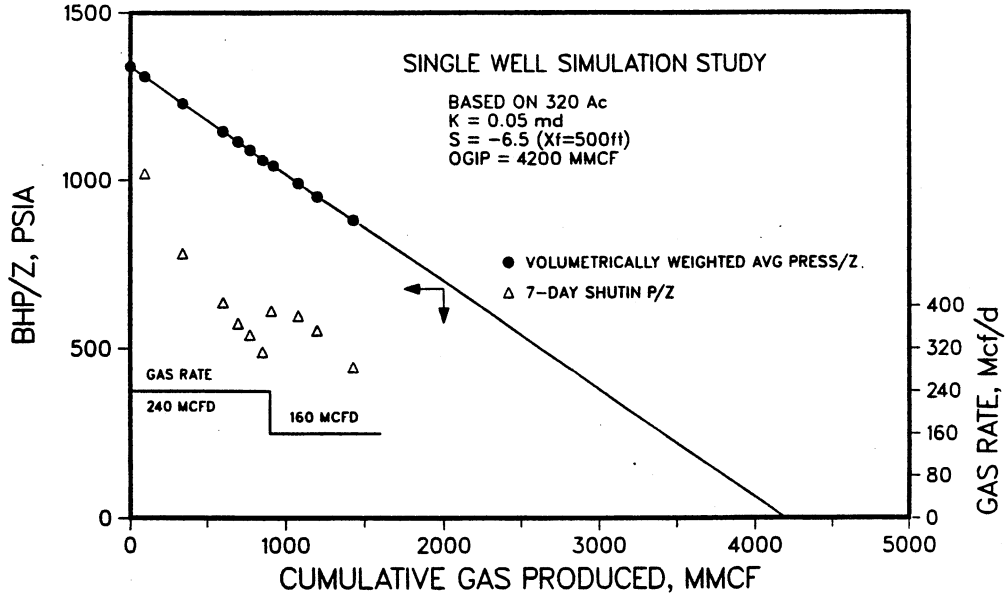

Fig. 22-Single-well simulation study of rate reduction effect on 7-day annual shut-in pressures.

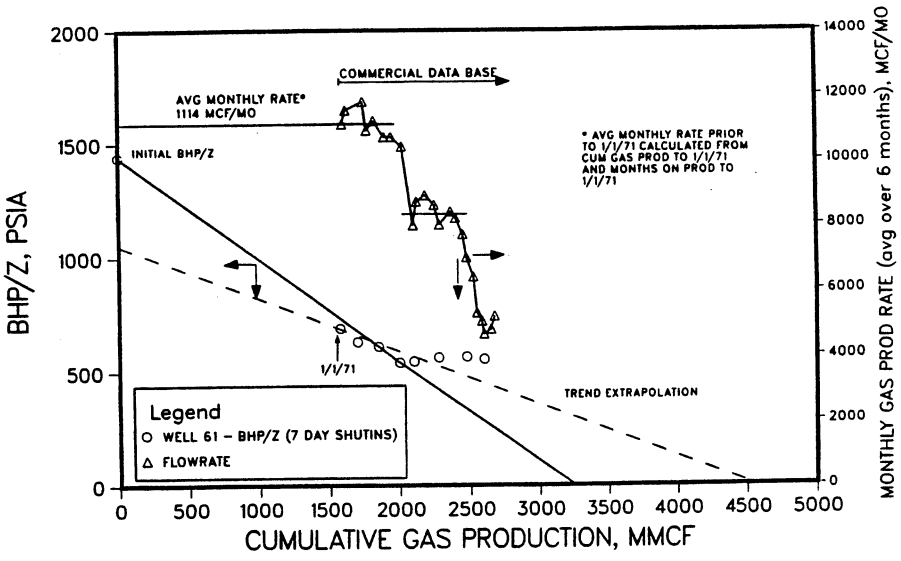

Fig. 23-San Juan field-well example of rate reduction effect on 7-day annual shut-in pressures.

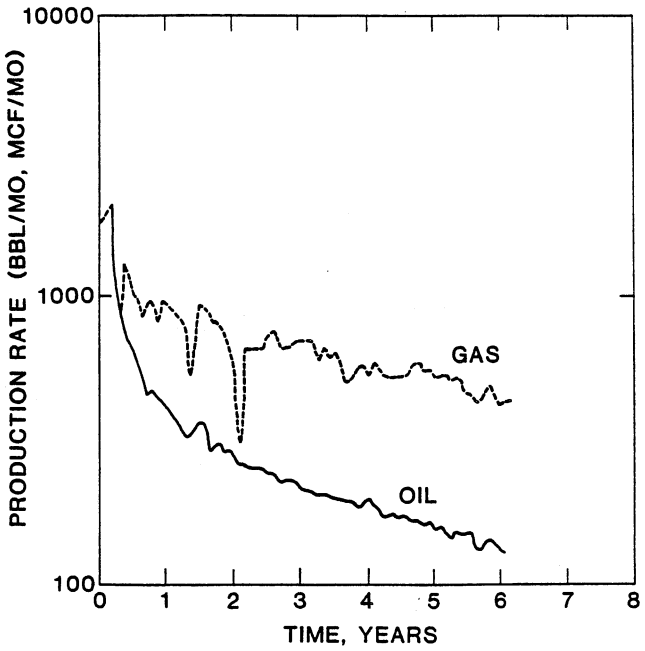

Fig. 24-Semilog plot of production history of Gentry and McCray's Oil Well Example No. 2 data.

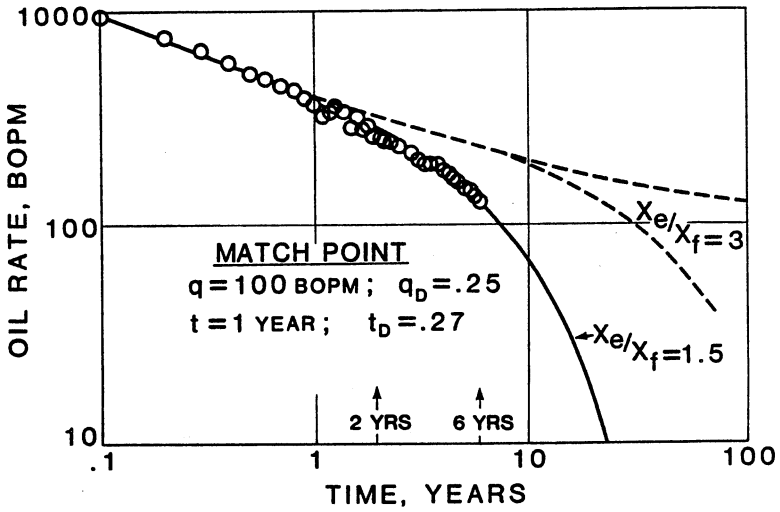

Fig. 25-Locke and Sawyer type-curve match of Gentry and McCray's Oil Well Example No. 2 data.

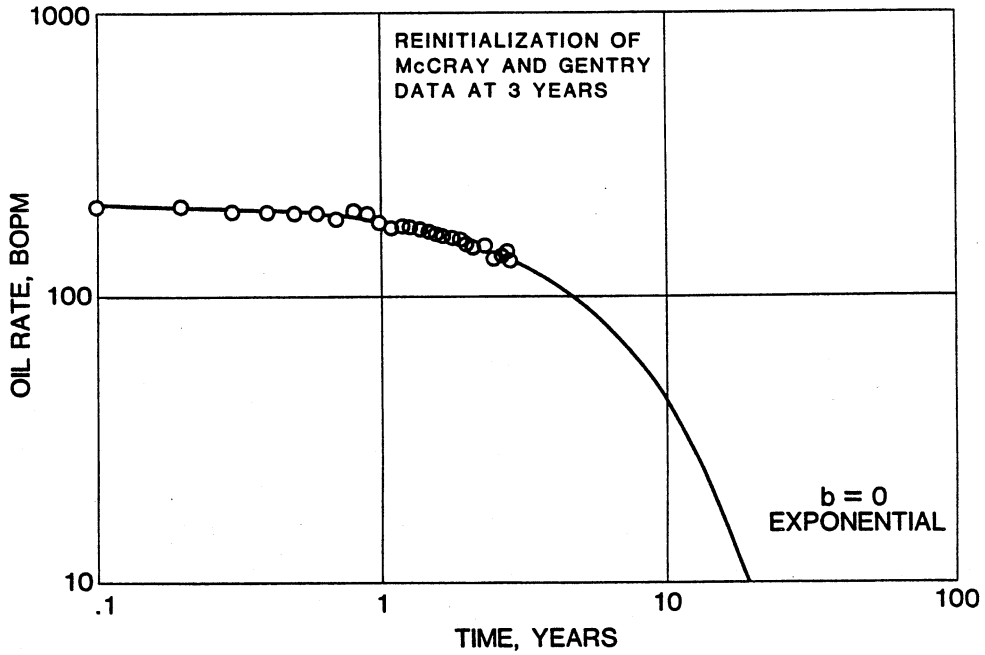

Fig. 26-Reinitialization of Gentry and McCroy's Oil Well Example No. 2 data at 3 years matched to an exponential, b=0.

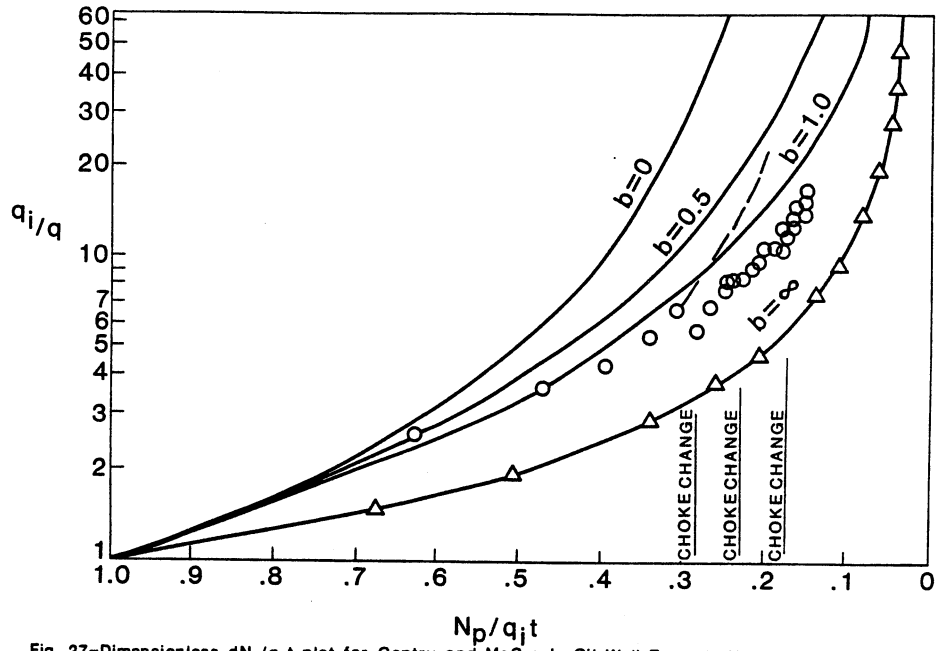

Fig. 27-Dimensionless $dN_q/q_i t$ plot for Gentry and McCray's Oil Well Example No. 2 data, indicating an apparent b between one and infinity.

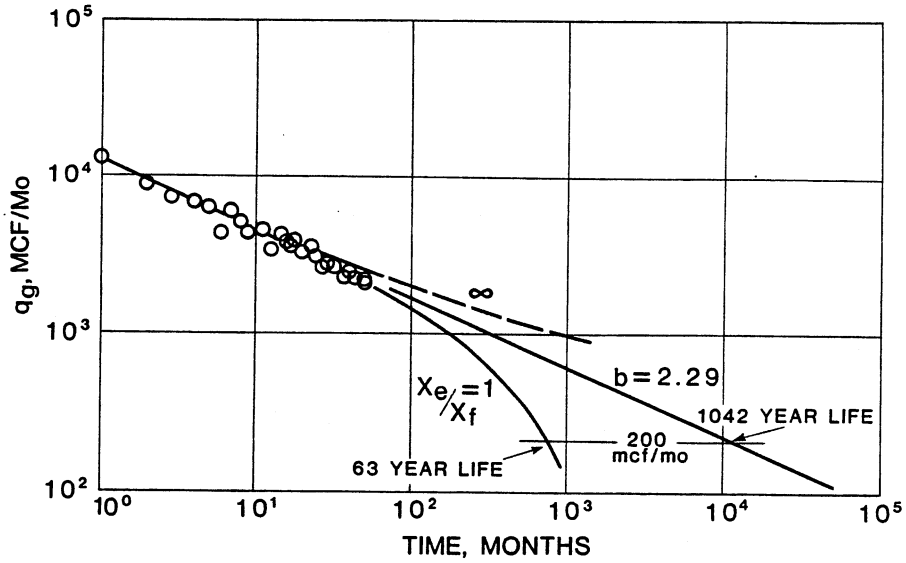

Fig. 28-Wattenberg field-well data matched to the Locke and Sawyer type curve and compared to a regression fit using an Arps equation with b=2.29.

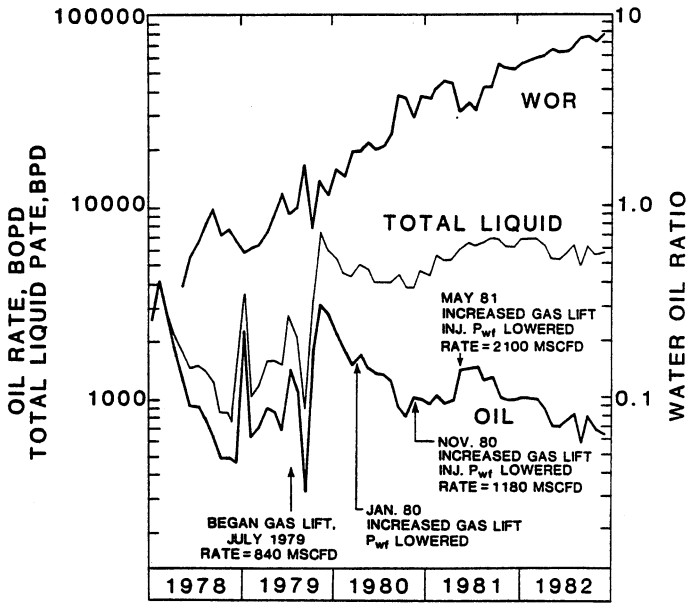

Fig. 29-Production performance of Field E.

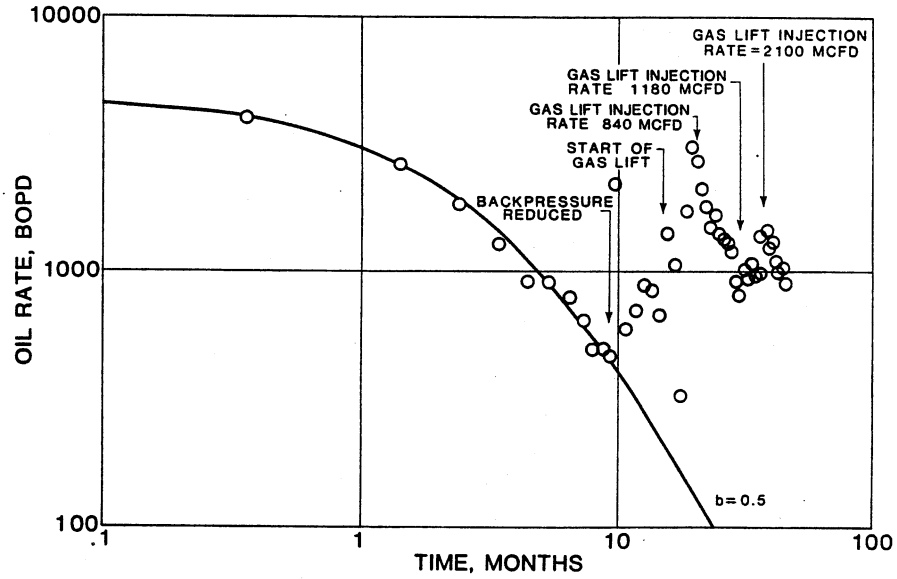

Fig. 30-Log rate vs. log time production performance plot of Field E.

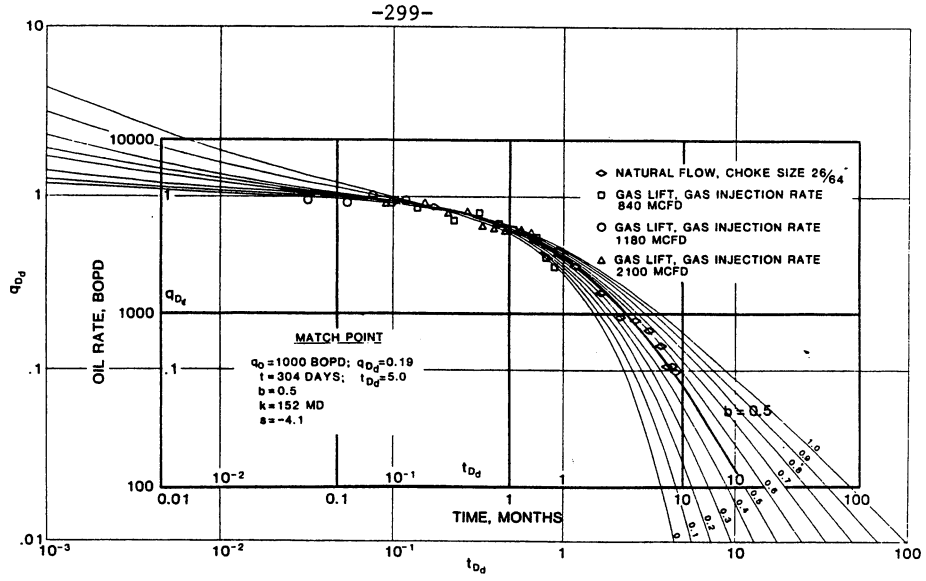

Fig. 31-Field E oil-rate-vs.-time data matched on the q_{dD}-t_{dD} type curve and the transfer of the q_{dD}-t_{dD} axes onto the real-time data plot.

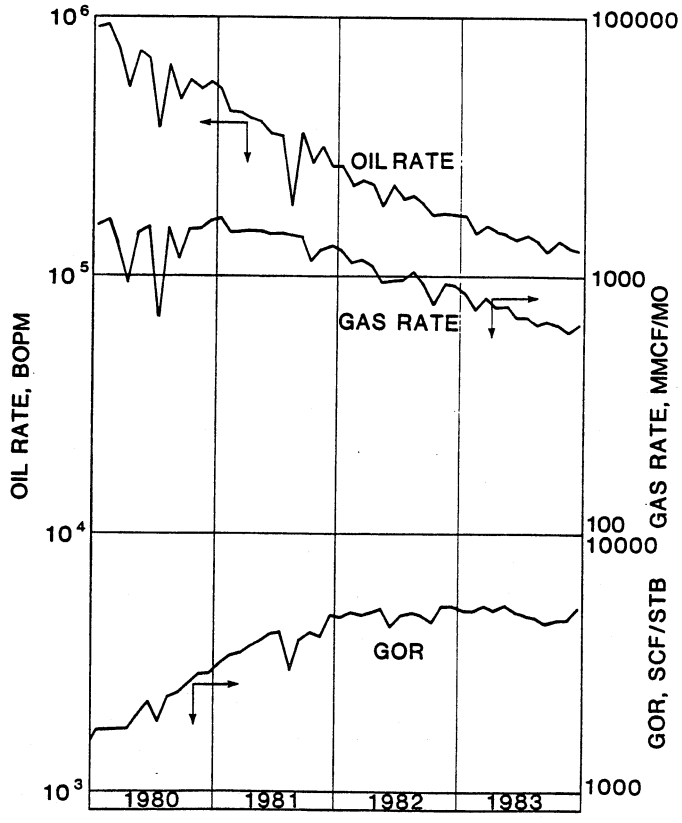

Fig. 32-Edda field production performance.

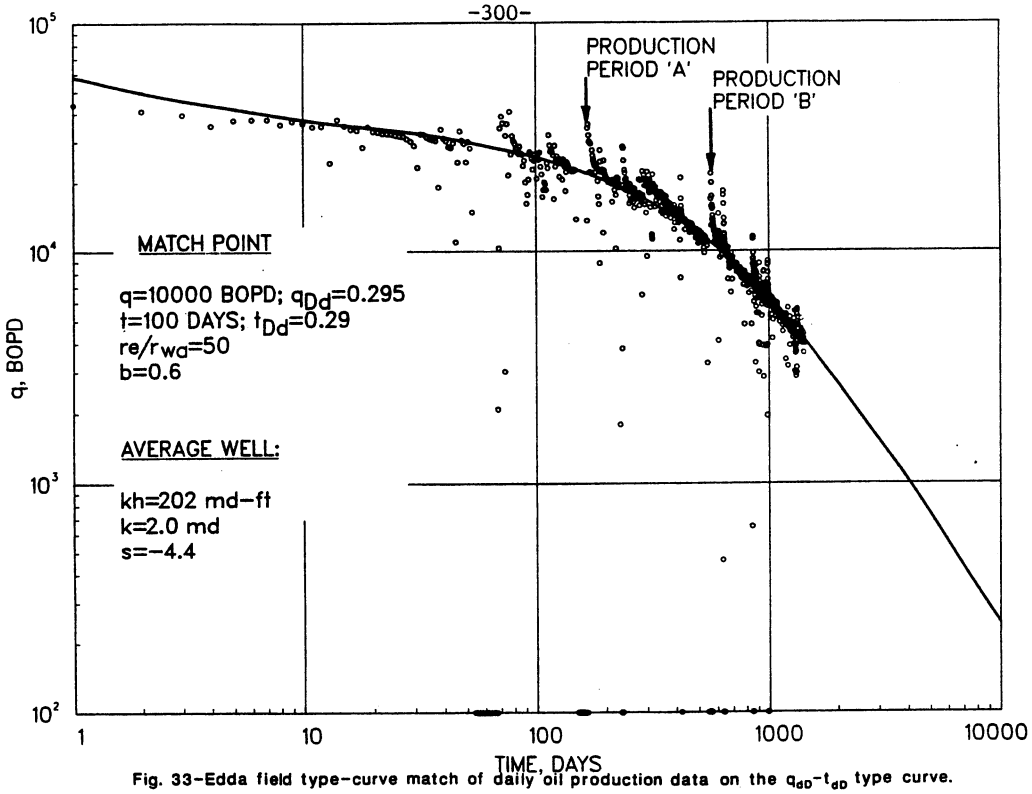

Fig. 33-Edda field type-curve match of daily oil production data on the q_{dD}-t_{dD} type curve.

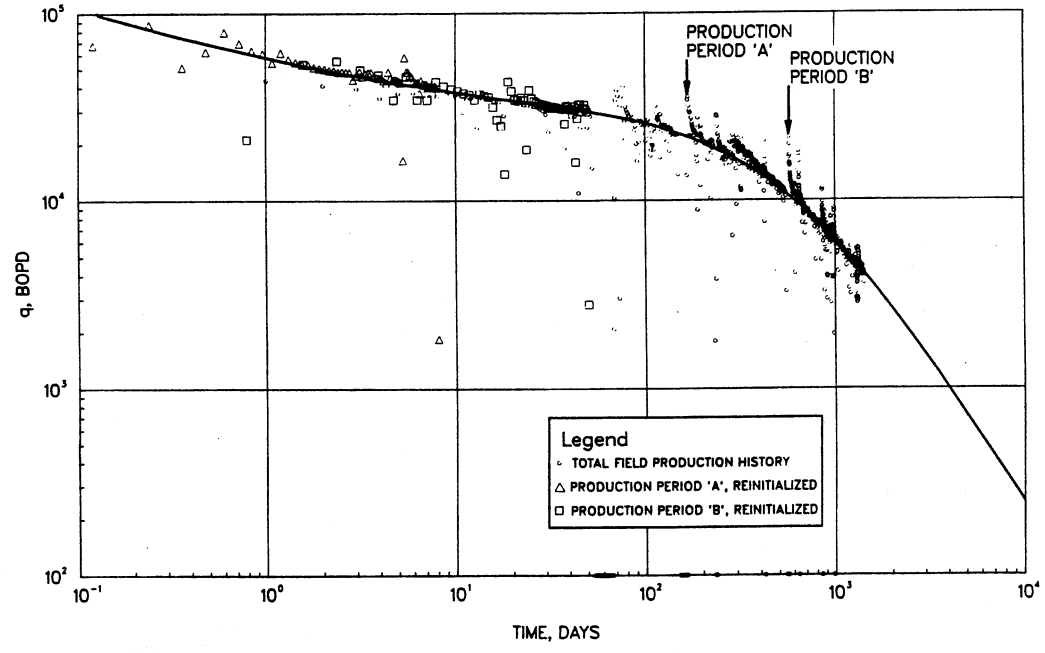

Fig. 34-Edda field- overlay of reinitialized production Periods A and B on the full-field, oil rate-time history.

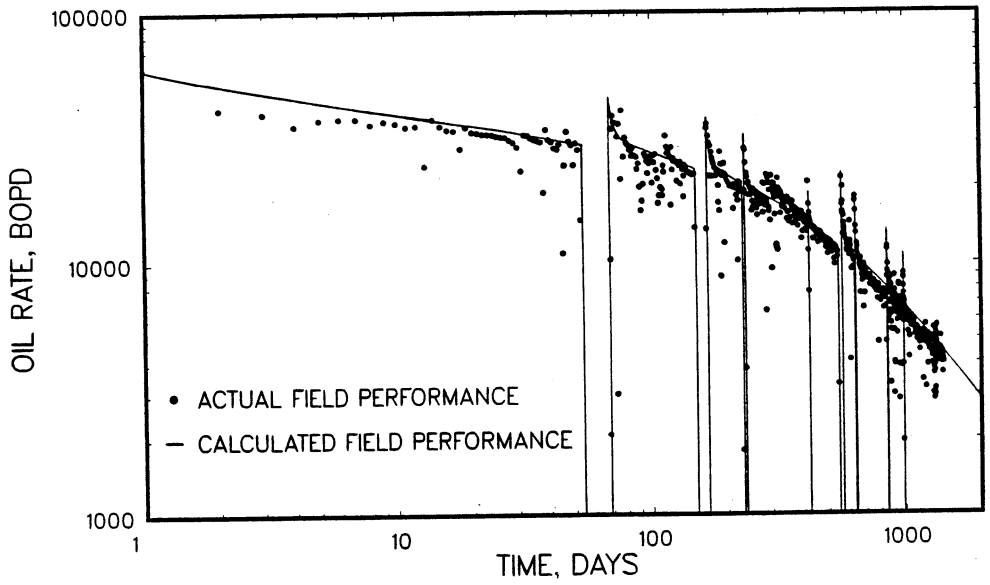

Fig. 35-Comparison of calculated Edda field performance based on the average well determined from the q_{dD}-t_{dD} type-curve match with actual field performance.

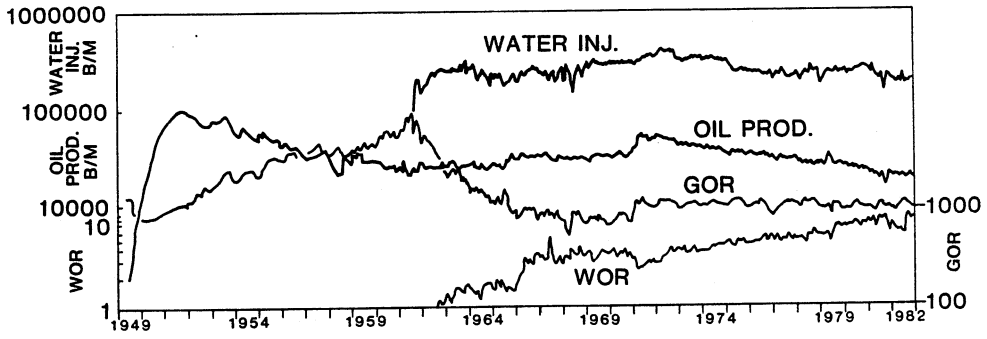

Fig. 36-Clyde Cowden lease-production performance.

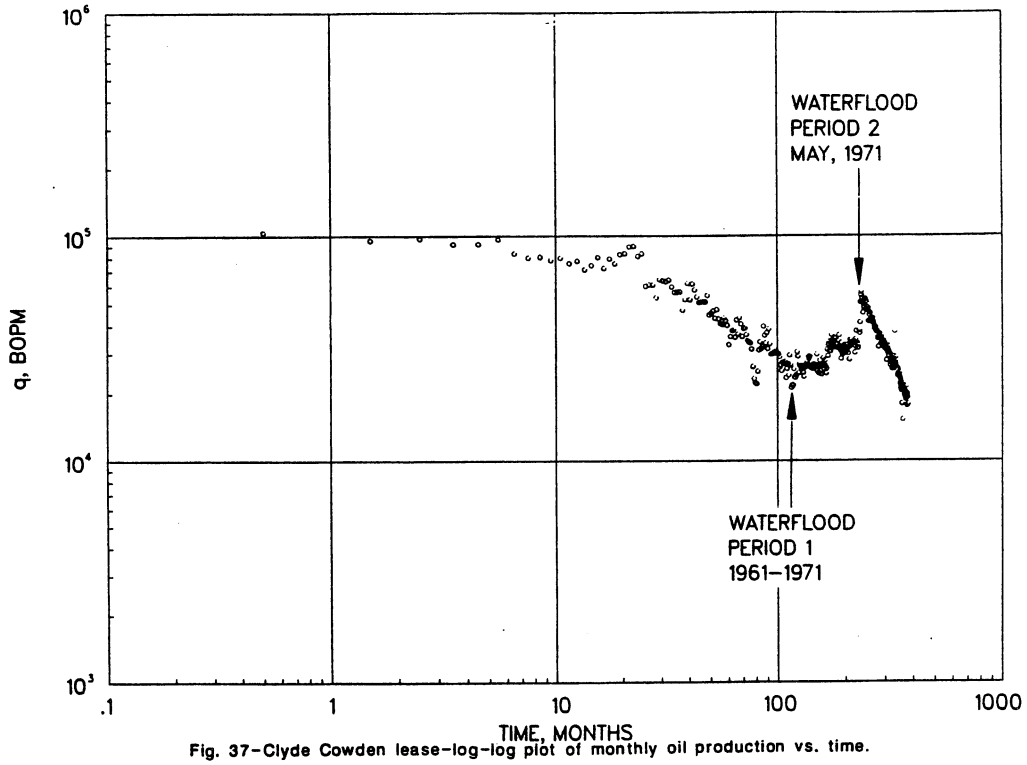

Fig. 37–Clyde Cowden lease–log–log plot of monthly oil production vs. time.

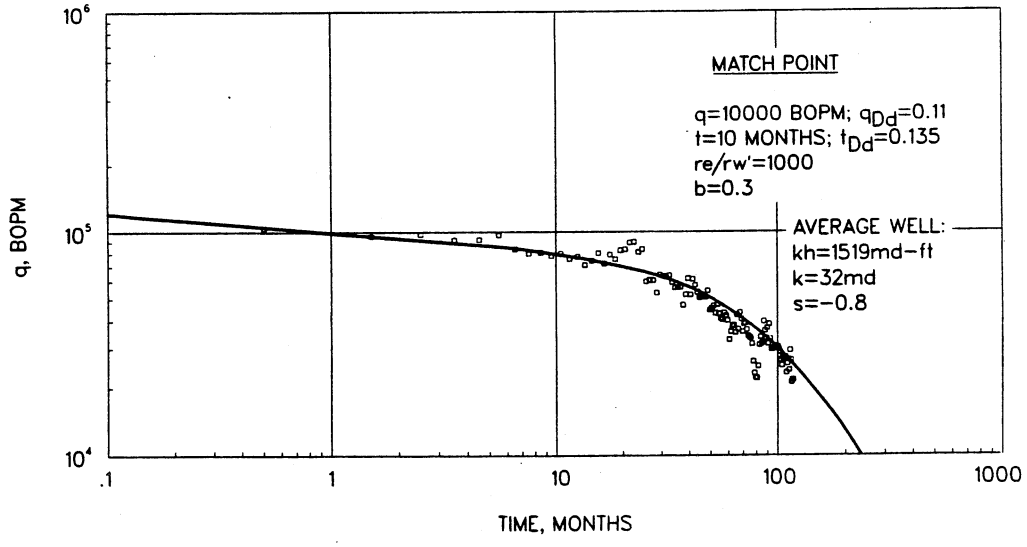

Fig. 38–Clyde Cowden lease–type–curve match of the primary production period.

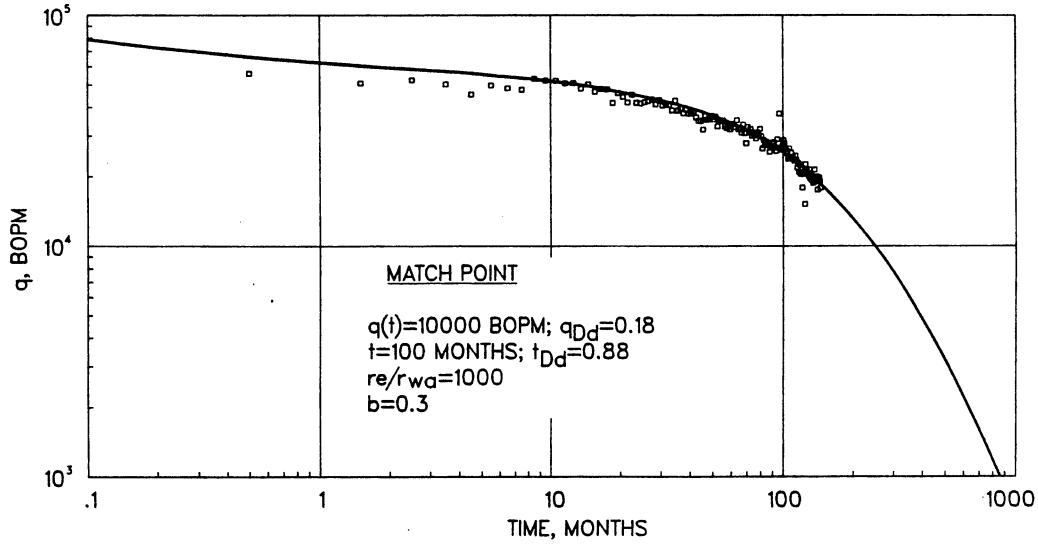

Fig. 39-Clyde Cowden lease-type-curve match of the reinitialized waterflood decline period.

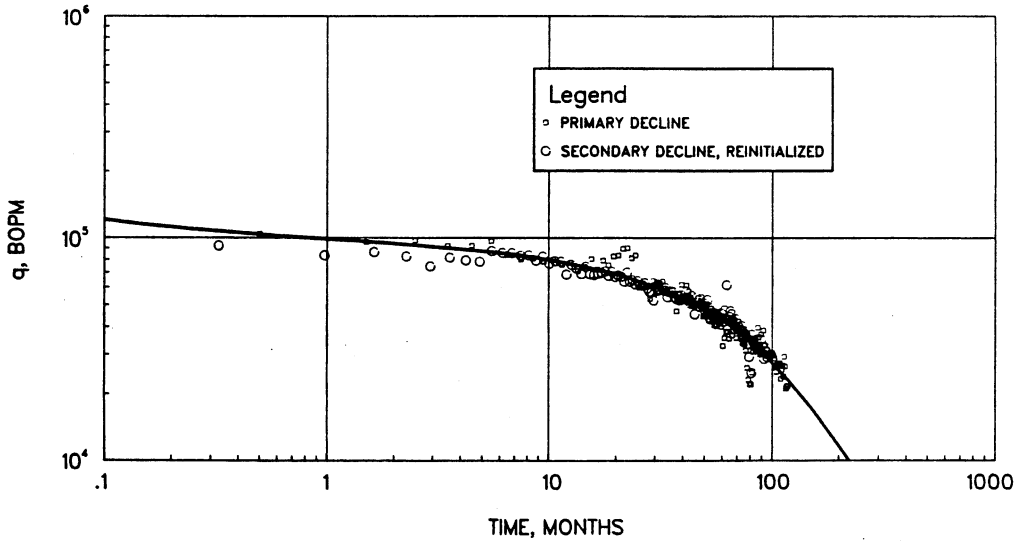

Fig. 40-Clyde Cowden lease-log-log overlay of primary and reinitialized waterflood periods on b=0.3.

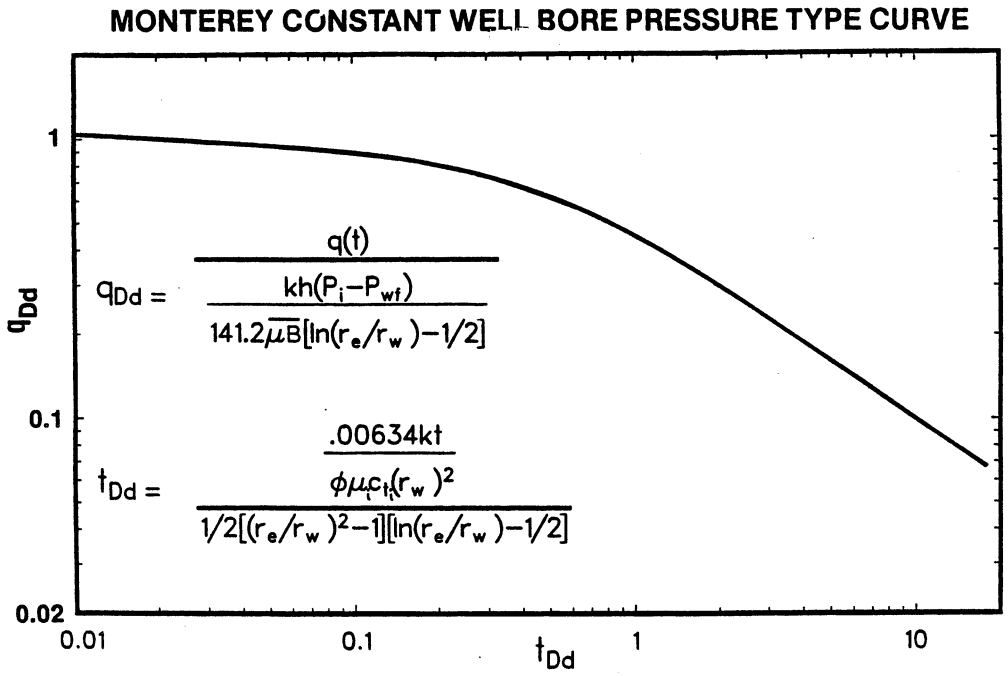

Fig. 41-Monterey constant-wellbore-pressure type curve.

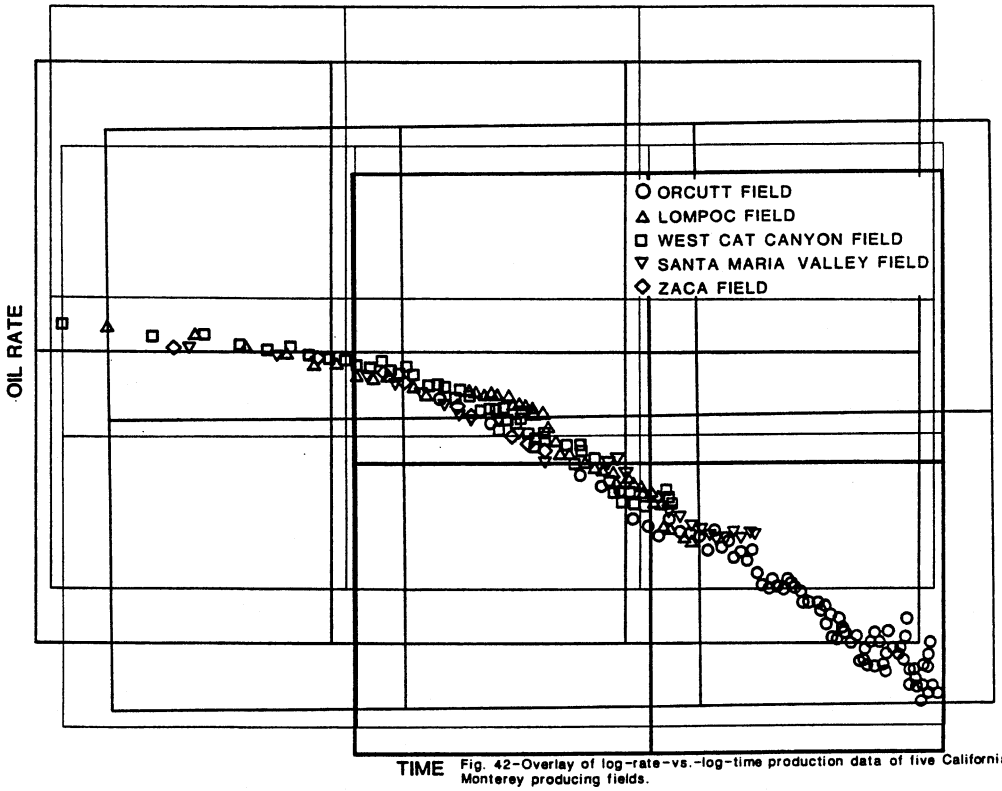

Fig. 42-Overlay of log-rate-vs.-log-time production data of five California Monterey producing fields.

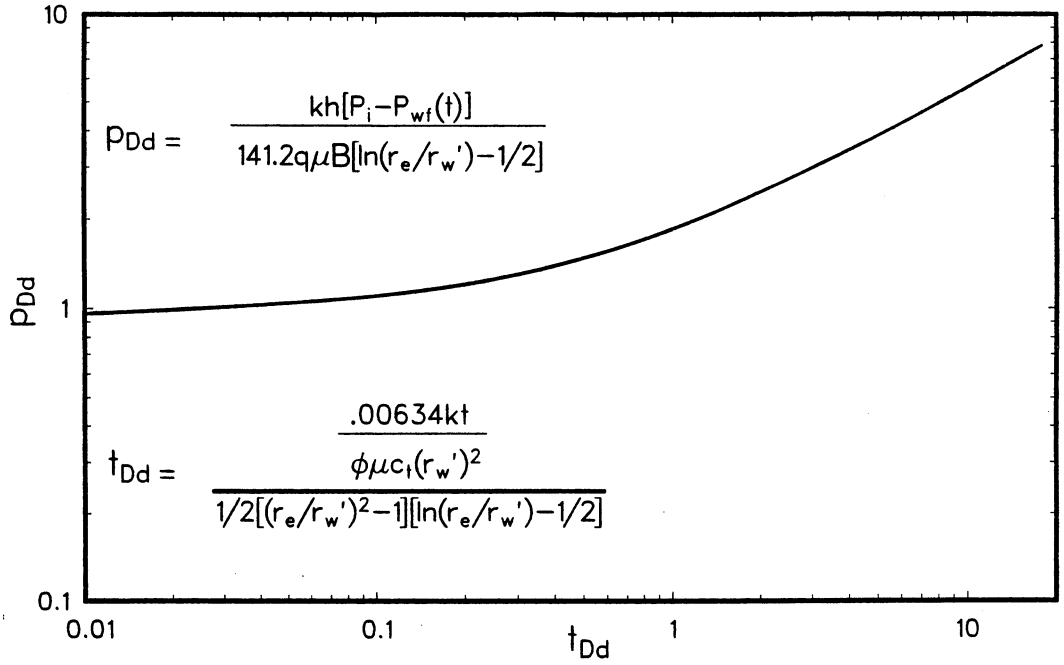

Fig. 43-Monterey constant-rate type curve.

SEMILOG PLOT OF THE MONTEREY CONSTANT WELLBORE PRESSURE SOLUTION

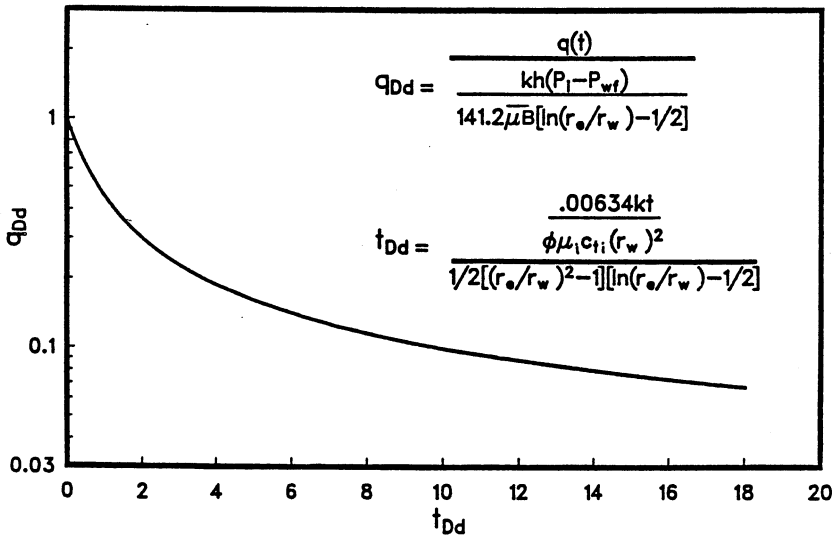

Fig. 44-Semilog plot of the Monterey constant-wellbore-pressure type curve.

RATE NORMALIZATION OF BUILDUP PRESSURE BY USING AFTERFLOW DATA

by

M. J. Fetkovich
M. E. Vienot

SPE, Phillips Petroleum Co.

SPE 12179

Original manuscript received in the Society of Petroleum Engineers office Oct. 5, 1983. Paper accepted for publication March 11, 1984. Revised manuscript received July 30, 1984. Paper first presented at the 1983 SPE Annual Technical Conference and Exhibition held in San Francisco Oct. 5-8.

RATE NORMALIZATION OF BUILDUP PRESSURE BY USING AFTERFLOW DATA

Summary

Field data indicate that in some instances significant afterflow occurs after a well is considered shut in. An analysis method for afterflow-dominated pressure buildup data is presented whereby the p_D - t_D model describing the transient behavior of the well can be directly obtained by matching a log-log plot of the rate-normalized pressure vs. time data to published type curves. The p_D - t_D model thus obtained allows a rigorous mathematical superposition analysis to be performed on the same data with results equivalent to those obtained from the normalized type-curve analysis.

This work demonstrates that rate normalization must be based on total afterflow rates, confirming with field data Perrine's assumption that total rate should be used in multiphase flow analyses. Dramatic changes in character are seen between the rate-normalized pressure vs. time and the conventional pressure vs. time log-log data plots for low permeability stimulated wells. Several field examples demonstrate the application of this simple and effective technique.

Introduction

Currently, wellbore storage type curves[1-4] based on the assumption of a constant wellbore storage coefficient are used to evaluate afterflow-dominated data from pressure alone. For pumping wells, the ability to calculate reliable buildup pressures and corresponding afterflow rates, along with the wellbore storage coefficient variation with time, has been reported in several papers.[5-9] More direct bottomhole measurements of afterflow and pressure buildup tests have been reported recently by Meunier et al.[10] In the U.S., wellbore storage effects often characterize pressure buildup tests because the majority of domestic wells are produced by rod pumps where afterflow dominates during the buildup. This type of completion can result in long periods of wellbore storage during test situations even for stimulated wells.

The first attempt to use both pressure and afterflow rate data was presented by Gladfelter et al.[5] in 1955. They suggested that the pressure rise after shut-in divided by the instantaneous change in rate caused by afterflow should be plotted vs. the logarithm of shut-in time. This resulted in a modified Miller-Dyes-Hutchinson (MDH) buildup plot. The validity of this approach was confirmed by Ramey[11] in 1965, and extended by him to include wellbore unloading effects during drawdown testing.

About this same time Winestock and Colpitts[12] proposed a similar rate normalization of pressure for drawdown analysis of gas during drawdown tests. Rate variations were not a result of wellbore storage effects but were more a result of a nearly constant wellbore pressure test condition. Their rate normalization of the pressure data was simply an attempt to make a constant rate analysis from essentially constant wellbore pressure data. A computer

study by Lee et al.[13] basically confirmed validity of the Winestock and Colpitts rate normalization analysis procedure. Additional discussion of the Gladfelter et al. and the Winestock and Colpitts normalization methods was given by Ramey[14] in 1976.

Rate-normalized type-curve plots of the Gladfelter et al. and Winestock and Colpitts example data show that after normalization virtually all the data were on the semilog straight line. Rate normalization linearized all the data in both instances. However, tests on low-permeability oil and gas wells with large negative skins often cannot be analyzed using their suggested rate-normalized pressure vs. logarithm of time plotting approach because the data may not reach the semilog straight line even after normalization.

A simple method of analyzing afterflow-dominated pressure buildup data is presented. The p_D - t_D model describing the transient behavior of the well may be obtained directly by matching a log-log plot of the rate-normalized pressure vs. time data to published type curves. The p_D - t_D model thus obtained allows a rigorous mathematical superposition analysis to be performed on the same data with results equivalent to those obtained from the normalized type-curve analysis.

Drawdown Rate Normalization Equations

Rate normalization techniques and procedures are best illustrated by first examining their application to drawdown data. Although the nature of the rate variation of drawdown data with time is different than that of afterflow rate variation, the end result is the same. Also, drawdown rate variations generally last much longer than afterflow rate variations.

The rate normalization equation given by Winestock and Colpitts for a gas well drawdown analysis can be written as

$$\frac{p_i^2 - p_{wfn}^2 - D'q_{gn}^2}{q_{gn}} = \frac{711(\mu_g z)T_r}{kh}\left[(\ln t_D + 0.809) + 2s\right], \quad . \; . \quad (1)$$

where

$$t_D = \frac{0.000264\ kt}{\phi\mu_g c_t r_w^2} \quad . \; . \; . \; . \; . \; . \; . \; . \; . \; . \; . \; . \; . \quad (2)$$

and the constant D' is related to the non-Darcy flow constant, D, by

$$D' = \frac{711(\mu_g Z)T_r}{kh}\ (2D). \quad . \; . \; . \; . \; . \; . \; . \; . \; . \; . \; . \quad (3)$$

Eq. 1 can be expressed in terms of the real gas pseudo-pressure, m(p), as

$$\frac{m(p_i) - m(p_{wfn}) - D'q_{gn}^2}{q_{gn}} = \frac{711T_r}{kh}\left[(\ln t_D + 0.809) + 2s\right], \quad . \; . \quad (4)$$

where

$$D' = \frac{711 T_r}{kh} (2D).$$

Winestock and Colpitts proposed a drawdown analysis technique wherein a plot of $(p_i^2 - p_{wfn}^2)/q_{gn}$ vs. logarithm of time is analyzed instead of a conventional plot of $p_i^2 - p_{wfn}^2$ vs. log t.

Eqs. 1 and 4 represent an approximation to superposition for a gradually changing flow rate condition. A rigorous superposition equation for any variation of rate was given by Odeh and Jones[15] with p_D being approximated by the logarithm of time as

$$\frac{p_i^2 - p_{wfn}^2 - D'q_{gn}^2}{q_{gn}} = \frac{711(\mu_g Z)T_r}{kh} \left\{ \frac{1}{q_{gn}} \left[\sum_{i=1}^{n} (q_{gi} - q_{gi} - 1) \cdot \ln(t_n - t_{i-1}) \right] + \ln \frac{k}{\phi \mu_g c_t r_w^2} - 7.432 + 2s \right\}. \quad (5)$$

A plot of

$$\frac{(p_i^2 - p_{wfn}^2)}{q_{gn}} \text{ vs. } \frac{1}{q_{gn}} \sum_{i=1}^{n} (q_{gi} - q_{gi-1}) \ln(t_n - t_{i-1})$$

should be linear, if $D' = 0$, with slope, m', and intercept, b, yielding kh and s, respectively. Flow capacity is evaluated from the slope, m', by

$$kh = \frac{711(\mu_g Z)T_r}{m'}, \quad (6)$$

and the skin from intercept b by

$$s = \frac{1}{2} \left(\frac{b}{m'} - \ln \frac{k}{\phi \mu_g c_t r_w^2} + 7.432 \right). \quad (7)$$

Odeh and Jones further recommend that if the plot bows, the data should be corrected for the quadratic effect $D'q^2$ until the plot is made linear. We demonstrate with a gas well drawdown example that an erroneous quadratic adjustment could be made if the logarithm of time approximation to p_D is used when not applicable, rather than using the correct $p_D - t_D$ model suggested by normalization.

A more general form of Eq. 5 in terms of $p_D - t_D$ after van Everdingen and Meyer[16] is

$$\frac{p_i - p_{wfn} - D'q_n^2}{q_n} = \frac{141.2\ \mu}{kh} \cdot \left\{ \frac{1}{q_n} \left[\sum_{i=1}^{n} (q_i - q_{i-1}) p_D (t_n - t_{i-1}) D \right] + s \right\}, \quad (8)$$

where

$$D' = \frac{141.2\ \mu}{kh} (D). \quad (9)$$

A plot of

$$\frac{p_i - p_{wfn}}{q_n} \text{ vs. } \frac{1}{q_n} \sum_{i=1}^{n} (q_i - q_{i-1}) p_D (t_n - t_{i-1}) D$$

should plot as a straight line if $D' = 0$, with slope m', from which kh can be evaluated by

$$kh = \frac{141.2\ \mu}{m'}, \quad (10)$$

and the skin from intercept b,

$$s = \frac{(kh)b}{141.2\ \mu} = \frac{b}{m'}. \quad (11)$$

Eq. 8 can be expressed in terms of the real gas pseudo-pressure as

$$\frac{m(p_i) - m(p_{wfn}) - D'q_{gn}^2}{q_{gn}} = \frac{1422T_r}{kh} \cdot \left\{ \frac{1}{q_{gn}} \left[\sum_{i=1}^{n} (q_{gi} - q_{gi-1}) p_D (t_n - t_{i-1}) D \right] + s \right\}, \quad (12)$$

which, if $D' = 0$, also should result in a straight line when plotted as

$$\frac{m(p_i) - m(p_{wfn})}{q_{gn}} \text{ vs. } \frac{1}{q_{gn}} \sum_{i=1}^{n} (q_{gi} - q_{gi-1}) p_D (t_n - t_{i-1}) D$$

with slope m' given by

$$m' = \frac{1422T_r}{kh}, \quad (13)$$

and intercept b equal to

$$b = \frac{1422T_r}{kh}(s). \quad \ldots\ldots\ldots\ldots\ldots\ldots \quad (14)$$

Solution of the superposition equation in terms of $p_D - t_D$ requires a trial-and-error calculation based on varying t_D/t. The initial estimate of t_D/t is normally obtained from a rate-normalized pressure type-curve analysis. The correct solution corresponds to that t_D/t yielding the minimum standard deviation between observed and backcalculated values of the rate-normalized pressure.

The first step in a varying rate drawdown analysis is to make a normalized log-log plot of $\Delta p/q$ vs. Δt to determine the correct $p_D - t_D$ model and whether a rate-normalized pressure vs. logarithm of time analysis can be performed.

Field Example of Drawdown Rate Normalization

Normalized Drawdown Analysis—Gas Well B. Gas Well B is a low-permeability gas well in West Virginia completed in the Onondega chert. It was hydraulically fractured with 62,000 gal [235 m^3] 3% gelled acid and 55,000 lbm [25 Mg] sand. After an 11-hour cleanup and an extended shut-in, a 72-hour drawdown followed by a 72-hour buildup test was conducted. Table 1 (from Ref. 17) shows both the drawdown pressure and rate data declining as a function of time. The test is neither a constant rate nor a constant wellbore pressure situation. Two methods of normalization are demonstrated with these data, rate-normalized pressure ($\Delta p/q$) for constant rate analysis and pressure-normalized rate ($q/\Delta p$) for constant wellbore pressure analysis.[17,18] Both techniques are presented to demonstrate the validity and utility of normalization in well test analysis.

Fig. 1 is a conventional pressure drawdown semilog plot in terms of real gas pseudopressure, m(p). A straight line was drawn through the last three points based on an "apparent" $\Delta m(p)$ vs. t type-curve match indicative of the beginning of a semilog straight line. Fig. 2 is a Winestock and Colpitts normalized pressure drawdown plot in terms of $\Delta m(p)/q_g$ vs. the logarithm of time. The data were not linearized using their suggested procedure. Note that the data have a continuously sweeping curve with no apparent straight-line section. This normalized plot is similar in shape to Winestock and Colpitt's unnormalized example data given in their paper.[12]

Examination of a rate-normalized log $\Delta m(p)/q_g$ vs. log t type-curve match (Fig. 3) shows that the semilog straight line section was just beginning at the end of the 72-hour drawdown test. This plot was matched on the infinite-conductivity vertical fracture solution. Using the slope through the last two points of the Winestock-Colpitts rate-normalized semilog plot, as indicated by the type-curve match, k = 0.038 md and skin s = -4.3 was obtained. This compares with k = 0.043 md and s = -4.3 (x_f = 46.5 ft [14 m]) for the rate-normalized pressure type-curve analysis.

If rate normalization of pressure is a valid method of analyzing gradual changes in rate to perform constant rate analysis, then pressure normalization

of rate should be valid for analyzing gradual changes in pressure to perform constant wellbore pressure analysis. Fig. 4 is a pressure-normalized rate, $q_g/\Delta m(p)$, vs. time type-curve plot of the same drawdown data. The data were fit to the infinite-conductivity vertical fracture constant wellbore pressure solution.[17] The constant wellbore pressure type-curve analysis yields $k = 0.039$ md and $x_f = 39.4$ ft [12 m] as compared with $k = 0.043$ md and $x_f = 46.5$ ft [14 m] from the constant rate type-curve analysis. These values compare well with those obtained from the Horner buildup test that followed (Table 2). It should be pointed out that pressure level and range being analyzed, this was expected.

Superposition Drawdown Analysis--Gas Well B. There seems to be doubt concerning the validity of normalization analysis since little use of the technique has appeared in recent literature. If a rigorous mathematical superposition analysis performed on the same data yields the same results as those obtained from the proper normalization analysis, we have validated the normalization approach through the use of field data.

Fig. 5 is an Odeh-Jones superposition plot of the drawdown data where the logarithm of time approximation to p_D is used. As expected, the data have the same continuously sweeping curve with no straight-line section that was seen on the Winestock and Colpitts logarithm of time plot (see Fig. 2). Recall that from the rate-normalized pressure type-curve match, only the last data point was found to be on the semilog straight-line portion; none of the data could be represented by a logarithm of time approach.

Fig. 6 represents a superposition analysis based on values of $p_D - t_D$ obtained from the infinite-conductivity vertical fracture solution. All points fall on a straight line. The calculated $p_D - t_D$ superposition value of permeability, $k = 0.043$ md, is the same as that calculated from the normalized type-curve analysis, whereas the fracture length, x_f, is 51.3 ft [15.6 m] compared with 46.5 ft [14.2 m]--essentially identical results.

If only a routine Odeh-Jones superposition plot based on the logarithm of time approximation to p_D were made, the data would next have to be corrected for the quadratic effect, $D'q^2$, in an attempt to linearize it finally. It is necessary to point out this effect on gas well drawdown data, as opposed to buildup data, since this same continuously sweeping curve can appear in afterflow-normalized buildup pressure data.

One further superposition example is given to illustrate that an exact physical flow model (such as the various vertical and horizontal fracture solutions) is not always required to determine reasonable reservoir parameters from transient analysis. Fig. 7 is a superposition plot based on values of $p_D - t_D$ from the original van Everdingen Hurst[19] solution with skin, $s = 0$ (Fig. 8). The concept of equivalent wellbore radius, r_w', is used to represent skin effect, particularly for the stimulated well situation. The results are close to those obtained from the other analyses (Table 2).

The extraordinary success we had using normalization techniques on oil and gas drawdown tests with both constant rate and constant wellbore pressure analyses prompted us to apply similar techniques to pressure buildup afterflow data.

Buildup Afterflow Rate Normalization Equations

The afterflow rate-normalized pressure equation proposed by Gladfelter et al.[5] to analyze pressure buildup data dominated by afterflow was given as

$$\frac{[p_{ws}(\Delta t) - p_{wf,s}]q_o}{q_o - q(\Delta t)} = \frac{70.6q_o\mu}{kh}\left[\ln\frac{0.000264\ k(\Delta t)}{\phi\mu c_t r_w^2} + 0.809 + 2s\right] \quad . \quad . \quad (15)$$

Cancelling q_o and expressing in the familiar logarithm base 10 form, we have their rate-normalized MDH equation

$$\frac{p_{ws}(\Delta t) - p_{wf,s}}{q_o - q(\Delta t)} = \frac{162.6\ \mu}{kh}\left[\log\frac{k(\Delta t)}{\phi\mu c_t r_w^2} - 3.23 + 0.87s\right] \quad . \quad . \quad (16)$$

Eq. 16 indicates that a plot of

$$\frac{p_{ws}(\Delta t) - p_{wf,s}}{q_o - q(\Delta t)} \quad \text{vs. } \log \Delta t$$

should be linear with slope equal to

$$m' = \frac{162.6\ \mu}{kh} \quad . \quad . \quad . \quad . \quad . \quad . \quad . \quad . \quad . \quad . \quad . \quad . \quad (17)$$

The skin is determined from

$$s = 1.1515\left\{\frac{p_{ws}(\Delta t) - p_{wf,s}}{m'[q_o - q(\Delta t)]} - \log\frac{k(\Delta t)}{\phi\mu c_t r_w^2} + 3.23\right\} \quad . \quad . \quad . \quad . \quad . \quad (18)$$

Note that buildup Eq. 16 is similar to Winestock and Colpitts' drawdown Eq. 1, except that the pressure difference now is normalized not by q but by Δq.

In 1974, Odeh and Jones[20] presented a method to analyze buildup afterflow rates following a constant rate semisteady state production period at rate q_o. The general equation describing the pressure change at any shut-in time, Δt_n, is

$$p_{ws}(\Delta t_n) - p_{wf,s} = \frac{70.6\ \mu}{kh}\left(\sum_{i=1}^{n} - (q_i - q_{i-1}) \cdot \ln(\Delta t_n - \Delta t_{i-1}) + (q_o - q_n)\left\{\ln\frac{0.000264k}{\phi\mu c_t r_w^2} + 0.809 + 2[s + D(q_o - q_n)]\right\}\right) \quad . \quad . \quad . \quad . \quad . \quad . \quad . \quad . \quad . \quad . \quad . \quad . \quad . \quad (19)$$

The linearized form of Eq. 19 is

$$\frac{p_{ws}(\Delta t_n) - p_{wf,s} - D'(q_o - q_n)^2}{q_o - q_n} = \frac{70.6\,\mu}{kh}\,\frac{-1}{q_o - q_n}\left[\sum_{i=1}^{n}(q_i - q_{i-1})\cdot \ln(\Delta t_n - \Delta t_{i-1})\right] + \ln\frac{0.000264k}{\phi\mu c_t r_w^2} + 0.809 + 2s, \quad \ldots\ldots \quad (20)$$

where

$$D' = \frac{70.6\,\mu}{kh}(2D) \quad \ldots\ldots\ldots\ldots \quad (21)$$

If non-Darcy flow is zero, a plot of

$$\frac{p_{ws}(\Delta t_n) - p_{wf,s}}{q_o - q_n} \text{ vs. } \frac{-1}{q_o - q_n}\sum_{i=1}^{n}(q_i - q_{i-1})\ln(\Delta t_n - \Delta t_{i-1})$$

should plot as a straight line with slope m', where

$$m' = \frac{70.6\,\mu}{kh}, \quad \ldots\ldots\ldots\ldots\ldots\ldots \quad (22)$$

and intercept b, from which the skin can be calculated, is given by

$$s = \frac{1}{2}\left(\frac{b}{m'} - \ln\frac{0.000264k}{\phi\mu c_t r_w^2} - 0.809\right). \quad \ldots\ldots\ldots \quad (23)$$

A more general form of Eq. 20, expressed in terms of dimensionless pressure and dimensionless time, is

$$\frac{p_{ws}(\Delta t_n) - p_{wf,s} - D'(q_o - q_n)2}{q_o - q_n} = \frac{141.2\,\mu}{kh}\,\frac{-1}{(q_o - q_n)}\left[\sum_{i=1}^{n}(q_i - q_{i-1})p_D(\Delta t_n - \Delta t_{i-1})_D\right] + s). \quad \ldots\ldots\ldots \quad (24)$$

When non-Darcy flow is zero, Eq. 24 should be linear when plotted as

$$\frac{p_{ws}(\Delta t_n) - p_{wf,s}}{q_o - q_n} \text{ vs. } \frac{-1}{q_o - q_i}\sum_{i=1}^{n}(q_i - q_{i-1})p_D(\Delta t_n - \Delta t_{i-1})_D$$

having slope

$$m' = \frac{141.2\ \mu}{kh} \quad \ldots\ldots\ldots\ldots\ldots\ldots\ldots (25)$$

and intercept

$$b = m' \cdot s. \quad \ldots\ldots\ldots\ldots\ldots\ldots\ldots (26)$$

As stated earlier concerning the solution of the drawdown superposition equation in terms of $p_D - t_D$, the solution of Eq. 24 also must be obtained through trial and error. The time conversion constant, t_D/t, which results in the minimum standard deviation between observed and backcalculated values of $[p_{ws}(\Delta t_n) - p_{wf,s}]/(q_o - q_n)$ is considered to give the best solution.

Note that if dimensionless time is defined in terms of fracture half-length, x_f, or equivalent wellbore radius, r_w', then t_D/t is used to determine x_f or r_w', from which skin can be obtained. If dimensionless time is defined in terms of x_f and if the plot of

$$\frac{p_{ws}(\Delta t_n) - p_{wf,s}}{q_o - q_n} \quad \text{vs.} \quad \frac{-1}{q_o - q_n} \sum_{i=1}^{n} (q_i - q_{i-1}) p_D(\Delta t_n - \Delta t_{i-1})_D$$

results in an intercept other than zero, an additional skin exists apart from that caused by stimulation. The composite skin is then the algebraic sum of the two skin values, $s_T = s_{xf} + s_d$.

To determine a $p_D - t_D$ model and whether semilog analysis techniques apply, it is necessary to make an afterflow-normalized pressure log-log plot of $\Delta p/\Delta q_t$ vs. Δt.

Field Examples of Afterflow Rate Normalization

Water Supply Well No. 1. An 18-hour buildup test was performed on a water well by using an acoustic liquid level monitor. The device, its use, and a review of field data obtained from it have been reported in the literature.[7,8] This single-phase flow test provided an excellent opportunity to apply the afterflow rate normalization procedure.

Fig. 9 is a log-log graph of both conventional Δp vs. Δt data and afterflow rate-normalized pressure data, $\Delta p/\Delta q$ vs. Δt. Early-time pressure data are clearly affected by wellbore storage. The conventional Δp vs. Δt log-log plot matched to the skin and storage type curve of Agarwal et al.,[1] at a $C_D = 1{,}000$ and skin = 0 (calculated $C_D = 826$), indicates the semilog straight line to begin about 200 minutes after shut-in. The permeability calculated from the match was 13.6 md.

The afterflow rate-normalized pressure log-log plot indicates that now all the normalized data fall on the semilog straight line. This is the expected result as demonstrated by Gladfelter et al.[5] However, as shown in later examples, afterflow rate normalization does not always normalize the data onto the semilog straight line. This at first was somewhat of a surprise--the idea of the well's real $p_D - t_D$ function being directly reflected by the

rate-normalized log-log data plot.

Fig. 10 is a graph of both conventional MDH plot of p_{ws} vs. log Δt and the afterflow rate-normalized pressure modified MDH plot of $\Delta p/\Delta q$ vs. log Δt. The conventional MDH plot has the usual character of a well with wellbore storage, with only a portion of the data existing on the semilog straight line. All the data on the $\Delta p/\Delta q$ modified MDH plot exist on the semilog straight line as was also indicated by the afterflow rate-normalized log-log data plot. The straight line drawn on the $\Delta p/\Delta q$ modified MDH plot was based on a least-squares regression fit of all the data. Permeability from the modified and conventional MDH plot is 13.1 and 13.7 md, respectively, and the skin is -0.2 and 0.

Since the afterflow rate-normalized pressure type-curve match indicated that all the data were on the semilog straight line, a superposition analysis based on the logarithm of time approximation to p_D was performed. As illustrated by Fig. 11 all the data were linearized by this superposition approach. The resulting permeability of 13.6 md and skin of zero are identical to the permeability and skin obtained from the normalized type-curve analysis. Table 3 compares results obtained from all analysis methods.

Brownscombe's Case 5. Case 5 of Ref. 8 was one of our early attempts to use normalization techniques with pressure buildup afterflow rate data. Fig. 12 is a log-log plot of both the conventional pressure Δp vs. Δt data and total fluid afterflow rate-normalized pressure data, $\Delta p/\Delta q_t$ vs. Δt. Note the dramatic change in early-time character from unit slope to half slope. The most interesting point observed is that the time to the start of the semilog straight line is satisfied by both the "1 1/2 log cycle rule" on the conventional Δp plot and the "double Δp rule" (p over q rule in this instance) on the afterflow rate-normalized plot. Total test duration was 77 hours with the time to the semilog straight line indicated to be 93 hours. The rate-normalized pressure type-curve match suggests the uniform-flux vertical fracture as a p_D - t_D model for a superposition analysis. Since none of the data lie on the semilog straight line portion of the vertical fracture solution, a logarithm of time approximation to p_D for analysis purposes would be invalid.

Fig. 13 is the total rate-normalized pressure type-curve plot along with its match point. Since a multiphase flow test is involved, the analysis procedure suggested by Perrine[21] and later by Martin[22] and Chu et al.[23] was necessary and gave a total value of $(kh/\mu)_t$ of 161 md-ft/cp [49 md·m/Pa·s] and a half fracture length, x_f, of 95 ft [29 m]. Note the early-time points approaching the half-slope portion from above, indicating a possible slightly positive skin on the fracture face.

Fig. 14 is a rate-normalized pressure MDH plot. A straight line was drawn through the last two points of the continuously sweeping data curve since none of the data were on the semilog straight line. The data were sufficiently close to the semilog straight line. The data were sufficiently close to the semilog straight line, although the calculated $(kh/\mu)_t$ of 156.4 md-ft/cp [47.6 md·m/Pa·s] compares well with that of 161.0 md-ft/cp [49 md·m/Pa·s] obtained from the normalized type-curve match. Similar results were obtained from a superposition plot (Fig. 15) where the logarithm of time approximation to p_D was used. Although no straight line existed, the data were close enough

to it so that a line through the last two points gave reasonable calculated results.

The question of a non-Darcy flow adjustment to linearize the data comes to mind since nearly all the afterflow is indicated to be gas. However, a superposition analysis based on $p_D - t_D$ from the vertical fracture solution as suggested by the rate-normalized type-curve analysis indicates that a non-Darcy flow adjustment is not required. Fig. 16 shows that the data are linearized when the correct $p_D - t_D$ model is used.

Table 4 compares results obtained from all the analysis methods. Note that results from the normalized type-curve analysis are essentially the same as those from the $p_D - t_D$ superposition, thus confirming with field data that normalization works for gradually changing rates.

Oil Well No. 1. Phillips' Oil Well No. 1 was hydraulically fractured in 1956 at initial completion and is currently under waterflood and on pump. A buildup test was run with an acoustic liquid level measuring device in Sept. 1979. All the pressure and afterflow data appearing in Table 5 come directly from the final test report. The wellbore storage coefficient has been calculated and added following the procedures appearing in Ref. 8 Table 6 lists pertinent reservoir and well data.

Fig. 17 is a log-log plot of the conventional Δp vs. Δt data and the total fluid afterflow rate-normalized pressure data, $\Delta p/\Delta q_t$ vs. Δt. As in the Case 5 example, the start of the semilog straight line is satisfied by the "1 1/2 cycle rule" on the conventional Δp plot and the "double Δp rule" on the afterflow rate-normalized pressure plot. Again, none of the data from the 67-hour buildup test are on the semilog straight line. The semilog straight line starts at approximately 100 hours (t_{Dxf} of 2.0 is used as start of semilog straight line).

Attempts at matching the conventional pressure vs. shut-in time log-log graph (Fig. 18) to any of the published wellbore storage type curves proved unsuccessful. However, the total fluid afterflow rate-normalized pressure vs. shut-in time log-log graph was matched to the uniform-flux vertical fracture solution (Fig. 19). Figs. 20 and 21 are log-log graphs of liquid and gas only afterflow rate-normalized pressure vs. shut-in time data. Neither of the individual phase normalization plots matched any of the published type curves. As expected for a multiphase-flow pressure-buildup test, a Perrine type of analysis would require that the normalization be based on total fluid (oil plus gas plus water) to obtain the correct $p_D - t_D$ model. In this case, the uniform-flux vertical fracture solution is matched with the total fluid normalization graph. This would appear to be a field data verification of the Perrine analysis method.

A rate-normalized pressure modified MDH plot (Fig. 22) was made and a straight line drawn through the last group of points of the continuously sweeping data curve. Similar sweeping curves with no clear straight-line sections were obtained on the conventional Horner plot (Fig. 23) and an Odeh-Jones logarithm of time superposition plot (Fig. 25). Straight lines drawn through the last group of points on each plot give reasonable calculated results.

Normally, in looking for a linear flow period, a pressure vs. $\sqrt{\Delta t}$ graph is made. In this case, a Δp vs. $\sqrt{\Delta t}$ plot does not result in a straight line but a total fluid afterflow rate-normalized pressure plot, $\Delta p/\Delta q_t$ vs. $\sqrt{\Delta t}$, does (see Fig. 24).

A $p_D - t_D$ superposition analysis based on the uniform flux vertical fracture solution, suggested by the rate normalized type-curve analysis, is shown in Fig. 26 for a t_D/t of 0.00034. A range of t_D/t values between 10^{-5} and 1 was investigated. A plot of t_D/t is identical to that obtained from the afterflow rate-normalized type-curve analysis.

Table 7 summarizes results from all methods of analysis. Note that the results obtained a normalized type-curve analysis and $p_D - t_D$ superposition are identical, again confirming with field data that normalization works.

On the basis of results from the $p_D - t_D$ or normalized type-curve analysis, the average reservoir pressure, $\bar{p}_R$, is calculated from an equation suggested by Ref. 20 but on a total fluid withdrawal basis:

$$\bar{p}_R = \frac{141.2 q_t \left[\ln \sqrt{\frac{2.25A}{C_A r_w^2}} + s \right]}{\left(\frac{kh}{\mu} \right)_t} + p_{wf,s} \quad \ldots\ldots (27)$$

For 40 acres [161 874 m^2], the well in the center of a square, $C_A = 30.883$ and $r_w = 0.31$ ft [0.095 m], we have

$$\bar{p}_R = \frac{141.2\ (328)[\ln\ (1{,}149.2) - 4.7]}{88.0} + 99.0$$

$$\bar{p}_R = 1235 + 99 = 1{,}334 \text{ psi } [9198 \text{ kPa}].$$

Conclusions

1. Normalization analysis techniques work for gradually changing rates and/or pressure data.

2. Normalized type-curve analysis identifies whether the semilog straight line exists and suggests the proper $p_D - t_D$ model for analysis purposes. Attempts at identifying linear flow, near wellbore permeability changes or boundaries, and special flow models such as dual porosity from early-time data affected by afterflow will require both accurate pressure and total afterflow fluid rate measurements.

3. The logarithm of time approximation to p_D for analysis of low-permeability stimulated wells is often invalid.

Nomenclature

b = intercept from superposition analysis
c_t = system total compressibility, psi^{-1} [kPa^{-1}]
C = wellbore storage coefficient, bbl/psi [m^3/kPa]
C_A = shape factor
C_D = dimensionless wellbore storage coefficient
D = non-darcy flow constant
D' = Dxm
h = formation thickness, ft [m]
k = permeability, md
m = slope of linear portion of conventional semilog plot, psi/cycle [kPa/cycle]
m' = slope of linear portion of a rate-normalized pressure semilog or superposition plot, psi/RB/D/cycle or psi/10^3 cu ft/D/cycle [kPa/res m^3/d/cycle] or [kPa/10^3 m^3/d/cycle]
$m(p)$ = real gas pseudopressure
p_i = initial pressure, psi [kPa]
p_{wf} = flowing bottomhole pressure, psi [kPa]
$p_{wf,s}$ = flowing bottomhole pressure just before shut-in, psi [kPa]
p_{ws} = shut-in bottomhole pressure, psi [kPa]
p_D = dimensionless pressure
$\bar{p}_R$ = average reservoir pressure, psi [kPa]
q_g = gas flow rate, 10^3 scf/D [10^3 std m^3/d] at 60°F [16°C] and 14.7 psia [101.4 kPa]
q_i = flow rate at the ith time period during a shut-in, RB/D [res m^3/d]
q_l = liquid rate, RB/D [res m^3/d]
q_n = flow rate during nth rate period, RB/D or Mscfd [res m^3/d] or [10^3 std m^3/d]
q_o = flow rate prior to shut-in, RB/D [res m^3/d]
q_t = total rate--gas and liquid, RB/D [res m^3/d]
$q(\Delta t)$ = afterflow rate at time Δt, RB/D [res m^3/d]
q_D = dimensionless flow rate
r_w = wellbore radius, ft [m]
r_w' = equivalent wellbore radius, ft [m]
s = skin factor, dimensionless
s_d = skin factor due to damage, dimensionless
s_{xf} = skin factor due to stimulation, dimensionless
t = time, hours
t_D = dimensionless time
t_{Dxf} = dimensionless time based on half-fracture length
t_H = Horner producing time
Δt = shut-in time, hours
T_r = reservoir temperature, °F [°C]
x_f = half-fracture length, ft [m]
z = gas deviation factor
μ = oil viscosity, cp [Pa·s]
ϕ = porosity, fraction

Subscripts

g = gas
i = time to the ith interval in a superposition analysis
l = liquid
n = time to the nth interval in a superposition analysis
t = total
w = wellbore

Acknowledgment

We wish to thank the Phillips Petroleum Co. for permission to publish this paper.

References

1. Agarwal, R. G., Al-Hussainy, R., and Ramey, H. J. Jr.: "An Investigation of Wellbore Storage and Skin Effect in Unsteady Liquid Flow: I. Analytical Treatment," Soc. Pet. Eng. J. (Sept. 1970) 279-90; Trans., AIME, 249.

2. McKinley, R. M.: "Wellbore Transmissibility From Afterflow Dominated Pressure Buildup Data," J. Pet. Tech. (July 1971) 863-72; Trans., AIME, 251.

3. Earlougher, R. C. Jr. and Kersch, K. M.: "Field Examples of Automatic Transient Test Analysis," J. Pet. Tech. (Oct. 1972) 1271-77.

4. Gringarten, Alain C. et al.: "A Comparison Between Different Skin and Wellbore Storage Type-Curves for Early-Time Transient Analysis," paper SPE 8205 presented at the 1979 SPE Annual Technical Conference and Exhibition, Las Vegas, Sept. 23-26.

5. Gladfelter, R. E., Tracy, G. W., and Wilsey, L. E.: "Selecting Wells Which Will Respond to Production-Stimulation Treatment," Drill. and Prod. Prac., API, Dallas (1955) 117-28.

6. Wilder, J. and Brownscombe, E. R.: "New Diagnostic Survey Improves Performance," Pet. Eng. (Jan. 1977) 58-73.

7. Godbey, J. K. and Dimon, C. A.: "The Automatic Liquid Level Monitor for Pumping Wells, "J. Pet. Tech. (Aug. 1977) 1019-24.

8. Brownscombe, E. R.: "Afterflows and Buildup Interpretation of Pumping Wells," J. Pet. Tech. (Feb. 1982) 397-405.

9. Bishop, D. F.: "Analysis of Pressure Buildups Taken from Fluid Level Entry--Lower Tyler Sands, Central Montana," paper SPE 10888 presented at the 1982 SPE Rocky Mountain Regional Meeting, Billings, MT, May 19-21.

10. Meunier, D., Wittman, M. J., and Stewart, G.: "Interpretation of Pressure Buildup Test Using In-Situ Measurement of Afterflow," paper SPE 11463 presented at the 1983 SPE Middle East Oil Technical Conference and Exhibition, Manama, Bahrain, March 14-17.

11. Ramey, H. J. Jr.: "Non-Darcy Flow and Wellbore Storage Effects in Pressure Build-Up and Drawdown of Gas Wells, "J. Pet. Tech. (Feb. 1965) 223-33; Trans., AIME, 234.

12. Winestock, A. G. and Colpitts, G. P.: "Advances in Estimating Gas Well Deliverability," J. Cdn. Pet. Tech. (July-Sept. 1965) 111-19.

13. Lee, W. J., Harrell, R. R., and McCain, W. D.: "Analysis Procedure for Variable-Rate Pressure Drawdown Data," J. Pet. Tech. (Jan. 1975) 115-16.

14. Ramey, H. J. Jr.: "Verification of the Gladfelter-Tracey-Wilsey Concept for Wellbore Storage-Dominated Transient Pressures During Production," J. Cdn. Pet. Tehc. (April-June 1976) 84-85.

15. Odeh, A. S. and Jones, L. G.: "Pressure Drawdown Analysis, Variable-Rate Case," J. Pet. Tech. (Aug. 1965) 960-64; Trans., AIME, 234.

16. van Everdingen, A. F. and Meyer, L. J.: "Analysis of Buildup Curves Obtained After Well Treatment," J. Pet. Tech. (April 1971) 513-24; Trans., AIME, 251.

17. Fetkovich, M. J. and Thrasher, T. S.: "Constant Well Pressure Testing and Analysis in Low Permeability Reservoirs," paper SPE 7928 presented at the 1979 SPE Symposium on Low Permeability Gas Reservoirs, Denver, May 20-22.

18. Fetkovich, M. J.: "Decline Curve Analysis Using Type Curves," J. Pet. Tech. (June 1980) 1065-77.

19. van Everdingen, A. F. and Hurst, W.: "The Application of the Laplace Transformation of Flow Problems in Reservoirs," Trans., AIME (1949) 186, 305-24.

20. Odeh, A. S. and Jones, L. G.: "Two-Rate Flow Test, Variable-Rate Case-Application to Gas-Lift and Pumping Wells," J. Pet. Tech. (Jan. 1974) 93-99; Trans., AIME, 257.

21. Perrine, R. L.: "Analysis of Pressure Build-up Curves," Drill. and Prod. Prac., API, Dallas (1956) 482-509.

22. Martin, John C.: "Simplified Equations of Flow in Gas Drive Reservoirs and the Theoretical Foundation of Multiphase Pressure Buildup Analyses," Trans., AIME (1959) 216, 309-11.

23. Chu, W. C., Reynolds, A. C. and Raghavan, R. A.: "Pressure Transient Analysis of Two-Phase Flow Problems," paper SPE 10223 presented at the 1981 SPE Annual Technical Conference and Exhibition, San Antonio, Oct. 4-7.

SI Metric Conversion Factors

acre	x	4.046 873	E+03	= m^2
^oAPI		141.5/(131.5 + ^oAPI)		= g/cm^3
bbl	x	1.589 873	E-01	= m^3
cp	x	1.0*	E-03	= Pa·s
cu ft	x	2.831 685	E-02	= m^3
ft	x	3.048*	E-01	= m
in	x	2.54*	E+00	= cm
psi	x	6.894 757	E+00	= kPa
psi^2	x	4.753 8	E+01	= kPa^2

* Conversion factor is exact.

TABLE 1

WEST VIRGINIA GAS WELL B, 72-HOUR DRAWDOWN DATA

Time (hours)	p_{wf} (psia)	Gas Rate (10^3 scf/D)	m(p) (10^6 psia^2/cp)	Δm(p) (10^6 psia^2/cp)	Δm(p)/q (10^3 psia^2/cp Mscfd)
0.0	4,185	0	1202.50	0	0
0.25	4,079	1,757	1153.95	48.55	27.63
0.75	4,025	1,468	1129.32	73.18	49.85
1.00	4,000	1,482	1117.95	84.55	57.05
2.00	3,926	1,494	1084.38	118.12	79.06
3.00	3,888	1,443	1067.20	135.30	93.76
6.00	3,794	1,443	1024.91	177.60	123.07
24.00	3,650	1,141	960.73	241.80	211.89
48.00	3,562	1,054	921.90	280.60	266.22
72.00	3,478	1,019	885.14	317.36	311.44

TABLE 2

WEST VIRGINIA GAS WELL B, SUMMARY OF ANALYSIS RESULTS

	kh (md-ft)	k (md)	Skin s	x_f (ft)
Conventional m(p) semilog	6.67	0.064	-4.0	-
Winestock-Colpitts graph (straight line through last two points)	4.03	0.038	-4.3	-
Δm(p)/q vs. t, log-log graph, infinite conductivity vertical fracture constant rate solution	4.50	0.043	-4.3	49.6
q/Δm(p) vs. t, log-log graph, infinite conductivity vertical fracture constant wellbore pressure solution	4.09	0.039	-4.0	39.4
Superposition based on logarithm of time approximation to $p_D - t_D$ (straight line through last two points only)	4.00	0.038	-4.4	-
Superposition based on ($p_D - t_D$), infinite conductivity vertical fracture constant rate solution	4.50	0.043	-4.3	51.3
Superposition based on ($p_D - t_D$), van Everdingen and Hurst, s = 0 constant rate solution	4.09	0.039	-4.5	-
Horner buildup analysis	4.52	0.043	-4.3	-

TABLE 3

WATER SUPPLY WELL NO. 1, SUMMARY OF RESULTS

	k (md)	Skin s
Wellbore storage type curve	13.6	0
Δp vs. log Δt MDH graph	13.7	0
$\Delta p/\Delta q$ vs. log Δt, modified MDH	13.1	-0.2
$\Delta p/\Delta q$ vs. Δt log-log graph Agarwal et al., skin and storage type curve	13.5	0
Superposition based on logarithm of time approximation to $p_D - t_D$ (straight line through all points)	13.6	0

TABLE 4

CASE 5 OF REF. 8, SUMMARY OF BUILDUP ANALYSIS RESULTS

	$\left(\frac{kh}{\mu}\right)_t$ (md-ft/cp)	$\left(\frac{k}{\mu}\right)_t$ (md/cp)	Skin s	x_f (ft)
Log $\Delta p/\Delta q_t$ vs. log Δt graph, uniform flux vertical fracture constant rate solution	161.0	4.47	-5.1	95.4
$\Delta p/\Delta q_t$ vs. log Δt, MDH graph (straight line through last two points)	156.4	4.34	-5.2	-
Superposition based on logarithm of time approximation to $p_D - t_D$ (straight line through last two points)	165.3	4.59	-5.2	-
Superposition based on ($p_D - t_D$), uniform-flux vertical fracture constant rate solution	163.4	4.54	-5.2	105

TABLE 5

OIL WELL NO. 1 TEST DATA

Shut-in Time Δt (minutes)	Liquid Level (ft)	Pressure		Afterflow Rates			Δp (psi)	$\left(\frac{\Delta p}{\Delta q}\right)_t$ (psi/RB/D)	Wellbore Storage Coefficient (bbl/psi)
		Surface (psi)	Bottomhole (psi)	Gas q_g (RB/D)	Liquid q_l (RB/D)	Total q_t (RB/D)			
0	7,277	40.9	99	257	71	328	0	0.0	0.0
3	7,269	41.3	103	229	59	288	4	0.100	0.161
5	7,263	41.5	105	219	59	278	6	0.120	0.197
10	7,248	42.1	111	202	60	262	12	0.182	0.156
15	7,234	42.8	116	183	61	244	17	0.202	0.176
20	7,219	43.4	122	168	61	229	23	0.232	0.137
25	7,205	43.9	128	154	62	216	29	0.259	0.129
30	7,190	44.5	133	142	62	204	34	0.274	0.146
35	7,176	45.0	139	131	63	194	40	0.299	0.115
40	7,161	45.6	145	122	63	185	46	0.322	0.110
45	7,147	46.1	151	112	64	176	52	0.342	0.105
50	7,132	46.6	156	105	64	169	57	0.358	0.120
55	7,118	47.1	162	98	64	162	63	0.380	0.094
60	7,103	47.6	168	91	65	156	69	0.401	0.092
70	7,074	48.6	180	82	65	147	81	0.448	0.088
80	7,045	49.5	192	72	66	138	93	0.489	0.083
90	7,019	50.4	202	67	61	128	103	0.515	0.092
100	6,994	51.3	212	62	57	119	113	0.541	0.086
110	6,970	52.1	222	58	55	113	123	0.572	0.081
120	6,948	52.9	231	55	50	105	132	0.592	0.084
173	6,851	56.8	272	41	43	84	173	0.709	0.085
236	6,756	60.5	315	27	36	63	216	0.815	0.075
308	6,665	64.0	356	19	31	50	257	0.924	0.069
390	6,579	67.5	395	15	26	41	296	1.031	0.066
583	6,413	74.3	472	9	20	29	373	1.247	0.061
694	6,341	77.4	505	7	16	23	406	1.331	0.061
814	6,274	80.4	536	6	14	20	437	1.419	0.058
945	6,213	83.3	564	5	12	17	465	1.495	0.060
1,034	6,155	86.1	591	4	11	15	492	1.572	0.037
1,234	6,098	88.5	621	3	10	13	522	1.657	0.065
1,393	6,041	90.6	648	2	9	11	549	1.732	0.049
1,562	5,983	92.7	674	2	9	11	575	1.814	0.050
1,741	5,926	94.7	700	2	8	10	601	1.890	0.050
1,929	5,868	96.6	726	1	8	9	627	1.966	0.048
2,127	5,811	98.4	752	1	8	9	653	2.047	0.048
2,334	5,754	100.3	777	0	8	8	678	2.119	0.049
2,552	5,696	102.1	830	0	7	8	704	2.200	0.047
2,778	5,639	103.8	828	0	6	7	729	2.271	0.047
3,015	5,582	105.6	853	1	6	7	754	2.349	0.046
3,180	5,547	106.8	867	0	5	6	768	2.385	0.053
3,240	5,535	107.2	873	1	5	6	774	2.404	0.042
3,300	5,523	107.6	878	1	5	6	779	2.419	0.050
3,360	5,511	108.0	883	1	5	6	784	2.435	0.050
3,420	5,499	108.4	888	1	5	6	789	2.450	0.050
3,480	5,488	108.6	899	0	5	5	800	2.477	0.021
3,540	5,477	108.9	904	0	5	5	805	2.492	0.042
3,600	5,466	109.1	908	0	5	5	809	2.505	0.052
3,660	5,455	109.3	913	0	5	5	814	2.520	0.042
3,720	5,444	109.5	917	0	5	5	818	2.533	0.052
3,780	5,434	109.7	922	0	5	5	823	2.548	0.042
3,840	5,423	109.9	926	0	5	5	827	2.560	0.052
3,900	5,413	110.1	930	0	4	5	831	2.573	0.052
3,960	5,493	110.4	935	0	4	4	836	2.580	0.038
4,020	5,383	110.5	939	0		4	840	2.593	0.042

TABLE 6

OIL WELL NO. 1 RESERVOIR PARAMETERS

Porosity, %	14.0
Thickness, ft	47.0
Wellbore radius, ft	0.31
Spacing, acres	40.0
System compressibility, psi^{-1}	20×10^{-6}
Reservoir temperature, ^{o}F	123.0
Oil gravity, ^{o}API	35.0
Oil viscosity, cp	3.18
Water viscosity, cp	0.56
Gas viscosity, cp	0.0155
Water cut, %	30.0
Casing ID, in.	4.953
Tubing OD, in.	2.375

TABLE 7

OIL WELL NO. 1, SUMMARY OF ANALYSIS RESULTS

	$\left(\frac{kh}{\mu}\right)_t$ (md-ft/cp)	Skin s	x_f (ft)
Wellbore storage type curve	no match obtained on published type curves		
Horner buildup analysis	76.2	-4.8	-
$\Delta p/\Delta q_t$ vs. log Δt, modified MDH analysis	85.6	-4.7	-
$\Delta p/\Delta q_t$ vs. Δt log-log graph, uniform-flux vertical fracture constant rate solution	87.5	-4.7	93.4
Superposition based on logarithm of time approximation to p_D - t_D (straight line through last points)	85.1	-4.6	-
Superposition based on p_D - t_D, uniform-flux vertical fracture constant rate solution	88.0	-4.7	93.1

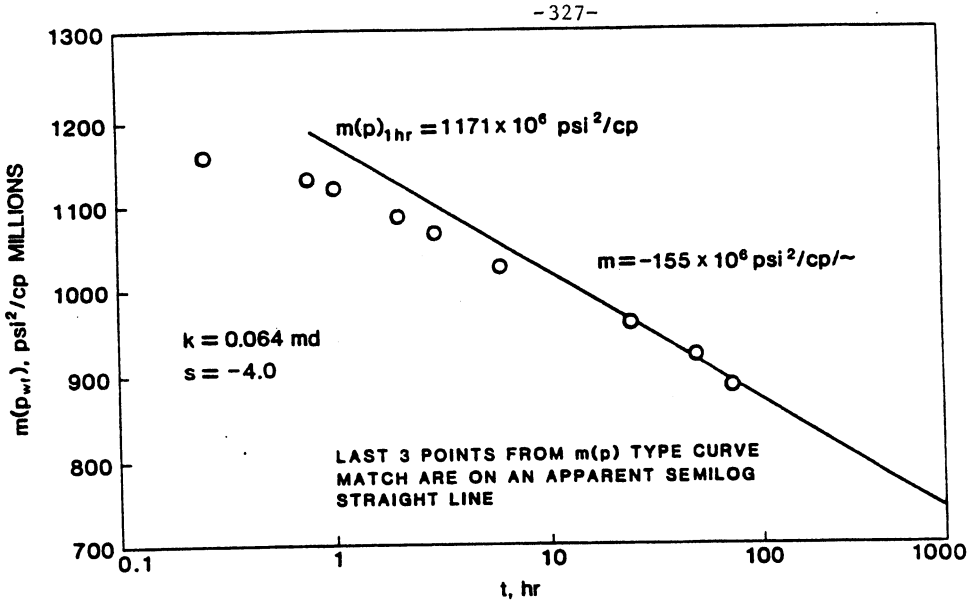

Fig. 1—Conventional *m(p)* drawdown semilog graph, West Virginia Gas Well B.

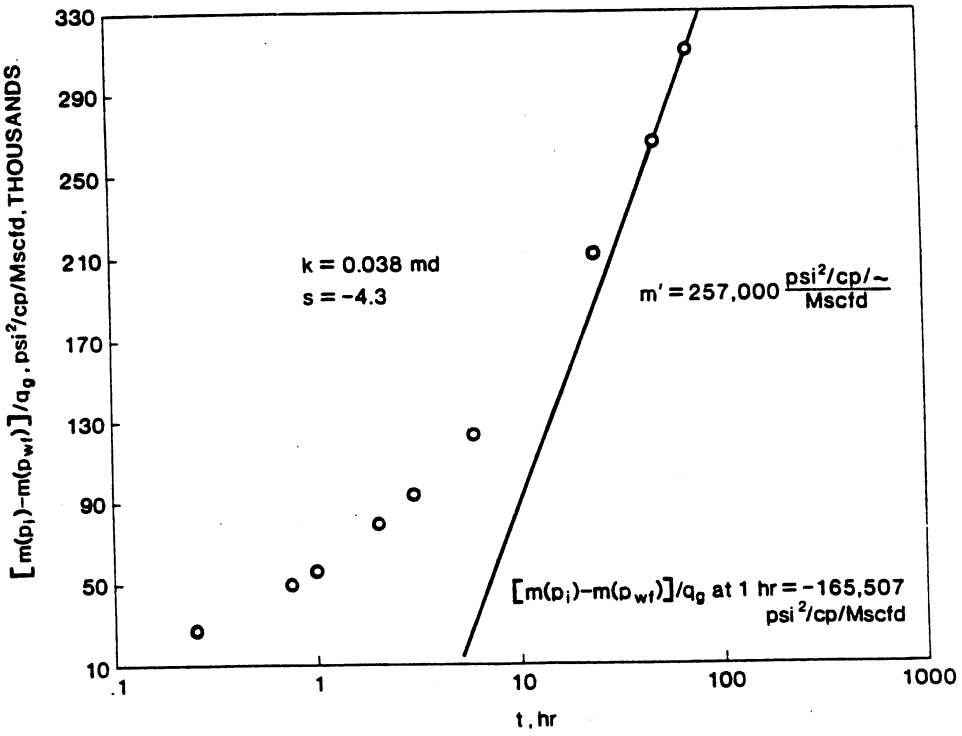

Fig. 2—Winestock-Colpitts graph, West Virginia Gas Well B.

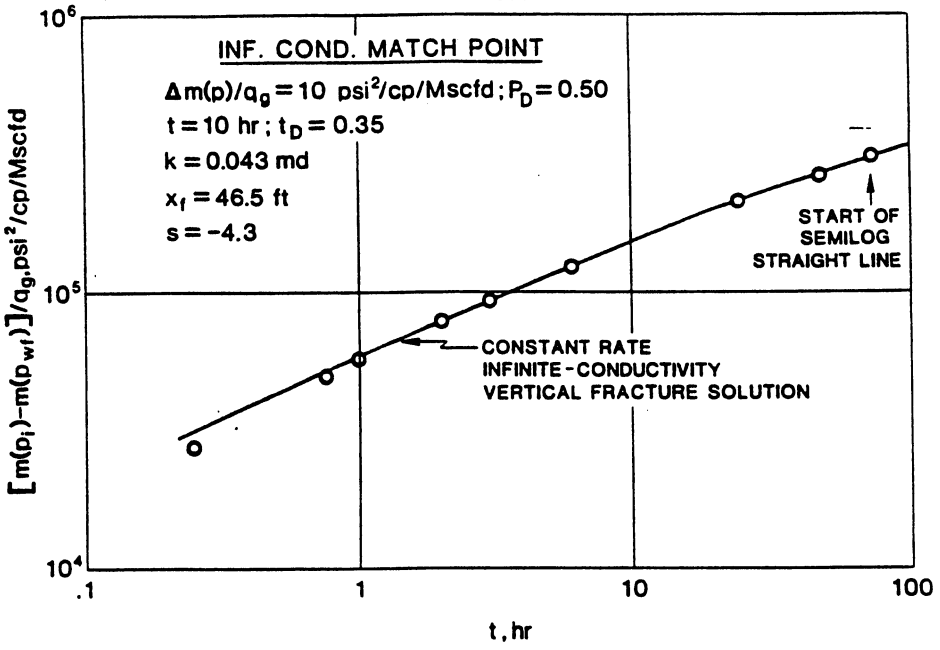

Fig. 3—Rate normalized log-log graph, West Virginia Gas Well B.

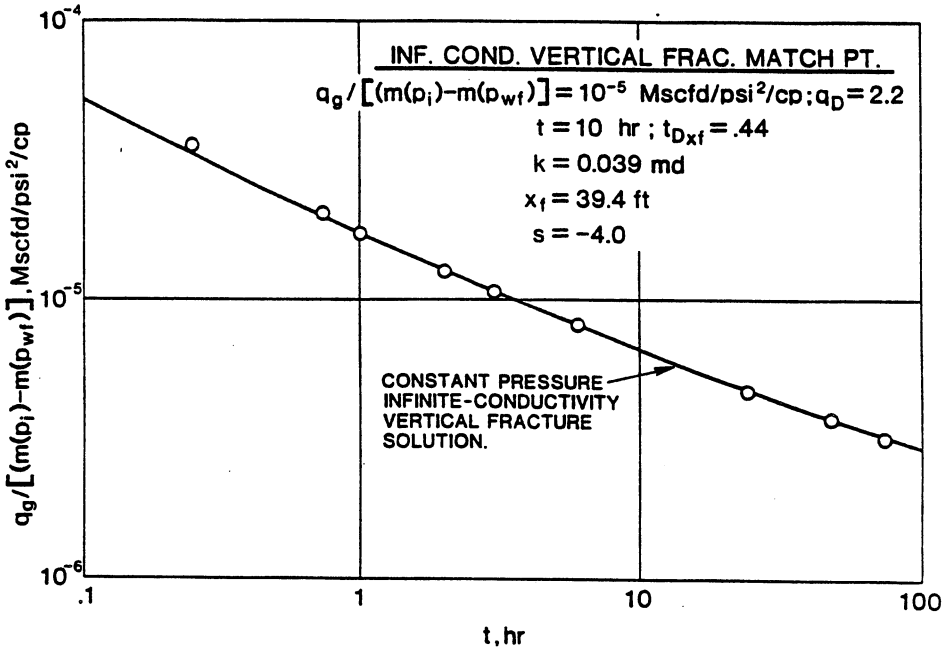

Fig. 4—Pressure normalized log-log graph, West Virginia Gas Well B.

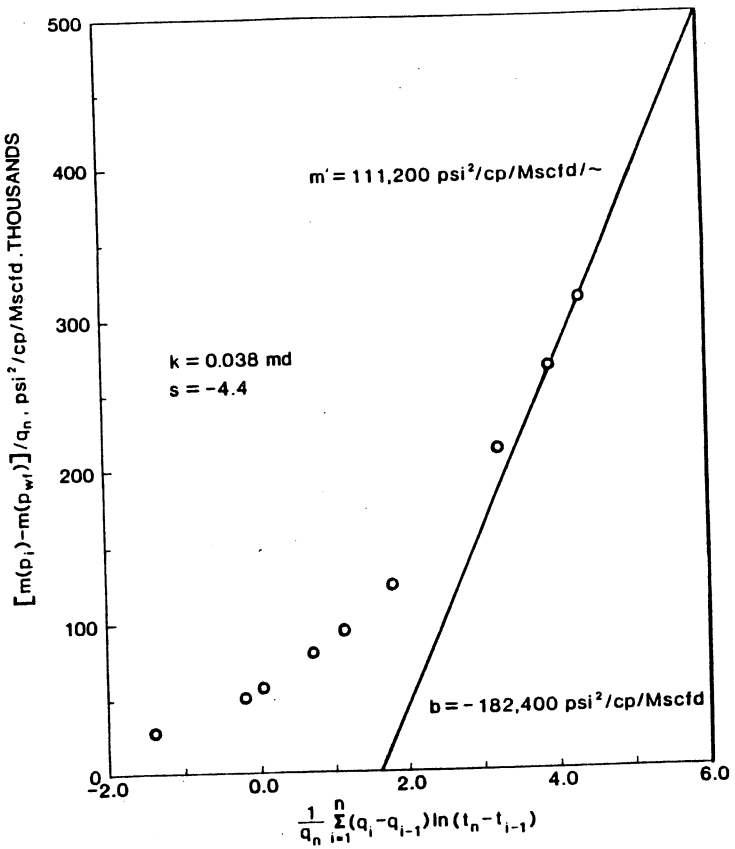

Fig. 5—Superposition based on logarithm of time approximation to p_D, West Virginia Gas Well B.

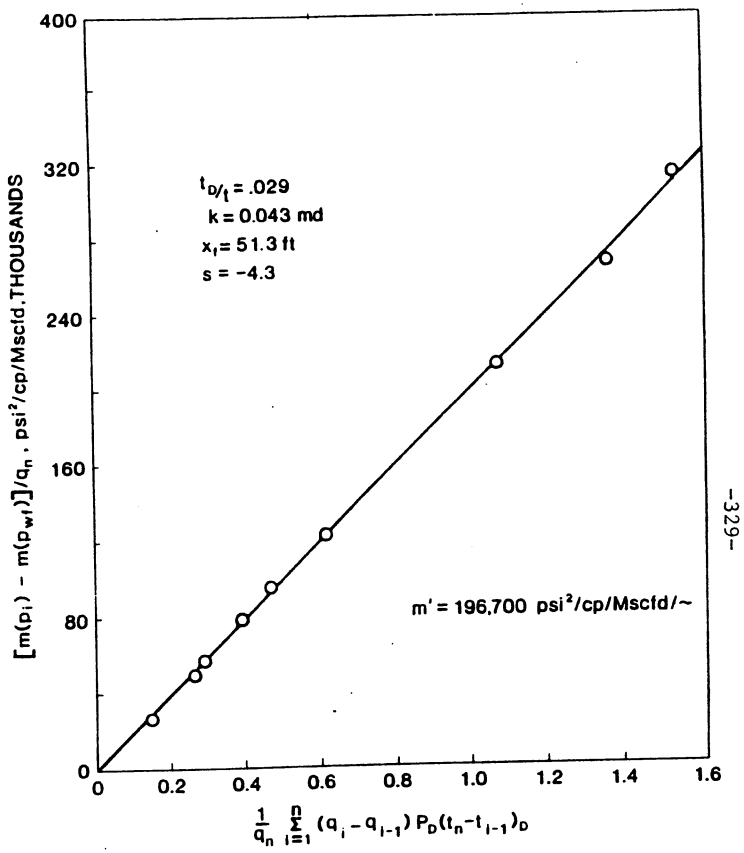

Fig. 6—Superposition based on infinite-conductivity vertical fracture p_D-t_D model, West Virginia Gas Well B.

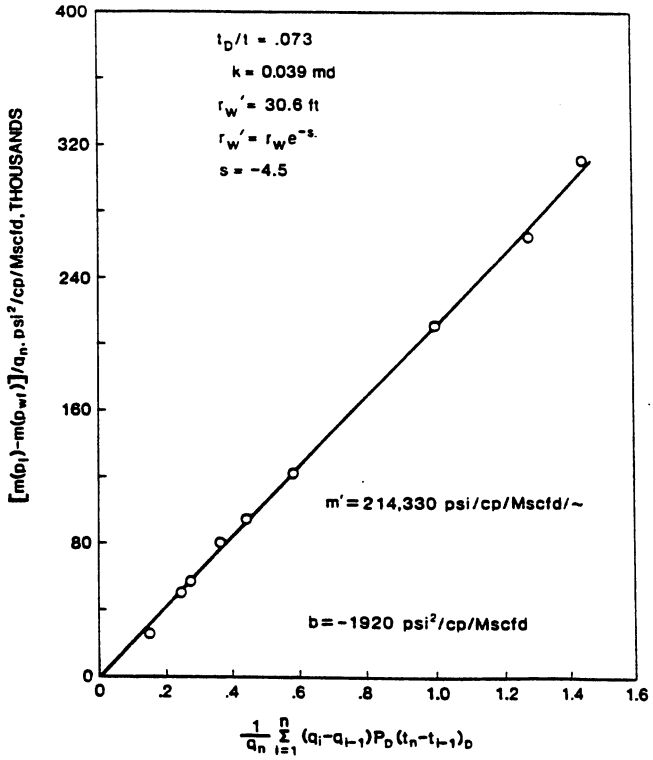

Fig. 7—Superposition based on van Everdingen-Hurst constant terminal rate solution, West Virginia Gas Well B.

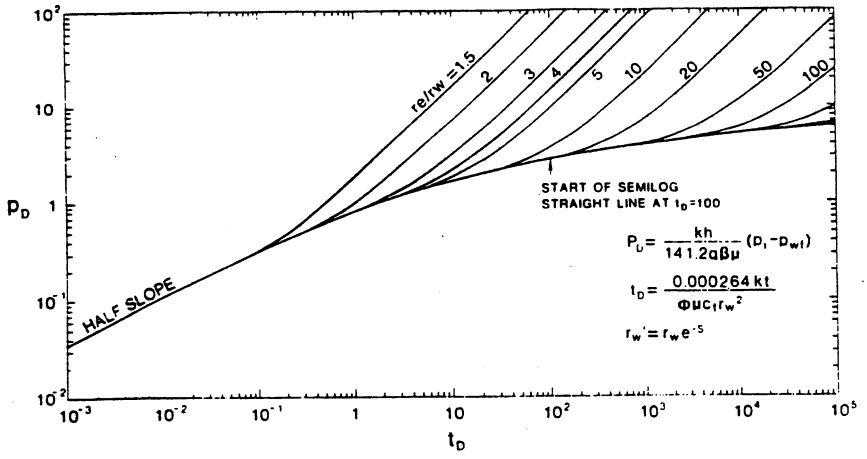

Fig. 8—van Everdingen-Hurst constant terminal rate solution, after Ref. 19.

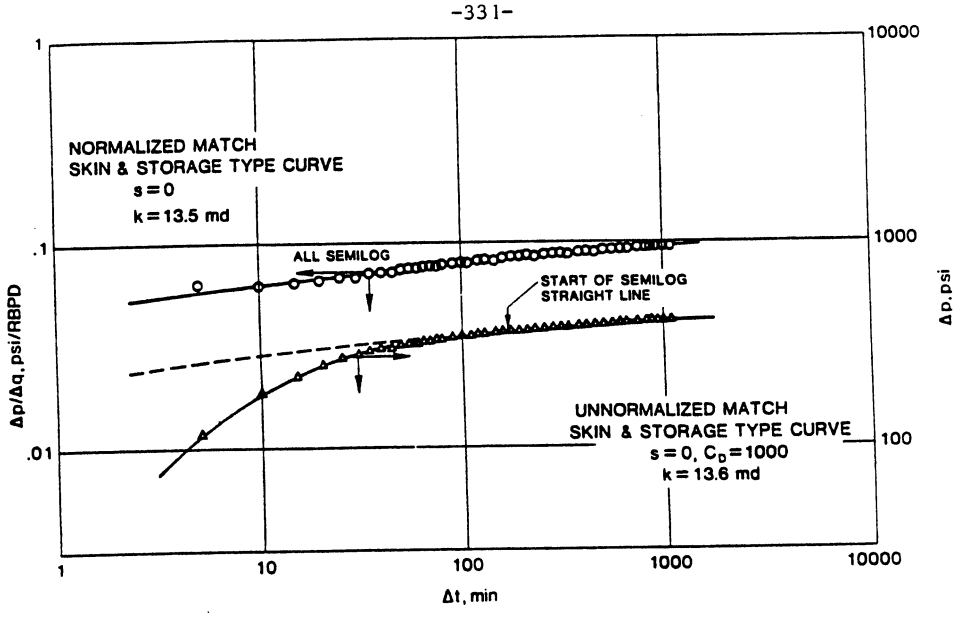

Fig. 9—Conventional pressure and afterflow rate normalized buildup log-log graphs, Water Supply Well No. 1.

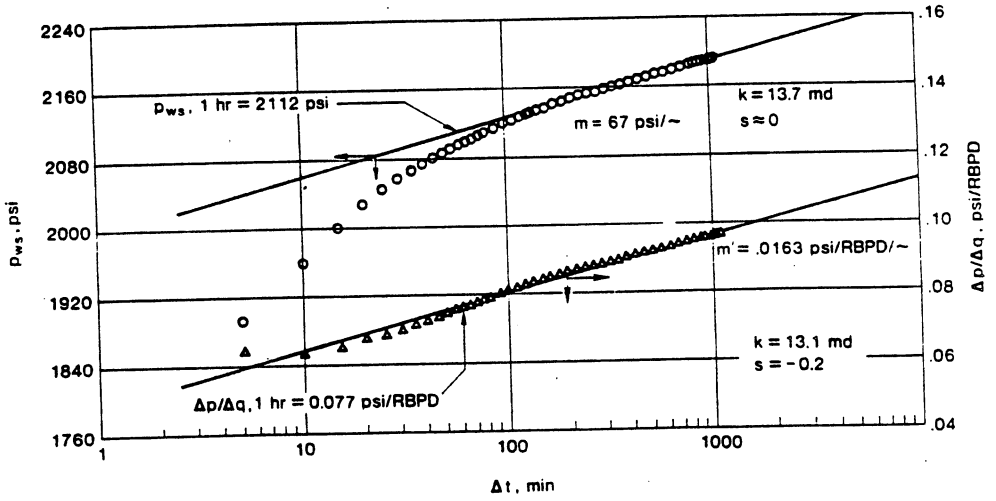

Fig. 10—Conventional pressure and afterflow rate normalized MDH graphs, Water Supply Well No. 1.

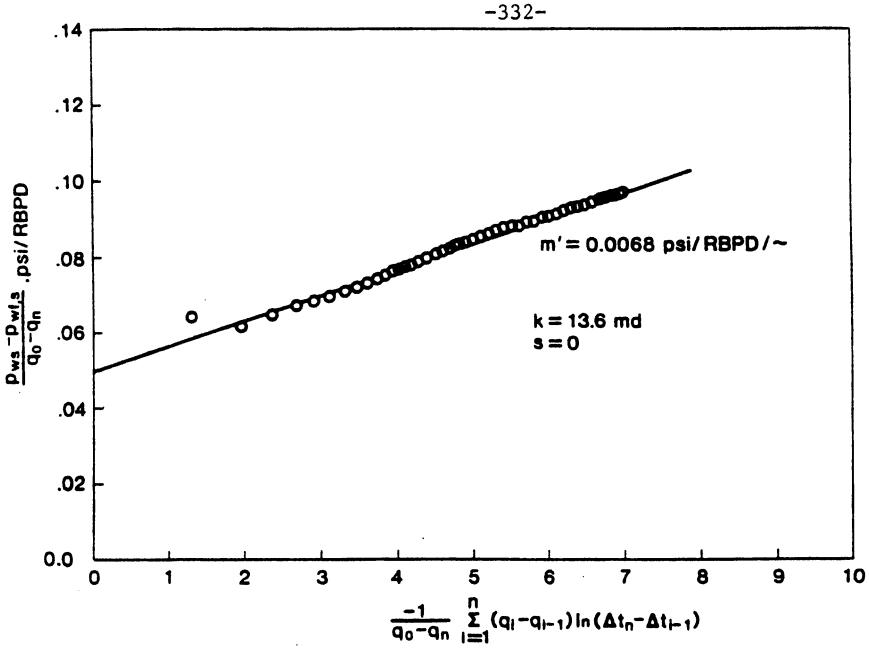

Fig. 11—Superposition based on logarithm of time approximation to p_D, Water Supply Well No. 1.

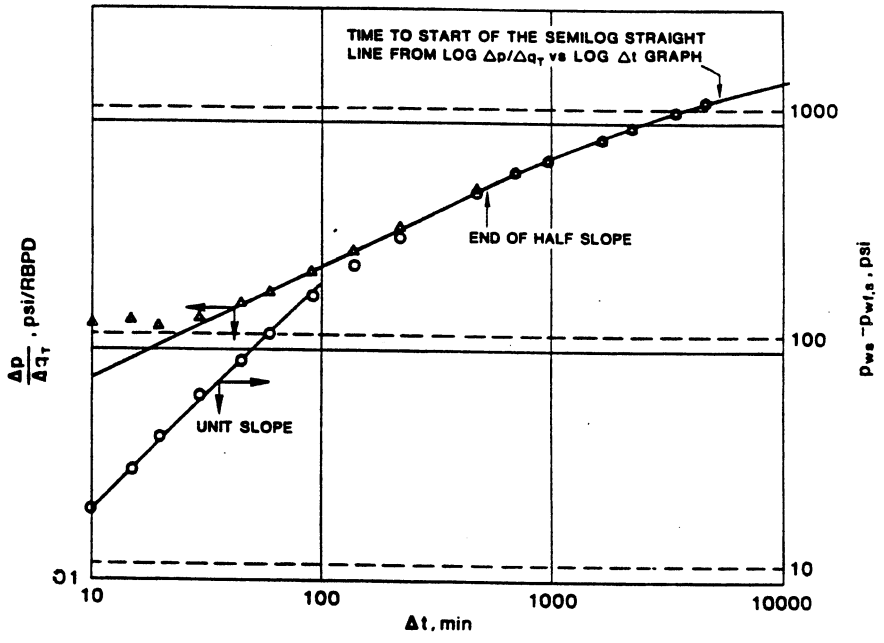

Fig. 12—Conventional and afterflow rate normalized buildup log-log graphs, Case 5 of Ref. 8.

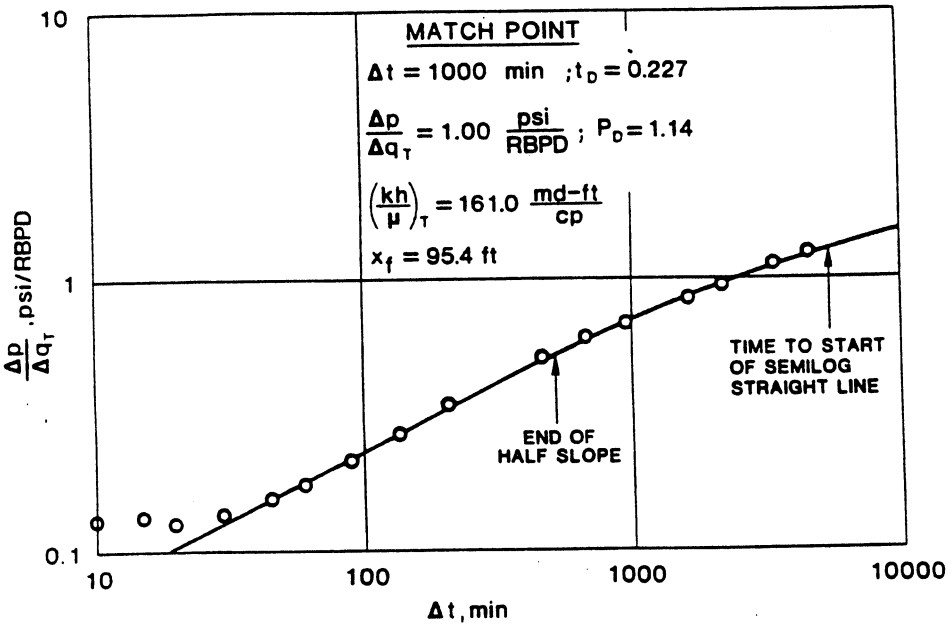

Fig. 13—Afterflow rate normalized log-log graph, Case 5 of Ref. 8.

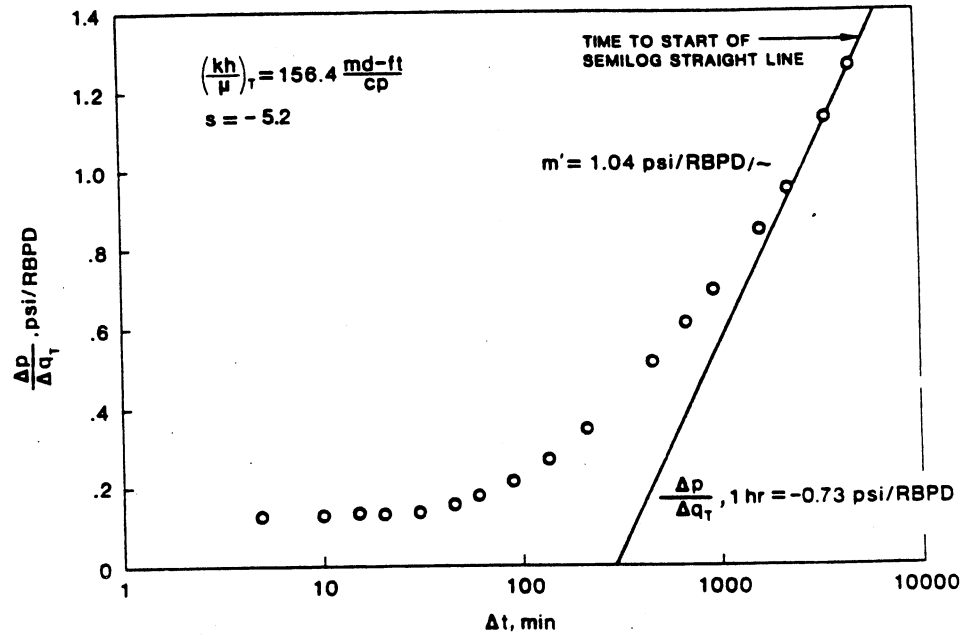

Fig. 14—Afterflow rate normalized MDH graph, Case 5 of Ref. 8.

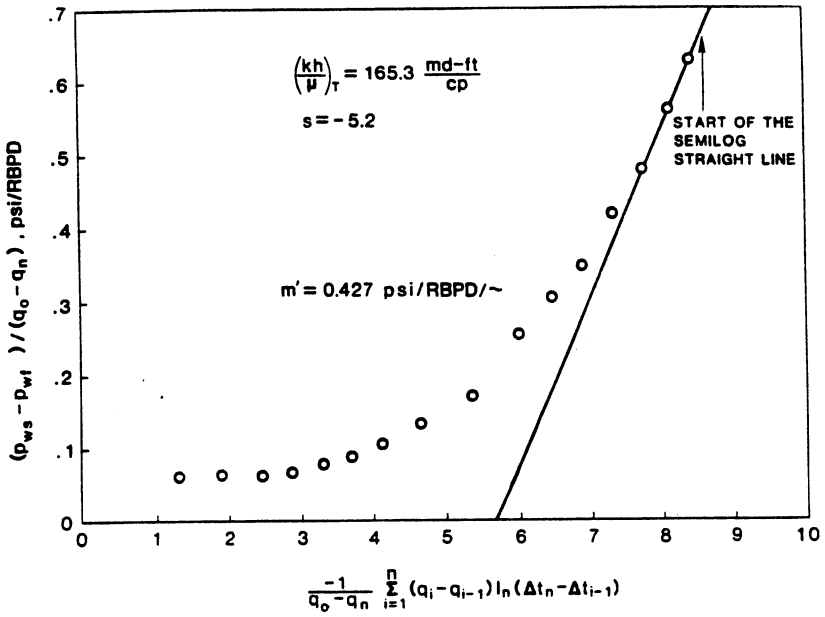

Fig. 15—Superposition based on logarithm of time approximation to p_D, Case 5 of Ref. 8.

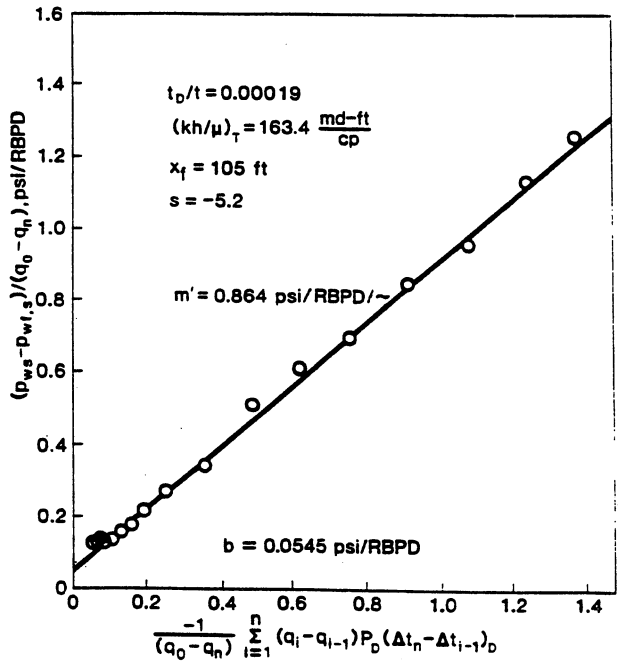

Fig. 16—Superposition based on uniform-flux vertical fracture p_D-t_D model, Case 5 of Ref. 8.

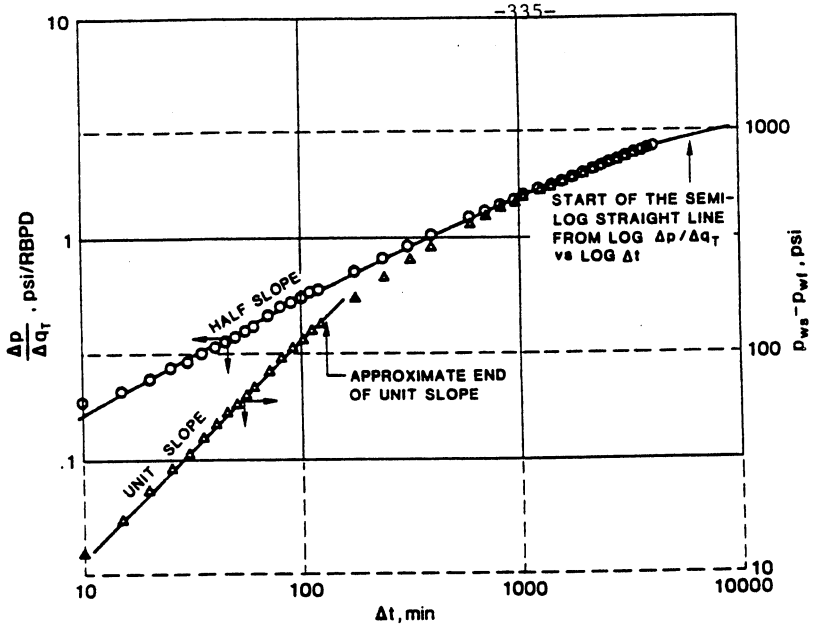

Fig. 17—Conventional pressure and afterflow rate normalized log-log graph, Oil Well No. 1

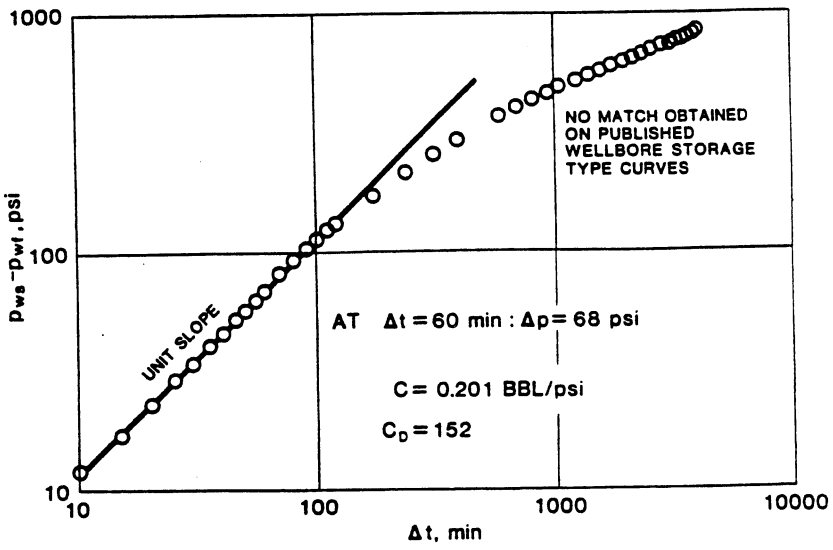

Fig. 18—Conventional pressure-time log-log graph, Oil Well No. 1.

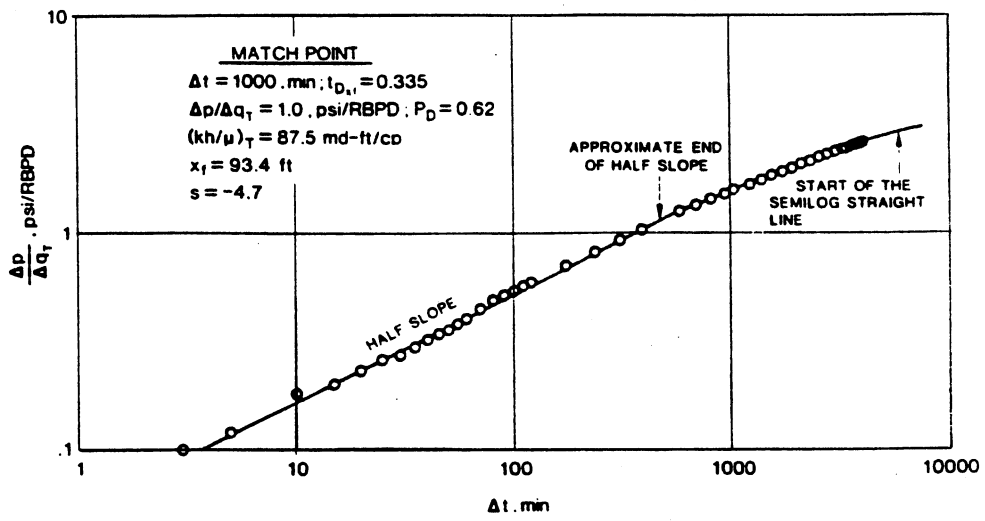

Fig. 19—Total afterflow rate normalized log-log graph, Oil Well No. 1.

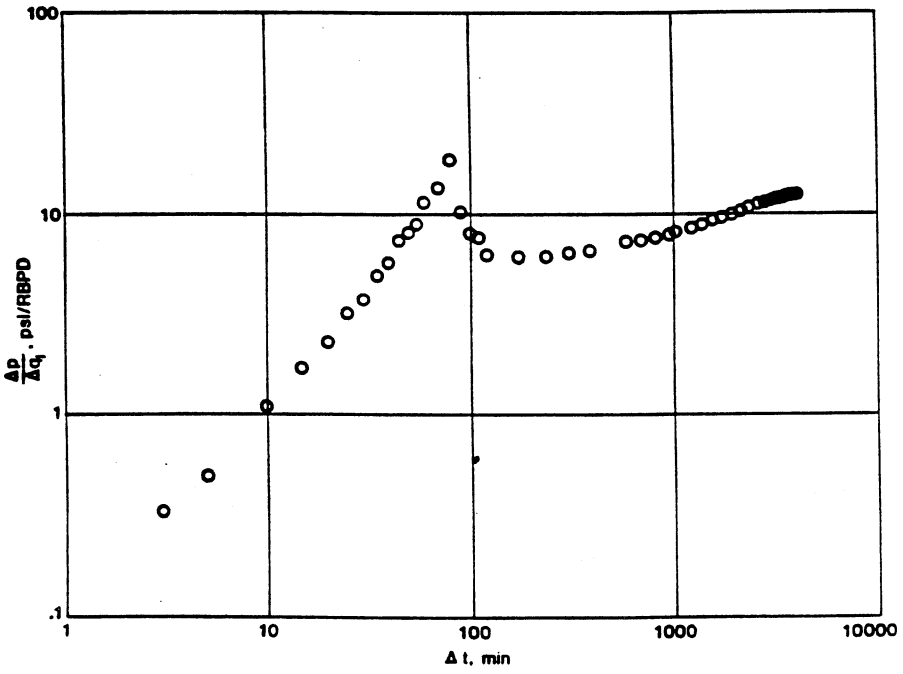

Fig. 20—Liquid afterflow rate normalized log-log graph, Oil Well No. 1.

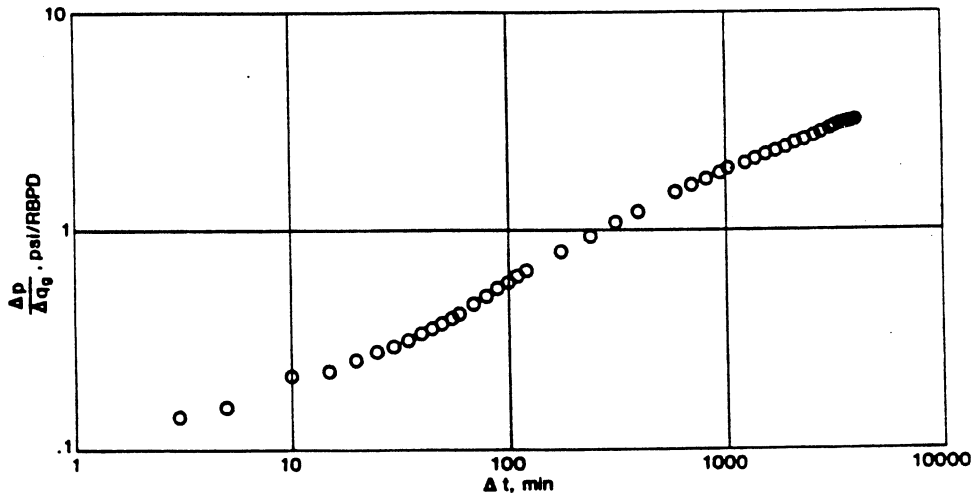

Fig. 21—Gas afterflow rate normalized log-log graph, Oil Well No. 1.

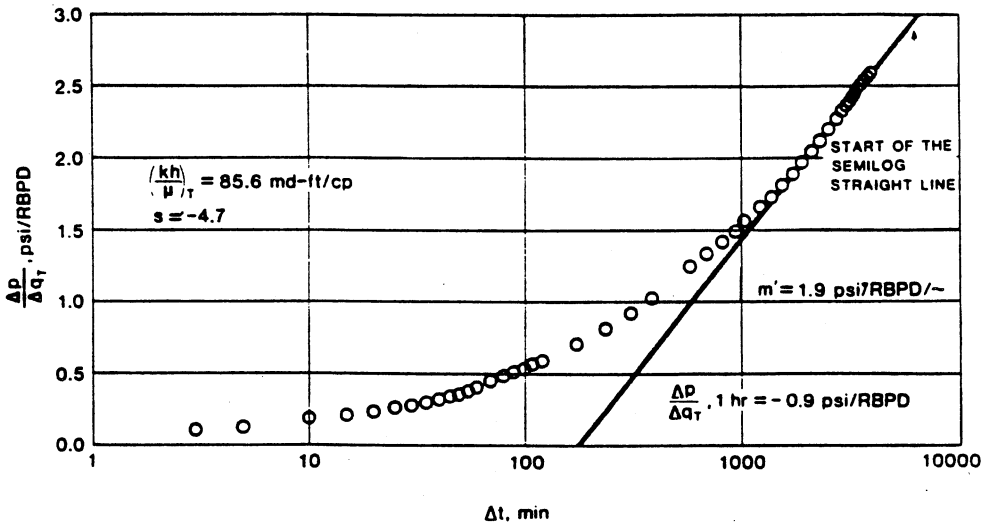

Fig. 22—Afterflow rate normalized MDH graph, Oil Well No. 1.

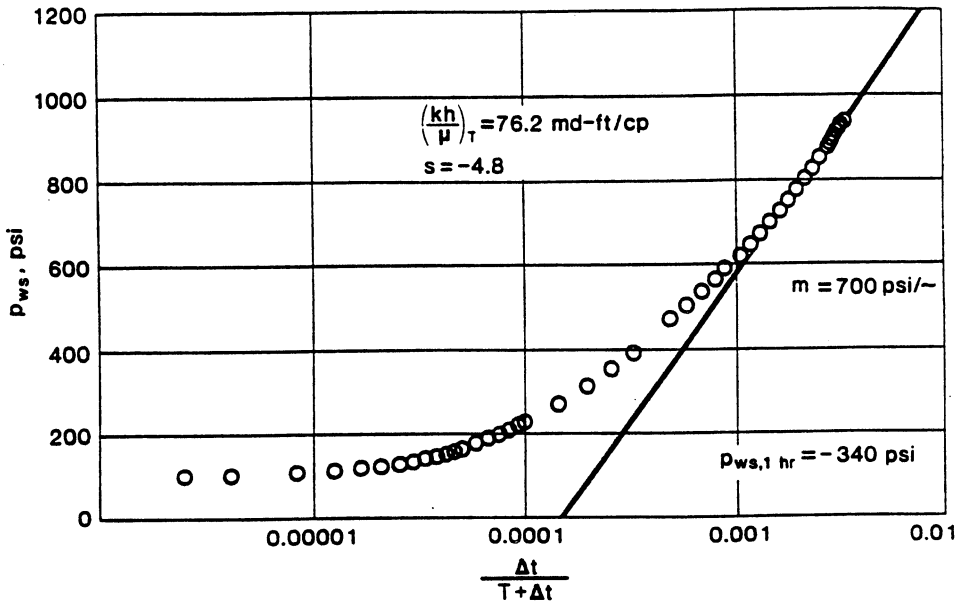

Fig. 23—Conventional Horner graph, Oil Well No. 1.

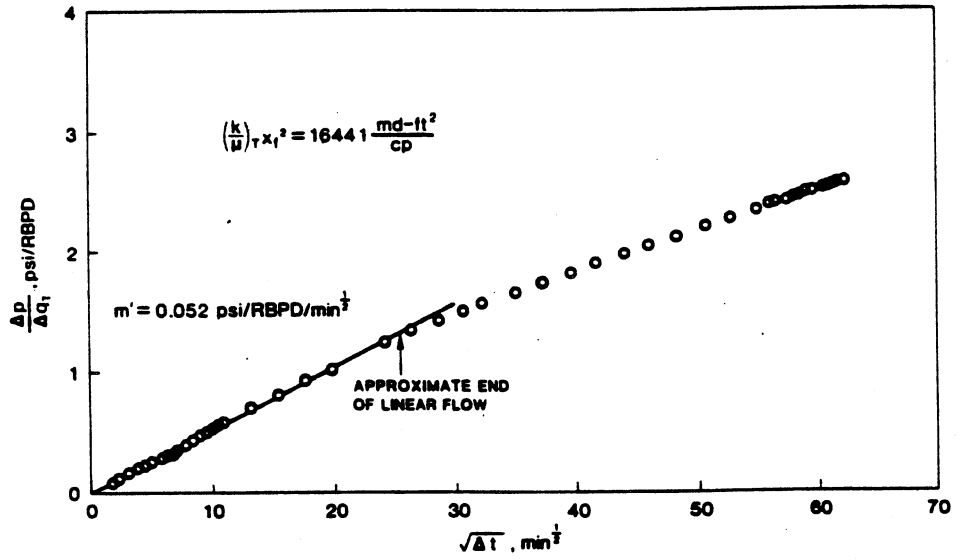

Fig. 24—Afterflow rate normalized pressure-square root of time graph, Oil Well No. 1.

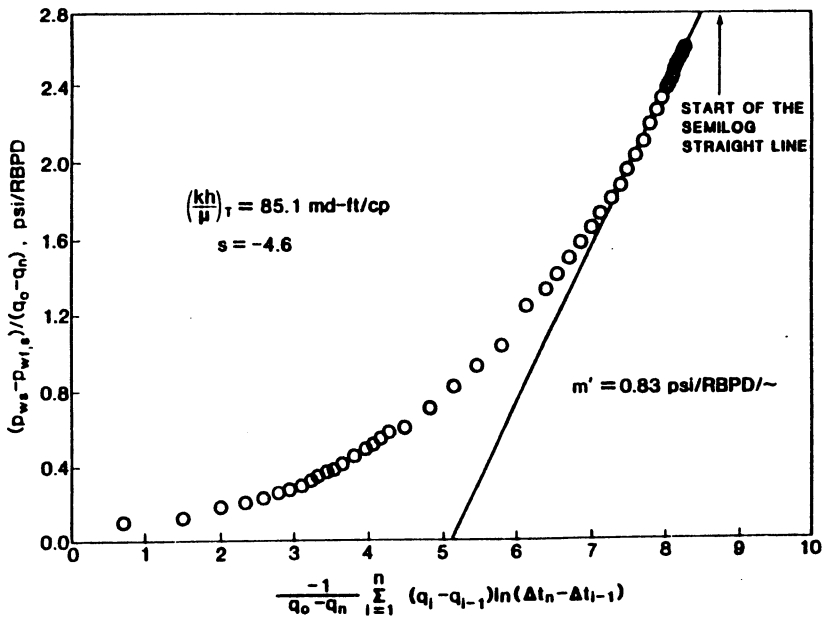

Fig. 25—Superposition based on logarithm of time approximation to p_D, Oil Well No. 1.

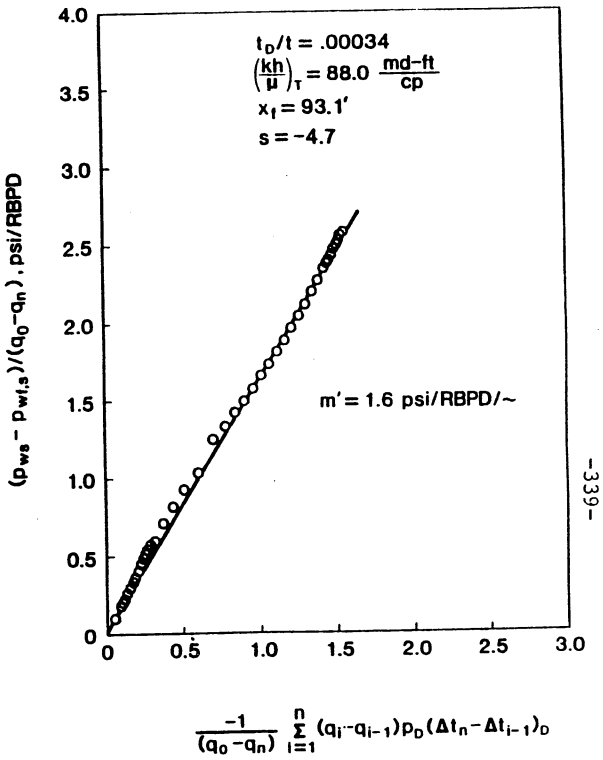

Fig. 26—Superposition based on uniform-flux vertical fracture p_D-t_D model, Oil Well No. 1.

SHAPE FACTOR, C_A, EXPRESSED AS SKIN, s_{CA}

by

M. J. Fetkovich
M. E. Vienot

SPE, Phillips Petroleum Co.

SPE 13304

Original manuscript (SPE 13304) received in the Society of Petroleum Engineers office April 9, 1964. Paper accepted for publication July 12, 1964. Revised manuscript received Sept. 27, 1964.

SHAPE FACTOR, C_A, EXPRESSED AS SKIN, s_{CA}

Summary

This work presents the conversion of the shape factor, C_A, to a pseudosteady-state skin term, s_{CA}. When the shape factor is expressed as a skin term, it becomes easier to see the effect that a well placement in a given drainage area will have on the well's performance. Skin factors for published drainage shapes and well locations are given.

Discussion

In attempting to calculate interference effects of well locations on production forecasts, it was found very convenient to express the shape factor, C_A, as a pseudosteady-state skin term, s_{CA}. When using pseudosteady-state flow equations, the effect of a well not located in the center of a radial or square drainage area becomes immediately apparent when the shape factor is expressed as a skin term.

The general pseudosteady-state equation in terms of C_A for oil, gas, or water can be written as

$$q = \frac{7.08kh\,(\bar{p} - p_{wf})}{(\mu\beta)\left(\ln\sqrt{\frac{2.2458A}{C_A r_w^2}} + s + Dq\right)} . \qquad ..(1)$$

By using an effective drainage radius, r_e', to maintain an equivalent reservoir volume

$$r_e' = \sqrt{\frac{A}{\pi}} \qquad ..(2)$$

and the shape factor for a well at the center of a circular drainage area ($C_A = 31.62$), we can obtain the familiar radial flow pseudosteady-state equation

$$q = \frac{7.08kh\,(\bar{p} - p_{wf})}{(\mu\beta)\left[\ln\left(\frac{r_e'}{r_w}\right) - \frac{3}{4} + s + Dq\right]} . \qquad ..(3)$$

Introducing a reference shape factor term, we can write

$$q = 7.08kh\,(\bar{p} - p_{wf})/\mu\beta\,\{\ln(r_e'/r_w) + \ln(2.656/\sqrt{C_{A,ref}})$$

$$+ [\ln(2.656/\sqrt{C_{A,new}}) - \ln(2.656/\sqrt{C_{A,ref}})] + s + Dq\}, \qquad ..(\ 4)$$

or

$$q = \frac{7.08kh\,(\bar{p} - p_{wf})}{(\mu\beta)\left[\ln\left(\frac{r_e'}{r_w}\right) + \ln\frac{2.656}{\sqrt{C_{A,ref}}} + \ln\sqrt{\frac{C_{A,ref}}{C_{A,new}}} + s + Dq\right]}. \qquad ..(\ 5)$$

Defining a pseudosteady-state skin factor, s_{CA}, as

$$s_{CA} = \ln\sqrt{\frac{C_{A,ref}}{C_{A,new}}}, \qquad .. (\ 6)$$

we have, referencing to the center of a circle (the classic analytical solution) with $C_{A,ref} = 31.62$,

$$q = \frac{7.08kh\,(\bar{p} - p_{wf})}{(\mu\beta)\left[\ln\left(\frac{r_e'}{r_w}\right) - 0.750 + s_{CA} + s + Dq\right]} \qquad .. (\ 7)$$

or, referencing to the center of a square (field and model situations) with $C_{A,ref} = 30.8828$,

$$q = \frac{7.08kh\,(\bar{p} - p_{wf})}{(\mu\beta)\left[\ln\left(\frac{r_e'}{r_w}\right) - 0.738 + s_{CA} + s + Dq\right]}. \qquad .. (\ 8)$$

Values of s_{CA} referenced to the center of a circle or square are tabulated in Table 1. Values of C_A in Table 1 were obtained from Ref. 1.

Constant wellbore pressure production forecasts for wells not in the center of a circle are made conveniently by using the concept of effective wellbore radius $r_w' = r_w e^{-s_{CA}}$ with q_{Dd} and t_{Dd} from Ref. 2 and $r_D' = r_e'/r_w'$.

Nomenclature

A = drainage area, ft^2 [m^2]
β = formation volume factor
C_A = shape factor
D = non-Darcy flow constant

Acknowledgment

We thank the Phillips Petroleum Co. for permission to publish this paper.

References

1. Earlougher, R. C. Jr.: Advances in Well Test Analysis, Monograph Series, SPE, Richardson, TX (1977).

2. M. J. Fetkovich: "Decline Curve Analysis Using Type Curves," J. Pet. Tech. (June 1980) 1065-77.

Table 1

SKIN FACTORS FOR VARIOUS DRAINAGE SHAPES

DRAINAGE SHAPE	SHAPE FACTOR C_A	$^{s}C_A$ REFERENCED TO A CIRCLE ⊙	$^{s}C_A$ REFERENCED TO A SQUARE ⊡	DRAINAGE SHAPE	SHAPE FACTOR C_A	$^{s}C_A$ REFERENCED TO A CIRCLE ⊙	$^{s}C_A$ REFERENCED TO A SQUARE ⊡
	31.62	0.000	-0.0116		10.8374	0.535	0.524
	30.8828	0.0116	0.000		4.5141	0.973	0.962
	31.6	0.0003	-0.0116		2.0769	1.361	1.350
	27.6	0.0680	0.0562		3.1573	1.152	1.140
	27.1	0.0771	0.0653		0.5813	1.998	1.986
	21.9	0.184	0.172		0.1109	2.826	2.815
	0.098	2.888	2.876		5.3790	0.886	0.874
	12.9851	0.445	0.433		2.6896	1.232	1.220
	4.5132	0.973	0.962		0.2318	2.458	2.446
	3.3361	1.125	1.113		0.1155	2.806	2.794
	21.8369	0.185	0.173	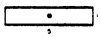	2.3606	1.297	1.286

h = formation thickness, ft [m]
k = permeability, darcy [m2]
P_{wf} = flowing bottomhole pressure, psia [kPa]
$\bar{P}$ = average reservoir pressure, psia [kPa]
q = surface flow rate, B/D [m^3/d]
q_{Dd} = decline curve dimensionless rate
r_e' = effective drainage radius, ft [m]
r_w = wellbore radius, ft [m]
s = skin factor
t_{Dd} = decline curve dimensionless time
μ = viscosity, cp [Pa·s]

MUSKAT'S CLUSTER WELLS EQUATION

by

M. J. Fetkovich

MUSKAT'S CLUSTER WELLS EQUATION

By M. J. Fetkovich

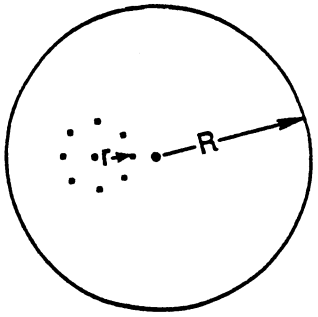

n = NUMBER OF WELLS IN THE CLUSTER
r = CLUSTER RADIUS
R = CLUSTER WELLS DRAINAGE RADIUS

$$\text{TOTAL } Q = \frac{2\ \pi kh\ (Pe - Pwf)}{\mu\beta\left[\text{LOG}\ \frac{R}{r} + \frac{1}{n}\ \text{LOG}\ \frac{r}{nrw}\right]}$$

$$q\ \text{WELL} = \frac{Q}{n} = \frac{2\ \pi kh\ (Pe - pwf)}{n\mu\beta\ \text{LOG}\ \left[\frac{R}{r} + \frac{1}{n}\ \text{LOG}\ \frac{r}{nrw}\right]}$$

$$\text{OR} \quad n\left[\text{LOG}\ \frac{R}{r} + \frac{1}{n}\ \text{LOG}\ \frac{r}{nr_w}\right] = n\ \text{LOG}\ \frac{R}{r} + \text{LOG}\ \frac{r}{nr_w}$$

$$\text{REDUCES TO} \quad \text{LOG}\ \frac{R^n}{nr^{n-1}\ r_w}$$

$$\text{OR} \quad \boxed{r_e' = \frac{R^n}{nr^{n-1}}}$$

8 WELL CLUSTER
UPPER BUNTER

$$R = \sqrt{\frac{A}{\pi}} = \sqrt{\frac{5739 \text{ ACRES} \times 43560}{\pi}} = 8920 \text{ FT.}$$

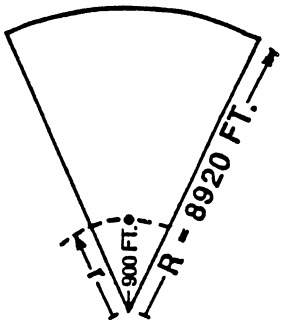

$$r_e' = \frac{R^n}{nr^{n-1}} = \frac{8920^8}{8(900)^7} = 10.47 \times 10^9 \text{ FT.}$$

MINIMUM POSSIBLE INTERFERENCE
8 WELLS EQUAL SPACING

717 ACRES/WELL

r_e = 3153 FT.

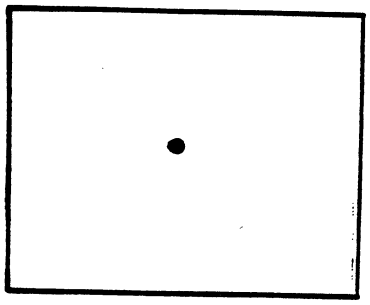

CALCULATED r FOR r_e' EQUAL TO THAT OF UNIFORM SPACING

$$r = \sqrt[n-1]{\frac{R^n}{nr_e'}}$$

$$r = \sqrt[7]{\frac{8920^8}{8(3153)}} = 7689 \text{ ft.}$$

EQUAL RESERVOIR INTERFERENCE INCREASED TUBING FRICTION DROP

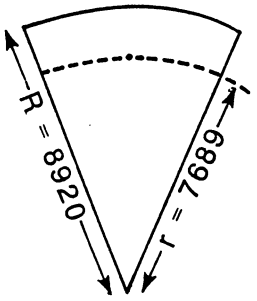

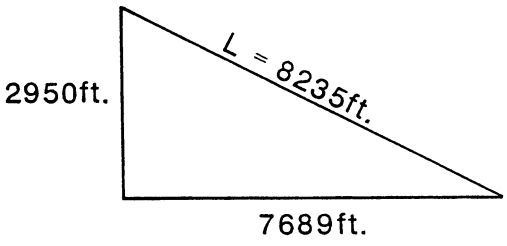

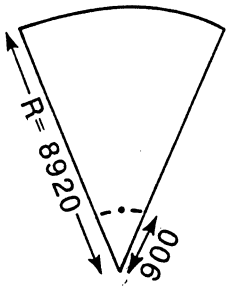

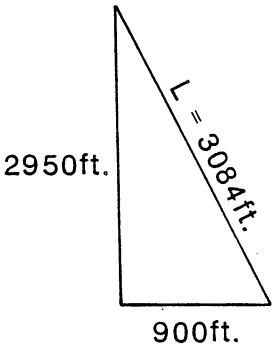

EFFECTIVE WELLBORE RADIUS
CLUSTER WELL

$$r_w' = r_w n \left(\frac{r}{R}\right)^{n-1}$$

OR

$$\frac{r_w'}{r_w} = n \left(\frac{r}{R}\right)^{n-1}$$

SINCE $$r_w' = r_w \, e^{-S}$$

OR $$\ln\left(\frac{r_w'}{r_w}\right) = -S$$

THEN $$-\ln\left[n \left(\frac{r}{R}\right)^{n-1}\right] = S$$

FOR THE 8 WELL CLUSTER (UPPER BUNTER)

SINGLE WELL SKIN

$$S = -\ln\left[8 \left(\frac{900}{8920}\right)^{7}\right] = +14$$

USED WITH NORMAL FLOW EQUATION AS

$$\left[\ln\left(\frac{R}{r_w}\right) + S\right] \text{ or } \ln\left(\frac{R}{r_w'}\right)$$

CASE STUDY OF A LOW PERMEABILITY VOLATILE OIL FIELD USING INDIVIDUAL-WELL ADVANCED DECLINE CURVE ANALYSIS

by

M. J. Fetkovich and M. E. Vienot
Phillips Petroleum Co.
R. D. Johnson and B. A. Bowman
Phillips Oil Co.

SPE Members

SPE 14237

This paper was prepared for presentation at the 60th Annual Technical Conference and Exhibition of the Society of Petroleum Engineers held in Las Vegas, NV, September 22-25, 1985.

CASE STUDY OF A LOW-PERMEABILITY VOLATILE OIL FIELD USING INDIVIDUAL-WELL ADVANCED DECLINE CURVE ANALYSIS

Abstract

This paper presents a detailed case history study of a low permeability volatile oil field located in Campbell County, Wyoming. The field was analyzed on an individual well basis using advanced decline curve analysis for 40 individual well completions. Well permeabilities, skins and original oil in place are calculated for each well from rate-time analysis using constant wellbore pressure type curve analysis techniques.

Original oil in place values calculated from rate-time analysis for individual wells are used with recoverable reserve projections from the decline analysis to obtain fractional recoveries for each well. Gas-oil ratios versus fractional recovery curves are also made for each well using historical cumulative production and the calculated oil in place values. Ultimate fractional recovery numbers and GOR vs fractional recovery curves, plotted for each well, are shown to suggest different rock types and reservoir fluids. Multi-well decline curve analysis shows the validity of the variables s (skin), k, OOIP, ultimate fractional recovery and GOR vs fractional recovery evaluated from each well's type curve evaluation. These variables must all give consistent and reasonable numbers when compared with each other. A single well analysis can easily give results that are not recognized as being invalid unless compared with other wells in the field.

The study also illustrates flowing and pumping well backpressure changes in a well's decline, the method of handling such changes, and their effect on ultimate recoverable reserves predictions. Conventional decline curve analysis can not handle backpressure changes because of its constraint that what controls the decline in the past will also continue in the future.

Introduction

In solution gas drive reservoirs, decline curve analysis of rate-time data for predicting future production and determining recoverable reserves for a fairly large number of wells is commonly done using the Arps[1] empirical equations and a computerized statistical approach to arrive at answers fairly quickly. For wells in high permeability reservoirs producing essentially wide-open, without future backpressure changes and without future stimulation treatments, the results obtained should be reasonably good providing the limits of the decline exponent b of between 0 and 1.0 are honored.

At the other extreme in analyzing rate-time data for predicting future production and recoverable reserves, a reservoir simulation study could be undertaken. However, this approach could take as much as a year to accomplish

and normally would not be considered acceptable, particularly for time-constrained property acquisition or sales situations where few of the detailed reservoir parameters necessary for a simulation study are available.

Many of the newer oil and gas fields being discovered and produced are in the low permeability classification, where transient behavior can last for years, and therefore are not amenable to analysis using the Arps equation alone. Also, a model study of such low permeability reservoirs would require a very fine grid system to correctly simulate and match the early transient rate-time decline data.

An approach to the problem of analyzing low permeability wells and total field rate-time decline has been given in papers [2,3,4,5,6] that illustrate methods of handling both the transient and depletion stages of rate-time decline. Well permeabilities, skins from stimulation treatments and original oil-in-place or original gas-in-place can be calculated for each well from rate time data using constant wellbore pressure type curve analysis techniques.

With a field case study of the School Creek Field in Campbell County, Wyoming, a low permeability volatile oil field, we will present a stepwise procedure for doing a total field study using individual well advanced decline curve analysis techniques. Original oil in place values calculated from rate-time analysis for individual wells are used with recoverable reserve projections from the decline analysis to obtain fractional recoveries for each well. Gas-oil ratio versus fractional recovery curves are also made for each well using historical cumulative production and the calculated oil in place values. Ultimate fractional recovery values and GOR versus fractional recovery curves, plotted for each well, are shown to suggest different rock types and reservoir fluids. Multi-well decline curve analysis shows the validity of the variables s (skin), k, OOIP, ultimate fractional recovery and GOR versus fractional recovery evaluated from each well's type curve match point. These variables must all give consistent and reasonable numbers when compared with each other. A single well analysis can often give results that are not recognized as being invalid unless compared with several other wells in the field. The study also includes and illustrates flowing and pumping well backpressure changes in a well's decline, the method of handling such changes and their effect on ultimate recoverable reserves predictions. Conventional decline curve analysis approaches do not consider backpressure changes and their effect on projected recoverable reserves.

School Creek Field - Wyoming

The School Creek Field is located on the eastern flank of the south central portion of the Powder River Basin in Campbell and Converse Counties, Wyoming. Following deposition of the underlying Skull Creek Shale, the lower Cretaceous sea receded from the area of the Powder River Basin. Subsequently, a wide-spread drainage system developed and carved its pattern into the Skull Creek Shale. As the lower Cretaceous sea transgressed east, Muddy deltaic sediments buried the previously deposited channel sediments as the sea continued to inundate the basin. Continuous basin fill by deposition of the overlying Mowry Shale resulted in the Muddy reservoir sands being ideally "sandwiched" between two marine hydrocarbon source shales.

In the School Creek Area, a north-south paleodrainage pattern was developed upon the underlying Skull Creek Shale and controlled the distribution of the productive tidal channel and point-bar sands of the lower Muddy formation. Younger upper Muddy marine facies units were then deposited as the Cretaceous sea transgressed east resulting in some well developed productive marine offshore bar sands within the field area.

In the School Creek Field, the Lower Muddy channel sands have 35 well completions with an average of 11 net feet of pay per well and an average porosity and water saturation of 13.6% and 39% respectively. Upper Muddy bar sands have 5 well completions with an average of 12 net feet of pay per well and an average porosity and water saturation of 22% and 14%, respectively. Production has also been established in secondary objectives, which include the Sussex, Turner, and Dakota formations. These wells are not included in this study.

Figure 1 is a plat showing the well locations, their relationship to the Channel Sand and Bar Sand and the three wells for which PVT samples were taken. Figure 2 is a type log for a School Creek Field Muddy formation completion.

The School Creek Field was discovered in 1980 when the Matheson E-1 well was drilled to 10,000 feet and completed in the Muddy formation. The initial reservoir pressure was approximately 3700 - 3600 psi. Basic fluid properties are given from three different PVT studies in Table 2 and Figure 3. Two quite different fluid samples were obtained in the Channel Sand: the Federal EE-1 sample with a bubble point pressure of 3400 psi, GOR of 1557 SCF/BBL and the Matheson E-1 sample with a bubble point pressure of 2705 psi, GOR of 736 SCF/BBL. Based on reported initial producing gas-oil ratios, the Federal EE-1 sample was used to represent wells in the southern portion of the field while the Matheson E-1 sample was used for wells in the northern portion of the field. The Federal J-1 sample was only used to represent the five Bar Sand well completions. Its bubble point pressure was 2838 psi with a gas-oil ratio of 1189 SCF/BBL.

Basic Decline Analysis Equations

The Arps[1] empirical decline equations that can be used for analysis and forecasting future production when depletion is clearly indicated are, for

$b > 0$

$$q(t) = \frac{q_i}{[1 + bD_i t]^{1/b}} \qquad ..(1)$$

and for $b = 0$ (exponential)

$$q(t) = \frac{q_i}{e^{D_i t}} \qquad ..(2)$$

where the limits of b are between 0 and 1.

For type curve analysis

$$q_{Dd} = \frac{q(t)}{q_i} \qquad ..(3)$$

and

$$t_{Dd} = D_i t \qquad ..(4)$$

From log-log type curve matching, the match of the rate-time data yields b, $t - t_{Dd}$, and $q(t) - q_{Dd}$. From these values q_i and D_i are evaluated and can then be used in the predictive equations 1 or 2 above to forecast future production and to obtain ultimate recoverable reserves.

As given in reference 3, we can also evaluate the productivity factor from $q(t) - q_{Dd}$ match point, the **same** match point as would be used with the above Arps equations.

$$P.F. = \frac{kh}{\left[\ln\left(\frac{r_e}{r_w'}\right) - \frac{1}{2}\right]} = \frac{141.2\ (\overline{\mu\beta})}{\overline{p}_R - p_{wf}} \cdot \frac{q(t)}{q_{Dd}} \qquad ..(5)$$

where r_w' is the effective wellbore radius incorporating the skin term, $r_w' = r_w\, e^{-s}$. The skin term can also include the effect of a shape factor C_A. See reference 7. If r_e/r_w' can be defined from a match of early transient data, we could then evaluate k and s of the well.

To evaluate pore volume[3], V_p, from the match point, we have

$$V_p = \pi\, r_e^2 h\phi = \frac{(\overline{\mu\beta})}{(\mu c_t)_{\overline{p}_R}\,(\overline{p}_R - p_{wf})} \cdot \frac{t}{t_{Dd}} \cdot \frac{q(t)}{q_{Dd}} \qquad ..(6)$$

which gives the pore volume at the **start** of the decline analysis.

In the above equations, $(\overline{\mu\beta})$ is normally evaluated at average pressure $(\overline{p}_R + p_{wf})/2$ while (μc_t) is evaluated at reservoir shut-in pressure $\overline{p}_R$.

In terms of an oil pseudo pressure, $m(p)_{oil}$, equations 5 and 6 can be written as

$$\frac{kh}{\left[\ln\left(\frac{r_e}{r_w'}\right) - \frac{1}{2}\right]} = \frac{141.2}{m(\overline{p}_R) - m(p_{wf})} \cdot \frac{q(t)}{q_{Dd}} \qquad ..(7)$$

and $$V_p = \frac{1}{(\mu c_t)_{\bar{p}_R} [m(\bar{p}_R) - m(p_{wf})]} \cdot \frac{t}{t_{Dd}} \cdot \frac{q(t)}{q_{Dd}} \quad ..(8)$$

Using a simple, practical engineering $m(p)_{oil}$ defined from inflow performance relationships, sufficient for decline curve analysis, (see Appendix), we would have for $\bar{p}_R \leq p_b$ (bubble point pressure)

$$\frac{kh}{\left[\ln\left(\frac{r_e}{r_w'}\right) - \frac{1}{2}\right]} = \frac{141.2\ (2\bar{p}_R)(\mu\beta)_{\bar{p}_R}}{(\bar{p}_R^2 - p_{wf}^2)} \cdot \frac{q(t)}{q_{Dd}} \quad ..(9)$$

and

$$V_p = \frac{2\bar{p}_R\ (\beta)_{\bar{p}_R}}{(c_t)_{\bar{p}_R}\ (\bar{p}_R^2 - p_{wf}^2)} \cdot \frac{t}{t_{Dd}} \cdot \frac{q(t)}{q_{Dd}} \quad ..(10)$$

Note that $\mu\beta$ is now evaluated at reservoir shut-in pressure, $\bar{p}_R$, as is (μc_t), which then allows cancellation of the viscosity terms in equation 10.

For cases where $p_{wf} < p_b$ and $\bar{p}_R > p_b$, as is the case for most of the School Creek Field wells in this study, the productivity factor is evaluated from

$$\frac{kh}{\left[\ln\left(\frac{r_e}{r_w'}\right) - \frac{1}{2}\right]} = \frac{141.2\ (\mu\beta)_{\bar{p}_R}}{\left[(\bar{p}_R - p_b) + \frac{(p_b^2 - p_{wf}^2)}{2p_b}\right]} \cdot \frac{q(t)}{q_{Dd}} \quad ..(11)$$

and

$$V_p = \frac{(\beta)_{\bar{p}_R}}{(c_t)_{\bar{p}_R}\left[(\bar{p}_R - p_b) + \frac{(p_b^2 - p_{wf}^2)}{2p_b}\right]} \cdot \frac{t}{t_{Dd}} \cdot \frac{q(t)}{q_{Dd}} \quad ..(12)$$

Equations 11 and 12 reduce to a simple Δp^2 form when $\bar{p}_R \leq p_b$ (see example equation A-9 in the Appendix).

To calculate a drainage radius from the pore volume, we have

$$r_e = \sqrt{\frac{V_p \times 5.615}{\pi h \phi}} \quad ..(13)$$

and oil in place at the start of the decline analysis is

$$OIP = \frac{V_p\ (1 - s_w)}{(\beta)_{\overline{p}_R}} \qquad ..(14)$$

Finally, the original oil in place is determined from

$$OOIP = OIP + N_p \qquad ..(15)$$

where N_p is the cumulative production to the start of the decline analysis.

Changes in Backpressure

Since many of the wells in the School Creek Field were evaluated under flowing conditions with more than one change in backpressure occurring, we have extended the single backpressure change superposition equation given in reference 2. Expressed in terms of $m(p)_{oil}$, for simplicity, we have

$$q(t) = \frac{kh\ [\ m(\overline{p}_R) - m(p_{wf1})\ ]}{141.2\left[\ln\left(\frac{r_e}{r_w'}\right) - \frac{1}{2}\right]} \left\{ q_{Dd}(t_{Dd}) \right.$$

$$+ \frac{m(p_{wf1}) - m(p_{wf2})}{m(\overline{p}_R) - m(p_{wf1})}\ q_{Dd}\ (t_{Dd} - t_{Dd1}) + \frac{m(p_{wf2}) - m(p_{wf3})}{m(\overline{p}_R) - m(p_{wf1})}$$

$$\cdot\ q_{Dd}\ (t_{Dd} - t_{Dd_2}) + \ . \ . \ . + \frac{m(p_{wfn-1}) - m(p_{wfn})}{m(\overline{p}_R) - (p_{wf1})}$$

$$\left. \cdot\ q_{Dd}\ (t_{Dd} - t_{Dd_{n-1}}) \right\} \qquad ..(16)$$

The rate change Δq for any backpressure change is a constant fraction of the initial rate at the same initial transient time period, as the rate change retraces the original q_{Dd} - t_{Dd} curve. The same value of the decline exponent b is used for all rate change superposition calculations.

$$\Delta q_1 = q_2 = q_1 \left[\frac{m(p_{wf1}) - m(p_{wf2})}{m(\overline{p}_R) - m(p_{wf1})} \right] \qquad ..(17)$$

and

$$\Delta q_2 = q_3 = q_1 \left[\frac{m(p_{wf2}) - m(p_{wf3})}{m(\overline{p}_R) - m(p_{wf1})} \right] \qquad ..(18)$$

Note that the $q_1/[m(\bar{p}_R) - m(p_{wf1})]$ is the initial productivity index in BOPD/psi or BOPD/psi^2, whichever is appropriate, times a Δp or $\Delta(p^2)$ term for successive flowing pressure changes.

For the more general expression used in this study for pressure above and below the bubble point pressure

$$\Delta q_1 = q_2 = \frac{q_1}{\Delta m(p)_1} \left[\frac{p_{wf1}^2 - p_{wf2}^2}{2p_b} \right] \quad ..(19)$$

and

$$\Delta q_2 = q_3 = \frac{q_1}{\Delta m(p)_1} \left[\frac{p_{wf2}^2 - p_{wf3}^2}{2p_b} \right] \quad ..(20)$$

where

$$\Delta m(p)_1 = (\bar{p}_R - p_b) + \left(\frac{p_b^2 - p_{wf1}^2}{2p_b} \right) \quad ..(21)$$

If and when $\bar{p}_R \leq p_b$ the expression reduces to the $\Delta(p^2)$ form. Similarly when $p_{wf} > p_b$ the Δp form is obtained. The Δp form would be appropriate for use with decline exponent values of b = 0 and Δp^2 form for b values greater than zero. For $\Delta(p^2)$, $\bar{p}_R \leq p_b$, the first backpressure change relationship becomes

$$\Delta q_1 = q_2 = \frac{q_1}{(\bar{p}_R^2 - p_{wf1}^2)} \cdot (p_{wf1}^2 - p_{wf2}^2) \quad ..(22)$$

For Δp, $p_{wf} > p_b$, the first backpressure change relationship becomes

$$\Delta q_1 = q_2 = \frac{q_1}{(\bar{p}_R - p_{wf})} \cdot (p_{wf1} - p_{wf2}) \quad ..(23)$$

Successive rate changes would be handled as shown in the previously given equations.

One should note that if $(\overline{\mu\beta})$ were correctly evaluated from $m(p)_{oil}$ using the inflow performance relationship discussed in the Appendix, all the decline curve analysis could be done directly in pressure terms i.e.

$$(\overline{\mu\beta}) = \frac{\bar{p}_R - p_{wf}}{m(\bar{p}_R) - m(p_{wf})} \quad ..(24)$$

A detailed example illustrating two backpressure changes is given for the Federal A-1 well, Figures 9 and 10 and Tables 9 and 9A. The example is carried out using the type curve match point and the basic Arps form of the decline equation. The procedure is quite simple using the concept of superposition given by equation 16.

A convenient equation[8] that can be used for calculating the <u>total</u> Δq as a result of n pressure changes is, for a Δp case,

$$P_{wfn} = P_{wf1} - \left\{ \frac{\bar{P}_R - P_{wf1}}{q_1} \left[\Delta q_1 + \Delta q_2 + \ldots + \Delta q_n \right] \right\} \quad ..(25)$$

for m(p)oil

$$P_{wfn} = \sqrt{P_{wf1}^2 - \frac{(2\bar{P}_R \; p_b - p_b^2 - P_{wf_1}^2)(\Delta q_1 + \Delta q_2 + \ldots + \Delta q_n)}{q_1}} \quad ..(26)$$

The Δq values are all specifically defined at a common point in time with respect to the initial rate q_1; 1 day or 1 month, for example. A one month time period is used in this study. The Federal A-1 example illustrates this point. (See Figure 9.) One can also back calculate intermediate flowing pressures and rate changes Δq while performance matching knowing the initial flowing pressure and rate, and the final flowing pressure. This also will be discussed with the Federal A-1 example.

Method of Decline Analysis

Log-Log Data Plots

The first step in approaching the rate-time log-log analysis in the study of the School Creek Field was to make a log-log plot of <u>all</u> the rate time data for each well. We next examined each well's plot to find when it actually started on decline. The rate time data was then reinitialized at the point of decline to t = 0 and a new log-log plot for each well was prepared. We have thus eliminated the constant rate or excess capacity time period which actually represents the constant rate solution instead of the constant wellbore pressure solution. <u>For log-log type curve analysis, we can't do decline analysis until the well is actually on decline</u>.

Based on the assumption that each well was draining its 160-acre spacing and that all wells had been equally stimulated - i.e., r_e/r_w' would then be the same for each well, a School Creek Field Type Curve was constructed by overlaying each well's log-log curve, with the axis all kept parallel, until a single curve was obtained. Figure 5 represents this attempt to obtain a total field type curve using data from 19 wells that exhibited a clear decline in their data. Note the "apparent" long transient period demonstrated by wells D-1, BA-1, and K-3. If this field type curve were valid, we would have a simple and quick method of preparing an oil production forecast and of determining ultimate recoverable reserves for these wells and the remaining completions. We would take the reinitialized log-log plot for each well, find the best match on the field type curve, and draw a line thru the data down the depletion stem of b = 0.30. Future rates would be read directly for the real time plot. Ultimate recovery would then be a summation of forecasted rates plus the cumulative production to the start of decline, plus any additional production as a result of placing the well on pump, where applicable.

To determine if the apparent transient stem was real, wells D-1, BA-1, and K-3 were all evaluated for k and skin (s) from a log-log type curve match on the

constant wellbore pressure solution (Figures 2 or 5 of reference 3). The evaluation of the match points lead to unreasonable values of permeability and, more specifically skins for all three wells. None of the wells were massively hydraulically fractured.

Well	K-md	s
D-1	0.017	-7.6
BA-1	0.040	-8.2
K-3	0.024	-8.0

It was therefore concluded that the data for these three wells was not really transient and should be placed in the early depletion period of the total field type curve. Figure 6 is our final School Creek Field Type Curve that does not exhibit a long transient stem. The field type curve is primarily a depletion type curve with a b = 0.30. (We will later discuss the b = 0.30 selected for this study.) Blind matching of log-log data to a type curve and extrapolation can sometimes lead to erroneous production forecasts. An evaluation of the match points to obtain reservoir variables for all wells being studied should give consistent and reasonable numbers when compared with each other thus confirming the validity of the forecast and the ultimate reserves numbers developed. The elimination of the apparent transient stem in this case is a good example of such a checking procedure. The composite type curve, Figure 4 of reference 2, was used for all match point evaluations performed in this study.

Basic Well and Reservoir Data

Table 1 lists basic individual well information and the match points obtained from a log-log type curve evaluation for 40 well completions. Three of the wells are commingled. The table lists first production, the start of decline analysis and the cumulative production to the start of the decline analysis. Initially, virtually all wells came on flowing with several on curtailed or restricted production before starting on decline. Many wells, because of early high gas-oil-ratios and gas disposition problems, were shut in for as much as a year before being returned to production. This accounts for the difference in time of as much as one year between first production and start of decline, with little cumulative production for some wells during this interval.

Reservoir shut-in pressures, $\bar{p}_R$, were generally assumed to be close to the original pressure of approximately 3600 psi, except in a few cases where bottomhole pressure surveys were available to indicate otherwise. Flowing pressures were estimated from general pressure surveys conducted on 10 wells in late 1982 and early 1983. Fluid levels shot on pumping wells indicated a minimum bottomhole flowing pressure of approximately 100 psi.

Porosity, thickness and water saturation for each well were furnished by a log analyst. Figure 4 is a permeability-porosity plot developed from 43 plug samples taken on four wells in the field. The core porosities, in general, are significantly less than the average values determined from log analysis. This will be discussed further under calculated r_e values.

The final four columns of the table list the match points obtained from the log-log type curve analysis for each of the well completions in terms of $t - t_{Dd}$ and $q(t) - q_{Dd}$ obtained using the composite type curve (Figure 4 of reference 2) and a decline exponent b = 0.30.

PVT Data

PVT properties required for evaluation of reservoir variables from the type curve match points are presented in Table 2 and also Figure 3. These are μ, β, and c_t, all evaluated at reservoir shut-in pressure, $\bar{p}_R$. The total compressibility term, c_t, was calculated using a water compressibility, c_w, of 3×10^{-6} psi^{-1} and pore volume compressibility, c_f, obtained from Hall's[13] correlation. The product $(\overline{\mu\beta})$ was "mechanically" evaluated at the average pressure $(\bar{p}_R + p_{wf})/2$.

Initially only two PVT samples were available for this study, the Federal EE-1 bottomhole samples to represent Channel Sand completions and the Federal J-1 bottomhole sample to represent Bar Sand completions. The Matheson E-1 PVT surface recombined sample became available only after our initial studies were virtually complete. This sample, because of the vastly different gas-oil-ratio (763 SCF/B versus 1557 SCF/B for the Federal EE-1 well) and because of being a surface recombined sample, had been labeled an unrepresentative sample. Inspection of initial GORs plotted for each well and a gas-oil-ratio versus fractional recovery curve, based on original oil in place developed from the match point evaluations, clearly suggested that the Matheson E-1 sample was valid. The final summary of the evaluation of reservoir variables from type curve analysis was made using the Federal EE-1 PVT data for all wells south of and including wells LL-1, H-1 and R-3. See Figure 1 and Tables 3 and 4. For wells to the north of these wells we used the PVT data from the Matheson E-2 well sample.

Because the study had been virtually completed when the Matheson E-1 sample results became available, we have included the results of all channel sand wells evaluated using both fluid samples. Basic patterns of evaluation results remained essentially the same between the northern and southern wells, i.e., higher percentage recoveries for the southern wells than the northern wells since their actual rate-time performance was based on the real fluid present, not what we selected to use for the final evaluation summary. The more undersaturated a well was, the less recovery would be obtained as compared with a well with a fluid saturated at its initial shut-in pressure, all else being equal. Tables 5, 6, 7, and 8 summarize the results of the match point evaluations based on $(\bar{p}_R - p_{wf})/(\overline{\mu_o\beta})$ and $m(p)_{oil}$ evaluation.

Calculated Results From Decline Curve Analysis

The final results of the type curve evaluation in terms of calculated reservoir variables are presented in Tables 3 and 4; the wells have been arranged on the basis of PVT areas. An $m(p)_{oil}$ evaluation was used for all results given in Table 3 and a $(\bar{p}_R - p_{wf})/(\overline{\mu_o\beta_o})$ evaluation for all values in Table 4.

Pore Volume (V_p)

The pore volume calculations are based on equations 6 and 12, where

$$V_p = \frac{(\overline{\mu\beta})}{(\mu c_t)_{\bar{p}_R} (\bar{p}_R - p_{wf1})} \cdot \frac{t}{t_{Dd}} \cdot \frac{q(t)}{q_{Dd}} \qquad ..(6)$$

and

$$V_p = \frac{(\beta)_{\bar{p}_R}}{(c_t)_{\bar{p}_R} \left[(\bar{p}_R - p_b) + \frac{(p_b^2 - p_{wf1}^2)}{2p_b} \right]} \cdot \frac{t}{t_{Dd}} \cdot \frac{q(t)}{q_{Dd}} \qquad ..(12)$$

Equation 6 would most certainly apply to reservoirs where the single phase liquid solution is applicable, i.e., where the decline curve exponent b = 0. The introduction of the $(\overline{\mu\beta})$ term evaluated at $(\bar{p}_R + p_{wf})/2$ with the Δp form is simply an attempt to account for solution-gas drive or two phase flow behavior. A rigorously derived $(\overline{\mu\beta})$ from m(p) concepts, as discussed previously, would be the approach to make equation 6 and 12 equivalent.

For solution gas drive reservoirs, Reference 2 demonstrates that the $\Delta(p^2)$ form of IPR (oil well backpressure curve with n = 1.0) used with a non-linear $\bar{p}_R$ versus N_p material balance relationship produces a decline exponent b = 0.33. Levine and Prats[9], in their simulation study of a solution gas drive reservoir producing under a constant wellbore pressure condition, presented a log q_D - log t_D type curve. (See their Figure 11.) The depletion stem of their type curve basically fits a decline exponent b $\cong$ 0.33. Figure 7 illustrates one of several wells in the School Creek Field that exhibited rate-time data in a sufficient stage of decline to help us establish a single decline exponent b $\cong$ 0.30. All our decline curve analysis and rate predictions were based on matching and forecasting on b = 0.30 for <u>all</u> wells. All forecasts for this study were done by graphical projection.

Figure 8 is a plot of percent recovery versus bottomhole flowing pressure for the Federal A-1 well. Using equations 6 and 12, the bottomhole flowing pressure was varied between 1600 psi to 100 psi and the pore volume V_p and OOIP calculated. Ultimate recovery was fixed at 36,000 BO for both $\Delta p/(\overline{\mu\beta})$ and $\Delta m(p)_{oil}$ cases to arrive at a percent recovery. Note the lack of sensitivity in percentage recovery for the $\Delta m(p)_{oil}$ case with the variation of bottomhole flowing pressure. Since the $\Delta m(p)_{oil}$ case is effectively a difference in pressures squared effect, we do not see a proportional increase in rate with drawdown as in the $(\overline{\mu\beta})$ case even though $(\overline{\mu\beta})$ was evaluated at each flowing pressure. This is virtually identical with the effect found for gas wells. The precise determination of flowing pressure, p_{wf}, may not then greatly affect our final results.

Oil in Place

Oil in place is calculated directly from V_p using equation 14

$$OIP = \frac{V_p (1 - s_w)}{(\beta)_{\bar{p}_R}} \qquad ..(14)$$

The calculated oil in place is at the start of decline which, when added to the cumulative production up to the start of the decline analysis, yields the original oil in place, OOIP, equation 15. The original oil in place is later used to calculate fractional oil recoveries, Table 10, and GOR versus fractional recovery, in an attempt to help identify or confirm different fluid properties used in the field analysis and also to possibly identify different rock types.

Calculated Drainage Radius (r_e)

A "calculated" drainage radius is determined from Vp with equation 13

$$r_e = \sqrt{\frac{V_p \times 5.615}{\pi h \phi}} \qquad ..(13)$$

The calculated value of r_e is not only a function of pore volume V_p determined from the type curve analysis match point, but also of porosity ϕ and thickness h. In this type of reservoir, with indicated thin "dirty" sands and possible limited areal extent, the value of average h used as determined for the logs may be too high. This would result in a calculated r_e value in some cases much less than r_e = 1490 feet for 160 acres. Also, very few of the core sample plugs obtained from wells in the field (see Figure 4) appear to approach the average porosity values reported from the log analysis listed on Table 1. If one were to build a simulation model of the School Creek Field, outlined in Figure 1, based on the log derived values of ϕ, h, and 160 acre spacing for each well, we would have to cut the pore volume to match the type curve analysis derived reservoir variables, specifically oil in place, that have already been history matched to the rate-time decline data.

To come up with calculated values of r_e, approaching on average the 160 acre field spacing, the ϕh product would have to be decreased. Otherwise, the rather tenuous conclusion that many wells are not draining the existing spacing could lead to a consideration of infill drilling.

Productivity Factor (P.F.)

The productivity factors for each well are calculated from equations 5 and 11,

$$P.F. = \frac{kh}{\left[\ln\left(\frac{r_e}{r_w'}\right) - \frac{1}{2}\right]} = \frac{141.2\ (\overline{\mu\beta})}{\overline{p}_R - p_{wf1}} \cdot \frac{q(t)}{q_{Dd}} \qquad ..(5)$$

where $(\overline{\mu\beta})$ is evaluated at average pressure $(\overline{p}_R + p_{wf})/2$

and

$$\frac{kh}{\left[\ln\left(\frac{r_e}{r_w'}\right) - \frac{1}{2}\right]} = \frac{141.2\ (\mu\beta)_{\bar{p}_R}}{\left[(\bar{p}_R - p_b) + \frac{(p_b^2 - p_{wf1}^2)}{2p_b}\right]} \cdot \frac{q(t)}{q_{Dd}} \qquad ..(11)$$

Since there is a lack of early time transient rate data to sufficiently define an r_e/r_w' stem, unique values of permeability and skin cannot be calculated for each well. We know that all completions were initially stimulated. The core data indicates an arithmetic average permeability of 0.650 md and a geometric average of 0.195 md, with a range of 0.2 md to 7 md. We also had one buildup test conducted on the KK-1 well where the final flowing pressure prior to shut-in was above the bubble point pressure. The analysis yielded a value of k = 2.5 md and s = -3.4.

A range of values of skin from 0 to -4 was selected to evaluate permeabilities for each well. When we fix r_w' on the basis of skin, $r_w' = r_w e^{-s}$, and having previously calculated r_e from the pore volume calculation we can then calculate kh and k from equations 5 and 11.

The ranges of values of k listed on tables 3 and 4 for various values of skin are surprisingly narrow within a given table and even between the two methods of calculation used. It should be pointed out that the values of permeability and skin calculated from the decline curve analysis are those at the <u>start</u> of the decline analysis.

If a good correlation from the core derived ϕ - k plot had been obtained and if log derived average porosities were considered reasonably reliable, we could have used it to determine k and then its corresponding skin from the tables for each well. Based solely on the KK-1 build-up analysis results and the fact that all wells were stimulated, one could also select the -3 skin columns on Table 3 or 4 to arrive at specific values of permeability at the start of decline for each well. There are no unreasonable values of permeabilities listed on either table. Nearly all lie within the range of the core permeabilities shown on Figure 4. Values of permeabilities in the 10s or 100s md on any well would, of course, be suspect.

<u>Example of Effect of Backpressure Change on Recovery and Decline</u>

The equations to calculate the change in producing rates with backpressure changes have been given previously as equations 16 -26. The Federal A-1 well produced against three different flowing pressures that resulted in two rate changes. Figure 9 is a log-log plot of the rate-time data with the solid line through the points calculated from the type curve match points used with the Arps hyperbolic decline equation. Only the first and last flowing pressure of 1400 psi and 100 psi, respectively, were known. Equation 26, solved in terms of Δq total with p_{wf3} = 100 psi yielded a total Δq = 747 BOPM. A trial and error calculation was then made varying Δq_1 until a best fit of both rate changes was obtained. This resulted in a p_{wf2} = 1069 psi.

Tables 9 and 9-A illustrate in detail the method of developing a forecast with two backpressure changes using the $m(p)_{oil}$ approach. Note specifically that since the rate-time decline is undergoing depletion, the Arps equation is used for all the calculations. One does not have to deal with the reservoir variables, kh, s, r_e/r_w', obtained from the match evaluations. This, however, would not be the case for a transient situation. Theoretically, the rates for the first few months should be calculated at the mid-point of the time interval, i.e., 0.5, 1.5, 2.5, to represent average monthly production rates. For simplicity of presentation of the superposition example, the rates have been evaluated at full month time intervals.

Table 9-A column 2 lists the rates for the initial flowing pressure, p_{wf1}, calculated from Arps' equation with b = 0.3, q_i = 4545.5 BOPM and D_i = 0.212 $mo.^{-1}$. The rate change as a result of a choke change to p_{wf2} = 1069 psi is listed in column 3. It is simply a constant fraction of the initial decline rates. The second backpressure change, when the well was placed on pump to p_{wf3} = 100 psi, is treated similarly. For superposition, columns 3 and 4 are retabulated at a time 1 month past the actual time of the pressure change. Total rate is then the sums of columns 2, 5, and 6. Adding the cumulative production to the start of decline analysis (2633 BO), we have

	N_p Ultimate, BO	
	$\Delta m(p)_{oil}$	$\Delta(p)$
No backpressure change	30,347	30,347
First backpressure change	32,667	34,668
Second backpressure change	35,858	47,226

The Δp numbers in the above table were generated for comparison by recalculating Δq_1 and Δq_2 on the basis of a Δp superposition using equation 23. From this approach, a procedure using actual production data (and its projected rates for a known initial flowing pressure) could be developed to determine the effect of a backpressure change on ultimate recovery, as follows:

Determine N_p at p_{wf1} to t = T, where T = total time of rate-time forecast,

$$\text{then} \quad \Delta N_{p1} = \frac{\Delta q_1}{q_1} \cdot \sum_{t=1}^{T-t\ @\ p_{wf_2}} q \text{ actual}$$

$$\text{and} \quad \Delta N_{p2} = \frac{\Delta q_2}{q_1} \cdot \sum_{t=1}^{T-t\ @\ p_{wf_3}} q \text{ actual}$$

where q actual may also be actual production plus that projected for the initial flowing pressure, p_{wf1}.

$$\text{Ultimate Recoverable} = N_p + \Delta N_{p_1} + \Delta N_{p_2}$$

Similarly, actual early time production rates instead of calculated values can be used to generate the rate-time superposition as illustrated in Table 9-A. This in essence would have the effect of including a downtime if any early time rate variations were due to downtime.

Figure 10 illustrates one more point about backpressure changes with regard to the decline exponent. As has been previously pointed out in references 2 and 3, the sum of two forecasts, both having the same value of decline exponent b, will rarely result in a total forecast having the same decline exponent. In general, the total forecast decline exponent will be larger. Reinitializing the rate-time data after the second backpressure change which also has b = 0.3 resulted in a decline exponent b = 0.40.

Finally, unless all wells are placed on pump at the same time, a backpressure change can cause a well's drainage radius to increase with respect to offset wells. The given superposition example implicitly assumes that r_e remains constant.

Commingled Wells

There are three wells in the School Creek Field where Bar Sand production and Channel Sand production are presently commingled. Figures 11 and 12 for the Federal K-1 well illustrate the method of analysis used to evaluate these wells. A difference curve was developed between the forecast rates of the Channel Sand production only and the commingled production which came on production later. Separate forecasts were then made and added together.

Summary of School Creek Field OOIP and Ultimate Recovery

Table 10 summarizes the results of the calculated original oil in place and ultimate recovery forecast for each well based on an $m(p)_{oil}$ and a $\Delta p/(\overline{\mu\beta})$ evaluation. The superposition of rates as a result of backpressure changes using Equations 19 and 23 have also been included where appropriate.

Channel Sand completion results are divided into the northern and southern areas of the field based on the two PVT samples discussed previously. Both evaluation methods indicate a much lower percentage recovery for wells in the northern portion of the field as compared with wells in the southern portion. Wells in the southern portion have percentage recoveries near twice those of wells to the north. This would be consistent solely on the basis of the difference in bubble point pressure between the two fluid samples. Values of percentage recoveries are always lower for the $m(p)_{oil}$ evaluation method. With regard to the additional recoverable reserves that could possibly be obtained by placing all wells on pump to a final bottomhole flowing pressure of 100 psi, the following table summarizes those results. (Nearly half of the wells were initially at or near 100 psi bottomhole flowing pressure at the start of decline.)

	Reserves for Initial Flowing Pressure	Increase of $m(p)_{oil}$ Reserves to p_{wf} of 100 psi		Increase of $\Delta p/(\overline{\mu\beta})$ Reserves to p_{wf} of 100 psi	
	STB	STB	% Increase	STB	% Increase
Northern Wells	223,900	15,594	7%	51,361	23%
Southern Wells	312,105	19,220	6%	67,605	22%
Total Field	819,484	68,354	8%	230,346	28%

If, in fact, the inflow performance relationship based on Δp^2 applies, the percentage increase as a result of placing all wells on pump to a final flowing pressure of 100 psi would be approximately 8% or 68,000 BO. If the inflow performance relationship were to follow a Δp (PI) behavior, the anticipated increase in reserves would be 28% or 230,000 BO. Perhaps the real increase in reserves due to lowering the final bottomhole flowing pressure lies somewhere between these two limits.

Individual Well Gas-Oil-Ratio Performance

Figures 13 thru 16 reflect gas-oil-ratio performance of individual wells in the field based on expressing the recovery factor in terms of each well's actual cumulative production divided by the OOIP calculated from the $m(p)_{oil}$ evaluation. Either method of calculating OOIP should show similar trends. Gas and oil rates are metered separately for each well and are not based on allocation from tests.

Figures 13 and 14 are on an expanded gas-oil-ratio scale in an attempt to help identify rock types in each area of the field. If one assumes the fluids are the same for each area, three different rock types and/or initial water saturations are possibly indicated in the southern portion of the field.

Figures 15 and 16, prepared on a scale where the entire gas-oil-ratio performance of each well can be shown clearly, indicate two different fluids, based mainly on the wells' peak gas-oil-ratio alone which is not a function of the method of calculating an OOIP number. Note that the gas-oil-ratio has turned over on several wells. The peak gas-oil-ratios for the northern wells is generally much lower than those of the southern wells. These gas-oil-ratio curves could be used in developing a gas forecast to go with the oil rate forecast developed from the decline curve analysis.

Conclusions

Original oil in place values can be calculated from rate-time analysis for individual wells and can also be used with reserves projections developed from the decline analysis to obtain fractional recoveries for each well in a field. These fractional recovery numbers should be reasonable, considering the fluid type and the permeability of the reservoir.

Each well's evaluation of the reservoir variables k, s (skin), OOIP and fractional recovery, obtained from individual well rate-time decline analysis, should give consistent and reasonable numbers when compared with other wells in the field. A single well analysis can give results that are not recognized as being invalid unless compared with other wells in the field.

Failure to consider a future lowering of a well's flowing bottomhole pressure from that causing a well's initial rate-time decline can result in underestimating ultimate recoverable reserves.

A method of treating future backpressure changes based on the superposition principle and an oil well inflow performance relationship is easily applied to decline curve analysis. An oil well inflow performance relationship can be utilized over an entire production forecast, not only at an instant in time.

Nomenclature

b = reciprocal of decline curve exponent (1/b)
β = formation volume factor res vol/surface vol
c_f = effective rock compressibility, psi^{-1}
c_t = total compressibility, psi^{-1}
c_w = water compressibility, psi^{-1}
D_i = initial decline rate, t^{-1}
e = natural logarithm base 2.71828
h = thickness, ft
k = effective permeability, md
k_{ro} = relative permeability to oil, fraction
$m(p)_{oil}$ = oil pseudo pressure, psi/cp
n = exponent of backpressure curve
N_p = cumulative oil production, STB
OIP = oil in place at start of decline analysis, STB
OOIP = original oil in place, STB
p_b = bubble point pressure, psia
$\overline{p}_R$ = reservoir shut-in pressure, at start of decline, psia
p_{wf} = bottomhole flowing pressure, psia
q_{Dd} = decline curve dimensionless rate
$q(t)$ = surface rate of flow at time t
r_e = external boundary radius, ft
r_w = wellbore radius, ft
r_w' = effective wellbore radius, ft
s = skin factor, dimensionless

S_w = water saturation
t = time, mo
t_{Dd} = decline curve dimensionless time
T = total time of forecast, mo
V_p = reservoir pore volume, ft^3
μ = viscosity, cp
ϕ = porosity, fraction of bulk volume

Acknowledgements

We wish to thank Phillips Petroleum Company for permission to publish to this paper. We also wish to thank U. G. Kiesow, M. D. Bradley, and S. D. Dunstan for their timely assistance in parts of this study.

References:

1. Arps, J. J.: "Analysis of Decline Curves", TRANS, AIME (1945) 160, 228-247.

2. Fetkovich, M. J.: "Decline Curve Analysis Using Type Curves," J. Pet. Tech (June 1980) 1065-1077.

3. Fetkovich, M. J., Vienot, M. E., Bradley, M. D., and Kiesow, U.G.: "Decline Curve Analysis Using Type Curves Case Histories," paper SPE 13169 presented at the 59th Annual Fall Meeting of SPE of AIME, Houston, Texas, September 1984.

4. Carter, R. D.: "Characteristic Behavior of Finite Radial and Linear Gas Flow Systems - Constant Terminal Pressure Case," SPE/DOE 9887 presented at the 1981 SPE/DOE Low Permeability Symposium, Denver, CO, May 27-29, 1981.

5. Carter, R.D: "Type Curves for Finite Radial And Linear Gas-Flow Systems: Constant Terminal Pressure Case," SPE 12917 presented at the 1984 Rocky Mountain Regional Meeting, Casper, WY, May 1984.

6. Da Prat, Giovanni, Cinco-Ley, Heber and Ramey, H. J. Jr.: "Decline Curve Analysis Using Type Curves for Two-Porosity Systems," Soc. Pet. Eng. J. (June 1981) 354-362.

7. Fetkovich, M. J. and Vienot, M. E.:"Shape Factor, C_A, Expressed as a Skin, S_{C_A}," J. Pet. Tech. (February 1985) 321-322.

8. Bradley, M. D.: Personal communication.

9. Levine, J.S. and Prats, M: "The Calculated Performance of Solution Gas Drive Reservoirs," Soc. Pet. Eng. J. (Sept. 1961) 145-152.

10. Fetkovich, M. J.: "The Isochronal Testing of Oil Wells", paper SPE 4529 presented at the 48th Annual Fall Meeting, Las Vegas, NV., Sept. 30 -October 3, 1973. (SPE Reprint Series No. 14,265).

11. Vogel, J. V.: "Inflow Performance Relationships for Solution Gas Drive Wells," J. Pet. Tech. (Jan. 1968), 83.

12. Whitson, C. H.: "Reservoir Well Performance and Predicting Deliverability," Unsolicited paper SPE 12518, U. of Trondheim.

13. Craft, B. C. and Hawkins, M. F., Jr.: "Applied Petroleum Reservoir Engineering, Prentice Hall, Inc. Englewood Cliffs, N.J. (1959) 132.

SI Metric Conversion Factors

acre	x	4.046873 E + 03	=	m^2
bbl	x	1.589873 E - 01	=	m^3
bbl/D	x	1.589873 E - 01	=	m^3/D
cp	x	1.0* E - 03	=	Pa·3
ft	x	3.048* E - 01	=	m
ft^3/D	x	2.831685 E - 02	=	M^3/D
md	x	9.869233 E - 04	=	μm^2
psi	x	6.894757 E - 03	=	MPa

* conversion factor is exact

Appendix

Oil Pseudo Pressure, $m(p)_{oil}$ For Decline Curve Analysis

Reference 10 introduced the concept of a pseudo-pressure m(p) for oil well drawdown tests similar to that now commonly used for gas wells. It was presented along with a general inflow performance relationship developed from multi-point test data of some 40 oil well tests.

A general inflow performance equation for decline analysis that treats flow both above and below the bubble point pressure for an undersaturated oil well assuming no non-darcy flow component is

$$q_o = J^* (\bar{p}_R - p_b) + J' (p_b^2 - p_{wf}^2) \qquad ..(A\text{-}1)$$

$$\text{where } J^* = \frac{kh}{141.2 \left[\ln \left(\frac{r_e}{r_w'} \right) - \frac{1}{2} \right]} \cdot \left(\frac{k_{ro}}{\mu_o \beta_o} \right)_{\bar{p}_R} \qquad ..(A\text{-}2)$$

$$\text{and } J' = J^* (\mu_o \beta_o)_{\bar{p}_R,\ p_b} \cdot \frac{a_2}{2} \qquad ..(A\text{-}3)$$

Assuming $(\mu_o\beta_o)$ is a constant value above the bubble point pressure equal to $(\mu_o\beta_o)_b$ (the basis for the constant PI assumption for flow above the bubble point pressure, P_b) then (See also Appendix of reference 10)

$$a_2 = \frac{1}{P_b\ (\mu_o\beta_o)_{P_b}} \qquad ..(A\text{-}4)$$

For $1/\mu_o\beta_o$ to go through a zero intercept on drawdown, we are really looking at a $(k_{ro})_{P_{wf}}/(\mu_o\beta_o)$, a pseudo $(\mu_o\beta_o)$. This then would reproduce field data log-log IPR curves with n = 1.00 and also Vogel's[11] Figure 7, a <u>computer</u> generated IPR. (Figure 17 in this paper.)

Thus

$$J' = \frac{J^*\ (\mu_o\beta_o)P_b}{2P_b\ (\mu_o\beta_o)P_b} = \frac{J^*}{2P_b} \qquad ..(A\text{-}5)$$

Substituting equation (A-5) into (A-1) we obtain the final form of the single phase and two phase IPR equation

$$q_o = J^*\left[(\bar{P}_R - P_b) + \frac{(P_b^2 - P_{wf}^2)}{2P_b}\right] \qquad ..(A\text{-}6)$$

or in terms of reservoir variables, with $k_{ro} = 1$ at start of decline analysis

$$q_o = \frac{kh}{141.2\left[\ln\left(\frac{r_e}{r_w'}\right) - \frac{1}{2}\right]} \cdot \frac{1}{(\mu_o\beta_o)_{\bar{P}_R}}\left[(\bar{P}_R - P_b) + \frac{(P_b^2 - P_{wf}^2)}{2P_b}\right] \qquad ..(A\text{-}7)$$

or in terms of $m(p)_{oil}$

$$q_o = \frac{kh}{141.2\left[\ln\left(\frac{r_e}{r_w'}\right) - \frac{1}{2}\right]} \cdot \left[m(\bar{P}_R) - m(P_{wf})\right] \qquad ..(A\text{-}8)$$

For the case of $\bar{P}_R \leq P_b$ we have from equation (A-7)

$$q_o = \frac{kh}{141.2\left[\ln\left(\frac{r_e}{r_w'}\right) - \frac{1}{2}\right]} \cdot \frac{1}{(\mu_o\beta_o)_{\bar{P}_R}} \cdot \frac{(\bar{P}_R - P_{wf}^2)}{2_{\bar{P}_R}} \qquad ..(A\text{-}9)$$

With $\bar{p}_R \leq p_b$ we can compare the Vogel and the Δp^2 inflow relationship in terms of $m(p)_{oil}$. We have

$$\Delta p^2 \text{ form: } m(p)_{oil} = \frac{1}{2\bar{p}_R} \cdot \left(\frac{k_{ro}}{\mu_o \beta_o}\right)_{\bar{p}_R} \cdot p^2 \qquad ..(A\text{-}10)$$

$$\text{Vogel form}^{12}\text{: } m(p)_{oil} = \frac{1}{9} \left(\frac{k_{ro}}{\mu_o \beta_o}\right)_{\bar{p}_R} \cdot \left(p + \frac{4p^2}{\bar{p}_R}\right) \qquad ..(A\text{-}11)$$

The Vogel Form would be extremely cumbersome if entered into the constant wellbore pressure solutions as an $m(p)_{oil}$ expression whereas the Δp^2 form results in a simple expression identical in form to the low pressure gas well backpressure equation. Oil well IPR curves, just as gas well backpressure curves are most applicable to the constant wellbore pressure solution conditions. A comparison of the Δp^2 form of IPR and Vogel's IPR equation (both these forms assume a non-Darcy flow component of zero) can be seen in Figure 17. The results shown on Vogel's Figure 7 are the only complete set of curves given in his paper with which we could make a comparison of the two methods when using the same match point. Vogel's points of match A thru H were used to develop the comparison. Note from the Figure 17 comparison that the Δp^2 form of the equation better fits his computer calculated IPR over the <u>entire range of depletion</u> than his own dimensionless form of the IPR equation. At very low flowing pressures approaching 0 flowing pressure, a region we seldom deal with, the Δp^2 form is slightly less than the simulation run result but still closer than using Vogel's dimensionless equation.

Reference 2 illustrates that when the Δp^2 form of the IPR equation is combined with a non-linear p versus N_p relationship for solution gas drive reservoirs, the expected decline curve exponent b = 0.333. This is practically the same value as that found and used in this study.

TABLE 1

SCHOOL CREEK FIELD, CAMPBELL - CONVERSE CO., WYOMING
BASIC RESERVOIR DATA AND DECLINE CURVE MATCH POINTS

	Well	Date (Mo - Yr) First Production	Date (Mo - Yr) Start of Decline Analysis	Well Status Pump or Flow	Well Status Date on Pump	N_p to Decline STB	$\bar{P}_R$ psia	P_{wf} psia	Log Data ϕ Fraction	Log Data h Feet	Log Data $(1-s_w)$ Fraction	Match Point w/(b=0.30) t mo	Match Point w/(b=0.30) t_{Dd}	Match Point w/(b=0.30) q(t) BOPM	Match Point w/(b=0.30) q_{Dd}
	A-1	6-81	9-81	F	12-83	2633	3500	1400	.137	9	.70	1	0.212	1000	0.220
	C-1	6-81	10-81	P	8-81	6226	3600	100	.138	15	.60	1	0.058	1000	0.680
	D-2	1-83	1-83	P	3-82	0	3600	500	.161	7	.52	1	0.156	10	0.110
	DD-1	6-82	3-83	F		7828	2900	600	.103	8	.60	1	0.354	1000	0.590
	EE-1	5-82	3-83	F		13839	3000	1000	.134	12	.50	1	0.313	1000	0.432
	F-1	10-83	10-83	P	6-83	0	3600	100	.100	11	.30	1	0.210	10	0.076
	FF-1	4-82	10-83	F		7642	3300	800	.145	10	.70	1	0.510	100	0.086
	G-1	6-82	7-82	P	11-83	289	3500	2000	.160	10	.60	1	0.100	100	0.270
	GG-1	6-82	9-82	F		3582	3600	1000	.120	5	.60	1	0.130	1000	0.430
	GG-2	6-82	6-82	P	11-83	0	3600	400	.125	14	.60	1	0.098	1000	0.914
	H-1	10-81	10-81	P	10-81	0	3600	100	.165	8	.60	1	0.083	1000	0.670
	I-1	9-81	9-82	F		3839	2900	700	.158	14	.70	1	0.290	1000	0.190
	J-1 (B)	5-82	5-83	F	9-83	1761	3600	1400	.240	17	.85	1	0.146	1000	0.205
	JJ-1	8-82	8-83	F		4287	3100	600	.149	13	.75	1	0.115	100	0.150
	K-1	5-82	6-82	F		501	3600	1000	.134	3.5	.60	1	0.075	1000	0.580
	K-1 (B)	3-83	3-83	F		0	3600	1000	.240	5	.90	1	0.185	1000	0.278
	K-4	5-82	12-82	P	12-82	7460	3300	100	.150	10	.60	1	0.210	1000	0.417
	KK-1	8-82	5-83	F		3643	3300	2000	.130	4	.50	1	0.229	1000	0.527
	KK-2	8-82	7-83	P	7-83	1535	3600	100	.140	38	.70	1	0.190	100	0.098
	LL-1	8-82	5-83	P	3-83	1468	3600	100	.132	10	.65	10	0.079	10	0.550
	LL-2 (B)	8-82	6-83	F		3327	3600	1000	.170	4	.70	1	0.250	100	0.098
	O-1	11-81	4-82	F		21473	3600	1600	.148	11	.75	1	0.178	1000	0.231
	Q-1	1-83	6-83	P	6-83	689	3600	100	.140	10	.50	1	0.144	100	0.310
	R-1	8-82	8-83	P	6-83	1635	3600	100	.123	6	.60	1	0.130	100	0.380
	R-2	9-82	8-83	P	3-83	1169	3600	100	.120	10	.60	1	0.092	100	0.670
	R-3	7-82	12-82	F		5443	3600	1000	.150	7	.60	1	0.063	1000	0.285
	R-3 (B)	5-83	5-83	F		0	3600	1000	.200	15	.90	1	0.115	100	0.047
	R-4	4-82	5-83	F		12237	3500	1200	.132	10	.60	1	0.118	100	0.070
	S-1	4-82	5-82	F		24533	3600	1000	.150	12	.70	1	0.115	1000	0.264
	S-1 (B)	5-83	5-83	F		0	3400	1200	.210	18	.85	1	0.205	1000	0.200
	T-1	3-82	6-83	F		23195	3300	1000	.142	20	.75	1	0.280	100	0.069
	T-2	5-82	8-83	F		8146	3300	1000	.158	15	.80	1	0.270	100	0.250
	T-3	5-82	7-83	P	7-83	1383	3600	100	.153	8	.75	1	0.200	100	0.280
	T-4	7-82	5-83	F		7692	3300	1200	.138	14	.55	1	0.239	100	0.201
	T-5	2-83	4-83	P	4-83	245	3600	100	.134	11	.65	1	0.300	100	0.088
Ford	A-1	6-82	7-82	F		1871	3600	1300	.143	15	.60	1	0.165	1000	0.330
Ford	B-1	9-82	2-83	P	11-82	319	3600	100	.152	17	.70	1	0.078	100	0.170
Math	B-1	10-80	10-81	P	10-80	10776	3300	100	.160	7	.52	1	0.0713	100	0.131
Math	D-1	5-82	5-82	P	3-82	0	3300	600	.143	5	.70	1	0.100	100	0.240
Math	E-1	7-81	12-81	P	12-82	7860	3500	1000	.152	16	.60	1	0.111	1000	0.188

TABLE 2

SCHOOL CREEK FIELD, CAMPBELL - CONVERSE CO., WYOMING

	Channel Sand PVT Data								Bar Sand PVT Data			
	Federal EE-1 PVT (p_b = 3400)				Matheson E-1 PVT (p_b = 2705)				Federal J-1 PVT (p_b = 2853)			
Well	@ $\bar{p}_R$ μ_o cps	@ $\bar{p}_R$ β_o RB/STB	@ p avg. $(\overline{\mu_o \beta_o})$ cps-RB/STB	@ $\bar{p}_R$ c_t x 10^{-6} psi^{-1}	@ $\bar{p}_R$ μ_o cps	@ $\bar{p}_R$ β_o RB/STB	@ p avg. $(\overline{\mu_o \beta_o})$ cps-RB/STB	@ $\bar{p}_R$ c_t x 10^{-6} psi^{-1}	@ $\bar{p}_R$ μ_o cps	@ $\bar{p}_R$ β_o RB/STB	@ p avg. $(\overline{\mu_o \beta_o})$ cps-RB/STB	@ $\bar{p}_R$ c_t x 10^{-6} psi^{-1}
A-1	0.150	1.90	0.366	27.4	0.46	1.47	0.647	15.7				
C-1	0.150	1.90	0.420	24.6	0.46	1.47	0.696	14.5				
D-2	0.150	1.90	0.400	22.1	0.46	1.47	0.677	13.2				
DD-1	0.200	1.70	0.431	24.5	0.43	1.48	0.707	15.0				
EE-1	0.200	1.70	0.405	21.6	0.44	1.48	0.682	13.4				
F-1	0.150	1.90	0.420	15.9	0.46	1.47	0.696	11.6				
FF-1	0.180	1.70	0.400	27.4	0.45	1.47	0.677	15.6				
G-1	0.150	1.90	0.344	24.5	0.46	1.47	0.638	14.2				
GG-1	0.150	1.90	0.378	24.5	0.46	1.47	0.658	14.7				
GG-2	0.150	1.90	0.405	24.5	0.46	1.47	0.682	14.7				
H-1	0.150	1.90	0.420	24.5	0.46	1.47	0.696	14.1				
I-1	0.200	1.70	0.425	27.5	0.43	1.48	0.702	15.5				
J-1 (B)									0.20	1.70	0.355	25.9
JJ-1	0.180	1.73	0.420	28.9	0.44	1.48	0.696	16.2				
K-1	0.150	1.90	0.378	24.5	0.46	1.47	0.658	14.5				
K-1 (B)									0.20	1.70	0.368	26.9
K-4	0.155	1.88	0.447	24.5	0.45	1.47	0.712	14.3				
KK-1	0.158	1.89	0.351	21.6	0.45	1.89	0.638	13.3				
KK-2	0.150	1.90	0.420	27.5	0.46	1.47	0.696	20.8				
LL-1	0.150	1.90	0.420	26.0	0.46	1.47	0.696	15.2				
LL-2 (B)									0.20	1.70	0.363	22.5
O-1	0.150	1.90	0.355	28.9	0.46	1.47	0.640	16.2				
Q-1	0.150	1.90	0.420	21.7	0.46	1.47	0.696	13.2				
R-1	0.150	1.90	0.420	24.6	0.46	1.47	0.696	14.7				
R-2	0.150	1.90	0.420	24.6	0.46	1.47	0.696	14.7				
R-3	0.150	1.90	0.378	24.5	0.46	1.47	0.658	14.3				
R-3 (B)									0.20	1.70	0.363	26.9
R-4	0.150	1.90	0.374	24.3	0.46	1.47	0.655	14.5				
S-1	0.150	1.90	0.378	27.4	0.46	1.47	0.658	15.5				
S-1 (B)									0.20	1.70	0.363	25.9
T-1	0.180	1.70	0.391	28.9	0.45	1.47	0.670	16.3				
T-2	0.180	1.72	0.391	30.4	0.45	1.47	0.670	16.7				
T-3	0.150	1.72	0.420	29.0	0.46	1.47	0.696	16.0				
T-4	0.180	1.90	0.382	23.2	0.45	1.47	0.672	13.9				
T-5	0.150	1.72	0.420	26.0	0.46	1.47	0.696	15.3				
Ford A-1	0.150	1.90	0.367	24.5	0.46	1.47	0.647	14.4				
Ford B-1	0.150	1.90	0.420	27.4	0.46	1.47	0.696	15.4				
Math B-1	0.158	1.88	0.437	22.1	0.45	1.47	0.712	13.1				
Math D-1	0.150	1.90	0.410	27.4	0.45	1.47	0.686	15.6				
Math E-1	0.150	1.90	0.382	24.4	0.46	1.47	0.672	14.2				

TABLE 3

SCHOOL CREEK FIELD - CALCULATED DECLINE CURVE ANALYSIS RESULTS
$m(p)_{oil}$ EVALUATION

	Well	Pore Vol. V_p RB	Start of Decline OIP STB	OOIP STB	Calculated r_e feet	$\frac{kh}{\ln \frac{r_e}{r_w'} - \frac{1}{2}}$	Prod. Factor s = 0 r_w' = .328 $\frac{k}{}$ - md	s = -1 r_w' = .892 $\frac{k}{}$ - md	s = -2 r_w' = 2.424 $\frac{k}{}$ - md	s = -3 r_w' = 6.588 $\frac{k}{}$ - md	s = -4 r_w' = 17.90 $\frac{k}{}$ - md	
	A-1	1104447	525927	528560	1265	7.8542	6.77	5.90	5.02	4.15	3.28	
	C-1	1144643	467201	473427	994	2.0567	1.03	0.89	0.76	0.62	0.48	
	D-2	29481	10429	10429	216	0.1297	0.11	0.09	0.07	0.05	0.04	
	F-1	35358	7216	7216	240	0.1840	0.10	0.09	0.07	0.05	0.04	
	G-1	272285	111137	111426	552	0.8261	0.57	0.49	0.41	0.32	0.24	
	JJ-1	315066	159662	143949	539	1.1995	0.64	0.54	0.45	0.35	0.27	
	K-1	1486687	606811	607312	2380	2.6253	6.29	5.54	4.79	4.04	3.29	
	K-4	603338	246261	253721	848	3.7869	2.79	2.41	2.03	1.65	1.27	
	Q-1	111090	37786	38475	377	0.4511	0.30	0.25	0.21	0.16	0.11	
	R-1	90143	36793	38428	467	0.3680	0.41	0.35	0.29	0.23	0.17	
	R-2	72243	29487	30656	328	0.2087	0.13	0.11	0.09	0.07	0.05	
Ford	A-1	968836	395443	397314	898	4.9183	2.43	2.10	1.78	1.45	1.12	Channel Sand
Ford	B-1	320561	152648	152967	471	0.8227	0.33	0.28	0.23	0.18	0.13	Matheson E-1 PVT
Math	B-1	617476	218427	229203	993	1.2054	1.29	1.12	0.95	0.78	0.61	
Math	D-1	208739	99399	99399	722	0.6806	0.98	0.84	0.71	0.57	0.44	
Math	E-1	2550551	1041041	1048901	1369	8.5120	4.17	3.64	3.11	2.57	2.04	
	DD-1	239364	84482	92310	721	1.9285	1.73	1.49	1.25	1.01	0.77	
	EE-1	436544	128395	142234	697	2.7416	1.64	1.41	1.18	0.95	0.72	
	FF-1	91086	37506	45148	335	1.0641	0.68	0.58	0.47	0.36	0.26	
	GG-1	791422	249923	253505	1535	1.7561	2.79	2.44	2.09	1.74	1.39	
	GG-2	461396	145704	145704	686	0.7718	0.39	0.34	0.28	0.23	0.17	
	H-1	734543	231961	231961	997	1.0406	0.98	0.85	0.72	0.59	0.46	
	I-1	821613	338311	342150	815	6.0868	3.18	2.75	2.31	1.88	1.44	
	KK-1	694523	183736	187379	1545	2.5211	5.02	4.38	3.75	3.12	2.49	
	KK-2	195445	72006	73541	256	0.7114	0.12	0.10	0.08	0.06	0.04	
	LL-1	72149	24682	26150	313	0.0126	0.01	0.01	0.01	.01	.01	
	O-1	1049477	414267	435740	1073	3.7613	2.60	2.25	1.91	1.57	1.23	
	R-3	2463966	778095	783538	2048	2.6496	3.12	2.74	2.36	1.98	1.60	Channel Sand
	R-4	374090	118134	130371	712	1.1906	0.86	0.74	0.62	0.50	0.38	Federal EE-1 PVT
	S-1	1302969	480041	504574	1137	2.8604	1.82	1.59	1.35	1.11	0.87	
	T-1	205575	89640	112835	360	1.3907	0.45	0.38	0.31	0.24	0.17	
	T-2	55937	26017	34163	205	0.3838	0.15	0.13	0.10	0.08	0.05	
	T-3	67939	26818	28201	315	0.2745	0.22	0.18	0.15	0.12	0.08	
	T-4	107785	34466	42158	316	0.4996	0.23	0.19	0.16	0.12	0.08	
	T-5	145800	49879	50124	420	0.7923	0.48	0.41	0.34	0.26	0.19	
	J-1 (B)	1198370	599185	600946	725	4.2095	1.78	1.54	1.29	1.04	0.79	Bar Sand
	K-1 (B)	614938	325555	325555	957	2.8428	4.25	3.68	3.11	2.55	1.98	PVT
	LL-2 (B)	154330	63548	66875	637	0.8064	1.43	1.22	1.02	0.82	0.62	
	R-3 (B)	585130	309774	309774	590	1.6814	0.78	0.67	0.56	0.45	0.34	
	S-1 (B)	930145	465072	465072	663	4.5877	1.81	1.56	1.30	1.05	0.79	

TABLE 4

SCHOOL CREEK FIELD - CALCULATED DECLINE CURVE ANALYSIS RESULTS
$(\bar{P}_R - P_{wf})/\overline{\mu_o \beta_o}$ EVALUATION

Well	Pore Vol. V_{RB}	Start of Decline OIP STB	OOIP STB	Calculated r_e Feet	Prod. Factor $\frac{kh}{\ln \frac{r_e}{r_w'} - \frac{1}{2}}$	s = 0 $r_w' = .328$ $\frac{k}{md}$	s = -1 $r_w' = .892$ $\frac{k}{md}$	s = -2 $r_w' = 2.424$ $\frac{k}{md}$	s = -3 $r_w' = 6.588$ $\frac{k}{md}$	s = -4 $r_w' = 17.90$ $\frac{k}{md}$	
A-1	898346	427784	430417	1141	6.3885	5.43	4.72	4.01	3.30	2.59	
C-1	755925	308541	314767	807	1.3583	0.66	0.57	0.48	0.39	0.30	
D-2	20959	7414	7414	182	0.0922	0.08	0.06	0.05	0.04	0.02	
F-1	23350	4765	4765	194	0.1215	0.07	0.05	0.04	0.03	0.02	
G-1	241168	98436	98725	519	0.7317	0.50	0.43	0.36	0.28	0.21	
JJ-1	226419	114739	119026	457	0.8621	0.45	0.38	0.31	0.25	0.18	
K-1	1147688	468444	468945	2091	2.0267	4.78	4.20	3.62	3.05	2.47	
K-4	394845	161161	168621	685	2.4783	1.77	1.52	1.28	1.03	0.78	
Q-1	73364	24954	25643	306	0.2979	0.19	0.16	0.13	0.10	0.07	
R-1	59530	24298	25933	379	0.2431	0.27	0.22	0.18	0.14	0.10	
R-2	47709	19473	20642	266	0.1379	0.09	0.07	0.06	0.04	0.03	Channel Sand
Ford A-1	779935	318341	320212	806	3.9593	1.93	1.66	1.40	1.14	0.87	Matheson E-1 PVT
Ford B-1	211699	100809	101128	382	0.5433	0.21	0.18	0.15	0.11	0.08	
Math B-1	404097	142946	153722	803	0.7889	0.82	0.71	0.60	0.48	0.37	
Math D-1	150804	71811	71811	613	0.4917	0.69	0.59	0.50	0.40	0.30	
Math E-1	1989906	812207	820067	1209	6.6410	3.20	2.79	2.37	1.96	1.54	
DD-1	183104	64625	72453	630	1.4752	1.30	1.12	0.93	0.75	0.56	
EE-1	346668	101961	115800	620	2.1772	1.28	1.10	0.92	0.73	0.55	
FF-1	73965	30456	38098	301	0.8641	0.55	0.46	0.37	0.29	0.20	
GG-1	707700	223484	227066	1451	1.5704	2.48	2.17	1.85	1.54	1.22	
GG-2	384481	121415	121415	626	0.6432	0.32	0.28	0.23	0.19	0.14	
H-1	587180	185425	185425	891	0.8319	0.77	0.67	0.56	0.46	0.35	
I-1	637459	262483	266322	717	4.7225	2.43	2.09	1.75	1.41	1.08	
KK-1	655552	173426	177069	1501	2.3797	4.72	4.12	3.53	2.93	2.34	
KK-2	156235	57560	59095	229	0.5687	0.09	0.08	0.06	0.05	0.03	
LL-1	57674	19731	21199	279	0.0101	0.01	0.01	.01	.01	.01	
O-1	995812	393084	414557	1045	3.5690	2.46	2.13	1.81	1.48	1.16	Channel Sand
R-3	2142759	874595	880038	1909	4.1245	4.81	4.22	3.64	3.05	2.46	Federal EE-1 PVT
R-4	338993	107050	119287	677	1.0790	0.77	0.66	0.55	0.45	0.34	
S-1	1169126	556727	581260	1077	4.4526	2.82	2.45	2.08	1.71	1.33	
T-1	169150	73757	96952	326	1.1444	0.37	0.31	0.25	0.19	0.14	
T-2	46026	21407	29553	186	0.3158	0.12	0.10	0.08	0.06	0.04	
T-3	68966	27223	28606	317	0.2787	0.22	0.19	0.15	0.12	0.08	
T-4	90675	28995	36687	289	0.4203	0.19	0.16	0.13	0.10	0.07	
T-5	116550	39872	40117	375	0.6334	0.38	0.32	0.26	0.20	0.15	
J-1 (B)	1040805	520402	522163	675	3.6561	1.53	1.32	1.10	0.89	0.67	Bar Sand
K-1 (B)	511535	270813	270813	872	2.3648	3.49	3.02	2.55	2.07	1.60	PVT
LL-2 (B)	128380	52862	56189	580	0.6708	1.17	1.00	0.84	0.67	0.50	
R-3 (B)	486739	257686	257686	538	1.3987	0.64	0.55	0.46	0.36	0.27	
S-1 (B)	787611	393805	393805	610	3.8847	1.52	1.30	1.09	0.87	0.65	

TABLE 5

SCHOOL CREEK FIELD - CALCULATED DECLINE CURVE ANALYSIS RESULTS
BASED ON FEDERAL EE-1 (CHANNEL SAND) AND $m(p)_{oil}$ EVALUATION

Well	Pore Vol. V_p RB	Start of Decline OIP STB	OOIP STB	Calculated r_e feet	Prod. Factor $\frac{kh}{\ln \frac{r_e}{r_w'} - \frac{1}{2}}$	s = 0 $r_w' = .328$ k - md	s = -1 $r_w' = .892$ k - md	s = -2 $r_w' = 2.424$ k - md	s = -3 $r_w' = 6.588$ k - md	s = -4 $r_w' = 17.90$ k - md
A-1	965906	355860	358493	1183	3.9091	3.34	2.91	2.47	2.04	1.60
C-1	1031488	325733	331959	944	1.0253	0.51	0.44	0.37	0.31	0.24
D-2	26889	7359	7359	207	0.0645	0.05	0.05	0.04	0.03	0.02
DD-1	239364	84482	92310	721	1.9285	1.73	1.49	1.25	1.01	0.77
EE-1	436544	128395	142234	697	2.7416	1.64	1.41	1.18	0.95	0.72
F-1	39437	6227	6227	253	0.0917	0.05	0.04	0.03	0.03	0.02
FF-1	91086	37506	45148	335	1.0641	0.68	0.58	0.47	0.36	0.26
G-1	237031	74852	75141	515	0.4046	0.28	0.24	0.20	0.16	0.12
GG-1	791422	249923	253505	1535	1.7561	2.79	2.44	2.09	1.74	1.39
GG-2	461396	145704	145704	686	0.7718	0.39	0.34	0.28	0.23	0.17
H-1	734543	231961	231961	997	1.0406	0.98	0.85	0.72	0.59	0.46
I-1	821613	338311	342150	815	6.0868	3.18	2.75	2.31	1.83	1.44
J-1 (B)	1198370	599185	600946	725	4.2095	1.78	1.54	1.29	1.04	0.79
JJ-1	232600	100838	105125	463	0.6463	0.34	0.29	0.24	0.19	0.14
K-1	1338189	422586	423087	2258	1.3020	3.10	2.73	2.36	1.99	1.61
K-1 (B)	614938	325555	325555	957	2.8428	4.25	3.68	3.11	2.55	1.98
K-4	531559	169646	177106	796	1.9689	1.44	1.24	1.04	0.85	0.65
KK-1	694523	183736	187379	1545	2.5211	5.02	4.38	3.75	3.12	2.49
KK-2	195445	72006	73541	256	0.7114	0.12	0.10	0.08	0.06	0.04
LL-1	72149	24682	26150	313	0.0126	0.01	0.01	0.01	.00	.00
LL-2 (B)	154330	63548	66875	637	0.8064	1.43	1.22	1.02	0.82	0.62
O-1	1049477	414267	435740	1073	3.7613	2.60	2.25	1.91	1.57	1.23
Q-1	103312	27187	27876	363	0.2249	0.15	0.12	0.10	0.08	0.06
R-1	82352	26006	27641	447	0.1834	0.21	0.17	0.14	0.11	0.08
R-2	65999	20842	22011	314	0.1040	0.07	0.06	0.05	0.03	0.02
R-3	2463966	778095	783538	2048	2.6496	3.12	2.74	2.36	1.98	1.60
R-3 (B)	585130	309774	309774	590	1.6814	0.78	0.67	0.56	0.45	0.34
R-4	374090	118134	130371	712	1.1906	0.86	0.74	0.62	0.50	0.38
S-1	1302969	480041	504574	1137	2.8604	1.82	1.59	1.35	1.11	0.87
S-1 (B)	930145	465072	465072	663	4.5877	1.81	1.56	1.30	1.05	0.79
T-1	205575	89640	112835	360	1.3907	0.45	0.38	0.31	0.24	0.17
T-2	55937	26017	34163	205	0.3838	0.15	0.13	0.10	0.08	0.05
T-3	67939	26818	28201	315	0.2745	0.22	0.18	0.15	0.12	0.08
T-4	107785	34466	42158	316	0.4996	0.23	0.19	0.16	0.12	0.08
T-5	145800	49879	50124	420	0.7923	0.48	0.41	0.34	0.26	0.19
Ford A-1	862420	272343	274214	848	2.4289	1.19	1.03	0.87	0.71	0.54
Ford B-1	275450	101481	101800	436	0.4101	0.16	0.14	0.11	0.09	0.06
Math B-1	552484	152815	163591	939	0.6388	0.68	0.59	0.50	0.41	0.32
Math D-1	181095	66719	66719	673	0.3457	0.49	0.42	0.35	0.29	0.22
Math E-1	2278011	719372	727232	1294	4.2598	2.07	1.81	1.54	1.27	1.01

TABLE 6

SCHOOL CREEK FIELD - CALCULATED DECLINE CURVE ANALYSIS RESULTS
BASED ON FEDERAL EE-1 PVT (CHANNEL SAND) AND $(\bar{p}_R - p_{wf})/\overline{\mu_o \beta_o}$ EVALUATION

Well	Pore Vol. V_p RB	Start of Decline OIP STB	Calculated OOIP STB	Calculated r_e feet	Prod. Factor kh / $\ln \frac{r_e}{r_w'} - \frac{1}{2}$	s = 0 r_w' = .328 k - md	s = -1 r_w' = .892 k - md	s = -2 r_w' = 2.424 k - md	s = -3 r_w' = 6.588 k - md	s = -4 r_w' = 17.90 k - md
A-1	892968	328988	331621	1138	3.6139	3.07	2.67	2.27	1.87	1.47
C-1	824552	260385	266611	843	0.8197	0.40	0.35	0.29	0.24	0.18
D-2	22683	6208	6208	189	0.0545	0.05	0.04	0.03	0.02	0.01
DD-1	183104	64625	72453	630	1.4752	1.30	1.12	0.93	0.75	0.56
EE-1	346668	101961	115800	620	2.1772	1.28	1.10	0.92	0.73	0.55
F-1	31525	4978	4978	226	0.0733	0.04	0.03	0.03	0.02	0.01
FF-1	73965	30456	38098	301	0.8641	0.55	0.46	0.37	0.29	0.20
G-1	231125	72987	73276	508	0.3945	0.27	0.23	0.19	0.15	0.11
GG-1	707700	223484	227066	1451	1.5704	2.48	2.17	1.85	1.54	1.22
GG-2	384481	121415	121415	626	0.6432	0.32	0.28	0.23	0.19	0.14
H-1	587180	185425	185425	891	0.8319	0.77	0.67	0.56	0.46	0.35
I-1	637459	262483	266322	717	4.7225	2.43	2.09	1.75	1.41	1.08
J-1 (B)	1040805	520402	522163	675	3.6561	1.53	1.32	1.10	0.89	0.67
JJ-1	187219	81164	85451	415	0.5202	0.27	0.23	0.19	0.15	0.11
K-1	1196626	377882	378383	2135	1.1643	2.75	2.42	2.09	1.75	1.42
K-1 (B)	511535	270813	270813	872	2.3648	3.49	3.02	2.55	2.07	1.60
K-4	420053	134060	141520	707	1.5559	1.12	0.96	0.81	0.65	0.49
KK-1	655552	173426	177069	1501	2.3797	4.72	4.12	3.53	2.93	2.34
KK-2	156235	57560	59095	229	0.5687	0.09	0.08	0.06	0.05	0.03
LL-1	57674	19731	21199	279	0.0101	0.01	0.01	.00	.00	.00
LL-2 (B)	128380	52862	56189	580	0.6708	1.17	1.00	0.84	0.67	0.50
O-1	995812	393084	414557	1045	3.5690	2.46	2.13	1.81	1.48	1.16
Q-1	82586	21733	22422	324	0.1798	0.12	0.10	0.08	0.06	0.04
R-1	65831	20789	22424	399	0.1467	0.16	0.14	0.11	0.09	0.06
R-2	52758	16661	17830	280	0.0832	0.05	0.04	0.04	0.03	0.02
R-3	2203310	695782	701225	1936	2.3694	2.77	2.43	2.09	1.75	1.42
R-3 (B)	486739	257686	257686	538	1.3987	0.64	0.55	0.46	0.36	0.27
R-4	338993	107050	119287	677	1.0790	0.77	0.66	0.55	0.45	0.34
S-1	1165131	429259	453792	1075	2.5579	1.62	1.41	1.19	0.98	0.77
S-1 (B)	787611	393805	393805	610	3.8847	1.52	1.30	1.09	0.87	0.65
T-1	169150	73757	96952	326	1.1444	0.37	0.31	0.25	0.19	0.14
T-2	46026	21407	29553	186	0.3158	0.12	0.10	0.08	0.06	0.04
T-3	68966	27223	28606	317	0.2787	0.22	0.19	0.15	0.12	0.08
T-4	90675	28995	36687	289	0.4203	0.19	0.16	0.13	0.10	0.07
T-5	116550	39872	40117	375	0.6334	0.38	0.32	0.26	0.20	0.15
Ford A-1	797412	251814	253685	815	2.2459	1.10	0.95	0.80	0.65	0.50
Ford B-1	220189	81122	81441	390	0.3279	0.13	0.11	0.09	0.07	0.05
Math B-1	418718	115816	126592	817	0.4842	0.51	0.44	0.37	0.30	0.23
Math D-1	153946	56717	56717	620	0.2939	0.41	0.36	0.30	0.24	0.18
Math E-1	2018793	637513	645373	1218	3.7751	1.82	1.59	1.35	1.11	0.88

TABLE 7

SCHOOL CREEK FIELD - CALCULATED DECLINE CURVE ANALYSIS RESULTS
BASED ON MATHESON E-1 PVT (CHANNEL SAND) AND $m(p)_{oil}$ EVALUATION

Well	Pore Vol. V_R RB	Start of Decline OIP STB	OOIP STB	Calculated r_e feet	Prod. Factor $\frac{kh}{\ln \frac{r_e}{r_w'} - \frac{1}{2}}$	s = 0 r_w' = .328 $\frac{k}{}$ - md	s = -1 r_w' = .892 $\frac{k}{}$ - md	s = -2 r_w' = 2.424 $\frac{k}{}$ - md	s = -3 r_w' = 6.588 $\frac{k}{}$ - md	s = -4 r_w' = 17.90 $\frac{k}{}$ - md
A-1	1104447	525927	528560	1265	7.8542	6.77	5.90	5.02	4.15	3.28
C-1	1144643	467201	473427	994	2.0567	1.03	0.89	0.76	0.62	0.48
D-2	29481	10429	10429	216	0.1297	0.11	0.09	0.07	0.06	0.04
DD-1	318987	129319	137147	832	3.3829	3.10	2.68	2.26	1.83	1.41
EE-1	558453	188666	202505	788	4.7868	2.91	2.51	2.11	1.71	1.31
F-1	35358	7216	7216	240	0.1840	0.10	0.09	0.07	0.05	0.04
FF-1	117453	55930	63572	380	1.9531	1.28	1.09	0.89	0.69	0.50
G-1	272285	111137	111426	552	0.8261	0.57	0.49	0.41	0.32	0.24
GG-1	867284	353993	357575	1607	3.5411	5.66	4.96	4.25	3.54	2.83
GG-2	503362	205454	205454	717	1.5493	0.80	0.68	0.57	0.46	0.35
H-1	834839	340751	340751	1063	2.0874	1.98	1.72	1.46	1.20	0.94
I-1	1189435	562571	566410	980	10.6782	5.72	4.96	4.20	3.43	2.67
J-1 (B)	1198370	599185	600946	725	4.2095	1.78	1.54	1.29	1.04	0.79
JJ-1	315066	159662	163949	539	1.1995	0.64	0.54	0.45	0.36	0.27
K-1	1486687	606811	607312	2380	2.6253	6.29	5.54	4.79	4.04	3.29
K-1 (B)	614938	325555	325555	957	2.8428	4.25	3.68	3.11	2.55	1.98
K-4	603338	246261	253721	848	3.7869	2.79	2.41	2.03	1.65	1.27
KK-1	974655	257845	261488	1830	6.2045	12.61	11.05	9.50	7.95	6.40
KK-2	169018	80485	82020	238	1.4271	0.23	0.19	0.15	0.12	0.08
LL-1	80723	35694	37162	331	0.0254	0.02	0.01	0.01	0.01	0.01
LL-2 (B)	154330	63548	66875	637	0.8064	1.43	1.22	1.02	0.82	0.62
O-1	1243778	634580	656053	1169	7.6629	5.35	4.65	3.96	3.26	2.56
Q-1	111090	37786	38475	377	0.4511	0.30	0.25	0.21	0.16	0.11
R-1	90143	36793	38428	467	0.3680	0.41	0.35	0.29	0.23	0.17
R-2	72243	29487	30656	328	0.2087	0.13	0.11	0.09	0.07	0.05
R-3	2775676	1132929	1138372	2174	5.3427	6.33	5.57	4.81	4.04	3.28
R-3 (B)	585130	309774	309774	590	1.6814	0.78	0.67	0.56	0.45	0.34
R-4	409477	167133	179370	745	2.3849	1.72	1.49	1.25	1.01	0.77
S-1	1514457	721170	745703	1226	5.7677	3.71	3.23	2.75	2.27	1.79
S-1 (B)	930145	465072	465072	663	4.5877	1.81	1.56	1.30	1.05	0.79
T-1	264822	135113	158308	408	2.5262	0.84	0.71	0.58	0.45	0.33
T-2	73983	40263	48409	236	0.6972	0.28	0.24	0.19	0.14	0.10
T-3	81065	41360	42743	344	0.5542	0.45	0.38	0.31	0.24	0.17
T-4	130935	48989	56681	348	0.9091	0.42	0.36	0.29	0.23	0.16
T-5	162061	71660	71905	443	1.5893	0.97	0.82	0.68	0.54	0.39
Ford A-1	968836	395443	397314	898	4.9183	2.43	2.10	1.78	1.45	1.12
Ford B-1	320561	152648	152967	471	0.8227	0.33	0.28	0.23	0.18	0.13
Math B-1	617476	218427	229203	993	1.2054	1.29	1.12	0.95	0.73	0.61
Math D-1	208739	99399	99399	722	0.6806	0.98	0.84	0.71	0.57	0.44
Math E-1	2550551	1041041	1048901	1369	8.5120	4.17	3.64	3.11	2.57	2.04

TABLE 8

SCHOOL CREEK FIELD - CALCULATED DECLINE CURVE ANALYSIS RESULTS
BASED ON MATHESON E-1 PVT (CHANNEL SAND) AND $(\bar{P}_R - P_{wf})/\overline{\mu_o \beta_o}$ EVALUATION

Well	Pore Vol. V_p RB	Start of Decline OIP STB	OOIP STB	Calculated r_e feet	Prod. Factor $\frac{kh}{\ln \frac{r_e}{r_w'} - \frac{1}{2}}$	s = 0 $r_w'_k$ = .328 md	s = -1 $r_w'_k$ = .892 md	s = -2 $r_w'_k$ = 2.424 md	s = -3 $r_w'_k$ = 6.588 md	s = -4 $r_w'_k$ = 17.90 md
A-1	898346	427784	430417	1141	6.3885	5.43	4.72	4.01	3.30	2.59
C-1	755925	308541	314767	807	1.3583	0.66	0.57	0.48	0.39	0.30
D-2	20959	7414	7414	182	0.0922	0.08	0.06	0.05	0.04	0.02
DD-1	228179	92505	100333	703	2.4199	2.17	1.87	1.56	1.26	0.96
EE-1	427729	144503	158342	689	3.6663	2.18	1.88	1.57	1.27	0.96
F-1	23350	4765	4765	194	0.1215	0.07	0.05	0.04	0.03	0.02
FF-1	87951	41882	49524	329	1.4626	0.94	0.79	0.65	0.50	0.35
G-1	241168	98436	98725	519	0.7317	0.50	0.43	0.36	0.28	0.21
GG-1	669523	273275	276857	1412	2.7337	4.30	3.75	3.21	2.66	2.11
GG-2	351874	143622	143622	599	1.0831	0.54	0.46	0.39	0.31	0.23
H-1	551330	225033	225033	864	1.3786	1.27	1.10	0.93	0.75	0.58
I-1	868886	410959	414798	837	7.8005	4.09	3.54	2.98	2.42	1.86
J-1 (B)	1040805	520402	522163	675	3.6561	1.53	1.32	1.10	0.89	0.67
JJ-1	226419	114739	119026	457	0.8621	0.45	0.38	0.31	0.25	0.18
K-1	1147688	468444	468945	2091	2.0267	4.78	4.20	3.62	3.05	2.47
K-1 (B)	511535	270813	270813	872	2.3648	3.49	3.02	2.55	2.07	1.60
K-4	394845	161161	168621	685	2.4783	1.77	1.52	1.28	1.03	0.78
KK-1	679465	179753	183396	1528	4.3254	8.59	7.51	6.43	5.35	4.27
KK-2	111620	53152	54687	193	0.9425	0.15	0.12	0.10	0.07	0.05
LL-1	53310	23572	25040	268	0.0168	0.01	0.01	0.01	0.01	.00
LL-2 (B)	128380	52862	56189	580	0.6708	1.17	1.00	0.84	0.67	0.50
O-1	1044348	532831	554304	1070	6.4343	4.44	3.85	3.27	2.69	2.10
Q-1	73364	24954	25643	306	0.2979	0.19	0.16	0.13	0.10	0.07
R-1	59530	24298	25933	379	0.2431	0.27	0.22	0.18	0.14	0.10
R-2	47709	19473	20642	266	0.1379	0.09	0.07	0.06	0.04	0.03
R-3	2142759	874595	880038	1909	4.1245	4.81	4.22	3.64	3.05	2.46
R-3 (B)	486739	257686	257686	538	1.3987	0.64	0.55	0.46	0.36	0.27
R-4	324438	132424	144661	662	1.8896	1.34	1.15	0.97	0.78	0.59
S-1	1169126	556727	581260	1077	4.4526	2.82	2.45	2.08	1.71	1.33
S-1 (B)	787611	393805	393805	610	3.8847	1.52	1.30	1.09	0.87	0.65
T-1	205561	104878	128073	359	1.9609	0.64	0.54	0.44	0.34	0.25
T-2	57427	31253	39399	208	0.5412	0.21	0.18	0.14	0.11	0.07
T-3	67547	34463	35846	314	0.4618	0.37	0.31	0.25	0.19	0.14
T-4	106495	39845	47537	313	0.7395	0.34	0.28	0.23	0.18	0.12
T-5	107026	47324	47569	360	1.0496	0.62	0.52	0.43	0.33	0.24
Ford A-1	779935	318341	320212	806	3.9593	1.93	1.66	1.40	1.14	0.87
Ford B-1	211699	100809	101128	382	0.5433	0.21	0.18	0.15	0.11	0.08
Math B-1	404097	142946	153722	803	0.7889	0.82	0.71	0.60	0.48	0.37
Math D-1	150804	71811	71811	613	0.4917	0.69	0.59	0.50	0.40	0.30
Math E-1	1989906	812207	820067	1209	6.6410	3.20	2.79	2.37	1.96	1.54

TABLE 9

EXAMPLE OF EFFECT OF BACKPRESSURE CHANGE ON DECLINE AND RECOVERY
FEDERAL A-1

$\bar{P}_R$ = 3500 psi; P_b = 2705 psi

Match Point, b = 0.30:

q(t) = 1000 BOPM; q_{Dd} = 0.220

t = 1 mo; t_{Dd} = 0.212

$$q_i = \frac{1000 \text{ BOPM}}{0.220} = 4545.5 \text{ BOPM}; \quad D_i = \frac{0.212}{1 \text{ mo}} = 0.212 \text{ mo}^{-1}$$

$$q(t) = \frac{q_i}{[1 + bD_it]^{1/b}} = \frac{4545.5 \text{ BOPM}}{[1 + 0.0636t]^{3.333}}$$

First backpressure change 1400 psia to 1069 psia @ t = 11 months

q_1 @ t = 1 mo = 3701 BOPM (See Figure 9)

$$\Delta q_1 = q_1 \frac{\left[\frac{P_{wf_1}^2 - P_{wf_2}^2}{2P_b}\right]}{\left[(\bar{P}_R - P_b) + \frac{(P_b^2 - P_{wf_1}^2)}{2P_b}\right]} = 3701 \frac{\left[\frac{1400^2 - 1069^2}{2(2705)}\right]}{\left[(3500-2705) + \frac{(2705^2 - 1400^2)}{2(2705)}\right]} = 313 \text{ BOPM}$$

Second backpressure change 1069 psia to 100 psia @ t = 16 months

$$\Delta q_2 = q_1 \frac{\left[\frac{P_{wf_2}^2 - P_{wf_3}^2}{2P_b}\right]}{\left[(\bar{P}_R - P_b) + \frac{(P_b^2 - P_{wf_1}^2)}{2P_b}\right]} = 3701 \frac{\left[\frac{1069^2 - 100^2}{2(2705)}\right]}{\left[(3500-2705) + \frac{(2705^2 - 1400^2)}{2(2705)}\right]} = 434 \text{ BOPM}$$

TABLE 9-A

EXAMPLE OF EFFECT OF BACKPRESSURE CHANGE ON DECLINE AND RECOVERY
FEDERAL A-1

	[1]	[2]	[3]	[4]	[5]	[6]	[7]
	t	q_1	Δq_1	Δq_2	Column [3]	Column [4]	q Total
			$\left\{\frac{313}{3701} \times [2]\right\}$	$\left\{\frac{434}{3701} \times [2]\right\}$	@ t = 12 mo	@ t = 17 mo	[2]+[5]+[6]
	mo	BOPM	BOPM	BOPM	BOPM	BOPM	BOPM
P_{wf_1}	1	3701	313	434			3701
	2	3050	258	358			3050
	3	2540	215	298			2540
	4	2135	181	250			2135
	5	1811	153	212			1811
	6	1548	131	181			1548
	7	1332	113	156			1332
	8	1154	98	135			1154
	9	1006	85	118			1006
	10	881	75	103			881
P_{wf_2}	11	776	66	91			776
	12	687	58	81	313		1000
	13	610	52	72	258		868
	14	544	46	64	215		759
	15	487	41	57	181		668
P_{wf_3}	16	438	37	51	153		591
	17	395	33	46	131	434	960
	18	357	30	42	113	358	828
	19	324	27	38	98	298	720
	20	295	25	35	85	250	630
	.	.	.	.	.	.	.
	.	.	.	.	.	.	.
	.	.	.	.	.	.	.
	58	26	2	3	4	7	37
	59	25	2	3	4	7	36
	60	24	2	3	4	6	34
	61	23	2	3	3	6	32
	62	22	2	3	3	6	31
Cum	(BO):	27,714	2,344	3,250	2,320	3,191	33,225

TABLE 10

SUMMARY OF SCHOOL CREEK FIELD OOIP AND ULTIMATE RECOVERY

	Can Include Flowing Pressure Changes						Initial P_{wf_1}	
	$m(p)_{oil}$			$(\bar{P}_R - P_{wf})/(\overline{\mu_o \beta_o})$				
Well	OOIP STB	Ultimate Reserves Forecast STB	Recovery Factor Percent	OOIP STB	Ultimate Reserves Forecast STB	Recovery Factor Percent	Ultimate Reserves Forecast STB	
A-1	528560	33719	6.4	430417	44270	10.3	28606	
C-1	473427	26692	5.6	314767	26692	8.5	26692	
D-2	10429	1032	9.9	7414	1032	13.9	1032	
(P&A) F-1	7216	848	11.8	4765	848	17.8	848	
G-1	111426	6343	5.7	98725	9309	9.4	4256	
JJ-1	163949	11122	6.8	119026	12120	10.2	10885	
K-4	253721	21282	8.4	168621	21282	12.6	21282	
Q-1	38475	3357	8.7	25643	3357	13.1	3357	
R-1	38428	3988	10.4	25933	3988	15.4	3988	
R-2	30656	2063	6.7	20642	2063	10.0	2063	
Ford A-1	397314	27538	6.9	320212	35289	11.0	24096	
Ford B-1	152967	8909	5.8	101128	8909	8.8	8909	
Math B-1	229203	22107	9.6	153722	22107	14.4	22107	
Math D-1	99399	5662	5.7	71811	5662	7.9	5662	
Math E-1	1048901	64832	6.2	820067	78333	9.6	60117	
Sub-Totals	3584071	239494	6.7	2682893	275261	10.3	223900	Channel Sand Matheson E-1 PVT
DD-1	92310	14182	15.4	72453	15040	20.8	13967	
EE-1	142234	23130	16.3	115800	25841	22.3	22091	
FF-2	45148	9430	20.9	38098	9911	26.0	9295	
GG-1	253505	28527	11.3	227066	34233	15.1	26719	
GG-2	145704	13280	9.1	121415	14300	11.8	13131	
H-1	231961	22243	9.6	185425	22243	12.0	22243	
I-1	342150	57238	16.7	266322	64346	24.2	54423	
KK-1	187379	19050	10.2	177069	31051	17.5	15018	
KK-2	73541	13769	18.7	59095	13769	23.3	13769	
LL-1	26150	3472	13.3	21199	3472	16.4	3472	
O-1	435740	46069	10.6	414557	60449	14.6	39046	
R-4	130371	21311	16.3	119287	22919	19.2	20205	
T-1	112835	28751	25.5	96952	30268	31.2	28229	
T-2	34163	7925	23.2	29553	8341	28.2	7782	
T-3	28201	7352	26.1	28606	7352	25.7	7352	
T-4	42158	9431	22.4	36687	10010	27.3	9198	
T-5	50124	6165	12.3	40117	6165	15.4	6165	
Sub-Totals	2373674	331325	14.0	2049701	379710	18.5	312105	Channel Sand Federal EE-1 PVT
J-1(B)	600946	53769	8.9	522163	70643	13.5	45938	
K-1(B+C)	932867	59999	6.4	739758	73780	10.0	55315	
LL-2(B)	66875	12373	18.5	56189	13421	23.9	12025	
R-3(B+C)	1093312	109671	10.0	1137724	134702	11.8	96732	
S-1(B+C)	969646	81207	8.4	975065	102313	10.5	73469	
Sub-Totals	3663646	317019	8.7	3430899	394859	11.5	283479	Bar and Channel PVT
Grand Totals	9621391	887838	9.2	8163493	1049830	12.9	819484	

Total Percent Recovery Factor = Total Reserves ÷ Total OOIP

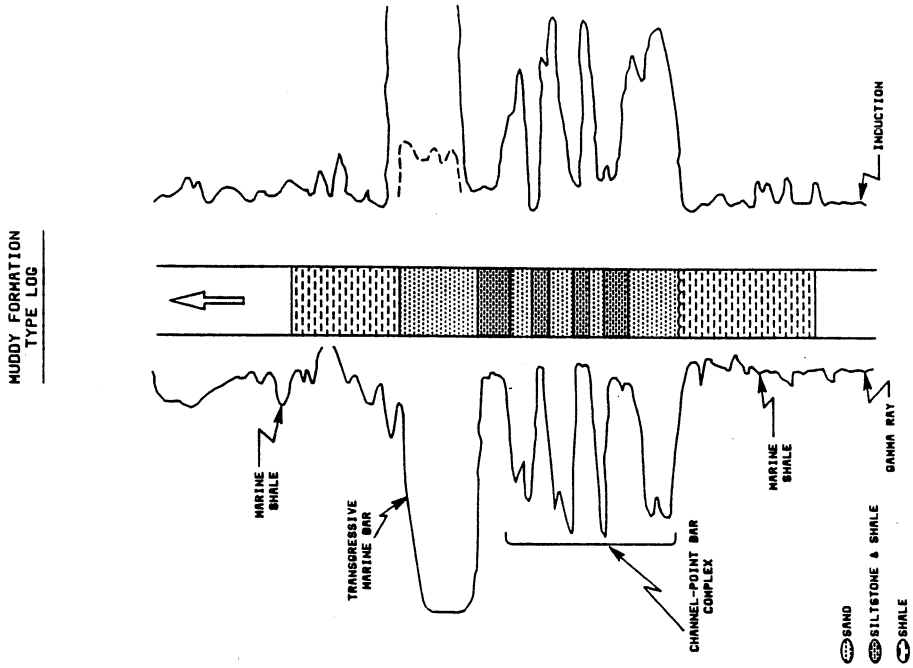

Fig. 2 Type log for a Muddy formation completion

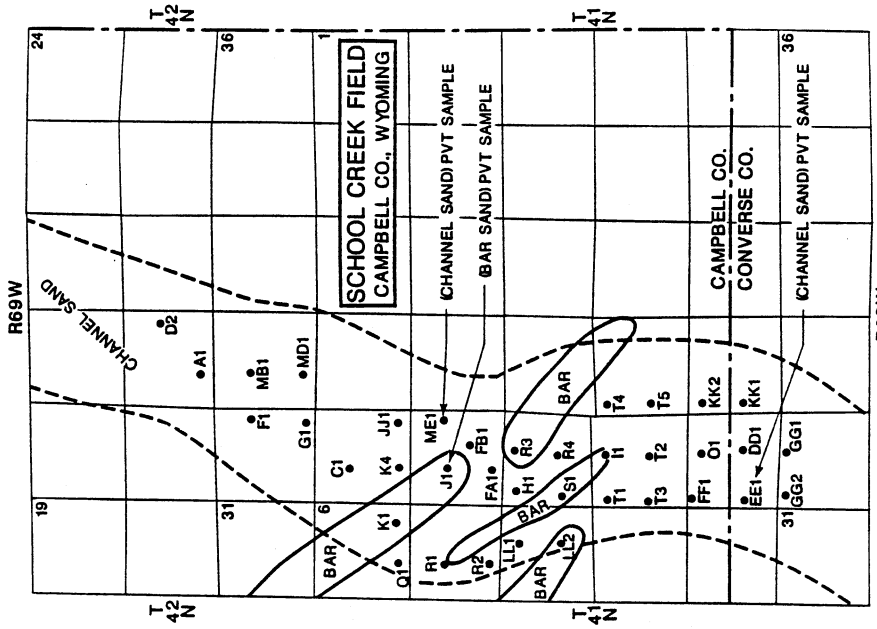

Fig. 1 - School Creek field well location map

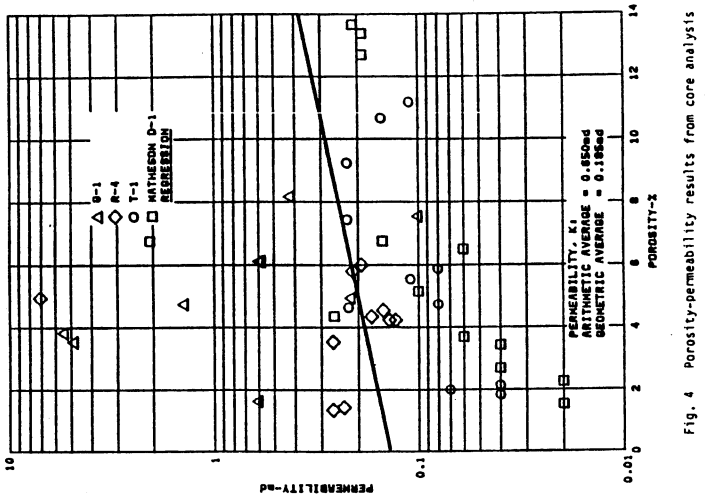

Fig. 4 Porosity-permeability results from core analysis

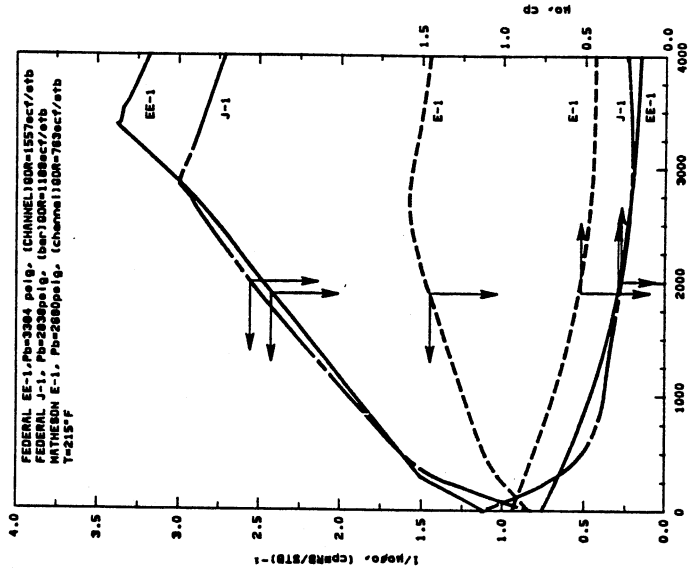

Fig. 3 PVT samples from the School Creek Field

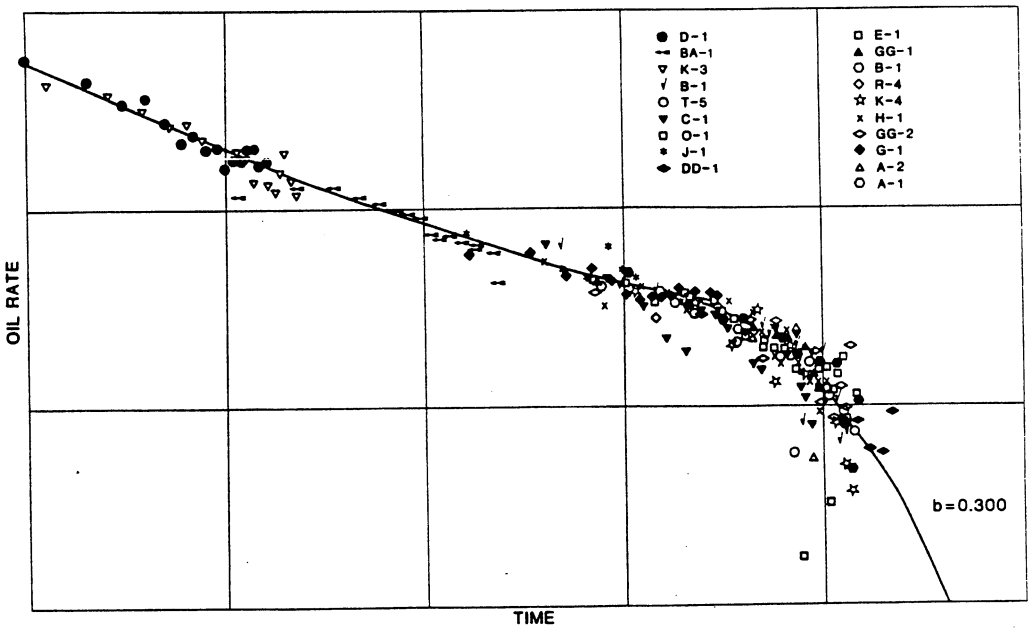

Fig. 5 - Initial School Creek field log-log type curve

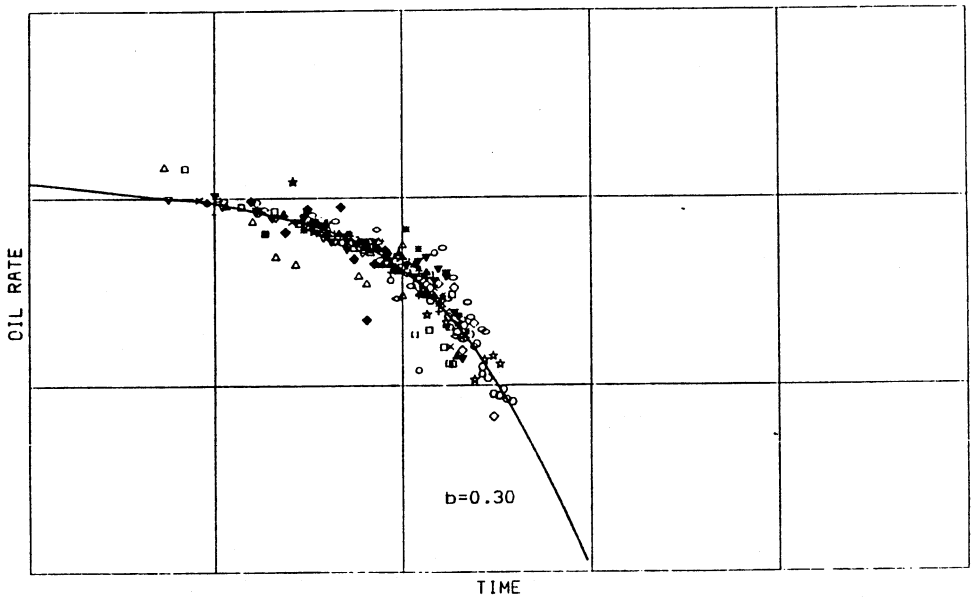

Fig. 6 - Final School Creek field log-log type curve

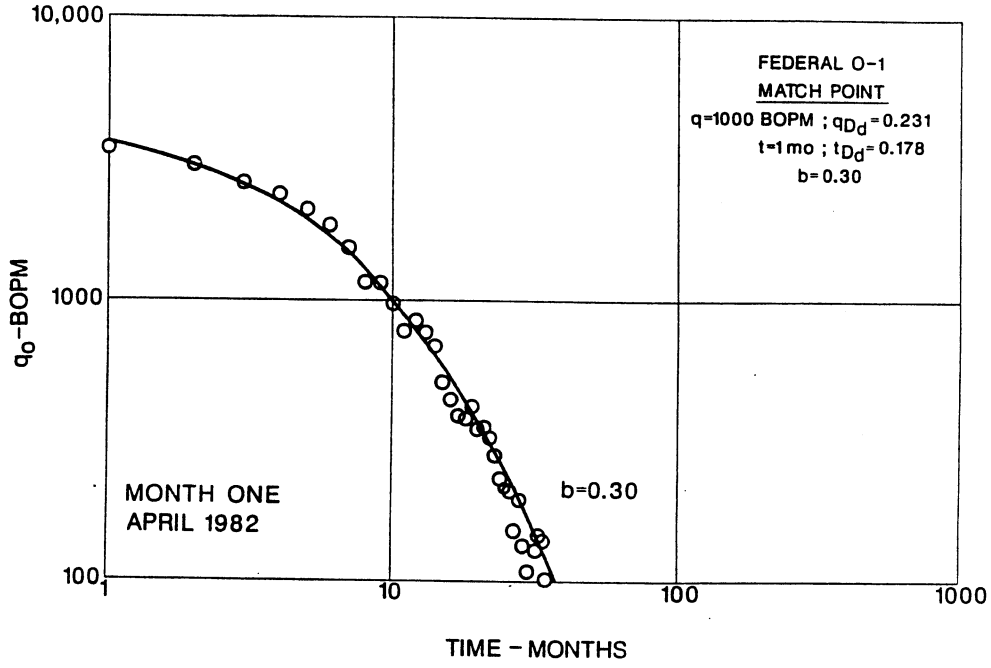

Fig. 7 - Decline exponent b=0.30 established from rate-time data

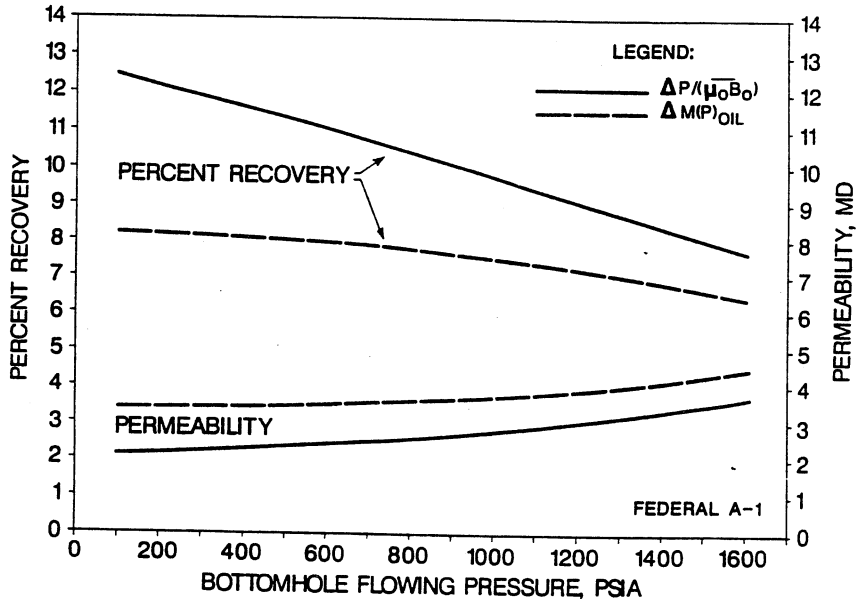

Fig. 8 - Sensitivity of calculated percent recovery and permeability to bottomhole flowing pressure

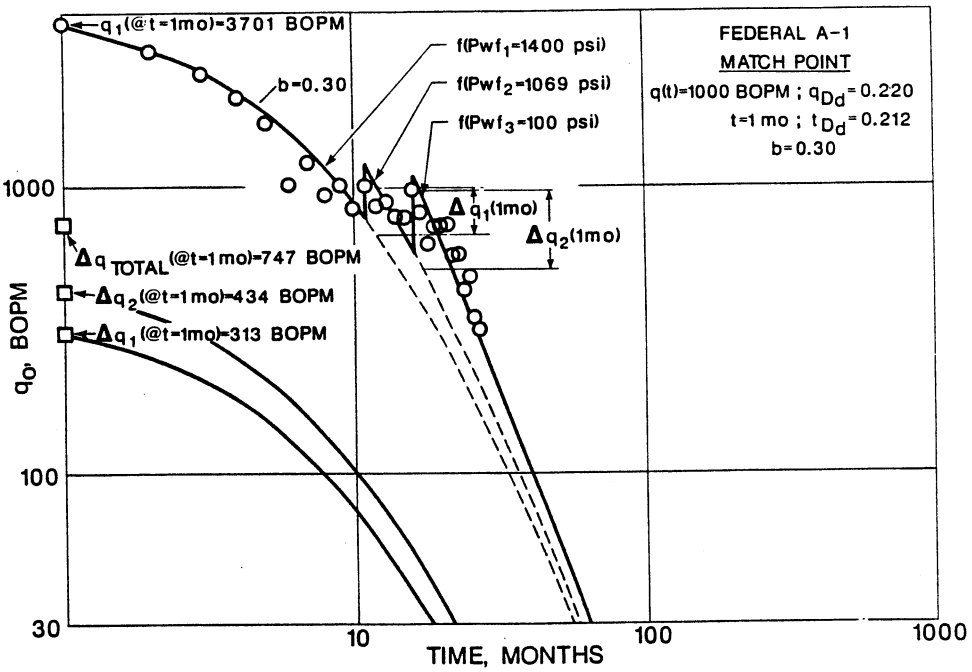

Fig. 9 - Example of effect of backpressure changes on recovery

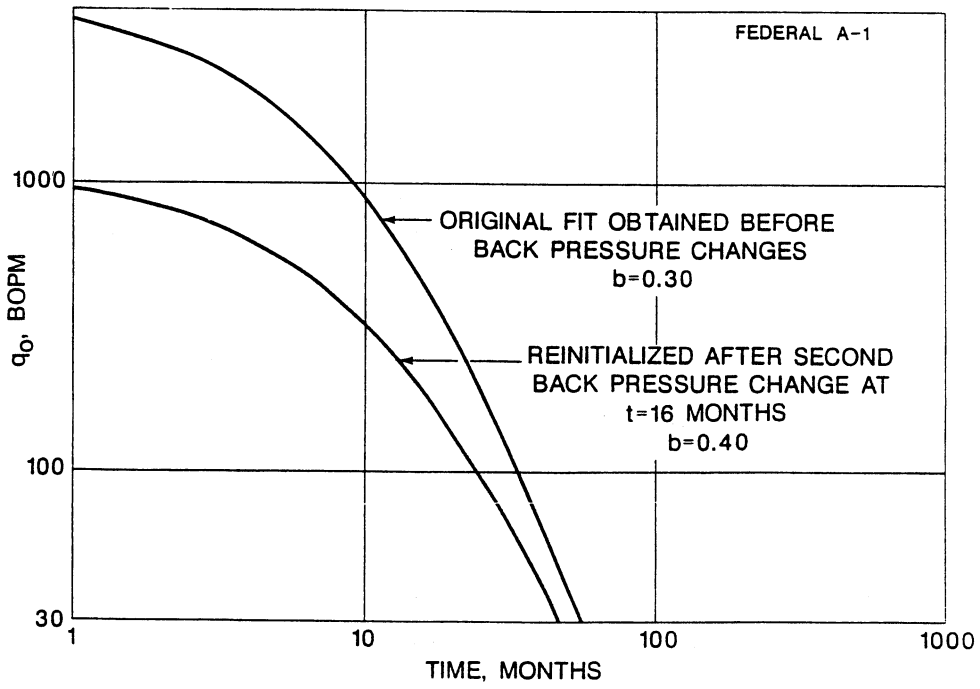

Fig. 10 - Example of backpressure changes on decline exponent, b

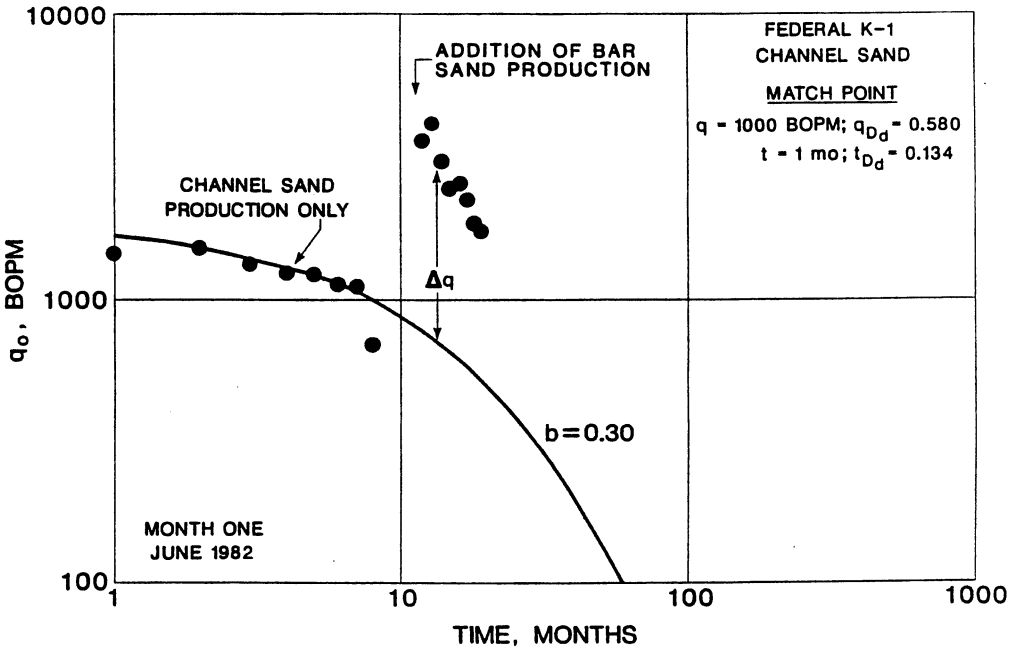

Fig. 11 - Rate-time data for a well commingled with another reservoir

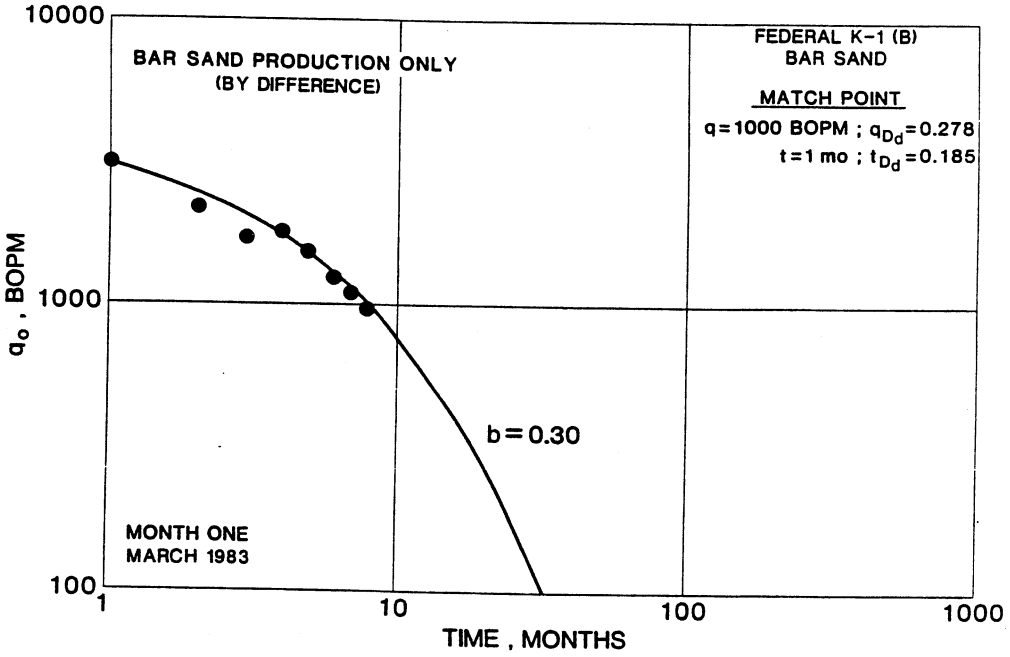

Fig. 12 - Decline data for a commingled well established by difference in production

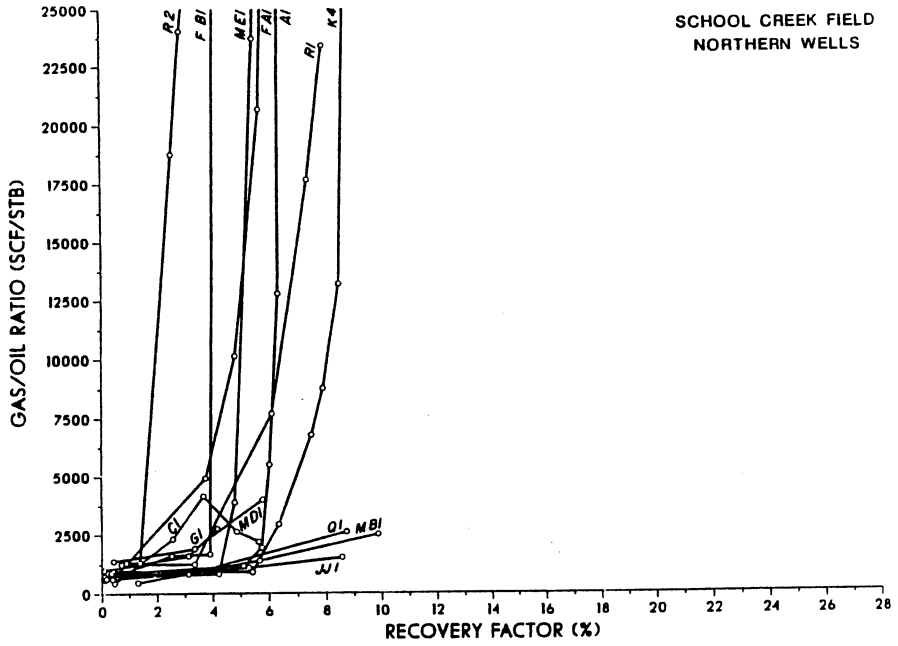

Fig. 13 - Individual well GOR performance, based on m(p) calculated OOIP

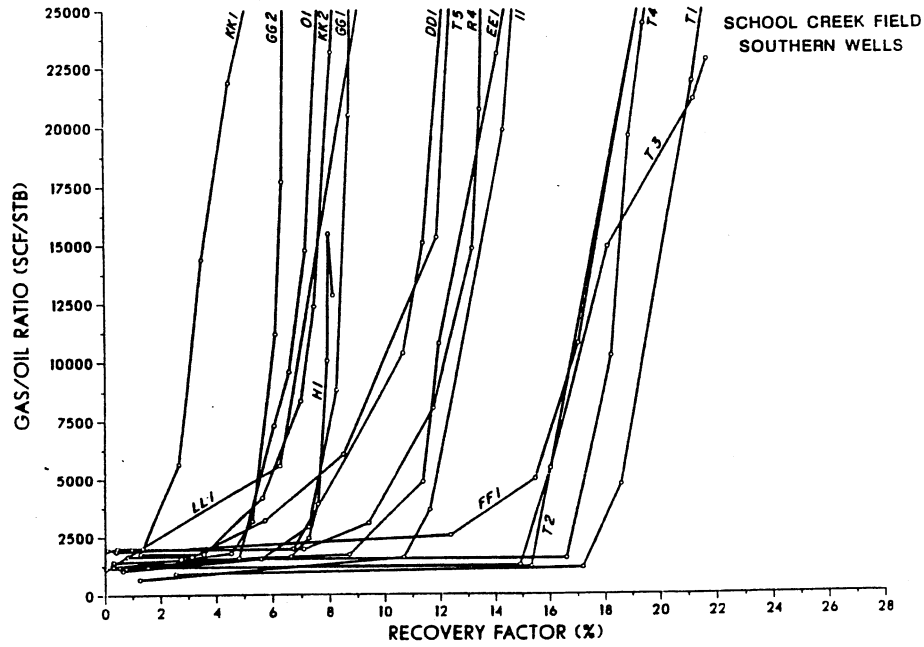

Fig. 14 - Individual well GOR performance, based on m(p) calculated OOIP

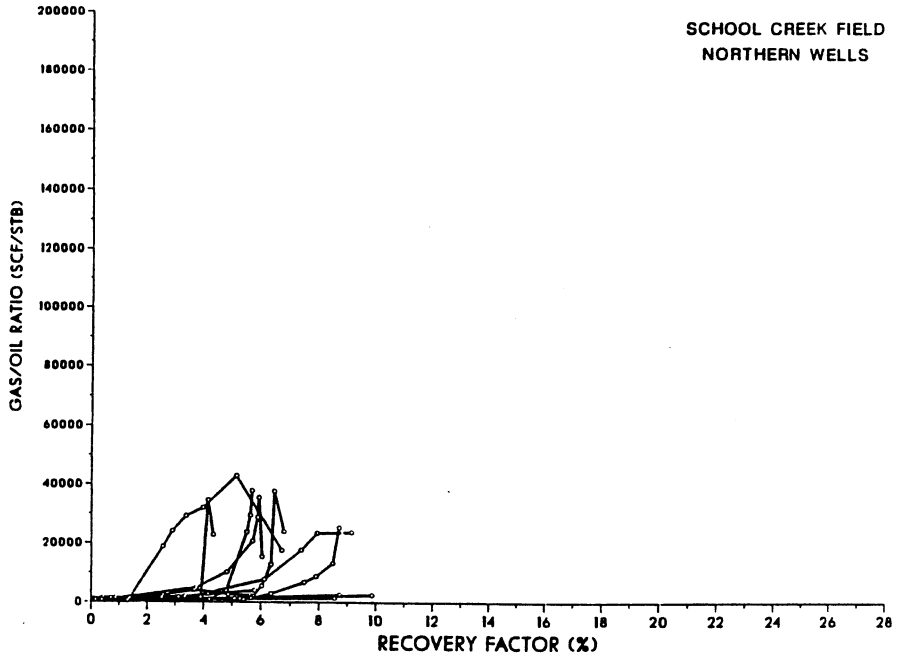

Fig. 15 - Individual well peak GOR performance, based on m(p) calculated OOIP

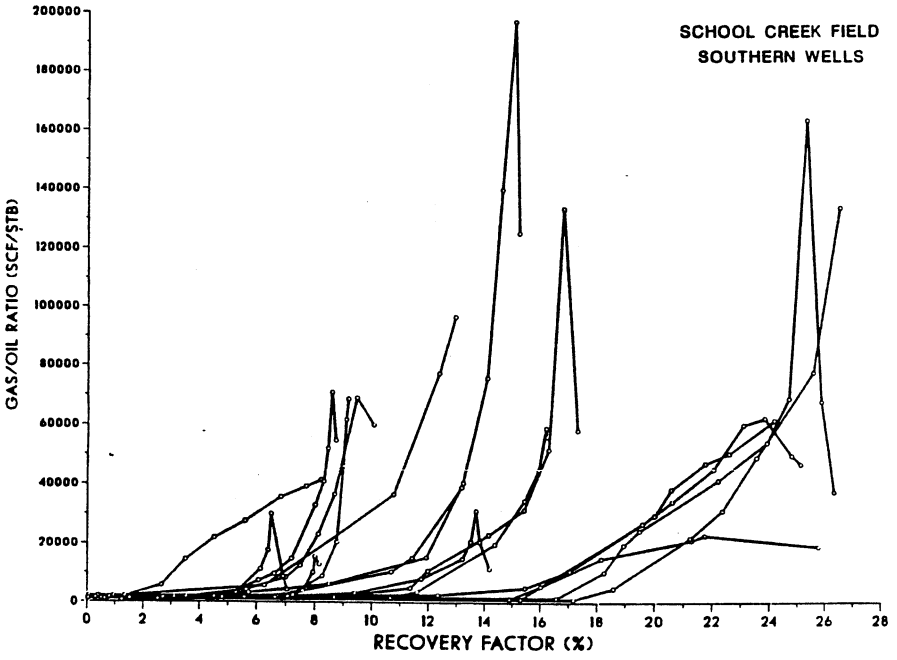

Fig. 16 - Individual well peak GOR performance, based on m(p) calculated OOIP

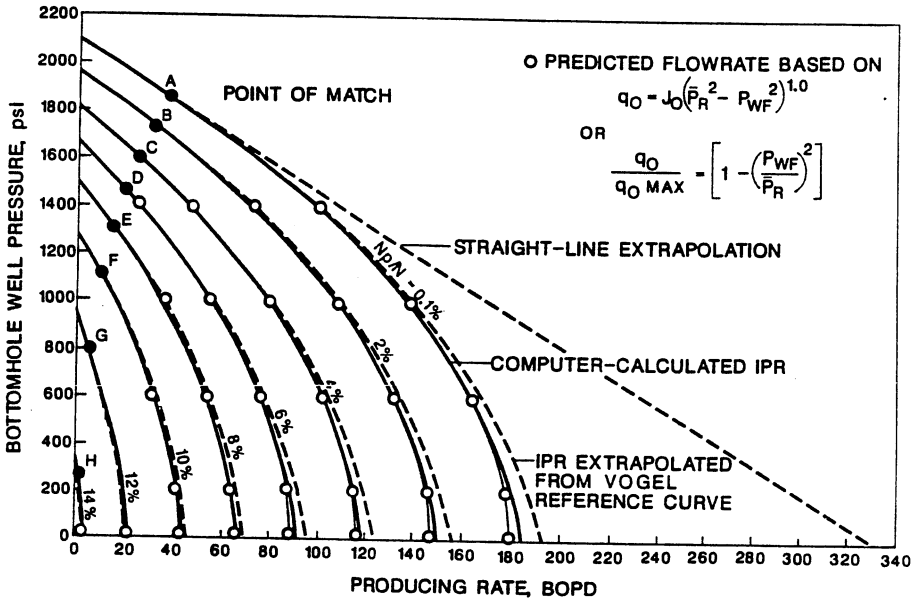

Fig. 17 - Comparison of inflow performance equations

OIL AND GAS RELATIVE PERMEABILITIES DETERMINED FROM RATE-TIME PERFORMANCE DATA

by

M. D. Fetkovich - Phillips Petroleum Co.
E. T. Guerrero - U. of Tulsa
M. J. Fetkovich and L. K. Thomas - Phillips Petroleum Co.

SPE Members

SPE 15431

This paper was prepared for presentation at the 61st Annual Technical Conference and Exhibition of the Society of Petroleum Engineers held in New Orleans, LA October 5-8, 1986.

OIL AND GAS RELATIVE PERMEABILITIES DETERMINED FROM RATE-TIME PERFORMANCE DATA

Summary

This paper presents a method of determining k_g/k_o, oil relative permeability, k_{ro}, and gas relative permeability k_{rg}, using oil and gas rate-time performance data from individual wells and from a total field. Advanced decline curve analysis is used to obtain original oil-in-place, N, and thus saturation; the Δp^2 form of an oil inflow performance equation is used to determine k_{ro} below the bubble point pressure.

The procedure was used on production data from several wells in a North Sea naturally fractured limestone volatile oil field. Results indicate the calculated oil and gas relative permeability curves differ from laboratory and correlation calculated curves. By analyzing the oil and gas relative permeability curves of each of the seven wells in the field, it was found that the degree of natural fracturing of a specific well influences the position of the oil and gas relative permeability curves. The results expressed as k_g/k_o curves appear to be consistent with the field case history findings of Arps for limestone reservoirs - i.e., as the degree of fracturing increases, the k_g/k_o curves become more unfavorable with respect to oil recovery.

Initial pressure surveys on each well determine its degree of fracturing while a later field-wide pressure survey confirms the oil-in-place calculated for each well using rate-time decline curve analysis.

Pressure-time data to make these calculations is seldom available for all wells in a field or, when available, is much less frequent than rate-time data. In contrast, the principal calculation methods shown in this paper use rate-time data, thus taking advantage of the most frequently collected and the most widely available information.

Introduction

The conventional approach to calculating gas-oil permeability ratio from field production performance data requires that reservoir pressures as a function of time be available.[1,2,3] Sufficient pressure data as a function of time for all individual wells in a field are seldom available to calculate each individual well's gas-oil permeability ratio. This is largely a result of the expense and loss of production that would be incurred in conducting pressure tests and the lack of reasonably accurate individual well oil and gas production data.

Total field performance derived gas-oil permeability ratio curves are usually based on averaging reservoir pressures from only a few wells and often do not provide adequate areal and time coverage of the entire field. The frequency of conducting pressure survey usually depends on the rate of pressure decline in the field, the expense of conducting the survey, and safety considerations.

When pressure as a function of time data are available, the Schilthuis[4] or Tarner[5] conventional "black-oil" material balance equation is used to solve for the original oil-in-place. For volumetric reservoirs, (a necessary assumption for calculation of the gas-oil permeability ratio curve), oil-in-place, N, using the material balance equation will calculate to be essentially constant as a function of time. Once the original oil-in-place is known, the gas-oil permeability ratio and oil or gas saturation can be calculated for each available reservoir pressure value.

Rate-time oil and gas production data should be available for all wells in a field on a monthly basis, either through direct measurement or through allocation based on reasonable accurate monthly separator tests. Rate-time analysis[6,7,8] is made with such production data to develop not only a gas-oil permeability ratio but also the relative permeabilities to oil and gas for individual wells. The method is used on production data from several wells in the Edda field, a North Sea naturally fractured limestone volatile oil field in the Greater Ekofisk Development.

Rate-Time Analysis Equations

Before the gas-oil permeability ratio and the oil and gas relative permeabilities can be calculated, the original oil-in-place, N, and productivity factor, PF, must be determined from rate-time performance data. Rate-time[6,7] decline analysis provides a method for calculating both the original oil-in-place and productivity factor on an individual well basis from production data for individual wells. This type of analysis utilizes the concept that once a well and its offsets have reached pseudo-steady state flow, a no flow boundary will result at a distance between all wells. The distance to the no flow boundaries for a well will depend on the flow rate of each offset well. Thus, the drainage volume of each well should remain constant if all wells are on decline and continue producing wide open against a common backpressure with no drastic changes in a well's production rate occurring.

To calculate the pore volume (oil-in-place) and productivity factor (productivity index) a log-log plot of oil production versus time is made. The rate-time plot is overlayed and matched on the Fetkovich type curve.[9] From a type curve match, the match point, $q(t) - q_{Dd}$ and $t - t_{Dd}$ is obtained.

The dimensionless flow rate is defined by

$$q_{Dd} = \frac{\dfrac{q(t)}{kh(p_i - p_{wf})}}{141.2(\overline{\mu_o B_o})[\ln(r_e/r_w') - 1/2]} \qquad \text{.....(1)}$$

and the dimensionless time is defined by

$$t_{Dd} = \frac{0.00634kt}{\phi(\mu c_t)_i r_w'^2} \cdot \frac{1}{1/2[(r_e/r_w')^2-1][\ln(r_e/r_w')-1/2]} \quad \text{.....(2)}$$

($p_i = \bar{p}_R$ at the start of decline analysis.)

The match points are used directly in the calculation of oil-in place and productivity factor.

Two forms of the rate-time pore volume and productivity factor equations are used in this study. One form assumes the oil decline rate below the bubble point pressure is proportional to $(\bar{p}_R - p_{wf})/\overline{\mu B_o}$.[7] The other form utilizes an m(p) of oil[7,10] approach - i.e., the oil rate with the reservoir pressure, $\bar{p}_R$, below the bubble point pressure declines as a function of $\bar{p}_R^2 - p_{wf}^2$. The first approach evaluates $(\overline{\mu_o B_o})$ at average pressure, $(\bar{p}_R + p_{wf})/2$, and will be called the Δp approach.

The flow rate equation for the Δp approach is

$$q_o = \frac{7.08kh}{[\ln(r_e/r_w')-1/2]} \cdot \frac{(\bar{p}_R - p_{wf})}{(\overline{\mu_o B_o})} \quad \text{.....(3)}$$

For the Δp approach, the pore volume can be calculated with the rate-time analysis match points from the following equation

$$V_p = \frac{5.615(\overline{\mu_o B_o})}{(\mu c_t)_{\bar{p}_R} (\bar{p}_R - p_{wf})} \cdot \frac{t}{t_{Dd}} \cdot \frac{q(t)}{q_{Dd}} \quad \text{.....(4)}$$

and oil-in-place is

$$N = \frac{V_p(1 - S_{wi})}{B_{oi}} \quad \text{.....(5)}$$

The productivity factor, PF, is defined as

$$PF = \frac{7.08\ kh}{\left[\ln\left(\frac{r_e}{r_w'}\right) - \frac{1}{2}\right]} = \frac{(\overline{\mu_o B_o})}{\bar{p}_R - p_{wf}} \cdot \frac{q(t)}{q_{Dd}} \quad \text{.....(6)}$$

A more rigorous method uses an m(p) of oil or an oil well inflow performance relationship as proposed by Fetkovich.[10] This will be referred to as the Δp^2 approach. The flow-rate equation for the Δp^2 approach is expressed as

$$q_o = \frac{7.08\ kh}{\left[\ln\left(\frac{r_e}{r_w'}\right) - \frac{1}{2}\right]} \left[\frac{p_b^2 - p_{wf}^2}{2p_b(\mu_o B_o)_{p_b}} + \frac{\bar{p}_R - p_b}{(\overline{\mu_o B_o})_{\bar{p}_R, p_b}}\right] \quad ...(7)$$

Using the rate-time match points, pore volume is calculated from the following equation

$$V_p = \frac{5.615\,[q(t)/q_{Dd}](t/t_{Dd})}{(\mu c_t)_{\bar{p}_R}\left[\frac{\bar{p}_R - p_b}{(\overline{\mu_o B_o})_{\bar{p}_R, p_b}} + \frac{(p_b^2 - p_{wf}^2)}{2p_b\,(\mu_o B_o)_{p_b}}\right]} \quad .....(8)$$

and oil-in-place is

$$N = \frac{V_p(1 - S_{wi})}{B_{oi}} \quad .....(5)$$

The productivity factor is

$$PF = \frac{7.08\ kh}{\left[\ln\left(\frac{r_e}{r_w'}\right) - \frac{1}{2}\right]} = \frac{q(t)/q_{Dd}}{\left[\frac{\bar{p}_R - p_b}{(\overline{\mu_o B_o})_{\bar{p}_R, p_b}} + \frac{p_b^2 - p_{wf}^2}{2p_b(\mu_o B_o)_{p_b}}\right]} \quad ..(9)$$

The oil-in-place calculated from rate-time analysis is then used with a reservoir material balance equation and the actual gas and oil production to calculate reservoir pressure. Then the gas-oil relative permeability ratio and gas saturation can be calculated. The rate-time productivity factor is used to calculate the oil relative permeability. Gas relative permeability values are calculated by multiplying the oil relative permeability by the gas-oil permeability ratio at the same gas saturation. These calculations will be discussed and demonstrated in detail later.

"Black Oil" Approach of Determining the Gas-Oil Permeability Ratio

The term "black oil" normally refers to reservoirs that have reservoir temperatures below 150°F, an initial solution GOR below 500 SCF/STB, and stock tank oil gravities below 35° API. Such a fluid will have little or no liquids drop out of the free gas phase when flashed through a separation process. Under "black oil" conditions, the Schilthuis or Tarner material balance equation is used with oil and gas production data and conventional laboratory and/or calculated PVT data to calculate a gas-oil relative permeability ratio for a well or a total field. Laboratory PVT analysis will give the oil viscosity, gas and oil formation volume factors and solution gas-oil ratios as a function of pressure that are needed in the material balance equation. Gas viscosity normally is calculated from a correlation. The laboratory PVT study also determines the bubble point pressure of the reservoir fluid.

When the reservoir pressure is below the bubble point pressure in a solution gas drive reservoir without water influx nor an initial gas cap, the following equation can be used to calculate reservoir pressure, $\bar{p}_R$, as a function of fractional recovery.

$$\frac{N_p}{N} = \frac{B_o - B_{oi} + (R_{si} - R_s) B_g + B_{oi} \left(\frac{C_w S_{wc} + C_f}{1 - S_{wc}} \right) (\bar{p}_{R_{bp}} - \bar{p}_R)}{B_o + (R_p - R_s) B_g} \qquad ....(10)$$

Determining N from rate-time analysis and using reported cumulative gas-oil ratio and cumulative oil production, we iterate on reservoir pressure using the above material balance equation until the right hand side equals the left hand side. We thus obtain reservoir pressure, $\bar{p}_R$, for every cumulative oil production period. After the reservoir pressure has been determined for each monthly production period, the pressure dependent terms, R_s, B_o, B_g, μ_g, and μ_o can be determined to then calculate the liquid saturation and gas-oil permeability ratio using the following equations.

$$S_L = \left(1 - \frac{N_p}{N} \right) \frac{B_o}{B_{oi}} (1 - S_{wc}) + S_{wc} \qquad ....(11)$$

or

$$S_g = 1 - S_L \qquad .....(12)$$

$$\frac{k_g}{k_o} = (R - R_s) \frac{\mu_g B_g}{\mu_o B_o} \qquad .....(13)$$

Compositional Calculation of Gas-oil Permeability

The classical black oil calculation of PVT data is based on a two component system (gas and oil) where gas is allowed to dissolve in oil, but oil is assumed to always exist in the liquid phase. This assumption is valid for low to medium gravity oil, but does not hold for volatile oils and gas condensates

since substantial amounts of the oil component can exist in the gaseous phase. Thus, black oil PVT data used in conjunction with separator oil and gas rates from a volatile oil reservoir will give incorrect material balance, oil saturations and gas-oil permeability ratios.

A composite (differential and flash) oil formation volume factor and solution gas-oil ratio can be calculated using a one-cell compositional material balance by flashing reservoir oil from each depletion step by itself through the separators. The following equations can be used to determine the oil formation volume factor and solution gas-oil ratio,

$$B_o = \frac{\text{Moles stock tank oil/molar density stock tank oil}}{\text{Moles reservoir oil/molar density reservoir oil}} \qquad .....(14)$$

$$R_s = \frac{379(5.615)(\text{moles gas from separators})}{\text{Moles reservoir oil/molar density reservoir oil}} \qquad .....(15)$$

The gas formation volume factor and liquid content of the gas phase, r_s, can be calculated by flashing reservoir gas through the separators,

$$B_g = \frac{379(5.615)(\text{moles gas from separators})}{\text{Moles reservoir gas/molar density of reservoir gas}} \qquad .....(16)$$

$$r_s = \frac{\text{Moles condensate from separator/molar density of stock tank condensate}}{379(5.615)(\text{moles separator gas})} \qquad .....(17)$$

The gas-oil permeability ratio can then be determined at a specific fractional oil recovery by using the following modified black oil equation (see Appendix for derivation),

$$\frac{k_g}{k_o} = \left(\frac{R - R_s}{1 - r_s R_s}\right) \frac{\mu_g B_g}{\mu_o B_o} \qquad .....(18)$$

A compositional material balance can also be used to directly calculate the gas-oil permeability ratio for a volatile oil reservoir using rate-time depletion data. At each time step the oil rate is set and k_g/k_o is varied until the computed gas-oil ratio equals the producing gas-oil ratio. The corresponding gas saturation is obtained from the flash of remaining fluids at the end of the time step. The compositional material balance program was used to directly calculate the k_g/k_o and S_g results reported for the Edda field study.

Oil and Gas Relative Permeability

With the reservoir pressure, $\overline{p}_R$, oil formation volume factor, and the historical oil flow rates (excluding condensate for volatile oil reservoirs) now available, the relative permeability to oil, k_{ro}, can be calculated. Rate-time analysis matching will give the q(t) and q_{Dd} needed to calculate the productivity factor using equations 6 or 9.

Once the productivity factor, PF, has been determined, the relative permeability to oil can be calculated by using the following equation for the Δp^2 approach.

$$k_{ro} = \frac{2\overline{p}_R(\mu_o B_o)\dfrac{q_o}{\overline{p}_R}}{PF\,(\overline{p}_R^{\,2} - p_{wf}^2)} \qquad \text{.....(19)}$$

and for the Δp approach

$$k_{ro} = \frac{q_o(\overline{\mu_o B_o})}{PF(\overline{p}_R - p_{wf})} \qquad \text{.....(20)}$$

For each production period - monthly for this study - an oil relative permeability value is calculated. The corresponding gas saturation is calculated by using equations 11, 12 for black oil systems or obtained from a compositional material balance run for volatile oil systems. Rate data immediately after a shut-in period is normally not used for low permeability reservoirs. After an extended shut-in, transient flow behavior will cause the production to be higher than would occur under pseudo-steady state flow conditions. This leads to invalid oil relative permeability values being calculated. After the relative permeability oil and gas-oil permeability ratio have been calculated, a value for gas relative permeability can be obtained. This is accomplished by multiplying the gas-oil permeability ratio by the oil relative permeability at the same gas saturation

$$k_{rg} = \frac{k_{rg}}{k_{ro}} \cdot k_{ro} \qquad \text{.....(21)}$$

In reality, the productivity factor, PF, could also include a rate dependent skin s (q, t) and a non-darcy flow term, $D_o q_o$, for completeness.[10] For simplicity, we have assumed these terms to be zero in calculating the relative permeability to oil. An s (q, t) term that would exist when $\overline{p}_R$ is above the bubble point pressure with drawdown below the bubble point pressure would vanish once the total reservoir pressure dropped below the bubble point pressure. In contrast, the D_o term if present should increase in the presence of an increasing gas saturation with depletion.

Production Performance Data From the Edda Field

Production performance data from the Edda field, which is the smallest of four overpressured volatile oil fields within the Greater Ekofisk development in the Norwegian Sector of the North Sea, is used in this study. Production from the Edda field started in December of 1979. Fig. 1 shows the wells and their location. The production data used in this study covers the same time period as that used in reference 6 to study the total Edda field decline.

Perforations in some of the Edda field wells are in the Ekofisk (Danian) chalk and Upper Cretaceous (Tor) chalk or Tor formation at approximately 11,000 feet. As indicated by production logs, the Tor formation provides the majority of the production with only a very small fraction coming from the Ekofisk formation when both formations are perforated. The Tor formation is considered to be much more highly fractured than the Ekofisk formation in the Greater Ekofisk area. The wells in the Edda field had calculated fracture intensities ranging from 28 in well C-2 to 1 in well C-5 Table 2. Fracture intensity is defined as the effective permeability determined from a pressure build-up test divided by the effective permeability of the matrix.

Initial gas-oil ratios and pressure buildup test results suggested that the Edda field may consist of two separate accumulations. The compositions of the reservoir fluid used for each of these two areas in this study are shown in Table 1. The PVT properties for the South Edda field (the field we will concentrate on) are shown in Figure 2. Examining the initial reservoir fluid compositions along with the initial solution gas-oil ratios and noticing the high fraction of low and intermediate hydrocarbon fractions, it was concluded that a black oil approach of calculating k_g/k_o, k_{ro}, and k_{rg} performance from the North and South Edda fields may not be appropriate.

Oil and gas-oil ratio production performance data are shown in Figures 3 through 9 for each of the seven producing wells in the Edda field. The allocated oil production (including condensate) is in stock tank barrels per day. The allocated gas-oil ratio is in standard cubic feet per stock tank barrel while the separator test GOR is in standard cubic feet per separator barrel.

The individual well peak oil production rates ranged from approximately 13500 BOPD TO 2000 BOPD. The gas-oil ratio for five of the South Edda field wells (wells C-2, C-5, C-9, C-11, and C-14) was initially around 1700 SCF/STB while the other two wells in the North Edda field (wells C-10 and C-15) had initial gas-oil ratios of approximately 2000 SCF/STB. This initial difference in GOR first suggested that the Edda field may consist of two separate reservoirs. (Also, when the only field wide pressure buildup tests were performed on the wells of the Edda field in September 1983, the two wells with the higher initial gas-oil ratios had significantly higher average reservoir pressures

than the other five wells.) In the rate-time analysis evaluations, a bubble point pressure of 6067 psi was used for the higher initial solution gas-oil ratio wells (2000 SCF/STB) and a bubble point pressure of 5045 psi was used for the lower initial solution gas-oil ratio wells (1700 SCF/STB). Initial gravities of the oil were approximately 41° API, ultimately increasing to 44° API. The producing gas-oil ratio increased steadily with time for wells C-2, C-5, and C-14, but increased only marginally for wells C-9, C-11, and C-15, and stayed approximately the same for well C-10.

Edda Field Individual Well Reservoir Parameters

The connate water saturation for each well in the Edda field was determined from resistivity logs. Log calculated average water saturations for the seven wells ranged from a low of 33.8% in well C-11 to a high of 47.8% in well C-5. The pay thickness of the oil zone for each well as calculated using a water saturation cutoff of 70%. Pay zone thickness ranged from a high of 120 feet in well C-9 to a low of 70 feet for well C-15. Porosity ranged from 20.8% to 25.3% and was calculated from a compensated neutron log. Table 2 summarizes these results for each well.

Total irreducible liquid saturation - water saturation plus residual oil - was determined from laboratory water flood tests on several Cretaceous core samples of different porosities. A plot was made which showed the effect of porosity on the total irreducible liquid saturation. Total irreducible liquid saturation for each well was determined by matching the compensated neutron log determined average porosity with the laboratory derived total irreducible liquid saturation versus porosity curve. The total irreducible liquid saturation values ranged from 63.5% for well C-15 to 53.5% for well C-2 (see Table 2). Residual oil saturation was approximated by subtracting the resistivity log determined irreducible water saturation from the laboratory determined total irreducible liquid saturation.

Because the fluids in the Edda field are contained in a fractured limestone rock system and the fracture permeability dominates fluid flow, a fracture intensity FI was calculated for each well. This was done to determine if the degree of fracturing in the well would affect the gas-oil permeability ratio curve and oil and gas relative permeability curves for each well. In order to calculate fracture intensity, the initial well test effective permeability and matrix effective permeability were determined. The reservoir effective permeability was determined from the initial pressure buildup tests. Effective permeabilities calculated from the build-up tests ranged from a high of 18 md to a low of 0.5 md. The effective permeability of the matrix was determined by flowing oil through core samples at irreducible water saturation. These permeabilities ranged from 0.66 md to 0.28 md. Each of the cores had different porosities from which a plot of porosity versus effective permeability was made. The effective matrix permeability for each well was then determined by using its average log derived porosity with the laboratory determined effective matrix permeability versus porosity plot. The fracture intensity was calculated by dividing the reservoir effective permeability from the pressure buildup test by the laboratory derived value. Well C-2 had the highest fracture intensity of 28 and well C-5 had the lowest value of 1. As should be expected, well C-2 had much greater production rates than well C-5. All well test effective permeability results, laboratory derived matrix permeability values, and fracture intensities for each of the seven Edda wells are given in Table 2.

Discussion of Results

Rate-Time Analysis

Rate-time analysis for each of the wells in the Edda field was performed by plotting and matching the oil production rate versus time to the log-log composite type curve of reference.[9] The log-log plots with their corresponding match point are shown in Figures 10 through 16 and summarized in Table 3. The oil production rate used on the log-log plot is the oil rate, excluding condensates, not the total liquid as would be measured from the separator. Note that the log-log plot on the oil rate, excluding condensate, and the oil rate, including condensate, for well C-9, indicates that the b exponent matched was 0.5 and 0.6 respectively. Further note that the match point would be the same for both curves.

This observation was used to obtain a first estimate of reservoir pore volumes for each of the wells in the Edda field. A compositional material balance computer run with rate-time calculated pore volume as input, calculated the historical k_g/k_o and gas saturation to match the actual rate and GOR performance. From the run we also obtained the surface oil production rate excluding condensate. A log-log plot of rate-time data with the oil rate, excluding the condensate, was then made to confirm or recalculate a new reservoir pore volume. Changes were usually negligible since much of the early time data used for the initial match did not have much free gas associated with it.

From an analysis of the individual well rate-time plots, five of the wells indicated a decline exponent b of 0.5, while well C-5 had a b exponent of 0 (exponential), and well C-14 had a b exponent of 0.2. References [6,7] suggest that all wells in the same reservoir should be expected to have approximately the same value of b exponent. Well C-14's b exponent of 0.2 cannot be readily explained, but well C-5's exponent of 0 is thought to be caused by the well flowing at an insufficient velocity to prevent wellbore liquid loading i.e., a high bottomhole backpressure, p_{wf}, has existed for the well for a long time. A well's decline exponent b is a function of the level of back-pressure.[9,11] (As p_{wf} approaches $\overline{p}_{Ri}$, b approaches 0.)

To determine the dimensionless flow rate, q_{Dd}, and dimensionless time, t_{Dd}, a match point is chosen. For convenience, the match points in this study were at a time of 1 month and a rate of 1000 BOPD for every well in the field. The dimensionless flow rates, q_{Dd}, ranged from a value of 0.64 for well C-5 to a value of 0.068 for well C-2, and the dimensionless time, t_{Dd}, ranged from 0.065 for well C-10 to 0.19 for well C-2. From the match point values, pore volume and the productivity factor for each well were calculated. The pore volume calculated using rate-time data was largest for well C-9, with 47,359,000 reservoir barrels and smallest for well C-5 with 11,210,000 reservoir barrels. The productivity factor was highest for well C-2 and lowest for well C-5, having values of 1.161 Darcy-ft and 0.123 Darcy-ft, respectively. All pertinent results obtained from rate-time analysis are shown in Table 3.

To confirm that the pore volume for each well from rate-time analysis was reasonable, the average reservoir pressure, $\overline{p}_R$, calculated from a

compositional material balance, using the rate-time calculated pore volume and actual oil and gas production rates, was compared with the average reservoir pressure obtained from the 1983 field-wide pressure buildup survey. See Figures 17-23. Pressure buildup results, in terms of p_{max}, p^* and $\overline{p}_R$, for each of the seven wells are shown in Table 3.

Separate compositional material balance runs were made with oil-in-place calculated from both the Δp and the Δp^2 pore volume equations (equations 4 and 8). The Δp pore volume equation always gave a calculated pore volume lower than the one calculated using the Δp^2 pore volume equation. (The area under the curve of $1/(\mu_o B_o)$ versus p from p_{wf} to $\overline{p}_R$ results in a smaller value than $\overline{(\mu_o B_o)}$ evaluated at $(\overline{p}_R + p_{wf})/2$ used with the Δp equation.) When using the pore volume equation, the compositional material balance computer program runs calculate a consistently lower average reservoir pressure.

Figures 17 through 23, show that when using the pore volume derived from the Δp^2 pore volume equation the material balance calculated average reservoir pressure for each well fell within the pressure buildup survey maximum shut-in pressure and p^* range. Good matches between the average reservoir pressure determined from the compositional material balance and buildup tests were found in wells C-9, C-11, and C-15 (Figures 19, 20, and 23). Pore volumes calculated using the Δp approach resulted in pressures which were always much less than the pressure found from the pressure buildup tests. The compositional material balance calculated average reservoir pressures for wells C-2 and C-14, using the pore volume obtained from the Δp pore volume equation, were even below the observed maximum shut-in pressure. Wells C-5, C-11, and C-14 fell within the maximum shut-in pressure and the p^* range using the Δp^2 calculated pore volume. Only Δp^2 calculated pore volume runs were made for the two wells in the North Edda field (wells C-10 and C-15).

Relative Permeability Ratio, k_g/k_o

To determine a gas-oil permeability ratio curve for each of the wells in the volatile oil Edda field, compositional material balance runs were made using the reported gas and oil production rates and the Δp^2 calculated pore volume determined from the rate-time match for each well. The gas-oil permeability ratio was determined by iterating on the gas-oil permeability ratio until the gas-oil ratio from production data matched the gas-oil ratio calculated from the material balance program. (For black oil reservoirs, k_g/k_o would be calculated directly using equation 13.) Gas-oil permeability ratio values were calculated for each monthly production period. When the reservoir pressure is above the bubble point pressure, the gas-oil permeability ratio is assumed equal to zero.

The calculated gas-oil permeability ratio versus gas saturation curves determined from the compositional material balance run for each of the wells in the Edda field are shown in Figures 24 through 30. Only for wells C-5 and C-10 were the gas-oil permeability ratio versus gas saturation curves demonstrating unusual behavior. Well C-5's gas-oil permeability ratio curve (see Figure 25) is considered unreliable because the well tended to load up with liquid and produced erratically. Well C-10 had an unusual curve (Figure 27) because the

producing gas-oil ratios for the well remain nearly constant (see also Figure 7). No explanation for this well's behavior has been found except that it appears to be in the North Edda field and exhibits the same flat GOR behavior as the C-15 well which is also in the North Edda field.

The most interesting result obtained from the individual well gas-oil permeability ratio curve study is that they all appear to be a function of fracture intensity. All of the well gas-oil permeability ratio curves have been normalized to the same average water saturation and plotted on Figure 31. Note that as the fracture intensity of the wells increase, the gas-oil permeability ratio curves become less favorable to oil flow, i.e., shift to the left. As can be seen from Figure 31, wells C-2 and C-14 which had fracture intensities of 28 and 18 respectively have the most unfavorable gas-oil permeability ratios. Well C-11 and C-15 have the lowest fracture intensities, and as would be expected, their relative permeability ratios are more favorable (were shifted more towards the right). The fact that gas-oil permeability ratio curves become unfavorable with higher fracture intensity suggests that capillary "end effects" may become a greater factor in naturally fractured reservoirs than in nonfractured systems. This end effect is caused by the capillary pressure discontinuity between the fracture and the matrix.

An average total South Edda field gas-oil permeability ratio curve was determined as a function of gas saturation, using the total gas and oil production of the South Edda field and the sum of the rate-time calculated individual well pore volumes, (Figure 32). The South Edda compositionally derived gas-oil permeability ratio curve was then compared using two different averaging methods, (Figure 33). The two averaging methods were least squares linear regression and volume averaging, as proposed by Guerrero.[3] (Actually Guerrero used a thickness weighted instead of volume weighted approach but the logic for using volume is similar.)

The linear regression technique attempts to make a best fit straight line from the individual well curves. The data from the wells in the South Edda field used to develop a total field gas-oil permeability ratio using the linear regression technique is shown in Table 5. As can be seen in Figure 33, the linear regression method's gas-oil permeability ratio approximation falls within the general area of the compositionally derived gas-oil permeability curve. However, because the gas-oil permeability ratio determined with this method forms a straight line, the gas-oil permeability ratio would be incorrect at high and low gas saturations.

The volume averaging technique averages the individual gas-oil permeability ratio curves by weighting each by pore volume. The data used to derive this curve are also shown in Table 5. At the same gas-oil permeability ratio an average field gas saturation is generated by using the following equation.

$$S_{gavg} = \frac{\sum_{i=1}^{n} S_{gi} V_{pi}}{\sum_{i=1}^{n} V_{pi}} \qquad \text{.....(22)}$$

A gas-oil permeability ratio curve generated using the volume averaged technique appears more reasonable than the linear regression method for two reasons: the curve will show characteristic curvature and the wells with the lower production rates (smaller drainage volumes) will not influence the shape of the curve as much as the wells with higher production rates (larger drainage volumes). As can be seen from Figure 33, the volume averaged gas-oil permeability ratio curve has almost the same shape as the compositional material balance derived gas-oil permeability ratio curve, but is shifted slightly towards higher gas saturation values. A volume averaged curve was also determined by normalizing each wells' curve to the South Edda field's average connate water saturation of 36.4 percent with virtually no difference.

k_g/k_o Determined From Correlations

The use of Corey's correlation[12] to develop a gas-oil permeability ratio curve requires a value for the pore size distribution index, λ, be known. The pore size distribution index can be determined from either an air-brine capillary pressure laboratory test or a log calculated capillary pressure curve. A log calculated capillary pressure curve was made by plotting water saturation as a function of depth for the C-9 well. The pore size distribution index for both the log and laboratory derived capillary pressure curve was calculated from a plot of capillary pressure versus effective water saturation. A λ of 2.063 was found using the laboratory capillary pressure curve.

The field performance compositionally and black oil derived gas-oil permeability ratio curve for well C-9 are compared with Corey's correlation and laboratory (unsteady-state) derived gas-oil permeability ratio curve (Figure 34). The laboratory curve was generated from the unsteady-state gas drive method on a Cretaceous core with 25.3% porosity and an effective permeability to oil at connate water saturation of 0.38 millidarcies. Corey's gas-oil permeability ratio curve was calculated using the pore size distribution index of 2.063. Neither the laboratory nor Corey's calculated gas-oil permeability ratio curves resembled well C-9's compositionally or black oil derived gas-oil permeability ratio curve. Laboratory and Corey's calculated gas-oil permeability ratio curves have almost no curvature and fall within a small gas saturation range. This suggests that laboratory and Corey derived gas-oil permeability ratio curve should not be used for naturally fractured reservoirs, as would be expected.

In order to show the effect of condensate production from a volatile oil reservoir on the gas-oil permeability ratio curve, both the black oil and compositionally calculated curves are plotted on Figure 34. The black oil gas-oil permeability ratio curve for well C-9 is shown to be below the compositional derived gas-oil permeability ratio curve. The calculated values for black oil and the compositionally derived gas-oil permeability ratio for each monthly production period of well C-9 is given in Table 4. As more free gas is produced from this volatile oil well, the calculated black oil and compositional gas-oil permeability ratio curves deviate to a much greater extent. This is primarily due to the increased amount of condensate being produced from the free gas phase as the reservoir pressure is lowered. When the black oil approach is used to calculate a gas-oil permeability ratio curve from field production data, a more favorable curve than actually exists in the reservoir will be obtained.

k_g/k_o Compared With Other Fields

One objective of this study was to determine if naturally fractured solution gas drive fields producing from the same formation would have gas-oil permeability ratio curves located in approximately the same region on a gas-oil permeability ratio versus gas saturation plot. In Figure 35, the South Edda field k_g/k_o curve is compared with Arps's limestone-dolomite-chert formations minimum, maximum and average curves.[13] All k_g/k_o curves in Figure 35 have been normalized to the same connate water saturation. Note that the total South Edda field gas-oil permeability ratio curve lies in approximately the same location as the fractured reservoirs found in Arps's limestone curves. To further emphasize this point, total field curves from other naturally fractured fields in the Greater Ekofisk area are compared with the Edda field curve and are also shown on Figure 35. The Edda field is the only oil field in the Greater Ekofisk area that produces exclusively from the more highly fractured tor (Cretaceous) formation. This would explain why the Edda field k_g/k_o is the most adverse curve. All of the Greater Ekofisk field gas-oil permeability ratio curves, normalized to the same water saturation, are in approximately the same location on a gas-oil permeability ratio versus gas saturation plot. All generally fall between Arps' average and maximum curves. The minimum Arps limestone curve represents highly naturally fractured reservoirs (fractured chert), and the average limestone curve represents a medium degree of fracturing.

Relative Permeability to Oil (k_{ro}) and Gas (k_{rg})

Relative permeability to oil, k_{ro}, was calculated in this study using an oil well inflow performance or Δp^2 backpressure equation (equation 19) and rate time performance data for the seven individual wells in the Edda field. Calculating the relative permeability to oil curves for individual wells gives some insight into how natural fractures influence fluid flow. An "average well" concept for a field would be required to calculate them from total field performance data. In the past, the only methods in which gas and oil relative permeability curves could be determined for naturally fractured reservoirs was by laboratory flooding of a fractured core,[14] using pseudo functions[15,16] or individual well history matching with simulation models. Very little information is given in any previously published literature on the shape of the oil relative permeability curve in an actual solution gas drive naturally fractured field case.

Relative permeability to oil curves were calculated for six of the wells in the Edda field using a constant bottomhole flowing pressure of 1500 psi. Results of these calculations are shown in Figures 36 through 41. The one well that did not have its oil relative permeability calculated was well C-10, because the gas-oil ratio was virtually constant. The C-10 well is considered to be in the North Edda field. The other North Edda well, C-15, also did not give a good relative permeability curve. The five wells which are located in the South Edda field, however, gave calculated oil relative permeability values that had distinguishable trends. Of these five wells, only C-2 seemed to have some oil relative permeability points which were scattered.

Calculating the gas relative permeability was the next step. This was accomplished by multiplying the calculated oil relative permeability by the previously determined gas-oil permeability ratio at the same gas saturation. One interesting result noticed by examining the gas relative permeability curves was that no critical gas saturation exists. This, however, should be expected for wells in a naturally fractured reservoir.

The conventional productivity index or Δp backpressure equation was also used to derive a relative permeability to oil equation (equation 20). One way in which to determine whether the Δp or the Δp^2, inflow performance, method of calculating oil relative permeability should be used is to conduct an isochronal test on a well in the field of interest. The Edda field and the Ekofisk field have similar fluid and rock characteristics. An Ekofisk field isochronal test was analyzed in a paper by Fetkovich.[10] The isochronal curve of the 2/4-2X well in the Ekofisk field was shown to give the Δp^2 oil backpressure equation for flows below the bubble point pressure. These results suggest that the Δp^2 form of the oil backpressure equation should be used to calculate the relative permeability to oil in the Edda field study.

Calculation of oil relative permeability was made on well C-9's production data using both the Δp and Δp^2 oil relative permeability equations. However, both were based on saturations and pressures, p_R, determined from the $\underline{\Delta p^2 \text{ calculated pore volume}}$ since the pore volume could also be determined from pressure performance data. The saturations are therefore the same for both the Δp and Δp^2 k_{ro} calculations. Data for these two calculations are shown in Table 6. A comparison of the oil relative permeability curves obtained using both the Δp and Δp^2 oil relative permeability equation is shown in Figure 42. The oil relative permeability calculated using the Δp equation gives lower oil relative permeability values than the Δp^2 equation. Therefore, if the Δp method is used for a reservoir exhibiting Δp^2 flow characteristics, a lower estimation of the oil and gas flow rates will be made.

The oil relative permeabilities of every well in the South Edda field, all normalized to the same water saturation and using the Δp^2 oil relative permeability equation, are plotted on Figure 43. The wells with the higher fracture intensity generally gave more favorable oil relative permeability curves at high gas saturations. Well C-2 had the highest fracture intensity of 28 and almost had the appearance of a straight line. This would indicate that the fractures are dominating flow because the oil relative permeability curve for fracture flow is normally represented by a straight line. Well C-5 had a fracture intensity of 1, indicating little or no natural fractures, and had an unfavorable oil relative permeability curve at high gas saturations. From well C-5's performance derived oil relative permeability curve, it is concluded that flow in this well is dominated by matrix flow. It resembles the oil relative permeability curves found in an unsteady-state matrix core plug, (see Figure 45).

In order to determine whether Corey's correlation derived gas and oil relative permeabilities can be used to approximate actual field oil and gas flow rates, they are compared to wells C-2 and C-14 performance derived relative permeabilities (Figure 44). The relative permeabilities for oil and gas

calculated using Corey's correlation are normalized to the same average water saturation that is used to normalize the performance calculated gas and oil relative permeability curves. The pore size distribution index varied between 0.1 to 1000. These values of 0.1 and 1000 were chosen to represent the most diverse cases of an extremely heterogeneous and homogeneous rock system, respectively. Calculated oil relative permeabilities for well C-2, which had the most favorable oil relative permeability curve, and well C-14, which had the least favorable oil relative permeability curve, are shown and compared on Figure 44. The dashed lines on Figure 44 represent the performance derived oil relative permeability curves of wells C-2 and C-14. Well C-14 matched fairly well with the homogeneous Corey's derived oil relative permeability curve which used a pore size distribution index of 1000. Well C-2 was to the left of Corey's derived oil relative permeability curves calculated using both pore size distributions of 0.1 and 1000. Note that only the oil relative permeability curve of well C-14 matched Corey's derived curve. The C-14 well fracture intensity of 18, and b exponent of 0.2, are lower than well C-2's fracture intensity of 28 and b exponent of 0.5. The major influence behind the difference between these two wells' oil relative permeability curve is thought to be the degree of fracturing. The gas relative permeability, shown also on Figure 44, calculated from Corey's equation deviated from performance derived gas relative permeability in that a critical gas saturation is assumed in Corey's equation and was not found in the performance derived values. Also, the gas relative permeability curve is much lower using Corey's equation as compared with the performance calculated gas relative permeability curve at low gas saturations. (For examples see Figures 45 and 46.)

Corey's correlation, laboratory, and performance calculated gas and oil relative permeability curves are compared for wells C-2 and C-9 in the Edda field on Figures 45 and 46. A water-wet laboratory calculated oil and gas relative permeability curve was used. The pore size distribution value of 2.063 was used in Corey's oil and gas relative permeability equations.

The performance derived gas relative permeability curves are significantly different from Corey's or laboratory derived gas relative permeability curves. This difference is partly caused by the laboratory and Corey's derived gas relative permeability curves always having a critical gas saturation. In the case of production performance from our naturally fractured solution gas drive reservoir, no critical gas saturation is seen to occur. Corey's and laboratory derived gas relative permeability curves might be used when attempting to approximate gas flow in an unfractured system, but should not be used in a naturally fractured system.

Both the oil relative permeability and gas-oil permeability ratio versus gas saturation curves derived from performance data for well C-9 were entered into a compositional material balance program along with pore volume from the rate-time analysis. A forecast was then made with the well producing wide-open against a minimum bottomhole flowing pressure of 1500 psia. A comparison between the actual oil production rate and gas-oil ratio and that computed from the compositional material balance program are shown in Figure 47. The comparison is excellent. The oil inflow performance equation used in the compositional material balance computer program to predict flow below the bubble point pressure is,

$$q_o = \frac{PF(\overline{p}_R^{\,2} - p_{wf}^2)k_{ro}}{2\overline{p}_R(\mu_o B_o)\overline{p}_R} \qquad \text{.....(23)}$$

Conclusions

1. Rate-time analysis can be used to determine the original oil in place, N, for an individual well. It was found that by entering the Δp^2 calculated pore volume obtained by rate-time analysis and the gas and oil production for each of the wells in the Edda field into the compositional material balance program, the average pressure computed from the compositional material balance matched quite well with pressure buildup average reservoir pressures.

2. Use of the black oil gas-oil permeability ratio equation for a volatile oil reservoir results in the calculation of a low gas-oil permeability ratio. In order to determine the gas-oil permeability ratio for a volatile oil reservoir, a correction term, designated r_s, can be introduced into the denominator of the black oil gas-oil permeability ratio equation, to correct for the amount of condensate being produced from the free gas phase.

3. As the fracture intensity is increased, the gas-oil permeability ratio becomes more unfavorable. Capillary end effects become more significant as the fracture intensity increases.

4. The Edda total field gas-oil permeability ratio curve was found to be in the same region as fractured limestone gas-oil permeability ratio curves shown in Arps' paper. Highly naturally fractured field gas-oil permeability ratio curves are closest to the minimum limestone Arps curve. Moderately naturally fractured reservoirs give gas-oil permeability ratio curves closer to the Arps average limestone curve.

5. The Δp^2 oil backpressure equation can be used to determine the relative permeability to oil from performance data.

6. Oil relative permeability curves derived from unsteady-state laboratory tests and Corey's correlation were found to be less favorable to oil flow than performance calculated oil relative permeability curves in the fractured limestone Edda field. The unsteady-state and Corey's correlation calculated oil relative permeabilities are not applicable to naturally fractured reservoirs.

7. As fracture intensity increases, the performance derived oil relative permeability curve approaches a straight line between 0% gas saturation and the irreducible liquid saturation. Low fracture intensity wells have oil relative permeability curves similar to laboratory determined matrix curves. Intermediate fracture intensity wells have oil relative permeability curves somewhere between the straight line found in highly naturally fractured reservoirs and the oil relative permeability curve of an unfractured system.

8. It was found that the unsteady-state and Corey's correlation derived gas relative permeability curves were much lower at small gas saturations than performance derived gas relative permeability curves.

Nomenclature

b = reciprocal of decline curve exponent
B_g = gas formation volume factor, RB/SCF
B_o = oil formation volume factor, RB/STB
B_{oi} = initial oil formation volume factor, RB/STB
C_f = effective rock compressibility, psi^{-1}
C_t = total compressibility, psi^{-1}
C_w = water compressibility, psi^{-1}
GOR = gas-oil ratio, SCF/STB
h = oil zone thickness, ft
k_g/k_o = gas-oil permeability ratio
k_{mat} = effective fluid permeability of the matrix, md
k_{rg} = relative permeability to gas, fraction
k_{ro} = relative permeability to oil, fraction
N = initial oil initially in place, STB
N_p = cumulative oil production, STB
$\bar{p}$ = average pressure, psia $(\bar{p}_R + p_{wf})/2$
p_b = bubble point pressure, psia
PF = productivity factor, md-ft, equations 6 and 9
p_{max} = maximum shut-in pressure, psia
$\bar{p}_R$ = reservoir average pressure, psia
p^* = pseudo pressure obtained from pressure buildup test, psia
PVT = pressure, volume, temperature variables (μ_o, μ_g, B_o, B_g)
p_{wf} = bottomhole flowing pressure, psia
q_{Dd} = decline curve dimensionless rate
q_o = average oil production rate, excluding condensate, STB/Day
$q(t)$ = surface rate of flow at time t, STB/Day
Q_o = average oil production rate, including condensate, STB/Day
r_e = external boundary radius, ft
r_s = condensate correction term, STB/SCF
r_w = wellbore radius, ft
r_w' = effective wellbore radius $r_w e^{-s}$, ft
R = instantaneous gas-oil ratio, SCF/STB
R_p = cumulative gas-oil ratio, SCF/STB
R_s = solution gas-oil ratio, SCF/STB
s = skin effect, dimensionless
s_g = gas saturation
S_L = total liquid saturation
S_o = oil saturation
S_{wc} = water saturation
t = time, days
t_{Dd} = decline curve dimensionless time
μ_g = gas viscosity, cp
μ_o = oil viscosity, cp
$(\overline{\mu_o B_o})$ = viscosity - formation volume factor product evaluated at $(\bar{p}_R + p_{wf})/2$, RB-cp/STB

$(\mu_o B_o)_{\bar{p}_R, p_b}$ = oil viscosity - formation volume factor, product evaluated at $(\bar{p}_R + p_b)/2$, RB-cp/STB

$(\mu_o B_o)_{\bar{p}_R}$ = oil viscosity - formation volume factor product evaluated at p_b, or $\bar{p}_R$ if below bubble point, RB-cp/STB

V_p = reservoir volume, ft^3
λ = pore size distribution index
ϕ = porosity, fraction of bulk volume

Subscripts

g = gas
i = initial
o = oil

Acknowledgements

We wish to thank Phillips Petroleum Company for permission to publish this paper. We also wish to thank our Stavanger Office and our co-venturers in the Greater Ekofisk Development for permission to publish the Edda field data.

References

1. Amyx, J.W., Bass, D.M., and Whiting, R.L.: "Petroleum Reservoir Engineering," McGraw-Hill, (1960).

2. Craft, B.C. and Hawkins, M.F., Jr.: "Applied Petroleum Reservoir Engineering," Prentice Hall, Inc., Englewood Cliffs, N. J. (1959).

3. Guerrero, E.T. and Stewart, F.M.: "Practical Reservoir Engineering #1," Oil and Gas Journal.

4. Schilthuis, R.J.: "Active Oil and Reservoir Energy," Trans AIME (1936) 118: 33-52.

5. Tarner, J.: "How Different Size Gas Caps and Pressure Maintenance Affect Ultimate Recovery," Oil Weekly (June 1944) 32.

6. Fetkovich, M.J., Vienot, M.E., Bradley, M.D., and Kiesow, U. G.: "Decline Curve Analysis Using Type Curves: Case Histories," paper SPE 13169 presented at the 59th Annual Fall Meeting of SPE of AIME, Houston, Texas, September 1984.

7. Fetkovich, M.J., Vienot, M.E., Johnson, R.D., and Bowman, B.A.: "Case Study of a Low Permeability Volatile Oil Field Using Individual-Well Advanced Decline Curve Analysis," paper SPE 14237 presented at the 60th Annual Technical Conference and Exhibition of the SPE, Las Vegas, NV, Sept. 1985.

8. Fetkovich, M.D.: "Oil and Gas Relative Permeabilities From Well and Reservoir Performance Data," Masters Thesis, U. of Tulsa, Tulsa, OK (1985).

9. Fetkovich, M.J.: "Decline Curve Analysis Using Type Curves," JPT (June 1980) 1065-1077.

10. Fetkovich, M.J.: "The Isochronal Testing of Oil Wells," paper SPE 4529 presented at the 48th Annual Fall Meeting, Las Vegas, Nev., Sept. 30 - Oct. 3, 1973.

11. Carter, R.D.: "Characteristic Behavior of Finite Radial and Linear Gas Flow Systems - Constant Terminal Pressure Case," SPE/DOE 9887 presented at the 1981 SPE/DOE Low Permeability Symposium, Denver, CO, May 27-29, 1981.

12. Corey, A.T., Rathjens, C. H., Henderson, J.H., and Wylie, M.R. J: "Three Phase Relative Permeability." Trans AIME (1956) 207, 349-351.

13. Arps, J.J. and Roberts, T.G.: "The Effect of the Relative Permeability Ratio, the Oil Gravity, and the Solution Gas-Oil Ratio on the Primary Recovery From a Depletion Type Reservoir," Trans AIME (1955) 204, 120-127.

14. Erlich, Robert: "Relative Permeability Characteristics of Vugular Cores - Their Measurement and Significance." paper SPE 3553 presented at the 46th Annual Fall Meeting of SPE of AIME, New Orleans, LA, Oct. 1971.

15. Jack, Hugh H., Smith, Owen J.E. and Matlax, C.C.: "The Modeling of a Three-Dimensional Reservoir With a Two Dimensional Reservoir Simulator - The Use of Dynamic Pseudo Functions," paper SPE 4701 presented at the SPE-AIME 47th Annual Fall Meeting, San Antonio, Tex., Oct. 1973.

16. Kyte, J.R. and Berry, D.W.: "New Pseudo Functions to Control Numerical Dispersion," paper SPE 5105 presented at the SPE-AIME 49th Annual Fall Meeting, Houston, Tex., Oct., 1974.

Si Metric Conversion Factors

bbl	x 1.589873	E-01	= m^3
bbl/D	x 1.589873	E-01	= m^3/D
c_p	x 1.0*	E-03	= Pa·3
ft	x 3.048*	E-01	= m
ft^3/D	x 2.831685	E-02	= M^3/D
md	x 9.869233	E-04	= μm^2
psi	x 6.894757	E-03	= MPa

* conversion factor is exact

Appendix

Modified Black-Oil Gas-Oil Permeability Ratio Equation for a Volatile Oil

Gas Rate $\quad q_g = q_g \text{ free} + (q_o \text{ free})\, R_s \quad \ldots A\text{-}(1)$

Oil Rate $\quad q_o = q_o \text{ free} + (q_g \text{ free})\, r_s \quad \ldots A\text{-}(2)$

GOR

$$GOR = \frac{q_g}{q_o} = \frac{\text{free} + q_o \text{ free } R_s}{\text{free} + q_g \text{ free } r_s} \qquad \ldots A\text{-}(3)$$

For black oil, r_s is equal to zero and the above equation reduces to:

$$GOR = \frac{q_g \text{ free}}{q_o \text{ free}} + R_s \qquad \ldots A\text{-}(4)$$

$$= \frac{k_g \, \mu_o \, B_o}{k_o \, \mu_g \, B_g} + R_s \qquad \ldots A\text{-}(5)$$

The k_g/k_o for the black oil gas can be calculated as follows:

$$\frac{k_g}{k_o} = \frac{\mu_g \, B_g}{\mu_o \, B_o} \quad (GOR - R_s) \qquad \ldots A\text{-}(6)$$

For a volatile oil case k_g/k_o can be calculated by rearranging equation A-3.

$$GOR = \frac{(q_g \text{ free}/q_o \text{ free}) + R_s}{1 + (q_g \text{ free}/q_o \text{ free}) r_s} \qquad \ldots A\text{-}(7)$$

$$GOR + GOR \left(\frac{q_g \text{ free } r_s}{q_o \text{ free}} \right) = \frac{q_g \text{ free}}{q_o \text{ free}} + R_s \qquad \ldots A\text{-}(8)$$

$$GOR + R_s = \frac{q_g \text{ free}}{q_o \text{ free}} \quad (1 - GOR * r_s) \qquad \ldots A\text{-}(9)$$

$$\frac{k_g}{k_o} = \frac{\mu_g \, B_g \, (GOR - R_s)}{\mu_o B_o \, (1 - GOR * r_s)} \qquad \ldots\ldots A\text{-}(10)$$

Note that when r_s is equal to zero (black oil), equation A-10 reduces to equation A-6.

TABLE 1

EDDA FIELD
INITIAL RESERVOIR COMPOSITIONS
(MOLE FRACTION)

COMPONENT	SOUTH EDDA	NORTH EDDA
C_1	0.5745	0.6210
C_2	0.0882	0.0826
C_3	0.0509	0.0471
i-C_4	0.0090	0.0078
n-C_4	0.0253	0.0236
i-C_5	0.0096	0.0075
n-C_5	0.0153	0.0125
C_6	0.0288	0.0098
C_{7+}	0.1917	0.1802
H_2S	0.0000	0.0000
N_2	0.0034	0.0035
CO_2	0.0033	0.0044
AVG.MOL. WT.	62.94	60.49
C_{7+} AVG. MW.	220.76	230.62
C_{7+} SP. GR.	0.8408	0.8430

	SEPARATOR CONDITIONS		
	1ST STAGE	2ND STAGE	STOCK TANK
PRESSURE - psia	1015	265	15
TEMPERATURE - °F	155	80	60

TABLE 2

RESERVOIR PARAMETERS OF THE EDDA FIELD

WELL NO.	OIL ZONE THICKNESS (feet)	POROSITY FRACTION	WATER SATURATION FRACTION	IRREDUCIBLE LIQUID SATURATION FRACTION	BUBBLE POINT PRESSURE (psia)	BUILD-UP k-md	k_{matrix} (ϕ-k PLOT) md	FRACTURE INTENSITY (FI) k_{bu}/k_{matrix}
C-2	110	0.253	0.372	0.535	5045	18.4	0.66	28
C-5	70	0.238	0.478	0.565	5045	0.7	0.50	1
C-9	120	0.246	0.347	0.550	5045	9.3	0.58	16
C-10	82	0.240	0.400	0.562	6067	2.7	0.50	5
C-11	90	0.241	0.338	0.560	5045	5.7	0.52	11
C-14	114	0.226	0.363	0.600	5045	7.3	0.40	18
C-15	115	0.208	0.412	0.635	6067	1.7	0.28	6

INITIAL RESERVOIR PRESSURE - 7115 psia
RESERVOIR TEMPERATURE - 270° F

TABLE 3

RATE TIME ANALYSIS RESULTS FOR THE EDDA FIELD WELLS

WELL NO.	MATCH POINTS FOR t=1 mo; q(t)=1000 BPD q_{Dd}	t_{Dd}	DECLINE EXPONENT "b"	PORE VOLUME 1000 BBLS	PRODUCTIVITY FACTOR (Darcy-ft)
C-2	0.068	0.190	0.5	42,520	1.161
C-5	0.640	0.072	0.0	11,210	0.123
C-9	0.080	0.145	0.5	47,359	0.984
C-10	0.350	0.065	0.5	29,113	0.166
C-11	0.220	0.080	0.5	31,214	0.359
C-14	0.135	0.100	0.2	41,757	0.588
C-15	0.285	0.067	0.5	33,818	0.203

1983 PRESSURE BUILD-UP SURVEY RESULTS FOR THE EDDA FIELD WELLS

WELL NO.	MAXIMUM SHUT-IN PRESSURE P_{max}-psia	P* psia	AVERAGE RESERVOIR PRESSURE $\bar{P}_R$-psia
C-2	1757.5	2414	2359
C-5	3460.6	--	--
C-9	1977.8	2776	2737
C-10	2685.2	4108	4053
C-11	2483.5	3689	3637
C-14	2686.9	3550	3511
C-15	2740.4	4204	4171

TABLE 4

COMPARISON OF BLACK OIL AND COMPOSITIONAL DERIVED RELATIVE PERMEABILITY RATIOS FOR WELL C-9 (IN THE EDDA FIELD)

N_p Oil & Cond STK/BBL	N_p Oil STK/BBL	$\bar{p}_R$ psia	GOR SCF/STB	R_s	r_s STB/MMSCF	B_o RB/STB	B_g RB/MSCF	μ_o cps	μ_g cps	Black Oil k_g/k_o	Modified Black Oil k_g/k_o	Compositional k_g/k_o	S_L * Black Oil Fraction	S_L Compositional Fraction
196227	196227	6791	1725	1725		1.9075		0.1934					1.0	1.0
579532	579532	6184	1725	1725		1.933		0.184					1.0	1.0
838408	838408	5804	1725	1725		1.952		0.179					1.0	1.0
1040251	1040251	5516	1725	1725		1.967		0.174					1.0	1.0
1194430	1194430	5319	1725	1725		1.980		0.171					1.0	1.0
1396393	1396393	5057	1725	1725		1.997		0.167					1.0	1.0
1576129	1576118	4889	1724	1641	73.9	1.954	0.785	0.180	0.0301	0.0056	0.0064	—	0.9774	0.9754
1679089	1679083	4804	1691	1596	71.2	1.931	0.792	0.186	0.0302	0.0063	0.0072	0.0063	0.9657	0.9620
1841146	1836008	4652	2266	1514	66.7	1.888	0.807	0.196	0.0303	0.0497	0.0585	0.0538	0.9453	0.9403
1942400	1929488	4556	2544	1463	64.0	1.861	0.817	0.202	0.0287	0.0674	0.0805	0.0805	0.9326	0.9271
2074118	2052821	4438	2518	1401	60.9	1.829	0.829	0.210	0.0283	0.0682	0.0806	0.0783	0.9173	0.9113
2196255	2165392	4329	2648	1345	58.2	1.800	0.842	0.218	0.0276	0.0772	0.0913	0.0903	0.9035	0.8972
2311216	2271062	4231	2669	1295	55.8	1.774	0.854	0.225	0.0270	0.0794	0.0933	0.0926	0.8911	0.8848
2415426	2364360	4137	3049	1248	53.7	1.749	0.867	0.232	0.0264	0.1016	0.1215	0.1217	0.8795	0.8734
2503709	2442579	4057	3170	1208	51.9	1.729	0.879	0.238	0.0258	0.1081	0.1294	0.1308	0.8701	0.8641
2585398	2513989	3981	3417	1171	50.3	1.709	0.890	0.244	0.0254	0.1218	0.1471	0.1491	0.8610	0.8556
2663909	2582055	3907	3575	1135	48.8	1.691	0.902	0.249	0.0250	0.1307	0.1583	0.1607	0.8527	0.8475
2737785	2642587	3835	3800	1101	47.3	1.673	0.914	0.254	0.0247	0.1434	0.1748	0.1775	0.8447	0.8400
2807114	2704020	3767	4007	1070	46.0	1.657	0.926	0.259	0.0243	0.1540	0.1888	0.1927	0.8374	0.8331
2874283	2760625	3700	4131	1039	44.7	1.641	0.938	0.264	0.0240	0.1607	0.1971	0.2014	0.8303	0.8265
2912327	2795038	3673	2766	1027	44.2	1.635	0.943	0.266	0.0235	0.0886	0.1009	0.1042	0.8272	0.8234
2984690	2858209	3610	3661	999	43.1	1.620	0.956	0.270	0.0236	0.1373	0.1630	0.1646	0.8203	0.8171
3034825	2900435	3562	4169	978	42.2	1.610	0.966	0.274	0.0232	0.1621	0.1967	0.2028	0.8156	0.8126
3093637	2949622	3504	4422	953	41.2	1.597	0.978	0.278	0.0231	0.1765	0.2158	0.2210	0.8098	0.8072
3139604	2986011	3450	5391	930	40.3	1.585	0.990	0.282	0.0228	0.2253	0.2878	0.2979	0.8047	0.8028
3188189	3025197	3396	5142	907	39.4	1.574	1.003	0.286	0.0226	0.2133	0.2675	0.2762	0.7999	0.7983
3231875	3060947	3351	4895	889	38.6	1.564	1.014	0.289	0.0224	0.2013	0.2482	0.2559	0.7955	0.7944
3277559	3097609	3299	5360	868	37.8	1.554	1.027	0.293	0.0222	0.2249	0.2820	0.2917	0.7911	0.7903
3319943	3132265	3255	5005	850	37.1	1.545	1.038	0.296	0.0220	0.2075	0.2548	0.2634	0.7871	0.7867
3354327	3159899	3217	5372	835	36.5	1.537	1.048	0.299	0.0218	0.2255	0.2805	0.2913	0.7837	0.7838
3398654	3197595	3177	4323	820	35.9	1.529	1.059	0.302	0.0216	0.1735	0.2054	0.2125	0.7800	0.7804
3441335	3226627	3139	5283	805	35.4	1.522	1.070	0.304	0.0215	0.2226	0.2738	0.2835	0.7766	0.7775
3480089	2358334	3098	5180	790	34.8	1.514	1.082	0.308	0.0213	0.2170	0.2647	0.2754	0.7731	0.7744
3515226	3287305	3063	5047	777	34.2	1.507	1.092	0.311	0.0212	0.2109	0.2549	0.2652	0.7699	0.7716
3548618	3315577	3033	4487	766	33.8	1.502	1.102	0.313	0.0210	0.1832	0.2160	0.2241	0.7675	0.7692
3581559	3343089	3001	4843	754	33.4	1.496	1.112	0.316	0.0209	0.2010	0.2398	0.2492	0.7647	0.7668
3614022	3369446	2967	5485	742	32.9	1.490	1.123	0.319	0.0208	0.2331	0.2844	0.2965	0.7620	0.7643
3644481	3394617	2937	5124	731	32.5	1.484	1.133	0.322	0.0207	0.2156	0.2587	0.2693	0.7593	0.7621
3670745	3416140	2910	5320	721	32.1	1.479	1.142	0.324	0.0205	0.2247	0.2710	0.2834	0.7571	0.7601
3699590	3439852	2881	5300	711	31.7	1.474	1.153	0.327	0.0205	0.2250	0.2704	0.2816	0.7548	0.7580
3727006	3462561	2854	5146	702	31.4	1.470	1.163	0.329	0.0203	0.2169	0.2587	0.2704	0.7528	0.7561
3753304	3484115	2827	5443	692	31.0	1.465	1.173	0.332	0.0202	0.2315	0.2785	0.2919	0.7506	0.7542

*S_L Based on N_p (Oil & Cond.) Surface Measured Production

TABLE 5

CALCULATED FIELD AVERAGE k_g/k_o CURVE USING THE LINEAR REGRESSION METHOD (SOUTH EDDA FIELD)

S_g	INDIVIDUAL WELL k_g/k_o					TOTAL FIELD
FRACTION	C-2	C-5	C-9	C-11	C-14	k_g/k_o
0.05	0.100	0.185	0.037	0.0230	0.0745	0.0818
0.06	0.116	0.210	0.051	0.0266	0.0968	0.0899
0.07	0.133	0.241	0.059	0.0298	0.117	0.0988
0.08	0.155	0.273	0.069	0.0351	0.140	0.108
0.09	0.175	0.310	0.078	0.0400	0.167	0.119
0.10	0.197	0.350	0.090	0.0445	0.194	0.131
0.11	0.218	0.387	0.111	0.0509	0.224	0.144
0.12	0.259	0.442	0.115	0.0576	0.251	0.158
0.13	0.278	0.543	0.125	0.0639	0.285	0.174
0.14	0.298	0.624	0.141	0.0676	0.320	0.191
0.15	0.318	0.800	0.153	0.0780	0.355	0.209
0.16	0.337	--	0.168	0.0870	0.391	0.230
0.17	0.355	--	0.182	0.100	0.426	0.253
0.18	0.375	--	0.199	0.105	0.466	0.278
0.19	0.393	--	0.215	0.111	0.505	0.305
0.20	0.412	--	0.230	0.120	0.562	0.335

$$\text{LOG } (k_g/k_o)' = - 0.0408 \text{ SL} + 2.789$$

CALCULATED FIELD AVERAGE k_g/k_o CURVE USING THE VOLUMETRIC AVERAGE METHOD (SOUTH EDDA FIELD)

	INDIVIDUAL WELL GAS SATURATION - S_q					PORE VOLUME AVERAGED
k_g/k_o	C-2	C-5	C-9	C-11	C-14	S_q
0.06	0.030	0.010	0.070	0.123	0.042	0.0589
0.07	0.035	0.014	0.080	0.138	0.049	0.0675
0.08	0.040	0.018	0.090	0.151	0.052	0.0747
0.09	0.043	0.020	0.099	0.163	0.059	0.0819
0.10	0.050	0.021	0.108	0.177	0.061	0.0890
0.11	0.055	0.025	0.116	0.189	0.064	0.0954
0.12	0.060	0.029	0.122	0.200	0.067	0.1012
0.13	0.065	0.031	0.131	0.208	0.071	0.1073
0.14	0.071	0.035	0.139	0.218	0.074	0.1136
0.15	0.078	0.039	0.148	0.226	0.079	0.1206
0.16	0.083	0.042	0.155	0.235	0.083	0.1265
0.17	0.089	0.045	0.161	0.242	0.089	0.1325
0.18	0.094	0.049	0.169	0.251	0.091	0.1381
0.19	0.100	0.052	0.178	0.259	0.095	0.1445
0.20	0.105	0.065	0.183	0.267	0.100	0.1506

TABLE 6

SOUTH EDDA FIELD'S WELL C-9'S CALCULATED k_{ro} USING Δp^2 AND Δp METHOD

				$\Delta p2$ Method		Δp Method *	
MONTH	S_L	$\bar{P}_R$ psia	q_o STB/Day	$(\mu_o B_o)\bar{p}_R$ STB-CP/RB	k_{ro}	$(\overline{\mu_o B_o})$ STB-CP/RB	k_{ro}
1	1.0	6791.3	6455	0.3689	1.0	0.4033	1.0
2	1.0	6184.4	12609	0.3564	1.0	0.4224	1.0
3	1.0	5804.1	8516	0.3487	1.0	0.4342	1.0
4	1.0	5516.3	6640	0.3427	1.0	0.4425	1.0
5	1.0	5319.3	5072	0.3388	1.0	0.4480	1.0
6	1.0	5056.9	6644	0.3339	1.0	0.4559	1.0
7	0.9754	4888.9	5912	0.3514	0.953	0.4603	0.8
8	0.9620	4803.5	3387	0.3585	0.569	0.4631	0.4
9	0.9403	4652.1	5162	0.3699	0.931	0.4672	0.7
10	0.9271	4555.5	3075	0.3767	0.580	0.4700	0.4
11	0.9113	4437.5	4057	0.3850	0.808	0.4741	0.6
12	0.8972	4329.3	3703	0.3927	0.776	0.4771	0.6
13	0.8848	4231.3	3476	0.3996	0.763	0.4801	0.6
14	0.8738	4136.7	3069	0.4061	0.706	0.4835	0.5
15	0.8641	4056.9	2573	0.4061	0.615	0.4859	0.4
16	0.8556	3980.7	2349	0.4162	0.586	0.4884	0.4
17	0.8475	3906.7	2239	0.4208	0.575	0.4908	0.4
18	0.8400	3835.4	2080	0.4250	0.533	0.4930	0.4
19	0.8331	3767.0	1932	0.4291	0.532	0.4961	0.4
20	0.8265	3700.3	1862	0.4329	0.530	0.4981	0.4
21	0.8234	3673.3	1132	0.4345	0.327	0.4986	0.2
22	0.8171	3610.1	2078	0.4381	0.620	0.5005	0.5
23	0.8126	3562.1	1389	0.4407	0.425	0.5024	0.3
24	0.8072	3503.5	1618	0.4439	0.510	0.5051	0.4
25	0.8028	3449.9	1197	0.4468	0.389	0.5063	0.3
26	0.7983	3396.2	1289	0.4497	0.431	0.5081	0.3
27	0.7944	3350.6	1176	0.4520	0.403	0.5110	0.3
28	0.7903	3299.4	1206	0.4547	0.426	0.5122	0.3
29	0.7867	3255.0	1140	0.4570	0.413	0.5135	0.3
30	0.7838	3217.0	909	0.4591	0.337	0.5151	0.2
31	0.7804	3176.8	1240	0.4610	0.471	0.5170	0.3
32	0.7775	3138.6	955	0.4631	0.371	0.5189	0.3
33	0.7744	3098.3	1043	0.4655	0.416	0.5204	0.3
34	0.7716	3062.9	953	0.4682	0.389	0.5217	0.3
35	0.7692	3032.8	930	0.4705	0.388	0.5224	0.3
36	0.7668	3001.3	905	0.4728	0.386	0.5240	0.3
37	0.7643	2966.9	867	0.4753	0.379	0.5246	0.3
38	0.7621	2936.7	828	0.4776	0.370	0.5260	0.3
39	0.7601	2910.0	708	0.4796	0.323	0.5263	0.2
40	0.7580	2880.9	780	0.4818	0.364	0.5281	0.3
41	0.7561	2854.1	747	0.4838	0.356	0.5285	0.2
42	0.7542	2827.3	709	0.4856	0.344	0.5295	0.2

* k_{ro} Δp method based on pressures, $\bar{p}_R$, determined from Δp^2 pore volume method

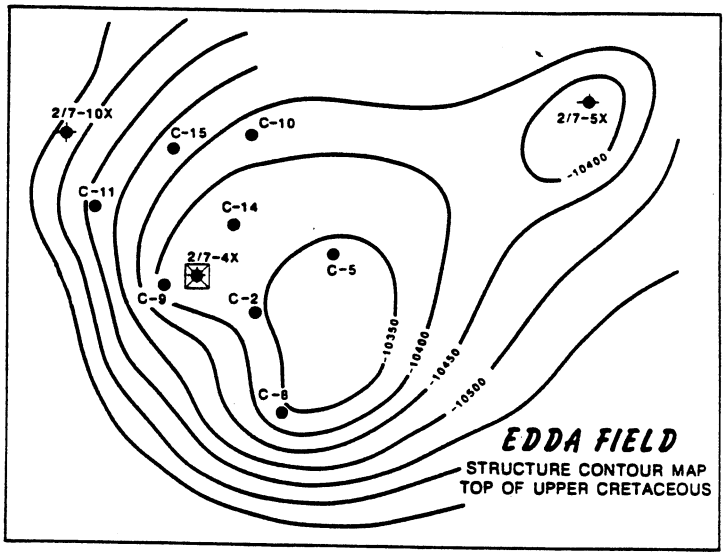

Fig. 1 Edda Field Well Location Map

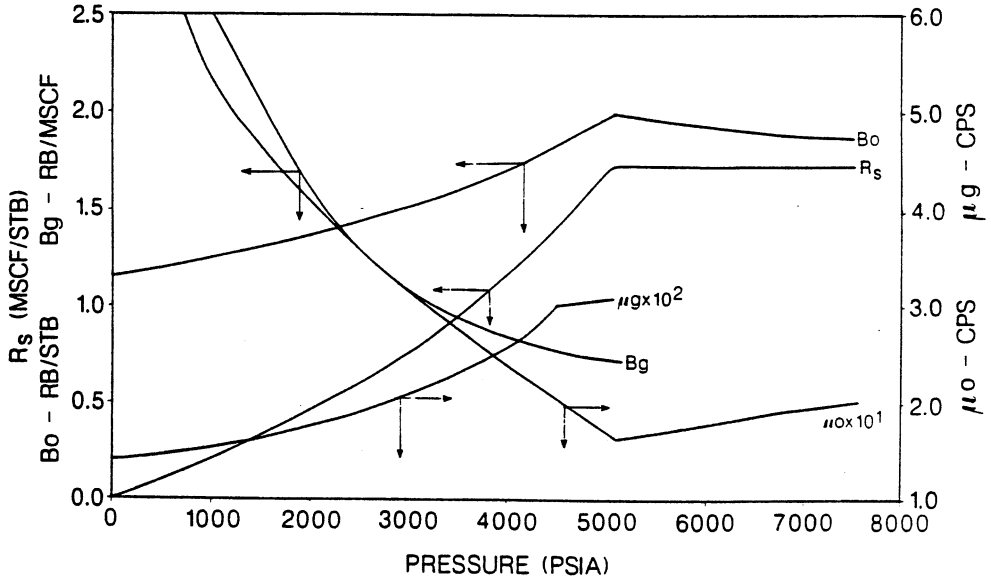

Fig. 2 South Edda Field PVT Data

EDDA FIELD
WELL NO. 2/7C-2

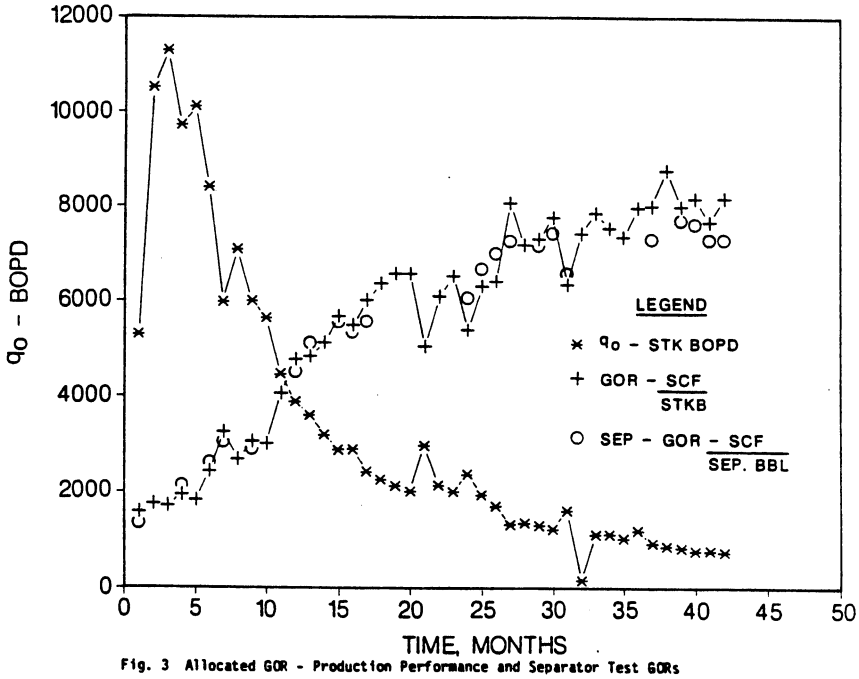

Fig. 3 Allocated GOR - Production Performance and Separator Test GORs

EDDA FIELD
WELL NO. 2/7C-5

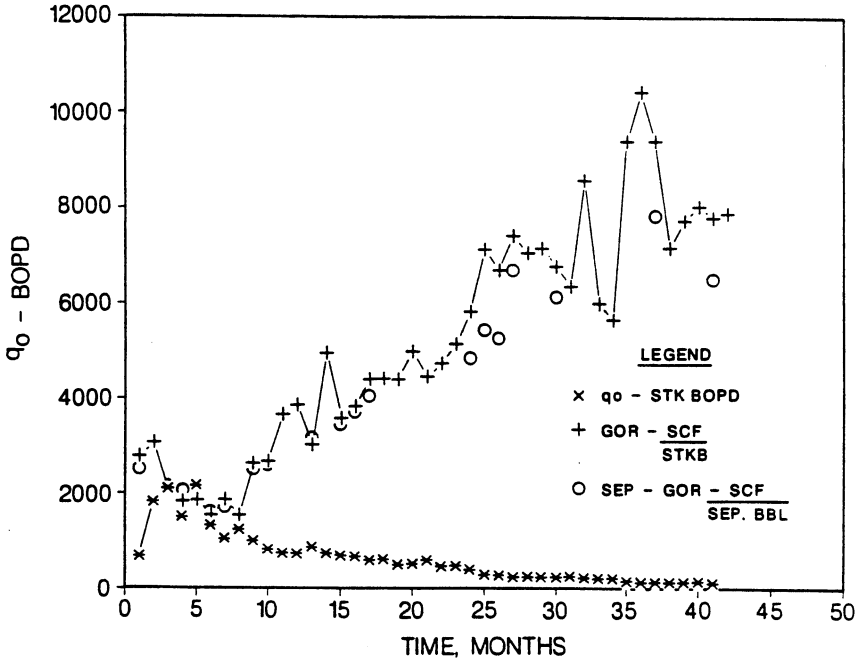

Fig. 4 Allocated GOR - Production Performance and Separator Test GORs

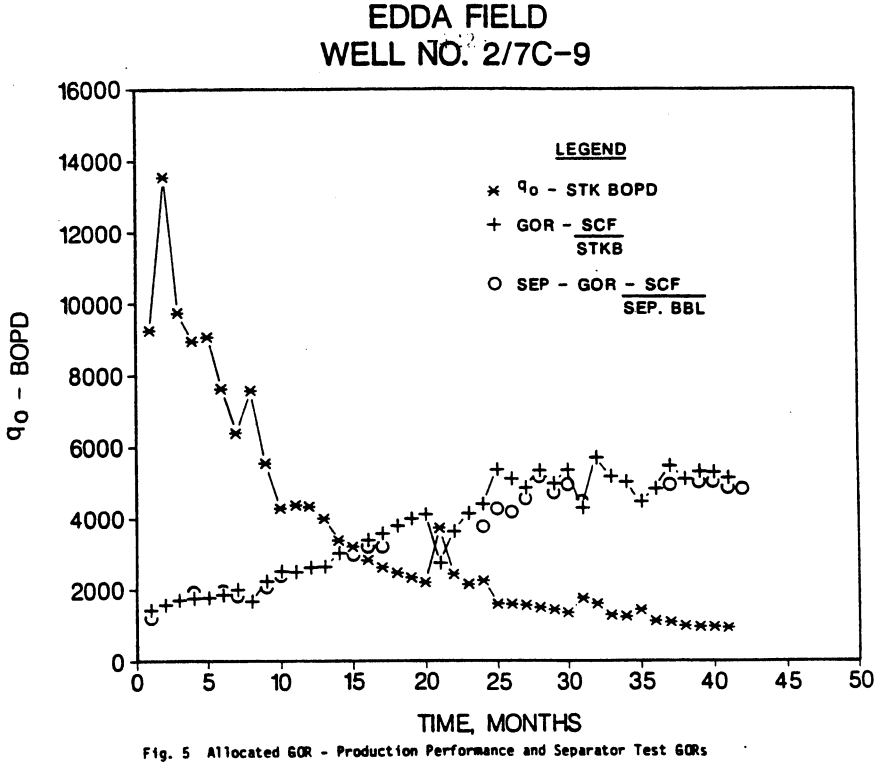

Fig. 5 Allocated GOR - Production Performance and Separator Test GORs

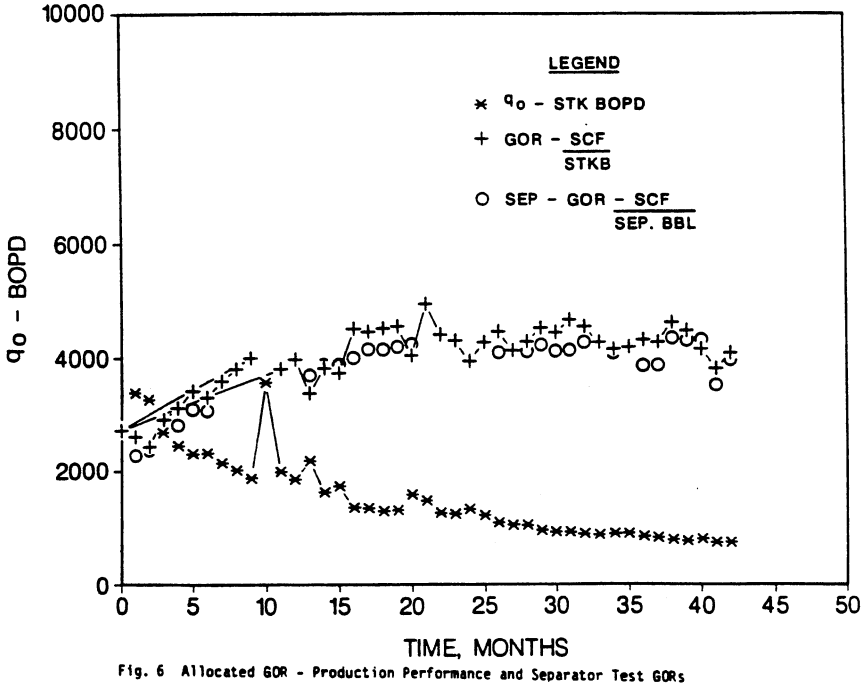

Fig. 6 Allocated GOR - Production Performance and Separator Test GORs

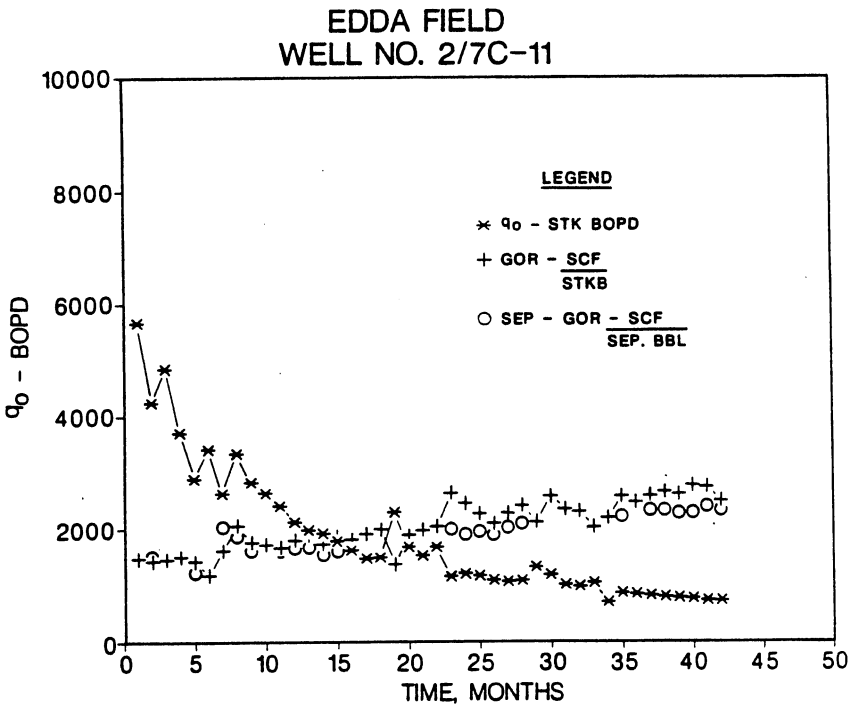

Fig. 7 Allocated GOR - Production Performance and Separator Test GORs

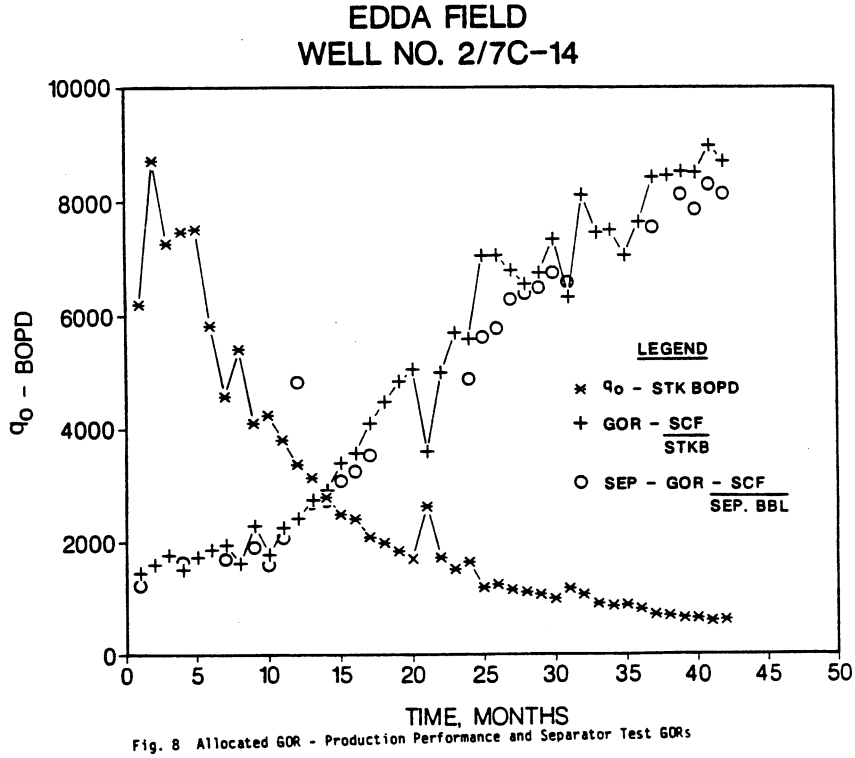

Fig. 8 Allocated GOR - Production Performance and Separator Test GORs

EDDA FIELD
WELL NO. 2/7C-15

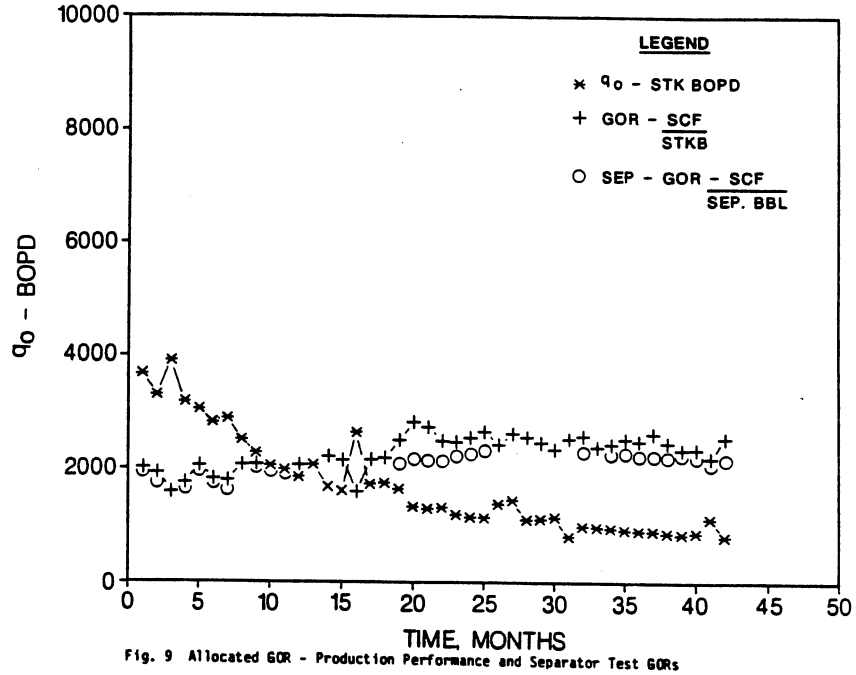

Fig. 9 Allocated GOR - Production Performance and Separator Test GORs

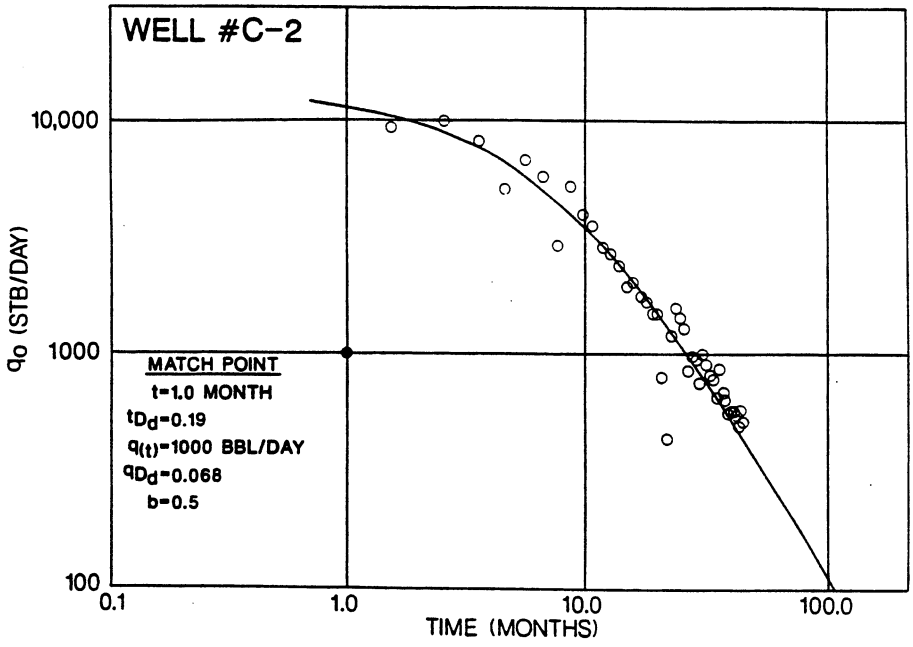

Fig. 10 Log Rate vs. Log Time Plot, Oil Rate Excludes Condensate

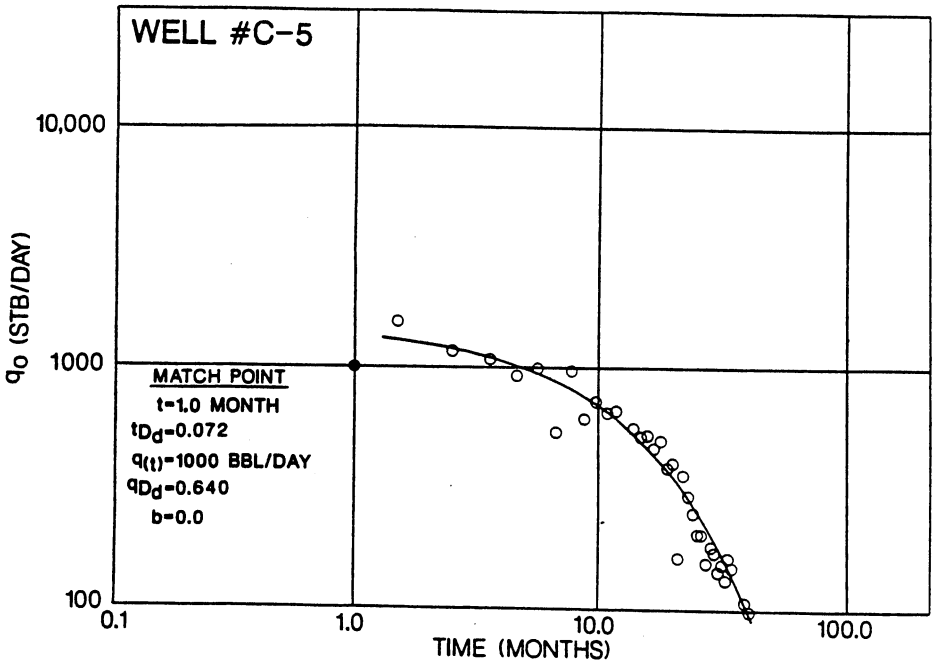

Fig. 11 Log Rate vs. Log Time Plot, Oil Rate Excludes Condensate

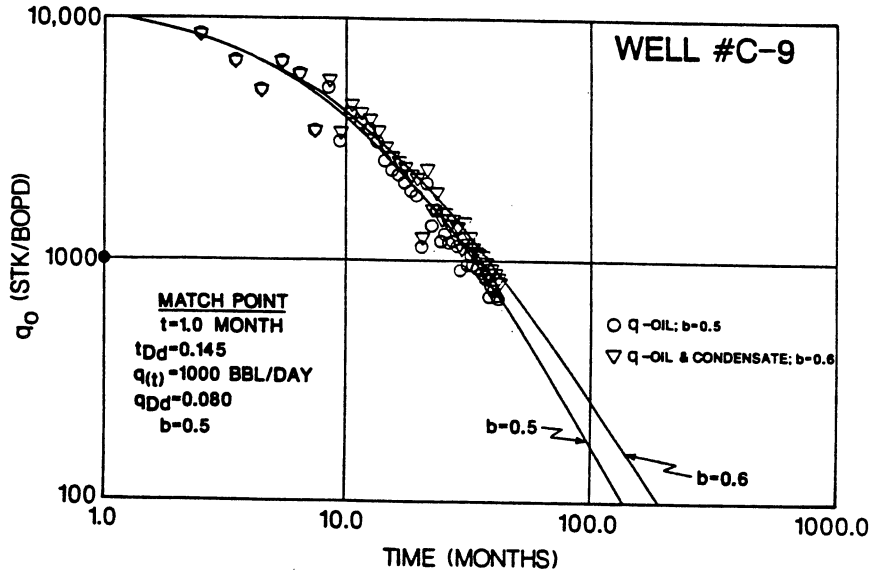

Fig. 12 Log Rate vs. Log Time Plots, Oil Rate Including and Excluding Condensate

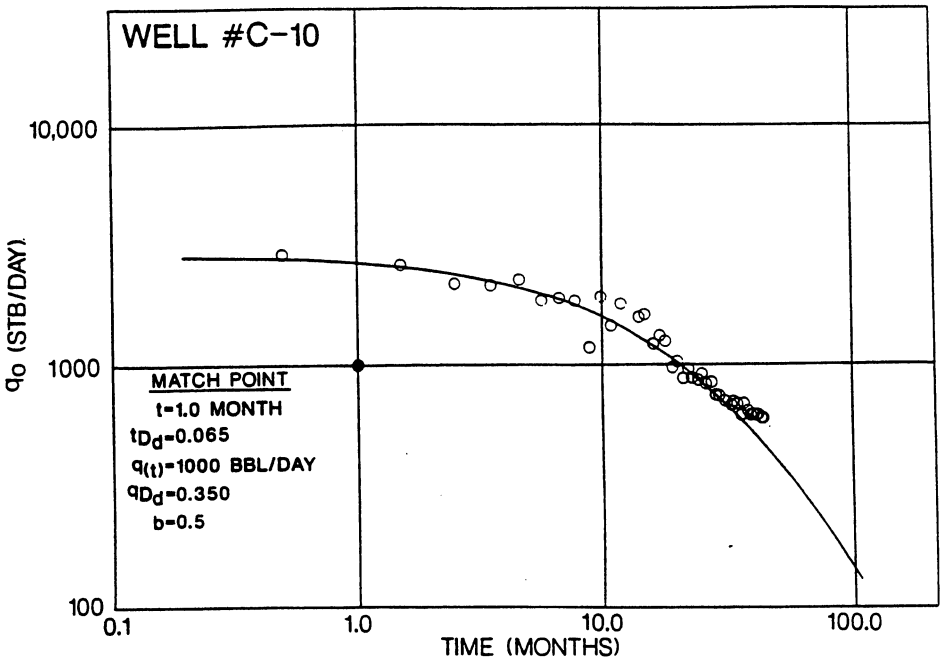

Fig. 13 Log Rate vs. Log Time Plot, Oil Rate Excludes Condensate

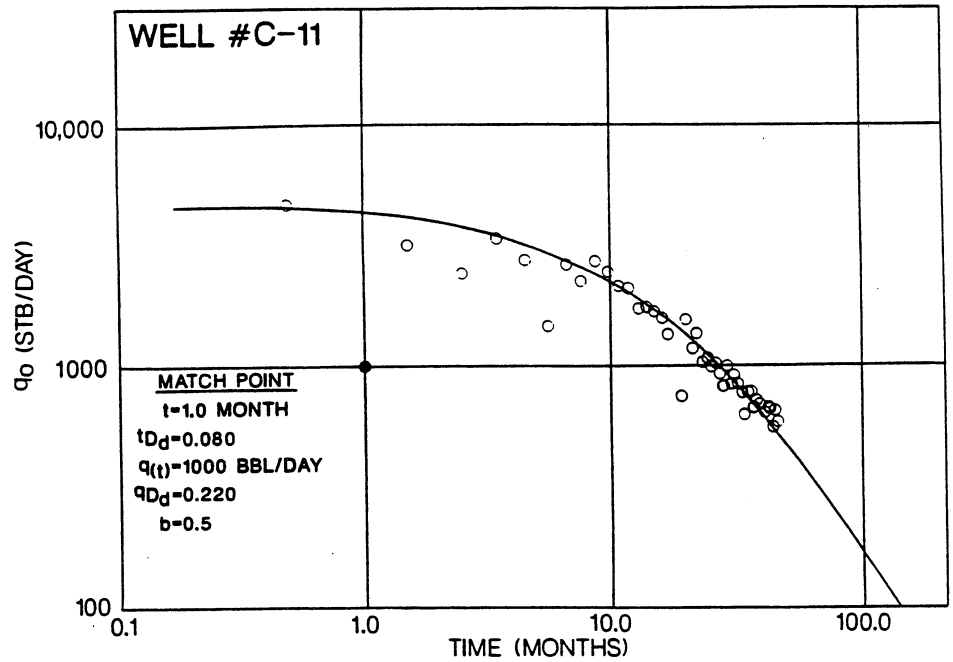

Fig. 14 Log Rate vs. Log Time Plot, Oil Rate Excludes Condensate

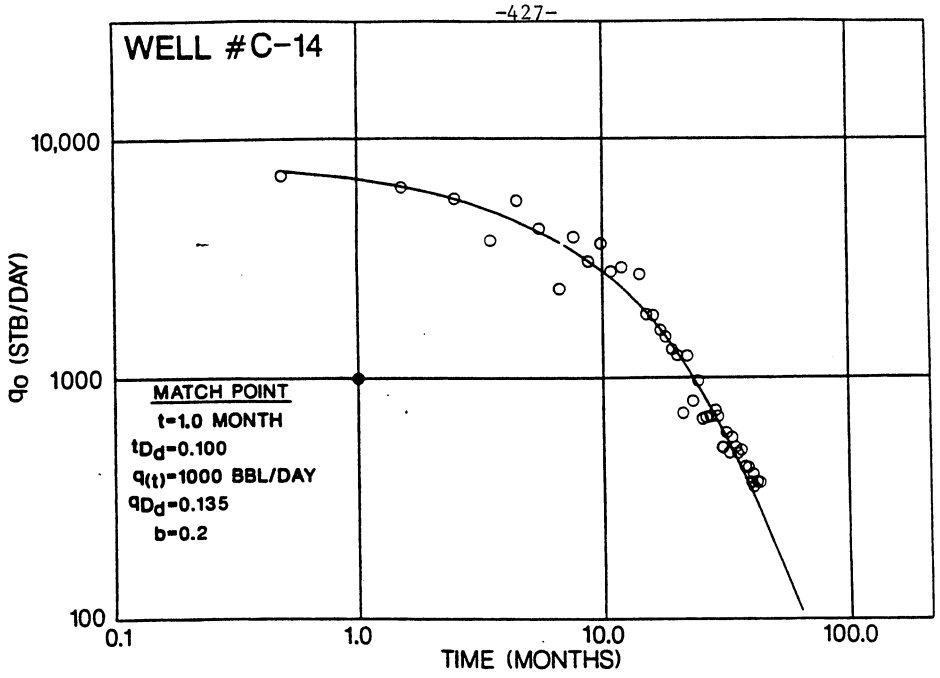

Fig. 15 Log Rate vs. Log Time Plot, Oil Rate Excludes Condensate

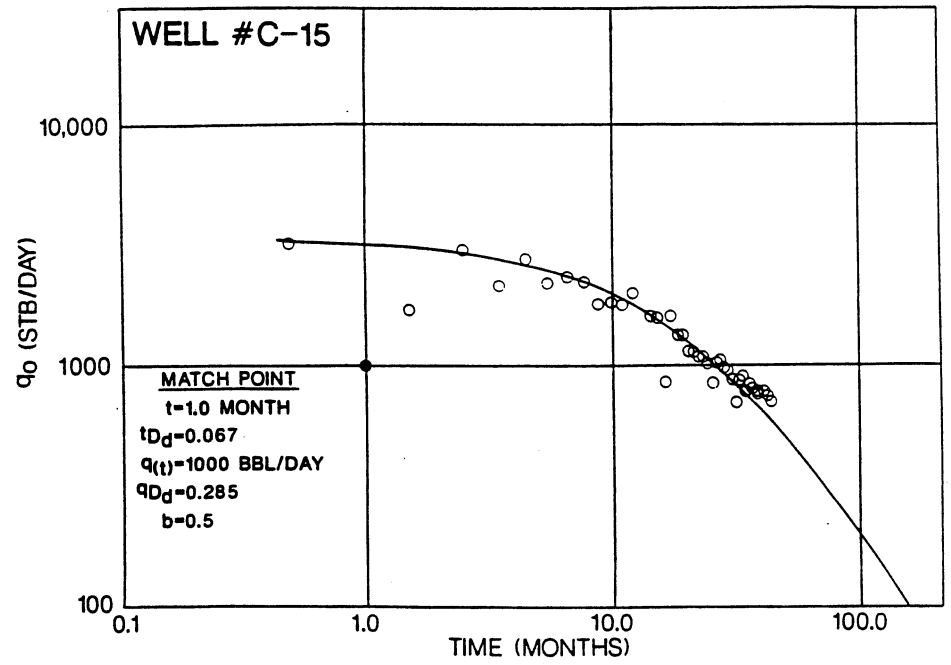

Fig. 16 Log Rate vs. Log Time Plot, Oil Rate Excludes Condensate

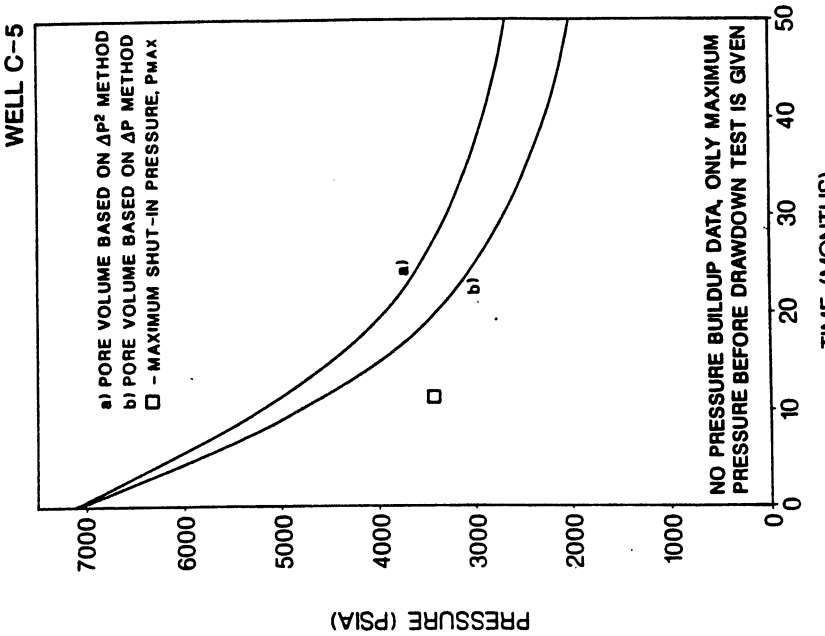

Fig. 18 Match of Pressure Build-up Data and Compositional M. B. Pressure Based on Rate-Time Calculated Pore Volume

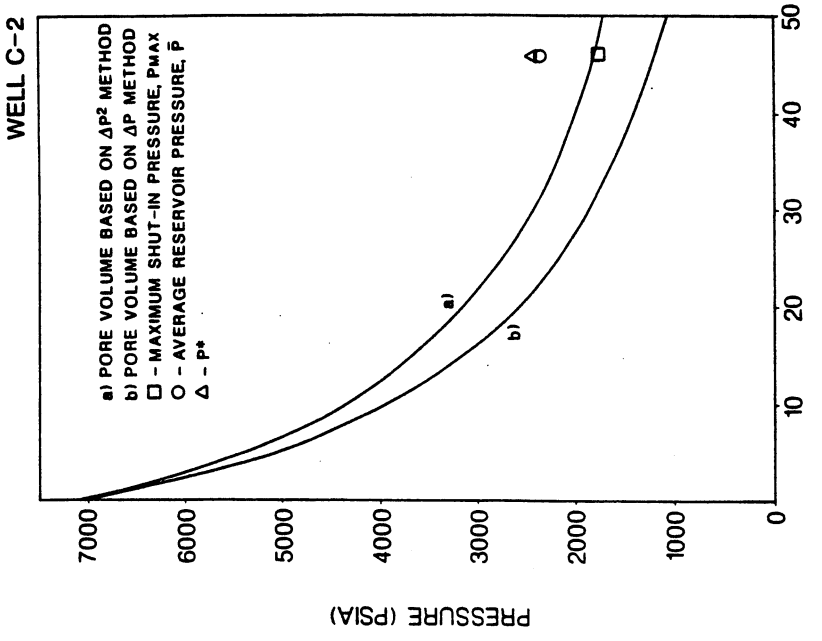

Fig. 17 Match of Pressure Build-up Data and Compositional M. B. Pressure Based on Rate-Time Calculated Pore Volume

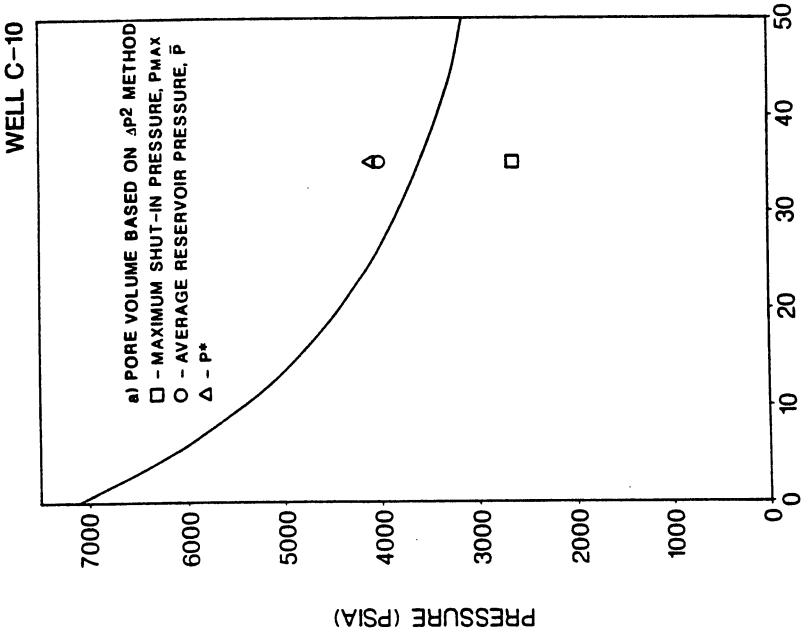

Fig. 20 Match of Pressure Build-up Data and Compositional M. B. Pressure Based on Rate-Time Calculated Pore Volume

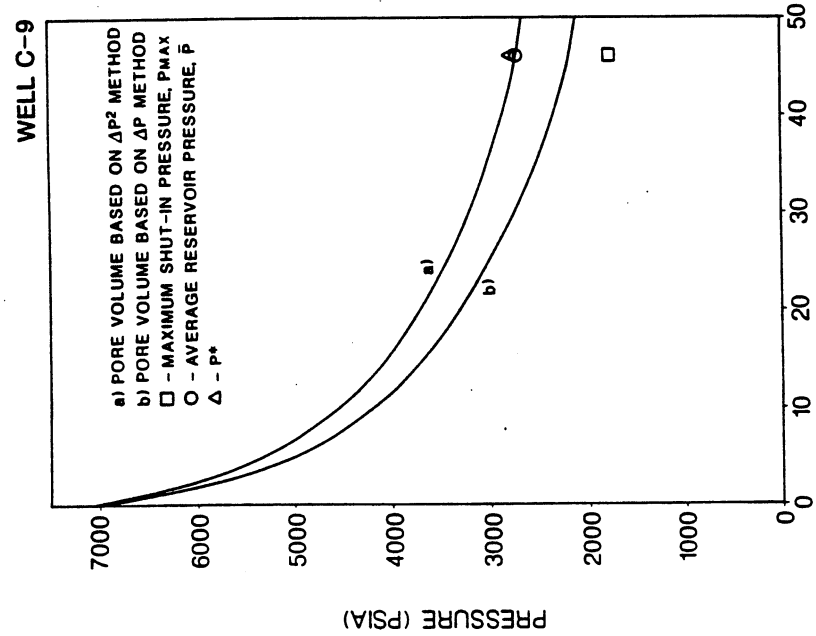

Fig. 19 Match of Pressure Build-up Data and Compositional M. B. Pressure Based on Rate-Time Calculated Pore Volume

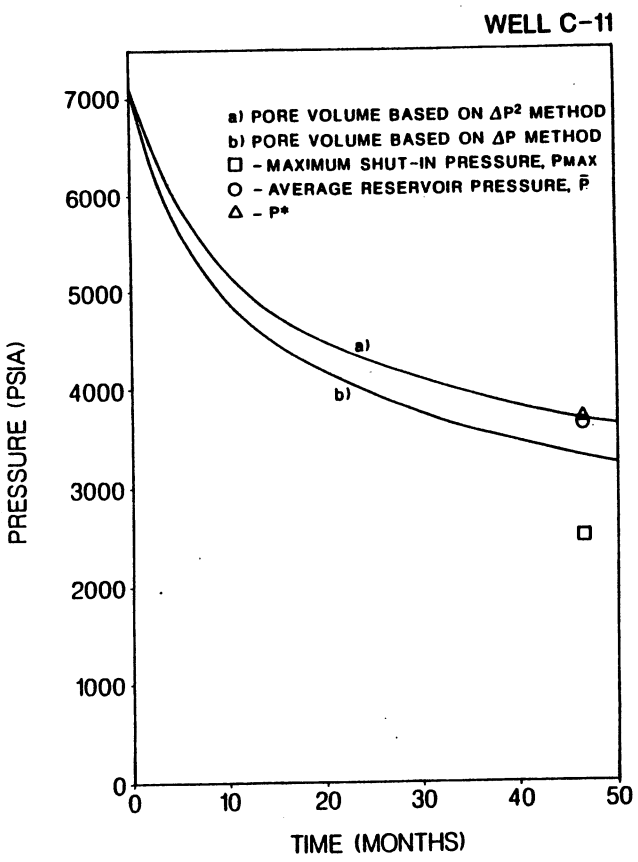

Fig. 21 Match of Pressure Build-up Data and Compositional M. B. Pressure Based on Rate-Time Calculated Pore Volume

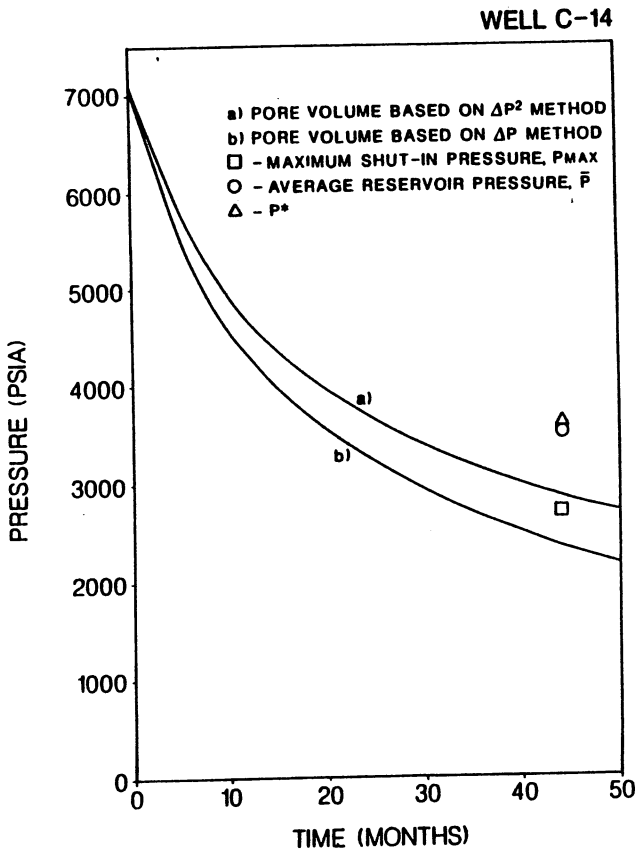

Fig. 22 Match of Pressure Build-up Data and Compositional M. B. Pressure Based on Rate-Time Calculated Pore Volume

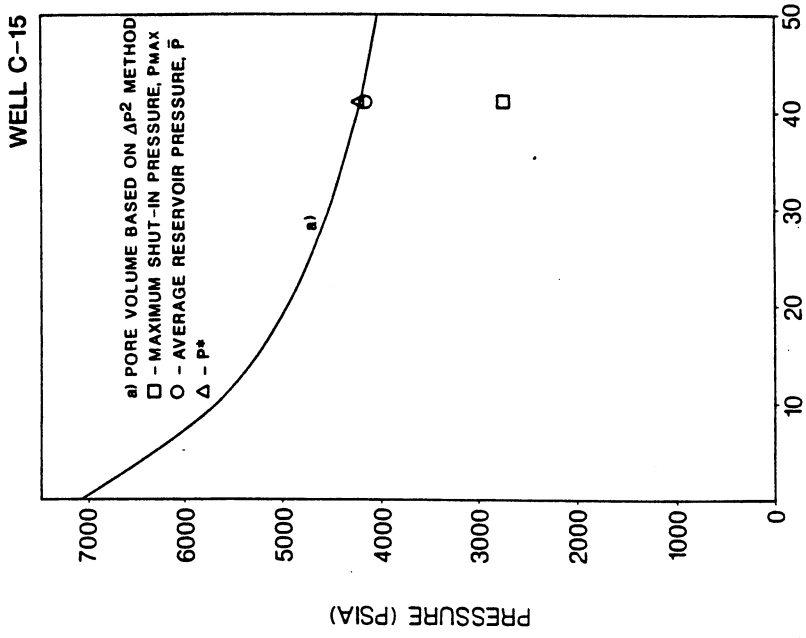

Fig. 23 Match of Pressure Build-up Data and Compositional M. B. Pressure Based on Rate-Time Calculated Pore Volume

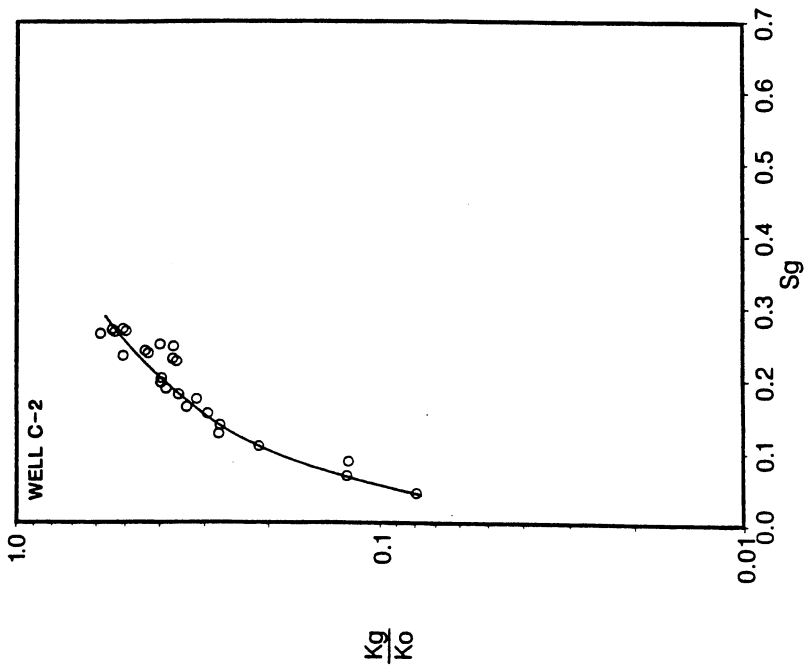

Fig. 24 Individual Well Performance Derived K_g/K_o Calculated Using a Compositional Material Balance With Rate-Time Calculated Pore Volume

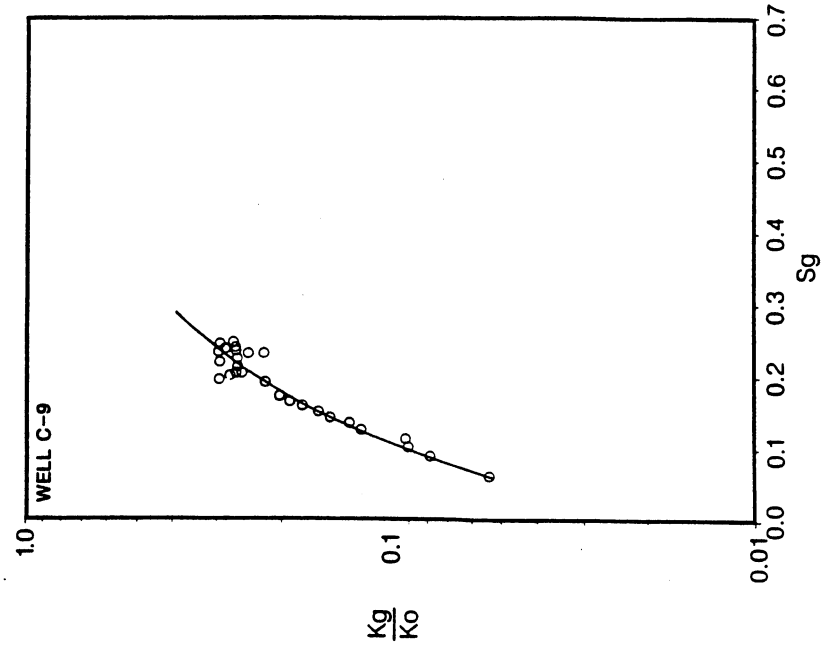

Fig. 26 Individual Well Performance Derived K_g/K_o Calculated Using a Compositional Material Balance With Rate-Time Calculated Pore Volume

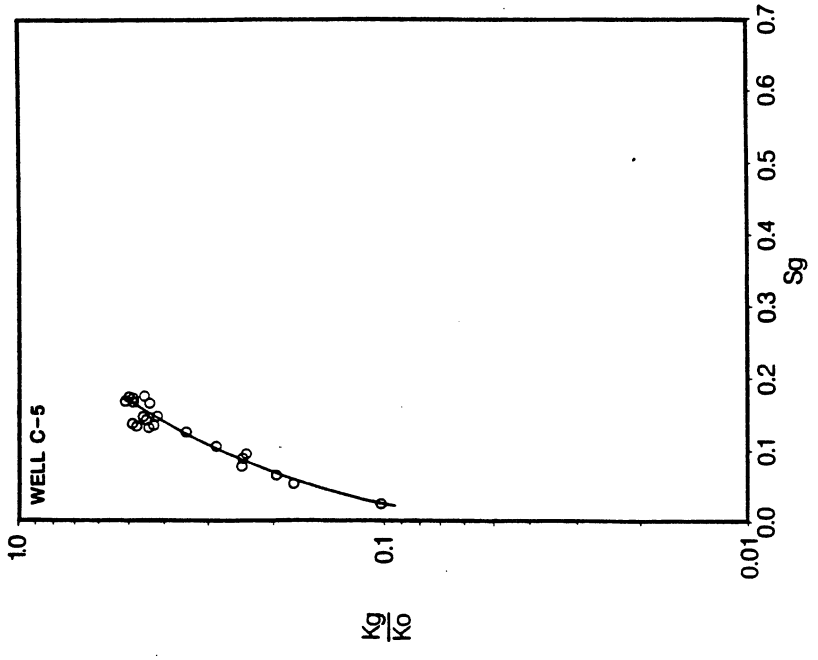

Fig. 25 Individual Well Performance Derived K_g/K_o Calculated Using a Compositional Material Balance With Rate-Time Calculated Pore Volume

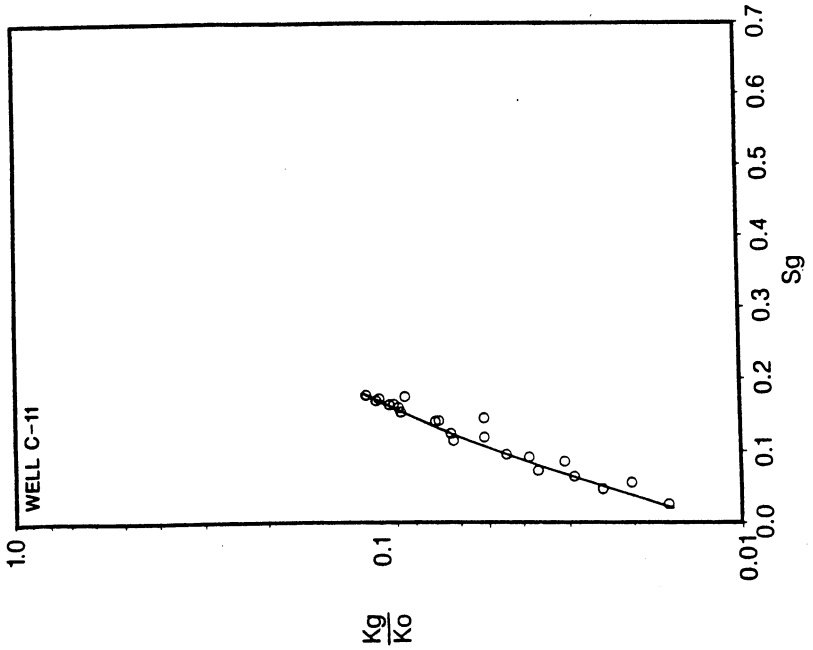

Fig. 28 Individual Well Performance Derived K_g/K_o Calculated Using a Compositional Material Balance With Rate-Time Calculated Pore Volume

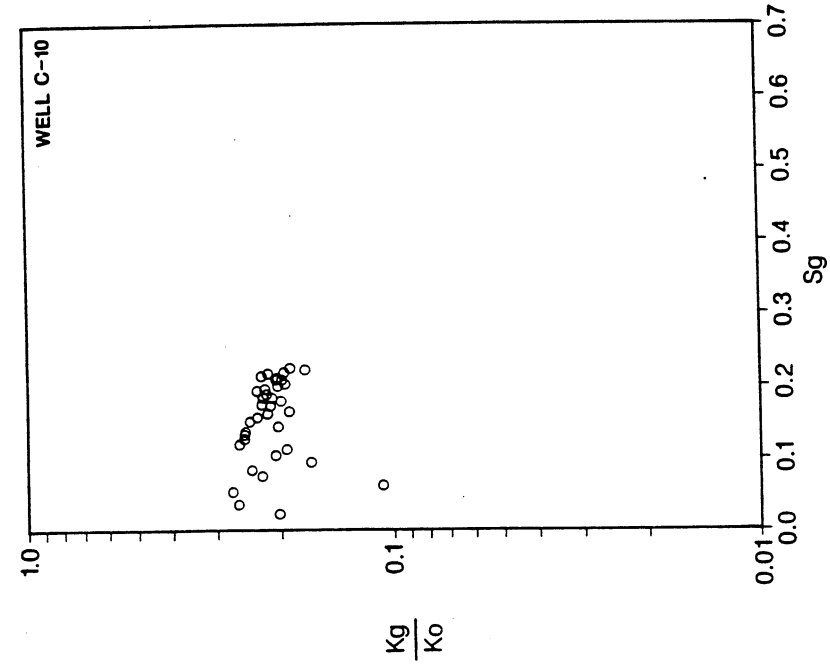

Fig. 27 Individual Well Performance Derived K_g/K_o Calculated Using a Compositional Material Balance With Rate-Time Calculated Pore Volume

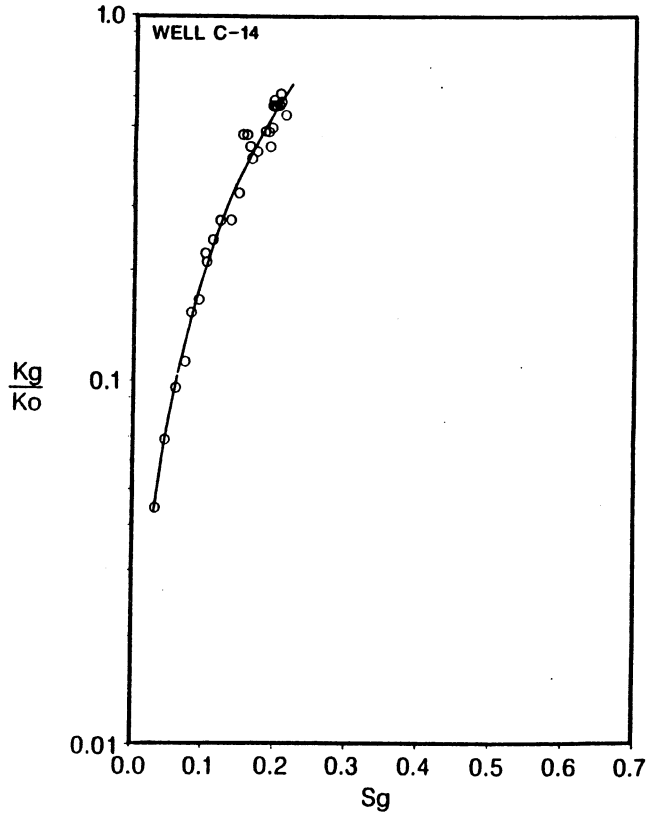

Fig. 29 Individual Well Performance Derived K_g/K_o Calculated Using a Compositional Material Balance With Rate-Time Calculated Pore Volume

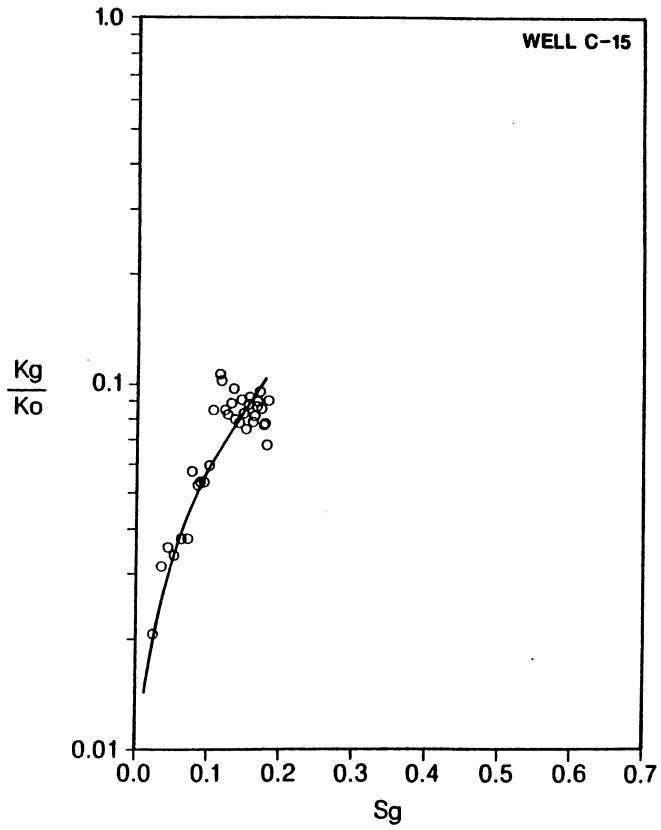

Fig. 30 Individual Well Performance Derived K_g/K_o Calculated Using a Compositional Material Balance With Rate-Time Calculated Pore Volume

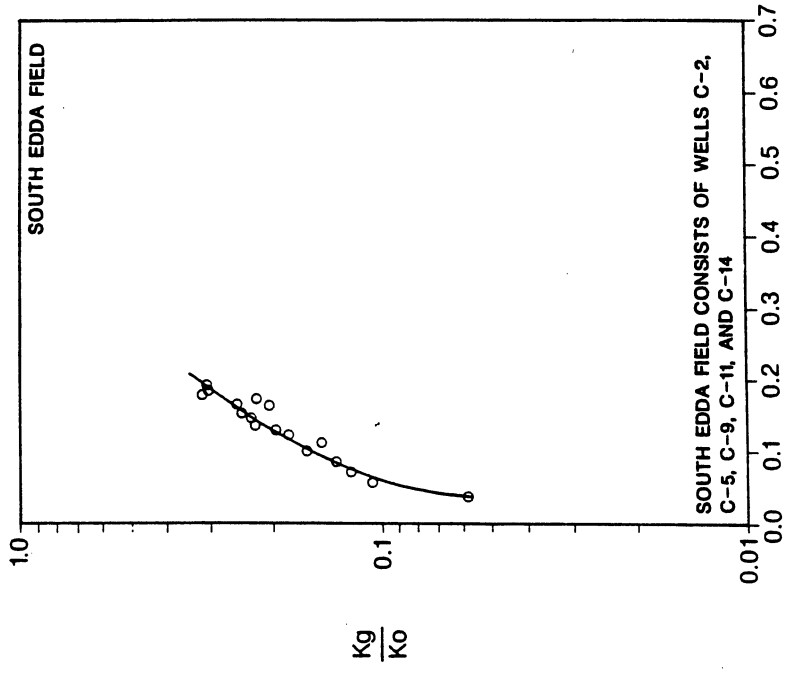

Fig. 32 Total Field Performance Derived K_g/K_o Calculated Using a Compositional Material Balance

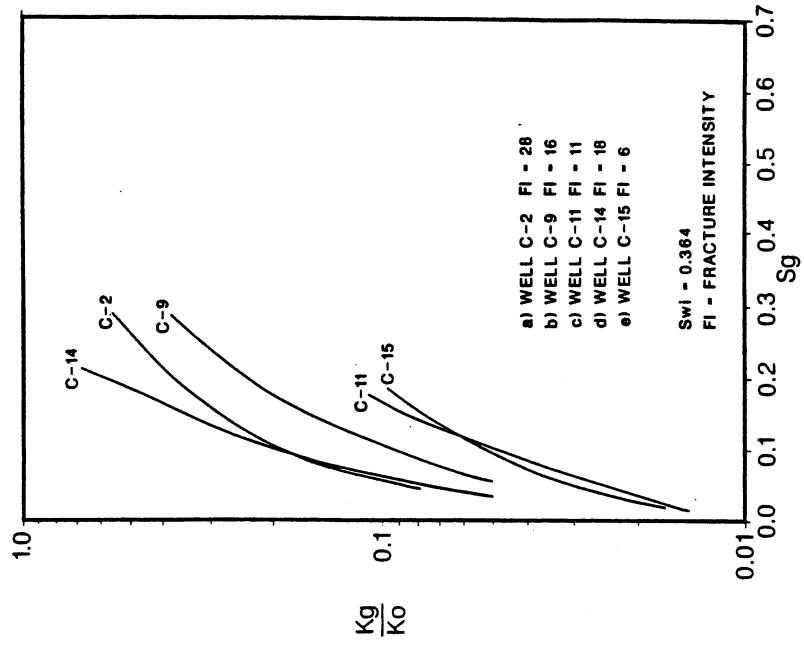

Fig. 31 Comparison of Individual Well Performance Derived K_g/K_o Curves Normalized to the Same Connate Water Saturation

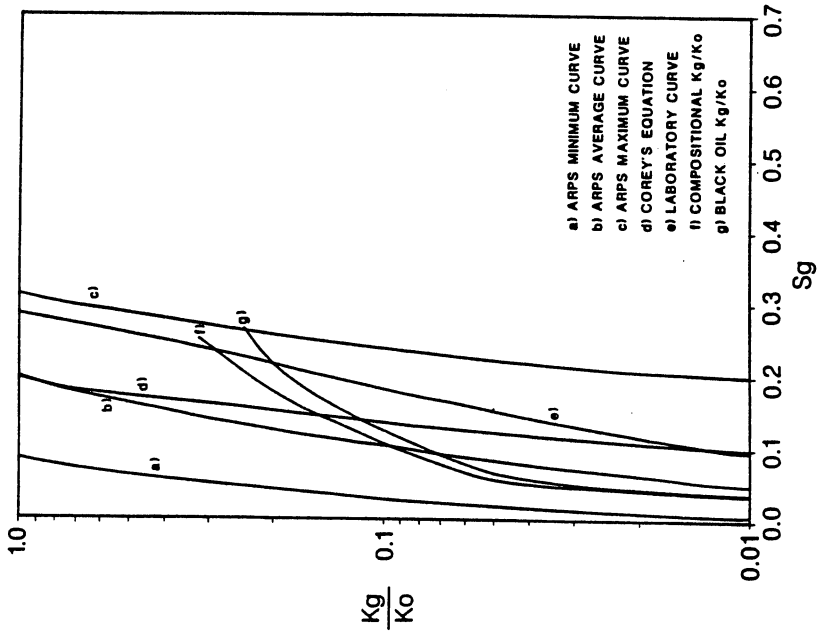

Fig. 34 Comparison of C.M.B. Derived K_g/K_o Curve With Corey's, Arps, Laboratory and Black Oil - Well C-9

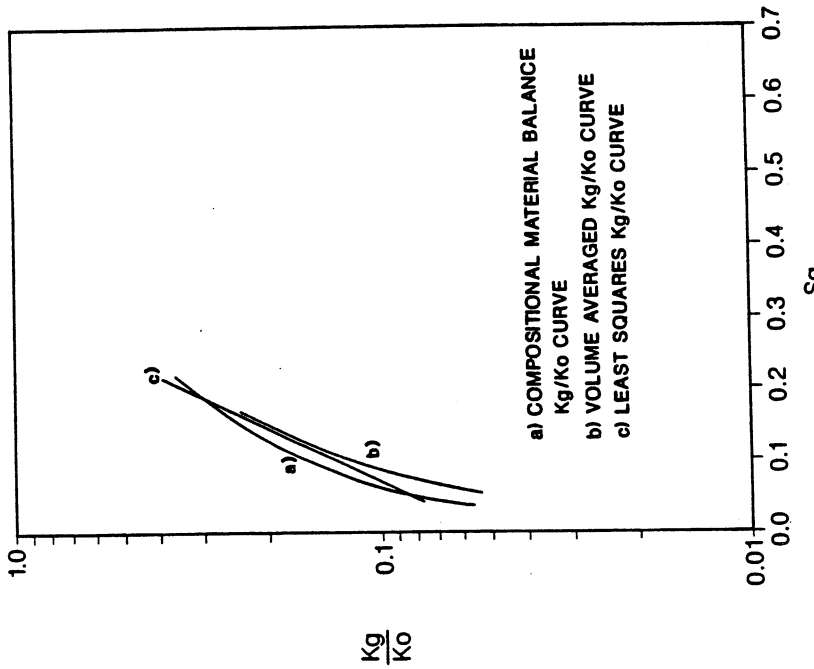

Fig. 33 South Edda Total Field K_g/K_o Curve Compared to a Five Well Volume Averaged and a Least Square K_g/K_o Curve

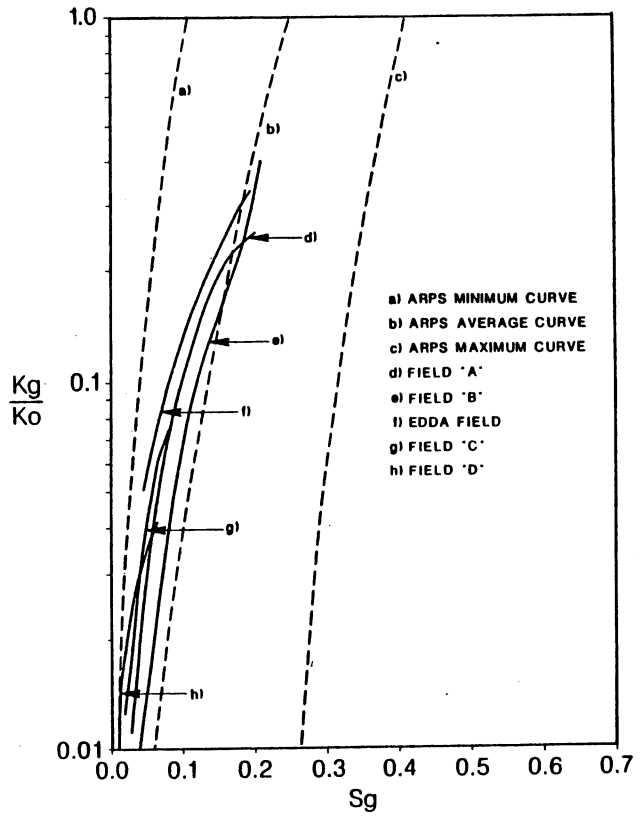

Fig. 35 Comparison of Greater Ekofisk Area Performance K_g/K_o Curves With the South Edda Field K_g/K_o Curve - All Normalized to S_{wi} = 0.364

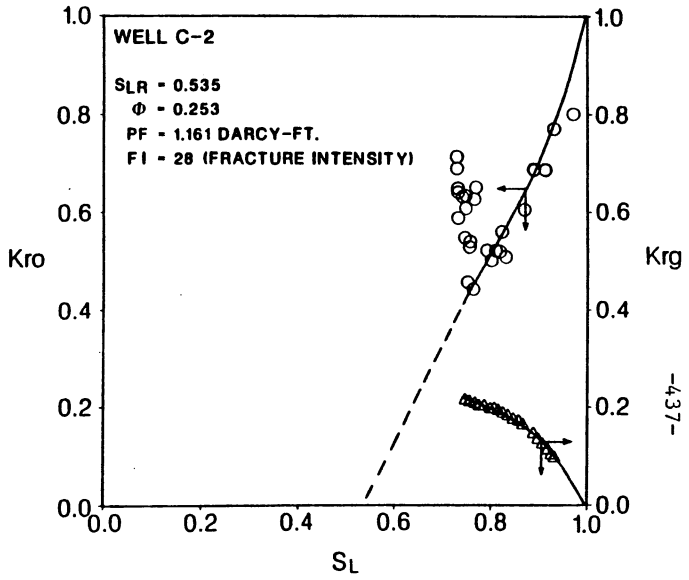

Fig. 36 Performance Derived K_{ro} and K_{rg}

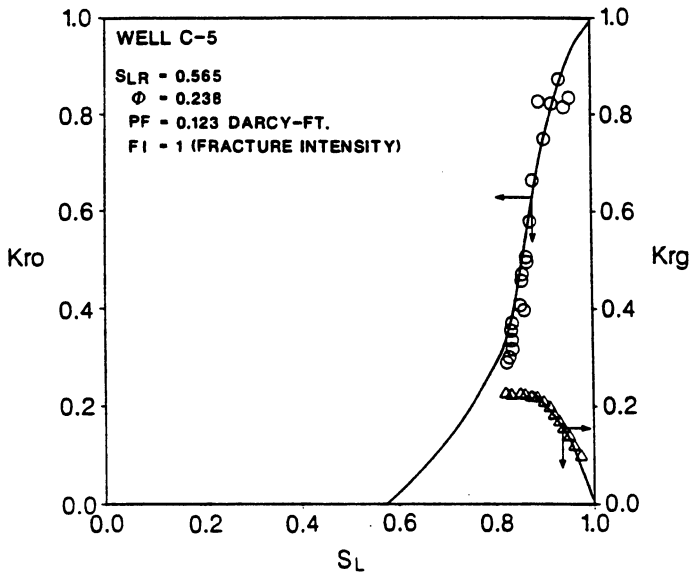

Fig. 37 Performance Derived K_{ro} and K_{rg}

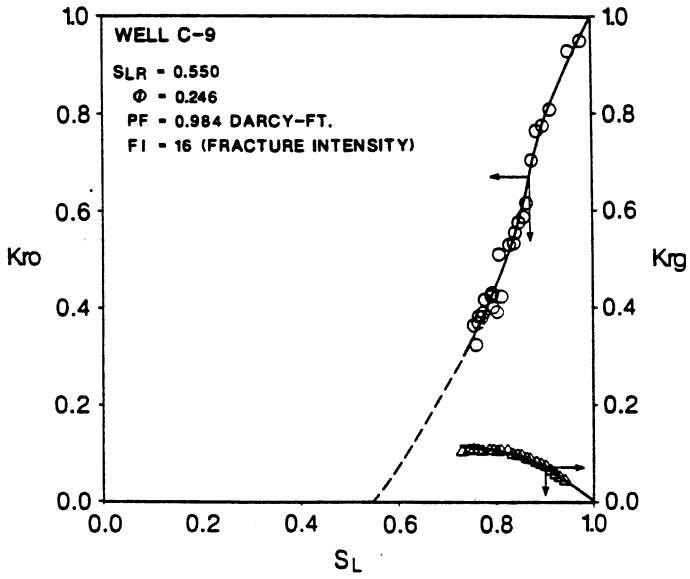

Fig. 38 Performance Derived K_{ro} and K_{rg}

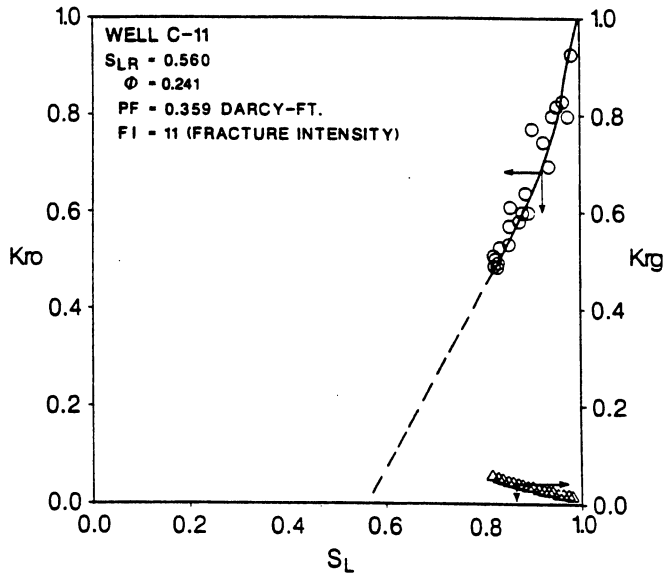

Fig. 39 Performance Derived K_{ro} and K_{rg}

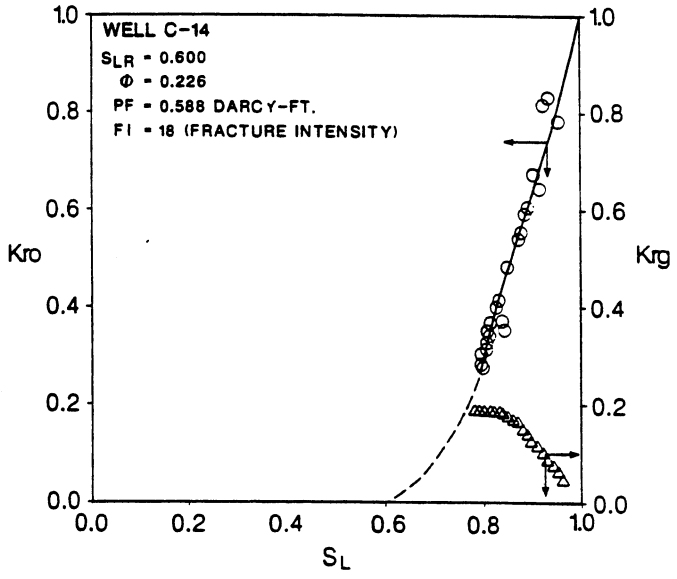

Fig. 40 Performance Derived K_{ro} and K_{rg}

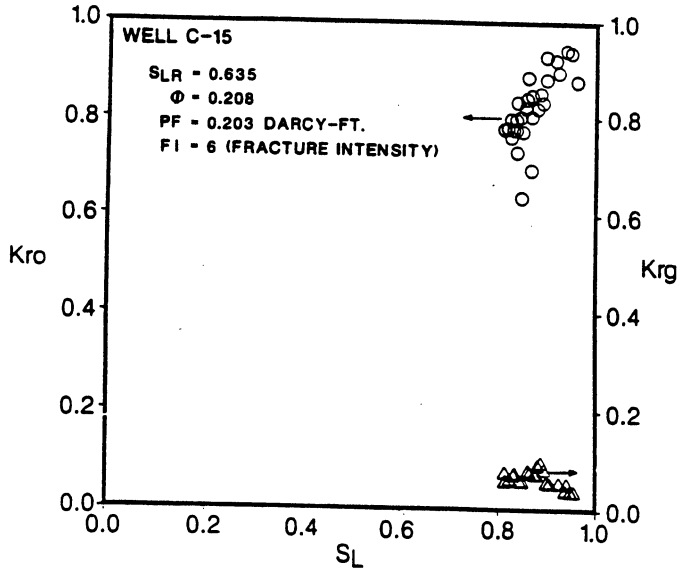

Fig. 41 Performance Derived K_{ro} and K_{rg}

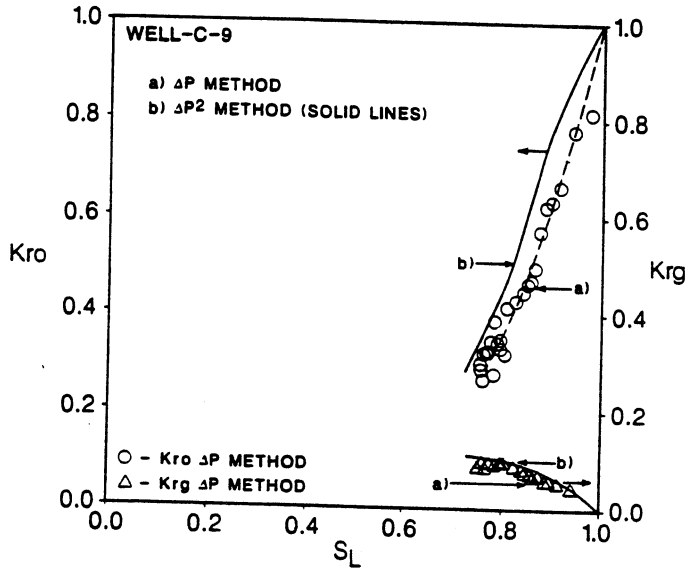

Fig. 42 Comparison of K_{ro} and K_{rg} Using the ΔP^2 and Δp Method

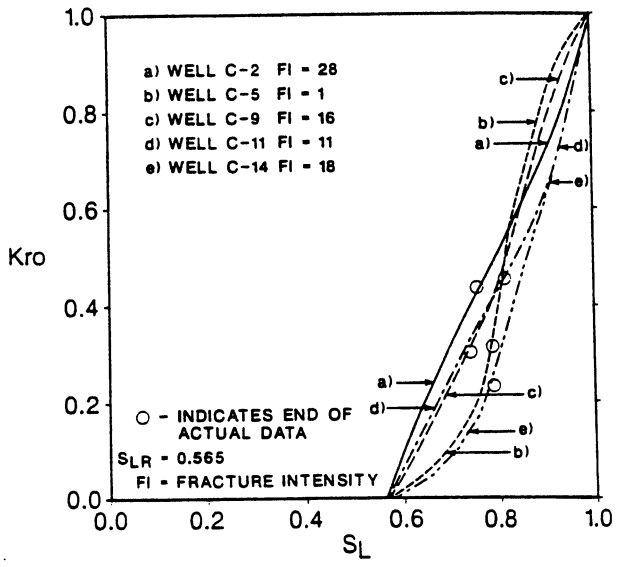

Fig. 43 Comparison of South Edda Field Wells Performance Derived K_{ro}, Normalized to the Same Irreducible Liquid Saturation

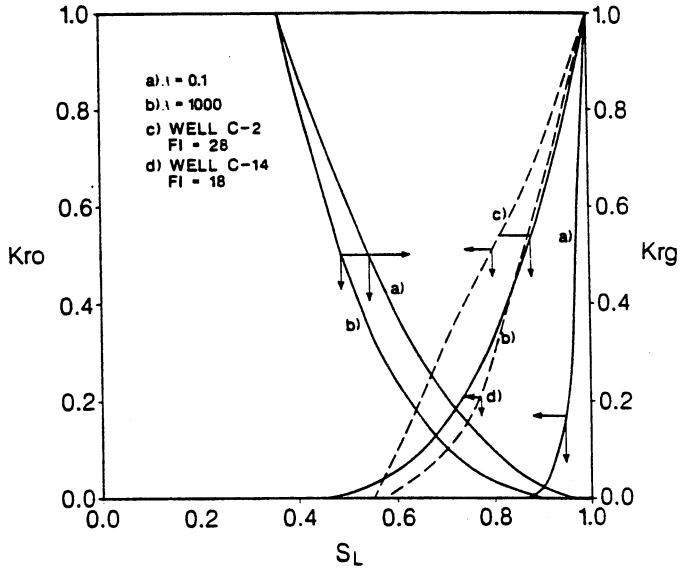

Fig. 44 Sensitivity of Corey's K_{ro} and K_{rg} Curves to the Pore Size Distribution Factor

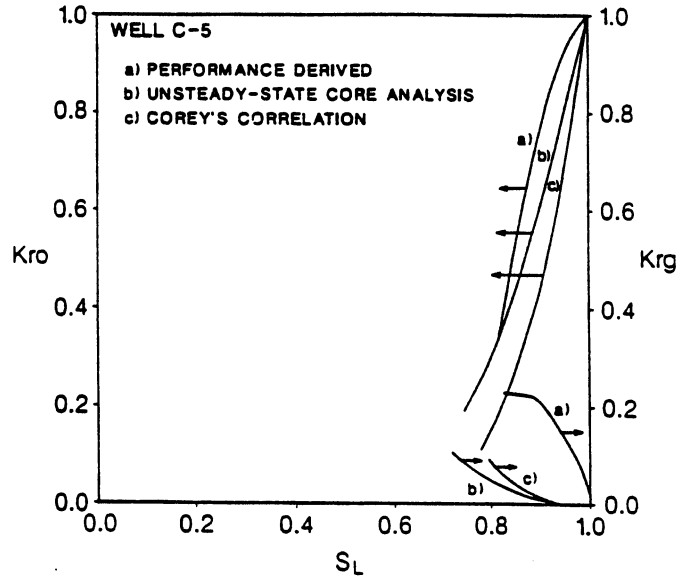

Fig. 45 Comparison of Performance Derived K_{ro} and K_{rg} Curves With Unsteady-State and Corey's Derived Curves

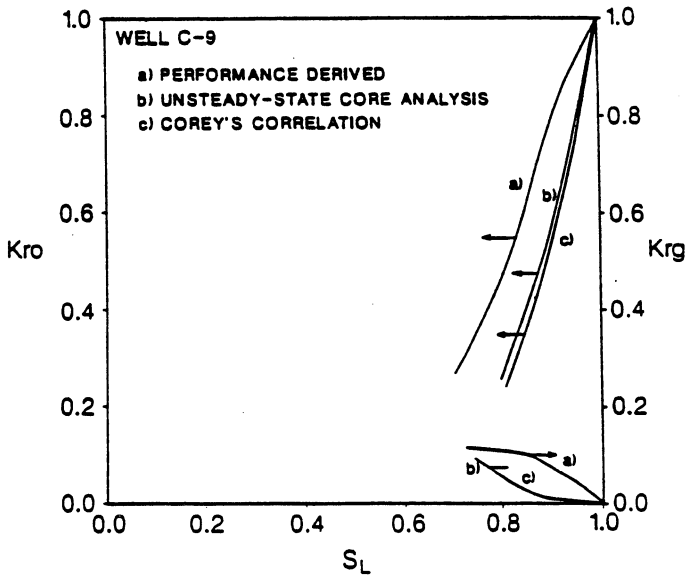

Fig. 46 Comparison of Performance Derived K_{ro} and K_{rg} Curves With Unsteady-State and Corey's Derived Curves

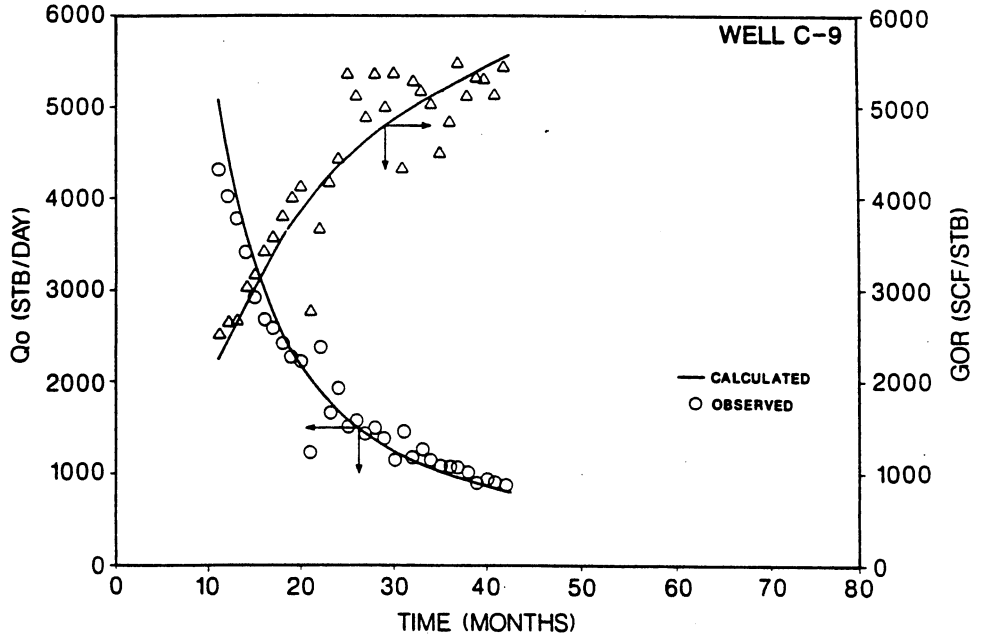

Fig. 47 Comparison of Gas-Oil Ratio and Oil Rates (Including Condensate) Obtained From Performance Derived K_{ro} and K_{rg} With Actual Oil Rates and GOR

DEPLETION PERFORMANCE OF LAYERED RESERVOIRS WITHOUT CROSSFLOW

by

M. J. Fetkovich
M. D. Bradley
A. M. Works
T. S. Thrasher

Phillips Petroleum Company

SPE Members

SPE 18266

This paper was presented at the 63rd Annual Technical Conference and Exhibition of the Society of Petroleum Engineers held in Houston, TX, October 2-5, 1988.

ABSTRACT

Based on actual field data, this paper presents a study of the depletion performance of a two-layered gas reservoir without crossflow that has produced for over 20 years at effectively a constant wellbore flowing pressure. The study demonstrates that a rate-time decline curve exponent "b" value ranging between 0.5 and 1 (harmonic) is a predicted response of a layered gas reservoir without crossflow. The actual rate-time performance data for the individual wells examined, and the field as a whole, exhibit a decline exponent b of approximately 0.9.

By means of graphical presentations of rate-time and pressure-cumulative production, this paper illustrates some of the depletion performance characteristics that identify no-crossflow layered reservoirs. These graphical presentations show very clearly the effect of changes in the layer volume, permeability, and skin (s) on the depletion performance of no-crossflow layered reservoirs.

Rigorous and simplified approaches to the problem result in essentially the same results. Both constant wellbore pressure and constant rate depletion performance are examined as a part of this study.

INTRODUCTION

Of all the papers written about noncommunicating layered reservoirs, only a few have attempted to deal with the subject of depletion - long term production forecasting. W. Tempelaar-Lietz[1] originally published an internal Shell report in 1953 on the effect of oil production rate from a volumetric reservoir with more than one layer. It was later published in the March 1961 SPEJ along with the classic Lefkovits et al.[2] paper on layered reservoirs. Lefkovits et al. modified the Tempelaar-Lietz constant rate two-layer single phase liquid depletion equations to account for two layers of unequal thickness. Fetkovich,[3] in 1974, applied the constant wellbore pressure single phase liquid solution to rate-time production data from a layered reservoir to demonstrate that when two noncommunicating layers, each characterized by a single phase liquid exponential decline, b = 0, were produced commingled, the result was an increase in b to 0.2.

Hypothetical solution gas drive reservoir studies for noncommunicating layers were conducted by Keller et al.[4] in 1949 to investigate the effects of recovery efficiency and gas-oil ratio behavior and by Gentry and McCray[5] in 1978 to study the effects of producing noncommunicating layers on the decline exponent, b. Both studies used single cell models that did not include transient effects. In addition, both used a conventional productivity index relationship, $PI = f(\Delta p)$, for defining a rate equation, instead of an IPR relationship that is a function of the difference in pressures squared, i.e., $PI = f(\Delta p^2)$. By their nature, more sophisticated multiphase flow studies would still have difficulty in assigning realistic k_{ro} and k_{rg} relationships for each layer. Further, the difficulty in obtaining the necessary field data such as individual well measured oil rates, gas rates, frequent bottomhole shutin pressures, and a non-linear $\bar{p}$ - N_p relationship presents a serious problem in verification. A similar problem exists for a single phase liquid situation in that few oil reservoirs are totally or even highly undersaturated and produced to abandonment by simple liquid expansion. Those that are highly

undersaturated often develop strong water drives because of the large reservoir pressure decline with small production volumes. Such fields are often immediately placed under waterflood. The single phase liquid solutions of Tempelaar-Lietz, however, could find application in very high-pressured gas reservoirs.

To date, we know of no published field case history that illustrates depletion performance characteristics, other than RFT layer pressures, to identify no-crossflow layered reservoir behavior. Single phase volumetric gas fields and wells offer the best opportunity for detection of layered reservoir responses in that only single phase flow exists. Furthermore, production data are measured separately for each well, and annual shut-in pressures are normally taken, sometimes with annual 48 or 72-hour deliverability tests. In our particular field study, rate-time data gave the first clue that we were dealing with a noncommunicating layered reservoir. The field has produced for over 20 years at effectively a low constant wellbore pressure, thus giving continuous, declining rate-time data for analysis. The total field and individual wells examined in our study exhibited a rate-time depletion decline exponent b approaching 1.0 with very little early time transient data evident. A gas well producing from a single homogeneous layer at a flowing wellbore pressure near zero has a maximum depletion decline exponent b = 0.5. [3,6]

The simplified rate-time and cumulative production-time equations of Reference 3, along with the $\overline{p}/z$ vs G_p equation, were first used to demonstrate that we were looking at a noncommunicating layered reservoir. Further confirmation and greater flexibility were then obtained using a conventional gas forecasting program based on gas material balance and a stabilized backpressure curve for each layer. In addition, a 100-cell, fully implicit radial model was used mainly to simulate annual 72-hour shutins and 48-hour deliverability tests and to verify the results obtained using the simplified approaches. All basic results and conclusions drawn in this paper can, however, be made using the simpler approaches described above. Both constant wellbore pressure and constant rate depletion were investigated. Graphical presentations of rate versus time and pressure versus cumulative production clearly demonstrate the effect of changes in the reservoir layer volumes, permeability (k), and skin (s), on the depletion performance of a two-layered system without crossflow.

FIELD DESCRIPTION

Development drilling began in our field of study in 1961; 212 gas wells had been drilled by early 1966. The reservoir consists of about 350 feet of gross sandstone thickness at a depth of 1800 feet. Initial reservoir pressure was approximately 428 psia. Other parameters include a reservoir temperature of 80°F, an average porosity of 15 percent, a water saturation of 51 percent, and a gas gravity of 0.7. A shale barrier averaging 50 feet in thickness has been clearly identified and correlated across the entire field. Core data indicate a bi-modal distribution with a permeability ratio between 10/1 and 20/1.

Wells were generally stimulated upon completion with 500 to 1000 gallons of 15% HCl, followed by a sand-frac which included 20,000 gallons of gel and 40,000 pounds of 20-40 sand. Stimulation results in terms of skin effect are shown in Table 1. Results obtained from several isochronal tests conducted on wells in the field are also summarized in Table 1. In most cases, the slope,

n, of the backpressure curve was found to be 1.0. Of the four tests that did not yield a backpressure slope of 1.0, one is actually a flow after flow test and the others showed indications that the wells had not adequately cleaned up after stimulation. All of our studies are based on the assumption that non-Darcy flow is not present in the reservoir, i.e., n = 1.0 for each layer.

The field came on production virtually wide open against an essentially constant wellbore pressure. A type curve analysis and regression fit of the total field rate-time production data yielded a decline exponent b of 0.89, practically identical to what we later found from individual well analysis.

WELL PERFORMANCE

To conserve space, we will present rate-time and pressure cumulative production data for two typical wells in the field that cover a range of gas-in-place. Additional field data are also presented in Fig. 1 in the form of a composite log-rate vs log-time overlay of 10 wells. This technique has also been applied to five California Monterey producing fields.[7] The similarity in b values for these two cases first suggested that we were looking at a no-crossflow layered reservoir particularly since both the field and the individual wells had the same decline exponent.

Figure 2 is a conventional semi-log plot of rate-time data for these two wells. The high initial percentage decline rate, decreasing to a much lower present percentage, is characteristic of wells experiencing hyperbolic decline with high decline exponents, b. As shown in Fig. 3, the log-rate vs log-time plots of these wells indicate little, if any, early transient production; the high values of b are the result of differential depletion of a layered reservoir.

The shape of the pressure cumulative production data, illustrated in Fig. 4, is typical of most other wells in the field. The rather large displacement between the measured annual 72-hour $\overline{p}/z$ points and the straight line connecting the initial and final points was first misinterpreted as the behavior of a low permeability reservoir. As shown in Table 1, our analysis of available isochronal test data yielded permeability values much too high to explain this departure. These $\overline{p}/z$ shapes are characteristic of a no-crossflow layered reservoir having a large contrast in layer permeabilities and volumes.

BASIC EQUATIONS

Rate-Time Equations

The depletion rate-time decline equation for a gas well[3] producing from any one layer at a constant wellbore pressure of zero, $p_{wf} = 0$, is

$$q_g(t) = \frac{(q_{gi})_{MAX}}{\left\{(2n-1)\left[\frac{(q_{gi})_{MAX}}{G_i}\right] t + 1\right\}^{\frac{2n}{2n-1}}} \qquad \ldots\ldots (1)$$

If a commingled well produces at a constant wellbore pressure, then the flow rate from each layer is independent of the flow rates of all the other layers and the total well production is the sum of each layer's production. Rate-time decline analysis for a two-layered system is performed with a log-log plot of total flow rate q_{gT} versus time where

$$q_{gT}(t) = q_{g1}(t) + q_{g2}(t) \qquad \ldots\ldots (2)$$

For n = 1, Darcy flow, Eq. 1 reduces to

$$q_g(t) = \frac{(q_{gi})_{MAX}}{\left\{\left[\frac{(q_{gi})_{MAX}}{G_i}\right] t + 1\right\}^2} \qquad \ldots\ldots (3)$$

Note that the exponent 2 is equal to the Arps[8] exponent 1/b or b = 0.5 for Eq. 3.

The pseudosteady-state backpressure equation with which Eq. 1 was derived is usually written as

$$q_g = C\,(\overline{p}^2 - p_{wf}{}^2)^n \qquad \ldots\ldots (4)$$

With n = 1 and p_{wf} = 0, Eq. 4, expressed in terms of reservoir variables, becomes

$$(q_{gi})_{MAX} = \frac{kh\,(p_i{}^2)}{1424\,(\overline{\mu Z})\,T\left[\ln\left(\frac{.472\,r_e}{r_w}\right) + s\right]} \qquad \ldots\ldots (5)$$

Combining Eqs. 2 and 3 for the rate-time performance of a two-layered system with a common wellbore flowing pressure of zero we have

$$q_{gT}(t) = \frac{(q_{gi})_{MAX1}}{\left\{\left[\frac{(q_{gi})_{MAX1}}{G_{i1}}\right] t + 1\right\}^2} + \frac{(q_{gi})_{MAX2}}{\left\{\left[\frac{(q_{gi})_{MAX2}}{G_{i2}}\right] t + 1\right\}^2} \qquad \ldots\ldots (6)$$

Only if $(q_{gi})_{MAX1}/G_{i1}$ is equal to $(q_{gi})_{MAX2}/G_{i2}$ will the b value of 0.5 for each layer yield a composite rate-time b value of 0.5.

$$q_{gT}(t) = \frac{(q_{gi})_{MAX1} + (q_{gi})_{MAX2}}{\left\{\left[\frac{(q_{gi})_{MAX}}{G_i}\right] t + 1\right\}^2} \qquad \ldots\ldots (7)$$

For the limiting case in which $(q_{gi})_{MAX2}$ approaches 0 in the low permeability layer, the total rate-time profile will, of course, be identical to that of the high permeability layer; each will have a b value of 0.5.

As defined in Reference 3, the ratio of decline curve dimensionless time to real time, t_{dD}/t, is equal to $(q_{gi})_{MAX}/G_i$. Layers having similar values of t_{dD}/t or $(q_{giMAX})/G_i$ will deplete at the same rate and could be treated as a single equivalent layer. We will use the ratio

$$\left[\frac{(q_{gi})_{MAX}}{G_i}\right]_R = \frac{\dfrac{(q_{gi})_{MAX1}}{G_{i1}}}{\dfrac{(q_{gi})_{MAX2}}{G_{i2}}} \qquad \ldots\ldots (8)$$

and the volume ratio

$$V_R = \frac{V_1}{V_2} = \frac{G_{i1}}{G_{i2}} \qquad \ldots\ldots (9)$$

as correlating parameters in our study. By convention, layer 1 is always the more permeable layer.

Assuming for simplicity that $p_{i1} = p_{i2}$ and $(\mu C_t)_{i1} = (\mu C_t)_{i2}$, and substituting reservoir variables as illustrated in Reference 3,

$$\left[\frac{(q_{gi})_{MAX}}{G_i}\right]_R = \frac{k_1/\phi_1}{k_2/\phi_2}\cdot\frac{\left[\ln\left(\dfrac{.472\ r_{e2}}{r_w}\right)+s_2\right]}{\left[\ln\left(\dfrac{.472\ r_{e1}}{r_w}\right)+s_1\right]}\cdot\frac{r_{e2}^2}{r_{e1}^2} \qquad \ldots (10)$$

Similar ratios were also suggested by Raghavan[9] except for the inclusion of the skin and r_e terms. It should be pointed out that the assumption of equal initial pressures is not necessary for the constant wellbore pressure cases since the layer production rates are independent of each other.

Cumulative-Time Equations

The cumulative production-time equation for a gas well producing from any one layer against a constant wellbore pressure of zero is

$$\frac{G_p(t)}{G_i} = 1 - \left\{(2n-1)\left[\frac{(q_{gi})_{MAX}}{G_i}\right]t + 1\right\}^{\frac{1}{(1-2n)}} \qquad \ldots\ldots (11)$$

For n = 1, Equation 11 reduces to

$$\frac{G_p(t)}{G_i} = 1 - \frac{1}{\left\{\left[\frac{(q_{gi})_{MAX}}{G_i}\right] t + 1\right\}} \quad \ldots\ldots (12)$$

Material Balance Equation

The material balance (M. B.) equation for any one layer is

$$\frac{\overline{p}}{z} = \frac{p_i}{z_i}\left[1 - \frac{G_p(t)}{G_i}\right] \quad \ldots\ldots (13)$$

For a two-layer system with equal initial pressure and fluids, the M. B. equation is

$$\left(\frac{\overline{p}}{z}\right)_T = \frac{p_i}{z_i}\left[1 - \frac{G_{p1}(t) + G_{p2}(t)}{G_{i1} + G_{i2}}\right] \quad \ldots\ldots (14)$$

For pressure-cumulative production analysis of a layered reservoir, each layer $\overline{p}/z$ and the total system $(\overline{p}/z)_T$ are all plotted versus the total well cumulative production, G_{pT}, where

$$G_{pT}(t) = G_{p1}(t) + G_{p2}(t) \quad \ldots\ldots (15)$$

LAYERED RESERVOIR PERFORMANCE FORECASTS

In order to better understand the depletion performance of our noncommunicating layered reservoir, a one well two-layered system was set up using reservoir variables from our field of study. The following data were used for both layers: r_e = 2979 ft, r_w = 0.30 ft, ϕ = 0.15, S_w = 0.514, S. G. = 0.7, T = 80°F, and p_i = 428 psia. A total well thickness, h, of 24 ft was used to obtain an average well original gas-in-place of 1.50 Bscf. All forecasts were made with a minimum bottomhole flowing pressure, p_{wf}, of 42.8 psia, 10 percent of the initial shutin pressure. Permeability ratios, K_R, ranging from 1/1 to 1000/1 were investigated along with layer volume ratios, V_R, of 1/1, 1/2, and 2/1. The low permeability layer was generally assigned a permeability of 1 md so that the effect of some early transients could be included in the forecasts. The permeability ratio level in our field is believed to be closer to 50 md/5 md resulting in negligible transient effects. Various combinations of skin (s) of +5, 0, and -3 were also investigated. As previously mentioned, non-Darcy flow was not included in our studies based on isochronal test data results. Realistic constant rate forecasts were made assuming typical onshore contract rates-of-take of 1 MMscfd/8.6 Bscf of original gas-in-place and 1 MMscfd/5 Bscf for offshore fields.

A conventional pseudosteady state gas deliverability computer program was

first used to develop all our forecasts. Using one month time steps, this program combines the backpressure equation with gas material balance for each layer. A 50 cell per layer fully implicit radial model was also used, primarily to simulate annual 72-hour shut-in pressures and to verify the results obtained from our deliverability program.

DISCUSSION OF RESULTS

Pressure Cumulative Production Graphs

The pressure-cumulative production graphs for layered reservoirs are unique in that individual layer and total system $\overline{p}/z$ is plotted versus the total commingled cumulative production from all layers, G_{pT}. This graph can be prepared for any number of layers. Figure 5 is such a plot for our two-layered system, assuming V_R = 1/1 or 0.750 Bscf/0.750 Bscf. In this case, K_R and $(q_{MAX}/G_i)_R$ are both equal to 10; K_R and $(q_{MAX}/G_i)_R$ will always be equal when the skins on both layers are equal (see Eq. 10). Production rates at constant wellbore pressure and two different realistic constant rate rates-of-take, i.e. 1 MMscfd/8.6 Bscfd and 1 MMscfd/5 Bscfd, produced identical results. Note that, for any given K_R, as long as the skins are equal on both layers, differential depletion will be identical for both layers. We also found this to be true for other values of V_R. Further, the pseudosteady state deliverability results and radial model results exactly overlay each other.

Another important observation to be made from Fig. 5 is that with V_R = 1, the respective distances between the total system $\overline{p}/z$ and each layer $\overline{p}/z$ are always equal for any value of cumulative production, G_{pT}. Both layer $\overline{p}/z$ values converge to the intersection of the minimum flowing pressure, p_{wf}/z, with the total system $\overline{p}/z$ line.

Fig. 5 also demonstrates two limiting conditions: when K_R = 1 or $(q_{MAX}/G_i)_R$ = 1, both layers will deplete equally and the $\overline{p}/z$ for each layer will overlay the total system $\overline{p}/z$ curve. At the other extreme, when $K_R \longrightarrow \infty$, or $(q_{MAX}/G_i)_R \longrightarrow \infty$, the maximum differential depletion envelope is described. It can be intuitively drawn by recognizing the fact that the vastly more permeable layer 1 will totally deplete while layer 2 remains at initial pressure; layer 2 will then deplete after layer 1 is no longer producing. The envelope can be constructed by first connecting p_i/z_i to G_{i1}. Call the intersection of this line and the horizontal line representing p_{wf}/z point A. Call the intersection of the vertical line passing through point A and the horizontal line representing p_i/z_i point B. Finally, connect point B to the point where p_{wf}/z and the total system $\overline{p}/z$ intersect. For example, see Fig. 8 where K_R = 1000.

Observations made in reference to Fig. 5 can also be made in reference to Fig. 6. The only difference is that V_R = 1/2 in Fig. 6; i.e., layer 1 contains 0.50 BSCF while layer 2 contains 1.00 BSCF. Note that for this volume ratio the vertical distance between the total system $\overline{p}/z$ line and the layer 1 $\overline{p}/z$ curve is twice that between the total $\overline{p}/z$ line and the layer 2 $\overline{p}/z$ curve. Again, this distance ratio is the same for any value of cumulative production, G_{pT}. By contrast, for V_R = 2/1, the distance between the total system and layer 1 $\overline{p}/z$ curves is half that between the total system and layer 2 $\overline{p}/z$ curves. In all cases, the vertical distance between the total system $\overline{p}/z$ line and each layer $\overline{p}/z$ curve is inversely proportional to their volume ratios.

Another useful plot suggested by Tempelaar-Lietz[1] for determining the volumes of gas recovered from each layer is shown in Fig. 7. In this case, V_R = 2/1; all other conditions are as discussed for Figs. 5 and 6. The cumulative production of layer 2 is plotted versus the cumulative production of layer 1. The straight line represents the case of $K_R = (q_{MAX}/G_i)_R = 1$, or the limit as q_T approaches zero. The curved line represents either constant wellbore pressure and constant rate production results.

A range of K_R from 1 to 1000 is illustrated in the pressure-cumulative production plot of Fig. 8. In each case, both layers are assumed to have equal skins and equal volumes. Similar results are obtained for V_R = 1/2 and 2/1. The degree of differential depletion between the two layers increases as $(q_{MAX}/G_i)_R$ increases and decreases as $(q_{MAX}/G_i)_R$ decreases. As $(q_{MAX}/G_i)_R$ approaches unity, the system will behave as a single layer.

Unequal Layer Skins

We have assigned a range of skin values to our individual well studies of +5, 0, and -3 to demonstrate the significance of $(q_{MAX}/G_i)_R$ as a correlation parameter. For K_R = 10 and V_R = 1, the following values of $(q_{MAX}/G_i)_R$ were obtained for various skin combinations:

s Layer 1	s Layer 2	K_R	$(q_{iMAX}/G_i)_R$
-3	0	10	15.5
0	5	10	15.9
-3	-3	10	10
0	-3	10	6.4
5	0	10	6.3

Figure 9 illustrates that when different layer skins result in the same value of $(q_{iMAX}/G_i)_R$, $\bar{p}/z$ versus G_{pT} curves for each layer exactly overlay. Similar results are obtained with regard to the decline exponent b.

Constant Rate Cases

To investigate the effect of rate sensitivity on differential depletion, three different constant rate forecasts were made along with a constant wellbore pressure case assuming K_R = 10, V_R = 1, and equal layer skins. Initial rates of 300 Mscfd based on a 1 MMscfd/5 Bscf rate of take, 175 Mscfd based on a 1 MMscfd/8.6 Bscf rate-of-take, and 10 Mscfd representing an economic limit rate were forecast.

The $\bar{p}/z$ vs G_{pT} graph, Fig. 10, demonstrates that differential depletion is not rate sensitive for our practical rates of interest. This is a result of the gas flow rates being a function of kh and a difference in pressures squared, i.e., $q_g = f(\Delta p^2)$. As p_{wf} approaches initial reservoir shut-in pressure ($\Delta p \longrightarrow 0$), as is the case for the 10 Mscfd forecast, the gas rate becomes a function of a difference in pressures, i.e., $q_g = f(\Delta p)$. Tempelaar-Lietz[1] found that for the single phase liquid case, where $q_o = f(\Delta p)$, differential depletion was sensitive to all rates of flow and that as the constant rate q approaches zero, both layers deplete equally, i.e., layer 1, layer 2, and the

total system pressures are all equal. Obviously, very high pressure gas wells will behave like the single phase liquid case, $q = f(\Delta p)$, and solution gas drive reservoirs below the bubble point should behave like the low pressure gas cases since oil well inflow performance[10] yields $q_o = f(\Delta p^2)$.

Figure 11 presents individual layer and composite flow rates for the above cases. Initially, layer rates are a function of kh. When the constant rate cases go on decline, the rates again become a function of kh. The 300 Mscfd case is not shown for clarity of presentation since it lies between 175 Mscfd and the constant p_{wf} case. Note that only for the 10 Mscfd case do the layer rates approach being equal, the constant rate definition of pseudosteady state for two layers of equal pore volume. At practical rates of production that eventually decline to the economic rate of 10 Mscfd, pseudosteady state is never achieved. Also included on this figure are the results obtained using the simple forecasting program based on gas material balance and a stabilized backpressure curve for each layer. The results are identical to the model results.

Field Shut-in Pressures

Routine field data available from layered gas wells consists of monthly commingled production rates, q_T, total system cumulative production, G_{pT}, and commingled shut-in pressures. In our field of study, 72-hr shut-in pressures are taken annually. Based on approximate field reservoir parameters (K_R = 10/1, V_R = 1/2, and $s_1 = s_2 = -3$) annual 72-hour shutin and 48-hour drawdown pressures were simulated using a two-layer radial reservoir model containing 50 cells in each layer. The constant wellbore pressure case results are shown in Fig. 12, and a 175 Mscfd constant rate case, based on a 1 MMscfd/8.6 Bscf rate-of-take, is shown in Fig. 13. As expected, both figures demonstrate that the commingled shut-in pressures, divided by z, basically follow the $\bar{p}/z$ curve of the more permeable layer. The 72-hour pressures for the constant wellbore pressure case are initially somewhat lower than those for the constant rate case because the 72-hour shut-in begins from a much lower flowing pressure prior to shut-in. After about 0.4 Bscf of recovery, the 72-hour pressure begins to exceed the more permeable layer pressure due to interlayer wellbore backflow. Note that trend plotting of the late-time 72-hour shut-in pressure points would overestimate the total original gas-in-place, G_{iT}.

Fig. 14 serves to illustrate the effect of a reduction in p_{wf} on the shape of the pressure-cumulative production plot. In this case, a constant p_{wf} of 192 psia ($\bar{p}/z$ = 200 psia) was maintained for the first 50 years, followed by a constant p_{wf} of 14.7 psia ($\bar{p}/z$ = 15.0 psia) thereafter. With this exception, all forecast assumptions are identical to those employed in Figs. 12 and 13. For a single layer gas reservoir of moderate to high permeability, a change in backpressure will not profoundly affect the shape of the pressure-cumulative production curve. For a layered reservoir without crossflow, however, the effect is dramatic as two distinct differential depletion envelopes become evident. Note that a flattening of the 72-hour shut-in points can be seen both before and after the backpressure change. Eventually, the 72-hour pressures asymptotically approach the minimum flowing wellbore pressure or abandonment pressure. Observed in several wells in our field of study, this flattening of measured shut-in pressures appears to be a characteristic signature of commingled layered reservoirs with contrasting layer

permeabilities. It is further magnified when the more permeable layer has a smaller volume than the less permeable layer. Shown in Fig. 15, Well L exhibits a flattening of 72-hour shut-in pressures before and after a line pressure change from 60 psig to 20 psig.

The rate-time companion plot of Fig. 14 is displayed in Fig. 16. The effect of the reduction in p_{wf} is equally pronounced. Interestingly, the total system production response following the backpressure change has the appearance of - but is not - an infinite acting transient spike. Figs. 14 and 16 also demonstrate the excellent agreement between results obtained from the backpressure curve-material balance program, a purely pseudosteady state approach for each layer, and results obtained from the 2-layer 50-cell radial model. As expected, with the ratio of $p_{wf}/\overline{p}$ being different for the two periods, the total system rate-time curve through the first 50 years exhibits a somewhat lower b value than the b value obtained by reinitializing the curve after the decrease in wellbore flowing pressure.

BACKPRESSURE CURVES

A stabilized backpressure curve and a material balance equation are frequently used to prepare long term production forecasts for single layer systems. The stabilized backpressure curve is only utilized during constant wellbore pressure production, i.e., the declining production period. A single stabilized backpressure curve relationship for multi-layer systems has never been defined, mainly because previous investigations of multi-layered systems are based on constant rate production - the rate never experiences decline.

Constant Wellbore Pressure

Depicted in Fig. 17, several different backpressure curves were developed from a radial model forecast, assuming $V_R = 1/2$, $K_R = 10/1$, $S_1 = S_2 = -3$, and a constant $p_{wf} = 42.8$ psia. Annual 72-hour shut-ins, each followed by a 48-hour drawdown, were also simulated to represent typical official test requirements, test data that would normally be available to construct a 48-hour depletion backpressure curve. (Drawdown and depletion backpressure curves are normally the same for low pressure gas wells. An isochronal test conducted at initial reservoir pressure is considered to be a drawdown backpressure curve.) The average reservoir pressure, p, used to define the backpressure curves in Fig. 17 represents either the simulated 72-hour shut-in pressure, or the volumetric average pressure for each layer and the total system.

Curve 1 represents the calculated position of the stabilized or pseudosteady state curve for layer 1 using the reservoir variables previously defined. The points that overlay the curve were obtained from the model run. Points that approach the stabilized curve from the right represent transient flow rates, or the shifting of the transient backpressure curve with time to pseudosteady state. The pressure, p, and rate, q, are those of layer 1 only.

Curve 2 represents the stabilized backpressure curve for layer 2, the low permeability layer. The previous discussion for layer 1 also applies to the layer 2 curve. Curve 3 is simply the sum of curves 1 and 2. Curve 4 represents the stabilized backpressure curve for the total system where $\overline{p}$ is the volumetric average pressure of the total system and q is the total flow rate from both layers. Clearly, curve 4 is not a straight line except at low

flow rates. We have therefore avoided the expression "pseudosteady state" when describing it. Curve 4 originates at the q_{MAXT} of curve 3 and asymptotically approaches a straight line of unit slope established from the layer 2 stabilized potential, q_{MAX2}, and the ratio of layer pore volumes, such that

$$(q)^*_{MAX} = (q)_{MAX2} \frac{G_{i1} + G_{i2}}{G_{i2}} \quad \ldots\ldots (16)$$

Since layer flow rates at these low levels become a function only of layer pore volumes, the position of this straight line asymptote was found to be independent of layer skins. (These points become much clearer by applying equations A-1 through A-10 to a fluid of small and constant compressibility rather than the fluid of high and variable compressibility used in our study.) We were unable to predict the layered reservoir stabilized curve limiting position from the constant rate long time solution of reference 2.

The shape of the layered system stabilized curve gives the appearance of a continuous loss in well performance that could be misinterpreted as a changing skin, a loss of reservoir permeability, or an infinite-acting transient decay.

This curve is identically reproduced, however, from pseudosteady state curves generated for each layer using a simple material balance-stabilized curve-deliverability program. For the permeability levels used in our study, early infinite acting transient effects appear to be negligible in long-term forecasting.

Curve 5 is based on the combined rate from both layers and the volumetric average pressure of the more permeable layer. We intuitively expect the commingled shut-in pressure to approach the pressure of the more permeable layer. (See also Fig. 12.) Curve 6 is a plot of the simulated annual 72-hour shut-in pressure and 48-hour drawdown flow rate obtained while producing against a constant bottomhole flowing pressure, p_{wf}, of 42.8 psia. Surprisingly, a perfectly straight line results having a backpressure curve slope, n, of 0.934. Recall that Darcy flow, n = 1, is assumed for each layer. Note that curve 6, the 48-hour depletion backpressure curve, does not reflect the shape of curve 4, the layered stabilized backpressure curve.

Constant Rate Production

The backpressure curves plotted for the constant rate case of 175 Mscfd, Fig. 18, assume $V_R = 1$. The $\overline{p}/z$-G_p and rate-time curves for this case are shown in Figs. 10 and 11. All previous discussions concerning the constant wellbore pressure case, Fig. 17, are applicable to Fig. 18. The only difference is the point at which each layer and the total system begin to go on decline. From the decline point on, the constant rate and constant wellbore pressure results for the same V_R ratio exactly coincide.

RATE-TIME DEPLETION BEHAVIOR

Figure 19 is a comparison of individual layer and total system rate-time responses for various ratios of $(q_{MAX}/G_i)_R$, or layer permeability ratios, since the layer skins are equal. It includes $(q_{MAX}/G_i)_R$ = 3, 10, 30, 100, and

1000. Only the contribution of layer 1, the high permeability layer, changes from case to case; the permeability of layer 2 is fixed at 1.0 md in each case. Further, each layer contains a gas-in-place of 0.75 Bscf, and each has been assigned a skin of -3.

The log rate vs log time profile for any single layer can be matched to a depletion b stem of 0.4. This result is commensurate with the expected behavior of a dry gas reservoir in the presence of a constant backpressure equal to 10% of the initial reservoir pressure. We have confirmed, however, that the same model correctly predicts a b value of 0.5 when the flowing bottomhole pressure, $p_{wf} = 0$.

As shown in Fig. 19, when two layers, each characterized by a b value of 0.4, are added together, the composite curve will yield a value of b much greater than 0.4. Only for the special case in which the ratio of q_{MAX} to initial gas-in-place is the same for each layer ($(q_{MAX}/G_i)_R = 1.0$), will the composite curve follow the same depletion stem described by each separate layer. Such cases reduce to a single-layered system.

For a given volume ratio, the greater the value of $(q_{MAX}/G_i)_R$, the greater the contrast between early layer producing rates. The low permeability layer will not contribute a significant fraction of the total rate until the high permeability layer is depleted. At late time, the total system curve and low permeability curve become indistinguishable. For the case of $(q_{MAX}/G_i)_R = K_R = 10$ or $(q_{MAX}/G_i)_R = K_R = 3$, the composite curve approximates a smooth hyperbolic decline. Differential depletion gives the total rate-time curve the appearance of a single, homogeneous system with a high b value. We know of no other mechanism to explain the occurence of nearly harmonic decline behavior observed in actual field data.

Note, however, that for cases in which the $(q_{MAX}/G_i)_R$ is greater than about 20, a double hump appearance is evident in the total rate-time curve. This double-depletion characteristic closely resembles the shape of the type curves developed by Da Prat[11] for single layered naturally fractured reservoirs. The early depletion of the high permeability layer appears analogous to fracture volume depletion; the late depletion of the low permeability layer can be considered analogous to matrix depletion. When attempting to identify a naturally fractured reservoir on the basis of double-depletion rate-time behavior, one must therefore consider the possibility of layering with no crossflow. In Monterey reservoirs, for example, the degree of fracturing is highly lithology dependent and any intra-layer fracture-matrix response may be overwhelmed by the layering response among lithologically disimilar zones of contrasting permeability.

Recall from Fig. 9 that when two separate layered systems have the same gas-in-place, share the same values of V_R, and $(q_{MAX}/G_i)_R$, each system will overlay the same $\overline{p}/z - G_{pT}$ curve. (As long as $(q_{MAX}/G_i)_R$ is constant, each system may have different layer permeabilities, porosities, and skins.) Fig. 20 demonstrates that such systems will also describe similar rate-time curves. In this case, $V_R = 1/1$ and $K_R = 10/1$ for both systems. For the system shown using open symbols, $S_1 = 0$ and $S_2 = +5$, resulting in $(q_{MAX}/G_i)_R = 15.9$. For the system represented by closed symbols, $S_1 = -3$ and $S_2 = 0$, yielding $(q_{MAX}/G_i)_R = 15.5$. Log rate versus log time type curves for these systems, based on radial model results, exactly match with a slight shift of both axes

due to differing layer skins. Only a minor difference is evident between the profiles of the low permeability layers; the undamaged layer traces a lower re/rw_a stem during the transient period. Note that the total system profiles, shown with square symbols, exactly overlie, each tracing a b stem of 0.8 through 100 years of production. Similar results are obtained using the pseudosteady state gas deliverability program.

Fig. 21 illustrates similar results for two other systems of equal $(q_{MAX}/G_i)_R$. Both systems assume $V_R = 1/2$ and $K_R = 10/1$ approximating the values for our field of study. The open symbols refer to the system in which $S_1 = +5$ and $S_2 = 0$, yielding $(q_{MAX}/G_i)_R = 6.3$. The closed symbols identify the system in which $S_1 = 0$ and $S_2 = -3$, resulting in $(q_{MAX}/G_i)_R = 6.4$. Again, composite profiles exactly coincide, this time approximating a b stem of 0.9.

Figs. 20 and 21 reveal that different values of V_R and $(q_{MAX}/G_i)_R$ produce different values of b. The complete spectrum of possible Arps b values for various differential depletion cases is shown in Table 2. All these results are based on a constant flowing pressure equal to 10 percent of the initial shut-in pressure. Several values of $(q_{MAX}/G_i)_R$, including 1.0, 3.0, 5.0, 10.0, 15.5, 30.0, 100.0, and 1000.0, were investigated in combination with volume ratios of 2/1, 1/1, and 1/2. Predictably, for any given V_R, the b value increases as $(q_{MAX}/G_i)_R$ increases, i.e., as the contrast in layer properties, primarily permeability, becomes more pronounced. For very large values of $(q_{MAX}/G_i)_R$, however, the double depletion decline develops and a constant b stem cannot be maintained. At both ends of the $(q_{max}/G_i)_R$ spectrum, therefore, the composite curve collapses to a single layer profile with a b of 0.4. The highest b values obtained in our study are for (q_{MAX}/G_i) ratios between 10 and 20. Further, for any given $(q_{MAX}/G_i)_R$, b increases as V_R decreases. Assuming $(q_{MAX}/G_i)_R = 10.0$, for instance, a V_R of 2/1 yields a b of 0.65, a V_R of 1/1 yields a b of 0.80, and a V_R of 1/2 yields a b of 1.0. For very low volume ratios, however, a constant b stem is again impossible to maintain.

Fig. 22 is a type curve overlay of six $(q_{MAX}/G_i)_R$ cases, including 1.0, 3.0, 5.0, 10.0, 15.5, and 30.0, all premising $V_R = 1/2$. Fig. 23 is a similar overlay of five V_R cases, including 2/1, 1/1, 1/2, 1/5, and 1/10, all assuming $(q_{MAX}/G_i)_R = K_R = 10/1$. In both figures, the axes of each individual rate-time plot are shifted so that all cases can be presented on a single Arps depletion type curve. Note in Fig. 22 that the radial model results generally begin to fall below a fixed b stem at late time. The higher the b stem indicated by the early depletion performance, the earlier in real time this drop-off occurs. For $V_R = 1/5$ and 1/10, shown in Fig. 23, the total system profile briefly exceeds a b of 1.0, only to fall back to a lower value of b later in depletion. Eventually, only the low permeability layer contributes to the total flow rate and the b value migrates to that of a single layer. Normal wellbore deterioration, liquid loading, etc., experienced even by a single layer completion, may, in fact, contribute to this migration. With the exception of cases involving low volume ratios, however, our results demonstrate that a fixed b stem will be sufficient for predicting flow rates to a practical economic limit. Nevertheless, caution should be exercised in using a fixed b value to predict reserves at late time for layered systems. We do not advocate the use of b stems greater than 1.0 for forecasting purposes.

A final point concerns the type curve matching procedure used on the curves generated in Figs. 22 and 23. We were unable to analytically predict exactly where to match each composite rate-time curve based on a total system kh. An approximate match could be obtained by first estimating q_{dD} using kh_T and $\overline{\mu\beta}$, and then shifting the curve from left to right along the time axis in order to match the appropriate early time re/rw_a stem. The best manual fit q_{dD} was in every case 5 to 10 per cent lower than the calculated q_{dD}. The problem lies in estimating the time to pseudosteady state for a layered system, making the t_{dD} match point difficult to evaluate. Further, the total system pore volume cannot be exactly estimated based on a type curve match of the total rate profile. If a gas well exhibits a b value greater than 0.5, indicating the presence of a layered system, individual layer pore volumes may be estimated by graphically desuperposing the total system curve from the high permeability layer with a b = 0.4 using a trial and error procedure.

DISCUSSION

Most reservoirs consist of several layers with reservoir properties varying to some degree between layers. Whether crossflow exists or does not exist between layers may be of considerable importance in long term forecasting. If crossflow exists, layers can be combined into a single equivalent layer using the average reservoir properties of the crossflowing layers. Even if crossflow does not exist, layers can still be combined into an equivalent single layer if each has the same diffusivity properties, or q_{MAX}/G_i. It should also be possible to reduce multi-layer systems into equivalent two-layer systems for rate-time analysis or production forecasting. All but the most permeable layer may be combined into a single layer of lesser permeability. We have made a few four-layer no-crossflow forecasts that compare closely to those obtained from our two-layer studies. As in the two-layer studies, the 72-hour shut-in pressures derived from a four-layer model track the most permeable layer. The decline exponent is also similar to that obtained for a two-layer system. We have had reasonable success in combining the four-layer cases into equivalent two-layer systems. In their studies of three-layer reservoirs, Lefkovits et al.[2] also found that "their behavior is like that of a two-layer reservoir." We also found that <u>limited</u> crossflow cases can behave similar to no-crossflow cases.

In a no-crossflow layered reservoir, or in a well with commingled reservoir completions, in order to significantly affect long-term production forecasts, <u>a contrast in layer permeabilities must exist</u>. More specifically, the contrast must be in the correlating parameters $(q_{MAX}/G_i)_R$ and V_R. Reservoirs most likely to develop these contrasts are naturally fractured reservoirs and very thick reservoirs. The Monterey, Spraberry, Altamont-Bluebell, and Austin Chalk, all described as naturally fractured reservoirs, exhibit <u>depletion</u> decline exponents approaching 1. The early, rapid rate decline observed in such reservoirs is usually interpreted as fracture volume depletion instead of the differential depletion of the <u>entire</u> naturally fractured layer or layers. This early rapid rate decline would be expected for a layered reservoir with no or very limited crossflow between layers. The single-layer naturally fractured or dual-porosity constant wellbore pressure solution of Da Prat et al.[11] does not result in a depletion decline exponent approaching 1. Although naturally fractured reservoirs are often thought to have vertical permeabilities equal to horizontal permeabilities (complete

crossflow throughout), depletion b values approaching 1 for such reservoirs suggest the presence of layering, with little or no crossflow between some or all layers. Prior to this study, the double depletion rate decline illustrated by Da Prat was considered to be one of the identifiable responses of naturally fractured reservoirs. This study, however, shows that a no-crossflow layered reservoir, without natural fracturing, can exhibit the same type of response.

Early recognition of a no-crossflow layered reservoir's precipitous rate and pressure cumulative production declines would require early individual layer tests, coring, and a good geological description. The relatively thick shale break observed in all wells in our field of study should have indicated the necessity for individual layer tests, both above and below the potential shale barrier. Individual layer tests along with the core data would have confirmed layer permeability contrasts and the potential for differential depletion. A vertical permeability test across the shale may also have been warranted. If high and low permeability layers are interbedded, as in many naturally fractured reservoirs, it may be difficult to test individual layers; pressure transient tests would reflect the kh of the high permeability layer(s). The kh of the low permeability layer(s) may not be detectable.

Obtaining RFT pressures on later development wells, replacement wells, or infill wells is another method that can be used for the early detection of differential depletion in layered reservoirs. Unfortunately, this is a one-time opportunity for a well. The multilayer testing procedures of Ehlig-Economides and Joseph[12] theoretically offer the opportunity to obtain layer pressures, permeabilities, and skins as frequently as necessary to define the pressure versus cumulative production curve for each layer.

Finally, if the most permeable layer(s) of a commingled no-crossflow reservoir were lost due to early water breakthrough, or were squeezed off after water breakthrough, we would expect the future rate decline exponent, b, to change, thereby reflecting the reservoir properties of the remaining layers. Late development or replacement wells may not experience the rapid initial declines exhibited by early development wells, particularly if lateral continuity exists.

No realistic physical gas reservoir system can produce and maintain a depletion decline exponent, b, greater than 1. Based on rate-time analysis of actual field data, we feel that this limit of b also applies to oil systems.

CONCLUSIONS

All of the following conclusions are applicable to our specific field of study. Most would be applicable to any no-crossflow layered reservoir. The use of the word layered in our conclusions always means a no-crossflow layered reservoir.

1.) A two-layered reservoir description for our field of study reproduces observed rate-time and pressure-cumulative production performance that a single layer description cannot reproduce.

2.) At practical rates of production, the rate-time and pressure-cumulative production performance is not rate sensitive.

3.) Rate-time and pressure-cumulative production responses for a layered reservoir can be correlated with $(q_{MAX}/G_i)_R$ and V_R. The magnitude of b may provide an indication of the permeability contrast and the volume ratio.

4.) The Arps' depletion decline exponents between 0.5 and 1 can be obtained with a layered reservoir description. A depletion decline exponent, b, greater than 1.0 cannot be developed and maintained using our two-layered reservoir description.

5.) Except for the special cases in which $(q_{MAX}/G_i)_R$ approaches unity or infinity, the composite depletion b value is always greater than that of a single layer system. Field and well rate-time data that exhibit higher than expected values of b (between 0.5 and 1.0 for gas reservoirs) suggest a layered reservoir system. Large initial percentage declines that are not attributable to infinite acting transient production, followed later by small percentage declines, are a characteristic of high b values and suggest a layered reservoir response.

6.) During the constant rate production period of a layered reservoir, the only performance characteristic that can be used to detect layering is the shape of the pressure cumulative production graph. The steeper the initial decline in $\bar{p}/z$, the smaller the volume ratio (G_{i1}/G_{i2}).

7.) Different combinations of layer skins can exhibit similar rate-time and pressure-cumulative production differential depletion responses.

8.) Shut in pressures obtained for layered reservoirs will track the pressure of the most permeable layer, more specifically, the layer with the highest value of q_{MAX}/G_i. Extrapolation of a shut-in $\bar{p}/z$ versus G_{pT} curve may possibly underestimate the gas-in-place, G_{iT}, at early times and overestimate the gas-in-place at late times. Similarly, semilog extrapolation of early rate-time data will underestimate recoverable reserves. Continuing to extrapolate late rate-time data along a fixed high value of b may overestimate recoverable reserves.

9.) The total system stabilized backpressure curve of a layered system is not a straight line. Annual deliverability tests, however, when plotted in the form of a depletion backpressure curve, will define a straight line. The slope of this backpressure curve is less than that of the individual layers.

10.) For our field of study, a simplified approach using a stabilized backpressure curve and a material balance equation for each layer yields the same basic results and conclusions as obtained from a radial model study.

NOMENCLATURE

b = reciprocal of decline curve exponent
B = FVF, res vol/surface vol
c_g = gas compressibility, psi^{-1} [kPa^{-1}]
C_t = total compressibility, psi^{-1} [kPa^{-1}]
C = gas-well backpressure curve coefficient
CAOF = calculated absolute open flow, Mscfd
e = natural logarithm

G_i = initial gas-in-place Bscf [std m^3]
G_p = cumulative gas production Bscf [std m^3]
h = thickness, ft [m]
J = productivity index, BOPD/psi [std m^3/kPa]
k = effective permeability, md
K_R = layer permeability ratio
n = exponent of backpressure curve
N_p = cumulative oil production, STB
N_{pi} = initial expandable oil-in-place at pressure p_i, STB (Eq. A-5)
$\bar{p}$ = average reservoir pressure, psia [kPa]
p_c = wellhead shut-in pressure, psig
p_i = initial reservoir pressure, psia [kPa]
p_{wf} = wellbore flowing pressure, psia [kPa]
$(q_i)_{MAX}$ = initial surface rate of flow from the stabilized curve
$(q^*)_{MAX}$ = Eq. 16
$q(t)$ = surface flow rate at time t
q_T = total constant rate from layers 1 and 2
r_e = external-boundary radius, ft [m]
r_{wa} = effective wellbore radius, ft [m]
r_w = wellbore radius, ft [m]
s = skin factor, dimensionless
S.G. = gas specific gravity
S_w = water saturation, fraction
t = time, days
t_{dD} = decline-curve dimensionless time
T = reservoir temperature, °R
V_R = layer volume ratio, (Eq. 9)
z = gas compressibility factor, dimensionless
μ = viscosity, cp [Pa·s]
ϕ = porosity, fraction of bulk volume

SUBSCRIPTS

g = gas
i = initial
o = oil
T = total of layers 1 and 2

ACKNOWLEDGMENTS

We thank Phillips Petroleum Co. for permission to publish this paper. We also wish to thank U. G. Kiesow and B. C. Nolen for their early efforts on this project. The necessary radial model logic revisions required to conduct this study were made by L. K. Thomas. Special thanks to Kay Patton for the excellent typing of this and several other papers previously published.

REFERENCES

1. Tempelaar-Lietz, W.: "Effect of Oil Production Rate on Performance of Wells Producing From More Than One Horizon," SPEJ (March 1961) 26-31.

2. Lefkovits, H. C., Hazebroek, P., Allen, E. E., and Matthews, C. S.: "A Study of the Behavior of Bounded Reservoirs Composed of Stratified Layers," SPEJ (March 1961) 43-58.

3. Fetkovich, M. J.: "Decline Curve Analysis Using Type Curves," JPT (June 1980) 1065-77.

4. Keller, W. O., Tracey, G. W., and Roe, R. P.: "Effect of Permeability on Recovery Efficiency by Gas Displacement," presented at the API meeting, Tulsa, OK., March 1949.

5. Gentry, R. W. and McCray, A. W.: "The Effect of Reservoir and Fluid Properties on Production Decline Curves," JPT (Sept. 1978) 1327-41.

6. Carter, R. D.: "Type Curves for Finite Radial and Linear Gas-Flow Systems: Constant-Terminal-Pressure Case," SPEJ (Oct. 1985) 719-28.

7. Fetkovich, M. J., Vienot, M. E., Bradley, M. D., and Kiesow, U. G.: "Decline Curve Analysis Using Type Curves - Case Histories," SPE Formation Evaluation, (Dec. 1987) 637-656.

8. Arps, J. J.: "Analysis of Decline Curves," Trans., AIME (1945)) 160, 228-47.

9. Raghavan, R.: "Behavior of Wells Completed in Multiple Producing Zones," paper SPE 14111 presented at the 1986 International Meeting on Petroleum Engineering, Beijing, China, March 17-29.

10. Fetkovich, M. J.: "The Isochronal Testing of Oil Wells," paper SPE 4529 presented at the 48th Annual Fall Meeting, Las Vegas, NV., Sept. 30 -Oct. 3, 1973. (SPE Reprint Series No. 14, 2651.)

11. Da Prat, Giovanni, Cinco-Ley, Heber, and Ramey, H. J. Jr.: "Decline Curve Analysis Using Type Curves For Two-Porosity Systems," SPEJ (June 1981) 354-362.

12. Ehlig-Economides, C. A. and Joseph, J.: "A New Test for Determination of Individual Layer Properties in a Multilayered Reservoir," SPE Formation Evaluation, (Sept. 1987) 261-283.

13. Fetkovich, M. J.: "A Simplified Approach to Water Influx Calculations - Finite Aquifer Systems," JPT (July 1971) 814-828.

APPENDIX - SINGLE PHASE LIQUID SOLUTIONS FOR TWO LAYERS

Constant Wellbore Pressure

Fetkovich[3,13] gives the pseudosteady-state constant wellbore pressure solution for single phase liquid flow for any one layer at a flowing pressure, p_{wf}, as

$$q(t) = \frac{q_i}{e^{\left[\frac{(q_i)_{MAX}}{N_{pi}}\right] t}} \qquad \ldots . \quad (A\text{-}1)$$

where

$$q_i = J\,(p_i - p_{wf}) \qquad \ldots\ (A\text{-}2)$$

and

$$(q_i)_{MAX} = \frac{q_i}{\left[1 - \frac{p_{wf}}{p_i}\right]} \qquad \ldots\ (A\text{-}3)$$

In terms of reservoir variables, we have

$$J = \frac{kh}{141.2(\overline{\mu B})\left[\ln\left(\frac{.472\ r_e}{r_w}\right) + s\right]} \qquad \ldots\ (A\text{-}4)$$

and

$$N_{pi} = \frac{\pi(r_e^2 - r_w^2)\ \phi h\ c_t\ p_i}{5.615\ B_i} \qquad \ldots\ (A\text{-}5)$$

(Note that N_{pi} is ultimate recovery and could also be defined as original oil-in-place multiplied by fraction recovery. This has application to volumetric solution gas drive reservoirs.)

Total production from a two-layered system is

$$q_T = q_1(t) + q_2(t) \text{ and } (q_i)_{MAXT} = (q_i)_{MAX1} + (q_i)_{MAX2} \qquad \ldots\ (A\text{-}6)$$

The cumulative production time equation from any one layer is

$$\frac{N_p(t)}{N_{pi}} = \left(1 - \frac{p_{wf}}{p_i}\right)\left\{1 - e^{-\left[\frac{(q_i)_{MAX}}{N_{pi}}\right] t}\right\} \qquad \ldots\ (A\text{-}7)$$

For a two-layered reservoir

$$N_{pT}(t) = N_{p1}(t) + N_{p2}(t) \qquad \ldots\ (A\text{-}8)$$

The material balance equation for any one layer is

$$p_i - \overline{p}(t) = \left[\frac{N_p(t)}{N_{pi}}\right] p_i \qquad \ldots\ (A\text{-}9)$$

and for the total reservoir of a two-layered system with equal initial pressure and fluids

$$p_i - \bar{p}(t) = \left[\frac{N_{p1}(t) + N_{p2}(t)}{N_{pi1} + N_{pi2}}\right] p_i \qquad \ldots . \text{(A-10)}$$

Constant Rate

The Tempelaar-Lietz[1] pseudosteady-state constant rate layer pressure drop equation as modified by Lefkovitz et al.[2] for two layers of unequal thickness given in terms of the constant rate q_T, $(q_i)_{MAX}$, N_{pi}, and p_i for each layer and the total system is for layer 1.

$$p_i - \bar{p}_1(t) = p_i\left(\frac{q_T}{N_{piT}}\right)t + \left\{p_i\left(\frac{q_T}{N_{piT}}\right)\frac{N_{pi2}\,[(q_i)_{MAX1}\,N_{pi2} - (q_i)_{MAX2}\,N_{pi1}]}{N_{piT}\,[(q_i)_{MAX1}\,(q_i)_{MAX2}]}\right.$$

$$\left.\left[1 - e^{-\frac{[(q_i)_{MAX}/N_{pi}]_1\,[(q_i)_{MAX}/N_{pi}]_2}{[(q_i)_{MAX}/N_{pi}]_T}\,t}\right]\right\} \qquad \ldots . \text{(A-11)}$$

The exponential term is common to equations that follow and will be expressed as e^{-xt} to conserve space.

For layer 2, the layer pressure drop equation is

$$p_i - \bar{p}_2(t) = p_i\left(\frac{q_T}{N_{piT}}\right)t - \left\{p_i\left(\frac{q_T}{N_{piT}}\right)\frac{N_{pi1}\,[(q_i)_{MAX1}\,N_{pi2} - (q_i)_{MAX2}\,N_{pi1}]}{N_{piT}\,[(q_i)_{MAX1}\,(q_i)_{MAX2}]}\right.$$

$$\left.\left[1 - e^{-xt}\right]\right\} \qquad \ldots . \text{(A-12)}$$

Equation A-9 is used to calculate the cumulative production, $N_p(t)$, from each layer and A-10 for the total system. Similar to the gas cases presented in this study, each layer pressure and the total system pressure are plotted versus the total cumulative production, $N_{pT}(t)$.

The flow rate for layer 1 is given by the following equation

$$q_1(t) = q_T\left\{\frac{N_{pi1}}{N_{piT}} + \frac{[(q_i)_{MAX1}\,N_{pi2} - (q_i)_{MAX2}\,N_{pi1}]}{N_{piT}\,(q_i)_{MAXT}}\,e^{-xt}\right\} \qquad \ldots \text{(A-13)}$$

and $q_2(t)$ can be obtained from

$$q_2(t) = q_T - q_1(t) \qquad \ldots . \text{(A-14)}$$

Equation A-13 corresponds to Eq. 13 of Ref. 2 and has been corrected for two typographical errors: N_{pi1}/N_{piT} should be followed by a + instead of - and A_1 in Ref. 2 should be $(A_1 + A_2)$ which converts to N_{piT} in the denominator of the second term of Eq. A-13.

It should be pointed out that Tempelaar-Lietz[1] found that a depletion comparison of his pseudosteady-state material balance approach for each layer with the rigorous solution "with the exception of the first few hours of production, errors of less than 2 percent are introduced by the steady-state approach." This is exactly what we found in our comparisons of the gas deliverability program and radial model results.

TABLE 1

INITIAL ISOCHRONAL TEST RESULTS

WELL	TEST DATE	WHSIP P_c psig	3 HOUR ISOCHRONAL TESTS CAOF mcfd	Slope n	kh md-ft	h ft	k md	s	*** h_1/h_2 = 1/2, k_1/k_2 = 10/1 k_1 md	k_2 md
A	10-19-60	384.5	16000	1.00	1498	64	23.4	-4.6	59	5.9
B	12-07-60	383.7	14600	1.00	1761	29	60.7	-5.2	152	15.2
C	01-27-61	386.4	13700	1.00	1332	37	36	-4.8	90	9.0
D	02-27-61	404.4	6200	0.78	1248	47	26.6	-4.0	66	6.6
E	03-06-61	379.9	3600	1.00	332	74	4.5	-3.8	11	1.1
F	03-09-61	408.1	8800	0.83	984	72	13.7	-4.5	34	3.4
G	01-23-63	419.5	3690	0.69*	565	29	19.5	-4.0	49	4.9
H	08-12-63	408.7	5800	1.00	225	39	5.8	-4.8	14	1.4
I	10-02-63	417.9	2000	0.86	215	23	9.3	-4.0	23	2.3
J	09-09-63	416.3	5900	1.00	397	41	9.7	-4.4	24	2.4
Arithmetic Averages		400.9	8029	0.92	856	46	20.9	-4.4	52	5.2
							18.8**			

* Flow after Flow Test

** $\frac{\Sigma kh}{\Sigma h}$

*** $k_1h_1 + k_2h_2 = kh_T$ and $h_1 + h_2 = h_T$
$k_1 = 10k_2$ and $h_2 = 2h_1$

TABLE 2

DECLINE EXPONENT b AS A FUNCTION OF $\left[\frac{(q)_{MAX}}{G_i}\right]_R$ AND V_R

$\left[\frac{(q)_{MAX}}{G_i}\right]_R$	V_R = 2/1	V_R = 1/1	V_R = 1/2
1	.4	.4	.4
3	.5	.55	.6
5	.6	.65	.7
10	.65	.8	1.0
15.5	.65	.8	1.0
30*	.6	.7	.8
100*	.5	.5	.5
1000*	.4	.4	.4

* Double depletion decline b listed in table is for the first depletion decline

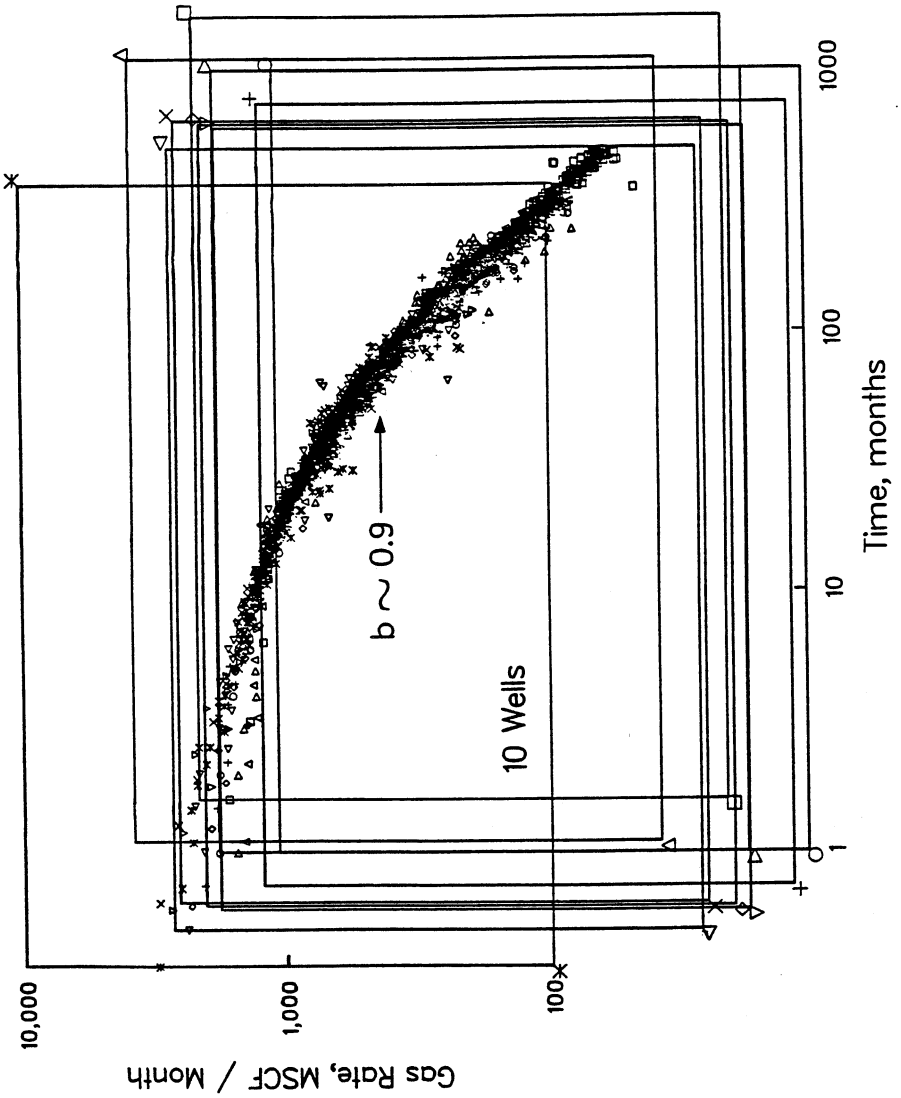

FIG. 1 OVERLAY OF LOG-RATE VS LOG-TIME PRODUCTION DATA OF TEN GAS WELLS

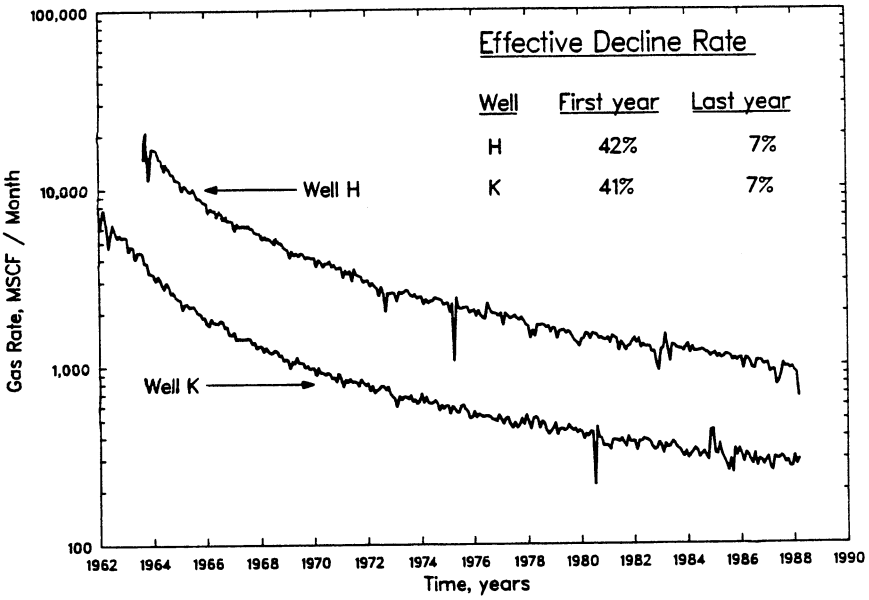

FIG. 2 SEMILOG PLOT OF RATE-TIME PRODUCTION DATA

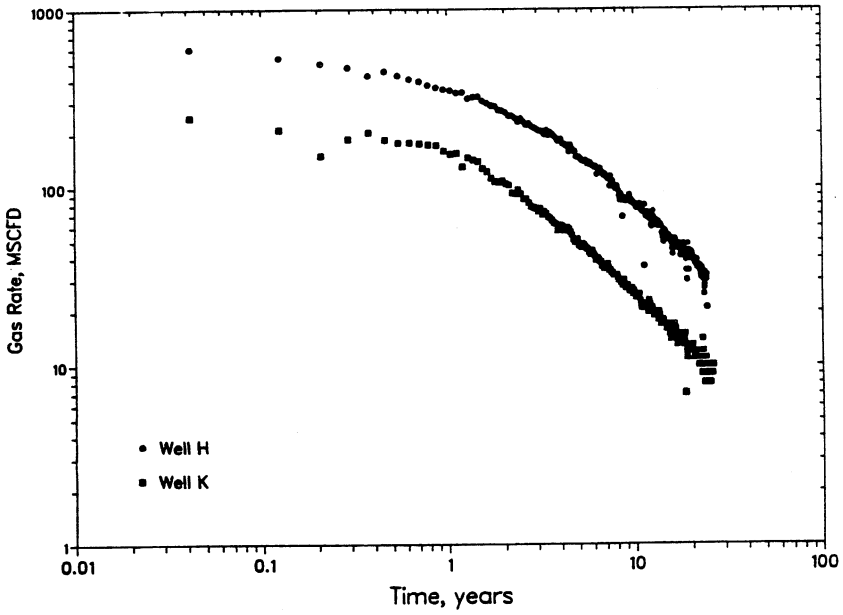

FIG. 3 LOG-RATE VS LOG-TIME PRODUCTION DATA

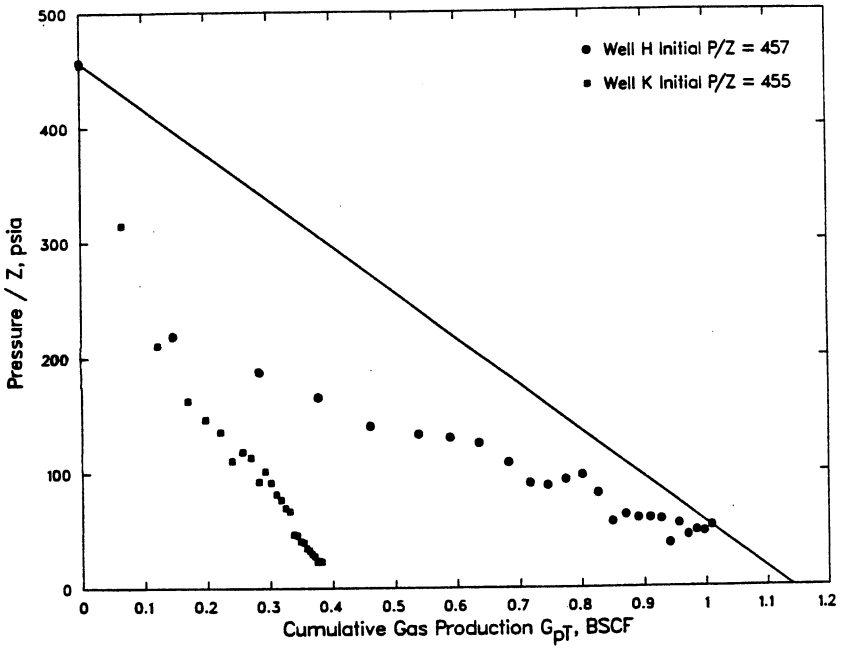

FIG. 4 P/Z VS CUMULATIVE PRODUCTION, 72-HOUR SHUT-INS

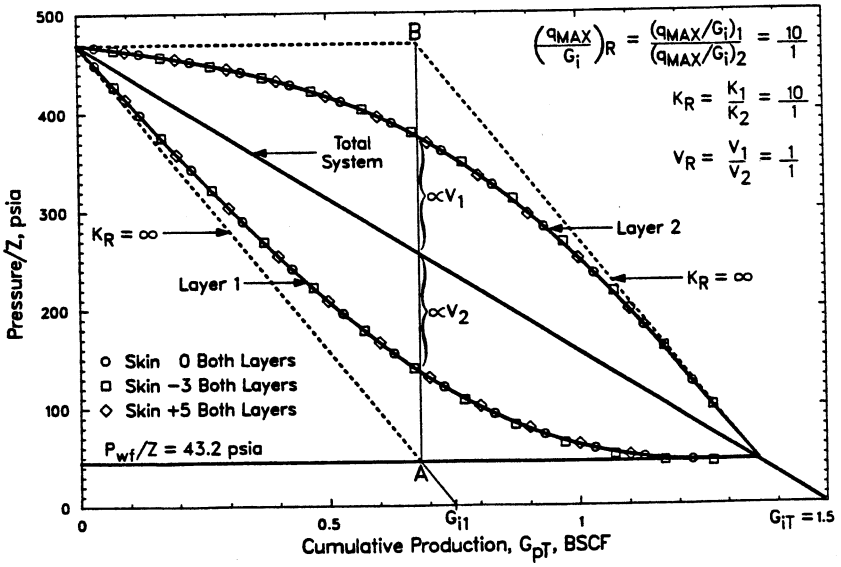

FIG. 5 P/Z VS CUMULATIVE PRODUCTION, LAYER SKINS EQUAL AND V_R = 1

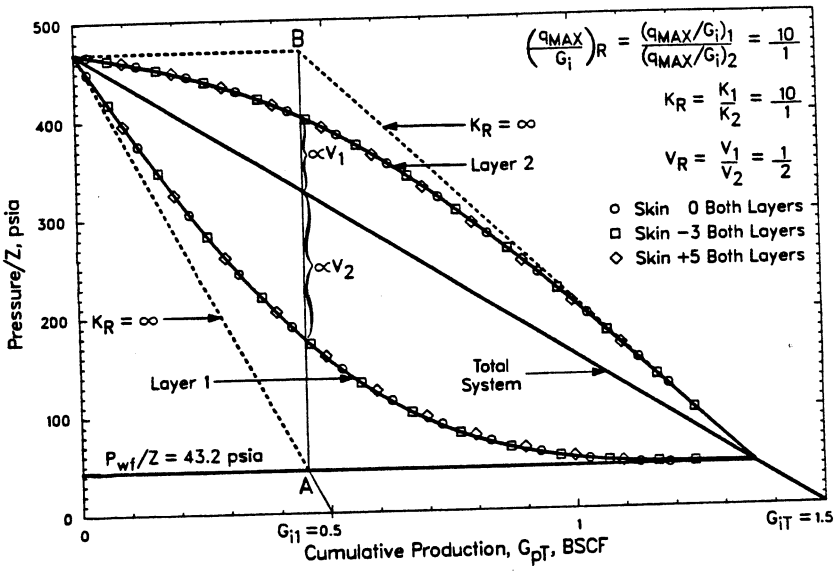

FIG. 6 P/Z VS CUMULATIVE PRODUCTION, LAYER SKINS EQUAL AND V_R = 1/2

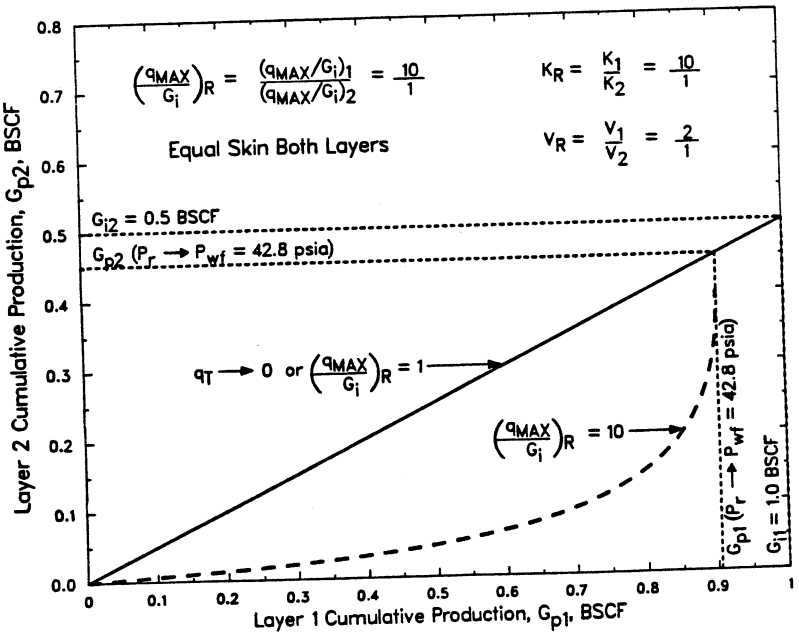

FIG. 7 TEMPELAAR-LIETZ PLOT OF G_p LAYER 1 VS G_p LAYER 2, V_R = 2/1

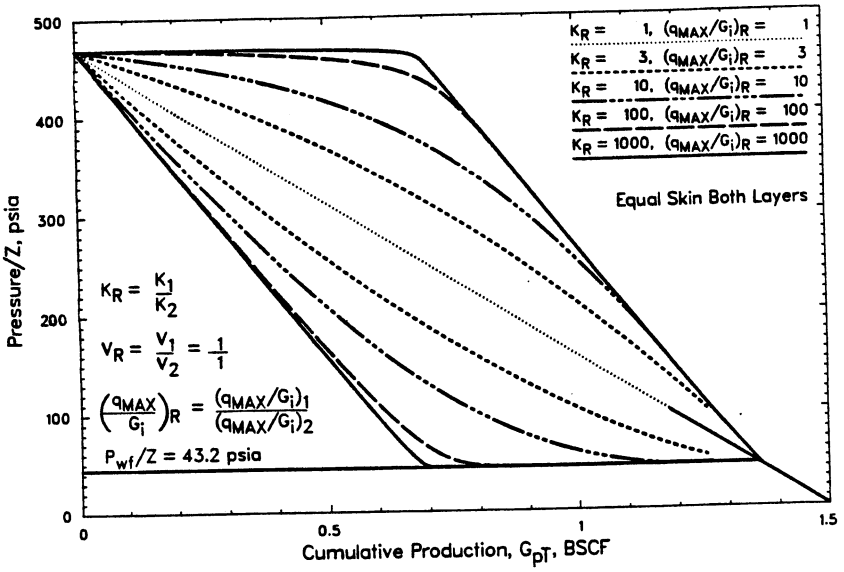

FIG. 8 P/Z VS CUMULATIVE PRODUCTION, LAYER SKINS EQUAL, V_R = 1 AND K_R RANGE 1 TO 1000

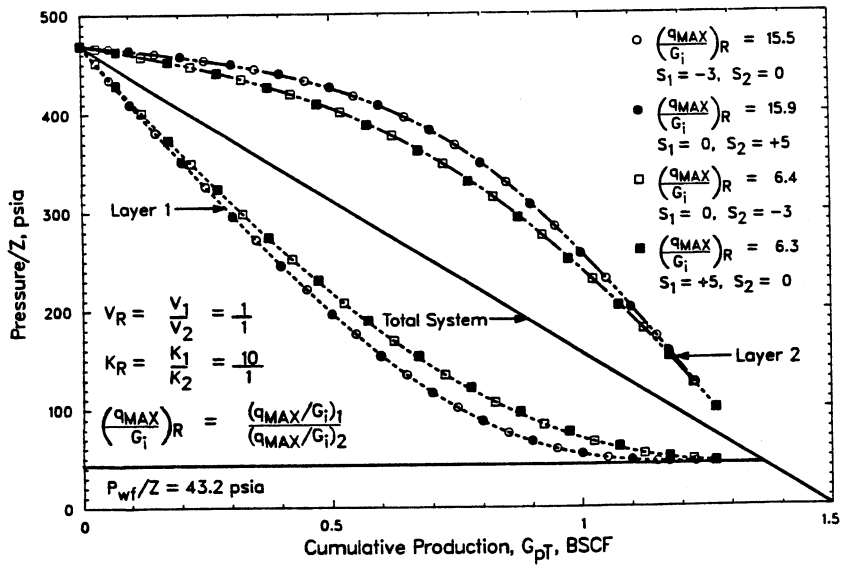

FIG. 9 EFFECT OF DIFFERENT LAYER SKIN (S) ON P/Z VS G_p CURVES, V_R = 1, K_R = 10

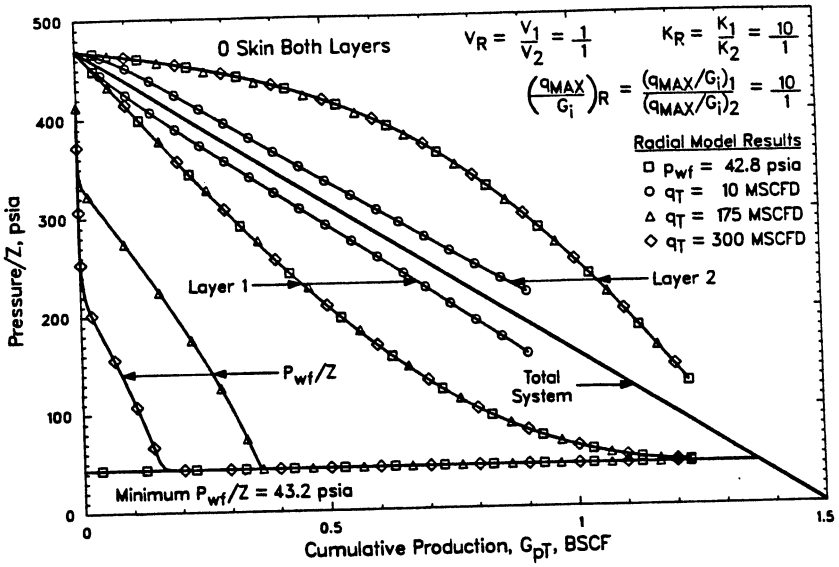

FIG. 10 EFFECT OF RATE ON DIFFERENTIAL DEPLETION

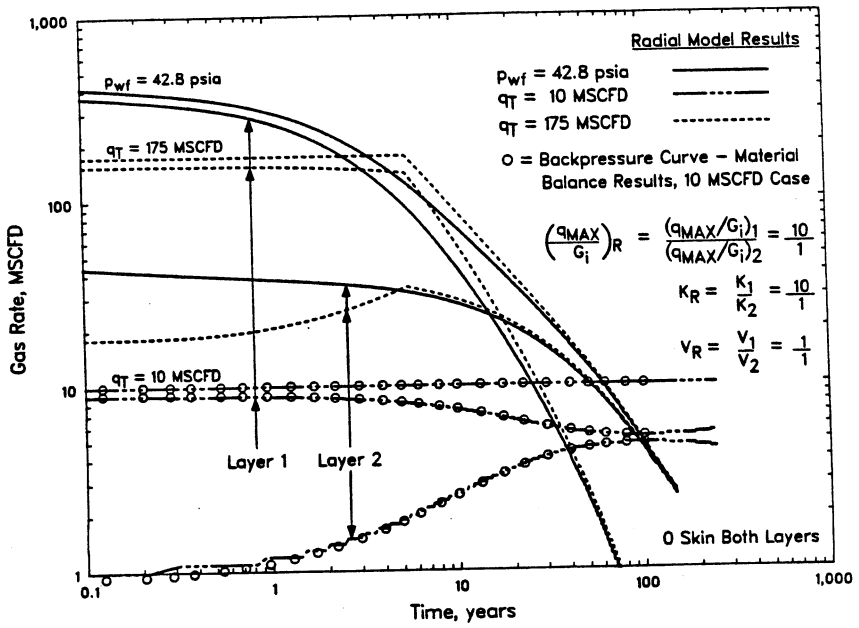

FIG. 11 LAYER AND COMPOSITE RATES VS TIME AT CONSTANT WELLBORE PRESSURE AND CONSTANT RATE

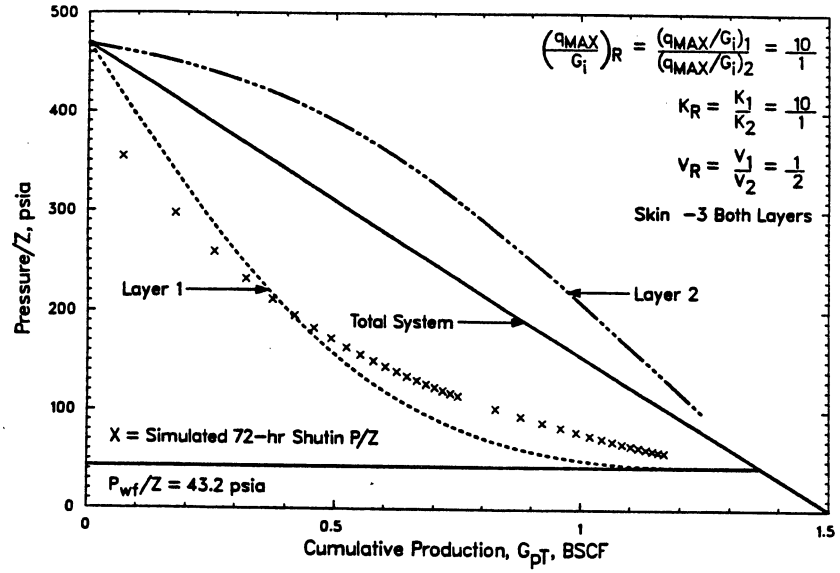

FIG. 12 SIMULATED 72-HOUR SHUT-IN P/Z COMPARED TO LAYER AVERAGE PRESSURE P/Z, CONSTANT WELLBORE PRESSURE CASE

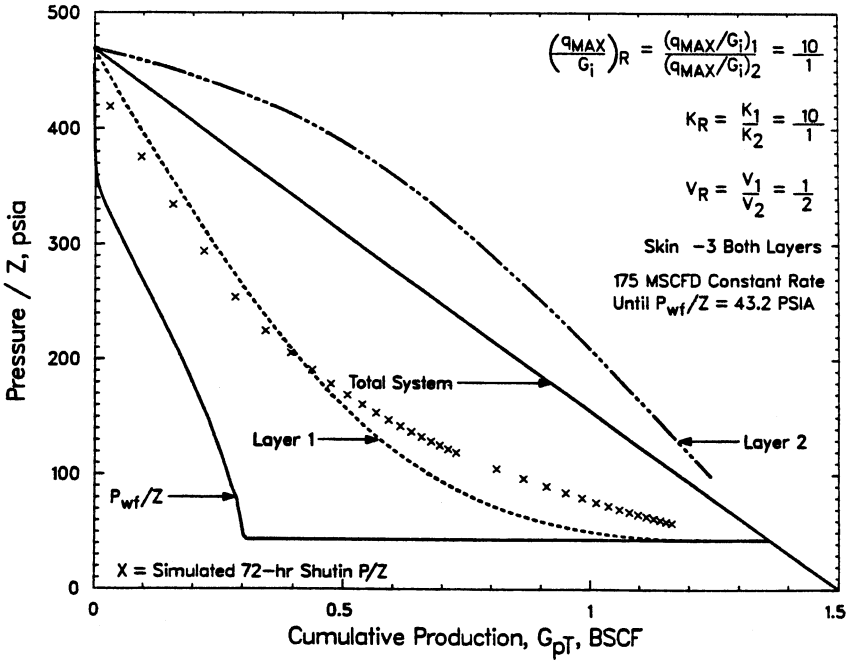

FIG. 13 SIMULATED 72-HOUR SHUT-IN P/Z COMPARED TO LAYER AVERAGE PRESSURE P/Z, CONSTANT RATE CASE

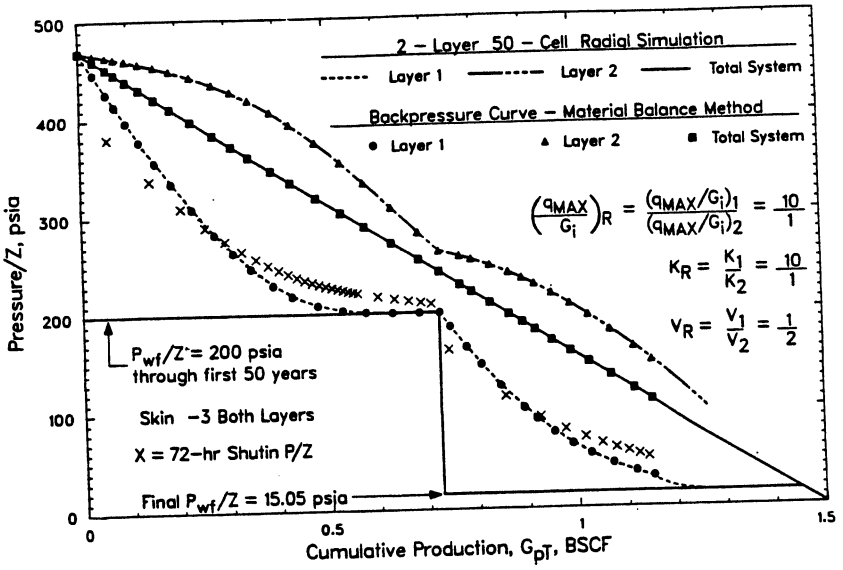

FIG. 14 EFFECT OF BACKPRESSURE, P_{WF}, CHANGE ON P/Z VS CUMULATIVE PRODUCTION GRAPH

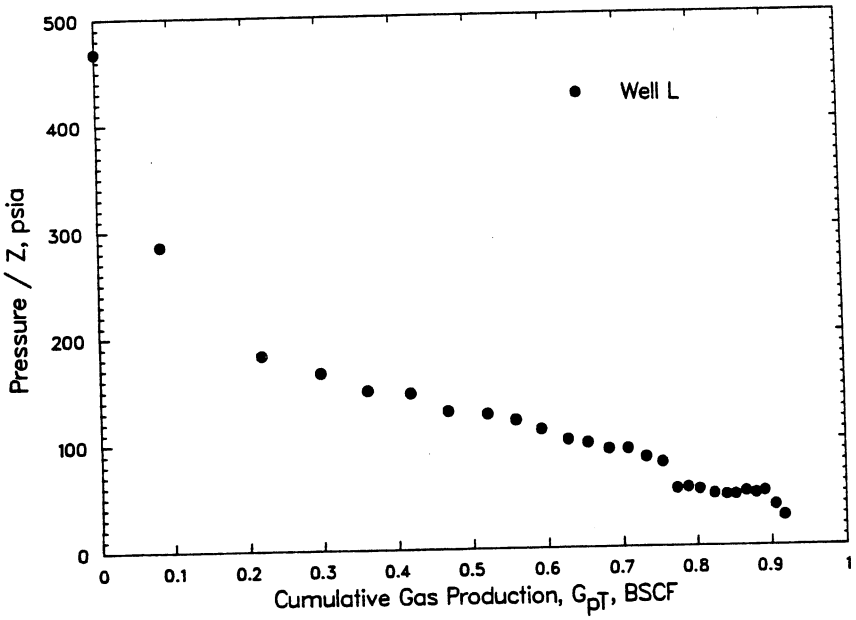

FIG. 15 FIELD EXAMPLE OF LINE PRESSURE CHANGE ON P/Z VS G_p GRAPH

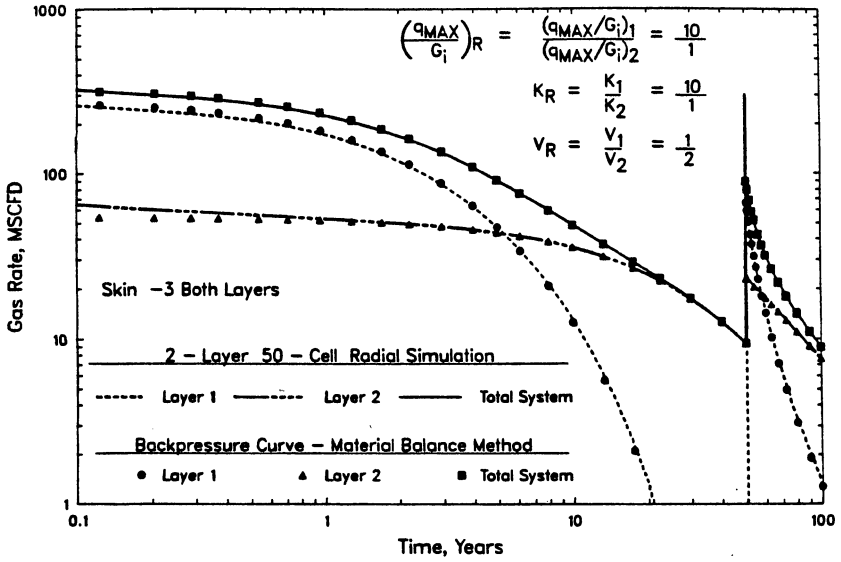

FIG. 16 EFFECT OF BACKPRESSURE, P_{WF}, CHANGE ON RATE-TIME PERFORMANCE

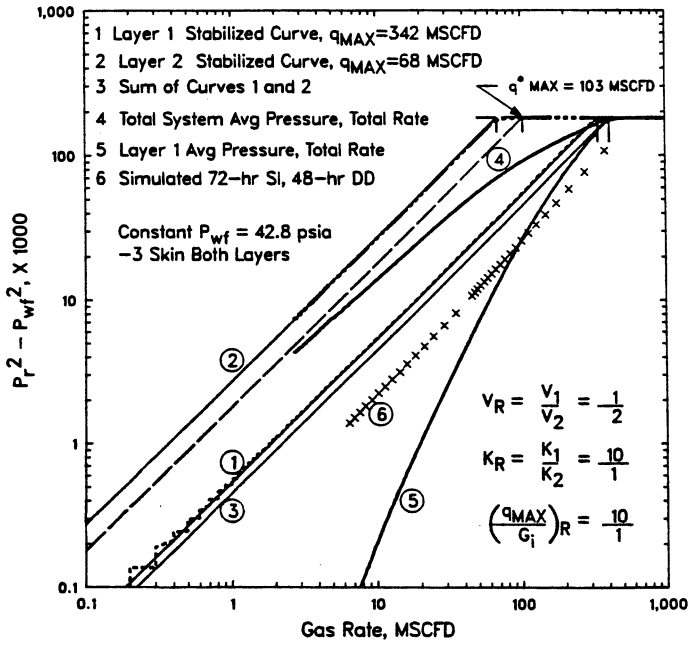

FIG. 17 LAYER AND COMPOSITE WELL BACKPRESSURE CURVE PERFORMANCE, CONSTANT WELLBORE PRESSURE

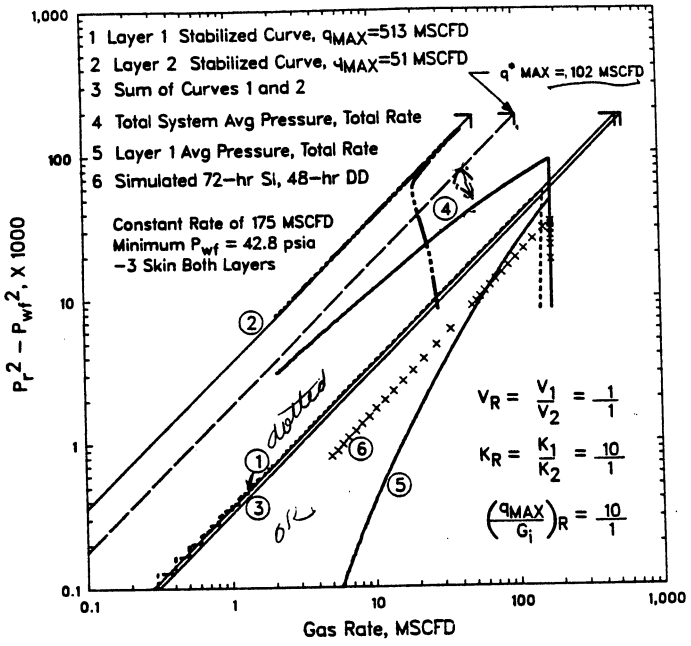

FIG. 18 LAYER AND COMPOSITE WELL BACKPRESSURE CURVE PERFORMANCE CONSTANT RATE AND CONSTANT WELLBORE PRESSURE

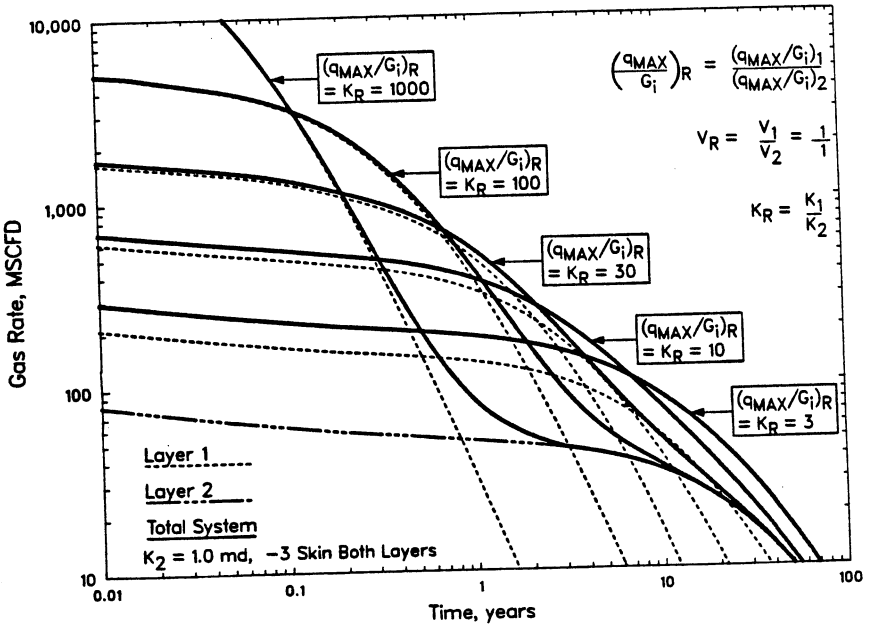

FIG. 19 EFFECT OF CHANGES IN $[q_{MAX}/G_i]_R$ RATIO ON TOTAL SYSTEM RATE AT $V_R = 1$

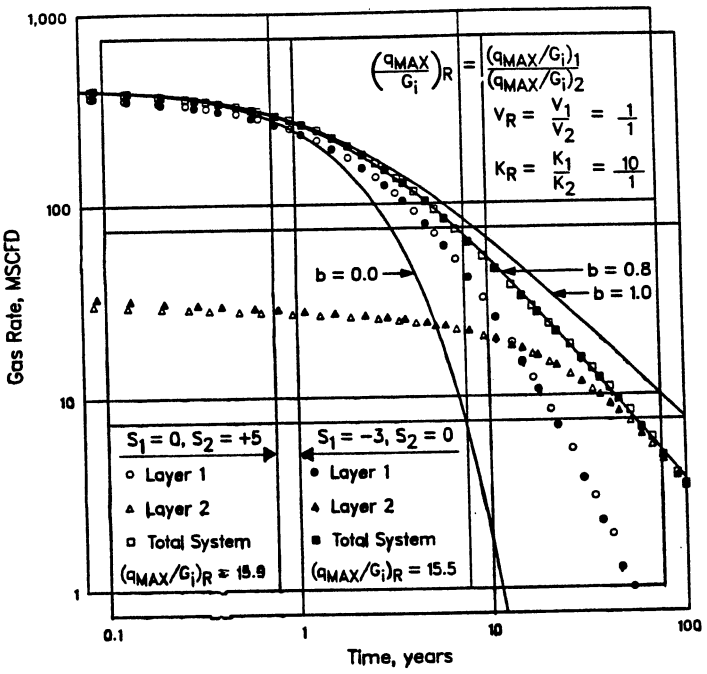

FIG. 20 EFFECT OF LAYER SKINS AT V_R = 1 AND K_R = 10 ON TOTAL SYSTEM DECLINE EXPONENT b

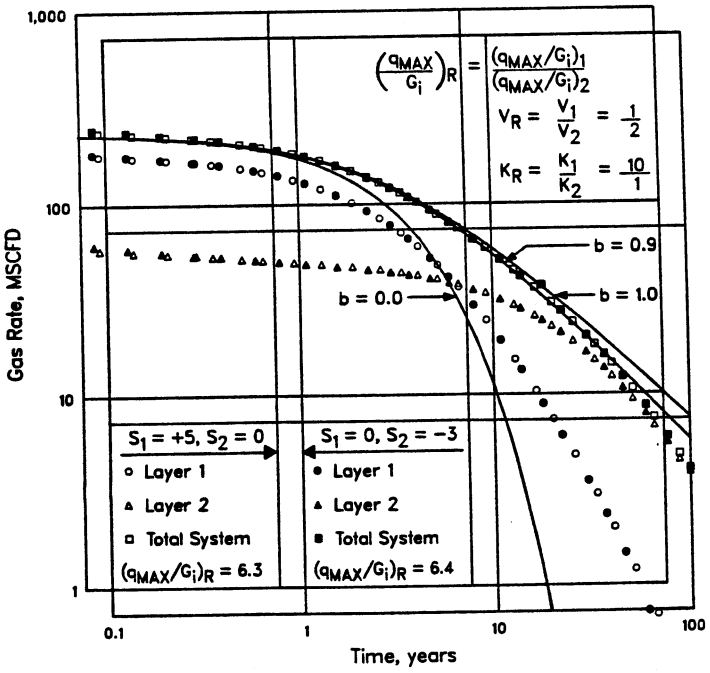

FIG. 21 EFFECT OF LAYER SKINS AT V_R = 1/2 AND K_R = 10 ON TOTAL SYSTEM DECLINE EXPONENT b

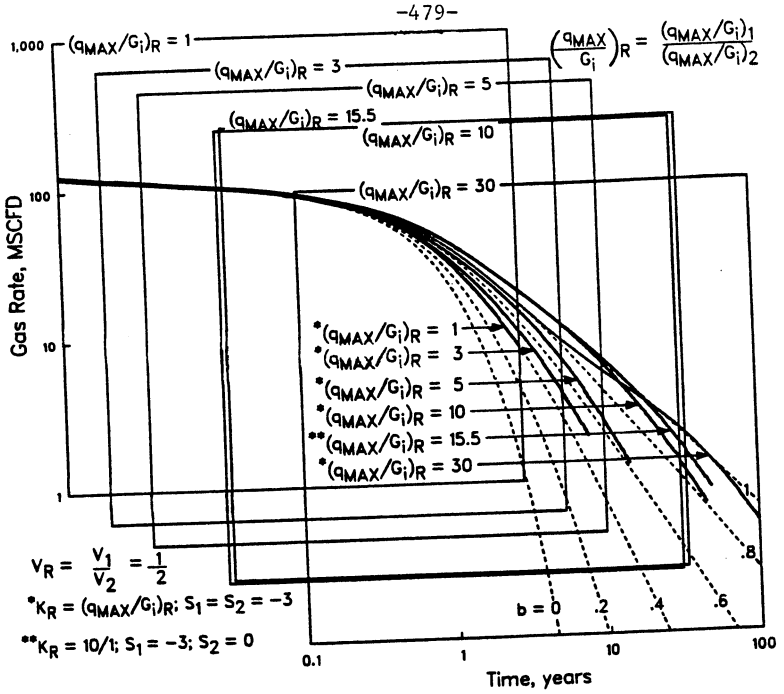

FIG. 22 COMPOSITE WELL DECLINES FOR $[q_{MAX}/G_i]_R$ BETWEEN 1 THRU 30 AT V_R = 1/2

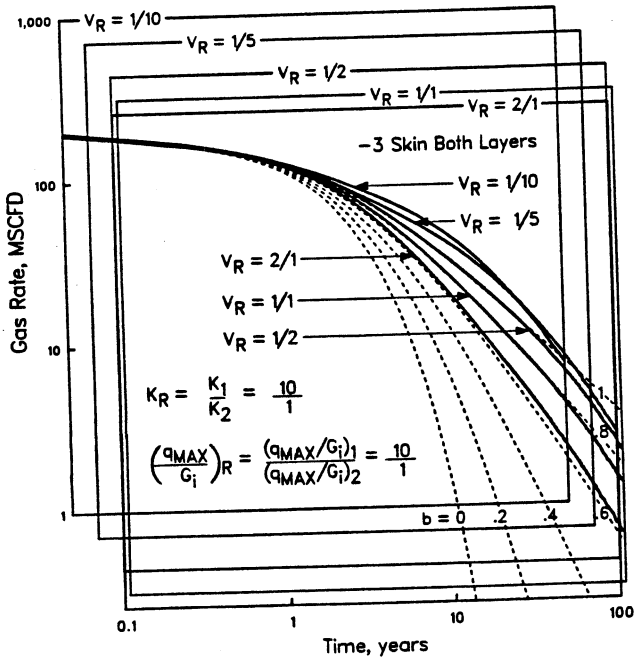

FIG. 23 COMPOSITE WELL DECLINES FOR V_R BETWEEN 2/1 THRU 1/10 AT $[q_{MAX}/G_i]_R$ = 10

DIMENSIONLESS FLOW RATE FUNCTIONS
PLANE RADIAL SYSTEM
INFINITE AND FINITE OUTER BOUNDARY,
CONSTANT-PRESSURE AT INNER BOUNDARY
∞ TO r_e/r_w = 100

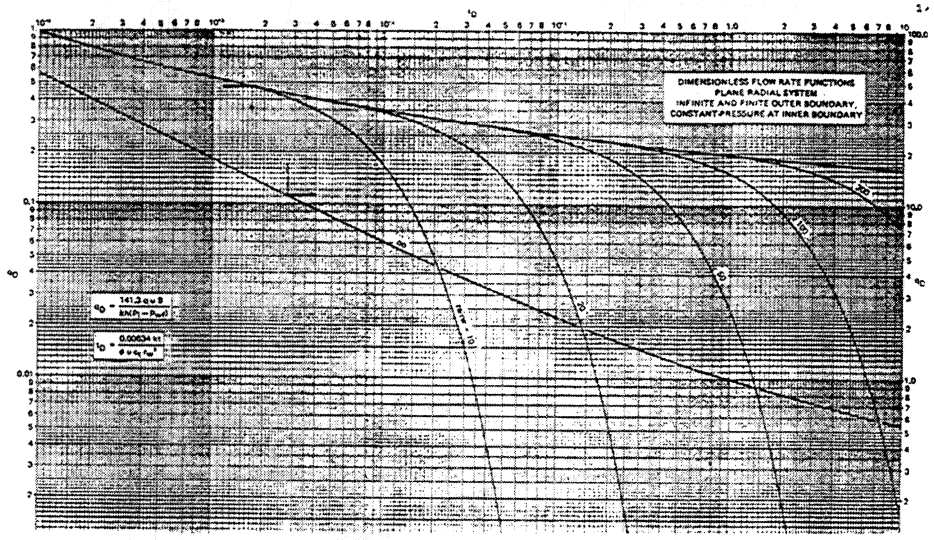

DIMENSIONLESS FLOW RATE FUNCTIONS
PLANE RADIAL SYSTEM
INFINITE AND FINITE OUTER BOUNDARY,
CONSTANT-PRESSURE AT INNER BOUNDARY
r_e/r_w = 100 TO r_e/r_w = 4000

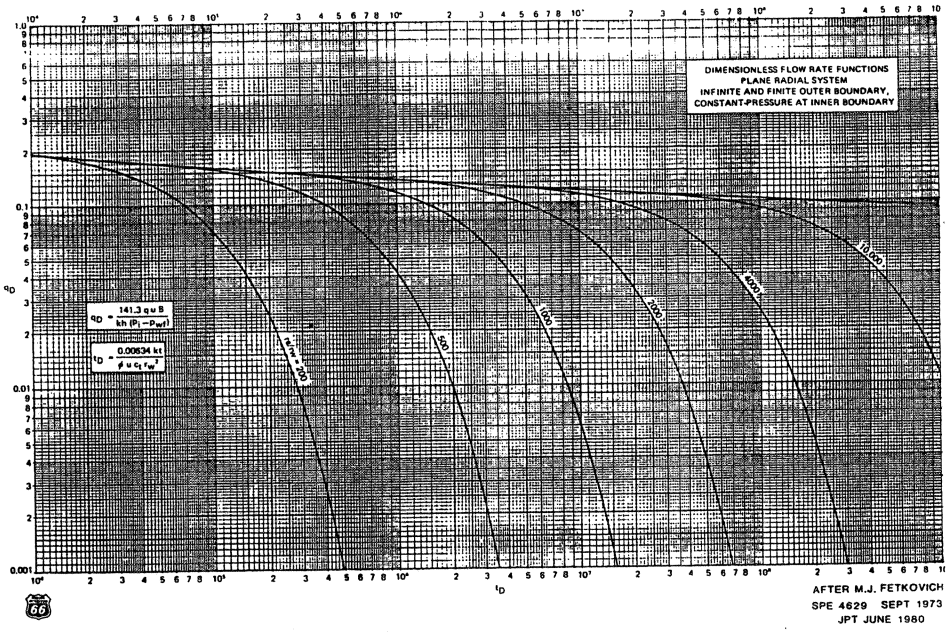

AFTER M.J. FETKOVICH
SPE 4629 SEPT 1973
JPT JUNE 1980

DIMENSIONLESS FLOW RATE FUNCTIONS
PLANE RADIAL SYSTEM
INFINITE AND FINITE OUTER BOUNDARY, CONSTANT-PRESSURE AT INNER BOUNDARY WITH INFINITE CONDUCTIVITY VERTICAL FRACTURE SOLUTION

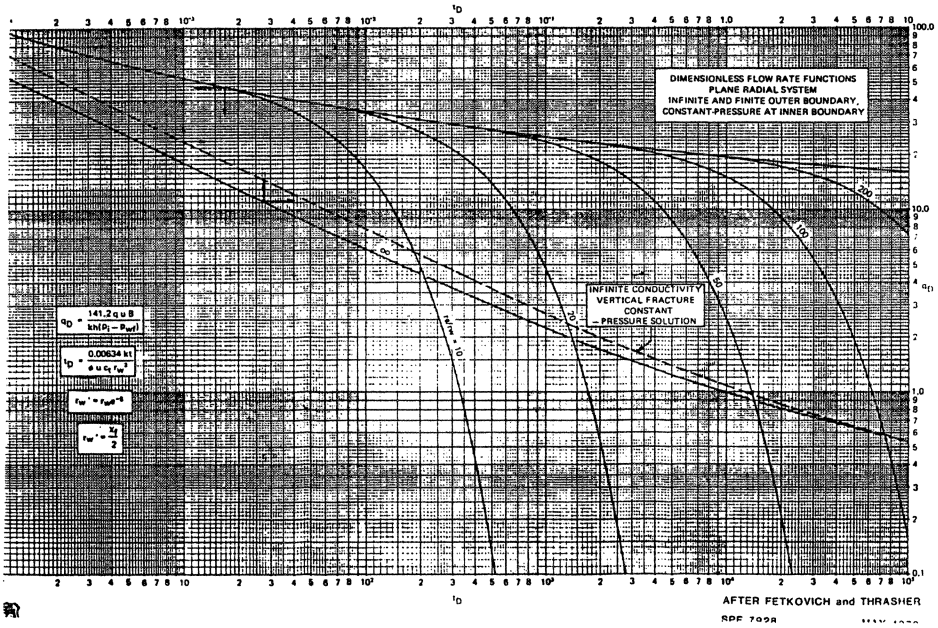

DIMENSIONLESS FLOW RATE FUNCTIONS
PLANE RADIAL SYSTEM
INFINITE AND FINITE OUTER BOUNDARY,
CONSTANT-PRESSURE AT INNER BOUNDARY
IN TERMS OF $q_{Dd} - t_{Dd}$

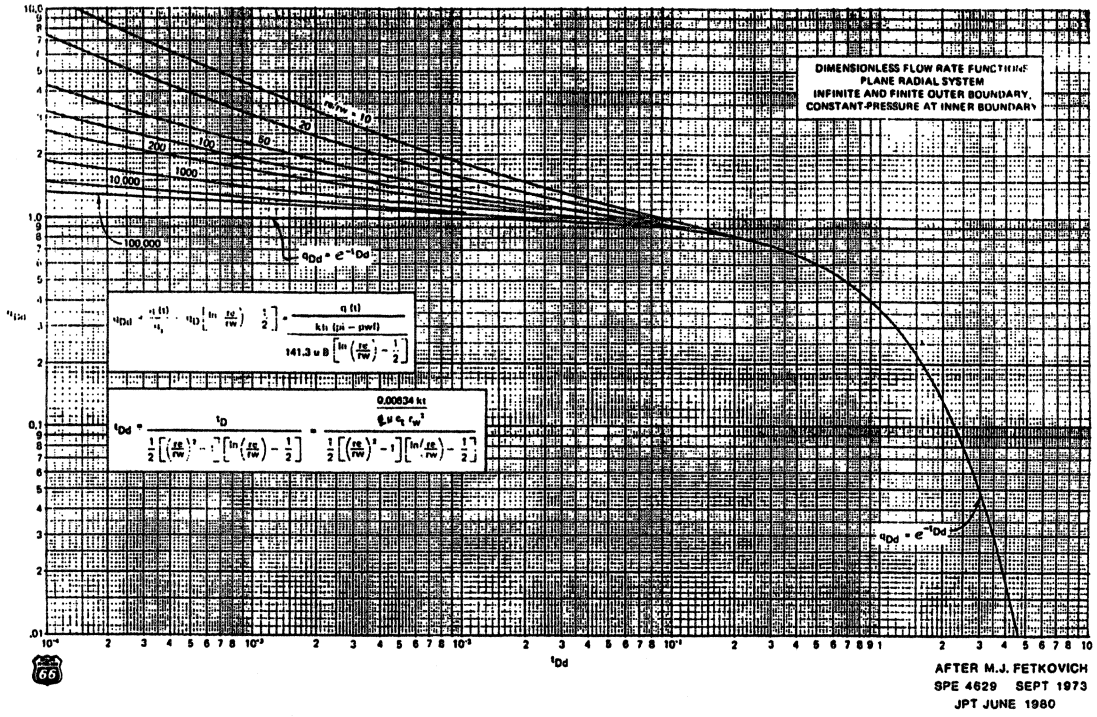

AFTER M.J. FETKOVICH
SPE 4629 SEPT 1973
JPT JUNE 1980

TYPE CURVES FOR ARPS EMPIRICAL RATE TIME DECLINE EQUATIONS UNITS SOLUTION (D_i = 1) FOR b = 0 TO b = 1.0

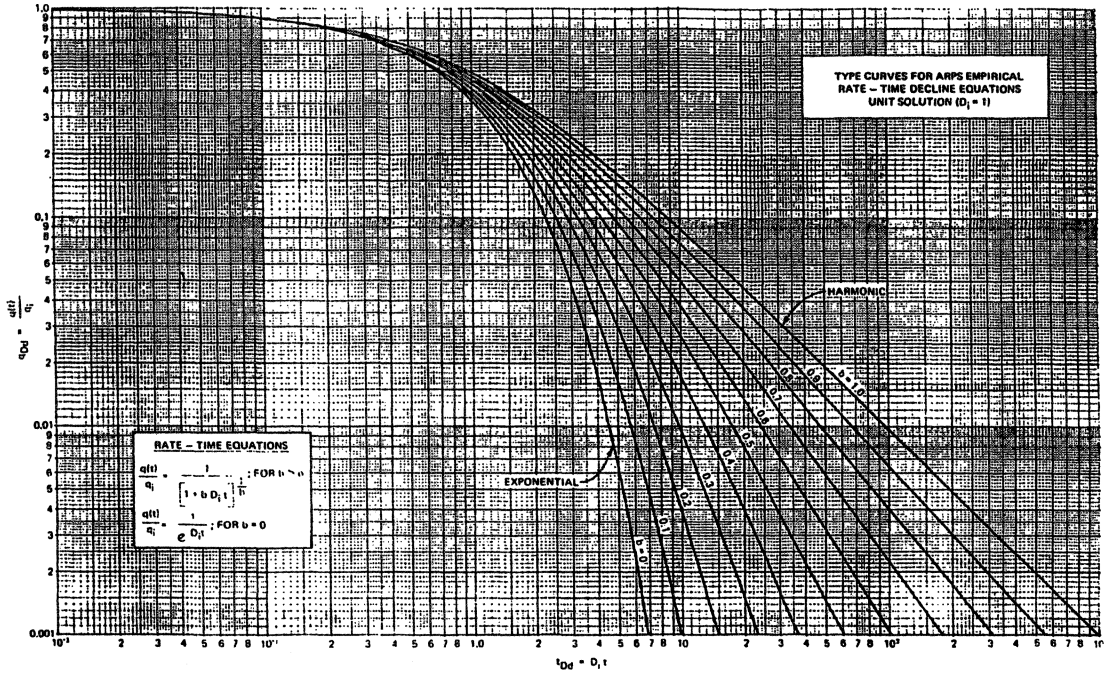

COMPOSITE OF THE
ANALYTICAL AND EMPIRICAL TYPE CURVES
FOR DECLINE CURVE ANALYSIS

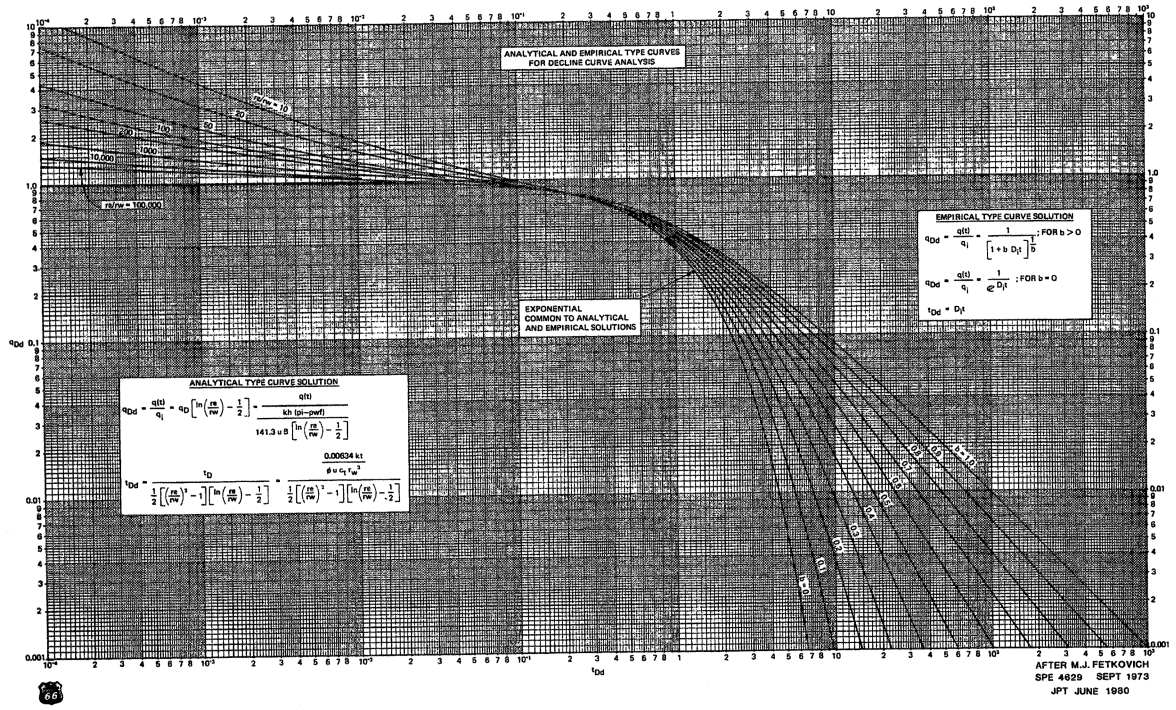

GAS RESERVOIR RATE-DECLINE TYPE CURVES WITH BACK PRESSURE FINITE SYSTEM WITH CONSTANT PRESSURE AT INNER BOUNDARY (p_{wf}) = CONSTANT @ r_w). EARLY TRANSIENT EFFECTS NOT INCLUDED AND Z = 1.0. BASED ON GAS WELL BACK PRESSURE CURVE SLOPE n = 1.00.

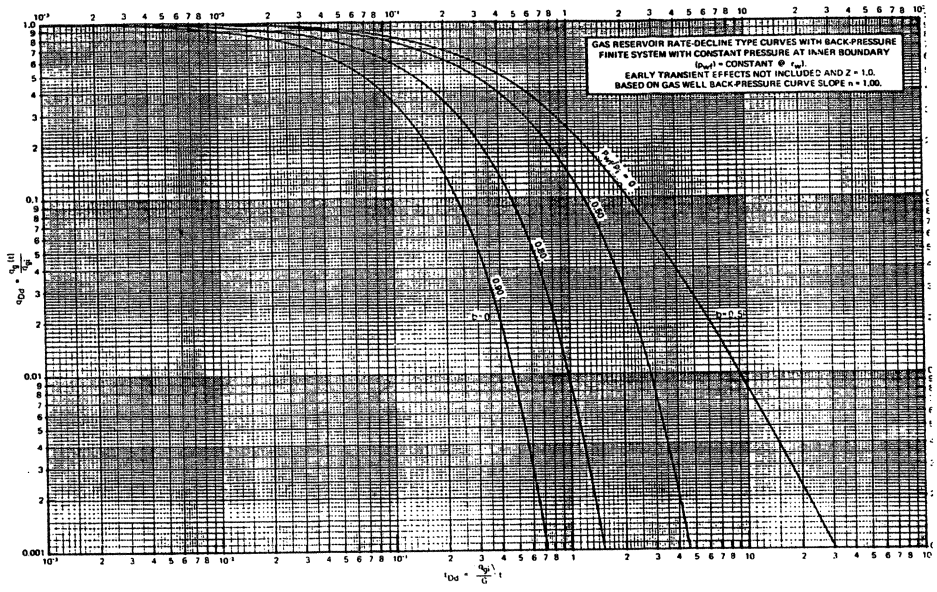

LOCKE AND SAWYER
TYPE CURVE FOR
INFINITE CONDUCTIVITY VERTICAL FRACTURE
CONSTANT-PRESSURE AT INNER BOUNDARY

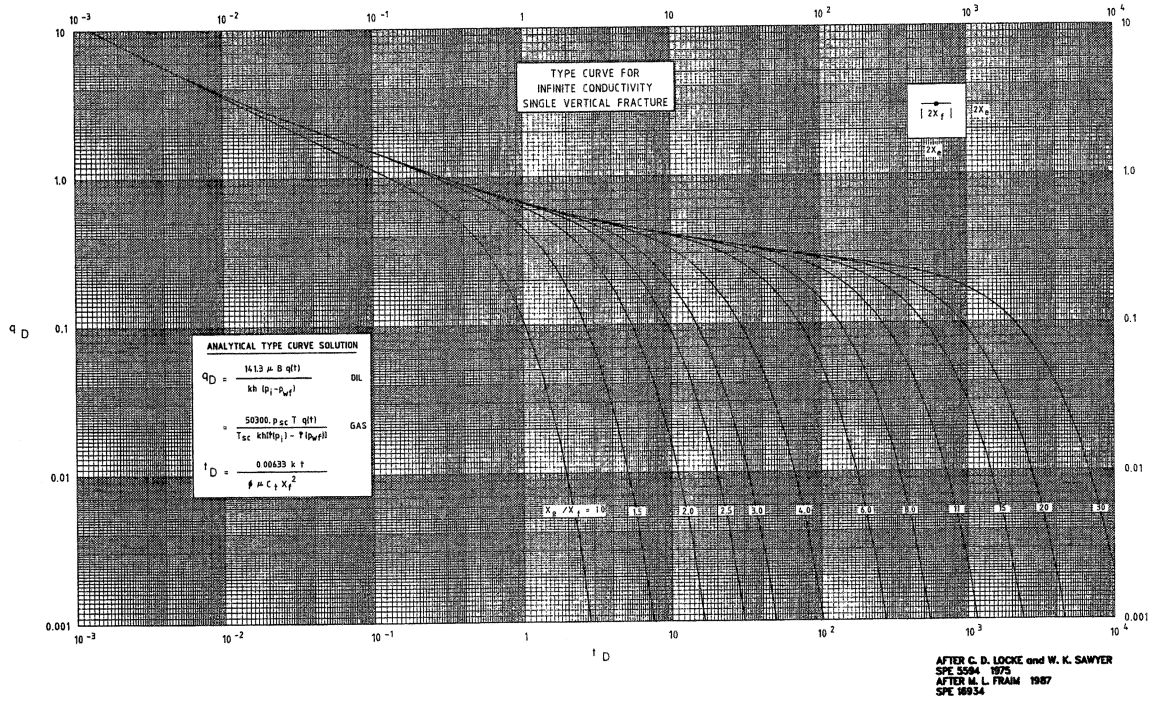

DIMENSIONLESS PRESSURE FUNCTION
PLANE RADIAL SYSTEM
INFINITE AND FINITE OUTER BOUNDARY TERMINAL RATE CASE
SKIN = 0
AFTER vanEVERDINGEN AND HURST

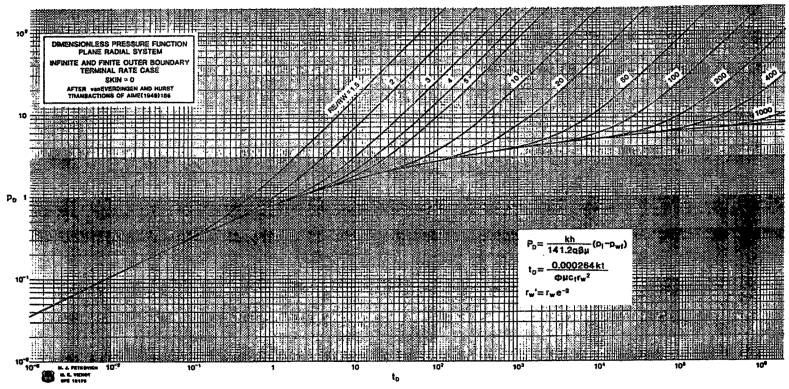

UNPROPPED FRACTURE
p_D VS t_{DL} FOR A VERTICALLY-FRACTURED WELL (ANALYTICAL SOLUTION.)

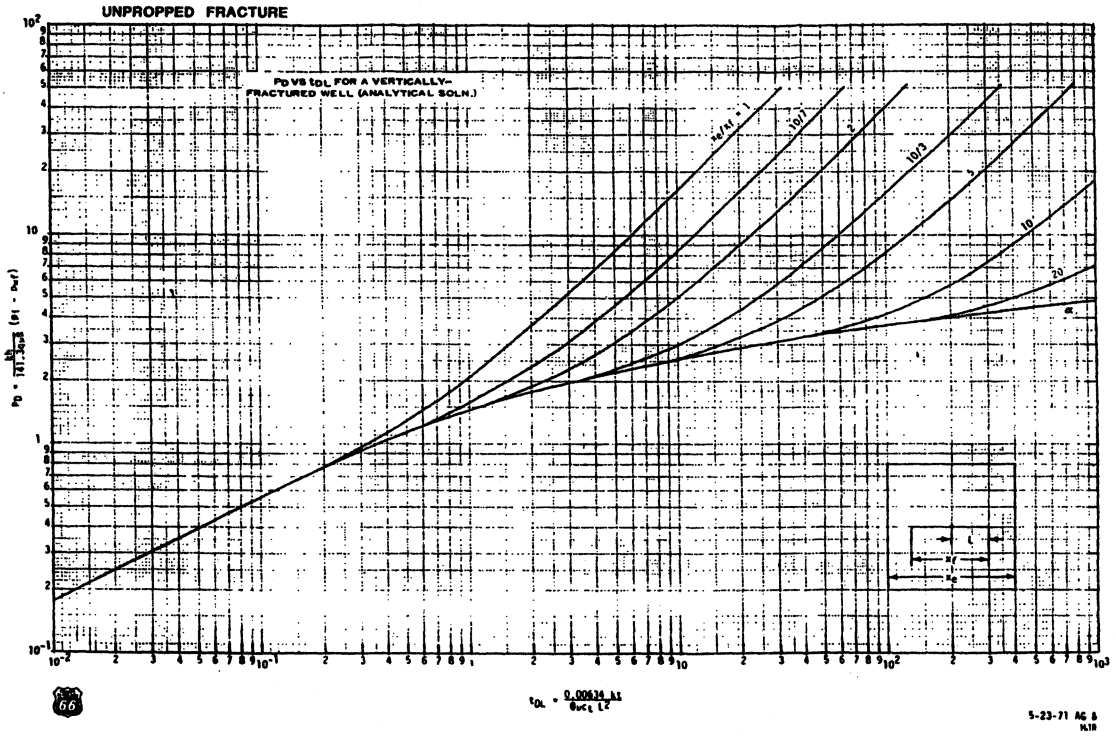

PROPPED FRACTURE
p_D VS t_{DL} FOR A VERTICALLY-FRACTURED WELL (ANALYTICAL SOLUTION.)